Topics in Current Chemistry 349

Jay S. Siegel
Yao-Ting Wu *Editors*

# Polyarenes I

Springer

# 349
# Topics in Current Chemistry

## Aims and Scope

The series Topics in Current Chemistry presents critical reviews of the present and future trends in modern chemical research. The scope of coverage includes all areas of chemical science including the interfaces with related disciplines such as biology, medicine and materials science.

The goal of each thematic volume is to give the non-specialist reader, whether at the university or in industry, a comprehensive overview of an area where new insights are emerging that are of interest to larger scientific audience.

Thus each review within the volume critically surveys one aspect of that topic and places it within the context of the volume as a whole. The most significant developments of the last 5 to 10 years should be presented. A description of the laboratory procedures involved is often useful to the reader. The coverage should not be exhaustive in data, but should rather be conceptual, concentrating on the methodological thinking that will allow the non-specialist reader to understand the information presented.

Discussion of possible future research directions in the area is welcome.

Review articles for the individual volumes are invited by the volume editors.

**Readership: research chemists at universities or in industry, graduate students**.

More information about this series at
http://www.springer.com/series/128

Jay S. Siegel • Yao-Ting Wu
Editors

# Polyarenes I

With contributions by

H.F. Bettinger · D.T. Chase · P.J. Evans · A.G. Fix · M.M. Haley · R. Jasti · J.S. Siegel · Z. Sun · C. Tönshoff · A.-F. Tran-Van · K.K. Wang · H.A. Wegner · J. Wu · Y.-T. Wu

Springer

*Editors*
Jay S. Siegel
School of Pharmaceutical Science and Technology
Tianjin University
Tianjin
China

Yao-Ting Wu
Department of Chemistry
National Cheng Kung University
Tainan
Taiwan

ISSN 0340-1022 ISSN 1436-5049 (electronic)
ISBN 978-3-662-43378-2 ISBN 978-3-662-43379-9 (eBook)
DOI 10.1007/978-3-662-43379-9
Springer Heidelberg New York Dordrecht London

Library of Congress Control Number: 2014955786



Printed on acid-free paper

Springer is part of Springer Science+Business Media (www.springer.com)

# Preface

The coming year (2015) will commemorate an important event in the history of chemistry, and – in particular – aromatic chemistry.

Exactly 150 years ago, on January 27, 1865, Adolphe Wurtz, formally presented August Kekulé's first benzene paper at a meeting of the Chemical Society of Paris. It was this event which was celebrated only 25 years later at the famous *Kekulé-Feier* or *Benzolfest* on March 11, 1890 in Berlin, in which Kekulé – after the plenary address of the vice-president of the Deutsche Chemische Gesellschaft, Adolf Baeyer, who was also Kekulé's first student – revealed his dreams to the public in which he had arrived at structural theory and the hexagonal structure of benzene (There is a vast amount of literature on the (two) dreams and the *Benzolfest* – from the psychological and historical viewpoints, from the importance of the benzene formula in organic chemistry and industry to the question of whether it was really Kekulé who was the first to propose this breakthrough. None of this will be repeated here; I just want to recommend to the reader the – in my view – most significant and clairvoyant monograph about this fascinating area of early organic chemistry: [1]).

The report on the Benzolfest in *Berichte der Deutschen Chemischen Gesellschaft* [2] is still a marvelous and highly enjoyable piece of chemical literature and – not the least – a tribute to international co-operation and friendship. It contains many deep insights into the nature of the scientific process and distinguishes itself by the humbleness and honesty of the speaker. Still, there are some conclusions which, I believe, are erroneous.

The most notable of these reads (in German): *Etwas absolut Neues ist noch niemals gedacht worden, sicher nicht in der Chemie*. (Absolutely new ideas have never been conceived, certainly not in chemistry). The first half of this quote, a paraphrase of a citation from the Old Testament (Ecclesiates 1:9) has been cited on many occasions, but it is – at best – only partly true.

To be sure, during most of the first century after the discovery of benzene (Faraday 1825) and Kekulé's hexagon structure (1865) the terms aromatic chemistry and benzene chemistry were practically synonyms, especially if the enormous success of the coal tar and dyestuffs industry is taken into account. It is a safe

assumption that Kekulé's dreams during these decades would have focused on the countless derivatives which can be prepared from this icon of organic chemistry. But, alas, Kekulé did nor dream any more, at least not in public.

The situation began to change when, as a consequence of quantum theory, and in particular the Hückel theory, nonbenzenoid aromatic molecules came onto the scene. These indeed represented many new aromatic (and antiaromatic) entities, whether neutral or charged. Clearly, this development, which ended in the 1960s and 1970s and was strongly driven by the introduction of new physical methods into organic chemistry (NMR spectroscopy!) as well as the development of computational chemistry represents the high point of aromatic chemistry of the twentieth century.

Interestingly, both benzenoid and nonbenzenoid aromatic compounds share a *structural* concept; namely, that all these systems were – by theory had to be! – planar. The origin of this obsession with planarity is manifold. It certainly goes back to benzene itself which in the minds of many chemists was a *rigid* entity. It is the tile-like chemical compound par excellence: just by putting these hexagonal moieties together one can build up an endless series of compounds: naphthalene, anthracene, phenanthrene, pyrene, coronene, the polyaromatic hydrocarbons (PAHs), etc., ad infinitum. All of them completely flat. The notion of rigidity of these compounds was also supported by the stiff molecular models usually employed by chemists in their daily work. And, of course, the Hückel rule seemed to demand planarity with all the axes of the overlapping p-orbitals oriented in parallel fashion for optimal effect.

Had Kekulé had access to an IR spectrometer (and also known the corresponding theory!) he would have noticed that the rigidity of his hexagon and its derivatives is rather limited, the out-of-plane bending vibrations being clearly recognizable in the region of ca. 1,000 $cm^{-1}$ and below in the IR spectrum, i.e., in a low energy section.

That in real life – in the laboratory of the synthetic chemist – the benzene rings do not have to be planar to display their aromaticity (as shown by their chemical and spectroscopic properties) became increasingly obvious when Cram´s seminal studies on cyclophanes began to appear, hydrocarbons which are characterized by "bent and battered" rings (Cram).

Other deliberate steps "out of the plane, into three-dimensional space" were also undertaken in the 1960s (see the corannulene synthesis by Lawton and Barth 1966). The real death blow to planar thinking, which is just another word for rigid thinking, came with the fullerene work of Kroto, Smalley, Krätschmer, and many others. I am sure that even Kekulé would have called these results "new."

From this paradigm change onwards, the benzene ring and all the aromatic and nonbenzenoid compounds derived therefrom – in whatever configuration or conformation – have become the building blocks for an endless variety of π-systems with planar or three-dimensional structures. The endless chemical space which can be constructed with double and triple bonds (in the simplest case) is becoming structurally as complex as the C–C single bond compounds. That many of these artifacts do not survive under the usual laboratory conditions most often has to do with their high reactivity, not their structural complexity.

To return to the title question: a modern day Kekulé would most likely not sit in front of a fancy fireplace or in a bus, but look at the marvelous aromatic molecules discussed in every single chapter of this book – and then start dreaming.[1]

Braunschweig, Germany Henning Hopf

## References

1. Rocke AJ (2010) Image and reality. The University of Chicago Press, Chicago
2. (1890) Ber Deutsch Chem Ges 23:1302. The speech is available on the net (in German): http://www.sgipt.org/wisms/geswis/chem/kek1890.htm

[1] Advice to younger readers: Kekulé in his Benzolfest speech did not recommend "dreaming" as a scientific method. In fact, he specifically addressed this problem by saying:

> "*Let us dream, gentlemen (chemists at that time were practically exclusively male), then we will possibly find the truth. But beware of publishing our dreams, before we have tested them with a wide-awake mind.*"

# Contents

**Beyond Pentacenes: Synthesis and Properties of Higher Acenes** ..... 1
Christina Tönshoff and Holger F. Bettinger

**Twisted Arenes** ..... 31
Kung K. Wang

**Synthesis, Structures, and Physical Properties of Aromatic Molecular-Bowl Hydrocarbons** ..... 63
Yao-Ting Wu and Jay S. Siegel

**Strategies in Organic Synthesis for Condensed Arenes, Coronene, and Graphene** ..... 121
Anne-Florence Tran-Van and Hermann A. Wegner

**Indenofluorenes and Derivatives: Syntheses and Emerging Materials Applications** ..... 159
Aaron G. Fix, Daniel T. Chase, and Michael M. Haley

**Closed-Shell and Open-Shell 2D Nanographenes** ..... 197
Zhe Sun and Jishan Wu

**Molecular Belts** ..... 249
Paul J. Evans and Ramesh Jasti

**Index** ..... 291

Top Curr Chem (2014) 349: 1–30
DOI: 10.1007/128_2013_437

Published online: 11 May 2013

# Beyond Pentacenes: Synthesis and Properties of Higher Acenes

**Christina Tönshoff and Holger F. Bettinger**

**Abstract** Acenes consist of linearly annulated benzene rings. Their reactivity increases quickly with increasing chain length. Therefore acenes longer than pentacene are very sensitive towards oxygen in the presence of light and thus these molecules have not been well studied or have remained elusive in spite of synthetic efforts dating back to the 1930s. This review gives an historical account of the development of the chemistry of acenes larger than pentacene and summarizes the recent progress in the field including strategies for stabilization of higher acenes up to nonacene.

**Keywords** Acenes · Alternant hydrocarbon · Polymer · Spectroscopy · Synthesis

## Contents

1 Introduction ..... 2
2 Hexacenes ..... 3
2.1 Parent Hexacene ..... 3
2.2 Substituted Hexacenes ..... 7
3 Heptacenes ..... 9
3.1 Parent Heptacene ..... 9
3.2 Substituted Heptacenes ..... 14
4 Octacene and Nonacene ..... 21
4.1 Parent Octacene and Nonacene ..... 21
4.2 Silylethynyl Substituted Nonacenes ..... 23
4.3 Thioaryl Substituted Nonacenes ..... 26
5 Conclusions and Outlook ..... 28
References ..... 28

C. Tönshoff and H.F. Bettinger (✉)
Institut für Organische Chemie, Universität Tübingen, Auf der Morgenstelle 18, 72076 Tübingen, Germany
e-mail: holger.bettinger@uni-tuebingen.de

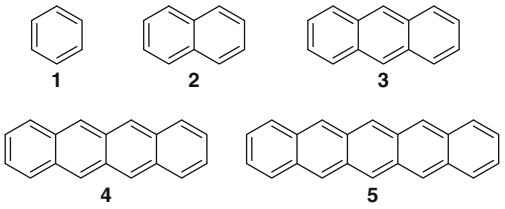


**Fig. 1** The smaller acene molecules **1**–**5**

## 1 Introduction

Acenes are polycyclic aromatic hydrocarbons that consist of linearly fused benzene rings. The smaller members of the acene series are well-known organic compounds. For example, benzene **1** was discovered by Michael Faraday in 1825, and the next highest homologue, naphthalene **2**, was isolated in 1819 from coal tar. Anthracene **3**, tetracene **4** (also known as naphthacene), and pentacene **5** follow as the next highest homologues (Fig. 1). Pentacene was first synthesized by Clar and John in 1930 [1]. The name "pentacene" was introduced by Philippi, who claimed its synthesis in 1929 [2]. Clar and John showed that Philippi's hydrocarbon was a dihydropentacene that could be turned into the blue pentacene by dehydrogenation [1]. Clar noticed the high radical character of his novel deep blue hydrocarbon and considered it to be the most stable radical known at that time [1]. As the name "pentacene" was taken by Philippi's hydrocarbon, Clar named his blue hydrocarbon 2,3,6,7-dibenzoanthracene-9,10-diyl in view of its radical character [1]. Clar later suggested that the polycyclic aromatic compounds consisting of linearly fused benzene units be called "acenes" [3].

To a large extent, current interest in the acene series is due to the fact that these molecules are valuable compounds in organic electronics. In particular, pentacene is at the focus of organic materials research [4, 5]. In contrast to the extremely well investigated pentacene, longer acenes are considerably less well studied. This is due to their low solubility and high reactivity. For example, the rate constant for the Diels–Alder reaction with maleic anhydride increases strongly with acene length (Table 1) [6]. The sites of addition in all cases are the hydrogen carrying carbon atoms of the central ring(s). These represent the most reactive sites of any given acene.

The enormous interest in pentacene has naturally led to the question of whether larger acenes could have even more favorable properties for materials applications. This has led to a revival of the chemistry of higher acenes in the last decade.

The strong interest in the acenes as potential semiconducting materials has led to a number of reviews of this field [7–11]. The purpose of the present account is to review the properties of the higher acenes, which we define for the purpose of this account as those that are larger than pentacene (Fig. 2).

**Table 1** Rate constants $k_2$ for the reaction of acenes with maleic anhydride

| Acene | $10^6$ $k_2$/L $mol^{-1}$ $s^{-1}$ |
|---|---|
| Benzene | No reaction |
| Naphthalene | No reaction |
| Anthracene | 2,270 |
| Tetracene | 94,200 |
| Pentacene | 1,640,000 |
| Hexacene | 6,570,000 |

Data taken from [6]

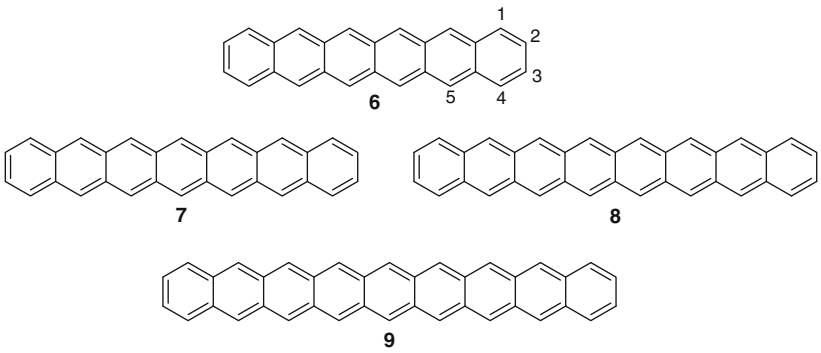


**Fig. 2** The higher acene molecules **6–9** discussed in this review

## 2 Hexacenes

### *2.1 Parent Hexacene*

The synthesis of this hydrocarbon with the formula $C_{26}H_{16}$ was first reported by Clar in 1939 [12]. It was obtained by dehydrogenation of 5,16-dihydrohexacene **10** during sublimation over copper powder at 300–320°C (Fig. 3). Clar described hexacene as a deep green compound with steel-blue surface reflections that is only poorly soluble in boiling xylene. This solution quickly loses its color due to the extreme sensitivity towards air and light. Immediate decoloration was also observed upon addition of maleic anhydride. Clar also noted that hexacene decomposes slowly upon heating to 300°C and upon vacuum sublimation at higher temperatures.

French chemist Charles Marschalk also synthesized hexacene in the late 1930s and reported properties similar to those described above [13]. An interesting correspondence between Clar and Marschalk is described in Clar's 1939 paper: in a September 1, 1938 letter by Marschalk to Clar, Marschalk communicates that he is on the way to the synthesis of heptacene. Clar described having finished and had already communicated the results of his work on hexacene to the chemical industry on April 2, 1938. Clar replied to Marschalk on September 11, 1938 that he had

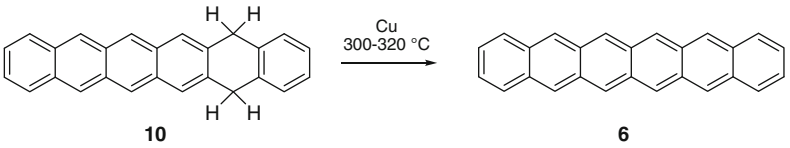


**Fig. 3** Synthesis of hexacene **6** from 5,16-dihydrohexacene **10** [12]

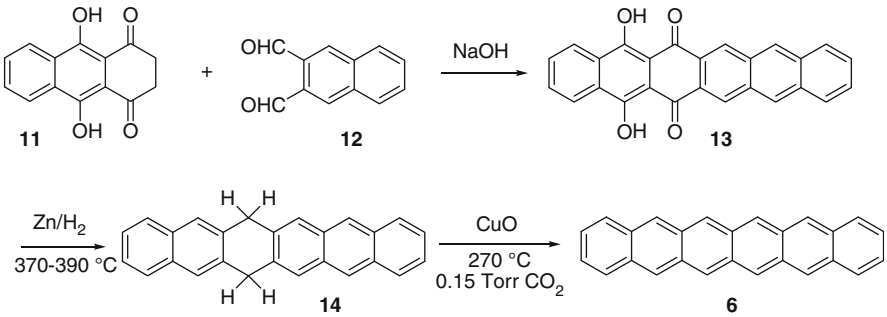


**Fig. 4** Three-step synthesis of hexacene **6** [17]

made hexacene, but would not be able to publish this result for technical reasons. Clar asked Marschalk to leave the investigation of hexacene to him. Marschalk agreed a few weeks later (September 28, 1938), and Clar expressed his gratitude to Marschalk in his paper.

A number of improved syntheses of hexacene have been reported since 1939 [14–17]. The improvements are related to the synthesis of dihydrohexacenes (like **14**), and the final step remains the catalytic dehydrogenation. An example (Fig. 4) is the three-step synthesis reported by Satchell and Stacey [17] that starts with an aldol condensation between 9,10-dihydroxyanthracene-1,4(2*H*,3*H*)-dione **11** and naphthalene-2,3-dicarbaldehyde **12**.

Due to its sensitivity to air and light, hexacene was not much investigated experimentally in the following decades. An X-ray crystallography investigation of small, extremely thin crystals that were invariably twinned allowed one to obtain the space group P-1 and unit cell dimensions, but the poor quality of the data precluded determination of bond parameters [18]. The absorption spectrum of hexacene received most attention. It was studied for crystalline material by Preuss and Zander [19], in solution by Wirz and co-workers [20] and Nijegorodov et al. [21], and in a solid argon matrix by Bettinger et al. [22]. The Wirz group also obtained solution spectra of the hexacene dication and dianion [20], as well as of its radical ions in the early 1980s [23]. The latter were also studied under matrix isolation conditions in solid argon [22]. The infrared spectrum of hexacene is also available [22]. Photoelectron spectroscopy studies have revealed the ionization potentials of hexacene [24, 25]. Biermann and Schmidt measured the second-order rate constant for the Diels–Alder reaction with maleic anhydride in 1980 (see above) [6].

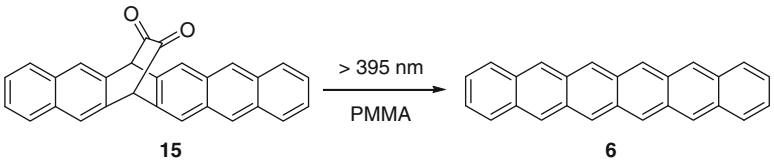


**Fig. 5** Photochemical generation of hexacene from α-diketone **15** [29]

The electrical conductivity of hexacene under pressure was studied in 1964 [26]. It was found to resemble the properties of pentacene in as much as the resistance decreased with pressure, but firm statements could not be made due to the limited supply of hexacene [26]. The conductivity of doped hexacene thin films was also investigated [27, 28]. Minakata et al. [27] found that doping with alkali metals, i.e., with electron donors, increased conductivity to $10^{-4}$ to $10^{-5}$ $\Omega^{-1}$ $cm^{-1}$, but much less so than observed for pentacene films. Likewise, the conductivity increased upon acceptor doping (iodine) [28]. The lower conductivity of doped hexacene compared to pentacene films was ascribed to structural disorder of the hexacene films, as these were amorphous while the pentacene films were crystalline. The hexacene thin films also showed optical properties that differed from pentacene: the initially green thin film of hexacene lost color within seconds after exposure to air, but upon doping with Rb the green color first regenerated and eventually the yellow color of hexacene-Rb formed. The doped yellow material turned gray during measurement of the UV/vis spectrum [27]. The iodine doped hexacene film also has a yellow color and a new absorption peak at 360 nm [28].

Mondal et al. reported an investigation of the photochemical synthesis of hexacene from an α-diketone **15** in 2007 (Fig. 5) [29]. A similar procedure was used successfully earlier for the photochemical formation of pentacene [30, 31].

Photolysis of a degassed toluene solution of **15** produced the absorption spectrum of hexacene in the early stages of conversion. However, the hexacene absorptions only increased initially; continued irradiation to effect a higher degree of conversion of the α-diketone **15** produced a hexacene dimer and oxygen adducts according to matrix assisted laser desorption ionization (MALDI) mass spectrometry [29]. The structure of the decomposition products could not be elucidated. Photogeneration of hexacene in oxygen saturated solutions indicated the formation of endoperoxides based on the typical singlet of the bridgehead protons between 6.0 and 6.1 ppm in the $^{1}$H-NMR spectrum [29]. The formation of oxygenated products indicates that hexacene in solution immediately reacts with trace amounts of oxygen during irradiation.

Neckers and coworkers could, however, generate hexacene photochemically after the photoprecursor had been embedded in a poly(methyl methacrylate) matrix (PMMA) [29]. Due to immobilization of the molecules, this matrix prevents photodimerization of hexacene and minimizes contact with ambient oxygen. Within the PMMA film (≈0.5 mm thick), hexacene is stable under ambient conditions overnight, but it is slowly oxidized by diffusion of molecular oxygen into the PMMA matrix [29].

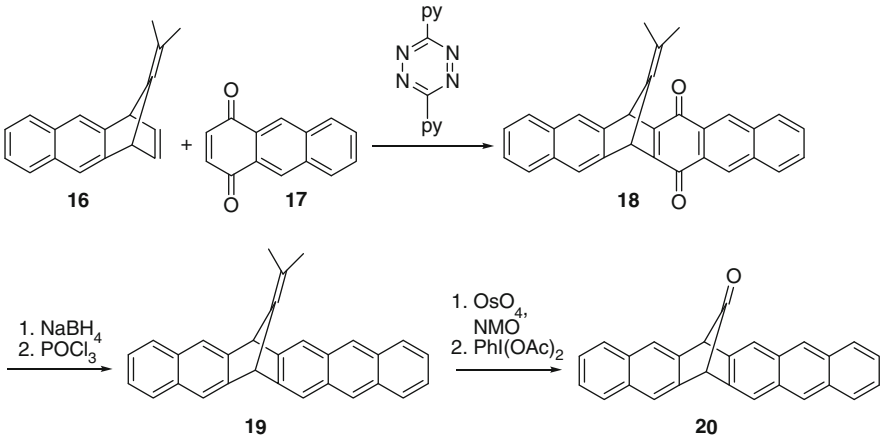


**Fig. 6** Synthesis of monoketone precursor **20** of hexacene [32]

Very recently, the synthesis of hexacene from a bridged monoketone precursor **20** was reported by Watanabe et al. [32]. Using Diels–Alder chemistry, the monoketone **20** was constructed from the isonaphthofulvene precursor **16** and anthracene-1,4-dione **17** (Fig. 6). After reduction and aromatization of the quinone **18** to give **19**, the double bond is oxidatively cleaved to yield **20**.

The photochemical decomposition ($\lambda = 365 \pm 30$ nm) of **20** in THF solution produced hexacene (Fig. 7) as identified by the typical vibrational progression of the *p* band. However, before quantitative conversion of the precursor was achieved, hexacene decomposed under the irradiation conditions. This observation is similar to that reported by Mondal et al. [29] using their α-diketone **15**.

Thermal decomposition of the bridged monoketone precursor **20** in the solid state, on the other hand, produced green-blue hexacene in a rather clean reaction, as indicated by cross-polarization magic angle spinning $^{13}$C NMR as well as by IR spectroscopy (Fig. 7) [32]. Watanabe et al. [32] succeeded in growing crystals of hexacene by vapor deposition. These were suitable for single-crystal X-ray crystallography. Hexacene crystallizes in the triclinic space group P-1, and the molecules pack in a herringbone motif similar to pentacene (Fig. 8) [32].

The authors investigated the chemical stability of solid hexacene in some detail [32]. They reported that hexacene is stable towards air in the dark both in the solid state and as a thin film. Irradiation of the thin film in air resulted in partial photodecomposition, as evidenced by a new UV/vis band at 430 nm and by detection of an endoperoxide by MALDI-TOF mass spectrometry [32]. However, even after 300 min of irradiation, substantial amounts of hexacene (about 70% of the original UV/vis intensity) remained. Watanabe et al. [32] explained the observation of a significantly increased stability of hexacene in the solid state compared to hexacene isolated in a PMMA matrix by the accessibility of the hexacene molecules. In the solid state predominantly the surface of the sample is oxidized, while in the PMMA matrix the single hexacene molecules can react with diffusing

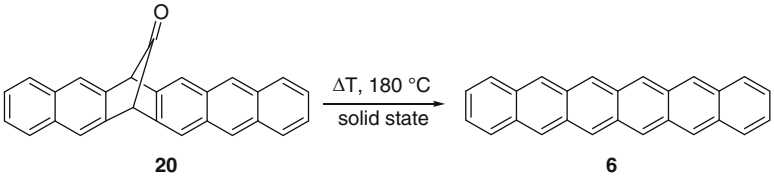


**Fig. 7** Synthesis of hexacene **6** from monoketone precursor **20** [32]

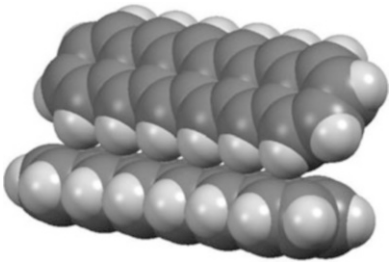

**Fig. 8** Two molecules of hexacene in the unit cell [32]

molecular oxygen. However, hexacene is also rather stable towards dimerization in the solid state [32], a reaction that was previously observed for silylethynyl substituted hexacenes in the solid state (see below) [33]. Watanabe et al. [32] explain this finding by different packing motifs: in contrast to parent hexacene, the silylethynyl substituted hexacenes crystallize in a face to face π stacking motif [33]. This latter motif is expected to favor dimerization [32].

Watanabe et al. also constructed field effect transistors from hexacene single crystals [32]. The authors report an averaged (14 devices) mobility of 0.88 $cm^2\ V^{-1}\ s^{-1}$ with a threshold at 34 V and an on/off ratio of $10^4$–$10^6$. The best hole mobility observed was 4.28 $cm^2\ V^{-1}\ s^{-1}$. The conductivity of crystalline hexacene ($2.21 \times 10^{-4}$ S $m^{-1}$) was slightly higher than that of pentacene [32]. The hole mobilities of hexacene thin films have been measured very recently [34].

## *2.2 Substituted Hexacenes*

### 2.2.1 Silylethynyl Substitution

One way to increase the persistence of reactive molecules is the introduction of bulky groups that can exert kinetic stabilization by increasing the barriers for decomposition reactions. In the case of the acenes, the most important of these reactions are oxidation via endoperoxide formation and dimerization. The introduction of silylethynyl groups was shown to be advantageous in pentacene

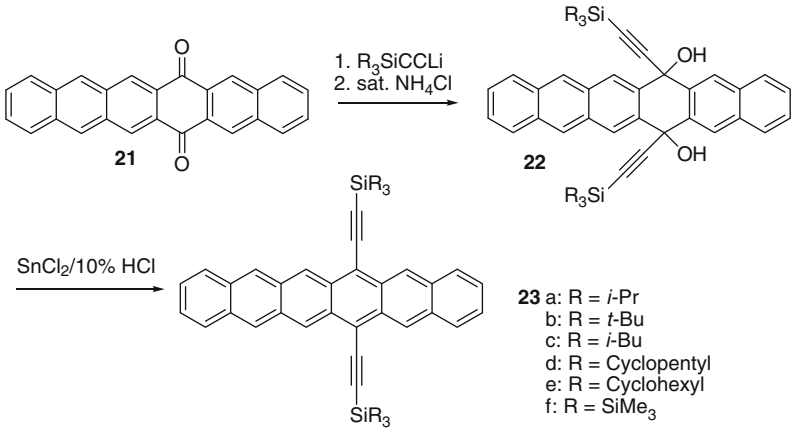


**Fig. 9** Synthesis of silylethynyl substituted hexacenes **23** [37]

chemistry [35, 36], and the group of Anthony has demonstrated that this strategy can result in an increased stability of the higher acenes.

In 2005, Payne et al. reported the first synthesis of a functionalized hexacene starting from quinone **21** (Fig. 9) [37]. The tri-*iso*-propylsilyl group (**23a**) is too small to stabilize the hexacene in solution or in the solid state. The bulkier tri-*tert*-butylsilyl (TTBS) group, however, provided sufficient stabilization to allow complete spectroscopic characterization of the corresponding hexacene derivative. Single crystal X-ray crystallography demonstrated that the acene unit is planar to within 0.1 Å and the alkyne groups are bent. This was ascribed to packing effects [37]. In spite of the stabilizing silylethynyl groups, the hexacene slowly decomposes in solution in the presence of air and light. The crystals, on the other hand, can be stored for several months in the dark [37].

The decomposition of the hexacenes was followed up by the Anthony group [33]. Particularly interesting results were obtained with the tri-*iso*-butylsilyl (TIBS) group that is smaller than the TTBS group investigated earlier. Under laboratory light, TIBS-hexacene was found to form a centrosymmetric dimer **24** interconnected between the C7 and C14 positions of both TIBS-hexacenes (Fig. 10) [33]. On the other hand, pure crystals of TIBS-hexacene kept under air in the dark produced a different dimer **25** with new bonds between the C7/C14 positions of one hexacene unit and the C8/C13 positions of the other hexacene molecule (Fig. 10) [33].

The centrosymmetric dimer **24** formed by reaction between the two most reactive sites (C7 and C14) and in this sense resembles the photodimers of parent anthracene, tetracene, and pentacene [38]. The dimer **25** formed in the dark reaction resulted from reaction of the most reactive ring of one monomer with the next to terminal ring of the other molecule [33]. Another interesting dimer **26** was isolated as a by-product of the hexacene synthesis by the Anthony group [33]. It is formed by Diels–Alder reaction between the reactive ring containing the C7 and C14 atoms and the alkynyl group of another TIBS-hexacene. As one intact hexacene unit is

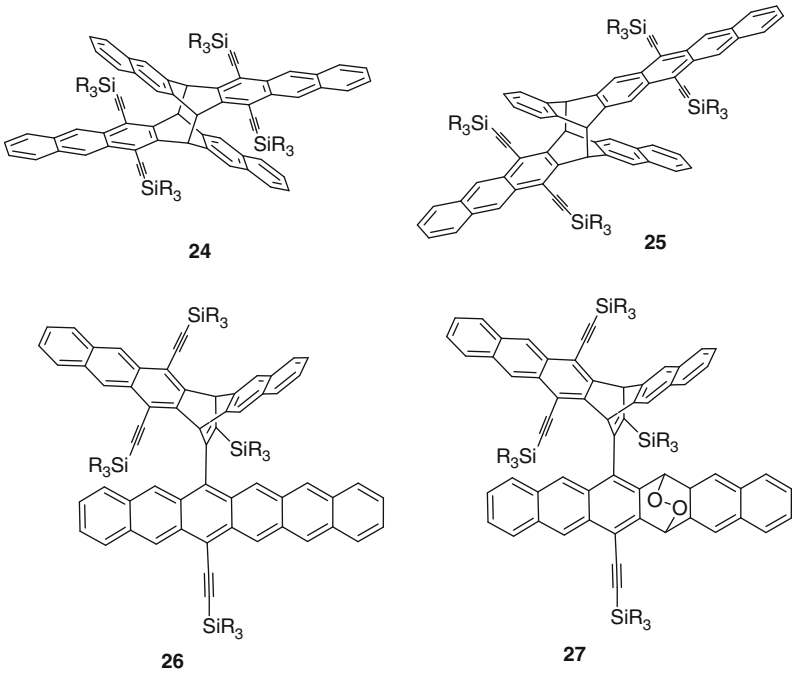


**Fig. 10** Dimers of TIBS-hexacene. *Top left*: product **24** obtained under laboratory light; *top right*: product **25** obtained under air in the dark; *bottom left and right*: Diels–Alder product **26** and its endoperoxide **27** [33]

present in **26**, the compound is green but turns yellow during column chromatography. This yellow product could be identified as an endoperoxide **27** by single-crystal X-ray crystallography [33].

The major pathway of decomposition of the silylethynyl substituted hexacenes is thus dimerization either in the light or in the dark. Endoperoxide formation is a mode of degradation only if one of the protecting ethynyl groups is compromised. Very recently Anthony and co-workers reported the synthesis of the 1,2,3,4-tetrafluoro as well as the 1,2,3,4,9,10,11,12-octafluoro derivatives of **23e** and the characterization of their charge transport properties [39]. The octafluoro compound was also investigated as an electron acceptor in organic bulk heterojunctions [40].

# 3 Heptacenes

## *3.1 Parent Heptacene*

In 1942 Clar reported the synthesis of heptacene [41]. As with hexacene, the key to the synthesis is the dehydrogenation of dihydroheptacenes (such as the 6,17-dihydro

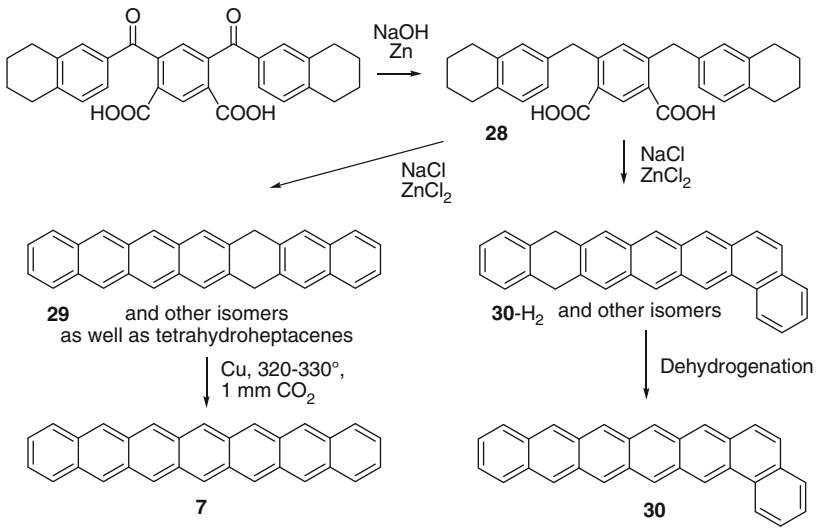


**Fig. 11** Synthesis of heptacene **7** or 1,2-benzohexacene **30** [41, 46]

derivative **29**) or tetrahydroheptacenes using copper bronze and a $CO_2$ stream at 310–320°C (Fig. 11). Clar describes that heptacene is extremely reactive and difficult to obtain in a pure state. He repeated the latter statement in some of his subsequent papers [42, 43]. Nonetheless, he describes heptacene as an almost black, grass green as a thin film, compound. It is said to be very poorly soluble in boiling 1-methylnaphthalene or phenanthrene with a green color. These solutions immediately decolorize upon contact with air or maleic anhydride. Clar observed bands in 1-methylnaphthalene solution in the visible at 736, 657, 594, 520, and 503 nm. He assigned the first three bands to the *p* band system and the last two to the $\alpha$ band system. Based on calculations, he predicted the longest wavelength absorption at around 840 nm and the $\beta$ band at 381 nm in this solvent.

With regard to the identity of the dihydroheptacenes there remains some ambiguity, as in the following year, 1943, Charles Marschalk [44] reiterated [45] that the orange-brown compound he had ascribed previously to 6,17-dihydroheptacene **29** does not isomerize to 7,16-dihydroheptacene, in contrast to Clar's [41] report. It also does not from heptacene under dehydrogenation conditions. However, he confirmed that among the hydrocarbon mixture Clar obtained from reductive cyclization of **28** there was an orange-brown compound that gave a highly reactive green hydrocarbon upon dehydrogenation with Pd/C in trichlorobenzene [44]. Its absorption spectrum agreed with that assigned by Clar [41] to heptacene [44].

Clar and Marschalk summarized their efforts towards heptacene in a joint paper in 1950 [46]. Dihydroheptacenes are confirmed not to give heptacene upon attempted dehydrogenation by copper or Pd/C. On the basis of similar UV/vis spectra the highly reactive green compound was assigned to 1,2-benzohexacene **30**. The authors suggested that reductive cyclization of **28** may have resulted in angularly annulated dihydrobenzohexacenes, such as **30**-$H_2$ displayed in Fig. 11 [46].

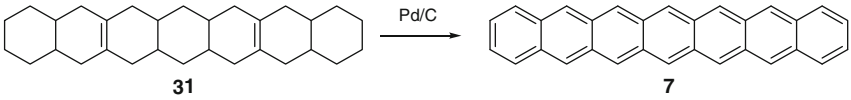


**Fig. 12** Catalytic dehydrogenation of hexacosahydroheptacene **31** was claimed to yield heptacene [15]

Another synthesis of a heptacene was reported by Bailey and Liao in 1955 [15]. These authors obtained heptacene in 76% yield by dehydrogenation of a hexacosahydroheptacene **31** with palladium-on-carbon at 340–375°C (Fig. 12). Bailey and Liao give a satisfactory elemental analysis and describe their product as greenish-black material that decomposes at approximately 400°C [15]. This work received criticism by Boggiano and Clar [42]. No further attempts at heptacene synthesis were described in the twentieth century, with the exception of a Ph.D. thesis [47].

A breakthrough was achieved by Neckers and co-workers who reported the first unequivocal synthesis of heptacene in 2006 [48]. This group used the Strating–Zwanenburg [49] reaction, i.e., the photobisdecarbonylation of the bridged α-diketone **37** [50, 51], in a PMMA matrix (Fig. 13) [48]. The heptacene photoprecursor **37** is accessible from 2,3-dibromonaphthalene **32** and 5,6,7,8-tetramethylidene-bicyclo[2.2.2]oct-2-ene **33**. First, the aryne generated from **32** undergoes Diels–Alder reactions with **33** and furnishes the hydrocarbon **34**. Aromatization of **34** to **35** is followed by oxidation of the etheno bridge. This was achieved by the osmium tetroxide catalyzed dihydroxylation of **35** and **36** and subsequent Swern oxidation.

Heptacene **7** was characterized by its UV/vis spectrum that shows the typical vibrational progression in the region of the *p* band ($\lambda_{max} \approx 760$ nm). Under ambient conditions, the compound isolated in the PMMA matrix disappears within 4 h presumably due to reaction with atmospheric oxygen molecules that diffuse into the matrix [48]. The persistence is less than that of hexacene under similar conditions. Note that photogeneration of heptacene in solution was not possible. In oxygen saturated solutions, oxygenated products rather than the hydrocarbons were obtained by Mondal et al. [48] according to MALDI-MS and $^1$H NMR investigations.

Further matrix isolation experiments were reported by Bettinger et al. using solid noble gas matrices (Ar and Xe) under cryogenic conditions [22, 52]. Heptacene was generated photochemically as reported by the Neckers group [48]. These experiments allowed measurement of the UV/vis absorption spectrum of heptacene between 200 and 800 nm (Fig. 14) and its IR spectrum (Fig. 15).

It was also observed that the acenes (including pentacene and hexacene) can undergo a photochemically (high energy line of a low pressure mercury lamp) initiated redox process that generates acene radical cations and radical anions within the same matrix (Fig. 16) [22, 52]. Assignment of the electronic transitions to the positively charged radical was possible by doping the noble gas matrix with better electron acceptors such as dichloromethane. This results in the suppression of

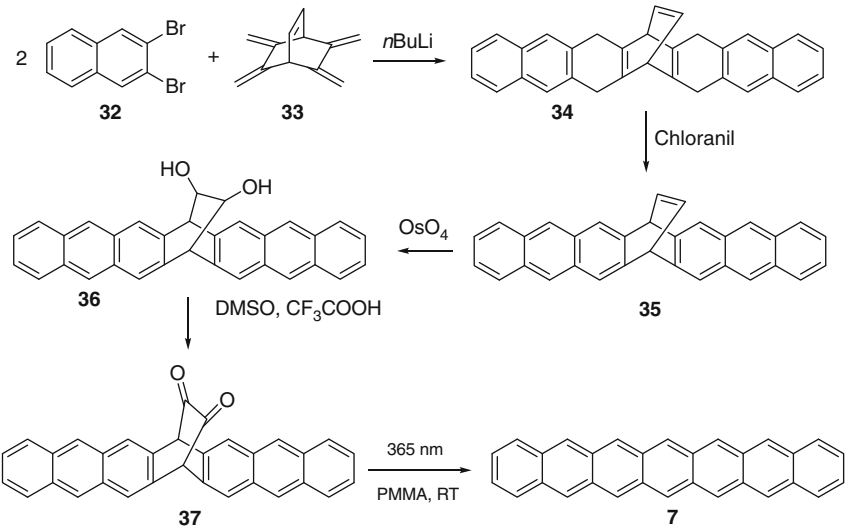


**Fig. 13** Photogeneration of heptacene **7** in a PMMA matrix from α-diketone **37** [48]

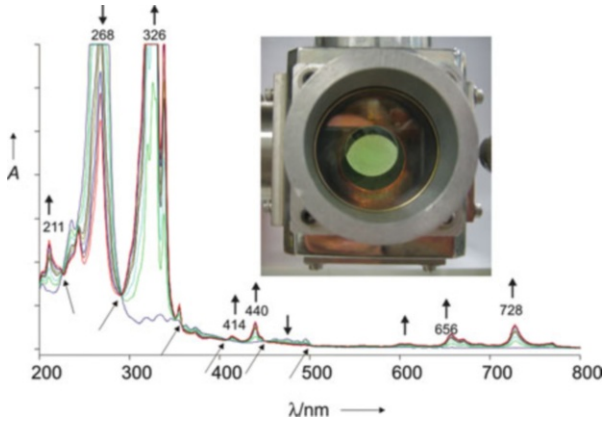


**Fig. 14** *Green color* of heptacene isolated in an argon matrix at 10 K. Reprinted with permission from [52]. Copyright 2007 Royal Society of Chemistry

acene radical anion formation and allows assignment of the remaining electronic transitions to radical cations. The longest wavelength absorption of the heptacene radical cation is observed at 2,134 nm in solid argon [22, 52].

An unexpected observation was made after the actual matrix isolation experiments: during warm-up of the optical substrate from 10 K to room temperature, the green color of the heptacene molecule (see inset of Fig. 14) disappeared and a yellow material was obtained at room temperature [22]. This differed from the behavior of pentacene and hexacene, which could be recovered from the optical substrate as blue and green materials, respectively. With heptacene, however,

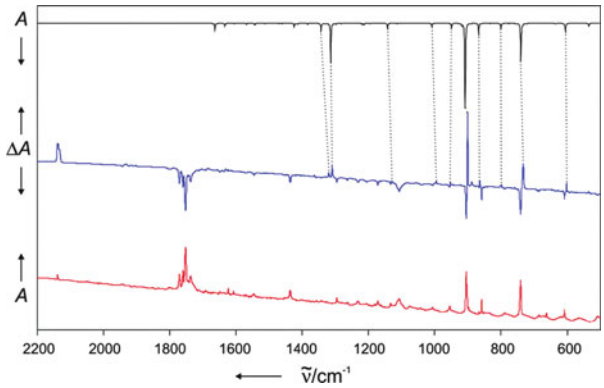


**Fig. 15** Mid-IR spectra (Ar, 10 K) of the photochemical decomposition of **7** and formation of heptacene. *Bottom* (*red*): IR difference spectrum after 2.5 h of irradiation ($385 < \lambda < 450$ nm); bands pointing downward decrease during irradiation and those pointing upward increase. *Middle* (*blue*): IR spectrum of **37** obtained after deposition for 75 min at 195°C. *Top* (*black*): IR spectrum computed for **7** at the RB3LYP/6-31G* level of theory scaled by 0.985. Reprinted with permission from [22]. Copyright 2009 American Chemical Society

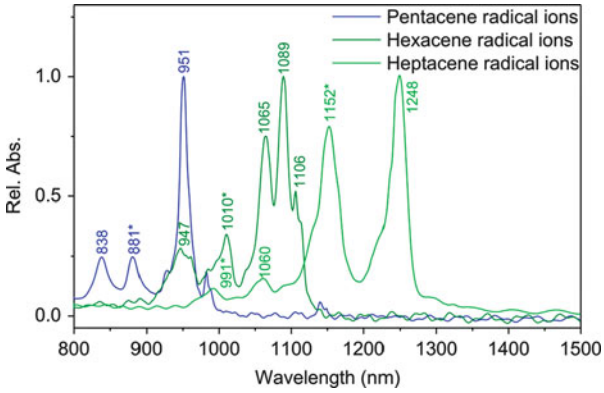


**Fig. 16** The SOMO-1 → SOMO transitions of the radical ions of acenes measured in solid argon at 10 K. Reprinted with permission from [22]. Copyright 2009 American Chemical Society

a yellow substance was washed from the substrate. This could be investigated by LDI-TOF-MS and showed the mass of the heptacene dimer among other signals at higher masses (presumably oxygenated products) [22]. As the concentration of oxygen is low in the matrix isolation system, oxidation occurs presumably after opening of the system to air and during sample preparation for MS measurements. Note that the colorless pentacene photodimer **38** (from a [4+4] cycloaddition, Fig. 17) is reported to be easily oxidized under ambient conditions, although it only consists of naphthalene subunits [38]. Hence, facile oxidation of heptacene dimers is also likely.

Anthony and co-workers reported that their silylethynyl hexacene dimers, although well defined in the solid state, only gave the mass of the monomer in

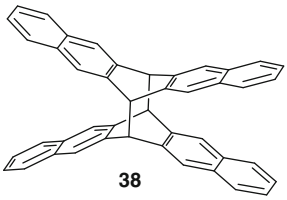


**Fig. 17** The [4+4] photodimer of pentacene (**38**)

LDI-TOF measurements [33]. The energy of dimerization of the substituted compounds is likely smaller than that of the parent acenes. It is not clear whether the dimer mass of heptacene observed is indeed due to the presence of (a structurally not characterized) heptacene dimer or to laser induced breaking of heptacene oligomers and polymers, but it is noted that the monomer mass was not observed [22]. A recent computational study by the Bendikov group shows that the dimerization of heptacene to the [4 + 4] dimer, a thermally forbidden reaction, is strongly exothermic [53].

A strongly bound ($E_{bind}$ = 24.4 kcal mol$^{-1}$; M06-2X/6-31G* level of theory) van-der-Waals dimer (**7-complex** in Fig. 18) exists that presumably forms without barrier [53]. The barrier for formation of the covalent dimer (**7M$_1$** in Fig. 18) from the van-der-Waals dimer (via transition structure **7T$_1$** in Fig. 18) is 12.3 kcal mol$^{-1}$ at M06-2X/6-31G* [53]. This is below the energy of two separated heptacene molecules. Hence, the energy gained by complex formation is enough to surmount the barrier for dimerization. One should note that the description of dispersion interactions in the anthracene dimer is problematic with density functional methods, even if empirical dispersion corrections are included [54]. The M06-2X functional has been shown to perform well for a number of systems, but how reliable the data are for heptacene dimerization is not clear at this time. Another problem for the reliable computation of heptacene dimerization may arise from the triplet instability of the spin-restricted Kohn–Sham (RKS) description of the heptacene molecule [55].

## *3.2 Substituted Heptacenes*

### 3.2.1 Silylethynyl Substituted Heptacenes

The first unambiguous report of a substituted heptacene was provided by Payne et al. in 2005 [37]. The authors synthesized silylethynyl substituted heptacenes similar to hexacenes: nucleophilic addition of lithium(silylacetylide) to heptacenequinone **39** followed by reduction of the diol by $SnCl_2$ (Fig. 19) [37].

As with hexacenes, the *i*-Pr group (TIPS) was too small to stabilize the heptacene. Even the *t*-Bu group (TTBS) resulted in a heptacene derivative that was described as being only marginally stable. Heptacene **40b** decomposed within a day in a rigorously oxygen-free solution, and even faster when the solution was

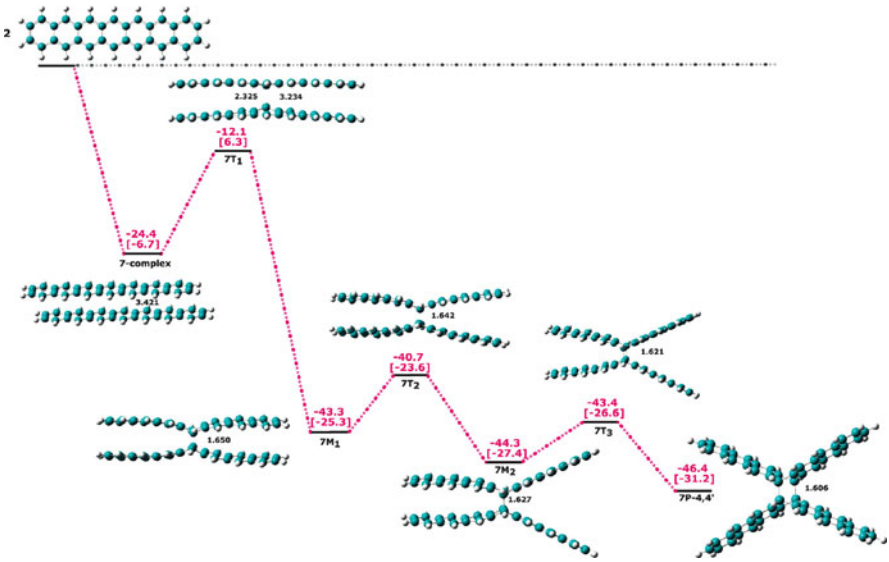


**Fig. 18** The potential energy surface for dimerization of heptacene under formation of the 4,4′ dimer as computed at the M06-2X/6-31G*+ZPVE level of theory. Lengths of newly formed C–C bonds are shown in *black*, energy data (in kcal $mol^{-1}$) in *red* (Gibbs free energy data, $\Delta G$, in *brackets*). Reprinted with permission from [53]. Copyright 2011 American Chemical Society

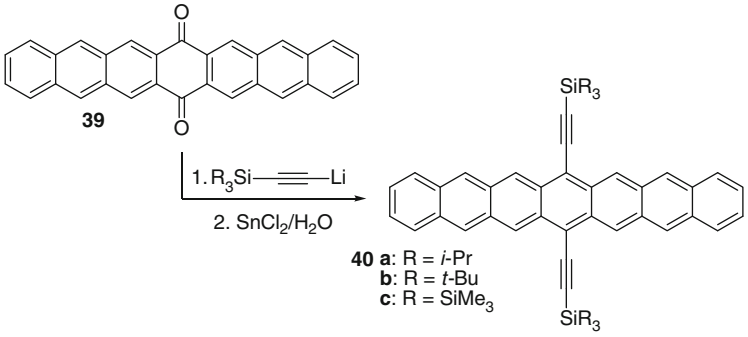


**Fig. 19** Synthesis of silylethynyl substituted heptacenes **40** [37]

concentrated [37]. Nonetheless UV/vis-NIR and $^1$H-NMR spectra could be obtained [37]. The still larger $SiMe_3$ group (TTMSS) allowed synthesis of a kinetically stabilized heptacene **40c** that could be investigated by single-crystal X-ray crystallography. Albeit the TTMSS groups were extensively disordered, the aromatic part of the molecule is essentially planar (Fig. 20) [37].

Heptacene **40c** decomposes within a few hours when its solution is in contact with air. The crystals, on the other hand, were reported to be stable for up to a week when exposed to air and laboratory lighting.

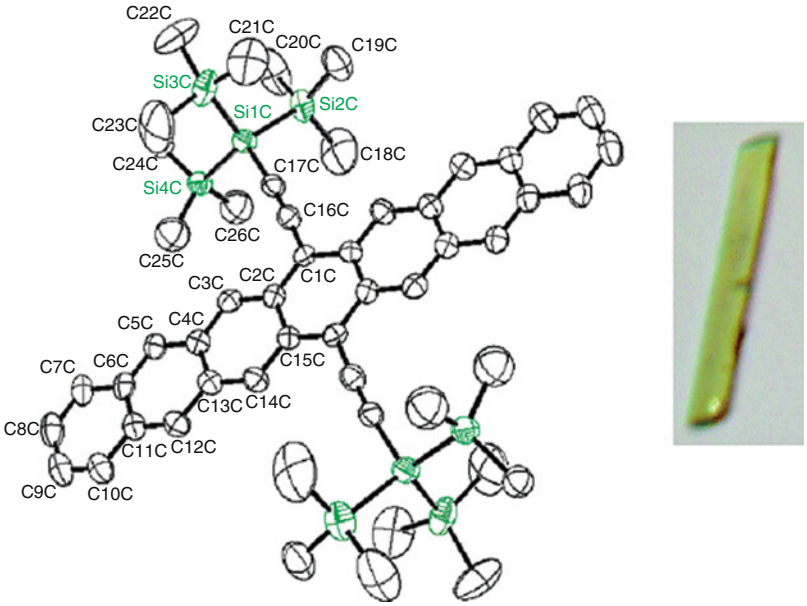


**Fig. 20** X-Ray crystal structure of heptacene **40c**. Reprinted with permission from [37]. Copyright 2005 American Chemical Society

A logical way of extending the lifetime of a heptacene is to increase the number of stabilizing groups. This approach was followed by Wudl's group [56] and by Qu and Chi [57]. The former group introduced four additional phenyl groups and reduced the size of the silyl groups by using TIPS. The synthesis started from 2,6-dibromo-anthraquinone **41** by introduction of the two TIPS-ethynyl groups (Fig. 21).

The double aryne generated from **42** by LiTMP induced HBr elimination was used in Diels–Alder reactions with diphenylisobenzofurane [56]. Reductive deoxygenation of the product **43** was achieved with Zn dust at 100°C. The heptacene **44** crystallized upon cooling of the reaction mixture [56]. Single crystal X-ray crystallography revealed that heptacene **44** shows an edge-to-face herringbone packing motif (Fig. 22) without π–π interactions. The molecules have an essentially planar heptacene backbone. The crystals are remarkably stable as they do not decompose within 21 days when exposed to laboratory atmosphere and light [56].

The acene could still be detected in solutions that were exposed to air for 41 h [56]. The oxidation of the heptacene results in a change of color of the solution from brown to orange. Based on UV/vis, $^{1}$H-NMR, and FAB-MS data, the authors suggested that the products of oxidation are endoperoxides, resulting from addition to the 6,17 or 8,15 positions (Fig. 23). These are the most reactive sites next to the 7,16 positions that are protected by the silylethynyl groups. Remarkably, dimerization of heptacene **44** was not observed [56]. This indicates that the four additional phenyl rings are sufficiently bulky to prevent dimerization. Thus, a combination of

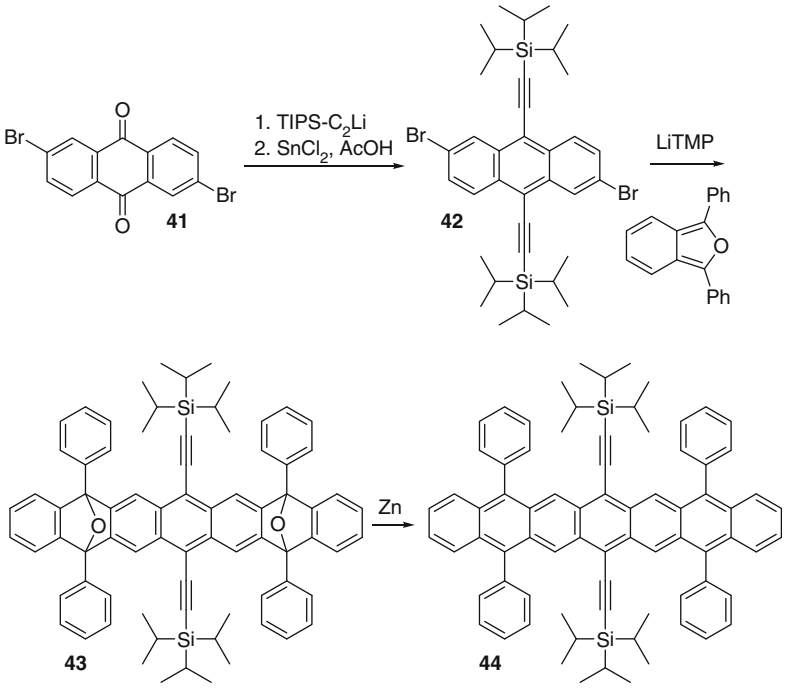


**Fig. 21** Synthesis of stabilized heptacene **44** [56]

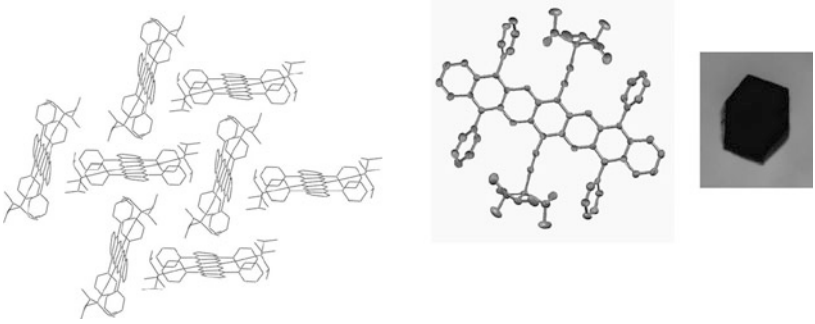

**Fig. 22** *Left*: crystal packing of heptacene **40**. *Right*: molecular structure of heptacene **40**. Reprinted with permission from [56]. Copyright 2008 John Wiley and Sons

the smaller TIPS-ethynyl groups (that were unable to stabilize the heptacene [37]) with four phenyl groups provides sufficient protection of the heptacene core.

Chun et al. also investigated the electronic structure of their heptacene **44** by UV/vis-NIR spectroscopy and cyclic voltammetry [56]. The heptacene shows one reversible reduction and one reversible oxidation step. The electrochemically derived HOMO-LUMO gap is 1.38 eV, in good agreement with the gap derived

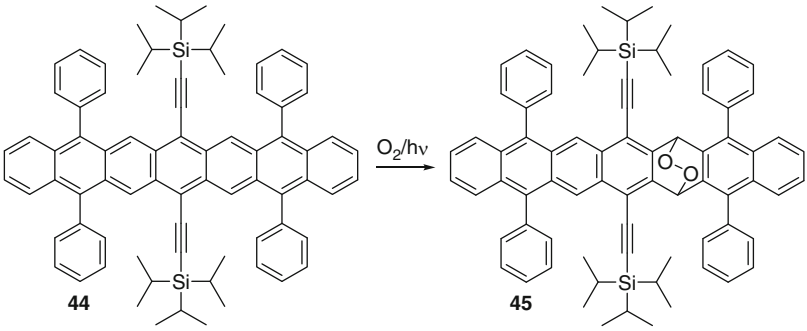


**Fig. 23** Endoperoxide formation upon irradiation of **44** in presence of oxygen [56]

from optical spectroscopy (1.35 eV, from the onset of the absorption). The HOMO and LUMO energies were given as −4.8 and −3.5 eV, respectively.

Qu and Chi added four electron-withdrawing *p*-trifluoromethylphenyl groups in addition to two TIPS-ethynyl groups to the heptacene core [57]. The synthesis of the required substituted heptacenequinone **49** was achieved by a Diels–Alder reaction of the transient isonaphthofuran with benzoquinone followed by dehydration. Addition of the TIPS-acetylide and subsequent oxidation with $SnCl_2/H_2O$ furnished the desired substituted heptacene **50** (Fig. 24) [57].

The substituents in **50** are increasing the stability of the heptacene core considerably. Half-lives of 1950, 200, and 100 min were estimated for oxygen-free toluene solutions of **50** under ambient light, white light (100 W), and UV light (4 W), respectively [57]. Even in the presence of oxygen, the heptacene **50** could still be detected after 47 h in toluene [57].

From electrochemical investigation of **50** the authors concluded that reversible reductions to the radical anion and the dianion and a reversible oxidation to the radical cation are possible [57]. The electrochemically determined HOMO and LUMO values are −4.93 and −3.61 eV, respectively. The electrochemical energy gap of 1.32 eV is in agreement with the optical gap (1.35 eV from the onset of absorption, $\lambda_{max} = 870$ nm) [57]. In summary, the four $CF_3$ groups considerably stabilize the heptacene by decreasing the energies of the frontier orbitals.

### 3.2.2 Aryl Substituted Heptacenes

The Wudl group investigated the ability of phenyl groups to stabilize the heptacene core (Fig. 25) [56].

Neither the 5,7,9,14,16,18-hexaphenylheptacene **51** nor the 5,9,14,18-tetraphenyl-9,16-bis[4-(2-ethylhexyloxy)phenyl]heptacene **52** could be isolated and characterized [56]. The former is barely soluble and easily oxidized, but the presence of the characteristic absorption in the NIR region can be considered as evidence for its (transient) existence, even if the typical vibronic transitions of the

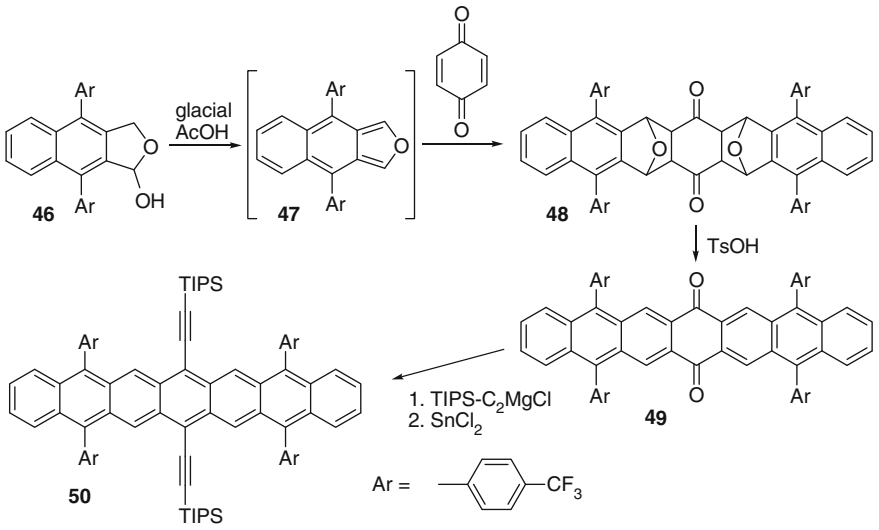


**Fig. 24** Synthesis of substituted heptacene **50** [57]

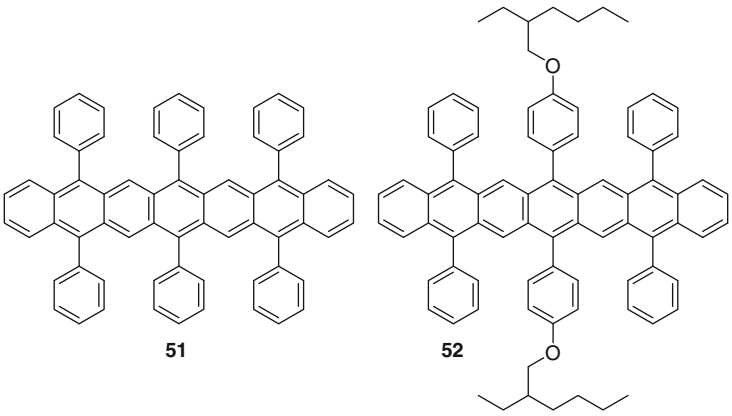


**Fig. 25** Aryl substituted heptacenes **51** and **52** investigated by Chun et al. [56]

*p* band are rather broad [56]. The more soluble derivative **52** is immediately oxidized upon exposure to air and light. As the color of the solution turns from brown to orange, the presence of a tetracene species was suggested [56].

The 2008 investigation by Chun et al. [56] nicely demonstrates that the introduction of bulky groups such as phenyl that may protect the acene from dimerization are not sufficient for stabilizing the heptacene core towards air oxidation in the presence of laboratory light. Two more aryl substituted heptacenes (**53** and **54**) were prepared and investigated by the Miller group in 2009 (Fig. 26) [58].

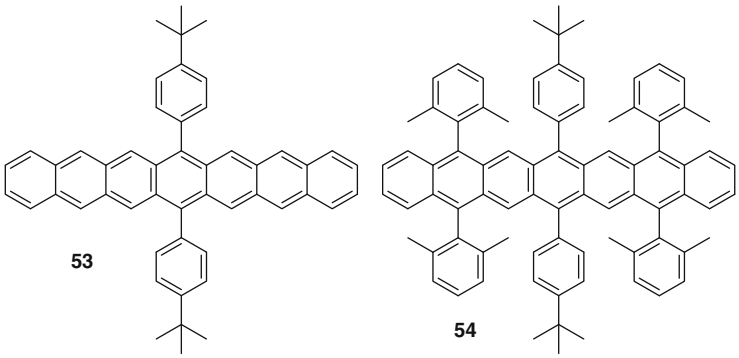


**Fig. 26** Aryl substituted heptacenes **53** and **54** [58]

As expected, the 7,16-di(*p-tert*-butylphenyl)heptacene **53** decomposed rapidly in solution in an ambient atmosphere in the presence of light, while the four additional *o,o*-dimethylphenyl substituents in **54** enhance the stability somewhat [58]. The half-life in the presence of light was not given, but appears to lie in the region of 10 min for this derivative from the displayed time dependence of acene absorption. The solids have "*significant lifetimes*" [58] and could be studied by LDI-TOF-MS. In addition to the molecular ion $M^+$, the less substituted derivative **53** also showed the presence of the oxygen adduct ($M^+ + 32$) and its fragment ($M^+ + 16$) [58].

### 3.2.3 Thioaryl Substituted Heptacenes

An approach to acene stabilization different to silylethynyl substituents was discovered by the group of Miller. In an investigation of the stability of pentacenes, Kaur et al. [59] identified thioalkyl and thioaryl groups as being superior to silylethynyl groups in stabilizing the aromatic core with respect to endoperoxide formation. The Miller group subsequently investigated the influence of thioaryl groups on the stability of the heptacene core [58]. The synthesis (Fig. 27) of two thioaryl substituted heptacenes was achieved by double Diels–Alder reactions of naphthoquinone and transient *o*-quinodimethane generated from **55**. The resulting heptacenetetraone **56** is either treated with 2,6-dimethylphenyllithium or reduced with $NaBH_4$. The resulting OH groups are removed in the usual way using $SnCl_2$.

In agreement with the earlier observations at the pentacene core, the two (*p-tert*-butylphenyl)thiophenyl substituents in **57** increase the stability of the heptacene towards oxidation [58]. An even larger increase in stability is observed with the presence of four *o,o*-dimethylphenyl groups as in **58** [58]. This heptacene derivative is stable for weeks in the solid state, for 1–2 days in solution in the dark, and for several hours under ambient conditions in the presence of laboratory light. The heptacene **58** could be fully characterized by NMR, UV/vis-NIR, fluorescence, and LDI-TOF-MS [58]. By the latter technique the absence of oxygenated derivatives

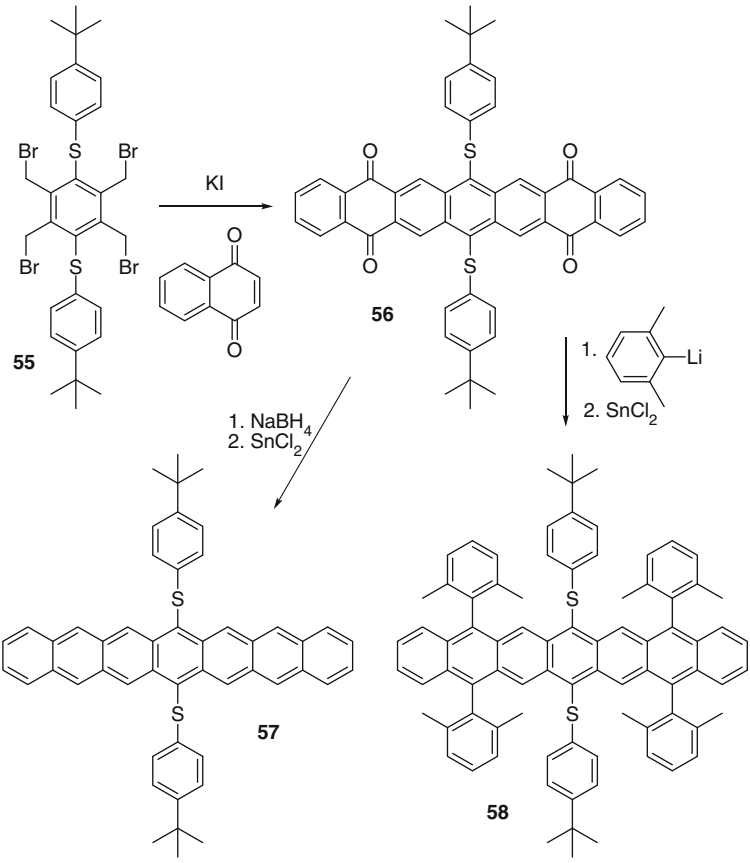


**Fig. 27** Synthesis of thioaryl substituted heptacenes **57** and **58** [58]

was demonstrated. The optical band gap of **58** was determined to be 1.37 eV (onset, $\lambda_{max} = 850$ nm) [58].

## 4 Octacene and Nonacene

### *4.1 Parent Octacene and Nonacene*

Larger acenes than heptacene have not been reported in the twentieth century. There have been attempts to synthesize these, e.g., by the group of Orville Chapman at UCLA, but these efforts have not met with success [47].

In view of the problems associated with the high reactivity of heptacene, it is likely that parent octacene and nonacene are too reactive to be isolated in

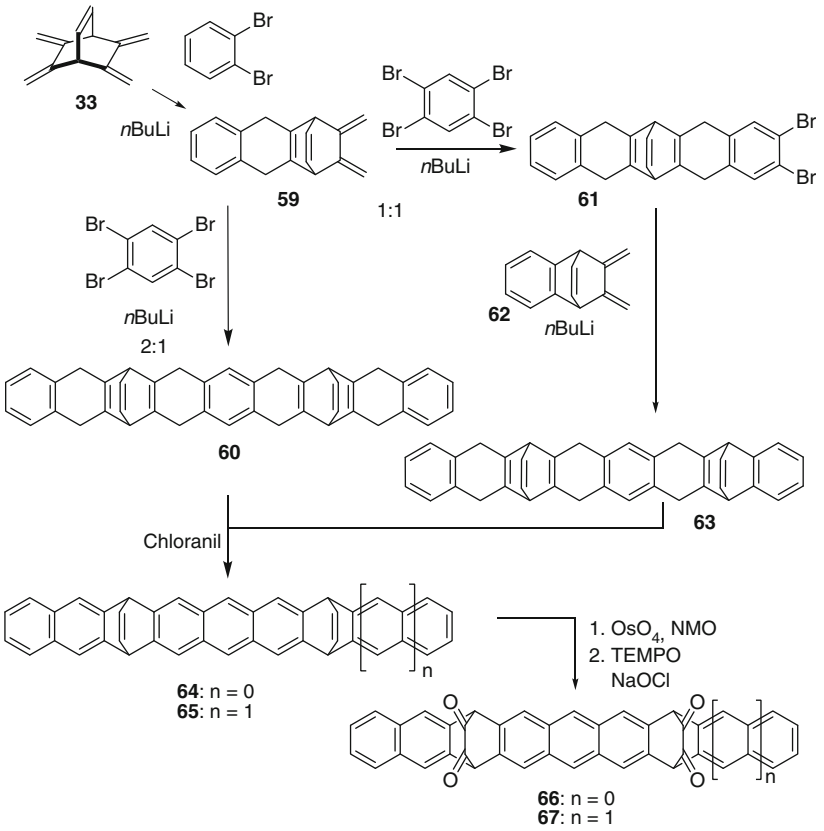


**Fig. 28** Synthesis of photoprecursors for octacene (**66**) and nonacene (**67**) [60]

substance. Motivated by the success of the photobisdecarbonylation strategy of bridged α-diketones in the synthesis of heptacene and smaller acenes under matrix isolation conditions [22, 48], we have developed a route to octacene and nonacene under matrix isolation conditions (Fig. 28) [60]. The key was to install two α-diketone bridges as in **66** and **67** to avoid having acene units larger than anthracene as otherwise problems associated with stability and solubility may hinder the synthesis of the required photoprecursors. The final step (Fig. 28), the oxidation of the diols to the α-diketones, proved to be most difficult and was achieved by Anelli oxidation [60].

Matrix isolation of the nonacene photoprecursor **67**, followed by irradiation ($\lambda > 395$ nm), produced an UV/vis spectrum that showed the typical vibrational structure of the *p* band in the region of a hexacene derivative (Fig. 29a). This behavior is in agreement with the photochemical decarbonylation of one of the two α-diketone bridges.

Further irradiation at shorter wavelengths ($\lambda = 305$–$320$ nm) resulted in decrease of the band associated with the hexacene derivatives into a set of new

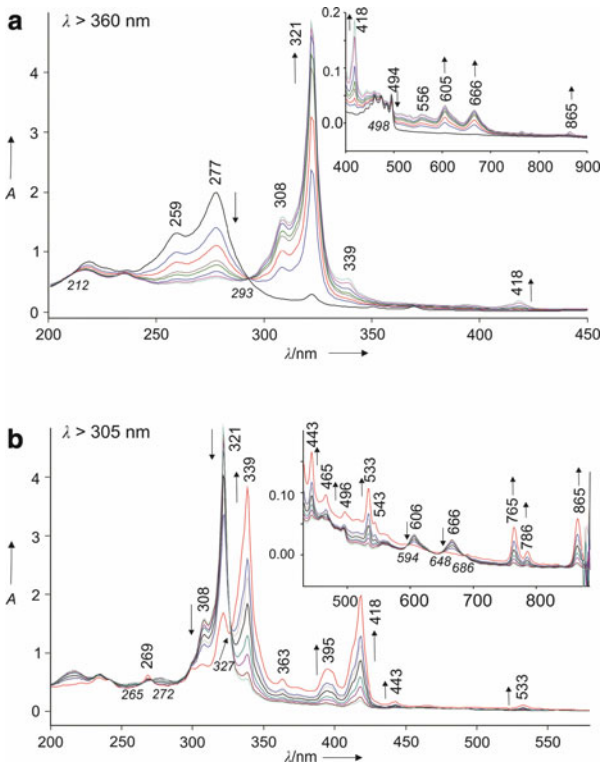


**Fig. 29** UV/vis spectra showing the transformation of **67** into **9**. The direction of *arrows* indicates increasing or decreasing bands under the respective irradiation conditions. The values for isosbestic points are given in *italics*. (**a**) Irradiation of **67** using visible light ($\lambda > 360$ nm) gives **68**. (**b**) Subsequent UV irradiation ($\lambda = 305$–$320$ nm) results in the photogeneration of **9**. The spectrum in *red* was measured after irradiation overnight and was not used for determining isosbestic points because the optical quality of the argon matrix deteriorates under these conditions resulting in baseline shifts. Reprinted with permission from [60]. Copyright 2010 John Wiley and Sons

bands that were associated with nonacene, e.g., the *p* band at 865 nm and the *β* band at 339 nm (Fig. 29b). Finally, short wavelength irradiation using the output of a low pressure mercury lamp ($\lambda = 254$ and 185 nm) produced the radical anion and radical cation of nonacene (Fig. 30) that is characterized by SOMO-1 → SOMO at longer wavelength than of any other acene studied under identical conditions. Thus the photogeneration of nonacene can be summarized as shown in Fig. 31 [60].

## *4.2 Silylethynyl Substituted Nonacenes*

Further significant progress was reported by the group of John Anthony in 2011 [61]. Purushothaman et al. [61] achieved the synthesis of the first crystalline nonacene derivatives **70** by exploiting the stabilizing effect of four silylethynyl

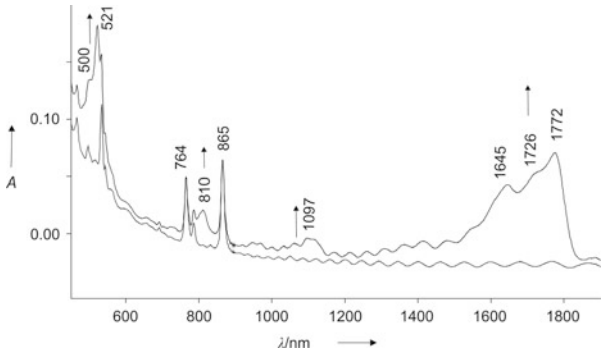


**Fig. 30** Vis/NIR spectrum obtained after irradiation ($\lambda = 185$ nm) of the nonacene sample prepared as described in the caption of Fig. 29. Reprinted with permission from [60]. Copyright 2010 John Wiley and Sons

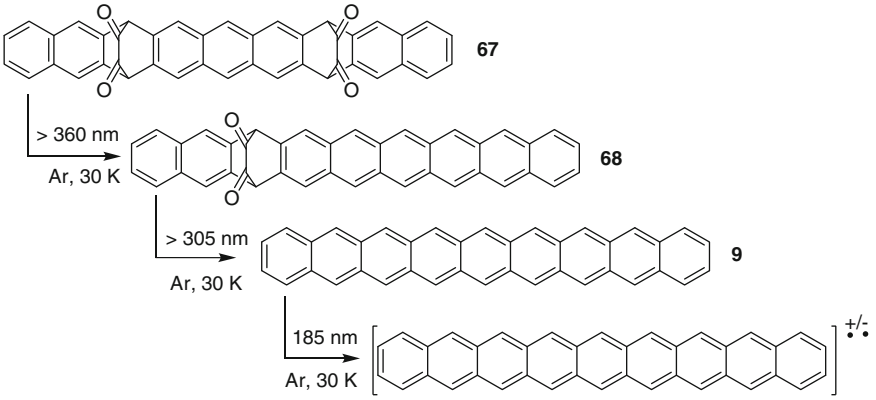


**Fig. 31** Photochemical conversion of nonacene precursor **67** to nonacene **9** and its ionization to the nonacene radical ions [60]

groups, of electron-withdrawing fluorine substituents at the terminal rings of the aromatic core, and of two 3,5-di(trifluoromethyl)phenyl groups at the central ring (Fig. 32) [61].

The key to success was the crystallization of the nonacene derivatives **70** from the reaction mixture of the final oxidation step. This approach avoided handling of the very unstable compounds in solution for an extended period of time. The solids thus obtained were stable when stored in the dark at 10°C over more than 2 days [61]. The crystals were suitable for X-ray crystallography and this demonstrated the presence of the nonacene aromatic core (Fig. 33). The quality of the datasets does not allow detailed bond lengths discussions, but reveals the stacking behavior of

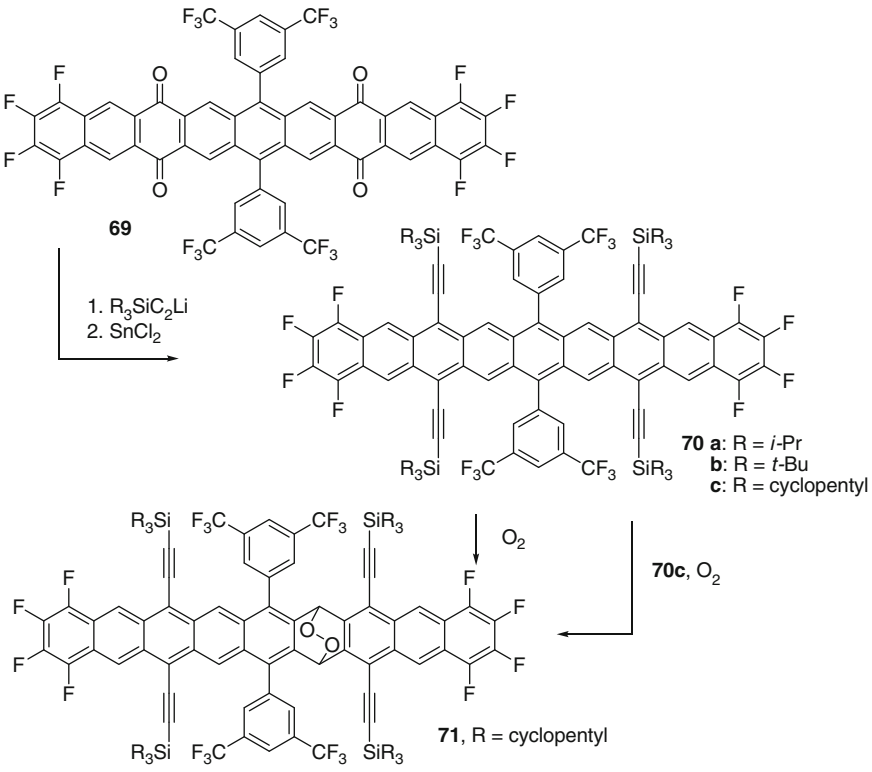


**Fig. 32** Synthesis of crystalline nonacenes **70** and their endoperoxides **71** [61]

these compounds. While **70a** adopted a 2D π stacked motif, **70b** and **70c** show 1D parallel "slipped" stacks [61]. The nonacene backbone is almost planar in **70b**, but it is warped in **70a** and more so in **70c** [61].

Dissolution of the crystals in toluene produces olive colored solutions of **70a–c** [61]. The measured UV/vis-NIR spectra (Fig. 34) resemble those of parent nonacene [60]. The authors stressed that nonacenes **70a–c** do not show fluorescence in the visible region (see below) [61]. The $S_0$–$S_1$ transitions of silylethynyl substituted acenes from anthracene to nonacene (without octacenes) are displayed in Fig. 34.

Note that Purushothaman et al. were unable to measure the $^1$H NMR spectra of their nonacene derivatives although they were sufficiently soluble [61]. The spectra improved over time and signals due to the photodecomposition product appeared. This decomposition product was independently generated and identified as the endoperoxide on ring 4 (**71**) based on X-ray crystallography (Fig. 32) [61]. Interestingly, the pure endoperoxide **71** fragments in the LDI-TOF-MS to the corresponding nonacene, and that is by far the most prominent mass signal [61].

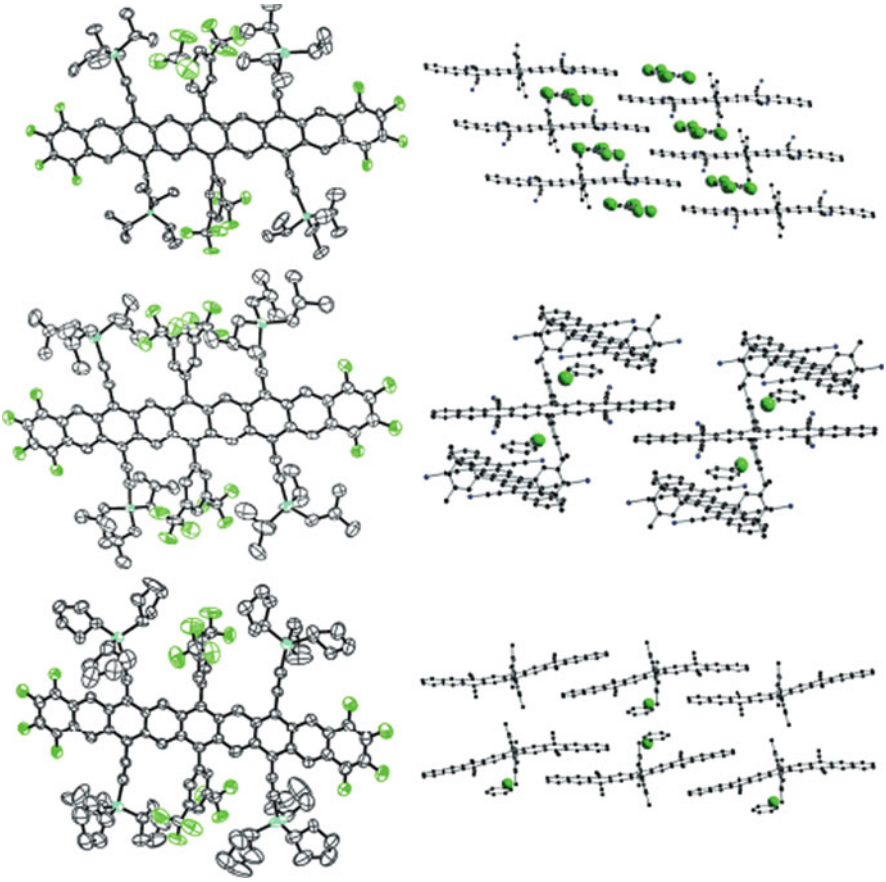

**Fig. 33** Thermal ellipsoid plots for **70a** (*top*), **70b** (*center*), and **70c** (*bottom*), and packing diagrams (*right*). F *green*, Si *blue*. Alkyl groups and fluorine substituents omitted from packing diagrams for clarity. Thermal ellipsoids set at 50% probability. Reprinted with permission from [61]. Copyright 2011 John Wiley and Sons

## *4.3 Thioaryl Substituted Nonacenes*

The Miller group also reported the synthesis of nonacene derivatives **75** and **76** using their thioaryl approach discussed above in the context of substituted heptacenes [62]. The synthesis is reminiscent of that of heptacene derivatives [58], with the key step being the Diels–Alder reaction between anthracenequinone **72** and the bis-ortho-quinodimethane precursor **73** (Fig. 35). The persistence of the less substituted derivative **76** is insufficient for characterization by solution phase methods. Derivative **75**, however, could be investigated by NMR, UV/vis-NIR, and fluorescence spectroscopies as well as by LDI-TOF-MS [62].

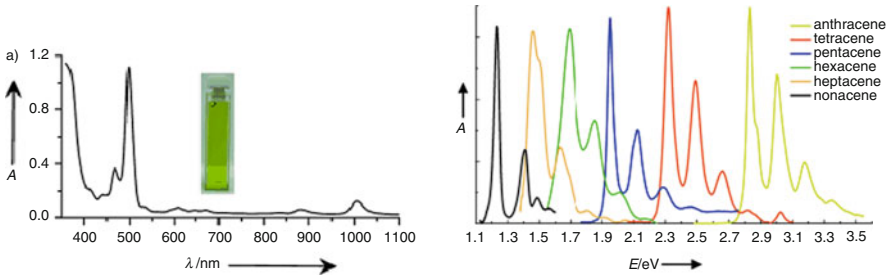


**Fig. 34** *Left*: UV/vis-NIR spectrum of nonacene **70c** measured in toluene at RT. *Right*: the long-wavelength portion of the absorption spectra for silylethyne-substituted acenes from anthracene to heptacene and nonacene **70c**. Reprinted with permission from [61]. Copyright 2011 John Wiley and Sons

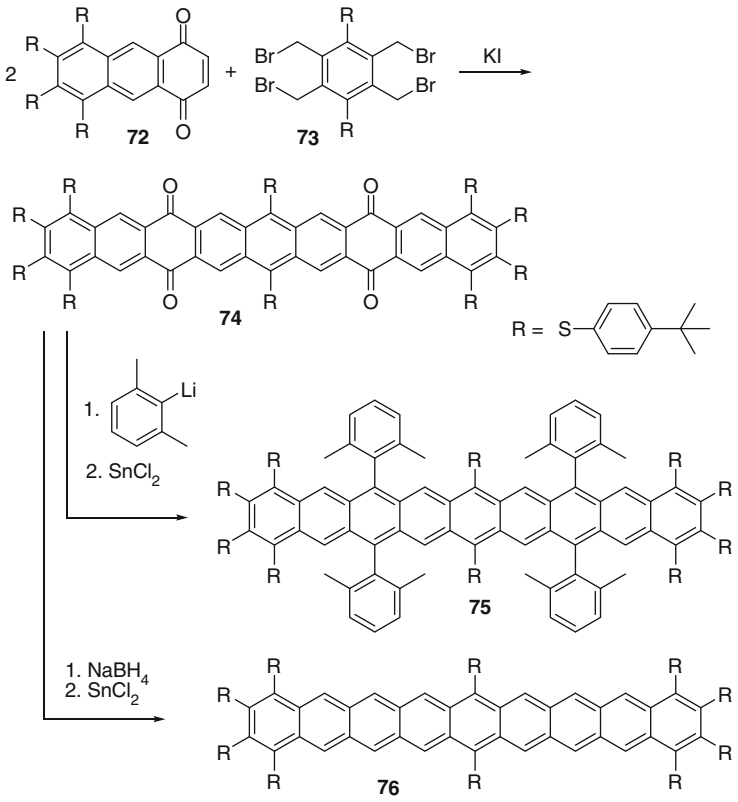


**Fig. 35** Synthesis of thioaryl substituted nonacenes **75** and **76** [62]

The data reported by Kaur et al.[62] are briefly summarized: the LDI-TOF-MS showed the mass required for the nonacene **75**. The UV/vis-NIR spectra showed weak absorptions at 1,033, 921, and 846 nm, along with strong ones at 655, 600, and 550 nm. A strong blood-red fluorescence with a maximum below 700 nm was observed. The electronic ground state of nonacene derivatives **75** and **76** was also investigated computationally [63]. As with the parent acenes larger than hexacene [55], an instability of the spin-restricted Kohn–Sham description was detected.

The identity of the nonacene **75** was challenged by the Anthony group on the basis of the very weak $S_0 \rightarrow S_1$ transition and the fluorescence in the visible [61]. Purushothaman et al. [61] argued that an alternant hydrocarbon such as nonacene **75** should emit from the $S_1$ state according to Kasha's rule. As the $S_0 \rightarrow S_1$ transition of **75** is in the NIR, no fluorescence in the visible should be observed. To support their argument, Purushothaman et al. measured the absorption and fluorescence spectrum of the endoperoxide **71** derived from their nonacene **70c**. Although the substituents differ from Miller's nonacene, the endoperoxide shows the typical vibrational fine structure of the *p* band of its pentacene chromophore (roughly 650, 600, and 550 nm). The endoperoxide is strongly fluorescent and emits just below 700 nm. The correspondence with the data reported by Kaur et al. [62] led the Anthony group to conclude that the observations reported for **75** *may arise from a decomposition product that makes the bulk of the sample* [61].

## 5 Conclusions and Outlook

The chemistry of higher acenes dates back to the 1930s. Yet significant improvements have only been made since the ground-breaking work of the Anthony group who employed silylethynyl groups for kinetic stabilization of the highly reactive π systems of hexacene, heptacene, and nonacene. The rediscovery of the Strating–Zwanenburg reaction for acene synthesis paved the way to the photogeneration of the parent acene systems in PMMA or cryogenic matrices. This approach made acenes up to nonacene available for spectroscopic study. It remains to be seen whether yet larger acenes can be generated.

**Acknowledgments** We are grateful for continued support from the Deutsche Forschungsgemeinschaft and the Fonds der Chemischen Industrie.

## References

1. Clar E, John F (1930) Ber Dtsch Chem Ges 63B:2967
2. Philippi E (1929) Monatsh Chem 53(54):638
3. Clar E (1939) Chem Ber 72:2137
4. Wang C, Dong H, Hu W, Liu Y, Zhu D (2012) Chem Rev 112:2208
5. Pron A, Gawrys P, Zagorska M, Djurado D, Demadrille R (2010) Chem Soc Rev 39:2577

6. Biermann D, Schmidt W (1980) J Am Chem Soc 102:3163
7. Anthony JE (2006) Chem Rev 106:5028
8. Anthony JE (2008) Angew Chem Int Ed 47:452
9. Würthner F, Schmidt R (2006) Chemphyschem 7:793
10. Bendikov M, Wudl F, Perepichka DF (2004) Chem Rev 104:4891
11. Zade SS, Bendikov M (2010) Angew Chem Int Ed 49:4012
12. Clar E (1939) Ber Dtsch Chem Ges 72B:1817
13. Marschalk C (1939) Bull Soc Chim Fr 6:1112
14. Clar E (1942) Ber Dtsch Chem Ges B 75B:1283
15. Bailey WJ, Liao C-W (1955) J Am Chem Soc 77:992
16. Lang KF, Zander M (1963) Chem Ber 96:707
17. Satchell MP, Stacey BE (1971) J Chem Soc C 468
18. Campbell RB, Robertson JM, Trotter J (1962) Acta Crystallogr 15:289
19. Preuss J, Zanker V (1974) Z Naturforsch Teil A 29:352
20. Angliker H, Rommel E, Wirz J (1982) Chem Phys Lett 87:208
21. Nijegorodov N, Ramachandran V, Winkoun DP (1997) Spectrochim Acta A 53:1813
22. Mondal R, Tönshoff C, Khon D, Neckers DC, Bettinger HF (2009) J Am Chem Soc 131:14281
23. Angliker H, Gerson F, Lopez J, Wirz J (1981) Chem Phys Lett 81:242
24. Boschi R, Clar E, Schmidt W (1974) J Chem Phys 60:4406
25. Schmidt W (1977) J Chem Phys 66:828
26. Aust RB, Bentley WH, Drickamer HG (1964) J Chem Phys 41:1856
27. Minakata T, Ozaki M, Imai H (1993) J Appl Phys 74:1079
28. Minakata T, Imai H, Ozaki M (1995) Polym Adv Technol 6:602
29. Mondal R, Adhikari RM, Shah BK, Neckers DC (2007) Org Lett 9:2505
30. Uno H, Yamashita Y, Kikuchi M, Watanabe H, Yamada H, Okujima T, Ogawa T, Ono N (2005) Tetrahedron Lett 46:1981
31. Yamada H, Yamashita Y, Kikuchi M, Watanabe H, Okujima T, Uno H, Ogawa T, Ohara K, Ono N (2005) Chem Eur J 11:6212
32. Watanabe M, Chang YJ, Liu S-W, Chao T-H, Goto K, IslamMd M, Yuan C-H, Tao Y-T, Shinmyozu T, Chow TJ (2012) Nat Chem 4:574
33. Purushothaman B, Parkin SR, Anthony JE (2010) Org Lett 12:2060
34. Watanabe M, Su W-T, Chen K-Y, Chien C-T, Chao T-H, Chang YJ, Liu S-W, Chow TJ (2013) Chem Commun 49:2240
35. Miller GP, Mack J, Briggs J (2000) Org Lett 2:3983
36. Anthony JE, Brooks JS, Eaton DL, Parkin SR (2001) J Am Chem Soc 123:9482
37. Payne MM, Parkin SR, Anthony JE (2005) J Am Chem Soc 127:8028
38. Berg O, Chronister EL, Yamashita T, Scott GW, Sweet RM, Calabrese J (1999) J Phys Chem A 103:2451
39. Purushothaman B, Parkin SR, Kendrick MJ, David D, Ward JW, Yu L, Stingelin N, Jurchescu OD, Ostroverkhova O, Anthony JE (2012) Chem Commun 48:8261
40. Kendrick MJ, Neunzert A, Payne MM, Purushothaman B, Rose BD, Anthony JE, Haley MM, Ostroverkhova O (2012) J Phys Chem C 116:18108
41. Clar E (1942) Chem Ber 75:1330
42. Boggiano B, Clar E (1957) J Chem Soc 2681
43. Clar E, McCallum A (1960) Tetrahedron 10:171
44. Marschalk C (1943) Bull Soc Chim Fr 10:511
45. Marschalk C (1941) Bull Soc Chim Fr 8:354
46. Clar E, Marschalk C (1950) Bull Soc Chim Fr 444
47. Fang T (1986) Heptacene, octacene, nonacene, supercene and related polymers, PhD Thesis, University of California, Los Angeles
48. Mondal R, Shah BK, Neckers DC (2006) J Am Chem Soc 128:9612
49. Strating J, Zwanenburg B, Wagenaar A, Udding AC (1969) Tetrahedron Lett 3:125
50. Mondal R, Okhrimenko AN, Shah BK, Neckers DC (2008) J Phys Chem B 112:11

51. Bettinger HF, Mondal R, Krasowska M, Neckers DC (2012) J Org Chem 78:1851–1857. doi:10.1021/jo301622f
52. Bettinger HF, Mondal R, Neckers DC (2007) Chem Commun 5209
53. Zade SS, Zamoshchik N, Reddy AR, Fridman-Marueli G, Sheberla D, Bendikov M (2011) J Am Chem Soc 133:10803
54. Grimme S, Diedrich C, Korth M (2006) Angew Chem Int Ed 45:625
55. Bendikov M, Duong HM, Starkey K, Houk KN, Carter EA, Wudl F (2004) J Am Chem Soc 126:7416
56. Chun D, Cheng Y, Wudl F (2008) Angew Chem Int Ed 47:8380
57. Qu H, Chi C (2010) Org Lett 12:3360
58. Kaur I, Stein NN, Kopreski RP, Miller GP (2009) J Am Chem Soc 131:3424
59. Kaur I, Jia W, Kopreski RP, Selvarasah S, Dokmeci MR, Pramanik C, McGruer NE, Miller GP (2008) J Am Chem Soc 130:16274
60. Tönshoff C, Bettinger HF (2010) Angew Chem Int Ed 49:4125
61. Purushothaman B, Bruzek M, Parkin SR, Miller A-F, Anthony JE (2011) Angew Chem Int Ed 50:7013
62. Kaur I, Jazdzyk M, Stein NN, Prusevich P, Miller GP (2010) J Am Chem Soc 132:1261
63. Gao X, Hodgson JL, Jiang D-E, Zhang SB, Nagase S, Miller GP, Chen Z (2011) Org Lett 13:3316

Top Curr Chem (2014) 349: 31–62
DOI: 10.1007/128_2012_361

Published online: 6 September 2012

# Twisted Arenes

**Kung K. Wang**

**Abstract** The nonbonded steric interactions of substituents at the crowded C4 and C5 positions of phenanthrene cause the aromatic system to twist out of planarity. Similarly, the presence of substituents at the C1 and C12 positions of benzo[*c*] phenanthrene and at the C1 and C14 positions of dibenzo[*c*,*g*]phenanthrene are responsible for the helical twists of the aromatic frameworks. Highly substituted acenes, such as octamethylnaphthalene and decaphenylanthracene, also exhibit substantial end-to-end twists. The X-ray structures of these compounds allow direct measurements of the extent of the structural distortions. The configurational stabilities of many twisted arenes have also been determined.

**Keywords** 1,12-Dimethylbenzo[*c*]phenanthrene • 1,14-Disubstituted dibenzo[*c*,*g*] phenanthrenes • 4,5-Dimethylphenanthrene • Helical aromatics

## Contents

1 Introduction ..... 32
2 Twisted Phenanthrenes and Related Compounds ..... 34
2.1 4,5-Dialkylphenanthrenes ..... 34
2.2 4,5-Diarylphenanthrenes ..... 36
2.3 4,5-Dihalophenanthrenes ..... 43
2.4 1,10-Disubstituted 4,7-Phenanthrolines ..... 44
2.5 1,10-Phenanthroline 1,10-Dioxides ..... 47
3 Twisted Benzo[*c*]phenanthrenes and Related Compounds ..... 47
3.1 1,12-Dialkylbenzo[*c*]phenanthrenes ..... 47
3.2 1,12-Diarylbenzo[*c*]phenanthrenes ..... 50
4 Twisted Dibenzo[*c*,*g*]phenanthrenes and Related Compounds ..... 52
4.1 1,14-Dialkyldibenzo[*c*,*g*]phenanthrenes ..... 52
4.2 1,14-Diaryldibenzo[*c*,*g*]phenanthrenes ..... 54

K.K. Wang
C. Eugene Bennett Department of Chemistry, West Virginia University, Morgantown, WV 26506-6045, USA
e-mail: kung.wang@mail.wvu.edu

4.3 1,14-Dimethoxydibenzo[*c*,*g*]phenanthrene and Related Compounds ..... 55
5 Twisted Naphthalenes, Anthracenes, and Higher Acenes ..... 56
5.1 Highly Substituted Naphthalenes ..... 56
5.2 Highly Substituted Anthracenes ..... 57
5.3 Highly Substituted Higher Acenes ..... 59
6 Conclusions and Outlook ..... 59
References ..... 60

## Abbreviations

| | |
|---|---|
| [α] | Specific rotation |
| Ar | Aryl |
| Boc | *tert*-Butoxycarbonyl |
| CD | Circular dichroism |
| DMF | *N*,*N*-Dimethylformamide |
| Et | Ethyl |
| HPLC | High-performance liquid chromatography |
| *i*-Pr | Isopropyl |
| LDA | Lithium diisopropylamide |
| Me | Methyl |
| *n*-Bu | Normal (primary) butyl |
| NMR | Nuclear magnetic resonance |
| Ph | Phenyl |
| *p*-Ts | *para*-Toluenesulfonyl |
| *t*-Bu | *tert*-Butyl |
| UV | Ultraviolet |
| VPO | Vapor pressure osmometry |

## 1 Introduction

Twisted arenes have attracted the attention of chemists for more than 70 years [1, 2]. It was readily recognized that the structure of 4,5-dimethylphenanthrene (**1**) is distorted due to nonbonded steric interactions of the two methyl groups occupying the crowded C4 and C5 positions (Fig. 1) [3–5]. Although the nature of the distortion was not apparent initially, bending the methyl groups away from each other and/or twisting the aromatic framework were considered as possible ways to relieve some of the strain. The X-ray structure of **1** now clearly indicates the presence of a significant helical twist in the phenanthrene system [5–7]. It has also been well established that the energy required to twist a polycyclic aromatic hydrocarbon is quite modest [8], and many examples of twisted arenes are known with some showing remarkable degrees of distortion.

In addition to **1** and the related phenanthrene systems, placing two substituents at the crowded C1 and C12 positions of benzo[*c*]phenanthrene, such as 1,12-dimethylbenzo[*c*]phenanthrene (**2**) [9, 10], also causes a significant twist of the

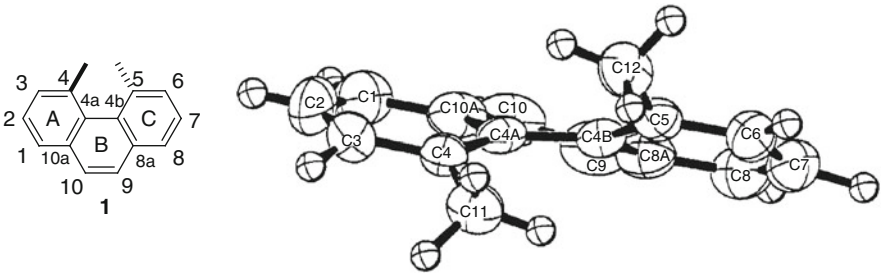


**Fig. 1** Structure and ORTEP drawing of 4,5-dimethylphenanthrene [5]. Reprinted with permission from [5]. Copyright (1987) American Chemical Society

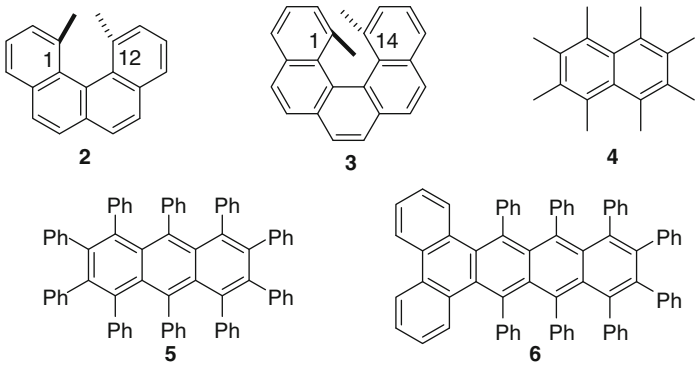


**Fig. 2** Structures of twisted arenes

aromatic system (Fig. 2). Similarly, 1,14-dimethyldibenzo[*c*,*g*]phenanthrene (**3**) and related molecules can also be expected to possess a twisted dibenzo[*c*,*g*] phenanthrene (pentahelicene) framework.

Highly substituted naphthalenes, such as octamethylnaphthalene (**4**), also exhibit significant twists of the aromatic system [11, 12]. The X-ray structure of decaphenylanthracene (**5**) shows a large end-to-end twist [13]. Higher acenes with overcrowded structures, such as octaphenyldibenzo[*a*,*c*]naphthacene **6** [14], have also been reported to show high degrees of twist.

The twisted structure of 4,5-dimethylphenanthrene (**1**) contributes to the chirality of the molecule. It was recognized early on that the ability to resolve the two enantiomers could provide supporting evidence for the nonplanarity of the aromatic system [1]. Determinations of the rates of racemization and the activation barriers of twisted chiral polyarenes have been actively pursued. Resolutions of the enantiomers to allow these investigations to proceed were achieved in several cases. In other cases, variable-temperature nuclear magnetic resonance (NMR) experiments were employed to provide insights into the configurational stabilities of the molecules. For practical applications, such as using these twisted compounds

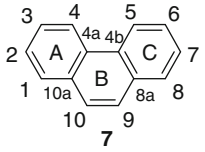


**Fig. 3** Structure of phenanthrene

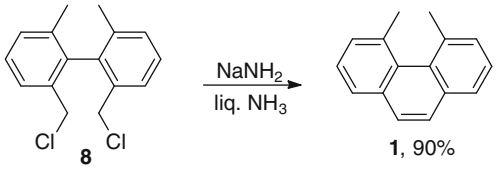


**Scheme 1** Synthesis of 4,5-dimethylphenanthrene [18]

as ligands to form organometallic complexes for asymmetric catalysis and for chiral molecular recognition, the configurational stability is of critical importance.

The strain energies in the twisted polyarenes have been determined by comparison of heats of combustion with those of the corresponding nonstrained isomers. In the case of 4,5-dimethylphenanthrene, the comparison was with that of 2,7-dimethylphenanthrene [15]. The bathochromic and hyperchromic shifts of the UV spectra of twisted arenes have been used to detect the presence of twisted distortion [16].

## 2 Twisted Phenanthrenes and Related Compounds

### *2.1 4,5-Dialkylphenanthrenes*

The X-ray structure of phenanthrene (**7**) shows that the aromatic system is nearly planar with a C4–C4a–C4b–C5 torsional angle ($\theta$) of only 2.6° (Fig. 3) [17]. The distortion is more pronounced in 4,5-dimethylphenanthrene (**1**) with a torsional angle $\theta$ of 31.5° [5]. The dihedral angle between the mean planes of the outer A and C rings (planes 1–2–3–4a–10a and 4b–5–6–7–8–8a) is 27.9°. The strain energy in **1** was determined to be 12.6 kcal/mol from comparison of its heat of combustion with that of 2,7-dimethylphenanthrene [15]. The enantiomers of **1** were separated by HPLC at cryogenic temperatures (−70°C to −80°C) on a chiral stationary phase. The activation barrier ($\Delta G^{\ddagger}$) for racemization was determined to be 16.1 kcal/mol at 25°C, indicating a rapid rate of inversion of configuration at this temperature [5].

The first synthesis of **1** from pyrene was developed by Newman and Whitehouse in 1949 [3]. An alternative synthetic procedure involving cyclization of 2,2′-bis (chloromethyl)-6,6′-dimethylbiphenyl (**8**) as a key step was reported in 1979 (Scheme 1) [18]. Other synthetic routes to **1** have also been developed [19–21].

Several analogs of **1** have been synthesized (Fig. 4), including 4,5,8-trimethyl-1-phenanthreneacetic acid (**9a**) bearing a $CH_2CO_2H$ group at the C1 position [22–24]. The presence of the carboxyl group provided a handle to allow partial resolution of the enantiomers of **9a**, giving the first evidence of a nonplanar structure. Separation

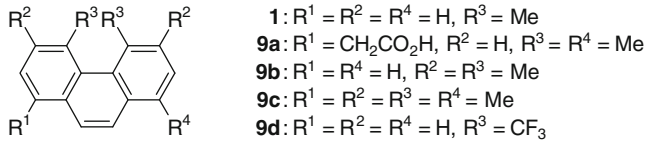


**Fig. 4** Structures of 4,5-disubstituted phenanthrenes

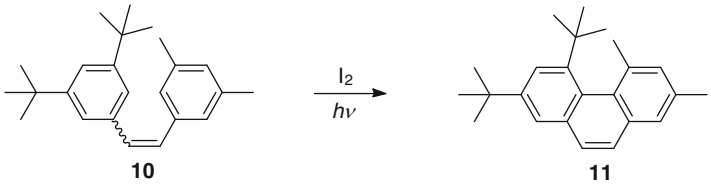


**Scheme 2** Photodehydrocyclization for 2,4-di(*tert*-butyl)-5,7-dimethylphenanthrene [25]

of the enantiomers by HPLC on silica coated with (+)-poly(tritylmethacrylate) was also achieved. By monitoring the helix inversion with a polarimetry, the activation energy ($\Delta G^{\ddagger}$) of racemization was determined to be 18.7 kcal/mol at −11°C [23]. It corresponds to a half-life of enantiomerization of 3 s at 24.8°C. The methylene hydrogen atoms in **9a** are diastereotopic, providing the opportunity to determine the activation energy of racemization by variable-temperature NMR studies and giving the activation energy of 18.6 kcal/mol at 78°C [23]. The higher activation energy of **9a**, compared to that of **1**, was attributed to the steric interactions of the substituents at the C1 and C8 positions with the hydrogens on C10 and C9, respectively, which contribute significantly to the helicity of **9a**.

The activation energy of racemization of **9b** ($\Delta G^{\ddagger}$ = 22.9 kcal/mol at 30°C) is also significantly higher than that of **1** [25]. The higher activation barrier was attributed to the buttressing effect of the methyl groups at the C3 and C6 positions in increasing steric crowing of the methyl groups at the C4 and C5 positions [5]. As a result, the torsional angle $\theta$ is increased to 32.9°. The combination of the buttressing effect and the presence of the two methyl groups at the C1 and C8 positions increases the activation barrier of **9c** to 25.1 kcal/mol at 49°C [23, 26]. With a sterically hindered *tert*-butyl group at the C4 position and a methyl group at the C5 position as depicted in 2,4-di-*tert*-butyl-5,7-dimethylphenanthrene (**11**), the activation barrier further increases to 26.6 kcal/mol at 80°C [25]. Phenanthrene **11** was synthesized by photochemically-induced dehydrocyclization reaction of the corresponding stilbene precursor **10** using $I_2$ as a dehydrogenation agent (Scheme 2).

Replacing the two methyl groups in **1** with two trifluoromethyl groups in **9d** increases the torsional angle $\theta$ to 34.0° [6]. With a sterically hindered *tert*-butyl group at the C4 position and methyl groups at C1, C5, and C8 positions as depicted in **12** (Fig. 5), the torsional angle $\theta$ further increases to 36.6° [27]. The total strain energy in **12** was estimated to be 34.0 kcal/mol at the ab initio HF-SCF level.

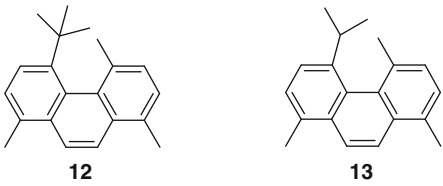


**Fig. 5** 4-*tert*-Butyl-1,5,8-trimethyl- and 4-isopropyl-1,5,8-trimethylphenanthrene [27–29]

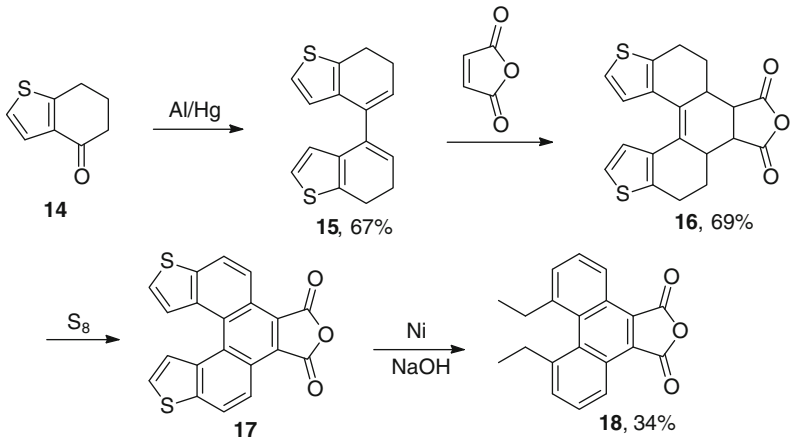


**Scheme 3** Synthesis of 4,5-diethylphenanthrene **18** [30]

Dianions of 4,5-dialkylphenanthrenes are stable and maintain their helicity [28, 29]. The dynamic NMR studies of **13** indicate that the activation barrier of racemization decreases substantially from 22.2 kcal/mol at 114°C to 15.4 kcal/mol at 46°C of its dianion ($\mathbf{13}^{2-}/2Li^{+}$). The lower activation barrier has been attributed to the elongation of the C9–C10 bond in the dianion.

A synthetic pathway for the 4,5-diethylphenanthrene derivative **18** was also reported (Scheme 3) [30]. Pinacolic reduction of **14** produced **15**, which in turn underwent a Diels–Alder reaction with maleic anhydride to give **16**. Aromatization followed by desulfurization then afforded **18** bearing the ethyl groups at the C4 and C5 positions.

## *2.2 4,5-Diarylphenanthrenes*

Photocyclization of 1-buten-3-yne **19** provided an efficient synthetic pathway to 4,5-diphenylphenanthrene (**20**) (Scheme 4) [31, 32]. Similarly, 4,5-diphenyl- (**21**), 4-(3,5-dimethylphenyl)-5-phenyl- (**22**), and 4,5-bi(3,5-dimethylphenyl)triphenylene (**23**) (Fig. 6) were also synthesized from the corresponding 1-buten-3-ynes [33]. Monobromination of **22** and **23** produced **24** and **25**, respectively.

Variable-temperature NMR studies of the NMR signals of the methyl groups of the 3,5-dimethylphenyl substituents in **22** and **23** provided the rotation barriers

**Scheme 4** Photocyclization for 4,5-diphenylphenanthrene [31, 32]

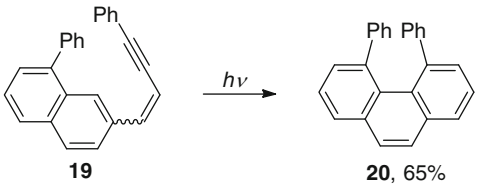


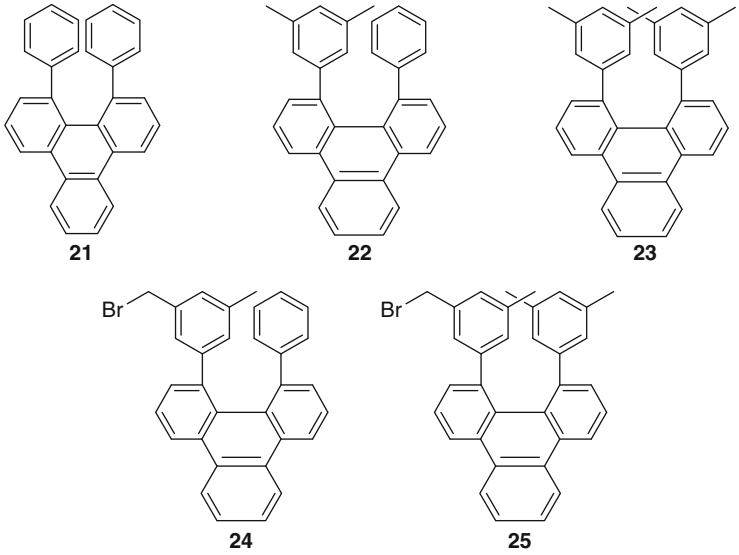


**Fig. 6** Structures of 4,5-diaryltriphenylenes [33]

around the carbon–carbon bonds attaching them to the triphenylene system. At the coalescence temperature of 16°C, the rotation barrier of **22** was determined to be 15.0 kcal/mol, whereas that of **23** was determined to be 14.8 kcal/mol at 14°C. Similarly, the rotational barriers of **24** and **25** were determined to be 15.3 and 14.8 kcal/mol, respectively.

The presence of diastereotopic hydrogen atoms on the methylene carbons of **24** and **25** also provided opportunities to determine the activation barriers for racemization. A barrier of 15.3 kcal/mol was determined for **24**, whereas that of **25** is too high to be determined by variable-temperature NMR studies. It was estimated that the activation barrier for racemization is larger than 21.1 kcal/mol for **25**. The similarity in the rotational barriers of **24** and **25** but very different racemization barriers suggest a molecular movement in which the phenyl groups turn around each other like cog wheels for racemization.

Overcrowded 4,5-bis(2-pyridyl)phenanthrenes **28a** and **28b** were prepared from the Diels–Alder reactions between 4*a*,5*a*-diazoniapentaphene diperchlorate (**26**) and ketene acetals **27a** and **27b**, respectively (Scheme 5) [16]. The X-ray structure

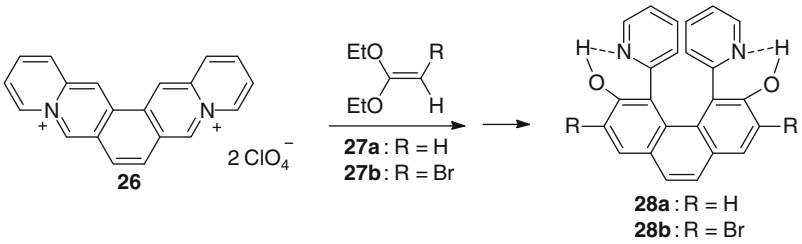


**Scheme 5** Synthesis of 4,5-bis(2-pyridyl)phenanthrene-3,6-diols [16]

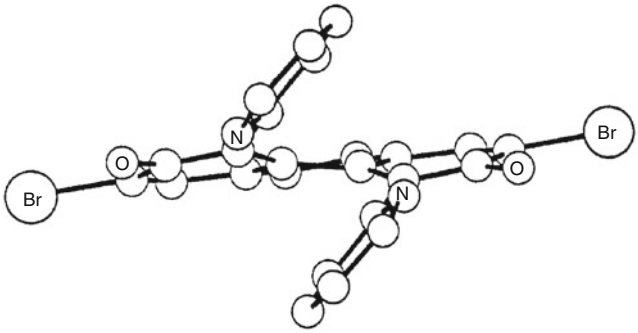


**Fig. 7** View of 2,7-dibromo-4,5-bis(2-pyridyl)phenanthrene-3,6-diol (**28b**) along the two fold symmetry axis [16, 34]. Reprinted with permission from [16]. Copyright (1971) American Chemical Society

of **28b** shows that each pyridine is intramolecularly hydrogen bonded to the neighboring hydroxyl group, creating a twofold axis of symmetry (Fig. 7) [34]. The two pyridyl groups are oriented essentially parallel to each other and are very close with a nonbonded intramolecular contact distance of 2.81 Å, which is shorted than the usual π-system van der Waals contact distance of ca. 3.4 Å between parallel aromatic hydrocarbons in crystals [35] or the graphite layer distance of 3.35 Å.

Similarly, 13,14-bis(2-pyridyl)pentaphene (**29**) (Fig. 8) was synthesized from condensation of **26** with benzyne, generated in situ from anthranilic acid and isoamyl nitrite [36]. Variable-temperature NMR studies of the mono- (**30**) and dimethylated pyridinium salts (**31**) indicated rapid rates of racemization on the NMR time scales below 79°C with the monomethylated **30** having an activation barrier of 16.6 kcal/mol at 30°C. A synchronous rotation with the pyridyl rings remaining parallel to each other was proposed as the molecular movement for racemization.

More recently, a three-step synthetic sequence for the 4,5-diarylphenanthrenyl derivatives **37a–c** was reported (Scheme 6) [37]. Condensation between benzannulated enediyne **32a** and diketone **33** produced propargylic diol **34a**. Reduction of **34a** with triethylsilane in the presence of trifluoroacetic acid furnished **35a**. Treatment of **35a** with potassium *tert*-butoxide promoted 1,3-prototropic shifts to generate, in situ, the benzannulated enyne-allene **36a**, which in turn underwent

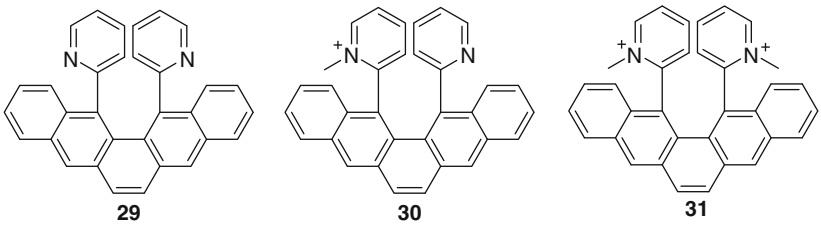


**Fig. 8** Structures of 13,14-bis(2-pyridyl)pentaphenes [36]

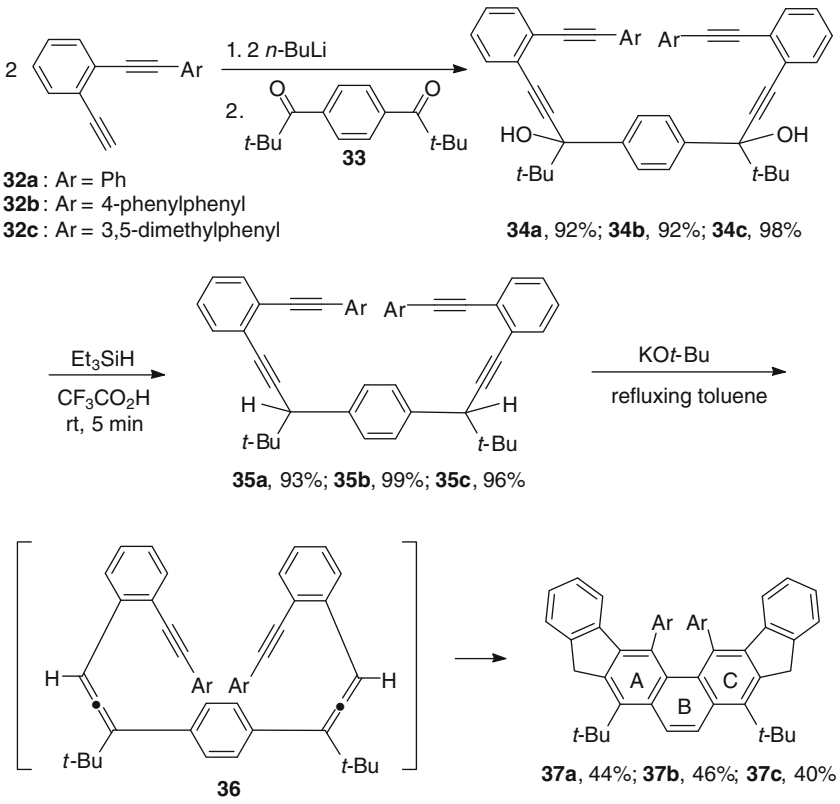


**Scheme 6** Synthesis of diindeno-fused 4,5-diarylphenanthrenes [37]

the Schmittel cascade cyclization reactions [38–40] leading to **37a**. Similarly, **37b** and **37c** were obtained from benzannulated enediynes **32b** and **32c**, respectively.

The X-ray structure of **37a** (Fig. 9) shows a severely twisted structure. As expected, the two phenyl groups are bent away from each other but are in essentially parallel orientation with a distance of ca. 2.9 Å. They are also orientated at a 53.1° angle from the central phenanthrenyl system. A pronounced 46.1° twist between the mean planes of rings A and C is much larger than that of **1** at 27.9°.

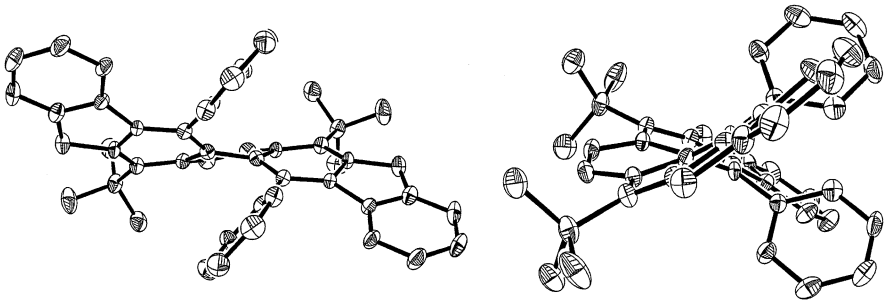

**Fig. 9** ORTEP drawings of the crystal structure of **37a** viewed from two different perspectives with hydrogen atoms omitted for clarity [37]. Reprinted with permission from [37]. Copyright (2001) American Chemical Society

The helical twist in **37a** is also manifested by the appearance of a set of AB $^{1}$H NMR signals with a large geminal coupling constant of 21.0 Hz from the diastereotopic methylene hydrogen atoms on the five-membered rings. The AB signals remain well separated and exhibit no line broadening at 125°C, indicating the rate of helix inversion is relatively slow on the NMR time scale. The activation barrier is estimated to be at least 19.4 kcal/mol, which is significantly higher than that of **24**. The buttressing effect from the two fused indeno rings at the 2,3- and 6,7-positions and the two sterically demanding *tert*-butyl groups at the 1- and 8-positions are responsible for the higher configurational stability. The higher configurational stability allowed the resolution of a derivative with a hydroxy group at the *para* position of each of the phenyl substituents. The enantiomers were found to be configurationally stable at 25°C for at least several days [41]. The $^{13}$C NMR spectra of **37a–c** also indicate restricted rotations of the aryl substituents at ambient temperature.

Treatment of **37a** with LDA followed by paraformaldehyde produced **38** as a mixture of three diastereomers (Scheme 7) [42]. The two consecutive Wagner–Meerwein rearrangements of **38** were promoted by $P_2O_5$ at 110°C, leading to 17,18-diphenyldibenzo[*a*,*o*]pentaphene (**39**) having an extended conjugation and bearing the two phenyl groups at the sterically most hindered positions. The two *tert*-butyl groups were removed during the course of the reaction.

The synthetic sequence outlined in Scheme 6 also found success in producing **40** bearing four phenyl substituents (Fig. 10) [43]. The X-ray structure of **40** if viewed from the direction perpendicular to the helical axis resembles that of a segment of a spiral staircase with the four phenyl groups as the four parallel steps or that of a single stranded DNA containing four bases. The two outer phenyl substituents on rings D and E are twisted toward opposite directions by 184.3°. The diindenophenanthrenyl system is severely distorted with a 29.3° twist angle between the mean planes of rings A and D and a more pronounced 59.2° twist angle between the mean planes of rings A and C.

Replacing the aryl substituents at the alkynyl termini in **35** with pyridyl, 2,2′-bipyridyl, and 2,2′;6′,2″-terpyridyl groups led to 4,5-diheteroarylphenanthrene

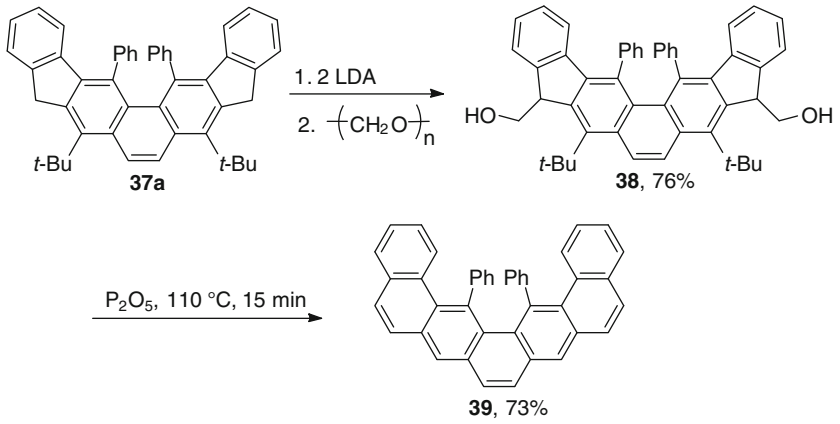


**Scheme 7** Ring expansions to 17,18-diphenyldibenzo[*a*,*o*]pentaphene (**39**) [42]

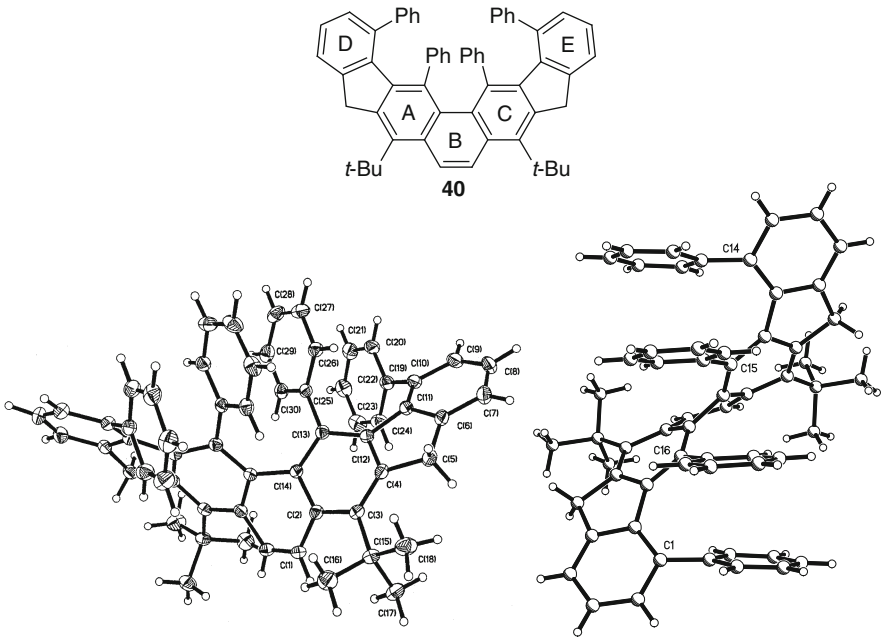


**Fig. 10** ORTEP drawing and molecular structure of molecular spiral staircase **40** [43]. Reprinted with permission from [43]. Copyright (2004) American Chemical Society

derivatives **41a**, **41b**, and **41c**, respectively (Fig. 11) [44]. The X-ray structures of **41a** and **41c** again exhibit helical twists of the diindenophenanthrenyl framework with the heteroaryl groups in parallel orientation with each other.

The presence of two terpyridyl groups in **41c** provides opportunities to form dinuclear ruthenium(II) bis(terpyridine) complexes **44a** and **44b** bearing helical

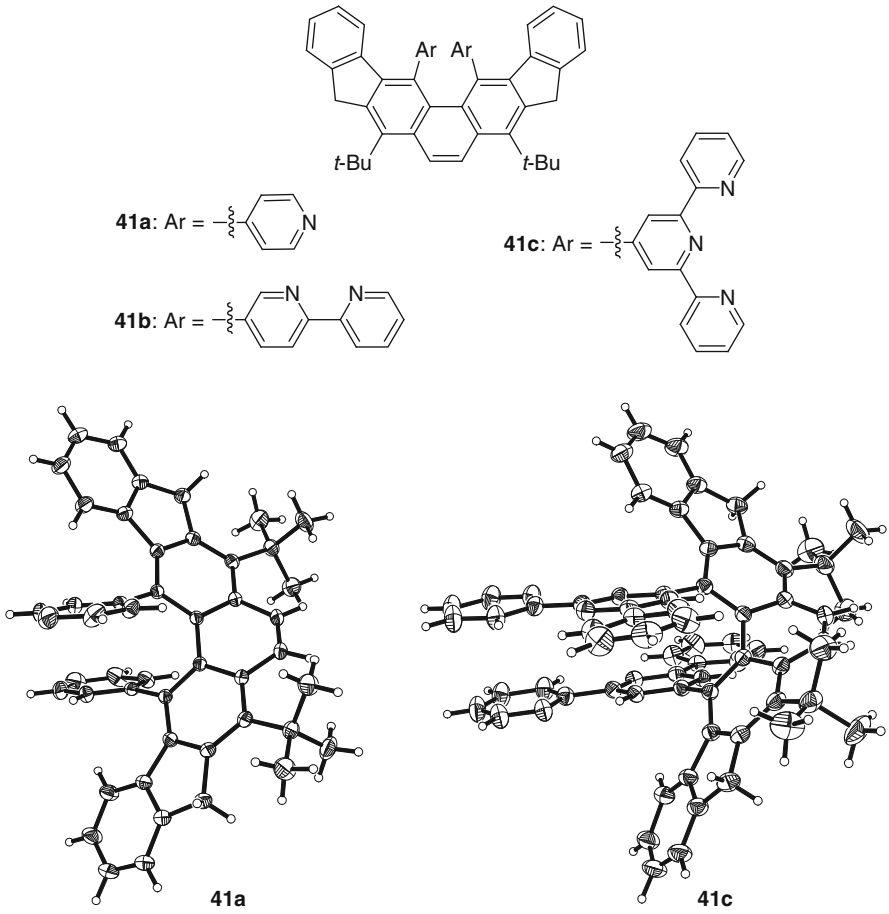


**Fig. 11** Structures and ORTEP drawings of 4,5-diheteroarylphenanthrenes **41a–c** [44]. Reprinted with permission from [44]. Copyright (2010) Royal Society of Chemistry

twists (Scheme 8). While there are many examples of ruthenium terpyridine complexes with liner and planar structures [45], such molecules with helical architecture are rare.

The close proximity of the acridine and acridan moieties in **45** provides the opportunity to generate **46** possessing a bridging hydrogen atom (C–H···C$^+$) between the methylacridan and methylacridinium groups (Fig. 12) [46]. The X-ray structure of **46** shows an unsymmetrical bridge with a distance of 1.08 Å for the localized C–H bond and a distance of 2.51 Å for H···C$^+$. The distance between the two carbon atoms is 3.14 Å. The C4-C4a-C4b-C5 torsional angle is 29.7°. The activation barrier for the hydride shift, determined by variable-temperature NMR studies, is 12.4 kcal/mol at 5°C.

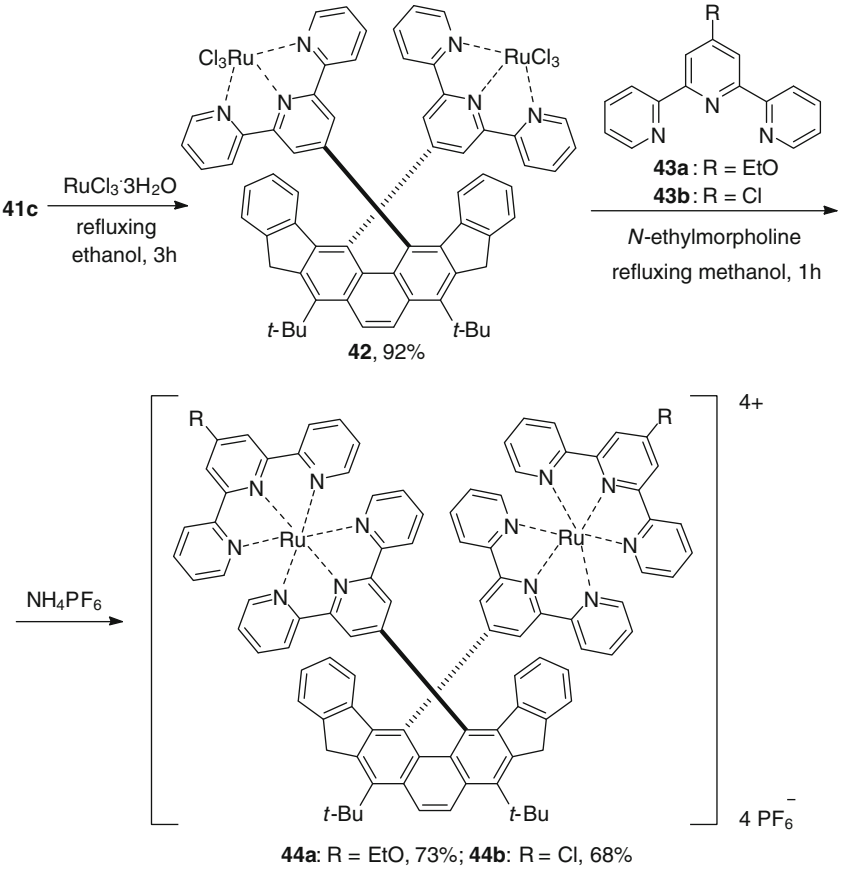


**Scheme 8** Synthesis of helical dinuclear ruthenium(II) bis(terpyridine) complexes [44]

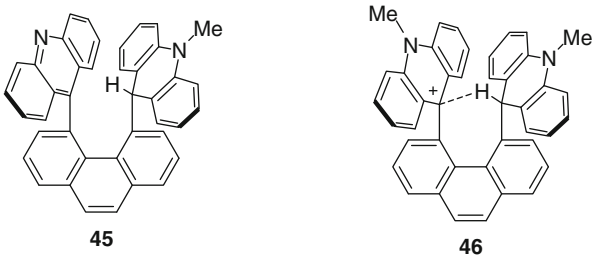


**Fig. 12** Structures of 4,5-disubstituted phenanthrenes **45** and **46** [46]

## *2.3 4,5-Dihalophenanthrenes*

The synthetic procedures for the four 4,5-dihalophenanthrenes **47a–d** (Fig. 13) have been reported. For **47a**, **47b**, and perhaps **47c**, the procedures are similar to that outlined in Scheme 1 [47–49]. Iodination of 4,5-dilithiophenanthrene produces

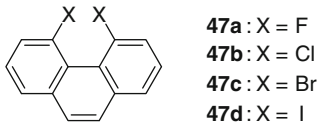


**Fig. 13** Structures of 4,5-dihalophenanthrenes

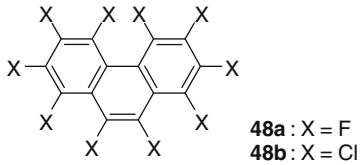


**Fig. 14** Structures of decafluorophenanthrene (**48a**) and decachlorophenanthrene (**48b**)

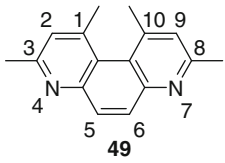


**Fig. 15** Structure of 1,3,8,10-tetramethyl-4,7-phenanthroline (**49**) [54]

diiodide **47d** [50]. The X-ray structures of **47a**, **47b**, and **47d** show twisted structures with torsional angles $\theta$ of 20.1°, 37.7°, and 34.6°, respectively [6, 50].

Decafluorophenanthrene (**48a**) [51, 52] and decachlorophenanthrene (**48b**) [53] (Fig. 14) have also been synthesized. The X-ray structure of **48b** shows a pronounced torsional angle $\theta$ of 41.9° [27, 53].

## *2.4 1,10-Disubstituted 4,7-Phenanthrolines*

As in 4,5-disubstituted phenanthrenes, substitutions at the sterically most hindered C1 and C10 positions of 4,7-phenanthroline as depicted in **49** (Fig. 15) cause helical twist of the aromatic structure [54]. The first example of such derivatives, 1,10-dicarboxy-3,8-diphenyl-4,7-phenanthroline (**50**), was reported in 1932 (Scheme 9) [55]. Condensation of *p*-phenylenediamine with benzaldehyde and then with pyruvic acid followed by cyclization produced **50**. Oxidation of **50** to tetracarboxydipyridyl **51** provided the supporting evidence for the formation of **50**.

More recently, 13,14-dimethyldibenzo[*b*,*j*][4,7]phenanthroline (**55**) was synthesized by the copper-catalyzed condensation reactions between 1,4-diiodobenzene (**52**) and 2-aminoacetophenone (**53**) to give **54** followed by sulfuric acid-promoted cyclization reactions (Scheme 10) [56]. Alternatively, **55** was also prepared by a one-pot procedure involving the $ZnCl_2$-catalyzed reactions between *N*,*N*′-diphenyl-*p*-phenylenediamine (**56**) and acetic acid (Scheme 11) [57, 58]. The enantiomers of **55** were separated by a chiral HPLC column and were found to undergo rapid racemization at room temperature. A slower rate of racemization was observed for the 13,14-diethyl derivative **57**. The X-ray structure of **57** confirmed the twisted aromatic framework.

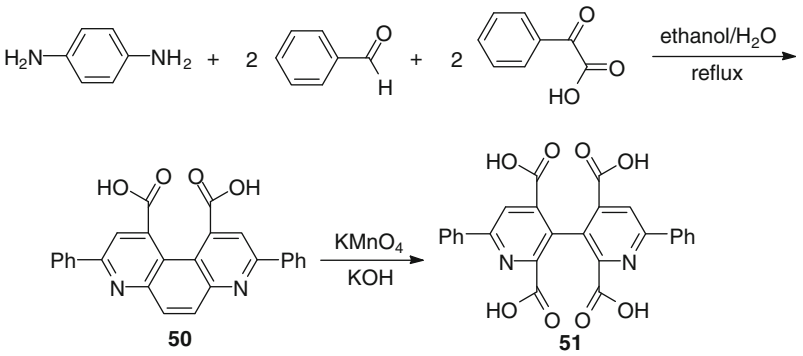


**Scheme 9** Synthesis of 1,10-dicarboxy-3,8-diphenyl-4,7-phenanthroline (**50**) [55]

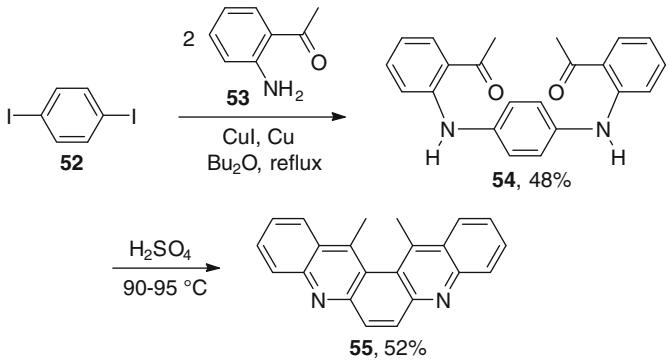


**Scheme 10** Synthesis of 13,14-dimethyldibenzo[*b*,*j*][4,7]phenanthroline (**55**) [56]

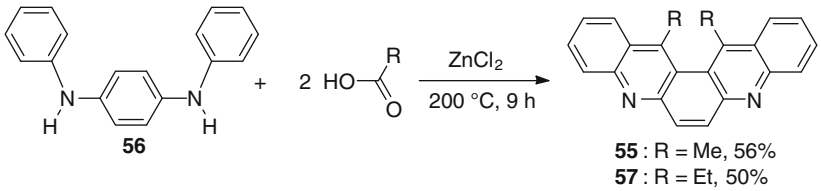


**Scheme 11** One-pot synthesis of 13,14-dialkyldibenzo[*b*,*j*][4,7]phenanthrolines [57, 58]

Treatment of diamine **56** with diacids **58** produced dibenzophenanthrolines **59a–c** bearing an additional 7-membered ring (Scheme 12) [57]. Attempts to separate **59a** and **59b** by chiral HPLC were unsuccessful, presumably because of rapid rates of racemization. The $^{1}$H NMR spectrum of **59c** also indicates a rapid rate of racemization. The presence of a stereogenic center at C13 of **59c** makes it possible to form two diastereomeric pairs, (*S*)-(*M*)/(*R*)-(*P*)-**59c** and (*S*)-(*P*)/(*R*)-(*M*)-**59c**. Only the racemic

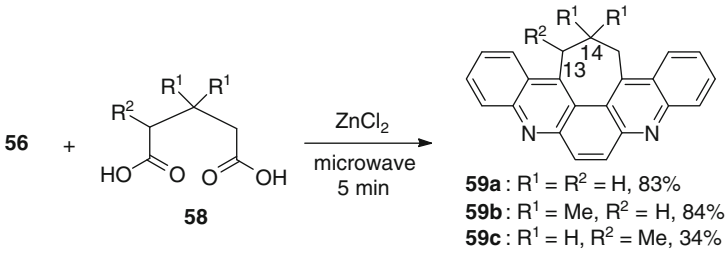


**Scheme 12** One-pot synthesis of dibenzo[*b*,*j*][4,7]phenanthrolines containing a trimethylene bridge [57]

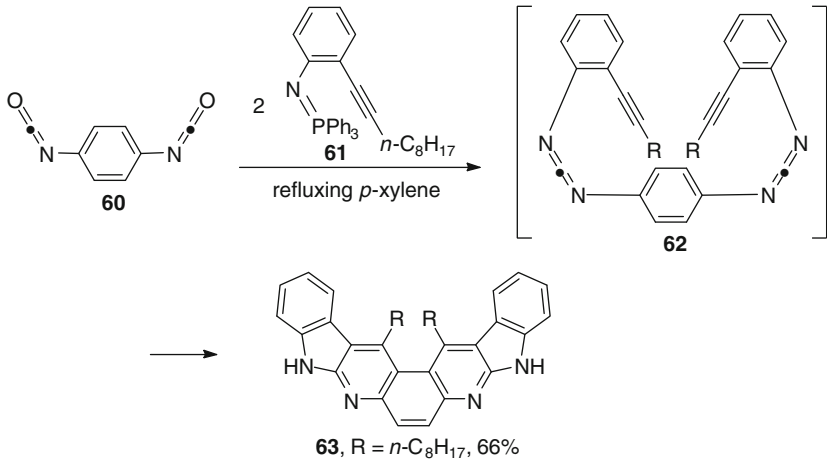


**Scheme 13** Synthesis of diindolophenanthroline **63** [59]

mixture of (*S*)-(*M*)/(*R*)-(*P*)-**59c** was produced exclusively. Since rapid equilibration between the two diastereomeric pairs can be expected, the exclusive formation of (*S*)-(*M*)/(*R*)-(*P*)-**59c** can only be attributed to their higher thermodynamic stability.

The cascade cyclization reactions of the benzannulated enyne-carbodiimide **62**, prepared in situ by the aza-Wittig reactions between 1,4-phenylene diisocyanate (**60**) and 2 equivalents of iminophosphorane **61**, produced diindolophenanthroline **63** (Scheme 13) [59]. The reaction mechanism is similar to that described for the benzannulated enyne-allene **36** in Scheme 6. The $^1$H NMR spectrum of **63** shows two sets of signals with equal intensity at $\delta$ 4.00 and 3.74, indicating the diastereotopic relationship of the two benzylic hydrogens on the same carbon atom and manifesting the presence of a helical twist. These two signals remain well separated and exhibit no line broadening at 110°C, indicating a relatively slow rate of racemization on the NMR time scale.

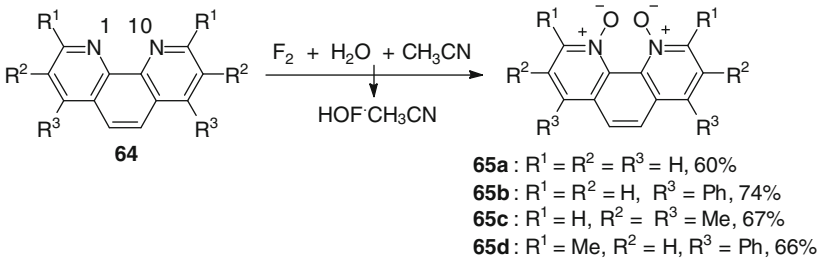


**Scheme 14** Synthesis of 1,10-phenanthroline 1,10-dioxides [60]

### *2.5 1,10-Phenanthroline 1,10-Dioxides*

Oxidations of 1,10-phenanthrolines **64** to form 1,10-phenanthroline 1,10-dioxides **65** were found to be unsuccessful with a variety of oxidizing agents except with $HOF{\cdot}CH_3CN$ (Scheme 14) [60]. On the other hand, 5,6-dihydro-1,10-phenanthrolines could be readily oxidized by a variety of oxidizing agents to form the corresponding dioxides, which upon dehydrogenation could also produce 1,10-phenanthroline 1,10-dioxides. The presence of two oxygen atoms at the sterically most hindered N1 and N10 positions could cause a helical twist of the molecule. However, variable-temperature NMR studies with a chiral europium shift reagent suggest a rapid rate of helix inversion on the NMR time scale.

## 3 Twisted Benzo[*c*]phenanthrenes and Related Compounds

### *3.1 1,12-Dialkylbenzo[c]phenanthrenes*

The X-ray structure of benzo[*c*]phenanthrene (**66**) (Fig. 16) shows significant structural distortion [61]. The acute dihedral angle between rings A and C is 18.1° and between rings A and D is 26.7°. Placing one or two substituents at the sterically most hindered C1 and C12 positions causes higher degrees of distortion.

The history of the chemistry of 1,12-dimethylbenzo[*c*]phenanthrene (**2**) resembles that of 4,5-dimethylphenanthrene (**1**). The first synthesis of **2** was reported by Newman and Wolf in 1952 [9]. The synthetic sequence included preparation of diacid **67** for the Friedel–Crafts acylation reactions to form diketone **68** (Scheme 15). Reduction followed by dehydration and dehydrogenation then produced **2**.

Similarly, 1,12-dimethylbenzo[*c*]phenanthrene-5-acetic acid (**69**) (Fig. 17) was later synthesized and resolved [62]. However, unlike 4,5,8-trimethyl-1-phenanthreneacetic acid (**9a**), which undergoes rapid helix inversion at room temperature, **69** is optically stable in refluxing mesitylene at 163°C for several days. The methyl ester of **69** was also found to be optically stable at temperature up to 250°C for 30 min.

**Fig. 16** Structure of benzo[*c*]phenanthrene [61]

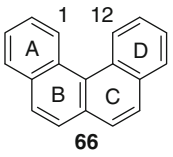


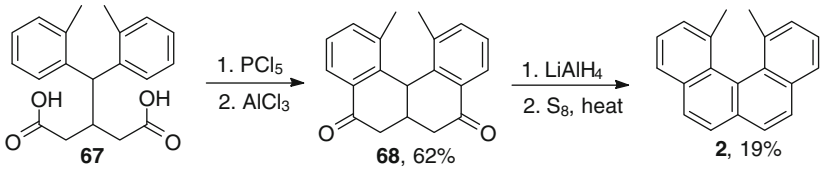


**Scheme 15** Synthesis of 1,12-dimethylbenzo[*c*]phenanthrene [9]

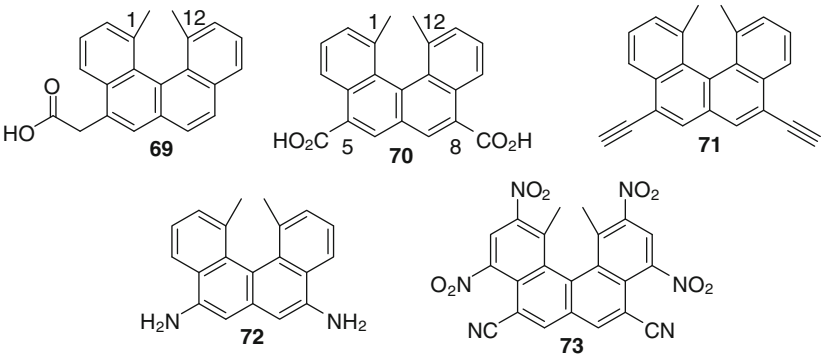


**Fig. 17** Structures of 1,12-dimethylbenzo[*c*]phenanthrenes

Several 5,8-disubstituted 1,12-dimethylbenzo[*c*]phenanthrenes, including diacid **70** [63, 64], diacetylene **71** [65], diamine **72** [66], and the tetranitro derivative **73** [66], have also been synthesized and resolved. The charge transfer complex between (*M*)-**73** and electron-rich (*M*)-**72** was found to be more stable than the complex between (*M*)-**73** and (*P*)-**72**.

A series of optically active macrocyclic amides, such as **74** (Fig. 18), consisting of one or more units of **70**, have been prepared [63]. A modest level of asymmetric induction using **74** as the catalyst for the addition reaction between aromatic aldehydes and diethylzinc was observed.

Trimer ($n = 3$) to nonamer ($n = 9$) of **75** (Fig. 19) containing *m*-phenylene spacers form thermally stable helix-dimers in non-polar solvents [67]. In hydrogen-bond breaking solvents, such as DMSO and THF, they dissociate into random-coil monomers.

Cyclic alkyne (*M*,*M*,*M*)-**76** (Fig. 20) was constructed from three units of (*M*)-**71** and three units of a *m*-phenylene derivative by the Sonogashira reactions [65]. The enantiomer (*P*,*P*,*P*)-**76** and its diastereomers (*M*,*P*,*M*)-**76** and (*P*,*M*,*P*)-**76** were likewise synthesized. Self-aggregation of (*M*,*M*,*M*)-**76** to form a dimer occurs in

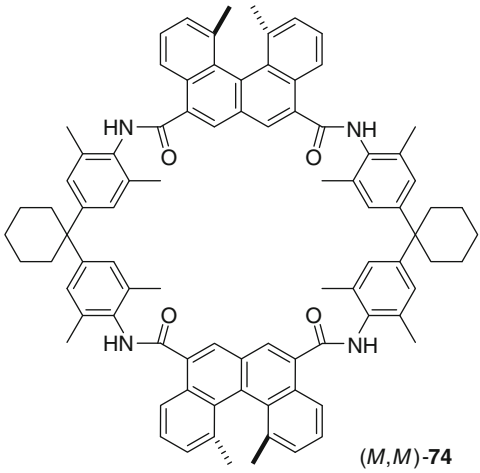


**Fig. 18** Structure of macrocyclic amide (*M*,*M*)-**74** [63]

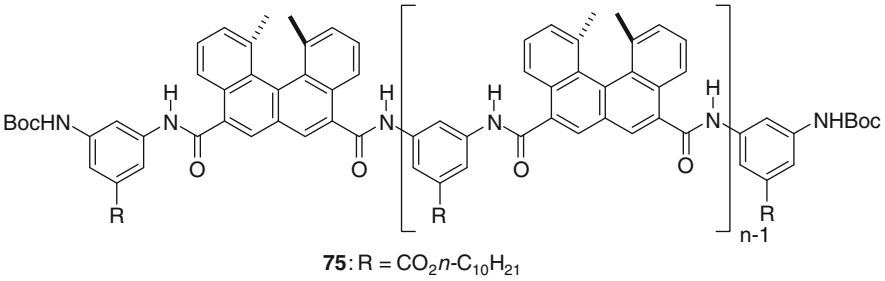


**Fig. 19** Structures of amidohelicene oligomers **75** [67]

chloroform and benzene at concentrations above 2 mM. The diastereomeric (*M*,*P*,*M*)-**76** forms aggregated dimer only above 15 mM. Effects of substituents and structures of linking groups on intra- and intermolecular aggregation by π–π interactions have also been investigated [68–70].

A series of optically active acyclic alkyne oligomers **77** (Fig. 21) containing two to nine units of (*P*)-**71** and bearing decyloxycarbonyl side chains have been synthesized [71]. In chloroform, heptamer ($n = 7$), octamer ($n = 8$), and nonamer ($n = 9$) form helical and dimeric structures, most likely double helices, whereas the lower oligomers form random-coil structures. Heptamer gradually unfolds to a random-coil structure in chloroform at room temperature.

CD and VPO studies reveal that acyclic alkyne pentamer (*P*)-**78** (Fig. 22) bearing perfluorooctyl side chains forms a homo-double-helix structure in trifluoromethylbenzene, a strong helix-forming solvent [72]. Unlike in chloroform, pentamer (*P*)-**77** ($n = 5$) also forms a homo-double-helix structure in trifluoromethylbenzene. Interestingly, the mixture of (*P*)-pentamer **78** and (*M*)-pentamer of **77** ($n = 5$) produces a hetero-double-helix dimer, indicating its higher stability over the homo-double-helix dimers of (*P*)-**78** and (*M*)-**77** ($n = 5$). On the other hand, the

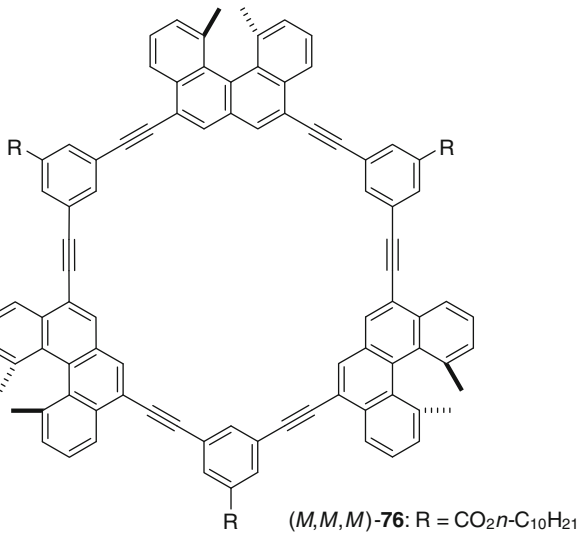


**Fig. 20** Structure of macrocyclic ethynylhelicene (*M*,*M*,*M*)-**76** [65]

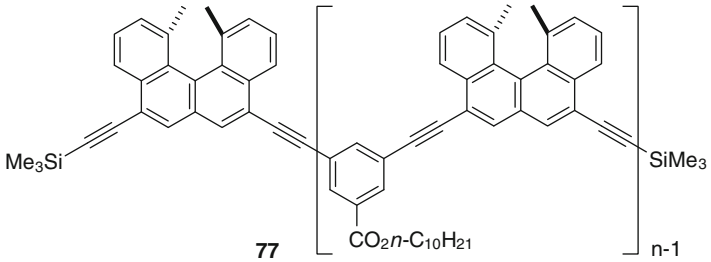


**Fig. 21** Structures of acyclic ethynylhelicene oligomers **77** [71]

hetero-double-helix dimer between (*P*)-**78** and (*P*)-**77** ($n = 5$) is not formed preferentially over the homo dimers. A systematic study of the side chain effect on the double helix formation has also been reported recently [73].

The structure and optical activity of 1,12-dimethyl-, 1,12-diethyl-, and 1,12-diisopropylbenzo[*c*]phenanthrene derivatives, (*P*)-**79a**, (*P*)-**79b**, and (*P*)-**79c** (Fig. 23), have also been investigated [74]. Interestingly, the ethyl and the isopropyl substituents cause less severe twists when compared to the methyl group. The acute dihedral angle of the mean planes of the two outer rings (rings A and D) is 47.9° for (*P*)-**79a**, 45.2° for (*P*)-**79b**, and 41.8° for (*P*)-**79c**.

## *3.2 1,12-Diarylbenzo[c]phenanthrenes*

The synthetic strategy outlined in Scheme 5 for 4,5-bis(2-pyridyl)phenanthrenes **28** also found success in the synthesis of 1,12-bis(2-pyridyl)benzo[*c*]phenanthrene **81** (Scheme 16) [75]. Condensation between 4*a*,10*a*-diazoniaanthra[1,2-*a*]anthracene diperchlorate (**80**) and 1,1-diethoxypropene led to **81** in 53% overall yield.

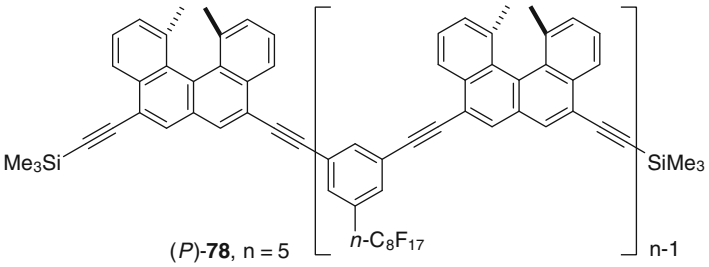


**Fig. 22** Structure of acyclic ethynylhelicene pentamer (*P*)-**78** [72]

**Fig. 23** Structures of 1,12-disubstituted benzo[*c*]phenanthrenes [74]

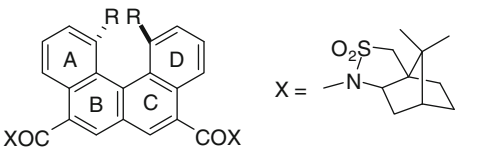


(*P*)-**79a**, R = Me; (*P*)-**79b**, R = Et; (*P*)-**79c**, R = *i*-Pr

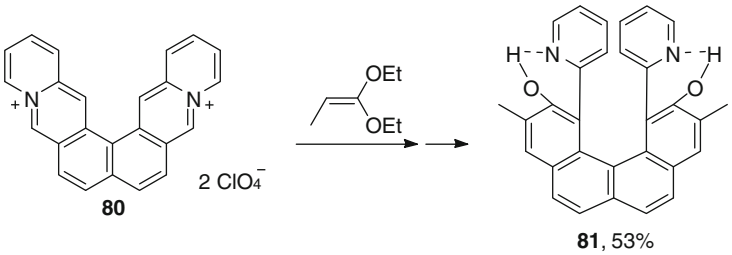


**Scheme 16** Synthesis of 1,12-bis(2-pyridyl)benzo[*c*]phenanthrene-2,11-diol **81** [75]

The cascade cyclization reactions of the benzannulated enyne-allenes outlined in Scheme 6 were also adopted for the synthesis of the diindeno-fused 1,12-diphenylbenzo [*c*]phenanthrene **85** (Scheme 17) [76]. The X-ray structure of **85** (Fig. 24) shows a twisted structure with a 59.9° acute dihedral angle between the mean planes of rings A and D. Each phenyl substituent is oriented at a 60.8° angle from the benzene ring to which it is attached but is roughly parallel to the opposite side of the twisted benzo[*c*] phenanthrene framework with a distance of ca. 2.94 Å at the closest point.

The $^{1}$H NMR signals of the two *ortho* hydrogen atoms on each of the phenyl substituents of **85** appear at $\delta$ 7.88 and 5.71, indicating that the two hydrogen atoms are in very different magnetic environments and the rate of rotation is relative slow on the NMR time scale at room temperature. Coalescence of the signals occurs at ca. 125°C, which corresponds to a rotation barrier of 18.5 kcal/mol. The AB signals of the methylene hydrogen atoms remain unaffected, indicating a slow rate of racemization on the NMR time scale.

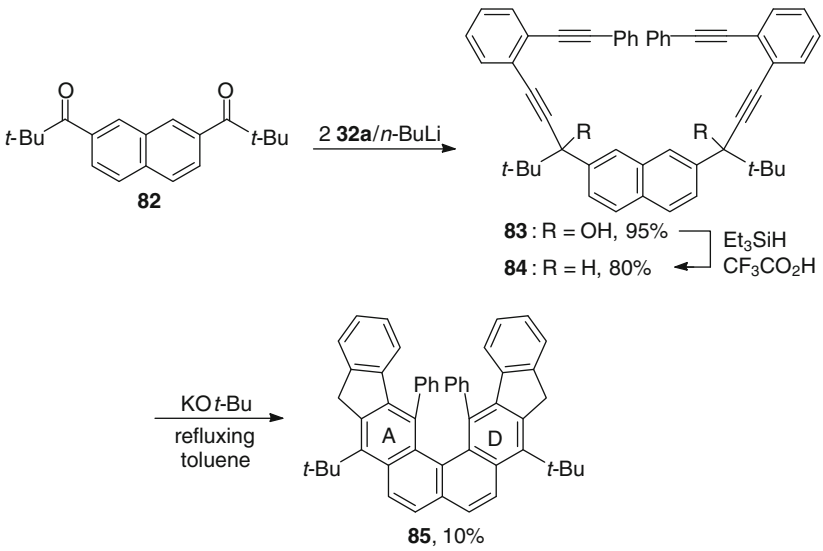


**Scheme 17** Synthesis of diindeno-fused 1,12-diphenylbenzo[*c*]phenanthrene **85** [76]

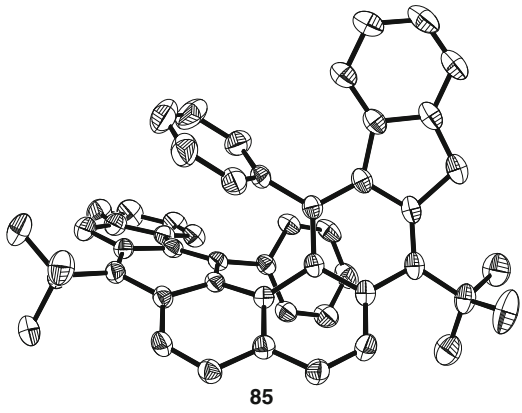


**Fig. 24** ORTEP drawing of the crystal structure of **85** with hydrogen atoms omitted for clarity [76]. Reprinted with permission from [76]. Copyright (2007) American Chemical Society

# 4 Twisted Dibenzo[*c*,*g*]phenanthrenes and Related Compounds

## *4.1 1,14-Dialkyldibenzo[*c,g*]phenanthrenes*

The X-ray structure of dibenzo[*c*,*g*]phenanthrene (pentahelicene, **86**) shows a pronounced structural distortion with a C14a–C14b–C14c–C14d torsional angle of 32° and an acute dihedral angle between the mean planes of the two outer benzene rings (rings A and E) of 50.6° (Fig. 25) [77]. The activation barrier for racemization is 24.1 kcal/mol at 40°C [78]. The half-life for racemization is ca. 14 h

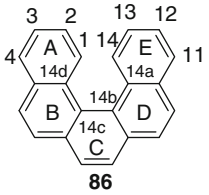


**86**

**Fig. 25** Structure of dibenzo[*c*,*g*]phenanthrene [77]

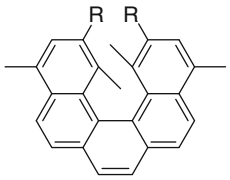


**87a** : R = Br
**87b** : R = CHO, 69%
**87c** : R = $CH_2OH$, 85%

**Fig. 26** Structures of 1,14-dimethyldibenzo[*c*,*g*]phenanthrenes [81, 82]

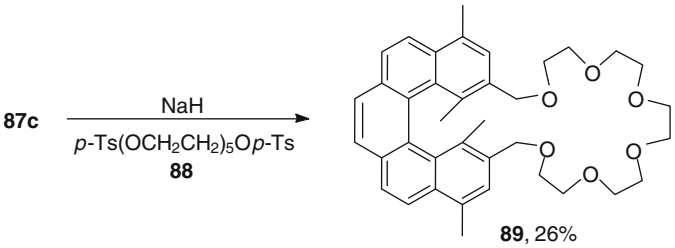


**89**, 26%

**Scheme 18** Synthesis of benzo[*c*]phenanthrene **89** bearing a crown ether [81]

at ambient temperature [77]. A computational study indicates that substitutions at C1 and C14 positions cause substantially higher activation barriers [79]. The X-ray structures of several substituted dibenzo[*c*,*g*]phenanthrenes have been reported [80].

While 1,14-dimethyldibenzo[*c*,*g*]phenanthrene has not been synthesized, 1,14-dimethyl derivative **87a** (Fig. 26) has been prepared by the photodehydrocyclization reaction of a stilbene-like precursor [81, 82]. Treatment of **87a** with *n*-butyllithium followed by DMF produced dialdehyde **87b** in 69% yield. Reduction of **87b** with lithium aluminum hydride gave diol **87c** in 85% yield. On exposure to sodium hydride and bistosylate **88**, diol **87c** was converted to **89** bearing a crown ether moiety (Scheme 18). Resolution of **89** to optically pure (*M*)-(−)-**89** and (*P*)-(+)-**89** was achieved with a chiral HPLC column. These 1,14-disubstituted dibenzo[*c*,*g*]phenanthrenes were optically stable, showing no optical change after refluxing in ethanol for 24 h. Selective chiral recognitions of one of the enantiomers of methyl phenylglycinate hydrochloride, 1-phenylethylamine hydrochloride, and 1,2-diphenylethylamine hydrochloride were observed.

Tetramethyl-substituted benzopentahelicene **90** (Fig. 27) was synthesized by the Diels–Alder reaction between a diene and benzyne followed by dehydrogenation [83].

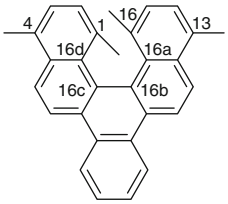


**90**

**Fig. 27** Structure of 1,4,13,16-tetramethylbenzopentahelicene **90** [83]

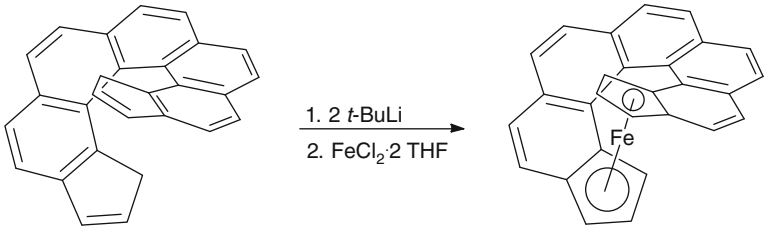


(*M*)-(−)-**91** (*M*)-(−)-**92**, 60%

**Scheme 19** Synthesis of optically active helical ferrocene (*M*)-(−)-**92** [84]

Computation using the semiempirical AM1 method shows a C16a–C16b–C16c–C16d torsional angle of 34.3° and a heat of formation for racemization of 33.7 kcal/mol, substantially higher than those of the derivatives without substitutions at C1 and C16 positions.

Optically active dibenzo[*c*,*g*]phenanthrene (*M*)-(−)-**91** bearing two fused cyclopentadienyl rings was synthesized by the photodehydrocyclization method with chirality being controlled during the cyclization process [84]. The optically active helical ferrocene (*M*)-(−)-**92** was obtained by treatment of (*M*)-(−)-**91** with *tert*-butyllithium followed by $FeCl_2$·2THF (Scheme 19).

## *4.2 1,14-Diaryldibenzo[c,g]phenanthrenes*

The photodehydrocyclization reaction was employed to produce 14,15-diphenyldibenzo[*f*,*j*]picene (**93**) (Fig. 28) in 0.8% yield [85]. The mass and $^1$H NMR spectra were used to support the structure assignment.

The diindeno-fused 1,14-diphenyldibenzo[*c*,*g*]phenanthrene **97** was synthesized by the cascade cyclization reactions of the benzannulated enediyne **96** (Scheme 20) [76]. As in the case of **85**, the X-ray structure of **97** (Fig. 29) shows profound twist with a 57.8° acute dihedral angle between the mean planes of rings A and E. Again, each phenyl substituent is oriented at a 60.2° angle from the benzene ring to which it is attached but is in roughly parallel orientation to the opposite side of the twisted dibenzo [*c*,*g*]phenanthrene framework with a distance of ca. 3.00 Å at the closest point.

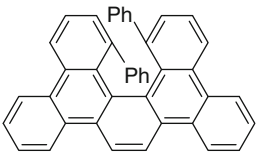


**93**

**Fig. 28** Structure of 14,15-diphenyldibenzo[*f*,*j*]picene (**93**) [85]

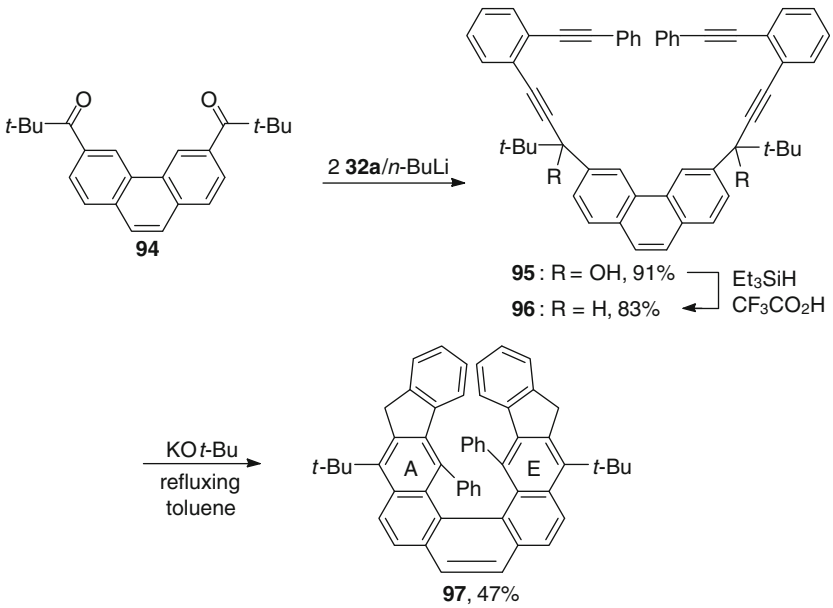


**Scheme 20** Synthesis of diindeno-fused 1,14-diphenyldibenzo[*c*,*g*]phenanthrene **97** [76]

Interestingly, the rotation barrier for the two phenyl substituents is only 12.9 kcal/mol at 20°C, smaller than the rotation barrier of 18.5 kcal/mol of **85**. Presumably the added strain at the transition state of rotation could spread over a more extended framework in **97**. As a result, the molecule could better accommodate the additional distortion caused by rotation. The AB signals of the methylene hydrogen atoms remain unaffected at 100°C, indicating a slow rate of racemization on the NMR time scale.

## *4.3 1,14-Dimethoxydibenzo[c,g]phenanthrene and Related Compounds*

The photodehydrocyclization reaction of a stilbene-like precursor was found to be efficient in producing 1,14-dimethoxydibenzo[*c*,*g*]phenanthrene [86]. Tandem radical cyclization reactions have also been used to produce a 1,14-dimethoxy

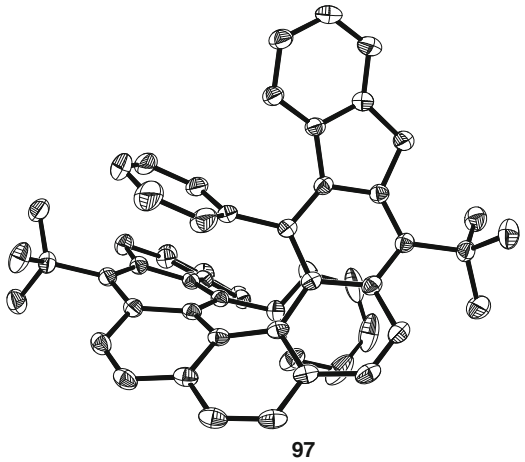


**Fig. 29** ORTEP drawing of the crystal structure of **97** with hydrogen atoms omitted for clarity [76]. Reprinted with permission from [76]. Copyright (2007) American Chemical Society

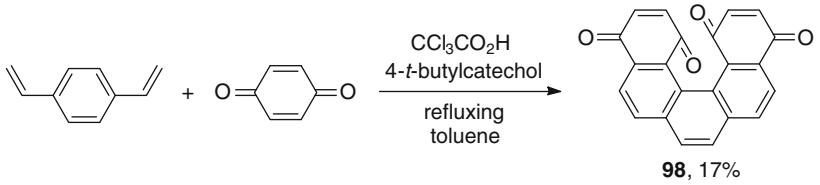


**Scheme 21** Synthesis of pentahelicenebisbenzoquinone **98** [88]

derivative [87]. Condensation between 1,4-diethenylbenzene and *p*-benzoquinone led to pentahelicenebisbenzoquinone **98** having oxygen atoms at C1 and C14 positions (Scheme 21) [88]. These oxygenated derivatives show higher configurational stability than the parent dibenzo[*c*,*g*]phenanthrene (**86**). The half-life for racemization at 25°C is ca. 6 years. Enantiopure pentahelicenebenzoquinones have likewise been synthesized [89, 90].

## 5 Twisted Naphthalenes, Anthracenes, and Higher Acenes

Twisted naphthalenes, anthracenes, and higher acenes have been reviewed recently [8]. Only a brief summary of representative examples is given in this section.

### *5.1 Highly Substituted Naphthalenes*

Naphthalenes with eight substituents usually show twisted structures. The twist can be attributed to nonbonded steric interactions between substituents on C1 and C8 and on C4 and C5. The distance between C1 and C8 in naphthalene is only 2.5 Å, which is invariably shorter than the sum of the van der Waals radii of the two

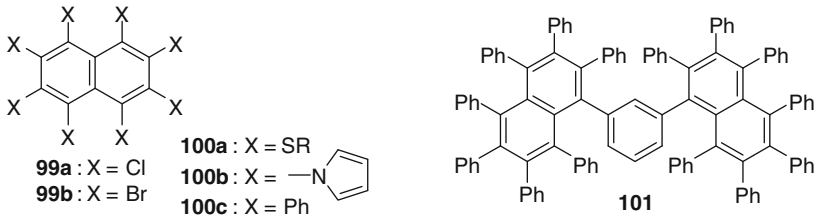


**Fig. 30** Structures of highly substituted naphthalenes

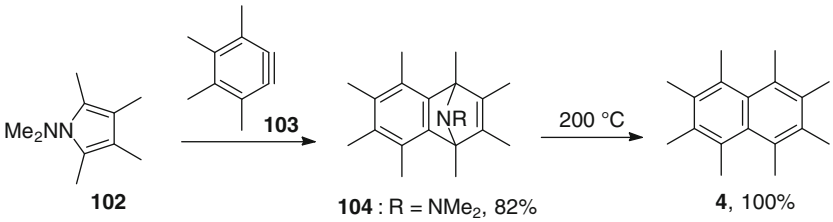


**Scheme 22** Synthesis of octamethylnaphthalene [11]

substituents. Octamethylnaphthalene (**4**) exhibits a 26° end-to-end twist [12]. Octachloro- (**99a**) [91] and octabromonaphthalene (**99b**) [92] (Fig. 30) show twists of 24° and 31°, respectively. Several highly twisted octakis(arylthio)naphthalenes **100a** and octapyrrolylnaphthalene (**100b**) have also been reported [8]. However, octaphenylnaphthalene (**100c**) has an essentially untwisted structure presumably due to the effect of crystal packing [13]. A large 35° twist was observed for the octaphenyl derivative **101** [93].

Condensation between *N*-dimethylaminopyrrole (**102**) and tetramethylbenzyne (**103**), generated in situ from 1,2-dibromo-3,4,5,6-tetramethylbenzene, to form the cycloadduct **104** followed by pyrolysis to form **4** (Scheme 22) [11] represents a general pathway for highly substituted naphthalenes.

Condensation between tetraphenylcyclopentadienone (**105**) and tetraphenylbenzyne (**106**), generated in situ by diazotization of tetraphenylanthranilic acid, to form **107** followed by decarbonylation to form **100c** (Scheme 23) [13] represents an alternative general pathway for highly substituted naphthalenes.

## *5.2 Highly Substituted Anthracenes*

Decamethylanthracene and related compounds were synthesized by a pathway similar to that outlined in Scheme 22 [11]. Decaphenylanthracene (**5**) was prepared by condensation between hexaphenylisobenzofuran (**108**) and tetraphenylbenzyne (**106**) to form **109** followed by deoxygenation with zinc dust in refluxing acetic acid (Scheme 24) [13]. The X-ray structure of **5** exhibits a 63° end-to-end twist.

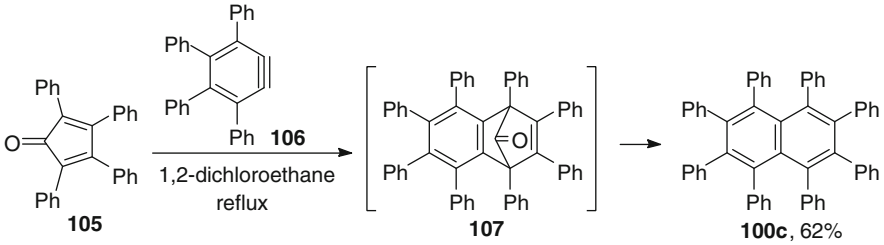


**Scheme 23** Synthesis of octaphenylnaphthalene [13]

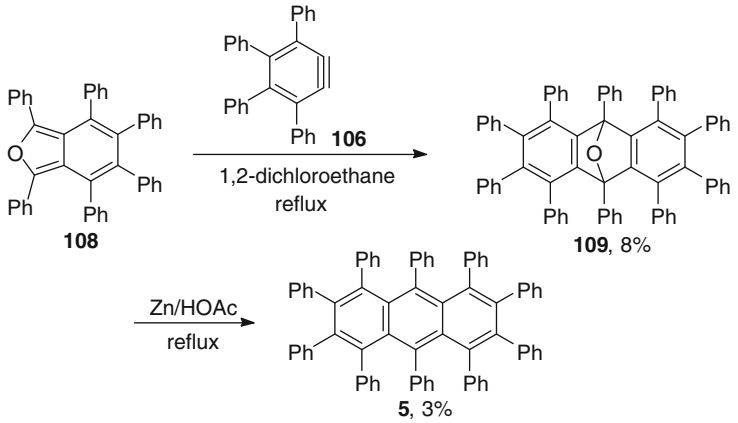


**Scheme 24** Synthesis of decaphenylanthracene [13]

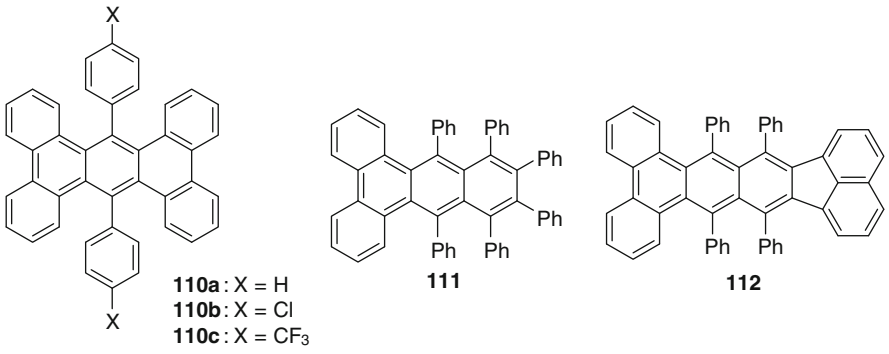


**Fig. 31** Structures of highly substituted anthracenes [94–96]

Benzannulated anthracenes **110a**, **110b**, and **110c** (Fig. 31) are highly twisted with end-to-end twists of 66°, 61°, and 70°, respectively [94, 95]. Similarly, crowded anthracenes **111** and **112** show twists of 60° and 57°, respectively [96].

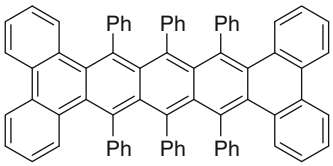


**113**

**Fig. 32** Structure of hexaphenyltetrabenzo[*a*,*c*,*l*,*n*]pentaacene **113** [97]

## *5.3 Highly Substituted Higher Acenes*

Several highly substituted higher acenes with high degrees of end-to-end twists have been reported. Octaphenyldibenzo[*a*,*c*]naphthalene **6** shows a 105° twist [14] and hexaphenyltetrabenzo[*a*,*c*,*l*,*n*]pentaacene **113** (Fig. 32) has the largest twist reported so far at 143.6° [97]. The enantiomers of **113** were resolved with very large specific rotations of $[\alpha]_D^{25} = +7440° \pm 150°$ and $[\alpha]_D^{25} = -7420° \pm 150°$, resembling those of helicenes. The activation barrier for racemization is 23.8 kcal/mol, which corresponds to a half-life of 9 h at room temperature.

# 6 Conclusions and Outlook

Synthetic methods have been developed to prepare twisted polyarenes with diverse structural features. A large number of X-ray structures have been reported, allowing direct measurements of the extent of distortion from planarity. However, the use of these twisted compounds for synthetic applications remains underdeveloped. While limited success has been achieved in using optically active twisted polyarenes as catalysts for asymmetric induction, a systematic study of this potentially fruitful area has not been undertaken. Molecular recognition is another area that is still in its infancy. Optical and electronic properties have not been exploited. However, there is no reason to believe that the chemistry of twisted polyarenes will not be as fruitful in the future as has been observed over the past 70 years. Because the future direction of the development of this fascinating class of compounds can barely be imagined, success can come from a wide variety of areas.

**Acknowledgments** The author thanks Professor Jeffrey L. Petersen for his assistance in obtaining several X-ray structures and the structural information given in this chapter. The financial support of the National Science Foundation (Grant CHE-0909613) is gratefully acknowledged.

## References


1. Newman MS (1940) J Am Chem Soc 62:2295
2. Haworth RD, Sheldrick G (1934) J Chem Soc 1950
3. Newman MS, Whitehouse HS (1949) J Am Chem Soc 71:3664
4. Badger GM, Campbell JE, Cook JW, Raphael RA, Scott AI (1950) J Chem Soc 2326
5. Armstrong RN, Ammon HL, Darnow JN (1987) J Am Chem Soc 109:2077
6. Cosmo R, Hambley TW, Sternhell S (1987) J Org Chem 52:3119
7. Imashiro F, Saika A, Taira Z (1987) J Org Chem 52:5727
8. Pascal RA Jr (2006) Chem Rev 106:4809
9. Newman MS, Wolf M (1952) J Am Chem Soc 74:3225
10. Hirshfeld FL, Sandler S, Schmidt GMJ (1963) J Chem Soc 2108
11. Hart H, Lai C-Y, Nwokogu GC, Shamouilian S (1987) Tetrahedron 43:5203
12. Sim GA (1982) Acta Crystallogr B38:623
13. Qiao X, Padula MA, Ho DM, Vogelaar NJ, Schutt CE, Pascal RA Jr (1996) J Am Chem Soc 118:741
14. Qiao X, Ho DM, Pascal RA Jr (1997) Angew Chem Int Ed Engl 36:1531
15. Frisch MA, Barker C, Margrave JL, Newman MS (1963) J Am Chem Soc 85:2356
16. Fields DL, Regan TH (1971) J Org Chem 36:2991
17. Kay MI, Okaya Y, Cox DE (1971) Acta Crystallogr B27:26
18. Newman MS, Lilje KC (1979) J Org Chem 44:4944
19. Wittig G, Zimmermann H (1953) Chem Ber 86:629
20. Bergmann ED, Pelchowicz Z (1953) J Am Chem Soc 75:2663
21. Bestmann HJ, Häberlein H, Eisele W (1966) Chem Ber 99:28
22. Newman MS, Hussey AS (1947) J Am Chem Soc 69:3023
23. Mannschreck A, Gmahl E, Burgemeister T, Kastner F, Sinnwell V (1988) Angew Chem Int Ed Engl 27:270
24. Munday R, Sutherland IO (1968) J Chem Soc B 80
25. Scherübl H, Fritzsche U, Mannschreck A (1984) Chem Ber 117:336
26. Mannschreck A, Hartmann E, Buchner H, Andert D (1987) Tetrahedron Lett 28:3479
27. Grimme S, Pischel I, Nieger M, Vögtle F (1996) J Chem Soc Perkin Trans 2 2771
28. Frim R, Goldblum A, Rabinovitz M (1992) J Chem Soc Perkin Trans 2 267
29. Frim R, Zilber G, Rabinovitz M (1991) J Chem Soc Chem Commun 1202
30. MacDowell DWH, Childers RL (1962) J Org Chem 27:2630
31. Tinnemans AHA, Laarhoven WH (1976) J Chem Soc Perkin Trans 2 1115
32. Tinnemans AHA, Laarhoven WH (1973) Tetrahedron Lett 817
33. Tinnemans AHA, Laarhoven WH (1979) Tetrahedron 35:1537
34. Smith DL, Barrett EK (1971) Acta Crystallogr B27:419
35. Robertson JM (1993) Organic crystals and molecules. Cornell University Press, Ithaca, pp 206–214
36. Fields DL, Regan TH, Graves RE (1971) J Org Chem 36:2995
37. Li H, Petersen JL, Wang KK (2001) J Org Chem 66:7804
38. Schmittel M, Strittmatter M, Vollmann K, Kiau S (1996) Tetrahedron Lett 37:999
39. Schmittel M, Strittmatter M, Kiau S (1996) Angew Chem Int Ed Engl 35:1843
40. Schmittel M, Vavilala C (2005) J Org Chem 70:4865
41. Kim D (2008) Ph.D. Dissertation, West Virginia University, Morgantown
42. Yang Y, Dai W, Zhang Y, Petersen JL, Wang KK (2006) Tetrahedron 62:4364
43. Dai W, Petersen JL, Wang KK (2004) Org Lett 6:4355
44. Wen B, Petersen JL, Wang KK (2010) Chem Commun 46:1938
45. Hofmeier H, Schubert US (2004) Chem Soc Rev 33:373
46. Suzuki T, Yoshimoto Y, Takeda T, Kawai H, Fujiwara K (2009) Chem Eur J 15:2210
47. Cosmo R, Sternhell S (1987) Aust J Chem 40:2137
48. Cosmo R, Sternhell S (1987) Aust J Chem 40:35
49. Cosmo R, Hambley TW, Sternhell S (1987) Tetrahedron Lett 28:6239

50. Bock H, Sievert M, Havlas Z (1998) Chem Eur J 4:677
51. Burdon J, Knights JR, Parsons IW, Tatlow JC (1974) Tetrahedron 30:3499
52. Kiplinger JL, Richmond TG (1996) J Am Chem Soc 118:1805
53. Herbstein FH, Kapon M, Merksamer R (1976) Acta Crystallogr B32:2205
54. Perkampus H-H, Köhler H (1960) Z Elektrochem 64:365
55. Woodruff EH, Adams R (1932) J Am Chem Soc 54:1977
56. Hellwinkel D, Ittemann P (1985) Liebigs Ann Chem 1501
57. Watanabe M, Suzuki H, Tanaka Y, Ishida T, Oshikawa T, Torii A (2004) J Org Chem 69:7794
58. Tanaka Y, Sekita A, Suzuki H, Yamashita M, Oshikawa T, Yonemitsu T, Torii A (1998) J Chem Soc Perkin Trans 1 2471
59. Shi C, Zhang Q, Wang KK (1999) J Org Chem 64:925
60. Carmeli M, Rozen S (2005) J Org Chem 70:2131
61. Lakshman MK, Kole PL, Chaturvedi S, Saugier JH, Yeh HJC, Glusker JP, Carrell HL, Katz AK, Afshar CE, Dashwood W-M, Kenniston G, Baird WM (2000) J Am Chem Soc 122:12629
62. Newman MS, Wise RM (1956) J Am Chem Soc 78:450
63. Okubo H, Yamaguchi M, Kabuto C (1998) J Org Chem 63:9500
64. Yamaguchi M, Okubo H, Hirama M (1996) Chem Commun 1771
65. Nakamura K, Okubo H, Yamaguchi M (2001) Org Lett 3:1097
66. Okubo H, Nakano D, Anzai S, Yamaguchi M (2001) J Org Chem 66:557
67. Amemiya R, Ichinose W, Yamaguchi M (2010) Bull Chem Soc Jpn 83:809
68. Saiki Y, Nakamura K, Nigorikawa Y, Yamaguchi M (2003) Angew Chem Int Ed 42:5190
69. Sugiura H, Takahira Y, Yamaguchi M (2005) J Org Chem 70:5698
70. Takahira Y, Sugiura H, Yamaguchi M (2006) J Org Chem 71:763
71. Sugiura H, Nigorikawa Y, Saiki Y, Nakamura K, Yamaguchi M (2004) J Am Chem Soc 126:14858
72. Amemiya R, Saito N, Yamaguchi M (2008) J Org Chem 73:7137
73. Saito N, Terakawa R, Shigeno M, Amemiya R, Yamaguchi M (2011) J Org Chem 76:4841
74. Sugiura H, Sakai D, Otani H, Teranishi K, Takahira Y, Amemiya R, Yamaguchi M (2007) Chem Lett 36:72
75. Fields DL, Regan TH (1973) J Heterocycl Chem 10:195
76. Zhang Y, Petersen JL, Wang KK (2007) Org Lett 9:1025
77. Kuroda R (1982) J Chem Soc Perkin Trans 2 789
78. Goedicke C, Stegemeyer H (1970) Tetrahedron Lett 937
79. Janke RH, Haufe G, Würthwein E-U, Borkent JH (1996) J Am Chem Soc 118:6031
80. Stammel C, Frohlich R, Wolff C, Wenck H, de Meijere A, Mattay J (1999) Eur J Org Chem 1709
81. Yamamoto K, Ikeda T, Kitsuki T, Okamoto Y, Chikamatsu H, Nakazaki M (1990) J Chem Soc Perkin Trans 1 271
82. Nakazaki M, Yamamoto K, Ikeda T, Kitsuki T, Okamoto Y (1983) J Chem Soc Chem Commun 787
83. Minuti L, Taticchi A, Marrocchi A, Gacs-Baitz E, Galeazzi R (1999) Eur J Org Chem 3155
84. Sudhakar A, Katz TJ (1986) J Am Chem Soc 108:179
85. Laarhoven WH, Boumans PGF (1975) Recl Trav Chim Pays Bas 94:114
86. Liu L, Yang B, Katz TJ, Poindexter MK (1991) J Org Chem 56:3769
87. Laarhoven WH, Guy IL, Nanson L (2006) Angew Chem Int Ed 45:2242
88. Katz TJ, Liu L, Willmore ND, Fox JM, Rheingold AL, Shi S, Nuckolls C, Rickman BH (1997) J Am Chem Soc 119:10054
89. Carreño MC, García-Cerrada S, Urbano A (2001) J Am Chem Soc 123:7929
90. Urbano A (2003) Angew Chem Int Ed 42:3986
91. Herbstein FH (1979) Acta Crystallogr B35:1661
92. Brady JH, Redhouse AD, Wakefield BJ (1982) J Chem Res (S) 137
93. Tong L, Ho DM, Vogelaar NJ, Schutt CE, Pascal RA Jr (1997) J Am Chem Soc 119:7291
94. Pascal RA Jr, McMillan WD, Van Engen D (1986) J Am Chem Soc 108:5652
95. Pascal RA Jr, McMillan WD, Van Engen D, Eason RG (1987) J Am Chem Soc 109:4660
96. Smyth N, Van Engen D, Pascal RA Jr (1990) J Org Chem 55:1937
97. Lu J, Ho DM, Vogelaar NJ, Kraml CM, Pascal RA Jr (2004) J Am Chem Soc 126:11168

Top Curr Chem (2014) 349: 63–120
DOI: 10.1007/128_2014_548

Published online: 6 May 2014

# Synthesis, Structures, and Physical Properties of Aromatic Molecular-Bowl Hydrocarbons

**Yao-Ting Wu and Jay S. Siegel**

**Abstract** This chapter summarizes the synthesis, physical properties, structure, and crystal packing of buckybowls. Buckybowls exemplify an intermediate class of polynuclear aromatic compounds between the closed-shell fullerenes and the flat extended arrays of graphene. These warped sheets can be seen as fragments of fullerenes or the end cap of single-walled carbon nanotubes; and, their curvature endows them with physical properties distinct from flat polynuclear hydrocarbons, which opens up unique possibilities for molecular bowls in various organic materials applications.

**Keywords** Buckybowl · Carbon nanotube · Corannulene · Sumanene

## Contents

1 Introduction ..... 64
2 Corannulene and Its Derivatives ..... 65
2.1 Corannulene and Simple Corannulene Derivatives ..... 65
2.2 Highly Substituted Corannulenes ..... 75
2.3 Cyclopentacorannulene, Acecorannulene and Annelated Corannulenes ..... 85
2.4 Benzocorannulene Family ..... 88
2.5 Indenocorannulene Family ..... 91
2.6 Other Corannulene Derivatives ..... 94
2.7 The Correlations Between Structures and Bowl-to-Bowl Inversion Barriers ..... 96

Y.-T. Wu (✉)
Department of Chemistry, National Cheng Kung University, No.1 Ta-Hsueh Road, 70101 Tainan, Taiwan
e-mail: ytwuchem@mail.ncku.edu.tw

J.S. Siegel (✉)
Institute of Organic Chemistry, University of Zurich, Winterthurerstrasse 190, CH-8057 Zurich, Switzerland

School of Pharmaceutical Science and Technology, Tianjin University, 92 Weijin Road, Nankai District, Tianjin 300072, People's Republic of China
e-mail: dean_spst@tju.edu.cn

3 Sumanene ..... 97
3.1 Sumanene and Simple Sumanene Derivatives ..... 97
3.2 Naphthosumanenes ..... 104
3.3 Hemifullerene ..... 105
4 Mixed Type Buckybowls ..... 106
4.1 Acenaphtho[3,2,1,8-*ijlkm*]diindeno[4,3,2,1-*cdef*:1′,2′,3′,4′-*pqra*]triphenylene ..... 106
4.2 Acenaphth[3,2,1,8-*fghi*j]-*as*-indaceno[3,2,1,8,7,6-*pqrstuv*]picene ..... 106
4.3 Circumtrindene ..... 108
5 Other Bulkybowls ..... 108
5.1 *as*-Indaceno[3,2,1,8,7,6-*pqrstuv*]picenes ..... 108
5.2 Tetrabenzopyracylene ..... 109
5.3 Tetraindenopyrene ..... 110
5.4 Highly Curved Fragment of $C_{70}$ and Higher Fullerenes ..... 110
5.5 Hexabenzocoronene-Based Buckybowl ..... 111
6 The Smallest Carbon Nanotube ..... 112
7 A Warped Nanographene ..... 112
8 Molecular Packing of Bowls in the Solid State ..... 113
9 Conclusion and Outlooks ..... 114
References ..... 115

## 1 Introduction

Introduction of five-membered rings into $sp^2$ carbon hexagonal π-networks enables formation of aromatic bowls, exemplifying the so-called Euler's rule [1]. Corannulene (**1**) and sumanene (**2**) are representative examples. Extending the curvature of such Euler's surfaces results in the formation of molecular carbon spheres or buckyballs. These architectural features are clearly seen in the icosahedral cage structure of buckminsterfullerene (**3**), which consists of 20 six-membered rings and 12 five-membered rings [2]; the five-membered rings provide the curvature. A related class of three-dimensional carbon surfaces, namely single-walled carbon nanotubes (SWNTs) [3], can be regarded as tubular polyhexagonal sheets with two Eulerean-curved end caps.

Compared to planar polycyclic aromatic hydrocarbons (PAHs), the curved structure of buckybowls endows them with additional interesting physical properties. For example, a bowl-shaped molecule has a dipole moment and a self complimentary shape that could lead to the formation of polar crystals. Moreover, buckyballs and carbon nanotubes are well known for their (potential) applications as electro-optical organic materials. Studies of buckybowls can provide fundamental information on buckyballs and carbon nanotubes.

The chemistry of corannulene-based [4–12] and sumanene-based buckybowls [4, 12–15] has been described in several review articles. In 2006 we published a review article focusing on the solution-phase synthesis of buckybowls, and the structures and physical properties of compounds thus prepared [7]. Since then, this research field has expanded dramatically and many important results have appeared; we update the contents herein, and introduce some important compounds, which are not furnished by solution-phase synthesis. Due to page limitations, some

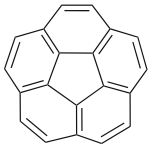

1

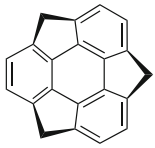

2

3

sub-topics such as metal complexes and surface chemistry are not directly addressed in this chapter.

## 2 Corannulene and Its Derivatives

The two key synthetic methods for preparing buckybowls can be classified as the solution-phase protocol and flash vacuum pyrolysis (FVP). Both methods have their advantages and limitations. The conventional solution-phase synthesis needs a special synthesis strategy to accommodate the additional strain energy of the bowl molecules; therefore, overcoming lengthy synthetic steps and low overall yields have been long-standing challenges. High-temperature pyrolysis routes can address some of the issues, but this strategy also suffers from several drawbacks: (1) modest yields, (2) almost no functional group tolerance, (3) small scale runs, and (4) the potential for thermal rearrangements of the molecule framework at high temperatures (1,000–1,300 °C) leading to undesired products [16]. Thus, the synthesis of buckybowls under mild synthetic conditions (in solution phase) on a kilogram scale became an important goal for facilitating the expansion of corannulene-based research. Fortunately, various halogenated corannulenes are accessible from corannulene, and metal-catalyzed/mediated reactions provide efficient methods in mild conditions for carbon–carbon bond formation (or ring closure) and enrich buckybowl chemistry.

### *2.1 Corannulene and Simple Corannulene Derivatives*

#### 2.1.1 Pioneering Syntheses

Corannulene (**1**) was synthesized by Lawton and Barth in 1966 [17, 18]. As mentioned by them: "Within its structural framework is an unusual strain resulting from the geometrical requirement that the bond angles deviate appreciably from the normal values found for benzenoid compounds." Thus, introduction of strain as late as possible is key to their synthetic strategy for the preparation of **1** [19]. Their synthesis started with acenaphthene, and after numerous synthetic steps the key intermediate **4** was obtained (Scheme 1). The diol acid **4** was converted to **5** upon

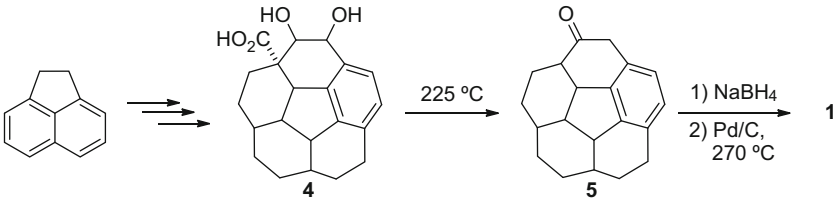


**Scheme 1** Synthesis of corannulene (**1**) based on Lawton and Barth's procedure [17, 18]

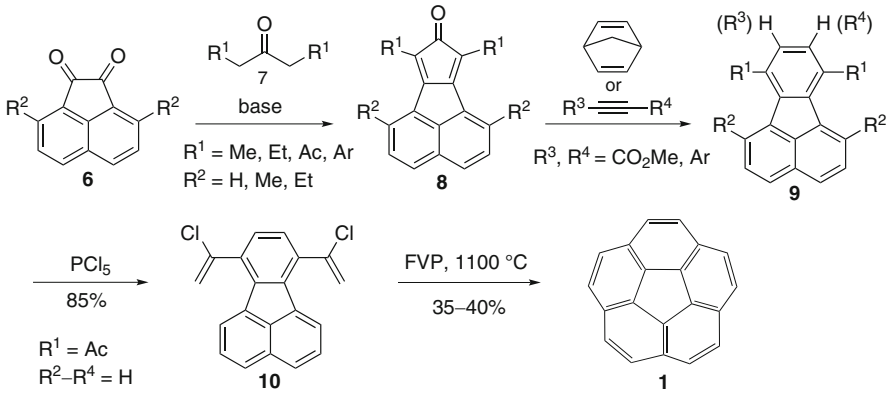


**Scheme 2** The FVP synthesis of corannulene (**1**) [20, 21]

acid dehydration followed by thermal decarboxylation. Sodium borohydride reduced the ketone, and the $sp^3$-hybridized framework was aromatized over palladium on charcoal. This synthetic approach takes 17 linear steps to prepare corannulene (**1**) in less than 1% overall yield. This classic work started the field of Eulerean carbon surfaces; however, the lengthy synthesis and the overall low yield limited further study of corannulene.

A few years later, high-temperature pyrolysis routes provided another way to achieve novel strained PAH target molecules (Scheme 2). One key reaction for the history and development of corannulene derivatives was the synthesis of acenaphthalene from 1-ethynylnaphthalene by Roger Brown [22–24]. This reaction suggested the possibility of using the rearrangement of the ethynyl unit or surrogates to a vinylidene reactive species. Larry Scott saw how to use this rearrangement to prepare **1** in an impressively short synthesis from commercially available starting materials, and his success sparked many others to join in the field. This practical and efficient method developed by Scott et al. required only three steps and produced **1** in a total yield of 26% [20, 21]. In the first step, the three starting materials, i.e., **6** ($R^2$=H), 2,4,6-heptanetrione (**7**, $R^1$=Ac), and norbornadiene, were heated with the catalyst, glycine, in toluene (Scheme 2). The Knoevenagel condensation between **6** and **7** afforded the cyclopentadienone derivative **8** ($R^1$=Ac, $R^2$=H), which underwent Diels–Alder reaction with norbornadiene to give 7,10-diacetylfluoranthene **9** ($R^1$=Ac, $R^2$=H) with loss of carbon monoxide and cyclopentadiene.

This synthetic approach has been widely used for preparing numerous fluoranthenes by chemists interested in tailor-made corannulenes (see below, Methods A–D). Notably, norbornadiene in the Diels–Alder reaction described above can be replaced with an alkyne to give 8,9-disubstituted fluoranthenes [25–29].

Treating **9** ($R^1$=Ac, $R^2$=H) with $PCl_5$ allowed transformation of the two methyl ketones in the side chains to chlorovinyl groups which occurred in 85% yield. Pyrolysis of **10** thus generated at high temperature furnished corannulene (**1**), presumably via a diethynyl intermediate produced by loss of hydrogen chlorides. Scott envisioned that terminal acetylenes would rearrange to vinylidene carbenes under these conditions and the carbenes would insert into the C–H bonds of the naphthalene fragment to close the two six-membered rings [21].

Although the obvious success of the preparation of corannulene by the FVP strategy comes from the small number of steps, the drawbacks, especially low functional group tolerance and small-scale runs, have to be improved. Automated or complete flow chemistry-based synthesis using the FVP technology has not yet been achieved but has good potential [30]; in contrast, greater advances have been made by finding mild scalable synthetic conditions in solution phase (see below, Methods A–D).

Shortly after the publication of the pyrolysis protocol, an alternative synthetic approach for synthesizing corannulene (**1**) in solution phase appeared. The key point of this strategy was a reductive coupling reaction to close the carbon–carbon bond across the 1,10 and 6,7 positions of 1,6,7,10-tetrakis(bromomethyl)-fluoranthene followed by dehydrogenation, but Wurtz type couplings were not initially observed [31], and standard pyrolysis was attempted to finish the synthesis. The successful example of a corannulene derivative made by a wholly solution phase synthesis was reported by the same group a few years later using a reductive coupling based on low-valent titanium chemistry [32]. Therein, 2,5-dimethylcorannulene (**13**) was prepared en route to a corannulene cyclophane.

Siegel and coworkers originally introduced the key step, i.e., Method A, on the basis of reductive benzylic coupling chemistry pioneered by Prakash and Olah [33] (Scheme 3). The synthetic approach started with 7,10-diethyl-1,6-dimethyl-fluoranthene (**11**), which was prepared according to Scheme 2 [32]. Bromination of **11** efficiently generated tetrabromide **12**. Under titanium-mediated conditions, **12** was converted to tetrahydrocorannulene **14**, oxidation of which furnished the desired 2,5-dimethylcorannulene (**13**). In addition to providing access to corannulene, this synthesis showed that solution phase methods could introduce substituents regioselectively, as in **13**, **15**, and **16**, which was not possible by means of pyrolysis methods [34].

Siegel's methodology for producing 2,5-dimethylcorannulene (**13**) was applied later independently by his group [34] and Rabiedau [35] for the synthesis of the corannulene parent compound (Scheme 4). Radical bromination of 1,6,7,10-tetramethylfluoranthene with NBS under forcing conditions yielded octabromide **17**, which underwent the ring closure by treating with reduced metals under anhydrous condition (Method B). Dichlorocorannulene **19** was synthesized in the same manner by the titanium-mediated protocol [34].

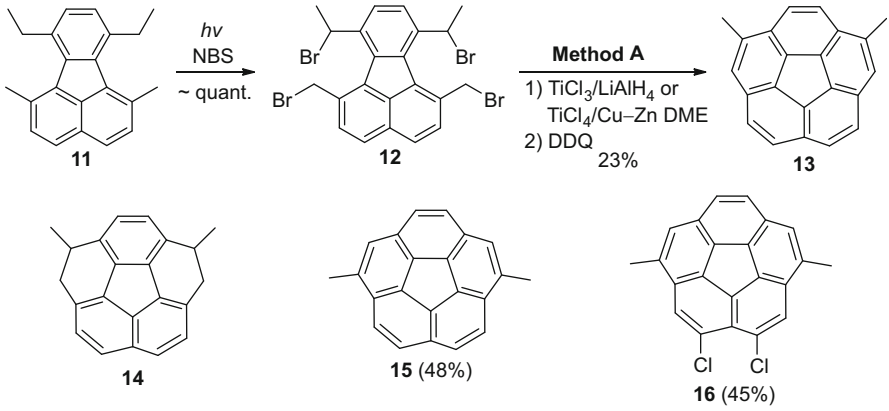


**Scheme 3** Synthesis of corannulene derivatives in solution phase by Method A [32, 34]

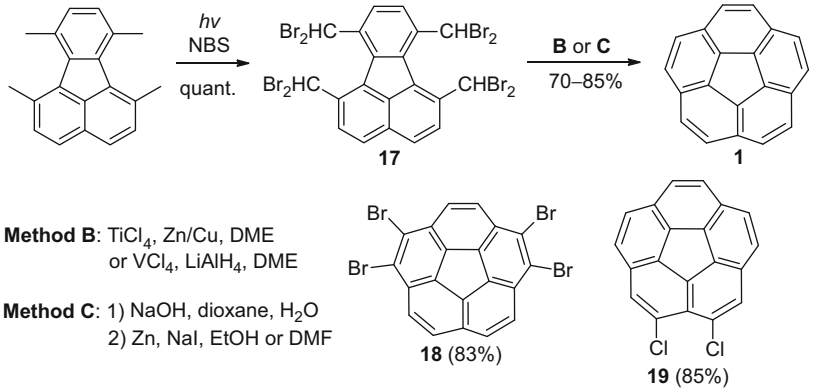


**Scheme 4** Synthesis of corannulene derivatives in solution phase by Methods B and C [34–38]

In a further refinement to the synthesis, Sygula and Rabideau discovered an appealing alternative method (Method C, Scheme 4) to prepare 1,2,5,6-tetrabromocorannulene **18** from **17** by the use of sodium hydroxide to deprotonate the remaining benzylic hydrogen and initiate carbon–carbon bond formation [36–38]. The desired molecule **1** was formed (90%) by treatment of **18** with zinc and potassium iodide [37, 38].

Under forcing bromination conditions, octabromide **17** forms from 1,6,7,10-tetramethyl fluoranthene bearing no flanking *ortho* substituents. Hexabromides **20** are obtained due to the steric hindrance of the flanking functional groups. Extension of the alkyl substituents (for example to ethyl) at the 1,6,7,10 positions also limits the degree of bromination. Nonetheless, ring closure of hexabromides **20** regioselectively to dibromocorannulenes **21** can be achieved by the base promoted procedure (Method C, Scheme 5) [25, 39, 40].

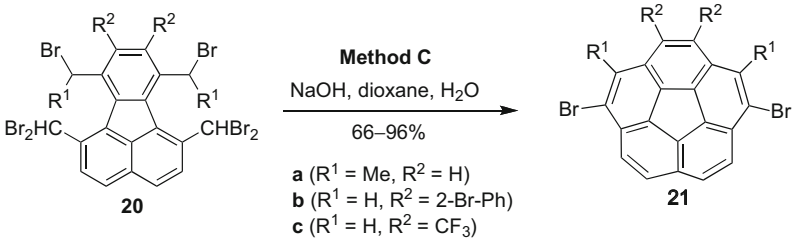


**Scheme 5** Synthesis of dibromo-substituted corannulenes derivatives by Method C [25, 39, 40]

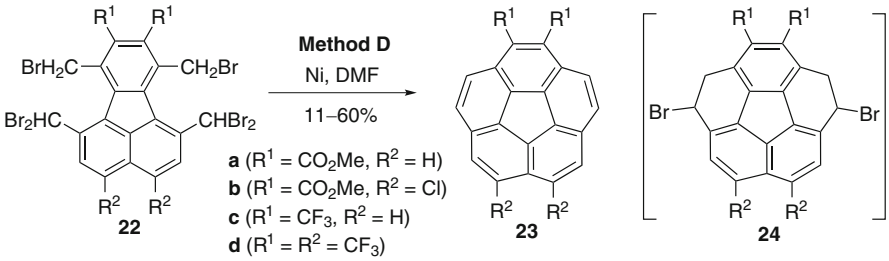


**Scheme 6** Preparation of corannulene derivatives **23** by Method D [26, 27, 40, 41]

Although methods A–C are efficient in generating corannulene derivatives, they would be problematic for sensitive functionality like the ester moiety. For example, cyclization of precursors **22** ($R^1$=$CO_2$Me) is doomed to failure under the reduction conditions of Methods A and B or in the presence of aqueous base as in Method C. A protocol developed by Sygula et al. formed the corannulene core by a nickel-mediated intramolecular coupling of benzyl and benzylidene bromides (Method D, Scheme 6) [26, 27]. In contrast to other methods presented above, this protocol provides higher tolerance of functional groups, especially esters. In the absence of ester moiety, corannulene derivatives such as **23c** and **23d** were obtained in low yield [40, 41]. Closure of two six-membered rings leads to completely debrominated products **23**. According to the postulated mechanism [42], dibromide **24** should be formed; however, it was not observed, probably due to a spontaneous double elimination of HBr giving **23** [26].

The aforementioned synthetic methods allow the formation of various corannulene derivatives in gram quantities. This scale makes the corannulene study appropriate for dedicated programs but does not make it a suitable article of commerce. Fortunately, corannulene (**1**) can now be obtained in kilogram quantities [43]. This large-scale and efficient production involves a number of important innovations, including (1) use of safer reagents, and (2) no column purification is required; for example, the preparation of the precursor, 3,8-dimethylacenaphthenequinone (**6**, $R^2$=Me, Scheme 2), from 2,7-dimethylnaphthalene is accompanied by a substantial amount of the undesired 4,7-dimethylacenaphthenequinone, which can easily be removed by treatment of the product mixture with the Girard's reagent.

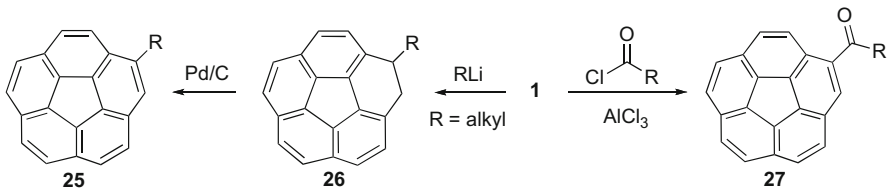


**Scheme 7** Preparation of mono-substituted corannulene derivatives directly from corannulene [46–48]

More recently, corannulene-$d_{10}$ was obtained by H/D exchange of corannulene (**1**). The exchange reaction can be conducted either in toluene-$d_8$ using the arenium acid $[\text{mesitylene}-\text{H}]^+$ as the catalyst [44] or in a mixture of DMF-$d_7$ and potassium *tert*-butoxide under microwave irradiation [45]. Both protocols gave corannulene-$d_{10}$ with a high degree of deuterium incorporation (>96%).

With kilogram quantities of corannulene in hand, many corannulene derivatives can be obtained from the parent compound. Monoalkyl substituted corannulene **25** was accessed from corannulene **1** by hydroalkylation and a subsequent dehydrogenation with Pd/C. Intermediates, 1-alkyl-1,2-dihydrocorannulenes **26**, were generated upon the treatment of **1** with the corresponding organolithium reagents in good to excellent yields (Scheme 7) [46]. However, the scope of this protocol is not broad enough, e.g., several alkyllithiums, such as methyllithium, do not give **26** (R=Me). Acylcorannulenes **27** can be obtained directly from corannulene by Friedel–Crafts acylation. Treatment of **1** with acid chlorides and $AlCl_3$ gave **27** in good to excellent yields [47, 48]. Reports of diacylation indicate that a mixture of isomers is formed. Issues of selectivity remain an open question.

For preparing mono-substituted corannulenes, functionalization of halocorannulene is ideal. Bromocorannulene (**28**-Br) was obtained in a good yield by the reaction of corannulene with bromine in the presence of a Lewis-acid catalyst (Scheme 8) [49], albeit still an issue to obtain really pure samples of **28**-Br. The reaction of corannulene with xenon difluoride gave fluorocorannulene (**28**-F), but the product has to be purified by reverse-phase HPLC [40]. Recent reports of Au(III)-catalyzed iodination [50] and chlorination [40] of corannulene using *N*-iodosuccinimide (NIS) and *N*-chlorosuccinimide (NCS), respectively, look promising as a methods for pure monohalo derivatives.

Methylcorannulene **25** (R=Me) was generated from **28**-Br by Ni-catalyzed methylation [34]. Alternatively, mono-substituted corannulenes **25** ($R=CMe_2OH$ or CHO) were also accessed by treatment of **28**-Br with *n*-BuLi forming the corannulyl lithium species and quenching with acetone [51] or DMF [52], respectively. Moreover, Negishi couplings and Sonogashira reactions of **28**-Br afford monoaryl and monoalkynyl substituted corannulenes **29** and **30**, respectively [53]. Treatment of **28**-Br with an excess of $NaNH_2$ and a catalytic amount of *t*-BuOK gave a buckybowl aryne (corannulyne), which was trapped by furan to yield a Diels–Alder product **31** in good yield [54]. Moreover, the reaction of *o*-trimethylsilylcorannulenyl triflate with cesium fluoride under mild conditions

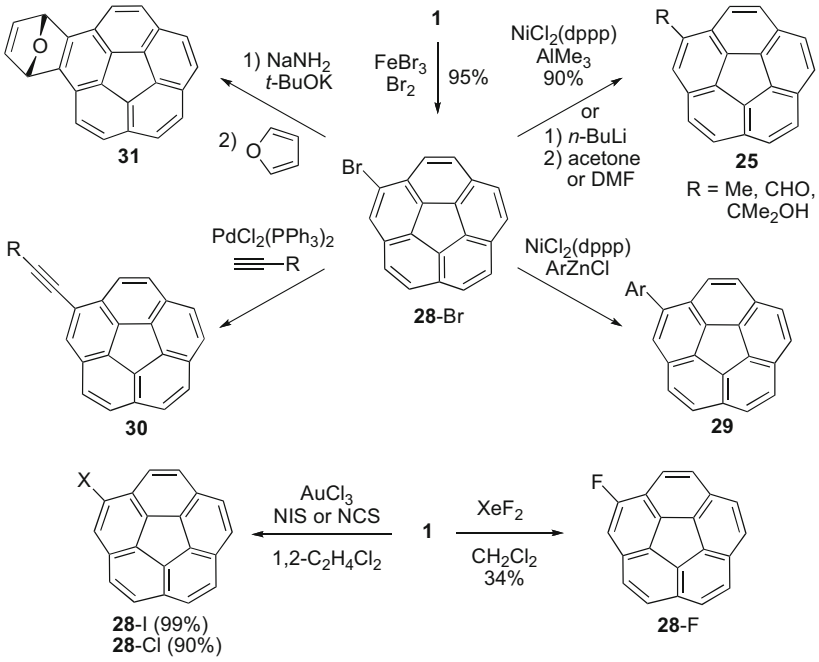


**Scheme 8** Synthesis of mono-substituted corannulenes from bromocorannulene [40, 49–54]

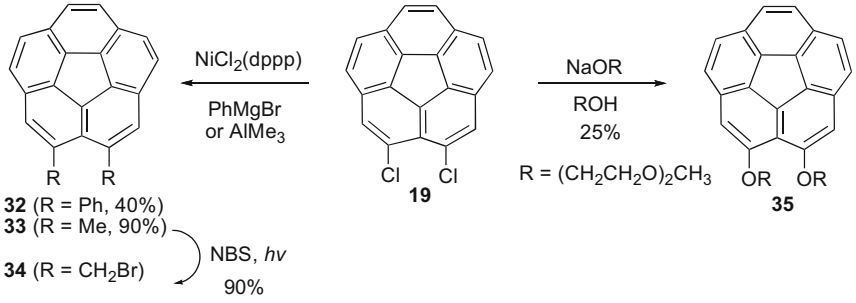


**Scheme 9** Synthesis of 2,3-disubstituted corannulenes [57]

also generated corannulyne in situ. Corannulyne so generated can undergo Pd-catalyzed [2+2+2] cyclotrimerization [55], as well as oligomerization [56].

Preparation of 2,3-disubstituted corannulene derivatives requires an alternative synthesis (Scheme 9) [57]. 2,3-Diphenylcorannulene (**32**) was generated by the Ni-catalyzed Kumada coupling of 2,3-dichlorocorannulene (**19**) with phenylmagnesium bromide. Similarly, the Ni-catalyzed methylation of **19** with trimethylaluminum yielded 2,3-dimethylcorannulene (**33**), from which the bis-(bromomethyl) derivative **34** was obtained by benzylic bromination with *N*-bromosuccinimide. Moreover, heating **19** in diethylene glycol monomethyl

ether with an excess of sodium hydride effected a nucleophilic aromatic substitution to form the 2,3-bis(diethylene glycol methyl ether) derivative **35**.

### 2.1.2 Structure and Properties of Simple Corannulene Derivatives

The curvature and rigidity of a buckybowl can be characterized by the bowl depth, POAV (π-orbital axis vector) pyramidalization angle [58–60], and bowl-to-bowl inversion barrier ($\Delta G^{\ddagger}_{inv}$). The experimental data of the first two are available by single-crystal X-ray crystallography of the desired bowl molecule. Because the barriers of many corannulene derivatives lie in the region of 7–20 kcal/mol, the $\Delta G^{\ddagger}_{inv}$ can be conveniently analyzed by variable temperature NMR study of a suitably derivatized molecule.

The C–C bonds in corannulene are conveniently classified as Rim, Flank, Hub, and Spoke (Fig. 1). X-Ray crystallographic analysis of **1** showed a hub-to-rim bowl depth of 0.87 Å [63, 64], as measured from the center of the five-membered ring to the plane containing the peripheral aromatic carbon atoms, and this is significantly shallower than would be expected for the polar cap within $C_{60}$ (ca. 1.5 Å) [65].

The bowl depth for simple corannulene derivatives strongly depends upon the kind, number, and position of substituent(s). Generally, they have smaller or comparable values to corannulene. The representative examples include **28**-F (0.87 Å) [40], **28**-Cl (0.86 Å) [40], **21c** (0.80 Å) [40], and **23c** (0.82 Å) [41]. 1,2,5,6-Tetrabromocorannulene **18** is an exception; its bowl depth was determined to be 0.91 Å [39].

The POAV pyramidalization angle of the carbon on the central five-membered ring (hub) in corannulene is 8.2°, in contrast to 11.6° for $C_{60}$. The rim carbons are predicted to be only slightly pyramidalized with pyramidalization angles in the range of 1–2°. Unlike the crystal structures of pyrene and related aromatic compounds of comparable surface area, the crystal structure of **1** is void of any aromatic face-to-face or bowl stacking. However, a mixture of corannulene and fullerene $C_{60}$ forms cocrystals [**1**·$C_{60}$] [66]. The shortest distances from $C_{60}$ to the concave surface of **1** and the convex surface of another **1** were determined to be 3.75 and 3.21 Å, respectively.

The bowl-to-bowl inversion process of corannulene (**1**) is defined as bowl form **1** converting to form **1′** via a planar transition structure $\mathbf{1}^{\ddagger}$ (Fig. 1). The difference in energy between **1** and $\mathbf{1}^{\ddagger}$ represents the bowl inversion energy ($\Delta G^{\ddagger}_{inv}$), which can be measured experimentally by variable temperature $^1$H NMR study of suitably-substituted corannulenes. Values of $\Delta G^{\ddagger}_{inv}$ were determined to lie in the range of 10.2–11.3 kcal/mol, depending on the substituent R. Benzylcorannulene [61], isopropylcorannulene [61], and bromomethylcorannulene [61] all exhibit a slightly higher $\Delta G^{\ddagger}_{inv}$ than 1-corannulenyl-1-methyl-1-ethanol [51]. The experimental value of $\Delta G^{\ddagger}_{inv}$ for the non-substituted parent **1** was estimated to be 11.5 kcal/mol although it cannot be directly measured due to symmetry [62]. A recent investigation indicated that the bowl-to-inversion barrier for corannulene can be

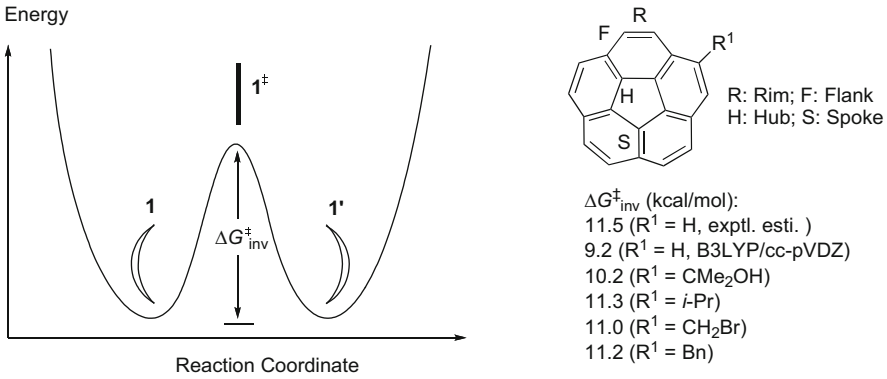


**Fig. 1** Energy diagram and $\Delta G^{\ddagger}_{inv}$ of the bowl inversion process of corannulenes [51, 61, 62]

reduced by tetracationic tetrapyriduna-tetrabenzyna-cyclododecaphane ($ExBox^{4+}$) [67]. Experimental studies were conducted with ethylcorannulene, and its inversion barrier was determined to be 10.8 and 8.71 kcal/mol in the absence and presence of $ExBox^{4+}$, respectively. The decrease in the inversion barrier (2.09 kcal/mol) determined experimentally is very close to the theoretical analysis (ca. 2.5 kcal/mol), which suggested the results are contributed by the stabilization of the planar transition-state structure (2.0 kcal/mol) and destabilization of the ground-state (0.5 kcal/mol).

As the hydrogens of the *peri* positions in **1** are replaced by larger moieties, the repulsion energy increases and $\Delta G^{\ddagger}_{inv}$ decreases relative to **1** (Table 1) [57, 62]. The order of barrier heights of some 2,3-disubstituted corannulenes determined experimentally follows oxygen (**35**, 9.9 kcal/mol) > phenyl (**32**, 9.4 kcal/mol) > bromomethyl (**34**, 9.1 kcal/mol), and all these examples exhibit lower barriers than other non-*peri* disubstituted corannulene derivatives, such as **36** (9.9 kcal/mol) and **37** (10.4 kcal/mol). The lower barriers found for the *peri*-substituted compounds compared to that found for the same substituents in isolated positions shows the special contribution from *peri* X/X repulsion. Substitution at the *peri* positions as well as the 1,6-positions leads to a further reduction in the barrier, for example compound **38** (8.7 kcal/mol). From an assumption of additivity in steric bulk, one can assess the steric size of a *peri* substituent as being roughly OR < Ph=Cl < Me.

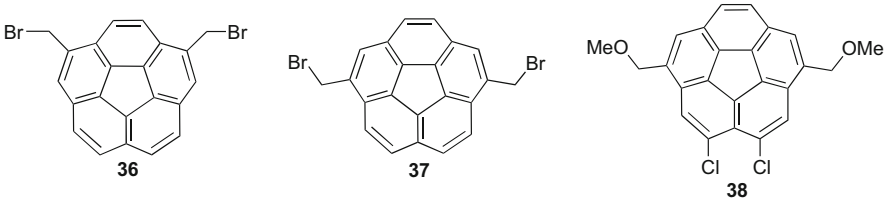

**Table 1** The inversion barrier (kcal/mol) and the bowl depth (Å) of some highly substituted corannulenes[a]

| Compound | R | $\Delta G^{\ddagger}_{inv}$ | Bowl depth | References |
|---|---|---|---|---|
| **41** | 3,5-$C_6(CH_3)_2H_3$ | – | 0.88 | [39] |
| **44** | Ph | – | 0.85 | [39] |
| **45** | Me | 8.7[b] | 0.85[b] | [62] |
| **45** | *t*-Bu | 4.5 | 0.72, 0.68[b] | [68] |
| **45** | $CF_3$ | – | 0.79 | [69] |
| **48** | SPh | – | 0.94 | Siegel et al., unpublished results |
| **49** | 3,5-$C_6(CH_3)_2H_3$ | – | 0.94 | [39] |
| **50** | Manisyl | 12.1 | 0.94 | [70] |
| **52** | Cl | – | 0.49[b], 0.51[c] | [71, 72] |
| **54** | Me | 2.2[b] | 0.58[b] | [62] |
| **55** | C≡C–*n*-Bu | – | 0.60 | [73] |
| **57** | 4-$C_6H_4Cl$ | 2.5 | 0.25 | [74] |
| **58a** | SPh | ≤8.28[b] | 0.49 | [75] |

[a]Based on experimental data and X-ray structure if not otherwise mentioned
[b]Calculated value
[c]The structure was determined by gas-phase electron diffraction

Corannulene (**1**) displays interesting electrochemical properties. The reduction states of **1** lie between those of the neutral hydrocarbon and the tetraanion ($\mathbf{1}^{4-}$/4$Li^+$). Reduction of **1** at −78°C with excess lithium metal in [$D_8$]-THF over a period of several days led to a series of three color changes, first to green, then to purple, and finally to brownish-red [76]. Quenching this solution with water gave tetrahydrocorannulene as the major product accompanied by small amounts of dihydrocorannulene and **1**. More recently, the structure of $[Na(DME)_3]^+[\mathbf{1}^-]$ was analyzed by X-ray crystallography, and its bowl depth (0.85 Å) was found to be slightly shallower than the parent **1** [77].

The first and second reduction potentials and the first oxidation potential of corannulene measured by CV (cyclic voltammetry) strongly depend on measured conditions, such as temperature, solvent, and electrolytes [34, 68, 78]. The third reduction potential was observed when the experiment was conducted with a suitable combination of solvent and electrolyte at low temperature (below 213 K) [68]. The reduction potentials of corannulene and their comparisons with other functionalized derivatives are presented in Table 3 (cf. Sect. 2.2.2).

The electrochemical properties of **1** allow it to give rise to electrochemiluminescence [69]. When a solution of **1** is treated with coreactants, such as benzoyl peroxide or arylamine, an intense blue light is generated. In addition, simple corannulene derivative 1,2-bis(trifluoromethyl)corannulene (**23c**) can potentially be applied as a electrically conductive material. The electron-accepting ability of trifluoromethyl groups cause **23c** to have charge-carrier mobility displays as $>0.9\ cm^2V^{-1}\ s^{-1}$ [41].

Stabilization of neutral radicals is another interesting property of bowl-shaped corannulene. The buckybowl neutral radicals **39** [52] and **40** [79] are stable as solids in air or as solutions in degassed toluene for long periods. Experimental results suggest spin delocalization of the radical species onto the corannulene moiety in **40** is more significant than **39**.

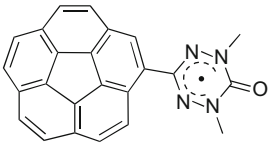


**39**

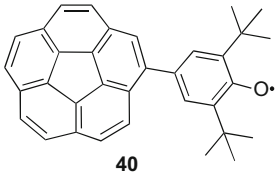


**40**

## *2.2 Highly Substituted Corannulenes*

Highly substituted corannulenes are not only important building blocks for new organic materials, they also provide the possibility to extend the aromatic system of the corannulene core. Direct multiple electrophilic aromatic substitution on corannulene has shown limited but important successes. In contrast, functionalization of multihalocorannulenes is a general route.

Two special chlorination procedures for pentachlorocorannulene and decachlorocorannulene open new avenues for the study of this area (see below). Already mentioned above, 1,2,5,6-tetrabromocorannulene (**18**) is a formal precursor of corannulene when using the Rabideau closure, but it is of direct importance for making various corannulene derivatives. The importance of multi-halocorannulenes stems from the variety and reliability of nucleophilic aromatic substitutions and related transition-metal catalyzed couplings with nucleophiles.

### 2.2.1 Synthesis

Already introduced in the chemistry of the 2,3-dichlorocorannulenes like **19** [34], nucleophilic aromatic substitution and related transition-metal catalyzed coupling chemistry transfers well with minor modifications to other halogenated corannulenes. Preparations of tetraethynylcorannulenes **41** [37–39] and tetraarylcorannulenes **42** [37, 38] were accessed by Pd-catalyzed Sonogashira and Suzuki reactions, respectively, in good to excellent yields (Scheme 10). Similarly, 1,2,5,6-tetramethylcorannulene (**43**) was obtained in good yield from **18** by the Ni-catalyzed protocol [37, 38]. Tetrasubstituted corannulene **44** with two kinds of functional groups was prepared from **21** by the Sonogashira reaction [39].

Limited alkyl groups can be regioselectively introduced on the corannulene core by Friedel–Crafts alkylation. For example, five sterically congested *tert*-butyl

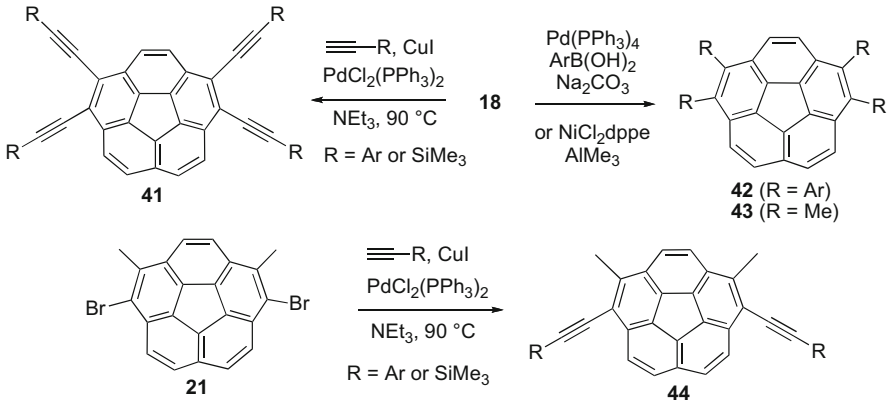


**Scheme 10** Synthesis of 1,2,5,6-tetrasubstituted corannulenes [37–39]

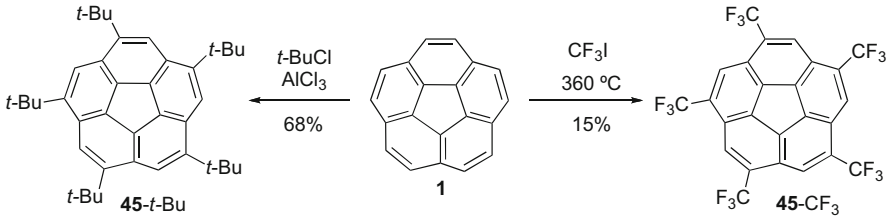


**Scheme 11** Synthesis of pentaalkylcorannulenes directly from corannulene [80, 81]

groups generated 1,3,5,7,9-penta-*tert*-butylcorannulene (**45**-*t*-Bu) in a symmetrical fashion (Scheme 11) [80]. Trifluoromethylations of corannulene (**1**) under harsh reaction conditions gave 1,3,5,7,9-pentakis(trifluoromethyl)corannulene (**45**-$CF_3$), accompanied by hexa- and hepta-substituted products [81]. The pure form of **45**-$CF_3$ was obtained by HPLC separation.

1,3,5,7,9-Pentachlorocorannulene (**46**) provides a general route for preparing pentasubstituted corannulenes selectively. A curious reaction between ICl and **1** gave **46** in roughly 50% yield [34, 49]. At that time, the cross-coupling reactions of aryl chlorides with various reagents were much more difficult than the corresponding bromides. Thus, synthesis of 1,3,5,7,9-pentasubstituted corannulenes from **46** presented several major challenges, among them overcoming the sparing solubility, activating the chloride for substitution, and completing the reaction five times on each molecule. Developing effective synthetic methods for coupling reactions with **46** was an accomplishment on a par with the most difficult substrates. Despite the expected low yields and poor reactivity, several solutions to this problem have been found [70, 82–94].

Very recently, 1,3,5,7,9-pentakis(Bpin)corannulene (**47**) was successfully prepared in Scott's laboratory (Scheme 12) [82]. In the presence of catalytic amounts of $[Ir(OMe)COD]_2$ and 4,4′-dimethylbipyridyl, the reaction of corannulene with bis

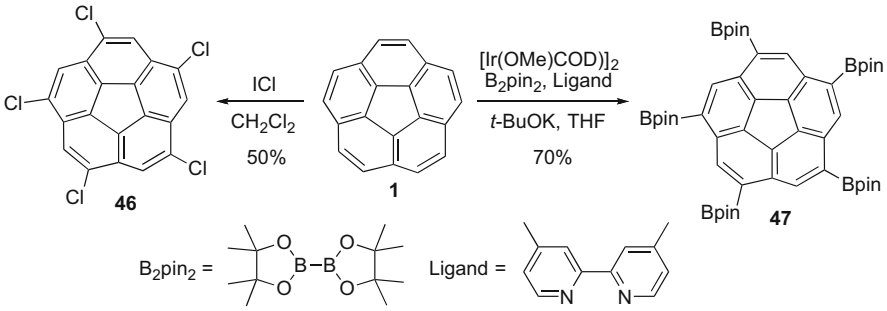


**Scheme 12** Synthesis of pentasubstituted corannulenes directly form corannulene [34, 49, 82]

(4,4,5,5-tetramethyl-1,3,2-dioxaborolan-2-yl)diborane ($B_2pin_2$) gave **47**, which can easily be separated from the two accompanying tetrasubstituted products. The selective formation of 1,3,5,7,9-pentakis(Bpin)corannulene (**47**) in the polyborylation conditions is caused by low steric repulsion between any two Bpin substituents, which does not violate the *ortho*/*peri*-prohibition, and the slow substituent redistribution process with the operation of a de-borylation/re-borylation. Compound **47** is a new precursor for synthesis of highly substituted corannulenes through further functionalization.

Siegel and coworkers were the first to study systematically transformations of pentachlorocorannulene **46** [83]. Pentaalkylcorannulenes **45** and pentaarylcorannulenes **50** were accessible by Ni-catalyzed cross-coupling reactions of **46** with organoaluminum and arylzinc reagents, respectively (Scheme 13). More recently, iron-catalyzed Kumada coupling also gave pentaalkylcorannulene derivatives **45** [84]. 1,3,5,7,9-Pentakis(trimethylsilylethynyl)corannulene **49** (R=$SiMe_3$) [83] was prepared from the cross-coupling of pentachloride **46** with a large excess of trimethylsilylethyne (ca. 50 equiv.) by using Eberhard's method [85] with a pincer catalyst at high temperature (ca. 165°C). At that time, the product was obtained in low yield. Later on, a modification of Nolan's procedure (Pd catalyst, ligand IPr) [86] developed by the same group made these reactions more efficient [39]. Pentaethynylcorannulenes **49** were obtained in 45–93% yields by the Stille coupling reaction of **46** with trimethylalkynylstannanes (eight examples) [39]. Reaction of **49** with tetracyanoethene (TCNE) yielded an electron-poor corannulene with five cyanobuta-1,3-dienyl branches [87]. Using the Nolan's procedure, the yields of pentaarylcorannulenes **50** were also improved, even with sterically congested manisyl moieties, and the products were obtained in up to 35% yield [70]. Moreover, the cross-coupling of **46** with less sterically congested arylboronic acids using Nolan's protocols [86] or Fu's catalytic system [Pd(*t*-Bu)$_3$, CsF] [88] allow a variety of functionalized pentaarylcorannulenes **50** [89, 90]. Direct nucleophilic substitution of **46** with nucleophiles makes it possible to produce **48**. The treatment of **46** with sodium arylthiolates gave 1,3,5,7,9-pentakis(arylthio)corannulene derivatives **48** (XR=SAr) [83, 91]. Formation of pentakis(diethylene glycol methyl ether)corannulene **48** (XR=O($C_2H_4O$)OMe) by

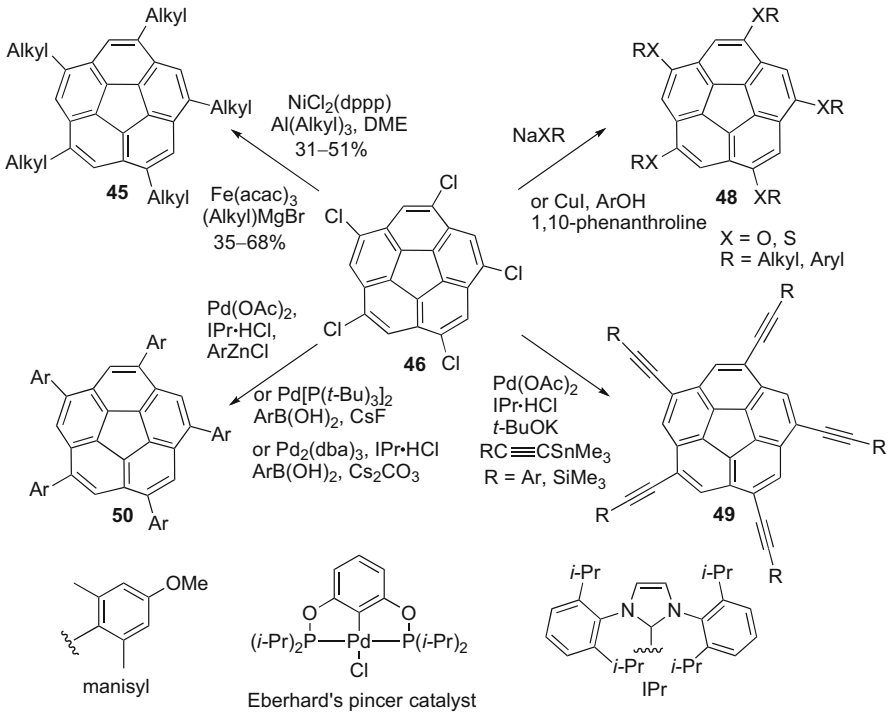


**Scheme 13** Synthesis of pentasubstituted corannulene derivatives from pentachlorocorannulene [39, 70, 83, 89–91, 93, 94]

the reaction of **46** with various sodium alkoxides required high temperature (180 °C) [83]. The reaction mechanism should be via a Meisenheimer complex [92] rather than an aryne intermediate. Recently, pentaalkoxycorannulenes [93] and pentaaryloxycorannulenes [94] were efficiently achieved by the Cu(I)-catalyzed Ullmann condensation reaction of **46** with aliphatic alcohols and substituted phenols, respectively. For the synthesis of pentaalkoxycorannulenes, a large excess of base (ca. 30 equiv.) was required to complete the substitutions.

Reactions of *sym*-penta(3-butynyl)corannulene **45** (alkyl=3-butynyl) with azides can generate triazole derivatives under the catalysis of Cu complexes. These interesting compounds provide potential applications in bioconjugated chemistry [95] and organic materials, which display liquid-crystalline behavior and organogelation properties [96].

Very recently, pentaalkylcorannulene derivatives were used as initiators to generate corannulene-core polymers by expansion of five pendant groups (Scheme 14) [97]. The first initiator **45**-PrOH was prepared by the Fe-catalyzed Kumada coupling of **46** with (3-((triisopropylsilyl)oxy)propyl)magnesium bromide, as presented in Scheme 13, and subsequent desilylation. The second initiator **45**-PrE was obtained by the reaction of **45**-PrOH with α-bromoisobutyryl bromide.

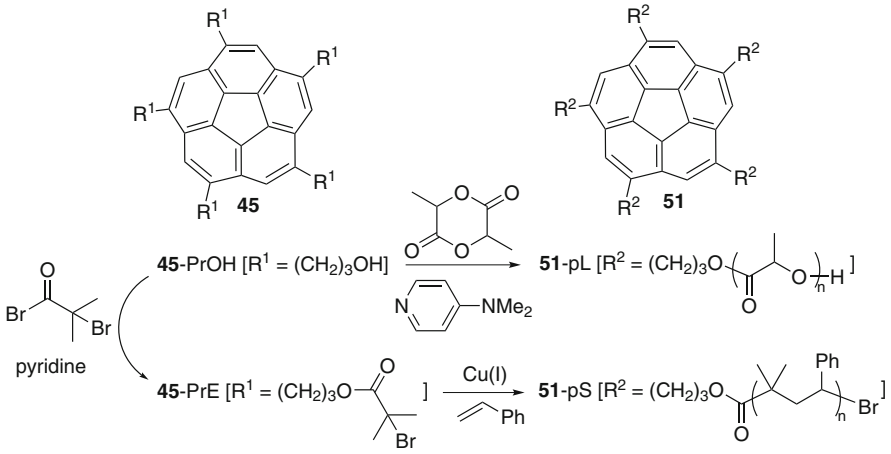


**Scheme 14** Synthesis of corannulene-core polymers **51** [97]

The initiators **45**-PrOH and **45**-PrE were then used to polymerize cyclic ester and styrenic monomers to give poly(lactide)s **51**-pL and polystyrene **51**-pS, respectively. Both polymerizations were observed under reasonable control over the molecular weight and chemical nature of the arms. Preliminary results demonstrated that these polymers are capable of forming a host–guest complex with $C_{60}$.

Balister conditions, using sulfonyl chloride, aluminum chloride, and sulfur dichloride, produced a sparingly soluble decachlorocorannulene **52** [34, 49], which should be generated via the intermediate **53** by loss of two chlorine molecules [98] (Scheme 15). In contrast to these confirmed perchlorinations of corannulene, Huang et al. reported a compound, isolated from electrical discharge in liquid chloroform, which they asserted to be **52** [99]; however, that product differs greatly in solubility, does not show the same NMR as authentic **52**, and has never been used to form authenticated decasubstituted products of corannulene. Therefore, the structure of the compound synthesized by the electrical discharge protocol is highly unlikely to be **52** and a proper structure determination is needed [71].

Several corannulene derivatives were obtained by metal-catalyzed coupling reaction of decachlorocorannulene (**52**). Decamethylcorannulene **54** was synthesized in 30% yield by methylations of **52** in the presence of $NiCl_2$(dppp) and trimethylaluminum [62]. Palladium-catalyzed cross-coupling reaction of **52** with an excess of stannylpentyne directly furnished **55** (ca. 10% yield), accompanied by an unexpected product **56** (ca. 18% yield). Structures of both compounds were verified by X-ray crystallography [73]. Apparently, **56** should be generated from **55** by the Bergman-type cyclization and subsequent cleavage of the rim bond.

Compared to metal-catalyzed functionalization of **52**, decaaryl-substituted corannulenes **57** were prepared by repetitive palladium-catalyzed arylation of corannulene with arylboroxin through C–H activation (Scheme 15) [74]. It was

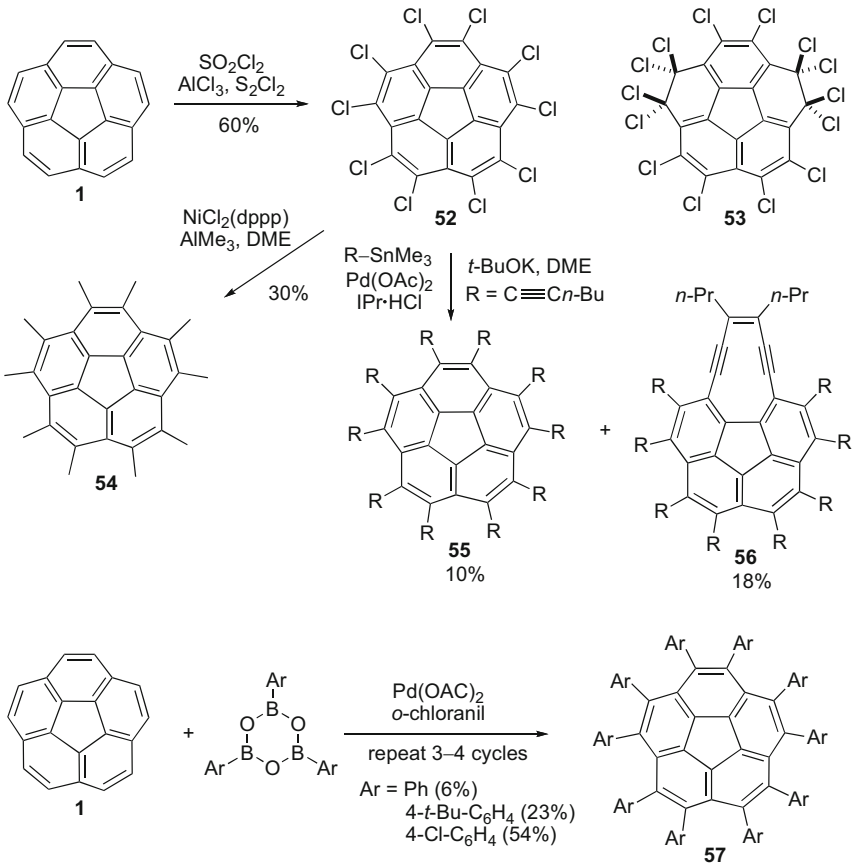


**Scheme 15** Synthesis of decasubstituted corannulene derivatives [34, 49, 62, 71, 74, 98, 99]

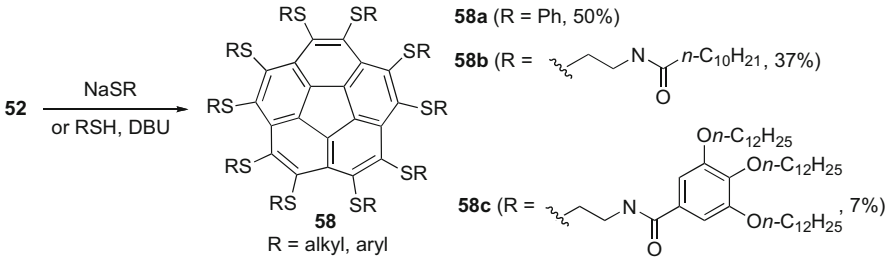


**Scheme 16** Synthesis of decakis(1-thio)corannulenes **58** [75, 100, 101]

observed that the arylation was not stopped at decaphenylcorannulene **57** (Ar=Ph) when phenylboroxin was employed, whereas (4-*tert*-butylphenyl)boroxin and (4-chlorophenyl)boroxin prevent the overarylation and allow decakis(4-*tert*-

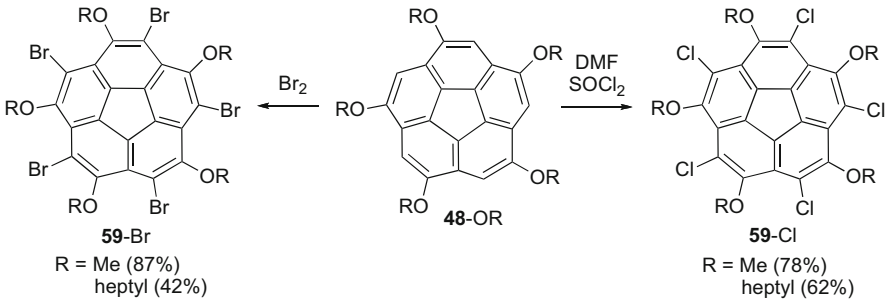


**Scheme 17** Synthesis of deca-heterosubstituted corannulenes **59** [93]

butylphenyl)corannulene and decakis(4-chlorophenyl)corannulene to be obtained in ca. 23% and 54% yields, respectively.

Reaction of decachlorocorannulene (**52**) with a variety of S-nucleophiles is a general protocol for synthesis of per(1-thio)-substituted corannulenes **58** (Scheme 16). Scott et al. efficiently prepared various decakis(1-alkylthio) corannulenes **58** by treating **52** with the corresponding sodium thiolates at room temperature [100]. Similarly, decakis(phenylthio)corannulene (**58a**) was obtained in 50% yield [75]. For the synthesis of **58b** and **58c**, the thiol species of the corresponding paraffinic components were ionized in situ by using DBU for the reaction with decachlorocorannulene (**52**). Corannulene derivatives **58b** and **58c** were found to form a liquid crystalline assembly [101].

Decasubstituted corannulenes can also be generated by functionalization of pentasubstituted corannulenes. The alkoxy groups on **48** increase electron density on corannulene to offer opportunities for halogenation to produce decahetero-substituted corannulenes **59** with two different substituents under mild conditions (Scheme 17). The treatment of pentaalkoxycorannulenes **48** with excess $Br_2$ or excess thionyl chloride afforded **59**-Br and **59**-Cl, respectively [93].

### 2.2.2 Structures and Properties of Highly Substituted Corannulenes

The structures and properties of highly substituted corannulenes strongly depend on the number and type of substituents. In the subclass of alkyl-substituted corannulenes, decamethylcorannulene (**54**) is much shallower than pentamethyl-corannulene **45**-Me (Table 1). The calculated $\Delta G^{\ddagger}_{inv}$ and bowl depth for **54** are only 2.2 kcal/mol and 0.58 Å, respectively [62]. Similarly, decakis(phenylthio)-corannulene (**58a**, 0.49 Å) [75] is flatter than pentakis(phenylthio)corannulene **48** (XR=SPh), which contains two different molecules to have the bowl depths 0.87 Å and 0.91 Å depending on orientations of the thiophenyl substituents (Siegel et al., unpublished results). Due to the fact that five phenylthio substituents are each oriented above and below the rim in **58a**, its inversion dynamics are complex. Moreover, the addition of bulky groups to the corannulene core also flattens the bowl. For example, the bowl depth of 1,3,5,7,9-penta(*tert*-butyl)corannulene

**Table 2** Photophysical properties of multiethynyl substituted corannulene derivatives[a] [39]

| Compound | Absorption $\lambda_a$ (nm) | Emission $\lambda_f$ (nm) | Quantum yield ($\Phi_f$) |
|---|---|---|---|
| **1** | 320 | 423 | 0.03 |
| **30** (R=Ph) | 400, 363−345 | 434, 415 | 0.20 |
| **44** (R=Ph) | 425, 378−359, 320 | 469, 446 | 0.75 |
| **41** (R=Ph) | 450, 400, 356, 305 | 500, 473 | 0.83 |
| **41** [R=3,4,5-$C_6H_2(OC_{12}H_{25})_3$] | 370 | 529 | 0.67 |
| **41** (R=$SiMe_3$) | 331 | 475, 449 | 0.17 |
| **49** (R=Ph) | 358, 324 | 485, 465 | 0.12 |
| **49** [R=3,4,5-$C_6H_2(OC_{12}H_{25})_3$] | 376, 332 | 542 | 0.37 |
| **49** (R=$SiMe_3$) | 339, 303 | 468, 452 | 0.05 |

[a]Measured in DCM

(0.72 Å) [80] is smaller than that of 1,3,5,7,9-pentamethylcorannulene (0.85 Å). Although the structure of lowly soluble decachlorocorannulene (**52**) has not yet been analyzed by X-ray crystallography, its bowl depth was determined to be 0.51 Å by gas-phase electron diffraction study [72], and 0.49 Å obtained at B3LYP/cc-pVDZ [71]. The bowl depth of deca-substituted corannulenes $C_{20}R_{10}$ strongly depend on the substituents, their values following the order arylethynyl > methyl > Cl ≅ SPh > Ar.

It was observed that 1,3,5,7,9-pentamanisylcorannulene **50** (R=manisyl) has an unusually large bowl depth (0.91 Å) and barrier to bowl inversion (12.1 kcal/mol) [70]. The increase of these values may be ascribed to van der Waals attractive forces among the *endo* methyl groups in the conformational ground state.

Notably, the number of attached arylalkynyl pendant groups correlates with an increase in the bowl depth of the corrannulene nucleus; the bowl depth for the multi-ethynylcorannulenes follows the sequence: **49** > **41** > **44** based on the crystallographic analysis [39].

Photophysical properties of a series of ethynyl substituted corannulenes have been systematically studied (Table 2) and they are tunable by varying the number and the kind of ethynyl substituents [39]. Most multi-ethynylcorannulenes in solution display high-quantum-efficiency luminescence and variable emission wavelengths. In contrast to the parent compound corannulene (**1**), the bathochromatic effects on absorption and emission wavelengths and the fluorescence quantum yields ($\Phi_f$) for the phenylethynyl-substituted series generally increase with the number of acetylene moieties. Pentakis(phenylethynyl)corannulene **49** (R=Ph) is the exception, and its low quantum yield can be explained by (1) the Ham effect [102], in which high symmetry leads to forbidden transitions between the ground and excited states, and (2) the deeper bowl depth, which causes the structure to deviate from planarity [103]. Moreover, arylethynyl substituents cause a greater red shift and higher quantum yield than (trimethylsilyl)-ethynyl groups. Additional electron-rich moieties on arylethynyl, such as 3,4,5-tridodecoxyphenyl, also strongly affect photophysical properties.

**Table 3** Reduction potentials of corannulene measured by cyclic voltammetry[a]

| Compound | Electrolyte/solvent | Reduction potential (V, vs ferronce) | References |
|---|---|---|---|
| **1** | TBAH/MeCN | −2.33, −2.95 | [34] |
| **1** | TBAH/MeCN (298 K) | −2.32, −3.03 | [78] |
| **1** | TBAP/MeCN | −2.31 | [81] |
| **1** | TMAB/DMF (213 K) | −2.30, −2.84, −3.43 | [78] |
| **15** | TBAH/MeCN | −2.34, −3.05 | [78] |
| **23c** | TBAH/THF | −1.66 | [41] |
| **23d** | TBAH/THF | −1.48 | [40] |
| **28**-F | TBAH/THF | −2.38 | [40] |
| **28**-Cl | TBAH/THF | −2.34 | [40] |
| **33** | TBAH/MeCN | −2.41, −3.01 | [34] |
| **43** | TBAH/MeCN | −2.43, −2.97 | [34] |
| **45**-Me | TBAH/MeCN | −2.49, −3.04 | [34] |
| **45**-$CF_3$ | TBAP/MeCN | −1.36 | [81] |
| **54** | TBAH/DMF | −2.58, >−3.11 | [34] |

[a]*TBAH* tetrabutylammonium hexafluorophosphate; *TBAP* tetrabutylammonium perchlorate; *TMAB* tetramethylammonium tetrafluoroborate. In comparisons of reduction potentials, the following conversion factors are used: $E(FeCp_2^+/FeCp_2)=E(NHE) - 0.665=E(SCE) - 0.424=E(Ag/AgNO_3) - 0.105$

The reduction potentials of corannulene and its derivatives are strongly affected by the kind and number of the substituents (Table 3). The methyl group is a weak electron-donating substituent. The addition of methyl groups to the corannulene nucleus shifted the reduction potentials to be more negative, especially decamethylcorannulene **54**-Me [34, 77]. The halogen substituent in monohalocorannulenes, such as **28**-F and **28**-Cl, does not change the reduction potential of corannulene significantly. Strong electron-withdrawing substituents, trifluoromethyl groups, cause the reduction potential of trifluoromethyl-substituted corannulene derivatives to make a large positive shift, compared to **1** [40, 41, 81]. Pentakis(trifluoromethyl)corannulene (**45**-$CF_3$) is a representative example.

Synthesis of a series of multi(phenylthio)corannulenes via direct nucleophilic substitution of corresponding halocorannulenes using sodium hydride as a base and thiophenol as the pro-nucleophile enabled a systematic study of their optoelectric properties as a function of substituent number and placement (Siegel et al., unpublished results). A linear dependence of the first reduction potential and the photophysical properties on the number of substituents was observed (Table 4). The first reduction potential measured by the cyclic voltammetry suggests an additivity factor of +0.10 V per phenylthio group on corannulene. Moreover, the bathochromic shift observed for the longest wavelength absorption $\lambda_{l,a}$ increases with rising substitution around the rim of **1**, with an additivity factor of ca. 10–15 nm per phenylthio group.

**Table 4** Selected physical properties of multi(phenylthio)corannulenes (Siegel et al., unpublished results)

| Compound | **1** | **60** | **61** | **62** | **63** | **48** (XR=SPh) | **58a** |
|---|---|---|---|---|---|---|---|
| 1st $Red_{CV}$ [V][a] | −2.45 | −2.43 | −2.09 | −2.28 | −1.95 | −1.58 | −1.49 |
| $\lambda_{l,a}$ (nm)[b] | 286 | 292 | 295 | 302 | 310 | 344 | 417 |
| $\lambda_{max,f}$ (nm)[b] | 422 | 448 | 456 | 460 | 496 | 492 | |

[a]Measured in THF
[b]Measured in acetonitrile

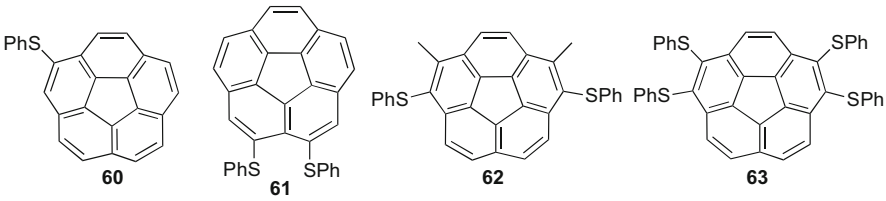


As described above, stable neutral buckybowl radicals **39** and **40** arise from hanging relatively stable radical bearing fragments onto corannulene. Charged *o*-semiquinone radical salts are not generally stable; however, the pronounced stabilization effect arising from highly *tert*-butyl substituted corannulene allowed the isolation of *o*-semiquinone radical salt **64**, which exists for a long time in an oxygen-free solution and the solid state under a nitrogen atmosphere. Negative charge densities are delocalized at both of the oxygen atoms and over the whole curved π network [104]. The sum of the absolute spin density on the corannulene skeleton of **64** (0.880) is larger than that of **39** (0.241) and **40** (0.553). In addition, the corannulyl backbone provides a suitable bridge for a strong intramolecular exchange interaction between two radical moieties. Corannulene-based neutral diradical **65** shows very strong intramolecular antiferromagnetic interaction through the corannulenyl backbone in the crystalline state, and has a singlet ground state and a thermally accessible excited triplet state [105].

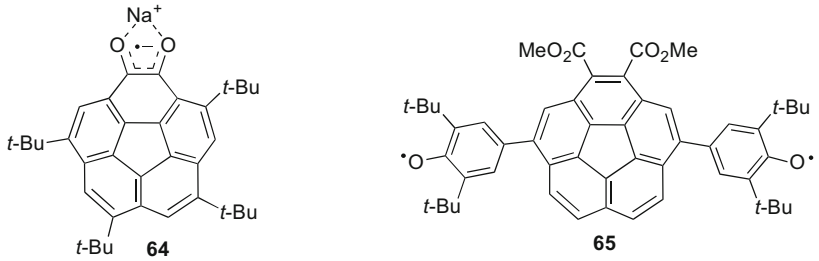

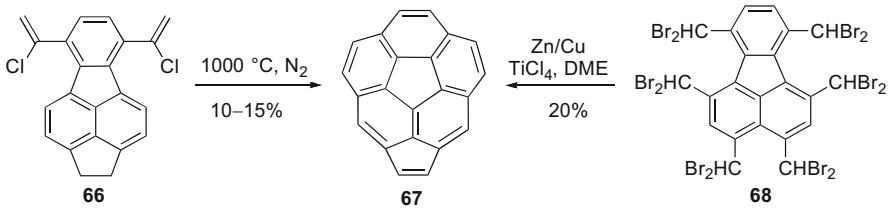


**Scheme 18** Synthesis of cyclopentacorannulene (**67**) [34, 106]

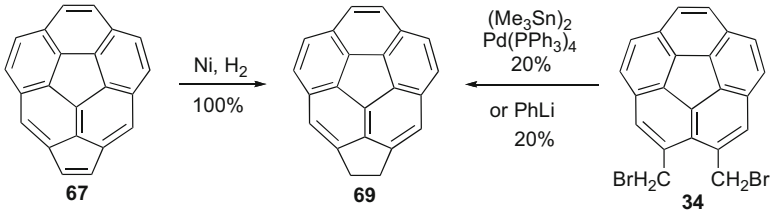


**Scheme 19** Synthesis of acecorannulene (**69**) [57, 62, 106]

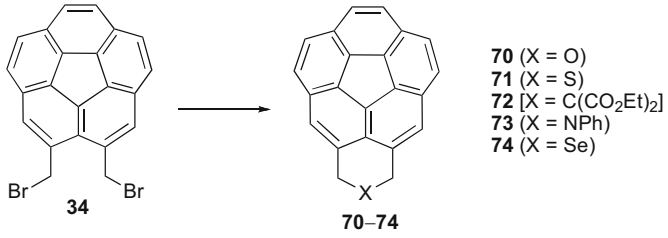


**Scheme 20** *peri*-Annelated corannulenes (heterocycles) [57]

## 2.3 *Cyclopentacorannulene, Acecorannulene and Annelated Corannulenes*

### 2.3.1 Synthesis

Cyclopentacorannulene (**67**) was obtained as a mixture with corannulene (in ratio 7:3) in 10–15% yield from dichloride **66** by flash vacuum pyrolysis at 1,000 °C (Scheme 18) [106]. In contrast, **67** could also be prepared, in 20% yield, by titanium-mediated carbenoid couplings of **68** in solution phase [34].

Acecorannulene (**69**) was generated in excellent yield from cyclopentacorannulene (**67**) by nickel-catalyzed hydrogenation (Scheme 19) [106]. Alternatively, **69** was also synthesized in the solution phase from dibromide **34** by either Pd-catalyzed Stille-type coupling [62] or by treatment with phenyllithium [57].

Various (heterocyclic) six-membered *peri*-annelated corannulenes **70–74** were accessed by the reaction of divalent nucleophiles with 2,3-bis(bromomethyl)-

**Table 5** The inversion barrier (kcal/mol) and the bowl depth (Å) of *peri*-annelated corannulenes

| | Exptl. | RHF/cc-pVDZ | | B3LYP/cc-pVDZ | | |
|---|---|---|---|---|---|---|
| Compound | $\Delta G^{\ddagger}_{inv}$ | $\Delta G^{\ddagger}_{inv}$ | Bowl depth | $\Delta G^{\ddagger}_{inv}$ | Bowl depth | References |
| **67** | – | 29.2 | 1.05 | 27.7 | 1.08 | [57] |
| **69** | 27.6[a] | 26.6 | 1.04 | 25.6 | 1.07 | [57, 61] |
| **70** | 17.3 | 14.8 | 0.91 | 14.7 | 0.95 | [57] |
| **71** | 13.9 | 12.1 | 0.86 | 11.8 | 0.90 | [57] |
| **72** | 15.5 | – | – | – | | [57] |
| **73** | 16.1 | 14.3 | 0.90 | 13.9 | 0.94 | [57] |
| **74** | 13.0 | – | – | – | | [57] |

[a]Determination from $[D_2]$-**69**

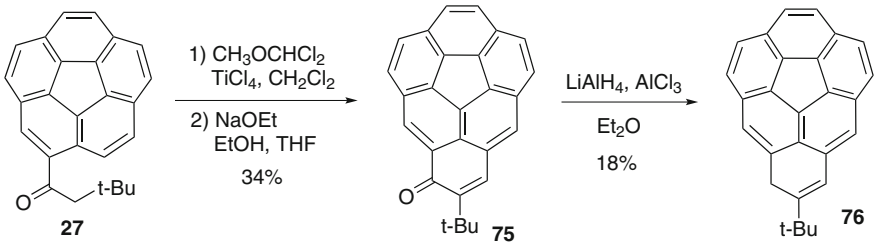


**Scheme 21** Synthesis of phenalene **76** [47]

corannulene (**34**) (Scheme 20) [57]. These compounds provide suitable models for systematically studying the influences of substituents and ring size on the inversion dynamics (Table 5).

Phenalene derivative **76** was synthesized from **1** in four steps (Scheme 21) [47]. Ketone **27**, which was generated in 99% yield by Friedel–Crafts acylation of **1** as shown in Scheme 7, underwent the *peri*-formylation and the subsequent intramolecular aldol condensation to give phenalenone derivative **75**. The treatment of **75** with a mixture of $LiAlH_4$ and $AlCl_3$ afforded **76**. It was observed that compound **76** is not stable in air because it generates **75** under aerobic conditions. In contrast, the anion $Li^{+}\cdot\mathbf{76}^{-}$, which was prepared by the treatment of **76** with an equimolar amount of *n*-BuLi, is highly stable in a degassed solution. The inversion barriers of **76** and its derivatives were systematically investigated based on computational analysis. The distribution of the negative charge on anionic **76** causes it to be flatter and easier to invert than the neutral. For example, the neutral radical species has a higher inversion barrier (12.6 kcal/mol) than that of the monoanion (11.3 kcal/mol).

Furan-fused corannulene **77** was efficiently prepared by a brief heating of **31** with 3,6-di(2-pyridyl)-1,2,4,5-tetrazine in chloroform (Scheme 22) [107]. Isocorannulenofuran **77** is a reactive diene for the Diels–Alder reaction (see Scheme 34) [108]. Difuran-fused corannulene **79** can be generated from *syn*/*anti*-**78**, which is prepared by treatment of a solution tetrabromocorannulene **18** in THF with *tert*-butyl

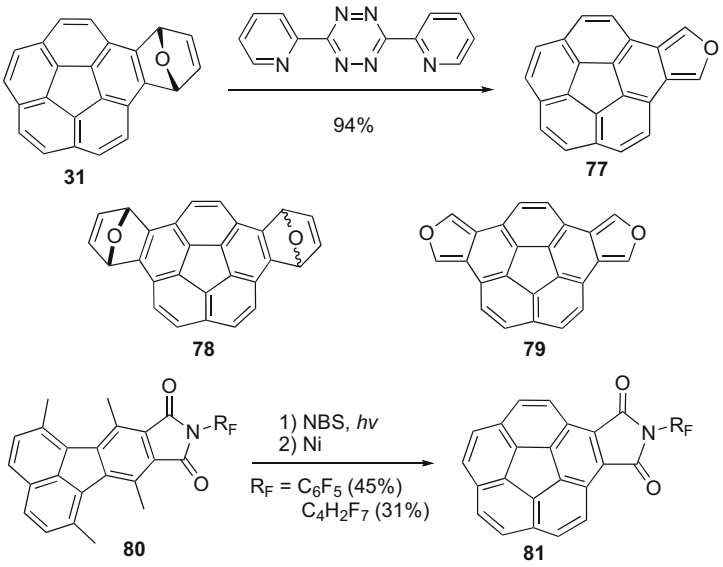


**Scheme 22** Synthesis of isocorannulenofuran **77** and imide-fused corannulenes **81** [107, 109, 110]

lithium [109]. Tetrabromocorannulene **18** is a corannuldiyne equivalent. The remaining two alkenyl moieties in **78** provide the possibility for the further Diels–Alder reaction with tetracyclone or **77**. Electron-poor N-substituted imide-fused corannulenes **81** were synthesized from fluoranthenes **80** by Method D in Scheme 6 [110].

Fluorine-containing annulated corannulenes **82** and **83** were synthesized by the reaction of corannulene with a large excess of 1,4-$C_4F_8I_2$ at 300°C, and the former as the major product was obtained in 15% yield [111]. Based on X-ray crystallography, the bowl depth of the corannulene core in **82** is around 0.78 Å, which is smaller than that of corannulene. Experimental results and theoretical studies indicated that **82** is a stronger electron acceptor than $C_{60}$.

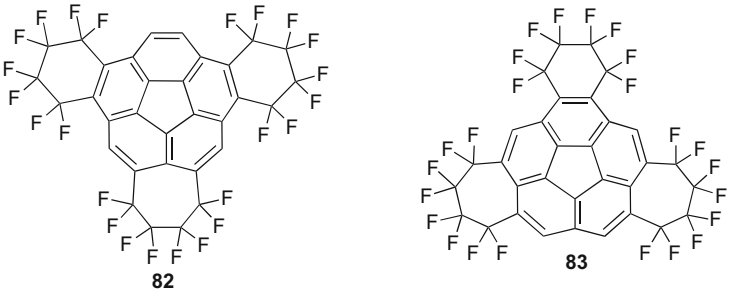

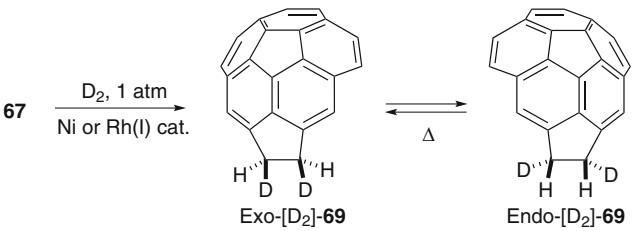


**Scheme 23** Synthesis of *exo*-dideuteriocyclopentacorannulene (*exo*-[$D_2$]-**69**) [61]

### 2.3.2 Structures and Properties of Annulated Corannulenes

Annulation of a five-membered ring to the rim of the corannulene framework significantly increases the curvature and rigidity of the system. Based on the crystallographic analysis, both the bowl depth (ca. 1.05 Å) [112] and the POAV pyramidalization angles (10.7°, 9.7°, and 9.0°) for the hub ring in **67** are larger than those for the parent compound **1**.

Computational studies of the bowl-to-bowl inversion barrier ($\Delta G^{\ddagger}_{inv}$) for **67** and **69** predict values of 27.7–30.9 and 25.6–28.9 kcal/mol, respectively (Table 5) [57, 113]. These results are consistent with the fact that **69** has less bowl strain and is shallower than **67**. Heterogeneous or homogeneous deuterogenation of **67** gave *exo*-dideuteriocyclopentacorannulene (*exo*-[$D_2$]-**69**) with the *exo* specificity (Scheme 23) [61]. The value of $\Delta G^{\ddagger}_{inv}$ for *exo*-[$D_2$]-**69** was determined to be ca. 27.6 kcal/mol based on the proton NMR studies.

The inversion barrier of (heterocyclic) *peri*-annelated corannulenes depends on the bridging groups. The methylene carbon–heteroatom bond length shortens along the series Se > S > C > N > O and the ring size contracts. This strained annelation leads to a slight increase in bowl depth, but, due to the high sensitivity of inversion barrier to bowl depth, there is a significant increase of $\Delta G^{\ddagger}_{inv}$. Therefore, $\Delta G^{\ddagger}_{inv}$ for the heterocyclic *peri*-annelated corannulenes follows the order: **70** > **73** > **72** > **71** > **74** (Table 5) [57]. The nitrogen-substituted series **73** was studied in greater detail [114]. *N*-Phenyl and *N*-butyl substituted 2,3-dihydro-1*H*-corannuleno[2,3-*cd*]pyridines display a value of $\Delta G^{\ddagger}_{inv}$ of about 16.5 kcal/mol, slightly higher than that of the NH derivative (16.1 kcal/mol).

## 2.4 *Benzocorannulene Family*

### 2.4.1 Synthesis

FVP synthesis of benzo[*a*]corannulene **85** was conducted with benzofluoranthene **84** [115] or [4]helicene precursor **86** [116] (Scheme 24). The former protocol is similar to the synthesis of corannulene (**1**) from fluoranthene **10** (Scheme 2). In the reaction with **86**, the reaction mechanism should involve a radical cascade

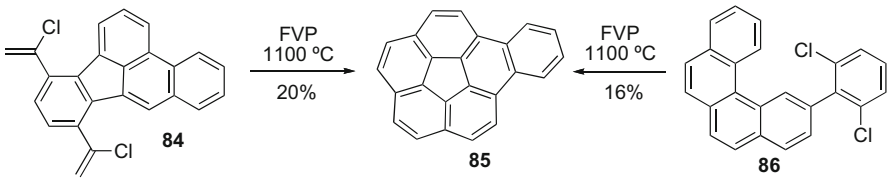


**Scheme 24** Synthesis of benzocorannulene **85** [54, 115, 116]

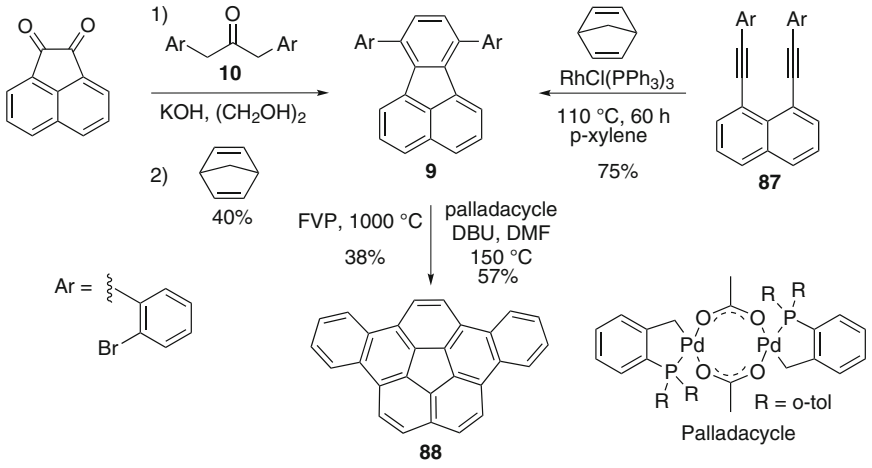


**Scheme 25** Synthesis of dibenzo[*a*,*g*]corannulene (**88**) [16, 117, 118]

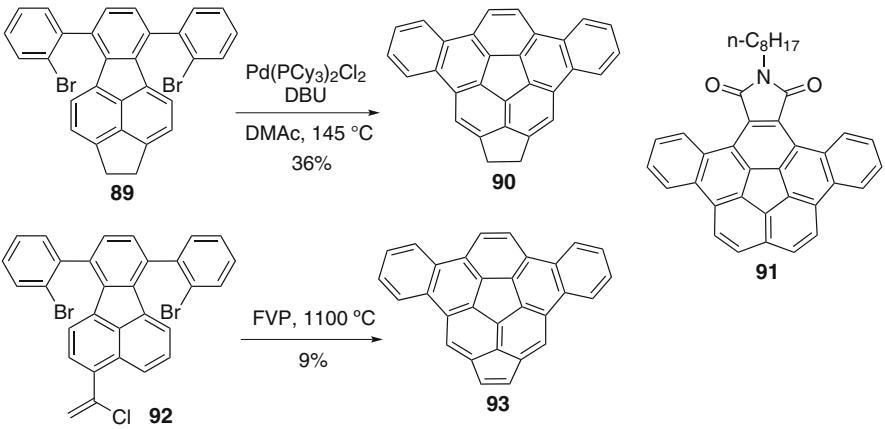


**Scheme 26** Synthesis of buckybowls **90** and **93** [119, 121]

cyclization and an aryl radical is generated by loss of a chlorine atom. Benzocorannulene **85** has also been prepared in the solution phase. Refluxing with $Fe_2(CO)_9$ in benzene, **31** was converted quantitatively to benzocorannulene **85** by cleavage of the 'endoxode' bridge [54].

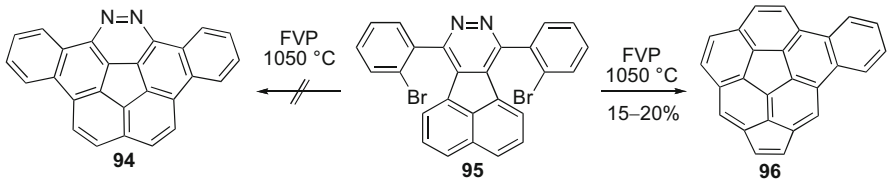


**Scheme 27** Synthesis of benzo[*g*]acecorannulene (**91**) [122]

Dibenzo[*a*,*g*]corannulene (**88**) was prepared from fluoranthene **9** under FVP conditions at 1,000 °C (Scheme 25) [117]. Compound **88** was also accessed from the same material by Pd-catalyzed intramolecular arylations [16]. In that report, Scott and coworkers tested various palladium catalysts, bases, and reaction conditions, and the best result (57% yield) was obtained under conditions employing the combination of palladacycle/DBU/DMF at 150 °C. A synthetic method has been reported to prepare 7,10-disubstituted fluoranthenes, including **9**, in good to excellent yields by Rh-catalyzed [(2+2)+2] cycloadditions of 1,8-di(ethynyl) naphthalenes **87** with NBD [118].

Similar to dibenzo[*a*,*g*]corannulene (**88**), 1,2-dihydrocyclopenta[*b*,*c*]dibenzo-[*g*,*m*]corannulene (**90**) [119] and *N*-octyldibenzo[*d*,*m*]-1,2-corannulimide (**91**) [120] were synthesized by Pd-catalyzed cyclization (Scheme 26). The OFET devices of **91** show interesting electron and hole motilities, and may have potential applications in organic electronic devices. Dibenz[*f*,*l*]acecorannulene (**93**) [121] can be directly prepared from **92** under FVP conditions.

Benzo[*g*]acecorannulene (**96**) is an unexpected product generated from **95**. According to the successful synthesis of dibenzo[*a*,*g*]corannulene (**88**) from 7,10-bis(2-bromophenyl)fluoranthene (**9**), an attempt was made to prepare *aza*-bowl **94** from **95**. However, this protocol gave **96** as the only identifiable product (Scheme 27) [122].

### 2.4.2 Structures and Properties

On the basis of crystallographic analysis, the corannulene cores in dibenzo[*a*,*g*]-corannulene (**88**) and *N*-octyldibenzo[*d*,*m*]-1,2-corannulimide (**91**) are shallow with a bowl depth of 0.83 and 0.65 Å, respectively [120, 123]. The cyclopenta-annulated buckybowl **90** is much deeper, and its bowl depth was determined as 1.03 Å. The maximum POAV pyramidalization angle of **90** was found to be 10.7°, which is very close to that of acecorannulene (**69**) [119]. However, the bowl inversion barrier for **90** was experimentally estimated as 23.5–23.6 kcal/mol, which is much smaller than that of acecorannulene (**69**, 27.6 kcal/mol).

Dibenzo[*a*,*g*]corannulene (**88**) and fullerenes $C_{60}$ and $C_{70}$ form cocrystals [**88**·$C_{60}$] and [(**88**)$_2$·$C_{70}$], respectively [123]. The bowl depth of the corannulene moiety in dibenzocorannulene are slightly deceased upon co-crystallization, and the

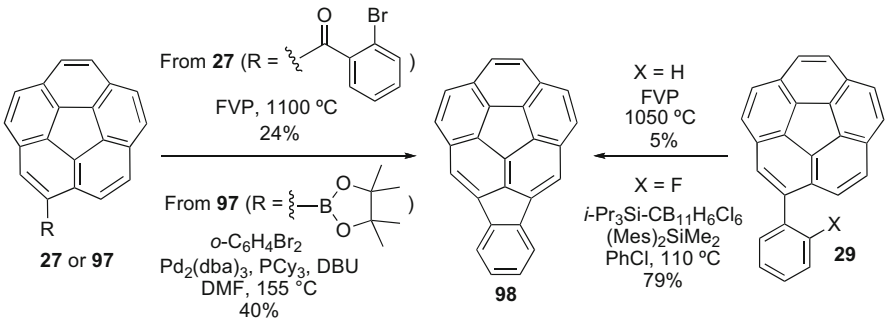


**Scheme 28** Synthesis of indenocorannulene **98** [48, 124–126]

values for [**88**·$C_{60}$] and [(**88**)$_2$·$C_{70}$] are determined to be 0.80 and 0.79 Å, respectively.

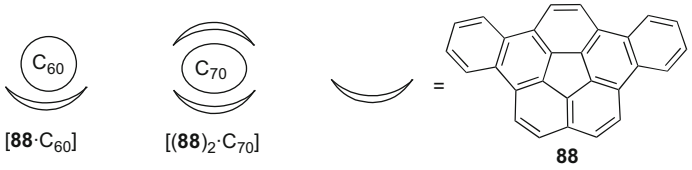


## *2.5 Indenocorannulene Family*

### 2.5.1 Synthesis

The FVP synthesis of indenocorannulene (**98**) was conducted with phenylcorannulene (**29**) [124] or 2-bromobenzoylcorannulene (**27**) [48] (Scheme 28). The cyclization of 2-bromobenzoylcorannulene (**27**) is more efficient than that of **29**. Compound **27** undergoes radical-type cyclization and subsequent decarbonylation to furnish **98**. In solution-phase synthesis, indeno[1,2,3]annelation of PAHs by a Suzuki-Heck-Type coupling cascade provided the extension of an aryl functional group with a junction of a five-membered ring in a single synthetic step [125].

In contrast to the FVP synthesis of indenocorannulene (**98**) from phenylcorannulene, the fluoro-substituted analogue **29** (X=F) turns out to be very efficient [126] (Scheme 28). Catalytic cyclization is initiated by reaction of a silyl cation with an aryl fluoride to generate a phenyl cation and, subsequently, Friedel–Crafts reaction to an intramolecular aryl coupling, flowed by deprotonation, to give **98**. The enabling feature of this reaction is the exchange of carbon–fluorine for silicon–fluorine bond enthalpies.

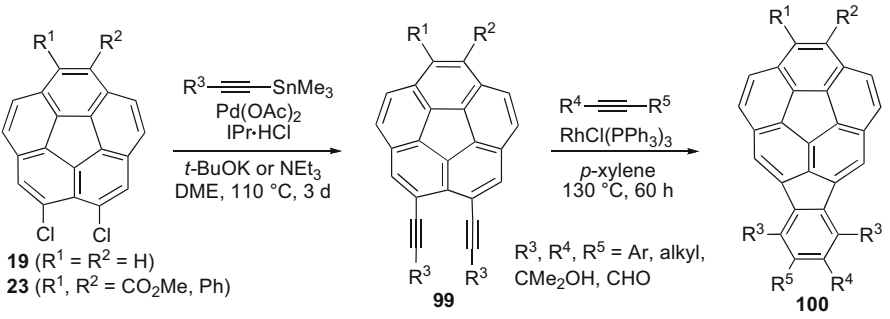


**Scheme 29** Preparation of highly substituted indenocorannulenes **100** [27]

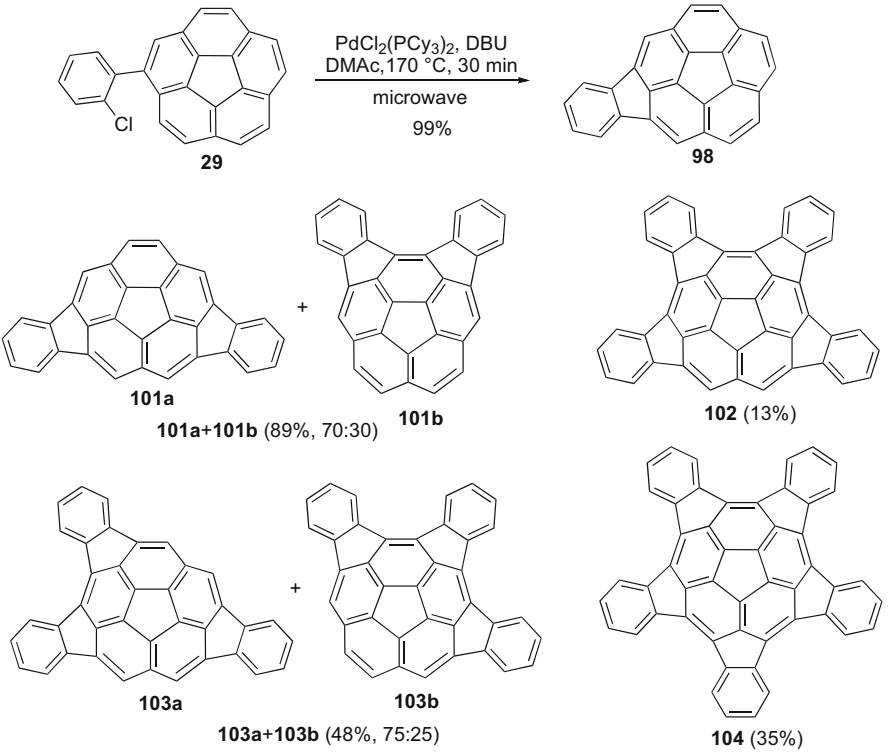


**Scheme 30** Synthesis of multi-indenocorannulenes [89, 128]

A rhodium-catalyzed protocol of alkyne cyclooligomerization provides an alternative route for the preparation of indenocorannulenes **100** [27] (Scheme 29). The key step of the synthesis starts with 2,3-diethynylcoranulenes **99**, which are accessed by Pd-catalyzed cross-coupling reactions of the corresponding 2,3-dichlorocorannulenes **19**/**23** with trimethyltin-substituted alkynes. The

**Table 6** POAV pyramidalization angles (deg) and bowl depths (Å) of indenocorannulene family[a]

| Compound | POAV[a] | Bowl depth | $\Delta G^{\ddagger}_{inv}$ (kcal/mol) | References |
|---|---|---|---|---|
| **98** | 8.9, 9.8, 11.2 | 1.07 | 29.8 (calcd.) | [27, 128] |
| **100** | 8.8, 9.8, 10.8 | 1.04 | >24 | [27] |
| **101a** | 10.4, 10.9, 11.2 | 1.21 | – | [128] |
| **101b** | 8.9, 9.8, 11.8 | 1.16 | – | [128] |
| **103a** | 11.1, 11.5, 12.0 | 1.30 | – | [128] |
| **103b** | 10.3, 11.8, 12.4 | 1.27 | – | [128] |
| **102** | 11.4, 12.1, 12.5 | 1.38 | – | [89, 128] |
| **104** | 12.7 | 1.43 | – | [89, 128] |

[a]POAV pyramidalization angles at the interior five-membered ring carbon atoms of the indenocorannulenes, and the values obtained by averaging the POAV angles of symmetry-related carbon atoms

'benzo' ring in **100** is formed by a formal [(2+2)+2] cycloaddition of the diynyl moiety in **99** with an external alkyne (Vollhardt and coworkers used the strategy of alkyne cyclotrimerization to make polycyclic aromatic compounds; for details, see [127]). This synthetic approach allows a variety of functional groups to be regioselectively introduced.

Scott and coworkers improved the synthesis of indenocorannulene **98** by conducting Pd-catalyzed intramolecular arylation reaction of (2-chlorophenyl)-corannulene **29** under microwave-assisted conditions (Scheme 30) [128]. The efficient condition allows a simple formation of multi-indenocorannulenes. Tetrakis-(2-chlorophenyl)corannulene **42** and pentakis(2-chlorophenyl)corannulene **50** were prepared by the Suzuki couplings of the corresponding halocorannulenes with 2-chlorophenyl boronic acid [89], as shown in Schemes 10 and 13. Subsequently, Pd-catalyzed cyclization of **42** and **50** gave tertaindenocorannulene **102** and pentaindenocorannulene **104**, respectively. Diindenocorannulenes **101** and triindenocorannulenes **103** were generated from regioisomeric mixtures of dibromocorannulenes and tribromocorannulenes, but the pure form of these products can be obtained. It should be noted that pentaindenocorannulene **104** is a possible precursor to the $C_5v$ end-cap of single-walled, "armchair" [5,5]nanotube.

### 2.5.2 Structures and Properties

The solid-state structures of the indenocorannulenes have been systematically studied. In contrast to the parent compound **98** [128], the substituted indenocorannulene **100** ($R^1$=$R^2$=$R^4$=$R^5$=$CO_2Me$, $R^3$=Ph) [27] is slightly flattened, revealed by comparing their bowl depths and the POAV pyramidalization angles (Table 6). Each additional indenoannulation increases the bowl depth and the curvature. Pentaindenocorannulene (**104**) is determined to have deepest bowl depth (1.43 Å) and the highest POAV pyramidalization angle (12.7°) [89, 128]. This curvature is significantly more pyramidalized than $C_{60}$.

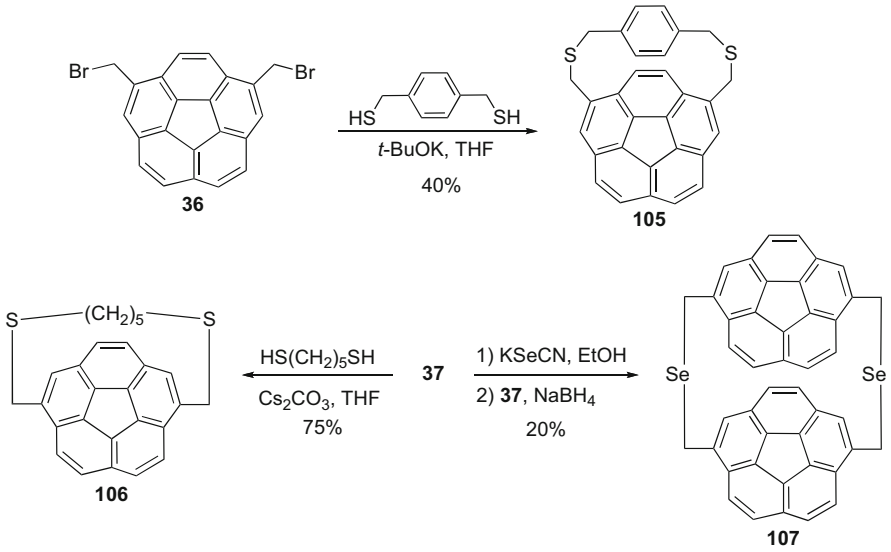


**Scheme 31** Synthesis of corannulene cyclophanes [32, 129]

## *2.6 Other Corannulene Derivatives*

### 2.6.1 Corannulene Cyclophane

Corannulene cyclophane **105** was prepared by treating **36** with a mixture of 1,4-bis (mercaptomethyl)benzene and potassium *tert*-butoxide (Scheme 31) [32]. Similarly, 1,5-pentadithiol/1,6-bis(bromomethyl)corannulene cyclophane (**106**) was prepared from **37** and 1,5-pentadithiol in 75% yield [129]. Synthesis of [3,3]seleno/1,6-dimethylcorannulene cyclophane (**107**), a cyclophane from two corannulenes, was not straightforward [129]. The key step is the in situ transformation of **37** to the bis(selenide anion), which reacts with the additional **37** to afford the seleno-bridged dimer **107**.

The bowl depths for **105** [32] and **106** [129] in the most stable form were determined to be 0.87 and 0.96 Å, respectively, based on theoretical analysis. The deep bowl depth of **106** is consistent with the experimental results showing that its solution structure indicates a very rigid conformation. Although no significant amount of strain is introduced by forming **105**, the molecule is conformationally restricted. The variable temperature proton NMR study sets the minimum limit for the barrier to benzene ring flip at $18 \pm 1$ kcal/mol. Thus, construction of the cyclophane effectively locks the structure into only one bowl form [129]. Two isomers – such as a head-to-tail form and a head-to-head form of **107** – are possible. The former is more stable than the latter by ca. 1.5 kcal/mol, and its calculated bowl depth is 0.86 Å, slightly flattened with respect to that of corannulene.

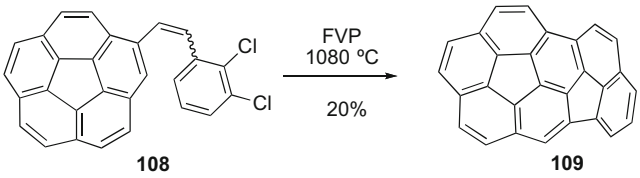


**Scheme 32** Synthesis of acenaphtho[1,2,3-*bcd*]corannulene (**109**) [48]

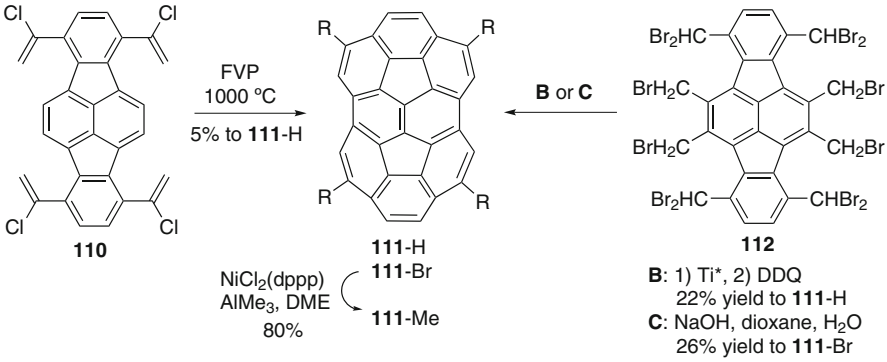


**Scheme 33** Synthesis of semibuckminsterfullerenes **111** [35, 130–132]

### 2.6.2 Acenaphtho[1,2,3-*bcd*]corannulene

The FVP synthesis of acenaphtho[1,2,3-*bcd*]corannulene (**109**) started with arylethenylcorannulene **108** (Scheme 32) [48]. A reaction mechanism was proposed in which the aryl radical, generated by chlorine atom loss one at a time, first closes a six-membered ring, and subsequently a five-membered ring, to yield **109**.

### 2.6.3 Semibuckminsterfullerene

Semibuckminsterfullerene (**111**) is a bowl-shaped polyarene comprising 50% of the $C_{60}$ skeleton. Similar to the synthesis of corannulene (**1**) shown in Scheme 2, Rabideau, Sygula, and co-workers subjected **110** to the cyclization under FVP conditions to prepare semibuckminsterfullerene (**111**-H) (Scheme 33) [130, 131]. A few years later the same group reported the solution-phase synthesis of semibuckminsterfullerenes **111**-H [35] and **111**-Br [132], which were easily accessed from dodecabromide **112** using the McMurry reaction and the carbenoid coupling, respectively. The four bromine substituents in **111**-Br were easily replaced by methyl groups to furnish tetramethyl derivative **111**-Me in good yield [132]. Based on crystallographic analysis, the highest POAV pyramidalization angle in **111**-Me was determined to be 11.6°, which is almost identical to buckminsterfullerene (11.64°).

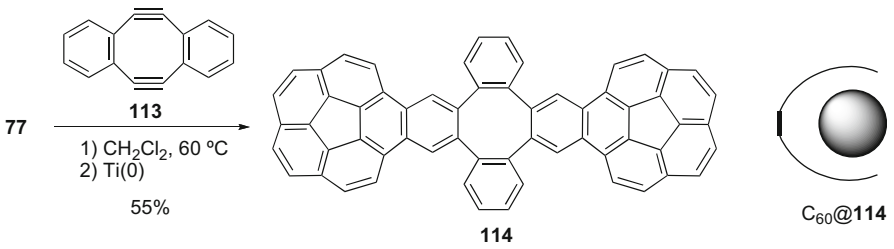


**Scheme 34** Synthesis of corannulene clip **114** [108]

### 2.6.4 Corannulene Clip

Two concave corannulene substituents fused to a tether make it possible to form a molecular catcher [108]. The designed molecule **114** was synthesized by the twofold Diels–Alder reactions of isocorannulenofuran **77** with dibenzocyclooctadiyne **113** and subsequently by deoxygenation with low-valent titanium (Scheme 34). Due to the non-planar shape of two corannulenyl moieties, **114** could have several conformations. A $^1$H NMR titration experiment indicated that buckycatcher **114** has a high binding affinity with $C_{60}$. The strong interaction between **114** and $C_{60}$ was also confirmed by the formation of crystals of inclusion complex $C_{60}$@**114**, which was generated from an approximately equimolar solution of both compounds in toluene. Based on X-ray crystallographic analysis, **114** in $C_{60}$@**114** acts as a molecular clip for the guest $C_{60}$.

## 2.7 *The Correlations Between Structures and Bowl-to-Bowl Inversion Barriers*

The correlations between structures and the bowl-to-bowl inversion barriers ($\Delta G^{\ddagger}_{inv}$) can be simply described as in Scheme 35 with a focus on bowl depth being directly related to the height of $\Delta G^{\ddagger}_{inv}$. Compounds of Class IA and Class IB (with a benzene ring fused to a rim of corannulene), where the bowl is shallower than that found for **1**, lead in general to a decrease of $\Delta G^{\ddagger}_{inv}$ relative to **1**. In contrast compounds of Class II lead in general to an increase of $\Delta G^{\ddagger}_{inv}$ relative to **1**. As the distance between two methylene groups in Class II decreases, the additional ring is more strained in the transition state to bowl inversion, which in part explains the observation that the value of $\Delta G^{\ddagger}_{inv}$ increases. Cyclopentacorannulene (**67**) and acecorannulene (**69**), with a direct connection between the *peri* carbon atoms, have the highest $\Delta G^{\ddagger}_{inv}$s within the simple annulated-corannulene family. The lower values of $\Delta G^{\ddagger}_{inv}$ for 1,2-dihydrocyclopenta[*b*,*c*]dibenzo[*g*,*m*]corannulene (**90**) and indenocorannulenes **98**/**100** compared to those of **67**/**69** is consistent with the principle of Class I, i.e., the shallower bowl gives rise to the lower inversion barrier.

In order to develop a quantitative structure–energy relationship, Siegel and co-workers investigated the correlation between bowl depth and barrier energy

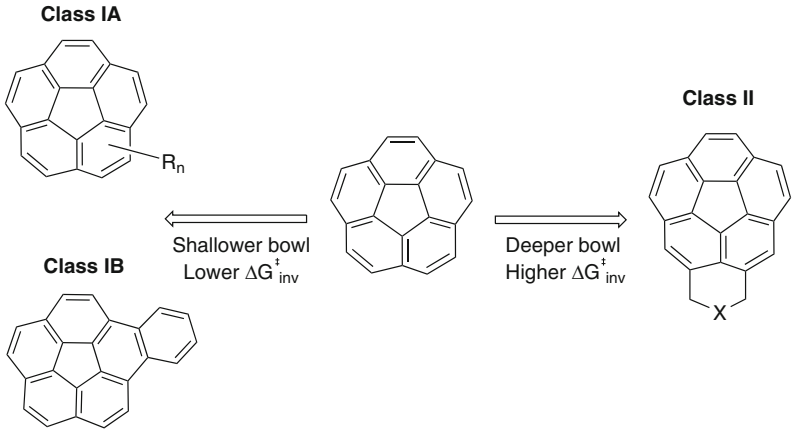


**Scheme 35** The correlations between structures and bowl-to-bowl inversion energy [57]

for some corannulene derivatives. They found the relationship can be empirically expressed as in (1). This simple quartic equation provided a reasonable fit to the experimental results [57]:

$$\left[\Delta G^{\ddagger}_{\text{inv}} = (\text{bowl depth}/0.87)^4 \times 11.5\ \text{kcal/mol}\right] \tag{1}$$

## 3 Sumanene

Sumanene (tricyclopenta[*def*,*jkl*,*pqr*]triphenylene, **2**) is a $C_{21}$-hydrocarbon containing three periphery methylene bridges, and it is also a basic bowl-shaped fragment of buckminsterfullerene. Sumanene (**2**) is named after "suman", the Hindi and Sanskrit word for a type of flower [133]. In contrast to corannulene, the chemistry of sumanene is relatively new because this compound was first successfully synthesized in the laboratory in 2003 [134].

### *3.1 Sumanene and Simple Sumanene Derivatives*

#### 3.1.1 Synthesis

In 1993, an attempt was made to synthesize sumanene (**2**) from tris(bromomethyl)-triphenylene under FVP conditions [133, 135]. Unfortunately, this protocol closed up to two five-membered rings. Ten years later, Sakurai et al. provided a new synthetic approach to prepare **2** in solution phase under mild conditions [134]. Similar to Lawton's synthetic strategy for corannulene, they first constructed the three-dimensional framework using tetrahedral $sp^3$ carbons and later aromatized the

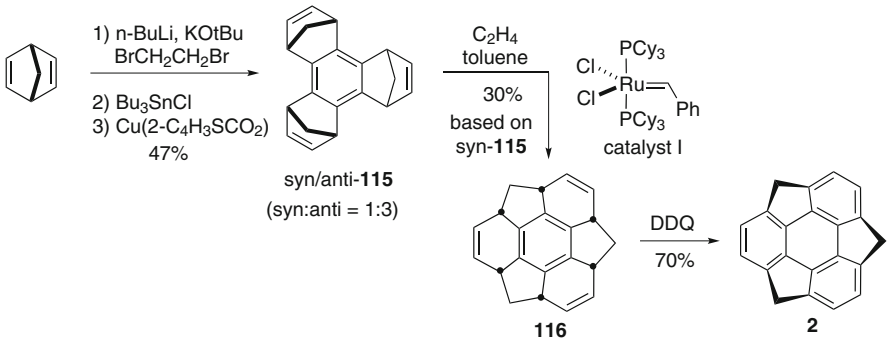


**Scheme 36** Synthesis of sumanene (**2**) [134]

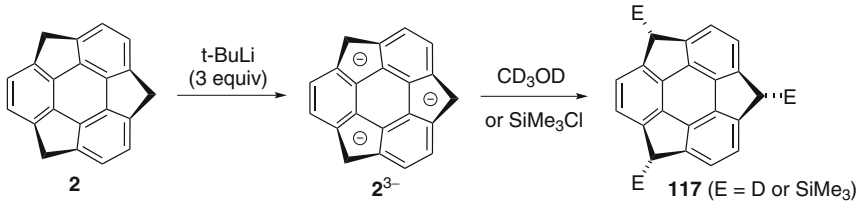


**Scheme 37** Synthesis of sumanene derivatives [136, 137]

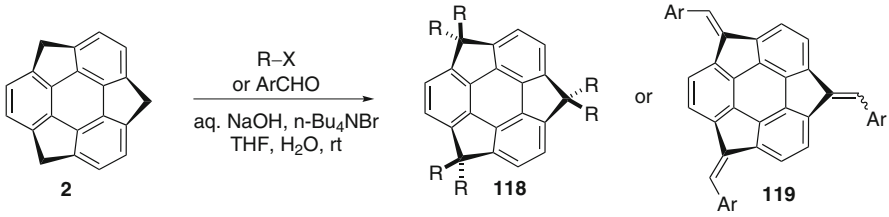


**Scheme 38** Synthesis of sumanene derivatives **118** and **119** [137, 138]

structure oxidatively to obtain the designed product. The successful synthesis started with trimerization of norbornadiene to give a mixture of *syn*- and *anti*-**115** (ratio 1:3) in a total yield of 47% (Scheme 36). Treatment of *syn*-**115** with catalyst **I** under an atmospheric pressure of ethylene furnished hexahydrosumanene **116** in 30% yield (based on *syn*-**115**) by ring-opening metathesis and subsequent ring-closing metathesis reactions. Finally, **2** was obtained by the oxidation of **116** with DDQ.

Generation of the mono-, di-, and trianion of **2** in [$D_8$]-THF depends on the amounts of *t*-BuLi used (Scheme 37) [136]. On the addition of 3 equiv. of *t*-BuLi, and subsequent treatment with excess amounts of $Me_3SiCl$, **2** was converted to tris-(trimethylsilyl) derivative *exo*-**117** (E=$SiMe_3$) as the sole isomer, in which all trimethylsilyl groups were selectively introduced at the *exo*-position. Similarly,

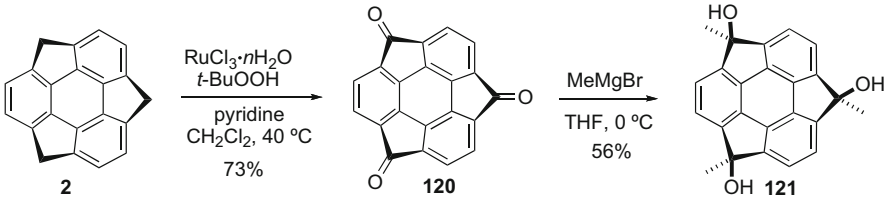


**Scheme 39** Synthesis and reaction of sumanenyl triketone **120** [139]

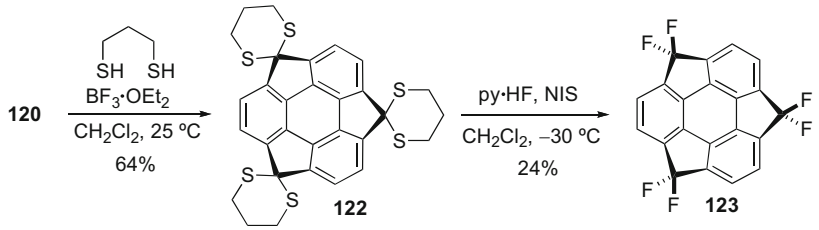


**Scheme 40** Synthesis and reaction of sumanenyl triketone **123** [140]

quenching trianion with $CD_3OD$ generated trideuterated sumanene *exo*-**117** (E=D) [137], which was used to determine the bowl inversion energy (see below).

Like fluorene, the three methylene moieties in sumanene can undergo alkylation or aldol condensation (Scheme 38). In the presence of a mixture of aqueous NaOH and $Bu_4NBr$, the reaction of **2** with allyl bromide or 4-methoxybenzyl chloride gave the corresponding hexa-alkylated sumanenes **118** [137]. Similarly, aldehydes yielded **119** in two regioisomeric forms [138].

In the presence of $RuCl_3$ and oxidant *t*-BuOOH, **2** was converted to triketone **120** in a good yield (Scheme 39) [139]. Consistent with the preferred *exo* attack at trigonal carbons of sumanene, reaction of **120** with methylmagnesium bromide selectively gave the product **121** as a single isomer, where all three methyl groups are at the *exo* positions.

Hexafluorosumanene **123** was prepared from sumanenetrione **120** via cyclic dithiane **122** (Scheme 40) [140]. Reaction of **122** with pyridine hydrofluoride (Olah's reagent) in the presence of *N*-iodosuccinimide gave **123** in 24% yield. The strong electron-withdrawing properties of fluorine substituents cause the first reduction potential of **123** to be shifted to −1.79 V from −3.21 V (vs ferronce) of the parent sumanenes (**2**).

Recently, a new synthetic protocol for synthesis of 9-arylfluorenes or 9,9-diarylfluorenes was reported wherein these products were furnished in good to excellent yields by Pd-catalyzed cross-coupling reactions of fluorene with haloarenes [141]. This synthetic method was also applied in the preparation of aryl-substituted sumanenes. Palladium-catalyzed arylation of sumanene (**2**) was conducted with 1-bromo-2,6-dimethylbenzene, and the desired xylylsumanene **124**-xyl was

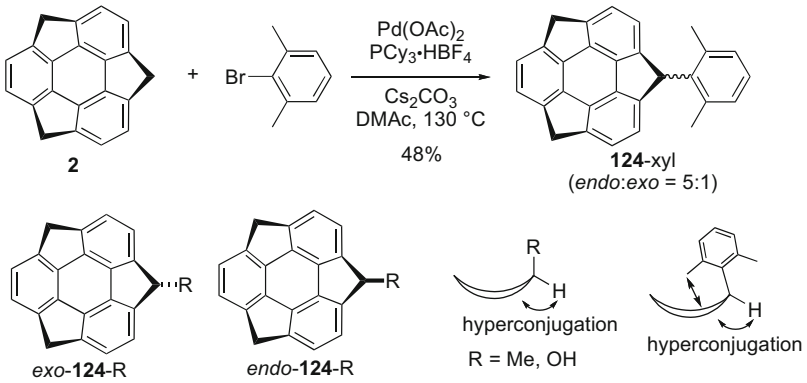


**Scheme 41** Synthesis of xylylsumanene **124**-xyl [141, 142]

successfully obtained in 48% yield (Scheme 41). Unlike **117** (E=$SiMe_3$), **124**-xyl was obtained as a mixture of *endo*- and *exo*-conformers in a 5:1 ratio.

A recent study indicated that the stereoelectronic effect of a curved aromatic structure dominates the stability of *endo*/*exo*-**124**-R (Scheme 41) [142]. Steric repulsion is the main factor to facilitate the conformer *exo*-**124**-$SiMe_3$, whereas some mono-substituted sumanenes, such as methylsumanene **124**-Me, hydroxysumanene **124**-OH, and 2,6-xylylsumane **124**-xyl, favor formation of the stable *endo*-conformation. In methylsumanene and hydroxysumanene, the hyperconjugation between the benzylic proton and the sumanenyl convex face causes the *endo* conformer to be more stable than the *exo* conformer. In **124**-xyl, the CH-π interaction, which is caused by the methyl group in xylyl substituent and the concave face of sumanene, favors the *endo*-conformer.

Mono-substituted sumanenes **125** can easily be obtained by electrophilic aromatic substitution reaction [143]. However, this protocol is unsuitable for preparation of di- and trisubstituted sumanenes due to the low regioselectivity. Trisubstituted sumanenes, such as $C_3$ symmetric triformylsumanene and its derivatives, were synthesized regioselectively by using suitable reaction intermediates *syn*-tri(norborneno)benzenes (cf. Scheme 36) [144].

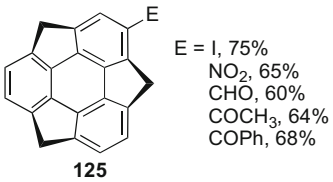


The enantioselective synthesis of a chiral buckybowl was reported by Sakurai and Higashibayashi in 2008 [145]. As in the synthesis of sumanene, $C_3$ symmetric *syn*-tris(norborneno)-benzene **126** is the key intermediate in this synthetic approach (Scheme 42). The synthesis started with enantiopure iodonorbornanone. The

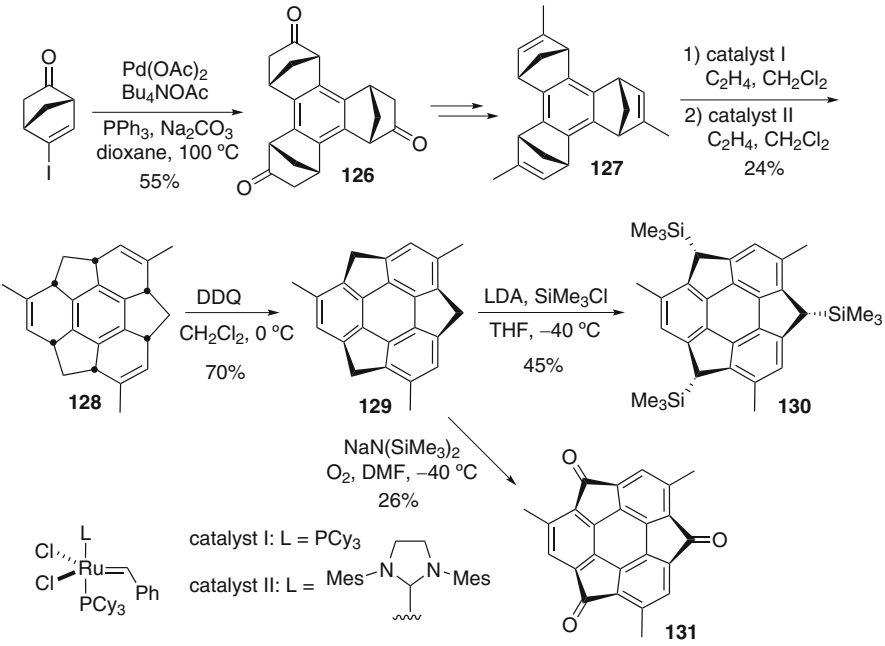


**Scheme 42** Synthesis of chiral sumanene derivatives [145–149]

Pd-catalyzed *syn*-selective cyclotrimerization yielded *syn*-tris(norborneno)benzene **126** [146–148]. This newly developed protocol is more efficient than the conventional method reported in Scheme 36. Triketone **126** was converted to **127**, which was then subjected to ring-opening and ring-closing metathesis reactions by treatment with catalysts **I** and **II**, respectively. The thus formed **128** underwent oxidative aromatization at low temperature to give *sym*-trimethylsumanene (*C*)-**129**. The bowl configuration of (*C*)-**129** was confirmed by CD spectral measurements. Treatment of (*C*)-**129** with LDA and subsequently with chlorotrimethylsilane at −40 °C yielded (*C*)-**130**, where all trimethylsilyl groups were *exo*-selectively introduced. In contrast to (*C*)-**129**, (*C*)-**130** has a high inversion barrier and was not diastereomerized, even at room temperature. Chiral HPLC analysis of (*C*)-**130** at room temperature enabled the determination of the enantiomeric excess (89% ee). Additionally, chiral buckybowl **129** was able to undergo oxidation under mild conditions (−40°C). Reaction of **129** with sodium hexamethyldisilazide under oxygen atmosphere gave **131** in 26% yield [149].

The sumanene-type heterobuckybowls such as trithiasumanene **132** and trisilasumanene **133** have also been prepared. The former was synthesized from a regioisomeric mixture of tris(chloroethenyl)benzotrithiophenes under FVP conditions at 1,000 °C [150]. In contrast, trisilasumanene **133** was prepared by threefold sila-Friedel–Crafts reactions [151]. The two heterobuckybowls provide a suitable model for systematically studying the influences of the ring size on the structure (Table 7).

**Table 7** POAV pyramidalization angles and bowl depths of sumanene and its derivatives

| Compound | POAV (deg)[a] | Bowl depth (Å)[b] | $\Delta G^{\ddagger}_{inv}$ (kcal/mol) | References |
|---|---|---|---|---|
| **2** | 8.8 | 1.11 | 19.6, 20.4[c] | [134, 136, 137] |
| **118** (R=$C_3H_5$) | – | – | 19.2 | [137] |
| **118** (R=MB[d]) | – | – | 18.2 | [137] |
| **123** | 9.6 | 1.24 | – | [140] |
| **129** | 9.1, 8.6 | 1.11 | 21.6 | [145, 152] |
| **131** | – | – | 23.3, 21.5 (calcd.) | [149] |
| **132** | 6.3 | 0.79 | – | [150] |
| **133** | | 0.23 | – | [151] |
| **139** | 10.8, 9.8 | 1.30 | 42.2, 39.9 (calcd.) | [153] |

[a]POAV angles at the hub six carbons of the sumanenes, and the values obtained by averaging the POAV angles of symmetry-related carbon atoms of sumanenes
[b]The bowl depth is gauged from the distance between hub and rim planes
[c]Determined by **117** (E = D)
[d]*MB* 4-methoxybenzyl

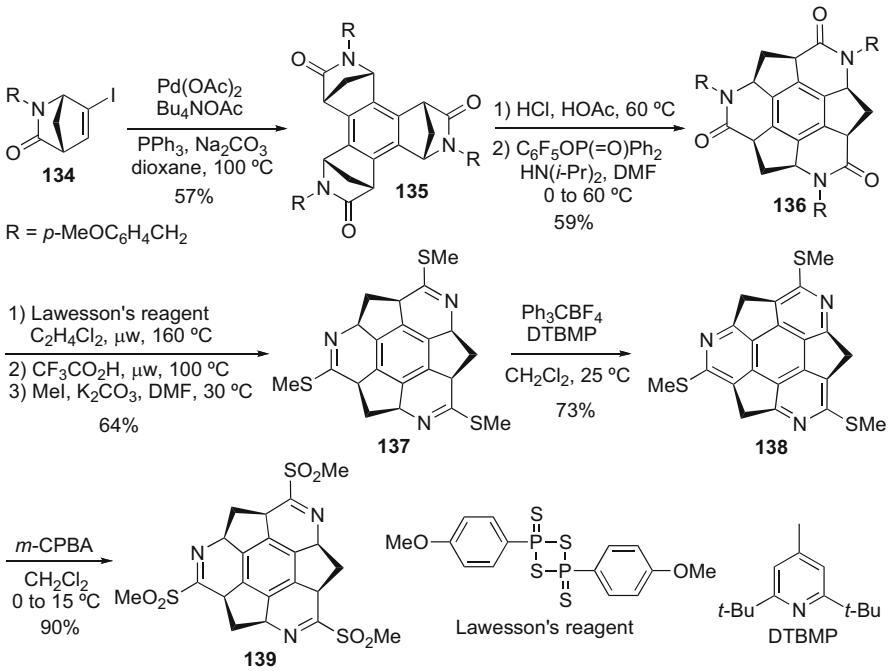


**Scheme 43** Synthesis of triazasumanenes [153]

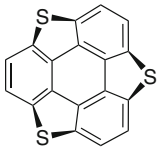


132

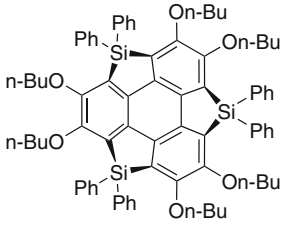


133

Sakurai and coworkers prepared *aza*-buckybowls, triazasumanene **138** and its derivative (Scheme 43) [153]. Similar to the synthesis of **129**, Pd-catalyzed cyclotrimerization of enantiopure (1*S*,4*R*)-**134** exclusively gave *syn*-**135**, which was hydrolyzed, followed by condensation, to furnish bowl-shaped lactam **136**. A three-step operation, including thiation reaction utilizing Lawesson's reagent, deprotection, and finally methylation, allowed **136** to generate thioimidate **137**. Three dihydropyridine rings were aromatized to afford (*C*)-(−)-**138** by treatment of a mixture of an oxidant $Ph_3CBF_4$ and a base 2,6-di-*tert*-butyl-4-methylpyridine (DTBMP). Similarly, the dextrorotatory enantiomer (*A*)-(+)-**138** was prepared from (1*R*,4*S*)-**134**. The structure of sulfone **139**, an oxidized derivative of **138**, was analyzed by X-ray crystallography.

### 3.1.2 Structures and Properties

The bowl inversion dynamics of sumanene (**2**) was studied by variable temperature NMR experiments, and its value was found to be 19.6 kcal/mol [134]. Chemical exchange NMR spectroscopy (EXSY) of **117** (E = D) also allows the determination of the bowl inversion barrier (ca. 19.7–20.4 kcal/mol), and the values depend on the solvent used [137]. These results show that **2** is much more rigid than corannulene. Unlike corannulene derivatives, the correlations between structures and bowl-to-bowl inversion barriers ($\Delta G^{\ddagger}_{inv}$) for substituted sumanenes have not been compressively studied. Based on the results currently available, substituents and their positions of the sumannenyl core affect $\Delta G^{\ddagger}_{inv}$ (Table 7). For example, hexa-alkylated sumanenes **118** show slightly lower bowl inversion barriers (18–19 kcal/mol) [137] than the parent sumanene, whereas $\Delta G^{\ddagger}_{inv}$ for (*C*)-**129** was found to have a higher inversion barrier (21.6 kcal/mol) [145]. Triketone **131** (23.3 kcal/mol) [149] has the highest inversion barrier of the simple carbon sumanene family, but the value is still much smaller than that for triazasumanene **139**. A chiral HPLC was used to investigate the racemization rate for a solution of enantiopure **139** in tetralin at 488 K, and the result of this experiment indicated the bowl inversion energy ($\Delta G^{\ddagger}_{inv}$) to be 42.2 kcal/mol.

Based on the crystallographic analysis, sumanene (**2**) and trimethylsumanene **129** have similar bowl depths (1.11 Å) and comparable POAV pyramidalization angles at the hub six carbons with a value around 8.8° [152]. Hexafluorosumanene **123** (bowl depth 1.24 Å, POAV angle 9.6°) is more curved than **2** and **129**. The

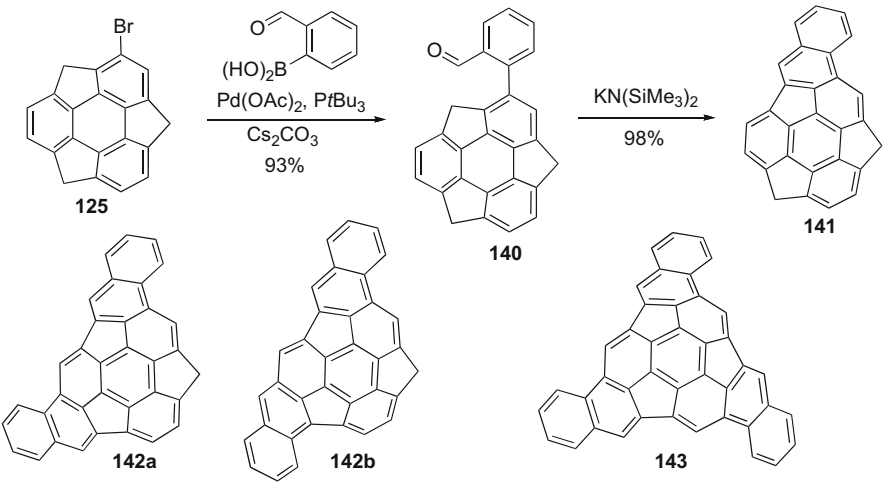


**Scheme 44** Synthesis of naphthosumanene derivatives [156]

bowl depth of heteroatom-substituted analogues **132** and **133** were determined to be 0.79 and 0.23 Å, respectively. The longer C–X bond length mainly causes their flattened structures. In contrast, triazasumanene **139** has a deeper bowl depth (1.30 Å) and a more curved structure. POAV pyramidalization angles of the hub carbons were determined as 9.8° and 10.8° [153].

The symmetry aligned columnar order of sumanene (**2**) in the solid state [136] allows it to have potential applications as an organic material. By using time-resolved microwave conductivity (TRMC) method, the charge carrier mobility of the needle-like single crystal of **2** demonstrated the large intracolumnar electron mobility (0.75 $cm^2\ V^{-1}\ s^{-1}$) and its remarkable anisotropy along the $\pi$-bowl stacking column axis [154].

Sumanene (**2**) and sumanenetrione (**120**) have similar bowl structures, but different electronic properties [155]. Their nanocrystals can form core–shell assemblies, and aggregates of **120** are wrapped by nanocrystals of **2**. The assemblies showed that amplified photoluminescence of sumanenetrione nanocrystals was caused by energy transfer from sumanene nanocrystals through the nanocrystalline interface.

## *3.2 Naphthosumanenes*

The methylene bridge of sumanene can be used for C–C bond formation for expanding the backbone of the π-bowl. The synthesis started with bromosumanene **125**, which was generated by selective monobromination of **2** with $HBr_3$•pyridine complex (Scheme 44) [156]. The Suzuki coupling of **125** with 2-formylphenylboronic

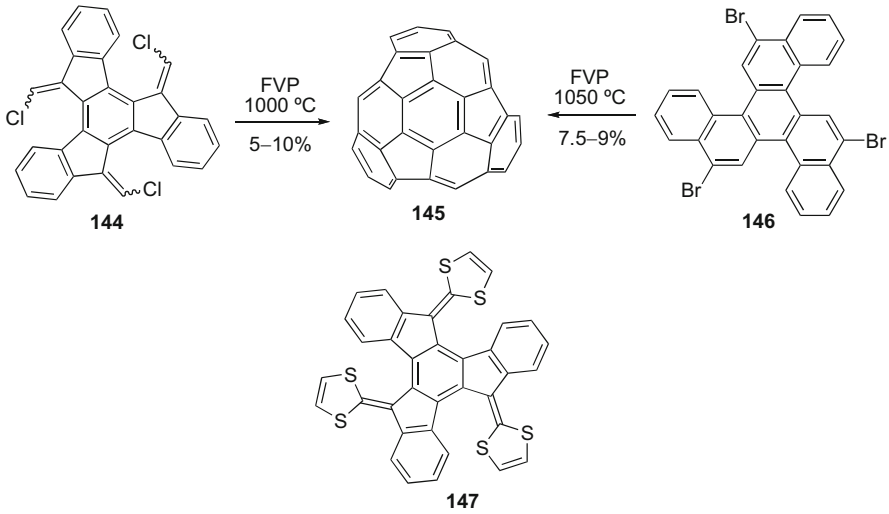


**Scheme 45** Synthesis of hemifullerene (**145**) [157, 158]

acid and subsequently the intramolecular benzannulation efficiently generated naphthosumanene **141**. Similarly, dinaphthosumanenes **142** and trinaphthosumanene **143** were accessed from dibromosumanenes and tribromosumanenes, respectively. Dibromosumanenes and tribromosumanenes were not formed regioselectively, and each contains two regioisomers. Therefore, dinaphthosumanenes were obtained as a mixture of **142a**/**142b** (55:45), but only one regioisomer of tribromosumanenes can finally give **143**. It should also be noted that the bowl-to-bowl inversion barrier for **141** was determined to be 32.2 kcal/mol by an EXSY experiment. Based on theoretical studies, the bowl-to-bowl inversion barrier and the maximum POAV pyramidalization angle for trinaphthosumanene (**143**) were suggested to be 63.8 kcal/mol and 10.8°, respectively.

## *3.3 Hemifullerene*

FVP synthesis of $C_3$-symmetric hemifullerene **145** was conducted with chlorinated tris-fulvene **144** [157] or tribenzotriphenylene **146** [158] (Scheme 45). The reaction mechanism of the latter should involve a radical-mediated cascade cyclization. An aryl radical, which is generated by bromine atom loss, undergoes 1,2-hydrogen shift and subsequent closure of the five membered ring. Two types of X-ray-quality crystals of **145** were obtained from the vapor phase and were verified as orthorhombic (**145**-*o*) and trigonal (**145**-*t*) [159]. Very recently the association of hemifullerene (**145**) with an electron-donating tetrathiafulvalene derivative **147**

**Scheme 46** Synthesis of buckybowl **149** [25]

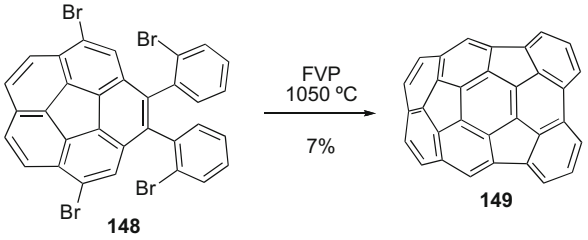


was investigated [160]. They form the supramolecular complex with a comparable binding constant to that for the association of **147** with $C_{60}$.

## 4 Mixed Type Buckybowls

A buckybowl containing both corannulenyl and sumanenyl fragments is described as a mixed buckybowl in this context. Pentaindenocorannulene (**104**) is one such example.

### *4.1* *Acenaphtho[3,2,1,8*-ijlkm*]diindeno[4,3,2,1*-cdef*:1′,2′,3′,4′*-pqra*]triphenylene*

Scheme 46 presents an unexpected formation of buckybowl **149** from corannulene derivative **148**, which was prepared by a protocol similar to Method C in Scheme 5 [25]. Under FVP conditions, **148** underwent cyclization to give hydrocarbon **149** through the formation of three C–C bonds. The key step in the cyclization should be 1,2-shift of the hydrogen atom of the rim radical, generated by the rupture of C–Br bond one at a time, for the formation of five-membered rings.

### *4.2* *Acenaphth[3,2,1,8*-fghi*j]*-as-*indaceno[3,2,1,8,7,6*-pqrstuv*]picene*

Buckybowl **151** (R=H) was first prepared by an inefficient route in which 7,12-bis-(2-bromophenyl)benzo[*k*]fluoranthene was cyclized under FVP conditions at 1,100 °C [161]. Later on, a new synthetic approach in solution phase made **151** easily accessible. The first step of the synthesis was Pd-catalyzed annellation of 1,8-bis(arylethynyl)naphthalene **87** (R=H) with iodobenzene to give benzo[*k*] fluoranthene **150** (Scheme 47) [28]. Cyclization of **150** was conducted with a mixture of DBU and $Pd(PCy_3)_2Cl_2$ to generate **151** (R=H) in 31% yield [162].

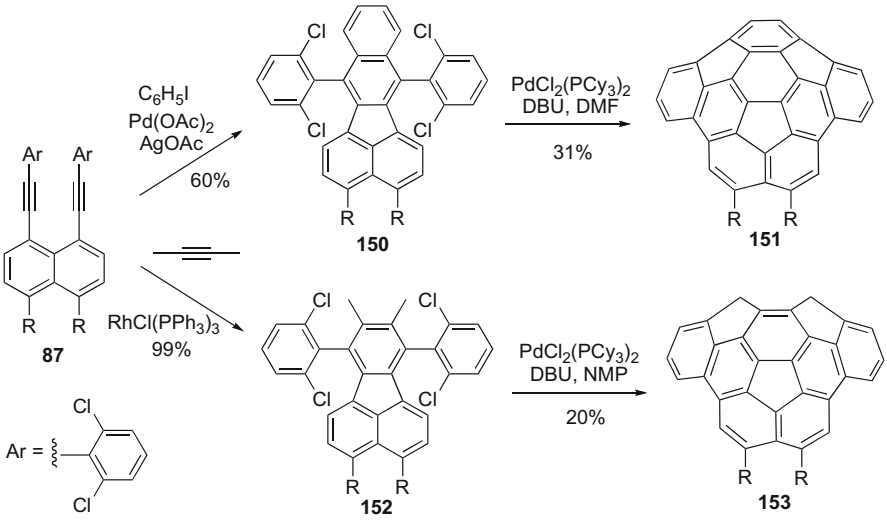


**Scheme 47** Synthesis of mixed buckybowls **151** and **153** [162, 164]

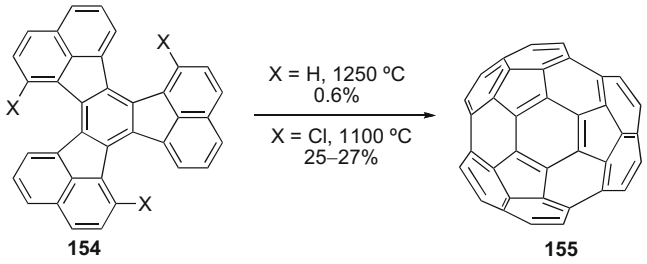


**Scheme 48** Synthesis of circumtrindene (**155**) [165, 166]

Moreover, a new methylene-bridged buckybowl **153** (R=H) was obtained from fluoranthene **152** (R=H) through benzylic and aryl C–H bond activation [163]. According to the crystallographic analysis, both buckybowls **151** (R=H) and **153** (R=H) have very high POAV pyramidalization angles and deep bowl depths [162, 164]. The maximum POAV pyramidalization angles for **151** and **153** was observed at carbon atoms in the central five-membered ring, both with the value of 12.8°. In **151**, bowl depths measured from the corannulene and sumanene cores were 1.24 and 1.48 Å, respectively. These values are significantly larger than those for the parent compounds corannulene (0.87 Å) and sumanene (1.11 Å). It should be noted that the highly curved structures for **151** and **153** correspond to their high bowl-to-bowl inversion barriers. The inversion barrier of the former was determined computationally to be 124.3 kcal/mol. The cyclopenta-annulation increases the bowl depth

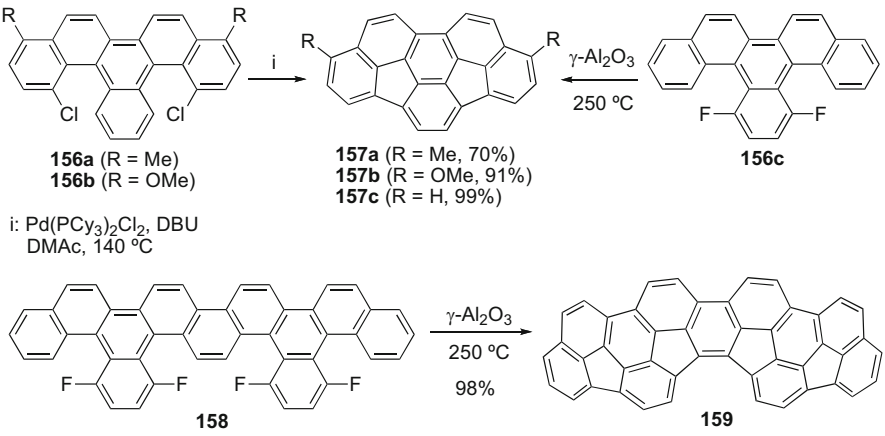


**Scheme 49** Synthesis of *as*-indaceno[3,2,1,8,7,6-*pqrstuv*]picene derivatives [168, 169]

and the bowl-to-bowl inversion barrier of buckybowls **151** (R–R=$C_2H_4$) and **153** (R–R=$C_2H_4$) [164] (Scheme 47).

### *4.3 Circumtrindene*

The FVP synthesis of circumtrindene (**155**) was conducted with decacyclene (**154**, X=H) at 1,250 °C, but this protocol gave the product in very low yield (Scheme 48) [165] because unfunctionalized aryl carbon atoms are inefficient for C–C bond formation. Trichlorodecacyclene **154** (X=Cl) dramatically improves the yield of **155** up to 27% [166]. Based on crystallographic analysis, the depth of the bowl is 3.107 Å and the POAV pyramidalization angles of the central hexagon are 11.9° and 12.4° [167].

## 5 Other Bulkybowls

### *5.1* as-*Indaceno[3,2,1,8,7,6-*pqrstuv*]picenes*

*as*-Indaceno[3,2,1,8,7,6-*pqrstuv*]picenes **157a** and **157b** were efficiently synthesized by Pd-catalyzed cyclization of dichlorobenzo[*s*]picenes **156a** and **156b**, respectively (Scheme 49) [168]. Recently, a new cyclization protocol through regiospecific HF elimination on fluoroarenes was developed [169]. Difluorobenzo-[*s*]picene **156c** in γ-$Al_2O_3$ at 250 °C was efficiently converted to indacenopicene **157c**. One obvious advantage of this solvent-free protocol is

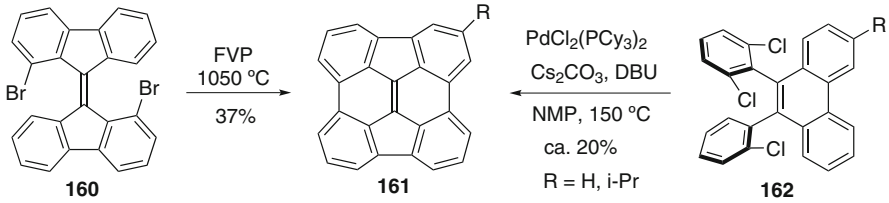


**Scheme 50** Synthesis of tetrabenzopyracylene **161** [170, 171]

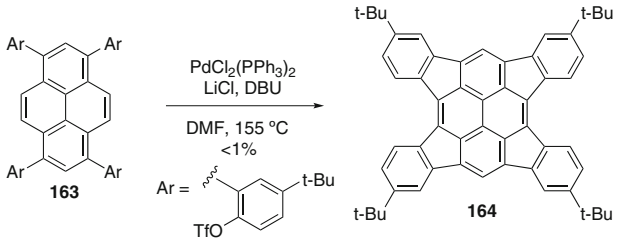


**Scheme 51** Synthesis of tetraindenopyrene **164** [174]

applicable to the production of highly insoluble fullerene precursors. For example, compound **159** was efficiently generated from the poorly soluble compound **158**.

The structure of 1,8-dimethyl-*as*-indaceno[3,2,1,8,7,6-*pqrstuv*]picene (**157a**) was analyzed by X-ray crystallography [168]. The maximum POAV pyramidalization angle was determined to be 8.4°, slightly greater than that of corannulene (8.2°).

## *5.2 Tetrabenzopyracylene*

In contrast to corannulene (**1**) and sumanene (**2**), tetrabenzopyracylene **161** is a less common fragment of $C_{60}$. The successful synthesis of **161** started with dibromobifluorenylidene **160** under FVP conditions (Scheme 50) [170]. The closure of two six-membered rings is the key step of this protocol and **160** was obtained in 37% yield. Alternatively, **161** was straightforwardly prepared in around 20% yield from 9,10-diarylphenanthrenes **162** by Pd-catalyzed intramolecular arylations [171]. The bowl-to-bowl inversion barrier for buckybowl **162** (R=*i*-Pr) was predicted to be approximately 7 kcal/mol [171, 172], which is consistent with the results of a variable-temperature proton NMR study. It should be noted that the central 6:6-bond in **161** underwent 1,2-addition with both electrophilic and nucleophilic reagents to give fullerene-type adducts [173]. The curvature and the Clar aromatic sextet theory reveal the high reactivity of the central alkenyl moiety.

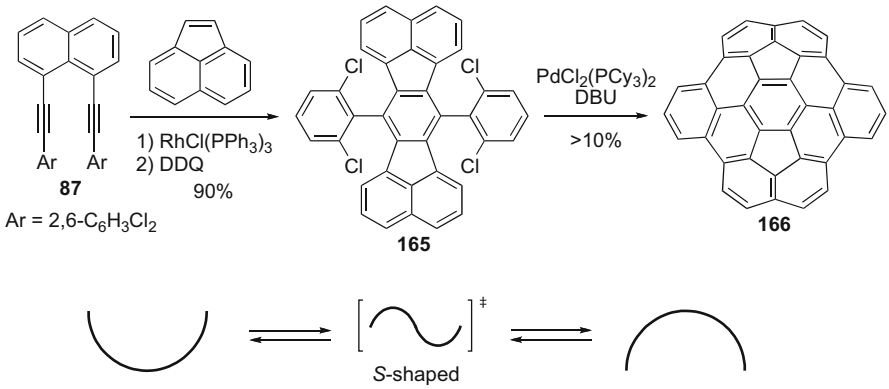


**Scheme 52** Synthesis and bowl-to-bowl inversion of buckybowl **166** [177]

## 5.3 Tetraindenopyrene

The chemistry of bowl-shaped fragments of $C_{60}$ has been intensively investigated, but that of bowl-shaped fragments of $C_{70}$ or higher fullerenes is almost completely unstudied. Tetraindenopyrene **164**, which is a fragment of $C_{70}$ [174], was prepared in very low yield from tetraarylpyrene **163** by Pd-catalyzed cyclization (Scheme 51). Based on theoretical studies, **164** was predicted to be a shallow bowl with a very low bowl-to-bowl inversion barrier (0.33 kcal/mol).

## 5.4 Highly Curved Fragment of $C_{70}$ and Higher Fullerenes

Buckybowl **166** is a highly curved subunit of $C_{70}$ and higher fullerenes, such as $C_{76}$, $C_{78}$, $C_{84}$, and others [175, 176]. The studied molecule **166** was easily synthesized from 1,8-bis(arylethynyl)naphthalenes **87** using a three-step synthetic approach (Scheme 52) [177]. 7,14-Diarylacenaphtho[*1,2-k*]fluoranthene derivative **165**, the key precursor in this synthesis, was efficiently prepared by simple rhodium-catalyzed [(2+2)+2] cycloaddition of **87** with acenaphthylene, and subsequently aromatized by treatment with 2,3-dichloro-5,6-dicyano-1,4-benzoquinone (DDQ). The Pd-catalyzed cyclization of **165** gave **166** in low yield. The low solubility of **166** in common organic solvents was mostly responsible for the unsatisfactory result. The curved structure of **166** was identified by X-ray crystallography and found to be a rigid bowl-shaped molecule with a deep bowl depth (ca. 2.30 Å). The maximum POAV pyramidalization angle of **166** was observed to be ca. 10.8°. Similar to semibuckminsterfullerene (**111**-H) [130], the bowl-to-bowl inversion of **166** proceeds via a non-planar transition structure. DFT computational studies indicated that the inversion route via an *S*-shaped transition structure has a lower

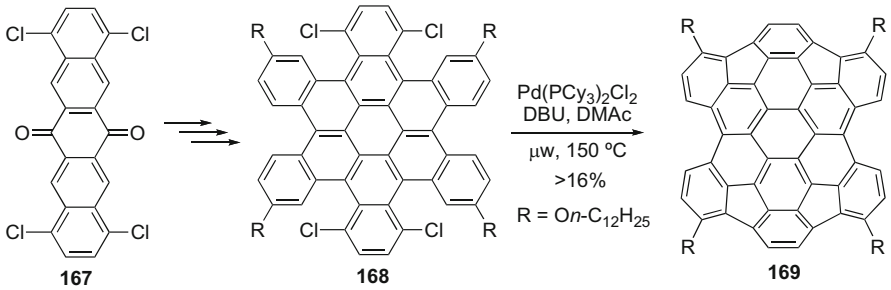


**Scheme 53** Synthesis of hexabenzocoronene-based buckybowl **167** [178]

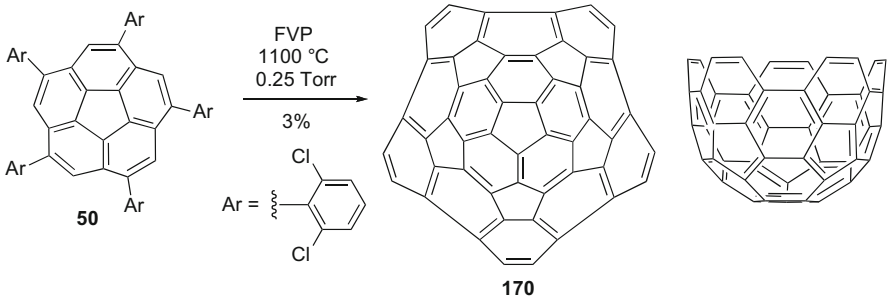


**Scheme 54** Synthesis of tubular molecule **170** [180]

barrier ($\Delta G^{\ddagger} = 79.8$ kcal/mol) than via a planar transition structure ($\Delta G^{\ddagger} = 116.3$ kcal/mol).

## 5.5 *Hexabenzocoronene-Based Buckybowl*

Buckybowl **169** is not a fragment of common fullerenes, such as $C_{60}$ and $C_{70}$ (Scheme 53) [178]. The synthesis started with pentacenequinone **167**, and the final step was microwave-assisted Pd-catalyzed cyclization of **168**. The maximum POAV pyramidalization angle of compound **169** was predicated to be 8.4° based on computational calculations. The bowl-to-bowl inversion barrier of **169** should be greater than 24 kcal/mol according to the result of a variable-temperature NMR experiment. It should also be noted that buckybowl **169** easily accepts electrons and associates strongly with $C_{70}$.

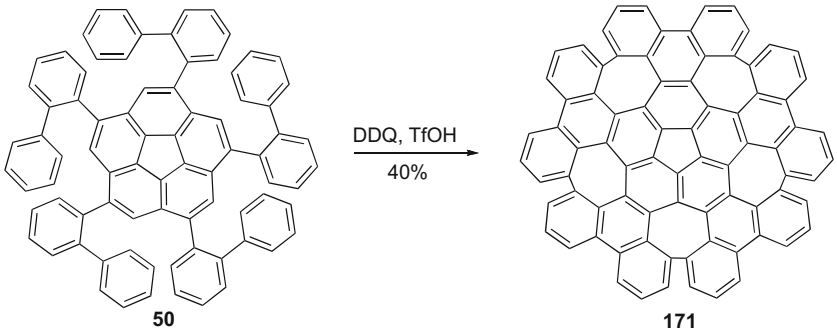


**Scheme 55** Synthesis of warped nanographene **171** [181]

## 6 The Smallest Carbon Nanotube

The structural properties of the corannulene-based series $(C_{10})_nH_{10}$ were theoretically studied [179]. The transition from a bowl to a tube increases with molecular size. Whereas corannulene (**1**) and $C_{30}H_{10}$ are seen as bowl-shaped compounds, $C_{40}H_{10}$ marks the onset of the tube regime, and $C_{50}H_{10}$ ends the character of the bowl regime. Recently, compound **170** ($C_{50}H_{10}$) has been synthesized in the Scott's laboratory (Scheme 54) [180]. The key precursor **50** was prepared by fivefold Negishi coupling of **46** with 2,6-dichlorophenylzinc chloride as shown in Scheme 13. Under FVP conditions, **50** was converted to **170** in 2–3% yield. Based on the crystallographic analysis, **170** has a nanotube structure with the bowl depth (tube length) of 5.16 Å. The average POAV pyramidalization angle of the central pentagon was observed to be 12.3° [180], which is very close to the computational result (12.2°) [179].

## 7 A Warped Nanographene

Nanographene **171** was prepared by cyclodehydrogenation of 1,3,5,7,9-pentakis (2-biphenylyl)corannulene **50**, which was synthesized by a Suzuki coupling of the resulting 1,3,5,7,9-pentakis(Bpin)corannulene (**47**) with 2-bromobiphenyl (Scheme 55) [181]. Based on X-ray crystallography, **171** adopts a warped structure, and the central corannulene moiety is very shallow with a bowl depth of 0.37 Å. The presence of five helical hexa[7]circulene moieties causes **171** to be chiral. Theoretical analysis indicated that activation energies for the inversion and the racemization are 1.7 and 18.9 kcal/mol, respectively.

**Table 8** Molecular packing of buckybowls

| Type | Compounds |
|---|---|
| **A** | **2** [136], **18** [39], **103a** [128], **123** [140], **145**-*t* [159], **155** [167] |
| **Quasi-A** | **44**-Ph [39], **101a** [128], **104** [89], **111**-Me [132], **151** [162, 164], **153** (R=H) [162], **161**-H [170], **166** [177] |
| **B** | **21c** [40], **23c** [41], **41** (R=3,5-$C_6H_3(CH_3)_2$) [39], **45**-$CF_3$ [81], **98** [128], **101b** [128], **103b** [128] **129** [152] |
| **Quasi-B** | **28**-F [40], **28**-Cl [40], **49** (R=3,5-$C_6H_3(CH_3)_2$) [39], **81**-$C_6F_5$ [110], **100** [27], **102** [89], **145**-*o* [159] |

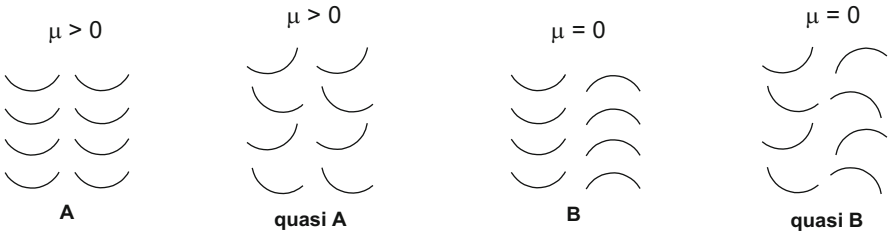


**Scheme 56** Schematic presentations of open geodesic bowls in crystals

## 8 Molecular Packing of Bowls in the Solid State

The curvature of buckybowls makes their solid-state packing very interesting but complex. Buckybowls can be polar because of the different electronic distributions within a curved surface [179]. Studies of the intermolecular interactions would be useful to clarify the generation of polar crystals by controlling solid-state packing. This kind of crystal engineering would allow buckybowls to make key advancements in materials chemistry. The types of molecular packing are summarized in Table 8 and Scheme 56. The ideal model for applications in materials science is Type **A**, bowl-in-bowl stacks where all columns are oriented toward the same direction, resulting in polar crystals. Similar to Type **A**, crystals of Type **Quasi-A** are also polar, but the bowls are slipped slightly from side to side within each stack. In contrast, crystals of Types **B** and **Quasi-B** are apolar because the neighboring columns are oriented toward opposite directions although they have bowl-in-bowl stacks.

In principle, all four packing types in Scheme 56 have bowl-in-bowl stacks. The molecule packing appears to depend on the size of the bowl surface area and the depth of the bowl, with larger and deeper favoring 1D columns, which would be encouraged to form by strong intermolecular interactions. As the aromatic molecular surface area becomes smaller, the molecular packing changes away from columnar. Recently, a theoretical investigation indicates that the dipole moment of a buckybowl should be an important factor to yield 1D columnar stacks [182]. It should also be noted that the periphery substituents can strongly affect crystal packing arrangements. For example, the molecular packing of corannulene is

highly disordered, but 1,2,5,6-tetrabromocorannulene (**18**) has perfect columnar order in Type **A** [39].

Although all four packing types have bowl-in-bowl stacks, the factors necessary to control the orientations of neighboring columns are still not well known. Even the same compound packs in different crystal systems. Trigonal crystals of hemibuckminsterfullerene (**145**-*t*) show as Type **A**, whereas orthorhombic crystals of hemibuckminsterfullerene (**145**-*o*) present as Type **quasi B**.

In contrast to the packing types described above, several compounds, such as pentakis(phenylthio)corannulene **48** (XR=SPh) (Siegel et al., unpublished results), pentaarylcorannulenes **50** (R=manisyl, 2,6-$C_6H_3Cl_2$) [70, 180], decaarylcorannulene **57** (R=4-$C_6H_4Cl$) [74], and decakis(phenylthio)corannulene **58a** [75], have bulky substituents at rim positions, which avoid the intermolecular interaction between any two corannulyl cores. Equally notable is that, unlike tetrakis(arylethynyl) corannulenes **41** and pentakis(arylethynyl)corannulenes **49** [39], decakis (1-pentynyl)corannulene (**55**) [73] does not present column-type packing. Although these compounds do not conform to the model bowl-in-bowl packing motif, some of them can furnish polar crystals. For example, pentamanisylcorannulene **50** [70] and decakis(1-pentynyl)corannulene (**55**) [73] form polar crystals as defined by their space groups of $P_1$ and $P_n$, respectively.

## 9 Conclusion and Outlooks

The syntheses, structures, and properties of buckybowls are highly interesting topics, and numerous scientists have been motivated to join the field. In comparison with our previous review article in 2006, investigations of buckybowls are full of vitality and many important achievements have been presented in the past 8 years.

Corannulene is the seed of buckybowl chemistry; its preparation has been improved from the milligram to the kilogram scale, and reactions have been conducted under mild conditions in the solution phase, in which many functional groups are tolerated. With these advantages, many corannulenyl derivatives and more expanded bowl-shaped molecules can easily be made for various studies. Thanks to the new synthetic protocols, many highly curved fragments of $C_{60}$, $C_{70}$ and higher fullerenes were synthesized, but improvements of reaction efficiency are still tough challenges for synthetic chemists. It must be emphasized that the developed synthetic strategies for generating buckybowls provide a reasonable basis for routes to furnish carbon tubes with homogenous molecular weight distributions.

The correlations between structures and bowl-to-bowl inversion barriers provide information on the inversion dynamics and design of a static bowl. Increase in the curve of buckybowls may also increase their molecular dipole moment. A high inversion barrier conveys a configurational stability to a chiral buckybowl, avoiding loss of enantiopurity through the bowl-inversion racemization process.

The presence of convex and concave surfaces in π-bowls causes the molecular packing complex. Control of their crystal packing to form polar crystals is

important not only for basic research in molecular engineering, but also for applications in materials science. However, the necessary factors and techniques to form polar crystals remain largely unknown. In the near future, more crystal examples will help to clarify the questions described above.

Redox chemistry and the photophysical properties of buckybowls have been intensively studied, and they can be tuned by changing molecular skeletons, as well as number and placement of substituents. The preliminary material investigations indicated that buckybowls can be used as liquid crystals and molecular electronics. Since the preparation methods have been dramatically improved, and investigations of physical properties have brought fruitful results, a wide range of applications of organic materials based on buckybowls can be looked forward to in the future. Progress from Lawton's seminal work to application in device technology has been verified by the recent patent on the use of numerous corannulene derivatives as OLEDs [183].

## References


1. Beck A, Bleicher MN, Crowe DW (1969) Excursions into mathematics. Worth, New York
2. Kroto HW, Heath JR, O'Brien SC, Curl RF, Smalley RE (1985) Nature 318:162–163
3. Iijima S (1991) Nature 354:56
4. Petrukhina MA, Scott LT (eds) (2011) Fragments of fullerenes and carbon nanotubes: designed synthesis, unusual reactions, and coordination chemistry. Wiley, Hoboken
5. Sygula A (2011) Eur J Org Chem 1611–1625
6. Tsefrikas VM, Scott LT (2006) Chem Rev 106:4868–4884
7. Wu YT, Siegel JS (2006) Chem Rev 106:4843–4867
8. Sygula A, Rabideau PW (2006) In: Haley MM, Tykwinski RR (eds) Carbon-rich compounds: from molecules to materials. Willey, Weinheim, pp 529–565
9. Scott LT (2004) Angew Chem Int Ed 43:4994–5007
10. Scott LT, Bronstein HE, Preda DV, Ansems RBM, Bratcher MS, Hagen S (1999) Pure Appl Chem 71:209–219
11. Mehta G, Rao HSP (1998) Tetrahedron 54:13325–13370
12. Schmidt BM, Lentz D (2014) Chem Lett 43:171–177
13. Amaya T, Hirao T (2012) Pure Appl Chem 84:1089–1100
14. Higashibayashi S, Sakurai H (2011) Chem Lett 40:122–128
15. Amaya T, Hirao T (2011) Chem Commun 47:10524–10535
16. Reisch HA, Bratcher MS, Scott LT (2000) Org Lett 2:1427–1430
17. Barth WE, Lawton RG (1966) J Am Chem Soc 88:380–381
18. Barth WE, Lawton RG (1971) J Am Chem Soc 93:1730–1745
19. Hopf H (2000) Classics in hydrocaron chemistry. Wiley, Weinheim, p 331
20. Scott LT, Hashemi MM, Meyer DT, Warren HB (1991) J Am Chem Soc 113:7082–7084
21. Scott LT, Cheng PC, Hashemi MM, Bratcher MS, Meyer DT, Warren HB (1997) J Am Chem Soc 119:10963–10968
22. Brown RFC, Harrington KJ, McMullen GL (1974) J Chem Soc Chem Commun 123–124
23. Brown RFC, Eastwood FW, Harrington KJ, McMullen GL (1974) Aust J Chem 27: 2391–2402
24. Brown RFC, Eastwood FW, Jackman GP (1977) Aust J Chem 30:1757–1767
25. Marcinow Z, Grove DI, Rabideau PW (2002) J Org Chem 67:3537–3539
26. Sygula A, Karlen SD, Sygula R, Rabideau PW (2002) Org Lett 4:3135–3137

27. Wu YT, Hayama T, Baldrige KK, Linden A, Siegel JS (2006) J Am Chem Soc 128: 6870–6884
28. Kung YH, Cheng YS, Tai CC, Liu WS, Shin CC, Ma CC, Tsai YC, Wu TC, Kuo MY, Wu YT (2010) Chem Eur J 16:5909–5919
29. Elliott EL, Orita A, Hasegawa D, Gantzel P, Otera J, Siegel JS (2005) Org Biomol Chem 3: 581–583
30. Albright LF, Crynes BL (eds) (1976) Industrial and laboratory pyrolyses, ACS Symposium Series 32. American Chemical Society, Washington
31. Borchardt A, Fuchicello A, Kilway KV, Baldridge KK, Siegel JS (1992) J Am Chem Soc 114:1921–1923
32. Seiders TJ, Baldridge KK, Siegel JS (1996) J Am Chem Soc 118:2754–2755
33. Olah GA, Prakash GKS (1976) Synthesis 607–608
34. Seiders TJ, Elliott EL, Grube GH, Siegel JS (1999) J Am Chem Soc 121:7804–7813
35. Sygula A, Rabideau PW (1999) J Am Chem Soc 121:7800–7803
36. Sygula A, Rabideau PW (2000) J Am Chem Soc 122:6323–6324
37. Xu G, Sygula A, Marcinow Z, Rabideau PW (2000) Tetrahedron Lett 41:9931–9934
38. Sygula A, Xu G, Marcinow Z, Rabideau PW (2001) Tetrahedron 57:3637–3644
39. Wu YT, Bandera D, Maag R, Linden A, Baldridge KK, Siegel JS (2008) J Am Chem Soc 130:10729–10739
40. Schmidt BM, Topolinski B, Yamada M, Higashibayashi S, Shionoya M, Sakurai H, Lentz D (2013) Chem Eur J 19:13872–13880
41. Schmidt BM, Seki S, Topolinski B, Ohkubo K, Fukuzumi S, Sakurai H, Lentz D (2012) Angew Chem Int Ed 51:11385–11388
42. Stanger A, Ashkenazi N, Boese R, Bläser D, Stellberg P (1997) Chern Eur J 3:208–211
43. Butterfield AM, Gilomen B, Siegel JS (2012) Org Process Res Dev 16:664–676
44. Duttwyler S, Butterfield AM, Siegel JS (2013) J Org Chem 78:2134–2138
45. Greene AK, Scott LT (2013) J Org Chem 78:2139–2143
46. Sygula A, Sygula R, Fronczek FR, Rabideau PW (2002) J Org Chem 67:6487–6492
47. Nishida S, Morita Y, Ueda A, Kobayashi T, Fukui K, Ogasawara K, Sato K, Takui T, Nakasuji K (2008) J Am Chem Soc 130:14954–14955
48. Preda DV (2001) Ph.D. Dissertation, Boston College, Chestnut Hill
49. Cheng PC (1996) Ph.D. Dissertation, Boston College, Chestnut Hill
50. Topolinski B, Schmidt BM, Kathan M, Troyanov SI, Lentz D (2012) Chem Commun 48: 6298–6300
51. Scott LT, Hashemi MM, Bratcher MS (1992) J Am Chem Soc 114:1920–1921
52. Morita Y, Nishida S, Kobayashi T, Fukui K, Sato K, Shiomi D, Takui T, Nakasuji K (2004) Org Lett 6:1397–1400
53. Jones CS, Elliott E, Siegel JS (2004) Synlett 187–192
54. Sygula A, Sygula R, Rabideau PW (2005) Org Lett 7:4999–5001
55. Yanney M, Fronczek FR, Henry WP, Beard DJ, Sygula A (2011) Eur J Org Chem 6636–6639
56. Yanney M, Fronczek FR, Sygula A (2012) Org Lett 14:4942–4945
57. Seiders TJ, Baldridge KK, Grube GH, Siegel JS (2001) J Am Chem Soc 123:517–525
58. Haddon RC, Scott LT (1986) Pure Appl Chem 58:137–142
59. Haddon RC (1988) Acc Chem Res 21:243–249
60. Haddon RC (1993) Science 261:1545–1550
61. Sygula A, Abdourazak AH, Rabideau PW (1996) J Am Chem Soc 118:339–343
62. Seiders TJ, Baldridge KK, Elliott EL, Grube GH, Siegel JS (1999) J Am Chem Soc 121: 7439–7440
63. Hanson JC, Nordman CE (1976) Acta Crystallogr B32:1147–1153
64. Petrukhina MA, Andreini KW, Mack J, Scott LT (2005) J Org Chem 70:5713–5716
65. Fedurco M, Olmstead MM, Fawcett WR (1995) Inorg Chem 34:390–392
66. Dawe LN, AlHujran TA, Tran HA, Mercer JI, Jackson EA, Scott LT, Georghiou PE (2012) Chem Commun 48:5563–5565

67. Juríček M, Strutt NL, Barnes JC, Butterfield AM, Dale EJ, Baldridge KK, Stoddart JF, Siegel JS (2014) Nat Chem 6:222
68. Bruno C, Benassi R, Passalacqua A, Paolucci F, Fontanesi C, Marcaccio M, Jackson EA, Scott LT (2009) J Phys Chem B 113:1954–1962
69. Valenti G, Bruno C, Rapino S, Fiorani A, Jackson EA, Scott LT, Paolucci F, Marcaccio M (2010) J Phys Chem C 114:19467–19472
70. Hayama T, Baldridge KK, Wu YT, Linden A, Siegel JS (2008) J Am Chem Soc 130: 1583–1591
71. Baldridge KK, Siegel JS (2008) Theor Chem Acc 120:95–106
72. Samdal S, Hedberg L, Hedberg K, Richardson AD, Bancu M, Scott LT (2003) J Phys Chem A 107:411–417
73. Hayama T, Wu YT, Linden A, Baldridge KK, Siegel JS (2007) J Am Chem Soc 129: 12612–12613
74. Zhang Q, Kawasumi K, Segawa Y, Itami K, Scott LT (2012) J Am Chem Soc 134: 15664–15667
75. Baldridge KK, Hardcastle KI, Seiders TJ, Siegel JS (2010) Org Biomol Chem 8:53–55
76. Ayalon A, Rabinovitz M, Cheng PC, Scott LT (1992) Angew Chem Int Ed Engl 31: 1636–1637
77. Filatov AS, Sumner NJ, Spisak SN, Zabula AV, Rogachev AY, Petrukhina MA (2012) Chem Eur J 18:15753–15760
78. Seiders TJ, Baldridge KK, Siegel JS, Gleiter R (2000) Tetrahedron Lett 41:4519–4522
79. Morita Y, Ueda A, Nishida S, Fukui K, Ise T, Shiomi D, Sato K, Takui T, Nakasuji K (2008) Angew Chem Int Ed 47:2035–2038
80. Sevryugina Y, Rogachev AY, Jackson EA, Scott LT, Petrukhina MA (2006) J Org Chem 71: 6615–6618
81. Kuvychko IV, Spisak SN, Chen YS, Popov AA, Petrukhina MA, Strauss SH, Boltalina OV (2012) Angew Chem Int Ed 51:4939–4942
82. Eliseeva MN, Scott LT (2012) J Am Chem Soc 134:15169–15172
83. Grube GH, Elliott EL, Steffens RJ, Jones CS, Baldridge KK, Siegel JS (2003) Org Lett 5: 713–716
84. Mattarella M, Siegel JS (2012) Org Biomol Chem 10:5799–5802
85. Eberhard MR, Wang Z, Jensen CM (2002) Chem Commun 818–819
86. Grasa GA, Nolan SP (2001) Org Lett 3:119–122
87. Wu YL, Stuparu MC, Boudon C, Gisselbrecht JP, Schweizer WB, Baldridge KK, Siegel JS, Diederich F (2012) J Org Chem 77:11014–11026
88. Littke AF, Fu GC (1998) Angew Chem Int Ed 37:3387–3388
89. Jackson EA, Steinberg BD, Bancu M, Wakamiya A, Scott LT (2007) J Am Chem Soc 129: 484–485
90. Pappo D, Mejuch T, Reany O, Solel E, Gurram M, Keinan E (2009) Org Lett 11:1063–1066
91. Mizyed S, Georghiou PE, Bancu M, Cuadra B, Rai AK, Cheng P, Scott LT (2001) J Am Chem Soc 123:12770–12774
92. Buncel E, Crampton MR, Strauss TJ, Terrier F (1984) Electron deficient aromatic and heteroaromatic-base interactions: the chemistry of anionic sigma complexes. Elsevier, New York
93. Pogoreltsev A, Solel E, Pappo D, Keinan E (2012) Chem Commun 48:5425–5427
94. Gershoni-Poranne R, Pappo D, Solel E, Keinan E (2009) Org Lett 11:5146–5149
95. Mattarella M, Berstis L, Baldridge KK, Siegel JS (2014) Bioconjugate Chem 25:115–128
96. Mattarella M, Haberl JM, Ruokolainen J, Landau EM, Mezzenga R, Siegel JS (2013) Chem Commun 49:7204–7206
97. Stuparu MC (2012) J Polym Sci A Polym Chem 50:2641–2649
98. Butterfield A (2008) M.S. Thesis, University of Zurich, Zurich
99. Huang R, Huang W, Wang Y, Tang Z, Zheng L (1997) J Am Chem Soc 119:5954–5955
100. Bancu M, Rai AK, Cheng PC, Gilardi RD, Scott LT (2004) Synlett 173–176

101. Miyajima D, Tashiro K, Araoka F, Takezoe H, Kim J, Kato K, Takata M, Aida T (2009) J Am Chem Soc 131:44–45
102. Ham JS (1953) J Chem Phys 21:756
103. Dey J, Will AY, Agbaria RA, Rabideau PW, Abdourazak AH, Sygula R, Warner IM (1997) J Fluoresc 7:231–236
104. Ueda A, Ogasawara K, Nishida S, Ise T, Yoshino T, Nakazawa S, Sato K, Takui T, Nakasuji K, Morita Y (2010) Angew Chem Int Ed 49:6333–6337
105. Ueda A, Nishida S, Fukui K, Ise T, Shiomi D, Sato K, Takui T, Nakasuji K, Morita Y (2010) Angew Chem Int Ed 49:1678–1682
106. Abdourazak AH, Sygula A, Rabideau PW (1993) J Am Chem Soc 115:3010–3011
107. Sygula A, Sygula R, Rabideau PW (2006) Org Lett 8:5909–5911
108. Sygula A, Fronczek FR, Sygula R, Rabideau PW, Olmstead MM (2007) J Am Chem Soc 129:3842–3843
109. Furrer F, Linden A, Stuparu MC (2013) Chem Eur J 19:13199–13206
110. Schmidt BM, Topolinski B, Roesch P, Lentz D (2012) Chem Commun 48:6520–6522
111. Kuvychko IV, Dubceac C, Deng SHM, Wang XB, Granovsky AA, Popov AA, Petrukhina MA, Strauss SH, Boltalina OV (2013) Angew Chem Int Ed 52:7505–7508
112. Sygula A, Folsom HE, Sygula R, Abdourazak AH, Marcinow Z, Fronczek FR, Rabideau PW (1994) J Chem Soc Chem Commun 2571–2572
113. Sygula A, Rabideau PW (1994) J Chem Soc Chem Commun 1497–1499
114. Steffens RJ, Baldridge KK, Siegel JS (2000) Helv Chim Acta 83:2644–2654
115. McMahon BJ (1997) B.S. Thesis, Boston College, Chestnut Hill
116. Peng L, Scott LT (2005) J Am Chem Soc 127:16518–16521
117. Bratcher MS (1996) Ph.D. Dissertation, Boston College, Chestnut Hill
118. Wu YT, Linden A, Siegel JS (2005) Org Lett 7:4353–4355
119. Marcinow Z, Sygula A, Ellern A, Rabideau PW (2001) Org Lett 3:3527–3529
120. Shi K, Lei T, Wang XY, Wang JY, Pei J (2014) Chem Sci 5:1041–1045
121. Weitz A, Shabtai E, Rabinovitz M, Bratcher MS, McComas CC, Best MD, Scott LT (1998) Chem Eur J 4:234–239
122. Tsefrikas VM, Arns S, Merner PM, Warford CC, Merner BL, Scott LT, Bodwell GJ (2006) Org Lett 8:5195–5198
123. Filatov AS, Ferguson MV, Spisak SN, Li B, Campana CF, Petrukhina MA (2014) Cryst Growth Des 14:756–762
124. Rai AK (1996) M.S. Thesis, Boston College, Chestnut Hill
125. Wegner HA, Scott LT, de Meijere A (2003) J Org Chem 68:883–887
126. Allemann O, Duttwyler S, Romanato P, Baldridge KK, Siegel JS (2011) Science 332: 574–577
127. Vollhardt KPC (1977) Acc Chem Res 10:1–8
128. Steinberg BD, Jackson EA, Filatov AS, Wakamiya A, Petrukhina MA, Scott LT (2009) J Am Chem Soc 131:10537–10545
129. Seiders TJ, Baldridge KK, Siegel JS (2001) Tetrahedron 57:3737–3742
130. Rabideau PW, Abdourazak AH, Folsom HE, Marcinow Z, Sygula A, Sygula R (1994) J Am Chem Soc 116:7891–7892
131. Clayton MD, Marcinow Z, Rabideau PW (1996) J Org Chem 61:6052–6054
132. Sygula A, Marcinow Z, Fronczek FR, Guzei I, Rabideau PW (2000) Chem Commun 2439–2400
133. Mehta G, Shahk SR, Ravikumarc K (1993) J Chem Soc Chem Commun 1006–1008
134. Sakurai H, Daiko T, Hirao T (2003) Science 301:1878
135. Sastry GN, Jemmis ED, Mehta G, Shah SR (1993) J Chem Soc Perkin Trans 2:1867–1871
136. Sakurai H, Daiko T, Sakane H, Amaya T, Hirao T (2005) J Am Chem Soc 127:11580–11581
137. Amaya T, Sakane H, Muneishi T, Hirao T (2008) Chem Commun 765–767
138. Amaya T, Mori K, Wu HL, Ishida S, Nakamura J, Murata K, Hirao T (2007) Chem Commun 1902–1904

139. Amaya T, Hifumi M, Okada M, Shimizu Y, Moriuchi T, Segawa K, Ando Y, Hirao T (2011) J Org Chem 76:8049–8052
140. Schmidt BM, Topolinski B, Higashibayashi S, Kojima T, Kawano M, Lentz D, Sakurai H (2013) Chem Eur J 19:3282–3286
141. Chen JJ, Onogi S, Hsieh YC, Hsiao CC, Higashibayashi S, Sakurai H, Wu YT (2012) Adv Synth Calal 354:1551–1558
142. Higashibayashi S, Onogi S, Srivastava HK, Sastry GN, Wu YT, Sakurai H (2013) Angew Chem Int Ed 52:7314–7316
143. Higashibayashi S, Baig RBN, Morita Y, Sakurai H (2012) Chem Lett 41:84–86
144. Shrestha BB, Karanjit S, Panda G, Higashibayashi S, Sakurai H (2013) Chem Lett 42: 386–388
145. Higashibayashi S, Sakurai H (2008) J Am Chem Soc 130:8592–8593
146. Higashibayashi S, Sakurai H (2007) Chem Lett 36:18–19
147. Reza AFGM, Higashibayashi S, Sakurai H (2009) Chem Asian J 4:1329–1337
148. Higashibayashi S, Reza AFGM, Sakurai H (2010) J Org Chem 75:4626–4628
149. Tsuruoka R, Higashibayashi S, Ishikawa T, Toyota S, Sakurai H (2010) Chem Lett 39: 646–647
150. Imamura K, Takimiya K, Otsubo T, Aso Y (1999) Chem Commun 1859–1860
151. Furukawa S, Kobayashi J, Kawashima T (2009) J Am Chem Soc 131:14192–14193
152. Higashibayashi S, Tsuruoka R, Soujanya Y, Purushotham U, Sastry GN, Seki S, Ishikawa T, Toyota S, Sakurai H (2012) Bull Chem Soc Jpn 85:450–467
153. Tan Q, Higashibayashi S, Karanjit S, Sakurai H (2012) Nature Commun 3:891
154. Amaya T, Seki S, Moriuchi T, Nakamoto K, Nakata T, Sakane H, Saeki A, Tagawa S, Hirao T (2009) J Am Chem Soc 131:408–409
155. Morita Y, Nakao S, Haesuwannakij S, Higashibayashi S, Sakurai H (2012) Chem Commun 48:9050–9052
156. Amaya T, Nakata T, Hirao T (2009) J Am Chem Soc 131:10810–10811
157. Abdourazak AH, Marcinow Z, Sygula A, Sygula R, Rabideau PW (1995) J Am Chem Soc 117:6410–6411
158. Hagen S, Bratcher MS, Erickson MS, Zimmermann G, Scott LT (1997) Angew Chem Int Ed 36:406–408
159. Petrukhina MA, Andreini KW, Peng L, Scott LT (2004) Angew Chem Int Ed 43:5477–5481
160. Gallego M, Calbo J, Aragó J, Calderon RMK, Liquido FH, Iwamoto T, Greene AK, Jackson EA, Pérez EM, Ortí E, Guldi DM, Scott LT, Martín N (2014) Angew Chem Int Ed 53:2170–2175
161. Clayton MD, Rabideau PW (1997) Tetrahedron Lett 38:741–744
162. Wu TC, Hsin HJ, Kuo MY, Li CH, Wu YT (2011) J Am Chem Soc 133:16319–16321
163. Hsiao CC, Lin YK, Liu CJ, Wu TC, Wu YT (2010) Adv Synth Catal 352:3267–3274
164. Chen MK, Hsin HJ, Wu TC, Kang BY, Lee YW, Kuo MY, Wu YT (2014) Chem Eur J 20: 598–608
165. Scott LT, Bratcher MS, Hagen S (1996) J Am Chem Soc 118:8743–8744
166. Ansems RBM, Scott LT (2000) J Am Chem Soc 122:2719–2724
167. Forkey DM, Attar S, Noll BC, Koerner R, Olmstead MM, Balch AL (1997) J Am Chem Soc 119:5766–5767
168. Wang L, Shevlin PB (2000) Org Lett 2:3703–3705
169. Amsharov KY, Kabdulov MA, Jansen M (2012) Angew Chem Int Ed 51:4594–4597
170. Bronstein HE, Choi N, Scott LT (2002) J Am Chem Soc 124:8870–8875
171. Chang HI, Huang HT, Huang CH, Kuo MY, Wu YT (2010) Chem Commun 46:7241–7243
172. Biedermann PU, Pogodin S, Agranat I (1999) J Org Chem 64:3655–3662
173. Bronstein HE, Scott LT (2008) J Org Chem 73:88–93
174. Wegner HA, Reisch H, Rauch K, Demeter A, Zachariasse KA, de Meijere A, Scott LT (2006) J Org Chem 71:9080–9087
175. Fowler PW, Manolopoulos DE (2006) An atlas of fullerenes. Dover Publications, Mineola

176. Thilgen C, Herrmann A, Diederich F (1997) Angew Chem Int Ed 36:2268–2280
177. Wu TC, Chen MK, Lee YW, Kuo MY, Wu YT (2013) Angew Chem Int Ed 53:1289–1293
178. Whalley AC, Plunkett KN, Gorodetsky AA, Schenck CL, Chiu CY, Steigerwald ML, Nuckolls C (2011) Chem Sci 2:132–135
179. Baldridge KK, Siegel JS (1997) Theoret Chem Acc 97:67–71
180. Scott LT, Jackson EA, Zhang Q, Steinberg BD, Bancu M, Li B (2012) J Am Chem Soc 134:107–110
181. Kawasumi K, Zhang Q, Segawa Y, Scott LT, Itami K (2013) Nat Chem 5:739–744
182. Filatov AS, Scott LT, Petrukhina MA (2010) Cryst Growth Des 10:4607–4621
183. Yamada N, Ueno K, Nishimura J, Okada Y (2010) Patent US 7,794,854 B2

Top Curr Chem (2014) 349: 121–158
DOI: 10.1007/128_2013_465

Published online: 25 October 2013

# Strategies in Organic Synthesis for Condensed Arenes, Coronene, and Graphene

**Anne-Florence Tran-Van and Hermann A. Wegner**

**Abstract** Graphene-type structures are without doubt one of the most exciting carbon-based materials known. Although graphene is mostly prepared by physical methods (CVD, exfoliation), organic synthesis represents a powerful alternative to access graphene-type structures in a selective and reproducible manner. Although graphene has been hyped as a "new" material, the resemblence to polycyclic aromatic hydrocarbons (PAHs) offers a long history in organic chemistry on which all new endeavors are built. In this review we demonstrate the state-of-the-art of organic synthetic strategies for the preparation of graphene-type structures on selected examples.

**Keywords** Catalysis · Coupling reactions · Graphene · Organic synthesis · Polycyclic aromatic hydrocarbons

## Contents

1 Introduction ..... 122
2 Synthetic Methods to Assemble Graphene-Type Structures ..... 122
2.1 Pioneering Synthesis of PAHs ..... 124
2.2 Syntheses via the Diels–Alder Reaction ..... 126
2.3 Cyclotrimerization ..... 132
2.4 Aryl–Aryl-Coupling Reactions ..... 137
2.5 Annulation Reactions ..... 142
2.6 Ring Closing Metathesis ..... 146

A.-F. Tran-Van
Departement für Chemie, Universität Basel, St.-Johanns Ring 19, 4056 Basel, Switzerland

H.A. Wegner (✉)
Institut für Organische Chemie, Justus-Liebig Universität, Heinrich-Buff-Ring 58, 35392 Giessen, Germany
e-mail: Hermann.A.Wegner@org.Chemie.uni-giessen.de

3 Synthetic Methods for the Extension of Graphene-Type Structures ..... 146
3.1 Polymerization Reactions ..... 147
3.2 Postfunctionalization of PAHs for the Extension to Graphene ..... 147
3.3 Direct Extension of PAHs by Diels–Alder Reaction ..... 148
4 Surface Assisted Methods for the Synthesis of Graphene-Type Structures ..... 149
5 Summary, Conclusions, and Outlook ..... 150
References ..... 152

## 1 Introduction

A material possessing no resistance, high stability, low weight, low toxicity, and high abundance – is this just a dream? Graphene – a network of pure carbon atoms just one atom thick – is the latest star in the sky of new materials [1–5]. The preparation of graphene currently relies largely on physical methods, such as micromechanical cleavage from highly ordered pyrolytic graphite, chemical vapor deposition (CVD) [6, 7], or chemical methods from graphene oxide [8]. Recently, surface based methods have also been developed, relying on the self-assembly of a mono-layer of molecules on a substrate followed by pyrolysis to form the graphene layer [9]. On closer inspection, graphene consists of anullated benzene rings and exhibits the structural characteristics of a polycyclic hydrocarbon (PAH). This class of compounds was an early area of study in organic chemistry, not only from a materials point of view but also in terms of the byproducts from combustion processes (Fig. 1). With this background, organic synthetic methods should be and have been applied to access defined graphene-type structures [10–13].

In this respect the application of organic synthetic methods to prepare graphene-type structures is still in its infancy. Early endeavours in this direction have recently been summarized [14–16]. Therefore this review aims mainly to give an overview of exemplary organic synthetic methodologies capable of assembling large polycyclic aromatics as graphene-type structures. We do not claim completeness. We will highlight the potential of the current status of organic chemistry in the light of graphene. We concentrate on flat six-membered ring structures, as bowl-shaped geometries are treated in a separate chapter in this book. The focus is on unsubstituted PAHs, only mentioning other examples in special cases.

## 2 Synthetic Methods to Assemble Graphene-Type Structures

Aromatic chemistry is as old as organic chemistry itself. In the beginning most aromatic compounds were isolated from coal tar and then further functionalized. Early on there were methods developed to assemble aromatic molecules from smaller precursors. The larger the compound the more difficult its synthesis. The

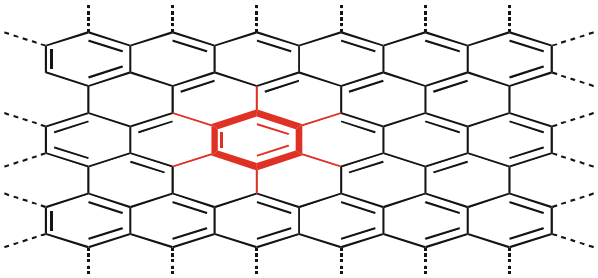

**Fig. 1** Graphene – a large polycyclic aromatic hydrocarbon

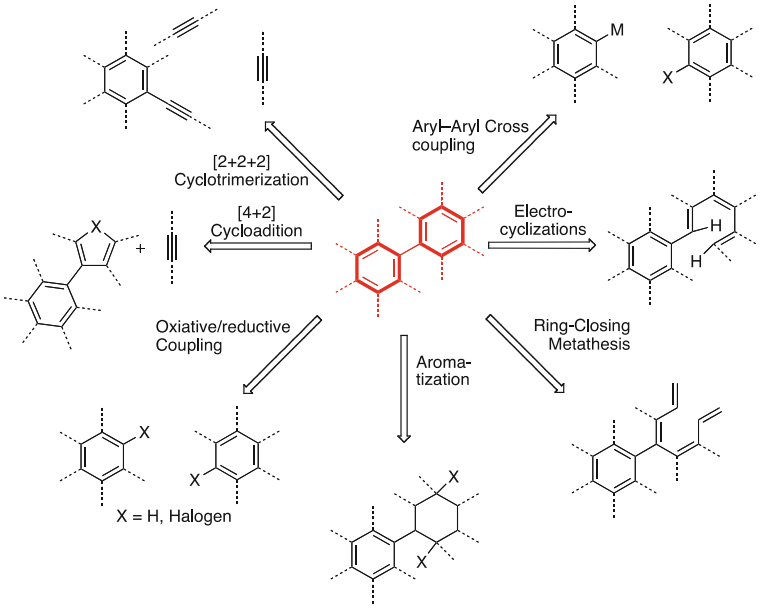


**Fig. 2** Organic synthesis strategies to assemble graphene-like structures

main challenge compared to other target orientated synthetic efforts, especially compared to the total syntheses of natural products, derives from the lack of functional groups in the final target. These have to be removed during preparation. Alternatively, unreactive bonds, such as C–H bonds, have to be activated to form new connections. Furthermore, for larger structures solubility becomes an issue, which is mostly addressed by adding solubilizing groups. Otherwise, heterogenous, biphasic conditions must be applied (Fig. 2).

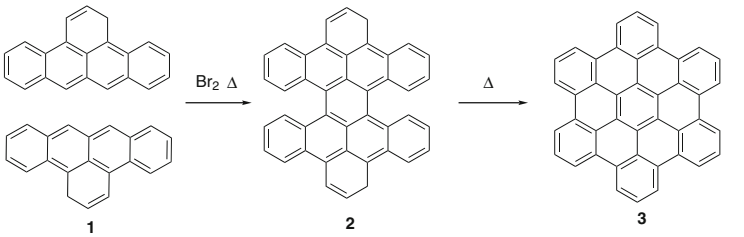


**Scheme 1** Synthesis of HBC via condensation of PAH fragments by Clar et al. [17]

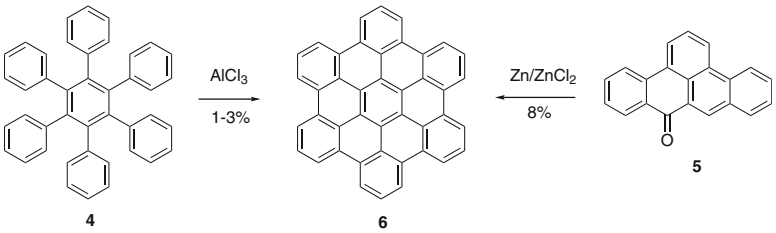


**Scheme 2** Synthesis of HBC by Halleux et al. [18]

## *2.1 Pioneering Synthesis of PAHs*

Polycyclic aromatic hydrocarbons (PAHs) were accessed originally by extraction from oil, tar, or coal as combustion byproducts. Hence, the first examples of syntheses of PAHs relied on reproducing such conditions with relatively harsh conditions such as high temperature. Therefore, products were obtained as mixtures of various isomers. Already at that time issues such as insolubility made the purification and characterization of the product a challenge.

Early work from Scholl et al. provided the first selective syntheses and characterizations of extended PAHs. One example is the synthesis of hexabenzocoronene (HBC) via dimerization of dibenzo-*peri*-naphthene by Clar et al. (Scheme 1) [17]. The synthesis proceeds through bromination to a perbromide, eliminating HBr upon heating. This observation was rationalized by the formation of the dimer **2** which, upon heating (melting) to 482°C, formed the insoluble and extremely stable HBC **3**.

In another synthesis of HBC **6** proposed by Halleux et al. [18] the molecule was synthesized via two different methods to prove unambiguously the structure of the desired product. One strategy was the cyclodehydrogenation of hexaphenylbenzene (**4**) which is a method still used by Müllen and co-workers. The second method was the condensation of dibenz[*1*,*9*;*2*,*3*]anthrone **5** with $Zn/ZnCl_2$ (Scheme 2) [18].

The addition of organometallic compounds to benzoquinone derivatives was an early approach for the synthesis of PAHs. The diol obtained was subsequently aromatized and cyclodehydrogenated to give the PAH [19–22]. An example of such an approach is depicted in Scheme 3. Clar et al. synthesized a cata-hexabenzocoronene **9** by this method.

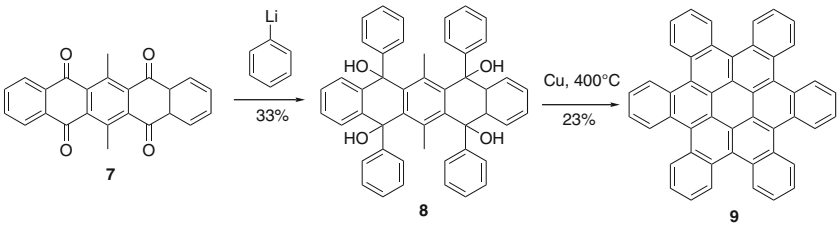


**Scheme 3** Synthesis of HBC by Clar et al.

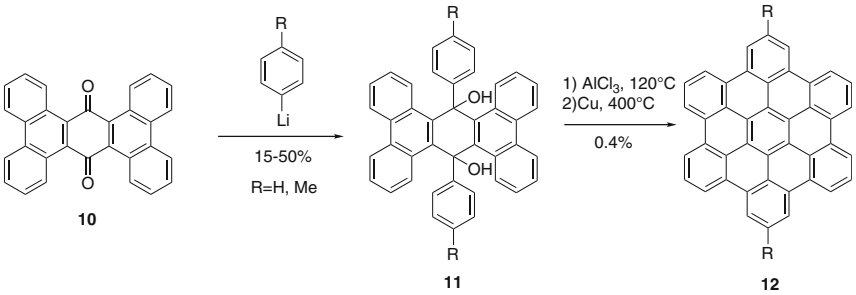


**Scheme 4** Synthesis of HBC by Schmidt et al. [23]

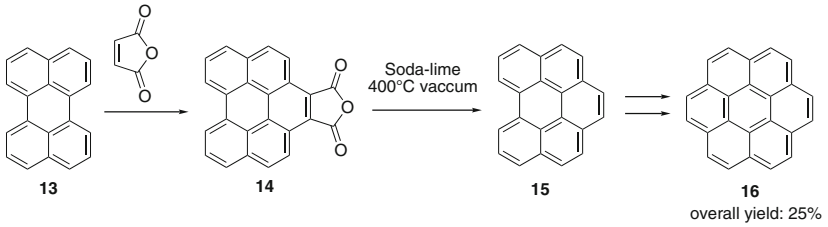


**Scheme 5** Synthesis of coronene **16** [22, 24]

The same approach was followed by Schmidt et al. to access substituted HBCs **12**, using a substituted phenyl-lithium reagent [23] (Scheme 4). For the first time, structure-property relationships could be systematically addressed with this reliable route to differently substituted HBCs. In this case the UV and IR spectroscopic properties were investigated. Indeed, a methyl substituent intensifies the 0–0 transition of the α band due to the different symmetry compared to the unsubstituted HBC (Symmetry $D_{6h}$). Additionally, the substitution increased its solubility.

The extension of PAHs using maleic anhydride in the presence of an oxidizing agent was also explored by Clar and Zander. The decarbonylation took place with soda-lime under vacuum sublimation. Coronene **16** and ovalene were synthesized by this method (Scheme 5) [22, 24].

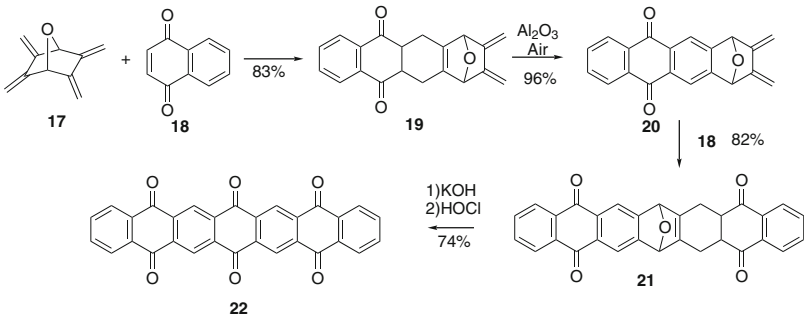


**Scheme 6** Synthesis of polyacene **22** via Diels–Alder [25]

Although milder conditions have been developed for the selective synthesis of PAHs since then, most of the methods developed during this pioneering work are still used to the present day. Moreover, progress in analytical methods has greatly enhanced the characterization of PAHs. The following sections illustrate more recent syntheses of PAHs, highlighting the advancement in organic chemistry based on the early roots described above.

## *2.2 Syntheses via the Diels–Alder Reaction*

The Diels–Alder reaction represents one of the most efficient methods for assembling six-membered carbon cycles. As this structural element is the characteristic of graphene-type structures, Diels–Alder reactions have been applied successfully for the synthesis of PAHs such as acene and coronene.

Various oligoacenes have been synthesized using quinone derivatives as the dienophile in Diels–Alder reactions. One example is the synthesis of a series of epoxypolyacenequinones **19**–**21** by Miller et al., via repetitive Diels–Alder/oxidation reactions with appropriate bis-dienes and quinones. The ether-bridge could be cleaved to give the desired acene **22** with up to 11 linearly annulated rings (Scheme 6) [25]. The final aromatization, however, has not been reported.

Another example of a Diels–Alder reaction of benzoquinone **24** with a substituted cyclopentadienone **23** is the synthesis of a molecular ribbon (Scheme 7) [26]. The compound is twisted in two directions and does not adopt a single longitudinal twist as originally intended. Again, no route for the aromatization has been described.

Arynes are also highly suitable dienophiles for the synthesis of PAHs via Diels–Alder reactions [27, 28]. For example, Kitamura et al. reported a new hypervalent iodide precursor **27** for the in situ generation of naphthyne, which can be trapped in a Diels–Alder reaction to form PAHs, such as **28** and **29** (Scheme 8) [29].

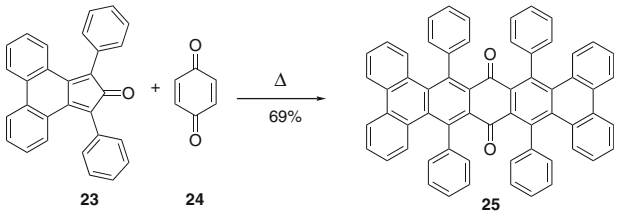


**Scheme 7** Synthesis of a twisted ribbon **25** [26]

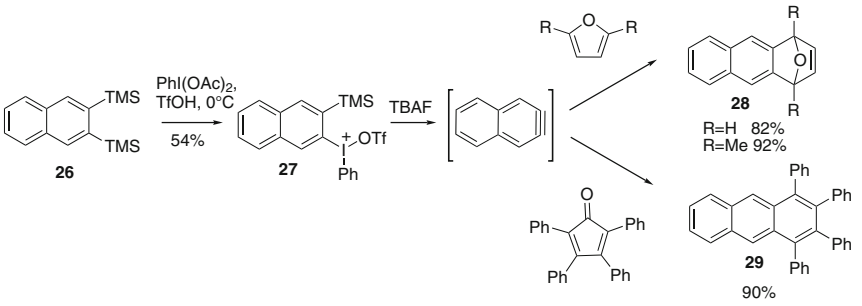


**Scheme 8** Synthesis of PAHs **28** and **29** using an aryne precursor [29]

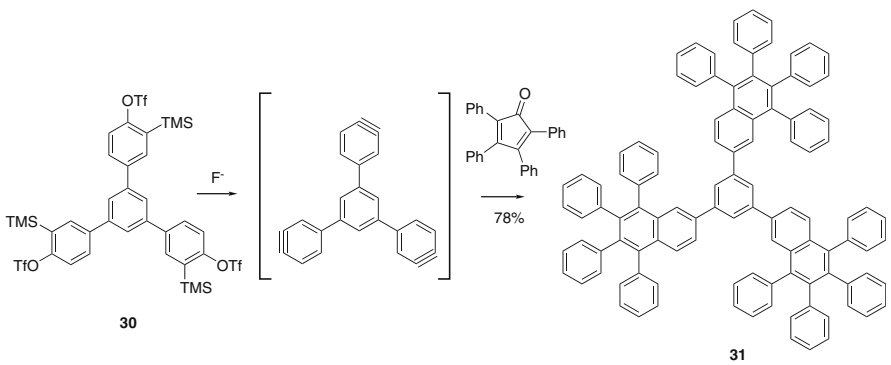


**Scheme 9** Synthesis of extended PAH **31** using an aryne Diels–Alder reaction [30]

Similarly, the trisaryne equivalent **30** underwent Diels–Alder reaction under mild conditions with different dienes, yielding various PAHs [30]. An impressive example is shown in Scheme 9, where 3 new aromatic rings are formed connecting in total 19 aromatic rings to form product **31**.

The synthesis of PAHs was also achieved by an intramolecular Diels–Alder reaction of an ene-diene stilbene derivative **32** (Scheme 10) followed by cyclodehydrogenation [31, 32].

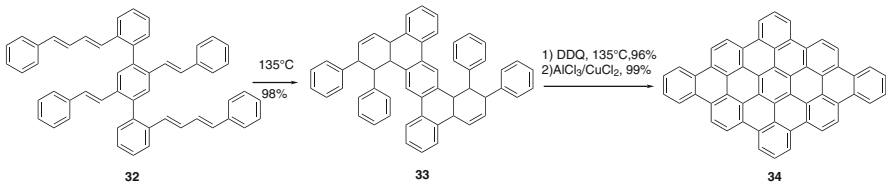


**Scheme 10** Synthesis of PAH **34** via intramolecular Diels–Alder reaction [31, 32]

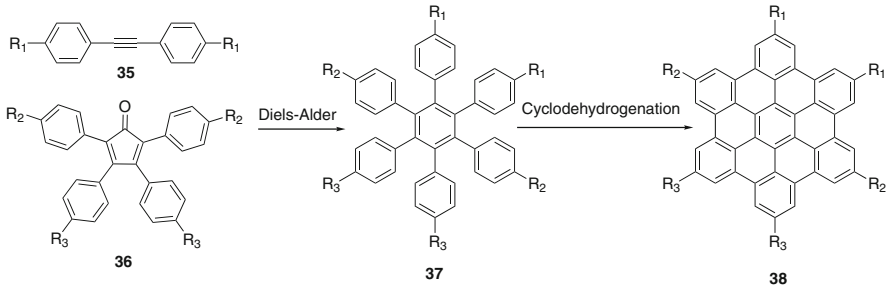


**Scheme 11** General strategy for the synthesis of HBCs **38** via Diels–Alder reaction followed by dehydrogenation

Over the last few decades Müllen and co-workers have perfected the Diels–Alder/cyclodehydrogenation sequences to synthesize graphene-type structures [10]. The general strategy is illustrated in Scheme 11 for the preparation of hexa-substituted HBCs **38**.

The advantage of this method is that it permits the selective synthesis of substituted HBCs. Without any functional groups, HBCs are insoluble in most organic solvents. The addition of solubilizing chains facilitated the characterization of those molecules. In addition, the processability of such HBCs allows for their application as functional materials. For example, alkyl substituted HBCs form discotic mesophases, which show liquid crystalline behavior [33].

Employment of the Diels–Alder/dehydrogenation strategy facilitated the synthesis of larger and larger graphene-type structures, such as the supernaphthalene **42** (Scheme 12) [34].

Müllen and coworkers took the method to the next level by iterating the Diels–Alder/dehydrogenation approach. This way the dendrimeric polyphenylenes are synthesized by repeated Diels-Alder reaction involving ethynyl-substituted tetraphenylcyclopentadienones **44** and a tetraethynylbiphenyl core **43**. Up to three generations of dendrimers have been synthesized by Diels–Alder/deprotection repeating sequences. An example is shown in Scheme 13 [35]. With a similar method, a 3-fold symmetric graphite disk consisting of 55 rings was prepared [36]. The large PAHs could only be characterized by MALDI spectrometry as their insolubility prevented the use of other analytical methods such as NMR spectroscopy.

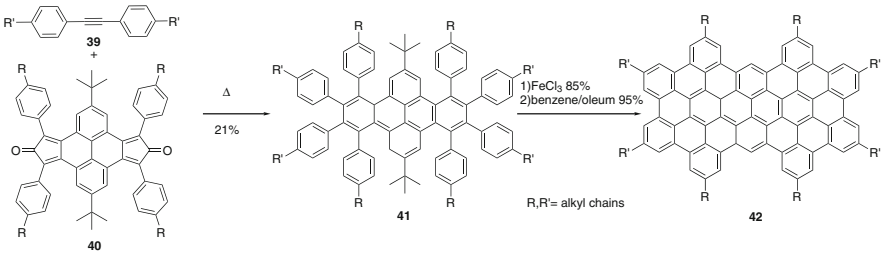


**Scheme 12** Synthesis of supernaphthalene **42** [34]

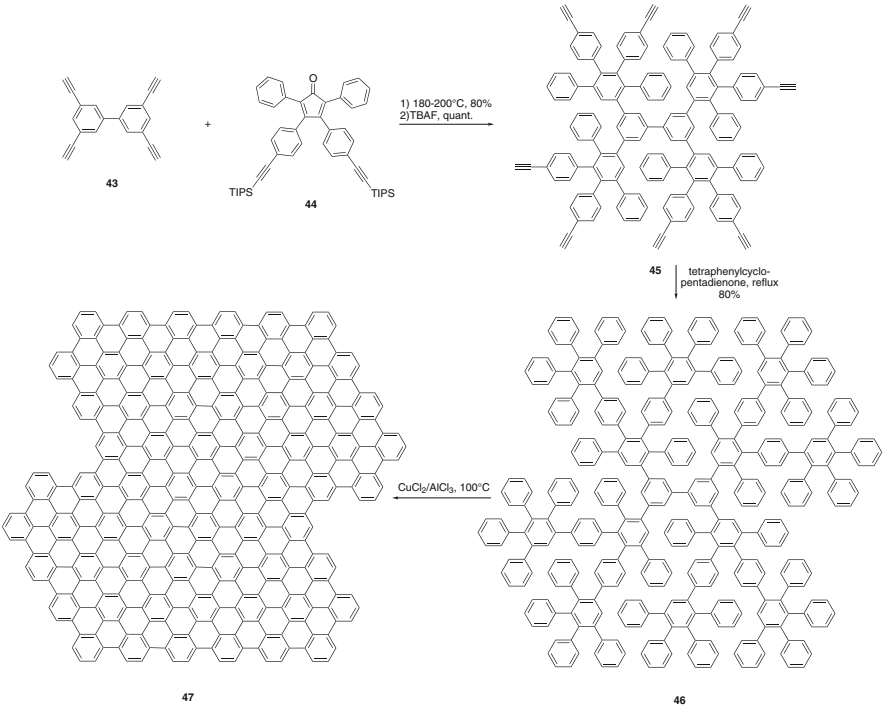


**Scheme 13** Iterative Diels–Alder/deprotection strategy for the synthesis of nano-graphene **47** [35]

Interestingly, even oligophenylenes with overlapping phenyl groups have been converted to planar graphene-type structures upon cyclodehydrogenation through a skeletal rearrangement [37, 38]. By changing the *meta* connection at the central benzene ring to *para* the supernaphthalene **50** was synthesized (Scheme 14).

Coronene **16** can be viewed as a "superbenzene." The series was continued with the synthesis of supernaphthalene **53** and supertriphenylene **56**, using different phenylacetylenes and tetraphenyl substituted cyclopentadienone. Two selected examples **53** and **56** are shown in Scheme 15 [39, 40].

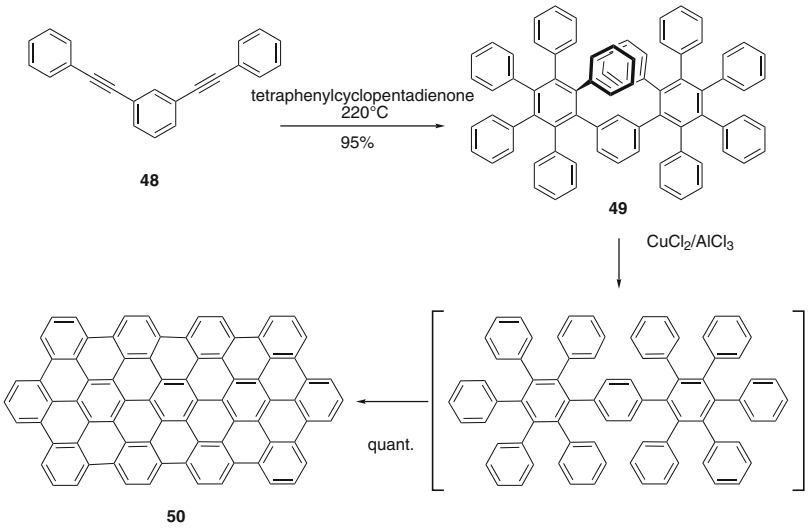


**Scheme 14** Synthesis of a graphene-type structure **50** via Ph-migration [37, 38]

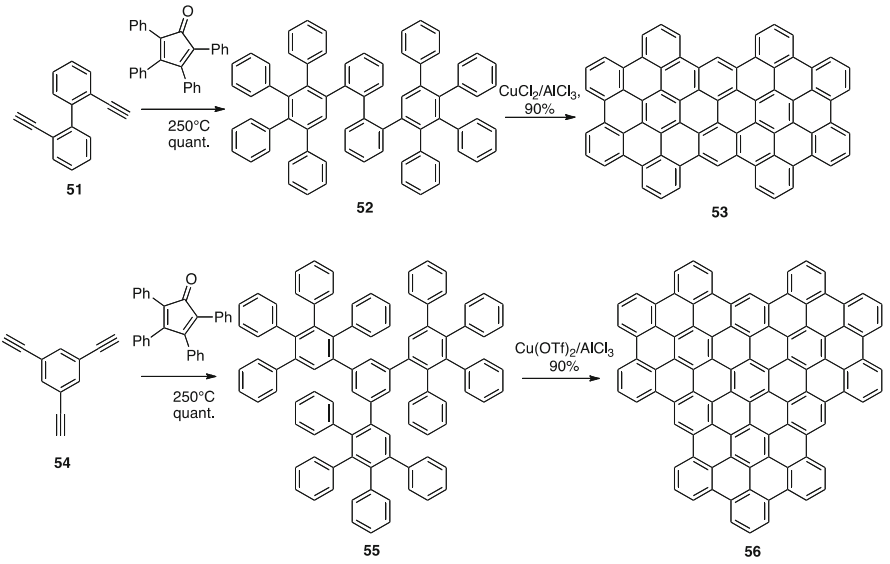


**Scheme 15** Synthesis of superbenzenoids **53** and **56** [39, 40]

The method was pushed to the extreme with the synthesis of a giant 222 carbon graphite sheet **63** by the Müllen group [41]. Two strategies were presented to access such a nano-graphene structure. The first pathway relied on a combination of Diels–Alder reactions involving cyclopentadienone derivatives and alkynes **61**, and a cyclotrimerization of alkyne **62**. The second strategy relied exclusively on

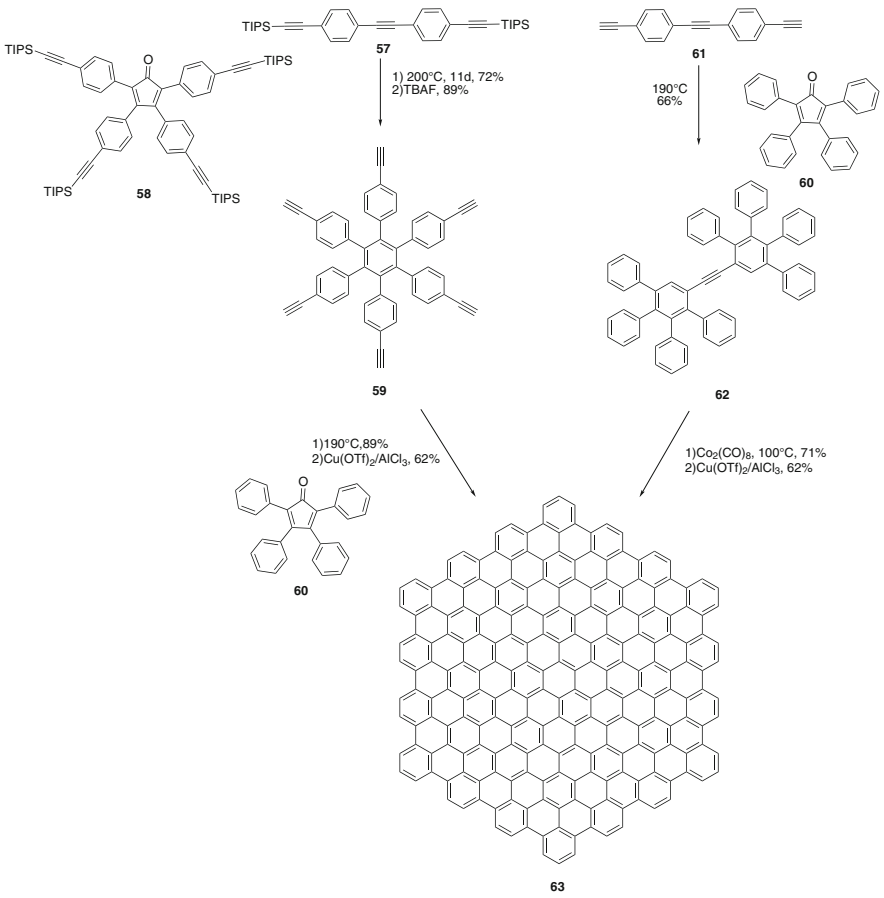


**Scheme 16** Synthesis of a giant 222 graphite sheet **63** [41]

Diels–Alder reactions. Bulky protecting group were used on the outer alkynes, encouraging a selective Diels–Alder reaction. However, the steric bulk slowed down the reaction rate, which required 11 days for complete conversion. The obtained polyphenylene was then planarized by cyclodehydrogenation to give the hexagonal graphene sheet **63** which was characterized by MALDI spectrometry (Scheme 16).

There are two main edge formations possible in graphene type structures as depicted in Fig. 3. It has been shown that the periphery of graphene plays a crucial role in its electronic structure, self-assembly behavior, and reactivity. Zig-zag and armchair edges also provide different reactive sites for further functionalization.

In the following, examples featuring the Diels–Alder/dehydrogenation strategy are presented. By choosing substituted cyclopentadienones and substituted alkynes, a myriad of graphene-type structures of different architectures varying in sizes and periphery can be accessed [42–44]. Thus, by modifying the cyclopentadienone **64**

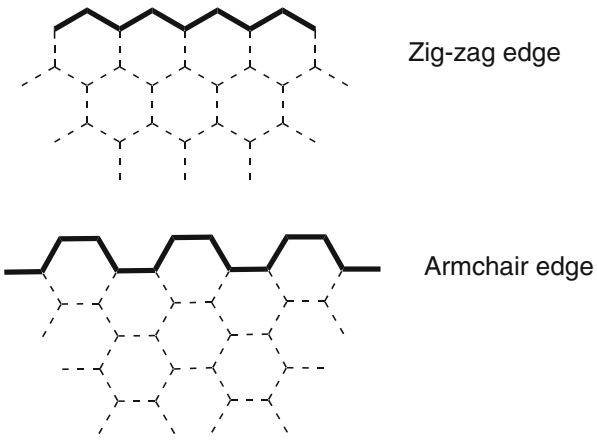


**Fig. 3** Different edges of graphene molecules

and **67** (Scheme 17, (1) and (2)) or the alkyne **70** and **75** (Scheme 17, (3) and (4)) or both (Scheme 17, (5)), PAHs with different edge types have been prepared. Introduction of different phenanthrenyl units into the precursor **75** allowed modification of the edge from fully armchair to partially zig-zag. Phenanthrene alkyne derivatives **75** were used for the PAHs with one zig-zag-edge, pyrene cyclopentadienones **79** for the two zig-zag edged PAHs. The synthesis was made using alkyl substituted building blocks to ensure solubility, thus facilitating the characterization and analysis of their properties. The properties of such zig-zag-edge molecules are enhanced over PAHs with an armchair edge obtained by the usual strategy.

## *2.3 Cyclotrimerization*

Alkyne cyclotrimerization is an elegant strategy for the synthesis of symmetrically substituted HBCs [45]. Similar to the Diels–Alder strategies described in the previous chapter, the product of the cycloaddition, the polyphenylene, can be cyclodehydrogenated to provide the final graphene-type structure. A general example is shown in Scheme 18.

With this method, a methoxy substituted polyphenylene precursor was synthesized. The molecule was adsorbed on a copper surface and the cyclodehydrogenation was thermally induced directly on the surface [46]. The synthesis of substituted HBCs permits tuning of the properties in this class of compounds, for example in a columnar supramolecular assembly [47]. The influence of substitution at the periphery with either oligoether (water soluble) or alkyl chains with different degrees of branching and different lengths has been studied [48].

The tuning of properties by synthesizing HBCs with functional groups also allows new applications. One example is the cyclotrimerization of double substituted tolane **85** (methylaryl and methoxyaryl protected arylamine), which yielded both possible isomers **86** and **87** in statistical yields (Scheme 19). These

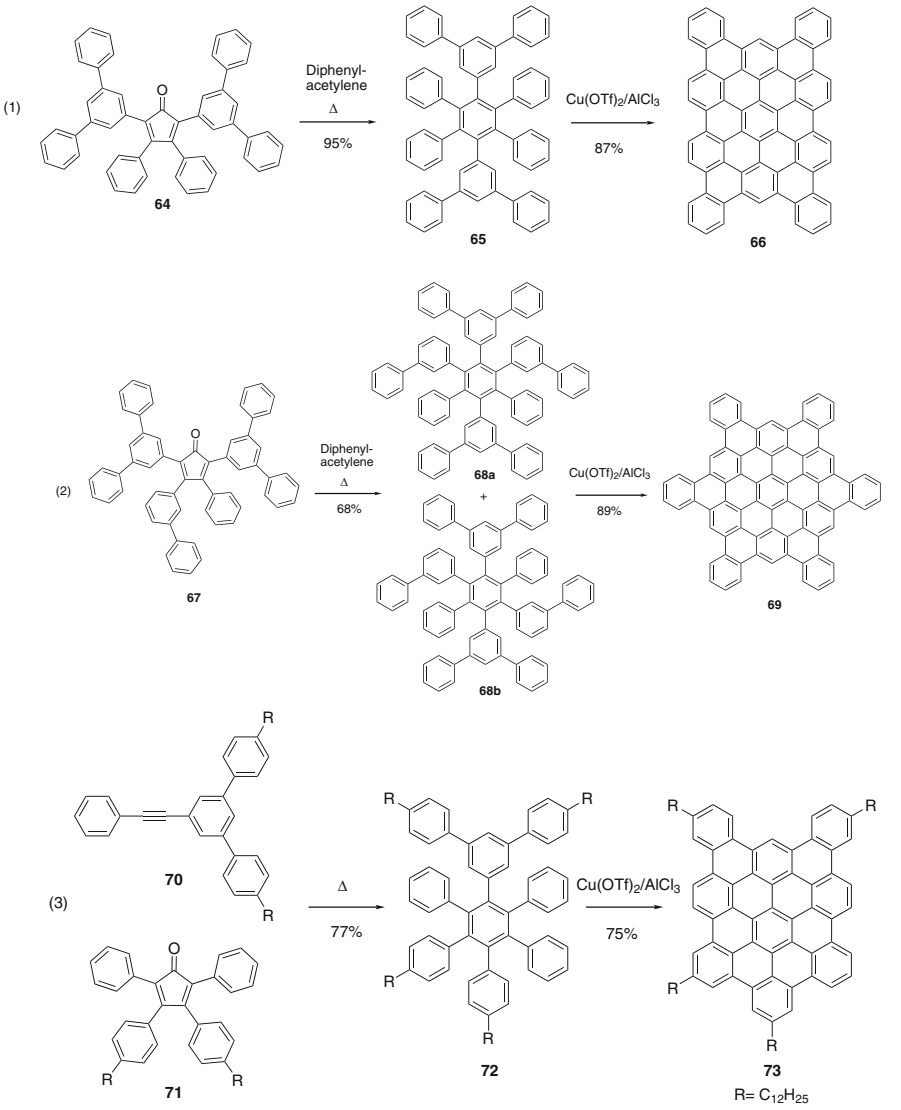


**Scheme 17** (continued)

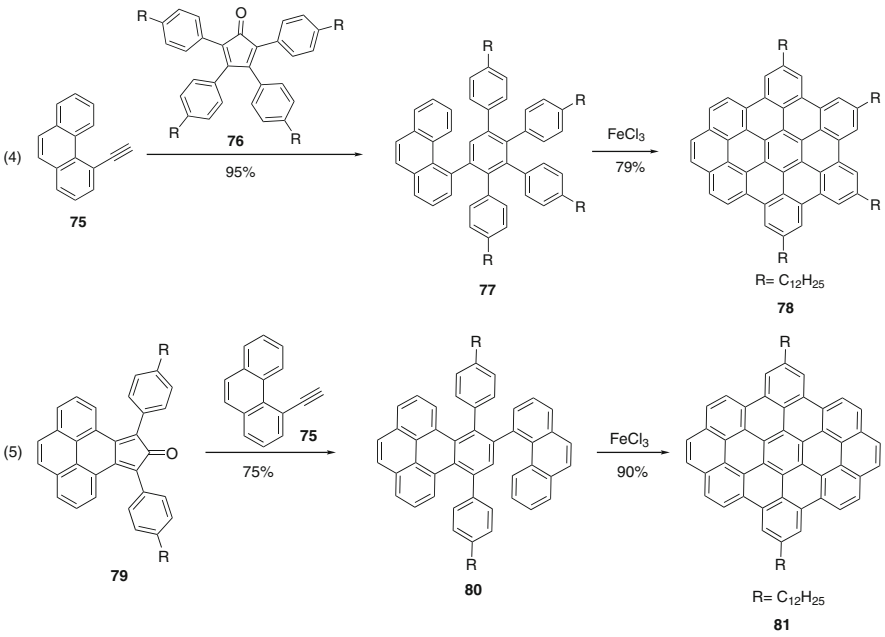


**Scheme 17** Preparation of graphene-type structures via the Diels–Alder/dehydrogenation strategy

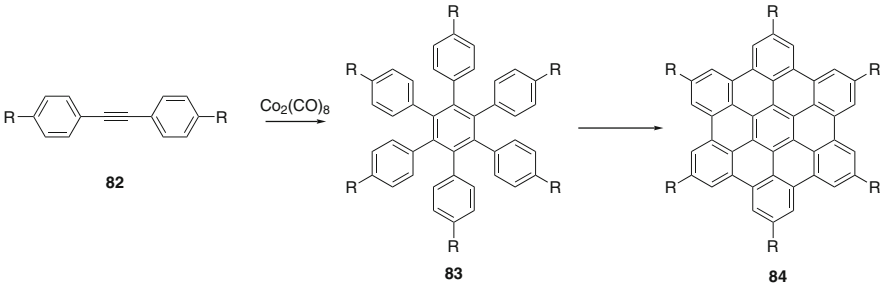


**Scheme 18** General concept for the synthesis of HBCs by alkyne cyclotrimerization

molecules with six redox-active triarylamine sites were used to study electron transfer pathways [49].

The versatility of the cyclotrimerization and the easy access to substituted phenylacetylene by modern coupling methods offers a wide range of variously decorated HBCs. An intriguing example is shown in Scheme 20. Permethoxylated hexa-*peri*-hexabenzocoronene (permethoxylated HBC) **90**, which results in a double concave conformation, was easily synthesized via cyclotrimerization of a hexamethoxysubstituted phenylacetylene **88** followed by the usual cyclodehydrogenation reaction [50]. The non-planarity of the system is explained by the steric

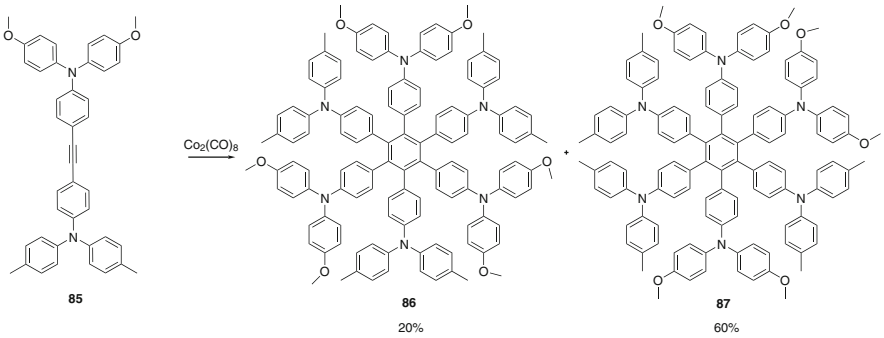


**Scheme 19** Cyclotrimerization of double substituted tolane **85** [49]

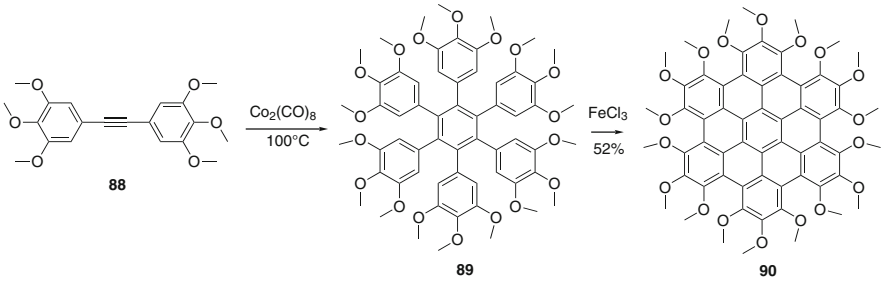


**Scheme 20** Synthesis of methoxy substituted HBC **90** [50]

hindrance between the methoxy groups at the periphery. X-Ray analysis of the complex of this **90** with fullerene or hexafluorobenzene illustrated the ability of this molecule to undergo host-guest chemistry.

A useful HBC building block has been designed for further functionalization, hexa(4-iodophenyl)-*peri*-hexabenzocoronene **93**. This compound was also prepared via cyclotrimerization of the silyl-protected alkyne **91**. With this iodo-HBC **93** further functionalization is possible despite its insolubility. Various functional groups can be attached via Sonogashira cross-coupling reactions, giving a starting point to a large series of compounds which form highly ordered columnar liquid crystals (Scheme 21) [51, 52].

Introduction of long ethylene glycol chains lead to an amphiphilic HBC [53]. This water soluble molecule can be used as a template for the fabrication of porous silica with defined nano-channels.

$C_3$ symmetric HBCs with alternating polar and apolar substituents can also be synthesized by statistical cyclotrimerization reaction of differently substituted diphenylacetylenes (e.g., ester vs. alkyl). The reaction produced a mixture of two isomers that were separated by column chromatography [54]. The synthesis was completed by cyclodehydrogenation to planarize the system. This substitution pattern has an influence on the packing mode, as the symmetry plays an important role in the self-assembling process.

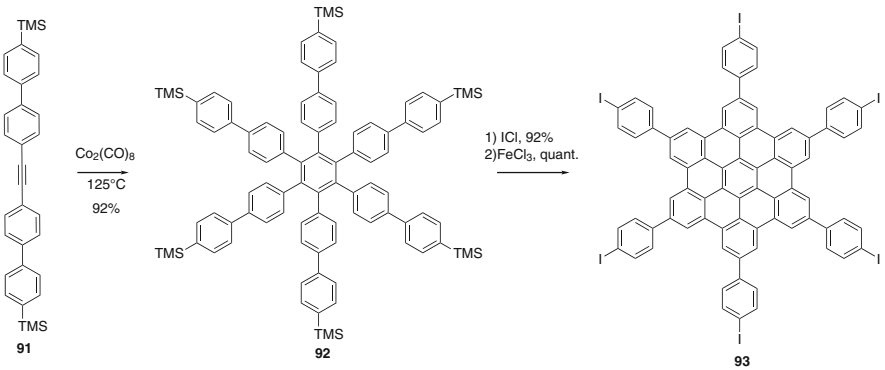


**Scheme 21** Synthesis of a substituted HBC **93** allowing further functionalization via Sonogashira cross-coupling reactions [51, 52]

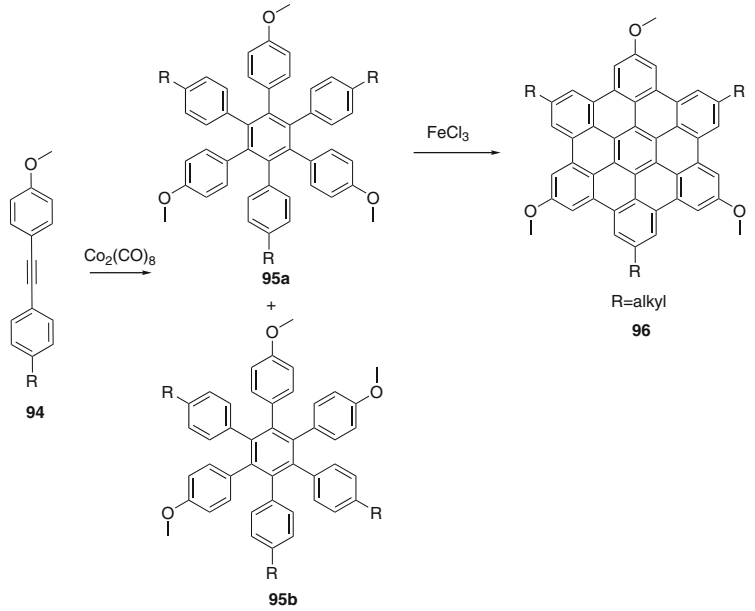


**Scheme 22** Synthesis of $C_3$ symmetric HBCs **96** [55]

Similarly, a $C_3$ symmetric *meta*-trimethoxy substituted hexaphenylbenzene precursor **95** with three alternating methoxy and alkyl (dodecyl) substituents was synthesized and planarized by cyclodehydrogenation (Scheme 22) [55]. A strong aggregation in solution was also observed (by NMR spectroscopy). In the solid state a complex helical superstructure was formed due to the influence of the methoxy groups in *meta* position as well as intermolecular interactions. After deposition on a surface, microfibers were obtained.

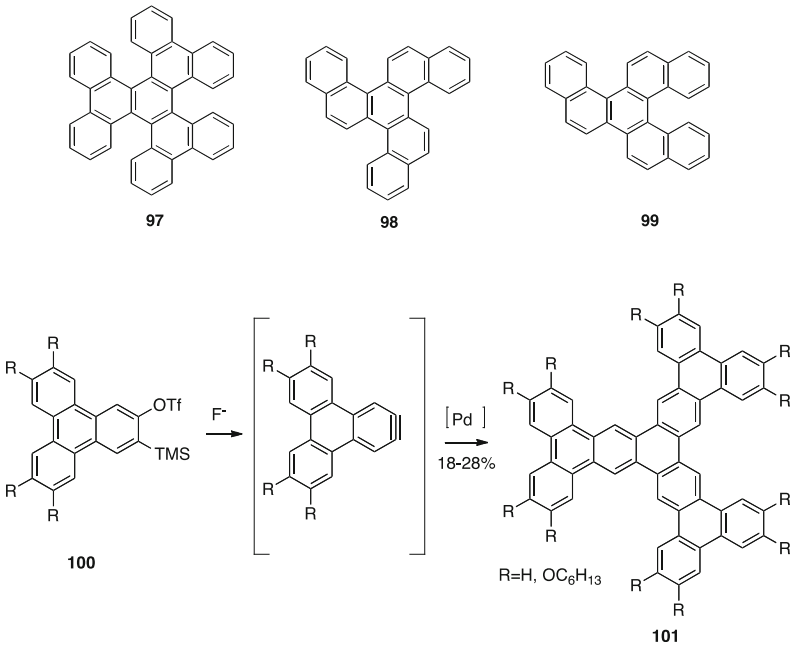


**Scheme 23** Examples of graphene-type structures assembled by trimerization of triphenylynes [56, 57]

In an analogous strategy, new graphene-type structures could be realized employing arynes as alkyne partners. The trimerization of naphtalyne and triphenylyne generated from the corresponding *ortho*-trimethylsilyl triflates gave various PAHs **97–99**, **101** as shown in Scheme 23 [56, 57].

## *2.4 Aryl–Aryl-Coupling Reactions*

### 2.4.1 Cross-Coupling Reactions

Without doubt, transition metal catalyzed cross-coupling reactions are one of the most efficient ways to join two aromatic fragments. This has also been recognized by awarding the Nobel Prize to Heck, Noyori, and Suzuki in 2010. Hence, it is not surprising that it has been used extensively to assemble PAHs. There have been numerous reviews on cross-coupling reactions. Therefore, the topic will not be elaborated on further here, despite the extraordinary importance of cross-coupling reactions [58–61]. In the area of molecular electronics, PAHs have been assembled by cross-coupling reactions for use in organic field effect transistors [62]. The effectiveness of this methodology is demonstrated by the examples shown below (Scheme 24) [63]. Twofold Suzuki coupling of the dibromoanthracene **104** with boronic ester **103** yielded trimer **105** (Scheme 25).

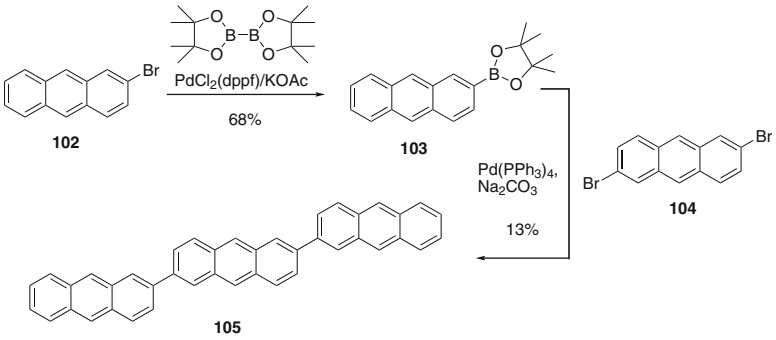


**Scheme 24** Example for a Pd-catalyzed cross coupling reaction for the synthesis of a trisanthracene **105** [63]

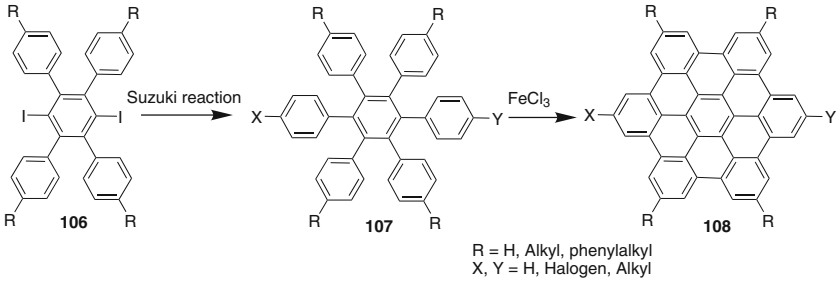


**Scheme 25** Suzuki cross-coupling reaction for the preparation of a *para*-substituted HBC **108** [64]

Similarly, a Suzuki reaction was applied to access the hexaphenylbenzene derivative **107** with two different substituents in *para* position. Dehydrogenation delivered the *para*-substituted HBC **108** [64].

### 2.4.2 Cross-Coupling Reactions Involving C–H Bond Activation

More recently, direct C–H functionalization has been developed [65] and also applied to the assembly of large aromatic structures [66]. The preparation involving C–H bond activation offers the great advantage that no pre-functionalization of the reaction partners is necessary. However, in most cases a suitable coordinating group must be present, limiting the application for the preparation of non-functionalized graphene-type structures [67]. In Scheme 26 a recent example has been presented, where a tethered aromatic C–H bond is connected via Pd-catalysis [68]. The immediate aromatization under acidic condition delivers the final PAH **111**. An example starting from bromostilbenes using Pd-catalysis has also been reported [69].

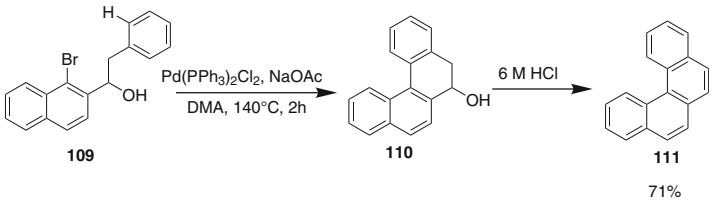


**Scheme 26** C–H Functionalization for the synthesis of graphene-type structures [68]

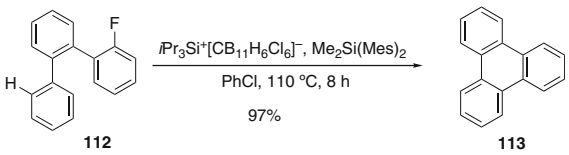


**Scheme 27** Proton-catalyzed, silane-fueled Friedel–Crafts coupling of fluoroarenes [71]

Most aryl–aryl coupling reactions involve transition metals and haloarenes. For the latter, iodine derivatives show the highest reactivity; fluorine is usually unreactive in this context [70]. Siegel and coworkers found a way to connect such unreactive C–F bonds with a C–H bond using a Si-reagent (Scheme 27) [71]. A Friedel–Crafts-type mechanism has been proposed, which is in itself a novelty. The driving force of this transformation is the formation of the very strong Si–F bond. Amsharov and coworkers were able to establish a similar reaction using a heterogenous Al-catalyst for the preparation of bucky-bowls [72].

Itami and coworkers established that pyrene can be selectively coupled with an arylboronic acid in an intermolecular fashion in the presence of a Pd-catalyst and stoichiometric amounts of chloranil as an oxidant [73]. With suitable coupling partners small graphene-type structures are accessible, which can be planarized using cyclodehydrogenation conditions (Scheme 28).

### 2.4.3 Oxidative/Reductive Coupling Reactions

Before the establishment of cross-coupling reactions, oxidative and reductive coupling reactions have been extensively used to build up large aromatic systems. The downside of this methodology, that only homo-coupling reactions can be realized, can now be seen as an advantage as it simplifies the preparation of the starting material. Also, the lack of functional groups in graphene-type structures makes obsolete the need to differentiate between different substituents. In particular, the option to connect two unfunctionalized aromatic building blocks adds greatly to its utility [74]. The Ullmann reaction represents a classical and effective tool to connect two halogen substituted aromatics under the influence of a metal as a

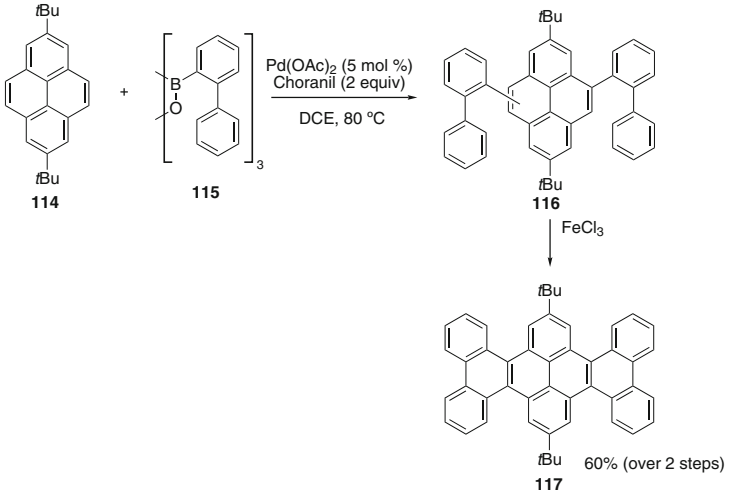


**Scheme 28** C–H functionalization of pyrene using Pd-catalysis [73]

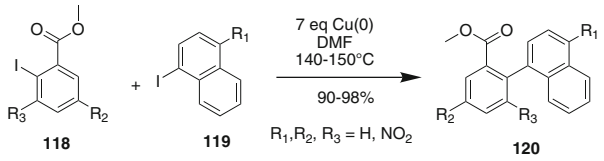


**Scheme 29** Example for an intermolecular Ullmann reaction [76]

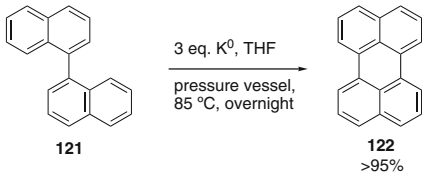


**Scheme 30** Reductive coupling of C–H bonds [77]

reducing agent [75]. In the example shown in Scheme 29, two different building blocks have been connected utilizing the different electronic properties of each of the coupling partners [76].

C–C bonds can also be built under reductive conditions. In this case elemental potassium, which is usually employed as a reducing agent, is able to connect two carbon atoms accompanied by the evolution of $H_2$ (Scheme 30). The exact mechanism is still under debate, although a radical chain reaction involving free hydrogen atoms ($H^{\bullet}$) in the two-step propagation cycle is proposed [77].

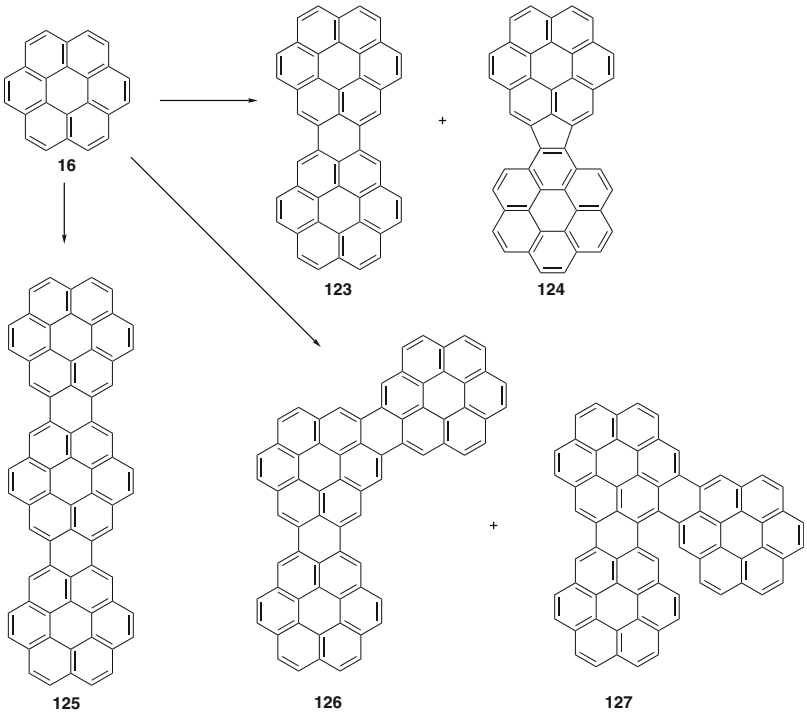


**Scheme 31** Selected products of the complex mixture of the intermolecular Scholl reaction of coronene **16** [81]

The more common way to connect two unfunctionalized aromatic rings is via the Scholl reaction, which has been employed early on in the synthesis of PAHs and has already been mentioned several times in this chapter [78]. In this case, a metal salt, such as $Fe(III)Cl_3$ [79] or $Al(III)Cl_3$, is employed which acts as the oxidizing agent. Examples shown earlier by the Müllen group feature this synthetic tool extensively, and it has proven its applicability to very large nano-graphene structures. Although very efficient in intramolecular coupling reactions, the Scholl reaction is less selective in intermolecular variations, giving rise to complex product mixtures [80]. In the example shown in Scheme 31, coronene **16** has been subjected to Scholl reaction conditions. Besides the dimers **123** and different isomers of trimer of coronene **125**–**127**, five-membered ring fusions have also been observed. A similar outcome has been observed by simply heating coronene to 550–600°C [81].

A nice feature of reductive as well as oxidative coupling reactions has been presented recently in the synthesis of quateranthene **132** (Scheme 32) [82]. After addition of the lithiated species of **128** into the bianthrone and dehydrogenation, base induced cyclization gave the intermediate **130**. Grignard addition to the ketone and subsequent reduction delivers **131**, which was then fully aromatized by a Scholl-reaction involving DDQ as an oxidant in the presence of $Sc(OTf)_3$.

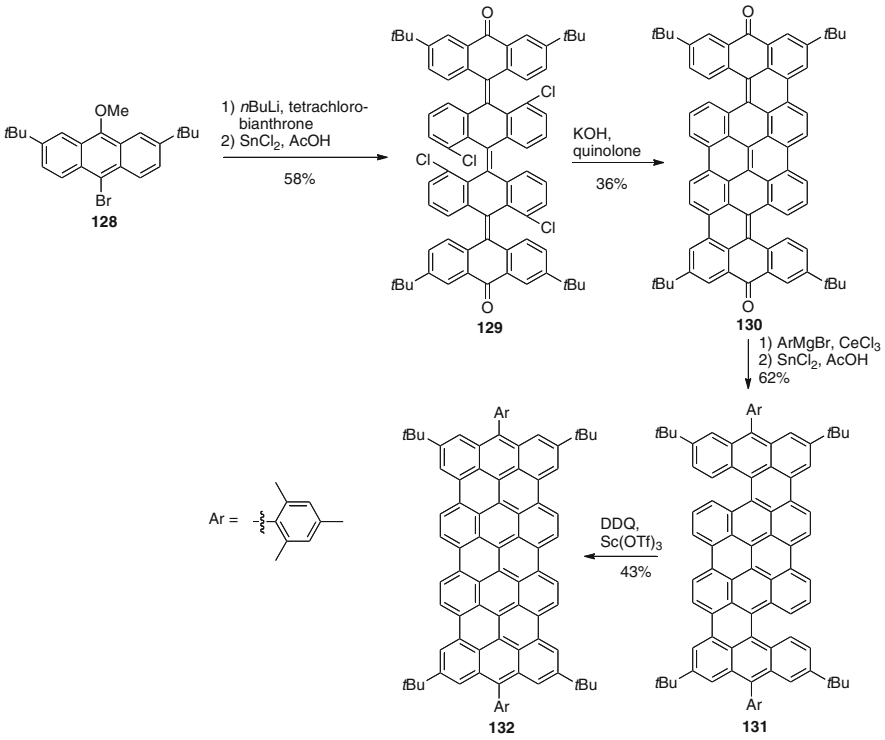


**Scheme 32** Synthesis of quateranthene **132** [82]

## *2.5 Annulation Reactions*

The extension of aromatic systems by annulation reactions is an effective way of extending smaller PAHs into larger graphene-like structures [83]. In this context multiple approaches have been devised.

### 2.5.1 Photocyclizations

Classical methods rely on electrocyclization reactions promoted by heat or, especially, by photochemical means, usually followed by an oxidation to deliver the aromatic compound. One of the most prominent routes is also known as the Mallory reaction, first reported in 1964 [84, 85]. Since then it has been further optimized [86] and applied, especially in the synthesis of helicenes [87], but also in a number of syntheses of graphene-type structures. Zhang et al. recently combined the Mallory reaction with a Scholl cyclization to access tetrabenzocoronene **135** (Scheme 33) [88]. A similar approach has been reported for the preparation of hexabenzocoronene [62].

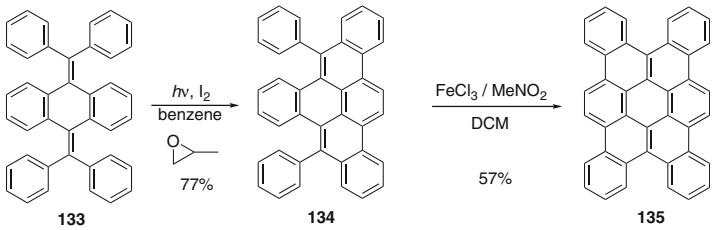


**Scheme 33** Mallory–Scholl reaction sequence for the synthesis of tetrabenzocoronene **135** [88]

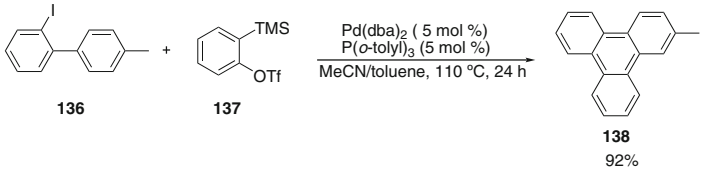


**Scheme 34** Pd-catalyzed cyclization reaction of an aryne intermediate [89]

### 2.5.2 Transition Metal Mediated Cyclizations

In the last two decades transition metal catalyzed cyclization/annulation reactions have also been reported. In most cases alkynes are cyclized within a biphenyl-containing substrate. Different modes of action for the transition metal can be distinguished. In the first case the metal undergoes an oxidative addition into an aryl–halogen bond and then performs the carbometallation of the alkyne. Here, an example by Larock and coworkers is presented, in which an in situ formed aryne species is cyclized with an iodo biaryl substrate **136** (Scheme 34) [89].

In the second case the metal acts as a π-Lewis acid activating the alkyne for a Friedel–Crafts-type cyclization [90]. With this approach small graphene-type structures can also be efficiently assembled (Scheme 35) [91].

Additionally, a mechanism via a metal–carbene intermediate has been observed. In the example shown in Scheme 36 a Ru catalyst was used to form four C–C bonds in one step for the synthesis of coronene **16** (Scheme 36) [92].

A different disconnection was recently presented by Wang and coworkers. In his approach bis(*N*-tosylhydrazone)s were cyclized using an Rh-catalyst [93]. The starting materials are easily accessible via Suzuki cross-coupling reaction (Scheme 37).

In all cases presented above, annulation reactions were limited to intramolecular arrangements. There are also transformations involving two independent reaction partners. In 2005 a Cr-mediated synthesis of PAHs from halobiaryls was published [94]. The 2,2′-dihalobiaryl starting material **150** is first treated with BuLi before addition of the Cr reagent. Final treatment with an acetylenic reaction partner delivers the phenanthrene core **151** (Scheme 38). Recently, Wu and coworkers presented a Pd-catalyzed version starting from 2,2′-diiodobiphenyls to access substituted phenanthrenes [95].

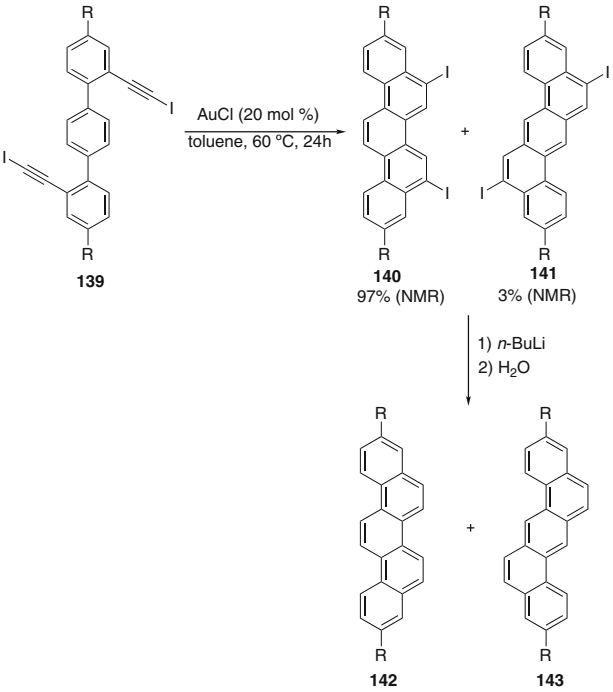


**Scheme 35** Au-catalyzed cyclization to access dibenzo[*a*,*h*]anthracene (*R* = *t*-Bu; no yield for the second step is given) [91]

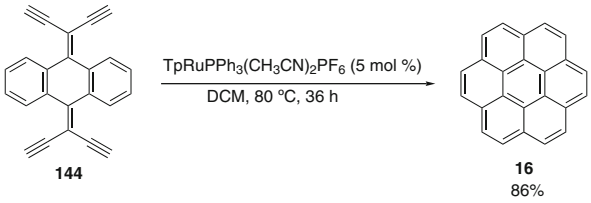


**Scheme 36** Synthesis of coronene via four-fold Ru-catalyzed cyclization [19]

To increase further the variability, methods starting from three or more reaction partners have been developed. Iodobenzene derivatives can be combined with an alkyne as well as an in situ formed aryne species under Pd-catalysis to efficiently form the phenanthrene core **154** (Scheme 39) [96].

The group of Wu showed that it is possible to perform a benzannulation on an unfunctionalized aromatic compound using two alkynes and a Pd catalyst (Scheme 40) [97]. The presence of electron-releasing groups increases the yield. If benzene is used as the starting material, only a low yield could be obtained. Two different mechanistic proposals are discussed, either involving a palladacyclopentadiene or participation of an Ar–Pd species in the first step of the cycle. AgOAc functions as the oxidizing agent to regenerate the Pd(II) species.

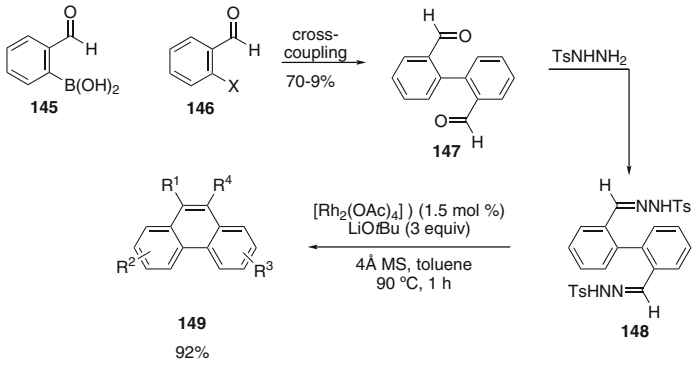


**Scheme 37** Formation of phenanthrene scaffold **149** by a Rh-catalyzed cyclization of bis (*N*-tosylhydrazone)s **148** (X=I, Br, Cl, OTf) [93]

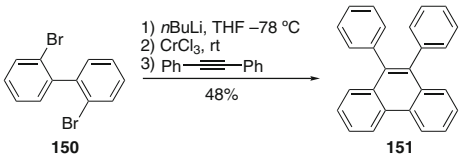


**Scheme 38** Cr-mediated synthesis of PAHs [94]

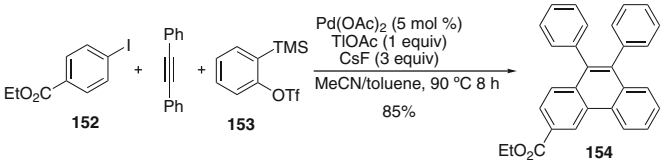


**Scheme 39** Pd-catalyzed cyclization of an aryliodide, alkyne and an in situ formed aryne [96]

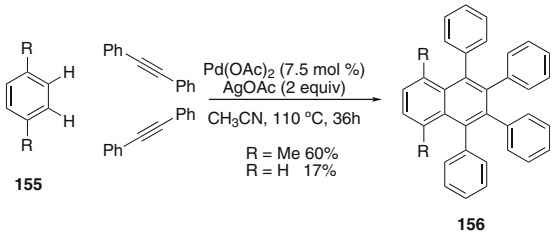


**Scheme 40** Pd-catalyzed annulation of unfunctionalized aromatics [97]

A Rh-based strategy was also put forward involving aryl boronic acids and air as the oxidizing agent with Cu as a co-catalyst for the oxidation (Scheme 41) [98]. Electron-rich as well as electron-poor boronic acids are well tolerated.

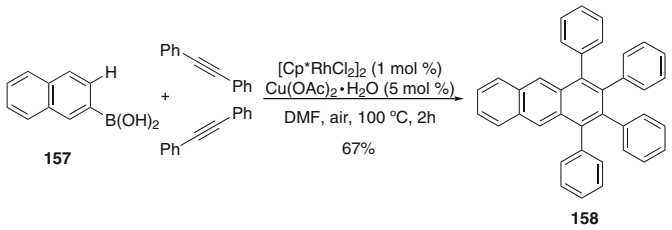


**Scheme 41** Rh-catalyzed annulation of aryl boronic acids [98]

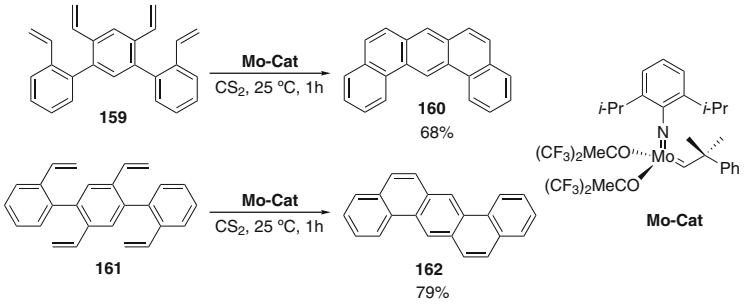


**Scheme 42** Metathesis as a means to build up graphene-type structures [102]

## *2.6 Ring Closing Metathesis*

Beside the coupling of two aromatic fragments or the cyclization of alkynes to form graphene-type structures, ring closing metathesis of olefins has been applied to the preparation of aromatic compounds [99, 100]. Not only simple monocyclic benzene derivatives can be synthesized [101] but also larger graphene-type structures have been realized using olefin metathesis. An impressive example by King and coworkers nicely demonstrates the utility of the metathesis reaction (Scheme 42) [102], once more justifying the award of the Nobel Prize in 2005 for this transformation.

# 3 Synthetic Methods for the Extension of Graphene-Type Structures

The perfect graphene sheet extends indefinitely, representing an ideal 2D polymer [103–105]. Most examples shown so far described the synthesis of distinct molecular PAHs. In order to harvest the unique properties of graphene, the small PAH fragments have to be further extended [106]. In principle most strategies explained above have the potential to achieve this goal. A small number of selected examples are illustrated below, demonstrating the basic concepts.

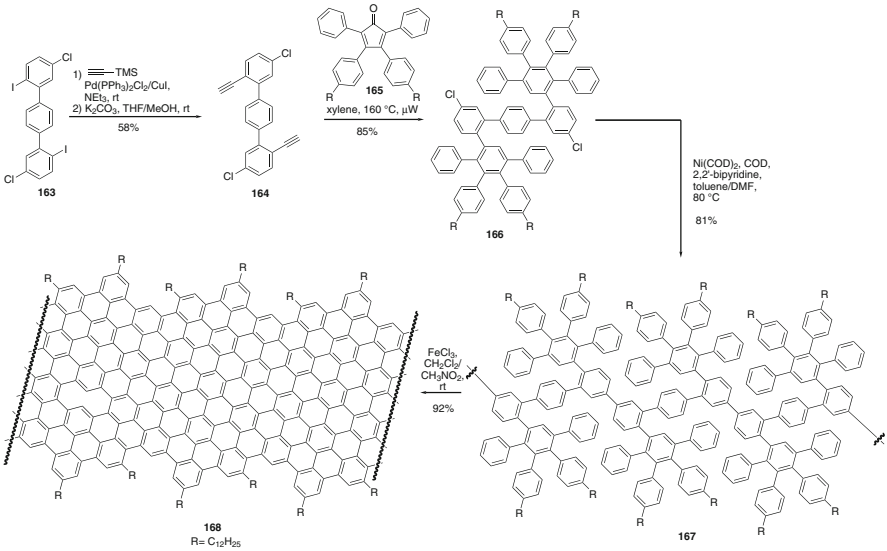


**Scheme 43** Synthesis of nano-graphene using cross-coupling, Diels–Alder, and dehydrogenation reactions [107]

## *3.1 Polymerization Reactions*

The creation of polymer-type PAHs requires a suitable choice of building blocks. Müllen and coworkers impressively demonstrated the synthesis of large nano-graphenes by combining cross-coupling, Diels–Alder, and dehydrogenation reactions (Scheme 43) [107]. First, a building block containing two acetylene units was prepared which was then subjected to Diels–Alder reaction with cyclopentadienone. A Ni-promoted Ullmann coupling provided the polymer **167**, which is then planarized into a graphene ribbon **168** upon aromatization.

Suzuki cross-coupling reactions have also been applied for the synthesis of graphene ribbons (Scheme 44) [108]. In the example shown the *para*-bisboronic ester **171** is polymerized to the intermediate **172**. Final dehydrogenation yielded the graphene ribbon **173**.

## *3.2 Postfunctionalization of PAHs for the Extension to Graphene*

Most PAHs have only unreactive C–H bonds at the periphery. For further extension the incorporation of synthetic handles is required to be able to make use of the tools described above. Classical aromatic substitutions (e.g., halogenation reactions) usually lack the selectivity required for efficient further synthetic elaborations.

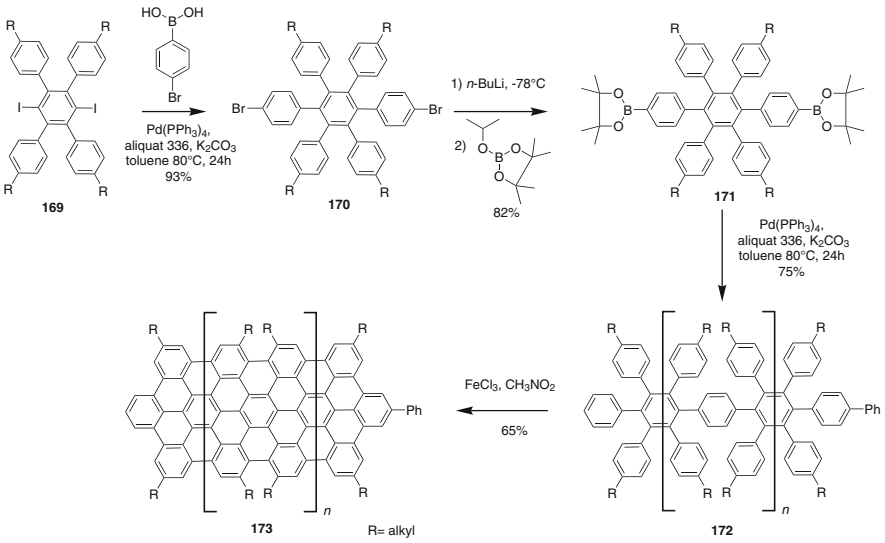


**Scheme 44** Preparation of a nano-graphene ribbon via Suzuki cross-coupling reaction [108]

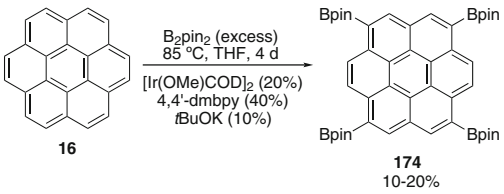


**Scheme 45** Selective Ir-catalyzed borylation of coronene **16** [109]

Recently, the group of Scott found that the direct borylation of PAHs proceeds in a reversible manner, finally delivering the thermodynamically most stable isomer [109]. With this methodology large PAHs can be selectively converted into boronates, which are suitable reaction partners for further transformations, such as Suzuki cross-coupling reactions (Scheme 45).

## *3.3 Direct Extension of PAHs by Diels–Alder Reaction*

In an ideal approach PAHs could be extended by simple addition of a $C_2H_2$-unit, followed by oxidation to the conjugated aromatic species. Usually, aromatic structures have been thought to be unreactive in such addition reactions. However, in 2012 the group of Scott found during their studies towards the elongation of carbon nanotube templates [110] that nitroethylene is a suitable dienophile in the

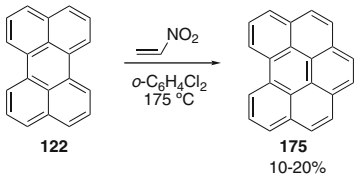


**Scheme 46** Extension of an armchair edge via Diels–Alder reaction [111]

Diels–Alder reaction to form bay regions on PAHs [111]. They also showed that pure acetylene effects the transformation, although the reaction is not as efficient (Scheme 46) [112].

Unfortunately, this strategy does not allow for the infinite growth of large graphene sheets from smaller PAHs fragments. For a successful reaction a bay region at the periphery must be present. While these are always regenerated in the case of carbon nanotubes, this is not true for 2D graphene-type structures.

The use of bifunctional dienophiles, such as parabenzoquinone, has been demonstrated as an efficient way to join PAHs to larger graphene-type structures [113].

## 4 Surface Assisted Methods for the Synthesis of Graphene-Type Structures

Solubility is the issue inhibiting the preparation of larger and larger PAHs from becoming more and more graphene like. For application purposes, e.g., in the area of molecular electronics, the final products have to be transferred to a surface to be able to address the compounds, ideally individually. Therefore, a preparation method directly on a surface would be highly useful [114]. Additionally, it would offer new possibilities in synthesis. Solubility would no longer be an issue. As described above, most transformations require a metal as catalyst or as mediator in stoichiometric amounts. This function can also be fulfilled by a metal surface. Furthermore, the structure of the surface can be utilized to enhance selectivity in the synthesis process. Modern microscope techniques also allow the direct observation of individual molecules on surfaces, allowing an easy in situ monitoring of the assembly.

Ten years ago the group of Müllen prepared PAHs and graphite islands, representing graphene-type structures, via surface-induced reaction of small molecules [115]. Although the reaction was unselective, the study demonstrated the general feasibility of such an approach (Scheme 47) [11, 14].

In collaboration with the group of Cai and Ruffieux, Müllen took the strategy a step further by employing a diiodobisanthracene derivative as a precursor for the formation of nano-ribbons [116, 117]. First, an Ullmann-type coupling on the surface connects the individual building blocks, which will then be dehydrogenated

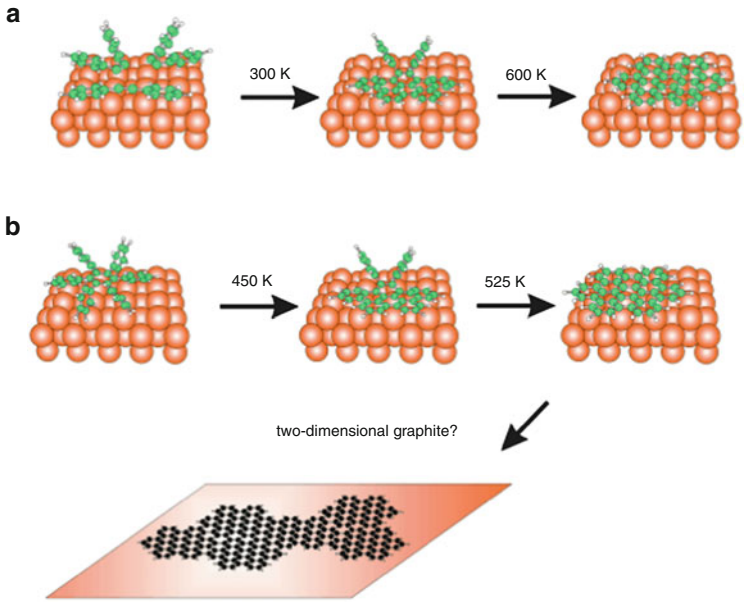


**Scheme 47** Proposed schemes for the thermally induced reactions of (**a**) diphenylacetylene and (**b**) hexaphenylbenzene on Cu(110) [115]

on the surface to form extended graphene ribbons. Depending on the monomers employed, different geometries of the final structures can be realized (Scheme 48).

A similar approach has also been put forward by the group of Hecht by presenting a suitable monomer to accomplish the on-surface polymerization [118].

Alternatively, small PAHs can be self-assembled on a surface and then connected via dehydrogenation to form high-quality large-area graphene. However, there is no direct control of the exact size and periphery of the prepared material [119].

## 5 Summary, Conclusions, and Outlook

The long history in organic chemistry of PAHs has been a solid basis for a continuous development of methods to access large graphene-type structures. The main drawback of applying organic synthetic methods towards the preparation of graphene consists in the low solubility of such structures in common organic solvents. Nevertheless, powerful strategies have been put forward in recent years, also combining classical approaches with new ideas, such as on-surface reactions.

Although the area is still in its infancy, not all efforts could be covered and a selection has been made to illustrate the progress and the potential of the current state-of-the-art in organic chemistry. The future will further enhance the possibilities to create new large PAHs with defined structures exhibiting the exciting properties of graphene. With a reliable method in hand to access

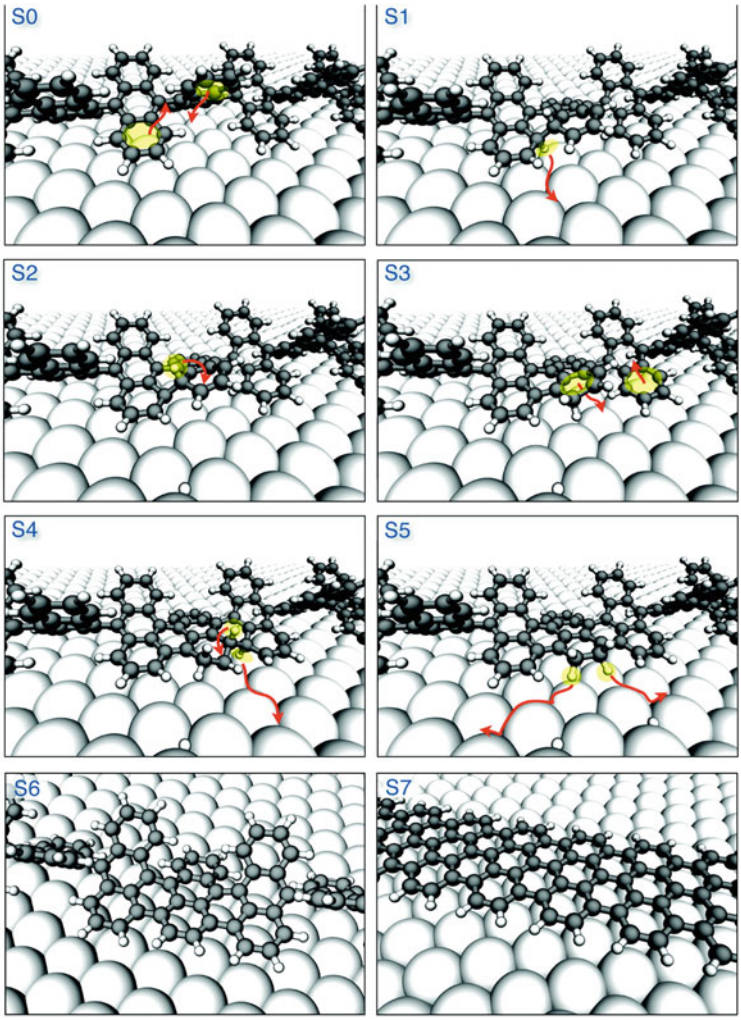


**Scheme 48** Preparation of graphene nanoribbons on a surface. Reprinted with permission from Blankenburg et al. [117]. Copyright 2013 American Chemical Society

graphene-type structures in a reproducible and efficient manner, applications of the magic material graphene will expand further and pave the way for commercial utilization.

**Acknowledgment** AFS is grateful for financial support by the COST action MP0901 "Designing novel materials for nanodevices: from theory to practice" and the Schweizer Bundesministerium für Bildung und Forschung. The authors thank Thomas Eaton, University of Basel, for proofreading the manuscript.

## References


1. Weiss NO, Zhou H, Liao L et al (2012) Graphene: an emerging electronic material. Adv Mater 24:5782–5825. doi:10.1002/adma.201201482
2. Zhu Y, James DK, Tour JM (2012) New routes to graphene, graphene oxide and their related applications. Adv Mater 24:4924–4955. doi:10.1002/adma.201202321
3. Enoki T, Takai K, Osipov V et al (2009) Nanographene and nanodiamond; new members in the nanocarbon family. Chem Asian J 4:796–804. doi:10.1002/asia.200800485
4. Katsnelson MI (2012) Graphene: carbon in two dimensions. Cambridge University Press, Cambridge
5. Choi W, Jo-won L (eds) (2013) Graphene: synthesis and applications. CRC, Boca Raton
6. Rao CNR, Subrahmanyam KS, Ramakrishna Matte HSS, Govindaraj A (2011) Graphene: synthesis, functionalization and properties. Mod Phys Lett B 25:427–451. doi:10.1142/S0217984911025961
7. Guo S, Dong S (2011) Graphene nanosheet: synthesis, molecular engineering, thin film, hybrids, and energy and analytical applications. Chem Soc Rev 40:2644. doi:10.1039/c0cs00079e
8. Gengler RYN, Spyrou K, Rudolf P (2010) A roadmap to high quality chemically prepared graphene. J Phys D Appl Phys 43:374015. doi:10.1088/0022-3727/43/37/374015
9. Gölzhäuser A (2012) Graphene from molecules. Angew Chem Int Edit 51:10936–10937. doi:10.1002/anie.201205955
10. Feng X, Feng X, Pisula W et al (2009) Large polycyclic aromatic hydrocarbons: synthesis and discotic organization. Pure Appl Chem 81:2203–2224. doi:10.1351/PAC-CON-09-07-07
11. Wu J, Gherghel L, Watson MD et al (2003) From branched polyphenylenes to graphite ribbons. Macromolecules 36:7082–7089. doi:10.1021/ma0257752
12. Fetzer JC (1989) Synthesis of large condensed polycyclic aromatic hydrocarbons. A review. Org Prep Proced Int 21:47–65
13. Skvarchenko VR (1963) Recent progress in the synthesis of monocyclic and polycyclic aromatic hydrocarbons. Russ Chem Rev 32:571–589
14. Clar E, Chen L, Zander M et al (2012) From nanographene and graphene nanoribbons to graphene sheets: chemical synthesis. Angew Chem Int Edit 51:7640–7654. doi:10.1002/anie.201201084
15. Mercuri F, Baldoni M, Sgamellotti A (2012) Towards nano-organic chemistry: perspectives for a bottom-up approach to the synthesis of low-dimensional carbon nanostructures. Nanoscale 4:369. doi:10.1039/c1nr11112d
16. Yan X, Li L-S (2011) Solution-chemistry approach to graphene nanostructures. J Mat Chem 21:3295. doi:10.1039/c0jm02827d
17. Clar E, Ironside CT, Zander M (1959) 28. The electronic interaction between benzenoid rings in condensed aromatic hydrocarbons. 1: 12-2 : 3–4 : 5–6 : 7–8 : 9–10 : 11-hexabenzocoronene, 1: 2–3 : 4–5 : 6–10 : 11-tetrabenzoanthanthrene, and 4 : 5–6 : 7–11 : 12–13 : 14-tetrabenzoperopyrene. J Chem Soc 142. doi: 10.1039/jr9590000142
18. Halleux A, Martin RH, King GSD (1958) 129. Syntheses dans la serie des derives polycycliques aromatiques hautement condenses. L'hexabenzo-1,12; 2,3; 4,5; 6,7; 8,9; 10,11-coronene, le tetrabenzo-4,5; 6,7; 11,12; 13,14-peropyrene et le tetrabenzo-1,2; 3,4; 8,9; 10,11-bisanthene. Helv Chim Acta 18:1178
19. Clar E, Guye-Vuillème JF, McCallum S, Macpherson IA (1963) Annellation effects in the pyrene series and the classification of absorption spectra. Tetrahedron 19:2185–2197
20. Clar E, Stephen JF (1965) Synthesis of 1:2, 3:4, 5:6, 7:8, 9:10, 11:12-hexabenzocoronene. Tetrahedron 21:467–470
21. Clar E, Mullen A (1971) Benzologues of terrylene. Tetrahedron 27:5239–5245
22. Clar E, Zander M (1957) 927. Syntheses of coronene and 1 : 2–7 : 8-dibenzocoronene. J Chem Soc 4616–4619

23. Hendel W, Khan ZH, Schmidt W (1986) Hexa-*peri*-benzocoronene, a candidate for the origin of the diffuse interstellar visible absorption-bands. Tetrahedron 42:1127–1134
24. Clar E (1948) Synthesis of ovalene. Nature 161:238–239
25. Thomas AD, Miller LL (1986) Repetitive Diels–Alder reactions for the growth of linear polyacenequinoid derivatives. J Org Chem 51:4160–4169
26. Pascal RA Jr, Van Engen D (1987) The solid state structure of 9,11,20,22-tetraphenyltetrabenzo[*a,c,l,n*] pentacene-10,21-dione: a longitudinally twisted molecular ribbon. Tetrahedron Lett 28:293–294
27. Pellissier H, Santelli M (2003) The use of arynes in organic synthesis. Tetrahedron 59:701–730
28. Sanz R (2008) Recent applications of aryne chemistry to organic synthesis. A review. Org Prep Proced Int 40:215–291. doi:10.1080/00304940809458089
29. Kitamura T, Fukatsu N, Fujiwara Y (1998) (Phenyl)[3-(trimethylsilyl)-2-naphthyl]iodonium triflate as a new precursor of 2,3-didehydronaphthalene. J Org Chem 63:8579–8581. doi:10.1021/jo9812476
30. Ikadai J, Yoshida H, Ohshita J, Kunai A (2005) Facile synthesis of polycyclic aromatic hydrocarbons via a trisaryne equivalent. Chem Lett 34:56–57. doi:10.1246/cl.2005.56
31. Müller M, Mauermann Düll H, Wagner M et al (1995) A cycloaddition–cyclodehydrogenation route from stilbenoids to extended aromatic hydrocarbons. Angew Chem Int Ed Engl 34:1583–1586
32. Müller M, Petersen J, Strohmaier R et al (1996) Polybenzoid $C_{54}$ hydrocarbons: synthesis and structural characterization in vapor-deposited ordered monolayers. Angew Chem Int Ed Engl 35:886–888
33. Iyer VS, Yoshimura K, Enkelmann V et al (1998) A soluble $C_{60}$ graphite segment. Angew Chem Int Ed Engl 37:2696–2699
34. Wasserfallen D, Kastler M, Pisula W et al (2006) Suppressing aggregation in a large polycyclic aromatic hydrocarbon. J Am Chem Soc 128:1334–1339. doi:10.1021/ja056782j
35. Morgenroth F, Kubel C, Müller M et al (1998) From three-dimensional polyphenylene dendrimers to large graphite subunits. Carbon 36:833–837
36. Wu J, Tomović Ž, Enkelmann V, Müllen K (2004) From branched hydrocarbon propellers to C3-symmetric graphite disks. J Org Chem 69:5179–5186. doi:10.1021/jo049452a
37. Müller M, Iyer VS, Kübel C et al (1997) Polycyclic aromatic hydrocarbons by cyclodehydrogenation and skeletal rearrangement of oligophenylenes. Angew Chem Int Ed Engl 36:1607–1610
38. Morgenroth F, Reuther E, Müllen K (1997) Polyphenylene dendrimers: from three-dimensional to two-dimensional structures. Angew Chem Int Ed Engl 36:631–634
39. Böhme T, Simpson CD, Müllen K, Rabe JP (2007) Current–voltage characteristics of a homologous series of polycyclic aromatic hydrocarbons. Chem-Eur J 13:7349–7357. doi:10.1002/chem.200601249
40. Iyer VS, Wehmeier M, Brand JD et al (1997) From hexa-*peri*-hexabenzocoronene to "superacenes". Angew Chem Int Ed Engl 36:1604–1607
41. Simpson CD, Brand JD, Berresheim AJ et al (2002) Synthesis of a giant 222 carbon graphite sheet. Chemistry 8:1424–1429
42. Kastler M, Schmidt J, Pisula W et al (2006) From armchair to zigzag peripheries in nanographenes. J Am Chem Soc 128:9526–9534. doi:10.1021/ja062026h
43. Wang Z, Tomović Ž, Kastler M et al (2004) Graphitic molecules with partial "zig/zag" periphery. J Am Chem Soc 126:7794–7795. doi:10.1021/ja048580d
44. Dötz F, Brand JD, Ito S et al (2000) Synthesis of large polycyclic aromatic hydrocarbons: variation of size and periphery. J Am Chem Soc 122:7707–7717. doi:10.1021/ja000832x
45. Yamamoto Y (2005) Recent advances in intramolecular alkyne cyclotrimerization and its applications. Curr Org Chem 9:503–519

46. Weiss K, Beernink G, Dötz F et al (1999) Template-mediated synthesis of polycyclic aromatic hydrocarbons: cyclodehydrogenation and planarization of a hexaphenylbenzene derivative at a copper surface. Angew Chem Int Ed Engl 38:3748–3752
47. Fechtenkötter A, Saalwächter K, Harbison MA et al (1999) Highly ordered columnar structures from hexa-*peri*-hexabenzocoronenes—synthesis, X-ray diffraction, and solid-state heteronuclear multiple-quantum NMR investigations. Angew Chem Int Ed Engl 38:3039–3042
48. Lee M, Kim J-W, Peleshanko S et al (2002) Amphiphilic hairy disks with branched hydrophilic tails and a hexa-*peri*-hexabenzocoronene core. J Am Chem Soc 124:9121–9128. doi:10.1021/ja017553
49. Lambert C, Nöll G (2002) Optically and thermally induced electron transfer pathways in hexakis [4-(*N*, *N*-diarylamino) phenyl] benzene derivatives. Chem-Eur J 8:3467–3477
50. Wang Z, Dötz F, Enkelmann V, Müllen K (2005) "Double-concave" graphene: permethoxylated hexa-*peri*-hexabenzocoronene and its cocrystals with hexafluorobenzene and fullerene. Angew Chem Int Ed 44:1247–1250
51. Wu J, Watson MD, Müllen K (2003) The versatile synthesis and self-assembly of star-type hexabenzocoronenes. Angew Chem Int Edit 42:5329–5333. doi:10.1002/anie.200352047
52. Wu J, Watson MD, Zhang L et al (2004) Hexakis(4-iodophenyl)-*peri*-hexabenzocoronene – a versatile building block for highly ordered discotic liquid crystalline materials. J Am Chem Soc 126:177–186. doi:10.1021/ja037519q
53. Wu J, Li J, Kolb U, Müllen K (2006) A water-soluble hexa-*peri*-hexabenzocoronene: synthesis, self-assembly and role as template for porous silica with aligned nanochannels. Chem Commun 48–50. doi:10.1039/b511868a
54. Feng X, Pisula W, Zhi L et al (2008) Controlling the columnar orientation of $C_3$-symmetric "superbenzenes" through alternating polar/apolar substitutents. Angew Chem Int Edit 47:1703–1706. doi:10.1002/anie.200703967
55. Feng X, Pisula W, Takase M et al (2008) Synthesis, helical organization, and fibrous formation of $C_3$ symmetric methoxy-substituted discotic hexa-*peri*-hexabenzocoronene. Chem Mater 20:2872–2874. doi:10.1021/cm800515s
56. Peña D, Pérez D, Guitián E, Castedo L (1999) Synthesis of hexabenzotriphenylene and other strained polycyclic aromatic hydrocarbons by palladium-catalyzed cyclotrimerization of arynes. Org Lett 1:1555–1557. doi:10.1021/ol990864t
57. Romero C, Romero C, Peña D et al (2006) Synthesis of extended triphenylenes by palladium-catalyzed [2+2+2] cycloaddition of triphenylynes. Chem-Eur J 12:5677–5684. doi:10.1002/chem.200600466
58. de Meijere A, Stulgies B, Albrecht K et al (2006) New interesting molecular topologies by way of modern cross-coupling reactions. Pure Appl Chem 78:813–830. doi:10.1351/pac200678040813
59. de Meijere A, Diederich F (eds) (2004) Metal-catalyzed cross-coupling reactions. Wiley-VCH, Weinheim
60. Nishihara Y (ed) (2012) Applied cross-coupling reactions. Springer, Heidelberg
61. Molnár Á (ed) (2013) Palladium-catalyzed coupling reactions. Wiley-VCH, Weinheim
62. Wu J (2007) Polycyclic aromatic compounds for organic field-effect transistors: molecular design and syntheses. Curr Organic Chem 11:1220–1240
63. Ito K, Suzuki T, Sakamoto Y et al (2003) Oligo(2,6-anthrylene)s: acene-oligomer approach for organic field-effect transistors. Angew Chem Int Edit 42:1159–1162
64. Yang X, Don X, Müllen K (2008) Efficient synthesis of symmetrically and unsymmetrically substituted hexaphenylbenzene analogues by Suzuki–Miyaura coupling reactions
65. Alberico D, Scott ME, Lautens M (2007) Aryl−aryl bond formation by transition-metal-catalyzed direct arylation. Chem Rev 107:174–238. doi:10.1021/cr0509760
66. Pascual S, de Mendoza P, Echavarren AM (2007) Palladium catalyzed arylation for the synthesis of polyarenes. Org Biomol Chem 5:2727. doi:10.1039/b707940k

67. Arockiam PB, Bruneau C, Dixneuf PH (2012) Ruthenium(II)-catalyzed C–H bond activation and functionalization. Chem Rev 112:5879–5918. doi:10.1021/cr300153j
68. Paul S, Jana R, Ray J (2010) Palladium-catalyzed intramolecular C–H activation: a synthetic approach towards polycyclic aromatic hydrocarbons. Synlett 2010:1463–1468. doi:10.1055/s-0029-1220070
69. Nassar-Hardy L, Deraedt C, Fouquet E, Felpin F-X (2011) A fully palladium-mediated construction of phenanthrenes and naphthoxindoles. Eur J Org Chem 2011:4616–4622. doi:10.1002/ejoc.201100477
70. Wegner HA (2012) Fluor als Abgangsgruppe in der organischen Synthese? Nachrichten aus der Chemie 60:880–883
71. Allemann O, Allemann O, Duttwyler S et al (2011) Proton-catalyzed, silane-fueled Friedel–Crafts coupling of fluoroarenes. Science 332:574–577. doi:10.1126/science.1202432
72. Amsharov KY, Kabdulov MA, Jansen M (2012) Facile bucky–bowl synthesis by regiospecific cove-region closure by HF elimination
73. Mochida K, Kawasumi K, Segawa Y, Itami K (2011) Direct arylation of polycyclic aromatic hydrocarbons through palladium catalysis. J Am Chem Soc 133:10716–10719. doi:10.1021/ja202975w
74. Scheuermann CJ (2010) Beyond traditional cross couplings: the scope of the cross dehydrogenative coupling reaction. Chem Asian J 5:436–451. doi:10.1002/asia.200900487
75. Hassan J, Sévignon M, Gozzi C et al (2002) Aryl–aryl bond formation one century after the discovery of the Ullmann reaction. Chem Rev 102:1359–1470
76. Suzuki H, Enya T, Hisamatsu Y (1997) Synthesis and characterization of some nitrobenzanthrones: suspected new mutagens in atmospheric environment. Synthesis 1273–1276
77. Rickhaus M, Belanger AP, Wegner HA, Scott LT (2010) An oxidation induced by potassium metal. Studies on the anionic cyclodehydrogenation of 1,1'-binaphthyl to perylene. J Org Chem 75:7358–7364. doi:10.1021/jo101635z
78. Rempala P, Kroulík J, King BT (2006) Investigation of the mechanism of the intramolecular Scholl reaction of contiguous phenylbenzenes. J Org Chem 71:5067–5081. doi:10.1021/jo0526744
79. Sarhan AAO, Bolm C (2009) Iron(III) chloride in oxidative C–C coupling reactions. Chem Soc Rev 38:2730. doi:10.1039/b906026j
80. Cataldo F, Ursini O, Angelini G, Iglesias-Groth S (2011) On the way to graphene: the bottom-up approach to very large PAHs using the Scholl reaction. Fuller Nanotub Car N 19:713–725. doi:10.1080/1536383X.2010.494787
81. Allen MJ, Talyzin AV, Tung VC et al (2011) Coronene fusion by heat treatment: road to nanographenes. J Phys Chem C 115:13207–13214. doi:10.1021/jp2028627
82. Konishi A, Hirao Y, Matsumoto K, Kurata H, Kishi R, Shigeta Y, Nakano M, Tokunaga K, Kamada K, Kubo T (2013) Synthesis and Characterization of Quarteranthene: Elucidating the Characteristics of the Edge State of Graphene Nanoribbons at the Molecular Level. J Am Chem Soc 135:1430–1437. doi:10.1021/ja309599m
83. Kotha S, Misra S, Halder S (2008) Benzannulation. Tetrahedron 64:10775–10790. doi:10.1016/j.tet.2008.09.004
84. Wood CS, Mallory FB (1964) Photochemistry of stilbenes. IV. The preparation of substituted phenanthrenes. J Org Chem 29:3373–3377
85. Jørgensen KB (2010) Photochemical oxidative cyclisation of stilbenes and stilbenoids—the Mallory-reaction. Molecules 15:4334–4358. doi:10.3390/molecules15064334
86. Liu L, Yang B, Katz TJ, Poindexter MK (1991) Improved methodology for photocyclization reactions. J Org Chem 56:3769–3775
87. Shen Y, Chen C-F (2012) Helicenes: synthesis and applications. Chem Rev 112:1463–1535. doi:10.1021/cr200087r
88. Zhang X, Jiang X, Zhang K et al (2010) Synthesis, self-assembly, and charge transporting property of contorted tetrabenzocoronenes. J Org Chem 75:8069–8077. doi:10.1021/jo101701k

89. Liu Z, Zhang X, Larock RC (2005) Synthesis of fused polycyclic aromatics by palladium-catalyzed annulation of arynes using 2-halobiaryls. J Am Chem Soc 127:15716–15717. doi:10.1021/ja055781o
90. Fürstner A, Davies PW (2007) Catalytic carbophilic activation: catalysis by platinum and gold π-acids. Angew Chem Int Edit 46:3410–3449. doi:10.1002/anie.200604335
91. Nakae T, Ohnishi R, Kitahata Y et al (2012) Effective synthesis of diiodinated picene and dibenzo[a, h]anthracene by AuCl-catalyzed double cyclization. Tetrahedron Lett 53:1617–1619. doi:10.1016/j.tetlet.2012.01.071
92. Shen H-C, Tang J-M, Chang H-K et al (2005) Short and efficient synthesis of coronene derivatives via ruthenium-catalyzed benzannulation protocol. J Org Chem 70:10113–10116. doi:10.1021/jo0512599
93. Xia Y, Liu Z, Xiao Q et al (2012) Rhodium(II)-catalyzed cyclization of bis(*N*-tosylhydrazone)s: an efficient approach towards polycyclic aromatic compounds. Angew Chem Int Edit 51:5714–5717. doi:10.1002/anie.201201374
94. Kanno K-I, Liu Y, Iesato A et al (2005) Chromium-mediated synthesis of polycyclic aromatic compounds from halobiaryls. Org Lett 7:5453–5456. doi:10.1021/ol052214x
95. Lin Y-D, Cho C-L, Ko C-W et al (2012) Palladium-catalyzed annulation of 2,2′-diiodobiphenyls with alkynes: synthesis and applications of phenanthrenes. J Org Chem 77:9979–9988. doi:10.1021/jo302013x
96. Liu Z, Larock RC (2007) Palladium-catalyzed, sequential, three-component cross-coupling of aryl halides, alkynes, and arynes. Angew Chem Int Edit 46:2535–2538. doi:10.1002/anie.200604969
97. Wu Y-T, Huang K-H, Shin C-C, Wu T-C (2008) Palladium-catalyzed formation of highly substituted naphthalenes from arene and alkyne hydrocarbons. Chem-Eur J 14:6697–6703. doi:10.1002/(ISSN)1521-3765
98. Fukutani T, Hirano K, Satoh T, Miura M (2009) Synthesis of highly substituted naphthalene and anthracene derivatives by rhodium-catalyzed oxidative coupling of arylboronic acids with alkynes. Org Lett 11:5198–5201. doi:10.1021/ol9021172
99. van Otterlo WAL, de Koning CB (2009) Metathesis in the synthesis of aromatic compounds. Chem Rev 109:3743–3782. doi:10.1021/cr900178p
100. Grubbs RH (2004) Olefin metathesis. Tetrahedron 7117–7140. doi:10.1016/j.tet.2004.05.124
101. Yoshida K, Toyoshima T, Imamoto T (2007) Efficient synthetic routes to aromatic compounds using ring-closing olefin metathesis followed by dehydration, oxidation, and tautomerization. Chem Commun 3774. doi:10.1039/b705581a
102. Bonifacio MC, Robertson CR, Jung J-Y, King BT (2005) Polycyclic aromatic hydrocarbons by ring-closing metathesis. J Org Chem 70:8522–8526. doi:10.1021/jo051418o
103. Schlüter AD, Sakamoto J (2012) Putting aromatic compounds to work: rational synthesis of organic 2D polymers. Pure Appl Chem 84:861–867. doi:10.1351/PAC-CON-12-01-10
104. Kissel P, Schlüter AD, Sakamoto J (2009) Rational monomer design towards 2D polymers: synthesis of a macrocycle with three 1,8-anthrylene units. Chem-Eur J 15:8955–8960. doi:10.1002/chem.200900781
105. Sakamoto J, van Heijst J, Lukin O, Schlüter AD (2009) Two-dimensional polymers: just a dream of synthetic chemists? Angew Chem Int Edit 48:1030–1069. doi:10.1002/anie.200801863
106. Schrettl S, Frauenrath H (2012) Elements for a rational polymer approach towards carbon nanostructures. Angew Chem Int Edit 51:6569–6571. doi:10.1002/anie.201201423
107. Schwab MG, Narita A, Hernandez Y et al (2012) Structurally defined graphene nanoribbons with high lateral extension. J Am Chem Soc 134:18169–18172. doi:10.1021/ja307697j
108. Yang X, Dou X, Rouhanipour A et al (2008) Two-dimensional graphene nanoribbons. J Am Chem Soc 130:4216–4217. doi:10.1021/ja710234t
109. Eliseeva MN, Scott LT (2012) Pushing the Ir-catalyzed C–H polyborylation of aromatic compounds to maximum capacity by exploiting reversibility. J Am Chem Soc 134:15169–15172. doi:10.1021/ja307547j

110. Fort EH, Scott LT (2011) Carbon nanotubes from short hydrocarbon templates. Energy analysis of the Diels–Alder cycloaddition/rearomatization growth strategy. J Mater Chem 21:1373. doi:10.1039/c0jm02517h
111. Fort EH, Scott LT (2010) One-step conversion of aromatic hydrocarbon bay regions into unsubstituted benzene rings: a reagent for the low-temperature, metal-free growth of single-chirality carbon nanotubes. Angew Chem Int Edit 49:6626–6628. doi:10.1002/anie.201002859
112. Fort EH, Scott LT (2011) Gas-phase Diels–Alder cycloaddition of benzyne to an aromatic hydrocarbon bay region: groundwork for the selective solvent-free growth of armchair carbon nanotubes. Tetrahedron Lett 52:2051–2053. doi:10.1016/j.tetlet.2010.10.033
113. Li J, Jiao C, Huang K-W, Wu J (2011) Lateral extension of π conjugation along the bay regions of bisanthene through a Diels–Alder cycloaddition reaction. Chem-Eur J 17:14672–14680. doi:10.1002/chem.201102120
114. Méndez J, López MF, Martín-Gago JA (2011) On-surface synthesis of cyclic organic molecules. Chem Soc Rev 40:4578. doi:10.1039/c0cs00161a
115. Beernink G, Gunia M, Dötz F, Öström H, Weiss K, Müllen K, Wöll C (2001) Synthesis of polycyclic aromatic hydrocarbons and graphite islands via surface-induced reaction of small molecules. Chemphyschem 2:317–320. doi:10.1002/1439-7641
116. Cai J, Ruffieux P, Jaafar R et al (2010) Atomically precise bottom-up fabrication of graphene nanoribbons. Nature 466:470–473. doi:10.1038/nature09211
117. Blankenburg S, Cai J, Ruffieux P, Jaafar R et al (2012) Intraribbon heterojunction formation in ultranarrow graphene nanoribbons. ACS Nano 6:2020–2025. doi:10.1021/nn203129a
118. Gille M, Viertel A, Weidner S, Hecht S (2013) Modular synthesis of monomers for on-surface polymerization to graphene architectures. Synlett 24:259–263. doi:10.1055/s-0032-1317959
119. Wan X, Chen K, Liu D et al (2012) High-quality large-area graphene from dehydrogenated polycyclic aromatic hydrocarbons. Chem Mater 24:3906–3915. doi:10.1021/cm301993z

Top Curr Chem (2014) 349: 159–196
DOI: 10.1007/128_2012_376

Published online: 25 October 2012

# Indenofluorenes and Derivatives: Syntheses and Emerging Materials Applications

**Aaron G. Fix, Daniel T. Chase, and Michael M. Haley**

**Abstract** The growing demand for flexible electronic devices and hydrogen storage materials has spurred a resurgence of interest in polyaryl hydrocarbons including graphene, acenes, fullerenes, polythiophenes, etc. Indenofluorenes are another polyaryl molecular scaffold that has shown utility in the organic and hybrid materials arena, with polymers incorporating the indeno[1,2-*b*]fluorene moiety being common in organic light emitting diodes. This review examines the syntheses and properties of the five distinct indenofluorene regioisomers, with a focus on small molecule applications in organic electronics of this intriguing and somewhat underexplored family of polyaryl hydrocarbons.

**Keywords** Acene · Indenofluorene · Organic electronics · Polyarene · Polycyclic aromatic hydrocarbon · Terphenyl

## Contents

1 Introduction ..... 160
1.1 Background ..... 160
1.2 Early Research ..... 162
2 Indeno[1,2-*a*]fluorenes ..... 165
2.1 Indeno[1,2-*a*]fluorene-7,12-diones ..... 165
2.2 Other Indeno[1,2-*a*]fluorenes ..... 166
3 Indeno[1,2-*b*]fluorenes ..... 167
3.1 Indeno[1,2-*b*]fluorene-6,12-diones ..... 167
3.2 Indeno[1,2-*b*]fluorene-6,12-olefins ..... 172
3.3 Fully-Conjugated Indeno[1,2-*b*]fluorene ..... 174
3.4 Other Indeno[1,2-*b*]fluorenes ..... 179

A.G. Fix, D.T. Chase, and M.M. Haley (✉)
Department of Chemistry and Materials Science Institute, University of Oregon, Eugene, OR 97403-1253, USA
e-mail: haley@uoregon.edu

4 Indeno[2,1-*a*]fluorenes ..... 183
4.1 Indeno[2,1-*a*]fluorene-11,12-diones ..... 183
4.2 Fully-Conjugated Indeno[2,1-*a*]fluorenes ..... 184
5 Indeno[2,1-*b*]fluorenes ..... 186
5.1 Indeno[2,1-*b*]fluorene-10,12-diones ..... 186
5.2 Fully-Conjugated Indeno[2,1-*b*]fluorenes ..... 187
5.3 Other Indeno[2,1-*b*]fluorenes ..... 187
6 Indeno[2,1-*c*]fluorenes ..... 189
6.1 Indeno[2,1-*c*]fluorene-5,8-diones ..... 189
6.2 Fully-Conjugated Indeno[2,1-*c*]fluorenes ..... 191
6.3 Other Indeno[2,1-*c*]fluorenes ..... 192
7 Conclusions ..... 192
References ..... 193

# 1 Introduction

## *1.1 Background*

Polycyclic aromatic hydrocarbons (PAHs), and polyarenes (PAs) in general, have been the subject of great interest for over 150 years, and constitute a significant cornerstone of the advancement of organic chemistry in the nineteenth and twentieth centuries [1, 2]. Initially discovered in the resins of fossil fuels, PAHs have been observed in a myriad of environments that range from natural mineral deposits to meteor rocks [3]. Isolation of PAH-rich tars and ashes has contributed not only to modern purification and separation techniques commonly used today, but has also brought forth fundamental concepts such as aromaticity, a topic that remains a neverending source of discussion in the literature. Furthermore, efforts to elucidate the reactivity of PAHs and PAs have resulted in the discovery of many novel reaction mechanisms and catalytic pathways that represent the foundation of modern physical organic chemistry.

In the last quarter century, PAH and PA research has made a remarkable return to the literature spotlight as compound accessibility and characterization has been made easier with the advent of modern synthetic methods and instrumentation, respectively [4–6]. One motivation for this resurgence lies with the unique optoelectronic properties that PAHs and PAs possess due to their inherently high levels of π-conjugation and delocalization. These attributes make PAHs and PAs useful for a variety of materials applications such as organic light-emitting diodes (OLEDs), field-effect transistors (OFETs), and photovoltaics (OPVs) [7, 8]. Such impetus has led to the development and expansion of various PAH classes, such as higher order acenes [9, 10] and condensed polycyclic aromatics [11–13]. Nontraditional structures that incorporate five-membered cyclopentyl rings (CP-PAHs) such as fullerenes [14] and buckybowls [15] have undergone rapid growth as well.

This review focuses on the pentacyclic indenofluorenes (IFs), another reemerging class of CP-PAHs, where the B and D rings are each a five-membered ring. First synthesized in the late nineteenth century by Gabriel [16], IF derivatives

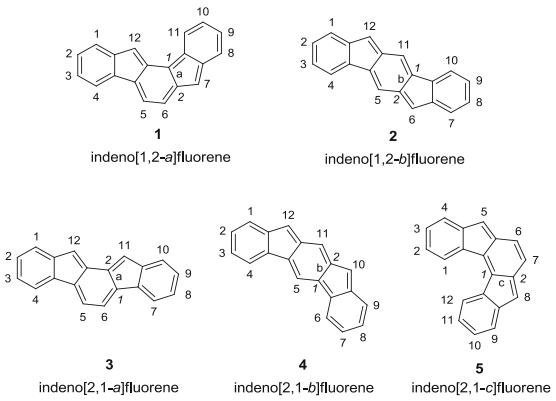


**Fig. 1** Nomenclature and numbering for indenofluorene isomers. *Italicized* numbers denote numbering for methylene bridge orientation, *non-italicized* numbers denote atom

were a sporadic topic in the literature for roughly 70 years [17–24] until the pioneering work by Deuschel [25, 26] and Chardonnens [27] in the 1950s devised a general strategy for their synthesis. However, at that time modern spectroscopic and structural identification techniques were rare in the scientific community; thus, IFs were not typically characterized beyond their melting points and elemental analyses. Outside their initial syntheses, IF development languished for another 40 years. A decade ago, following the realization of CP-PAHs as viable organic materials, interest in the IF scaffold resumed. Since then derivatized IFs have been recognized as potential candidates for stable emissive materials [28–34] and more recently identified as a semiconducting material in devices [35–37].

The indenofluorene family is comprised of five structural isomers which can be difficult to discern as multiple naming and numbering strategies as well as graphical presentations have been employed over the last century to describe their shape and structure (Fig. 1). Current nomenclature uses a bracketed set of numbers and a letter to distinguish one isomer from another where the set of numbers refer to the orientation of how the indene group faces the fluorene and the letter corresponds to the edge of the indene/fluorene ring fusion. Both "1,2" isomers exhibit an *anti* relationship between the methylene bridges of the five-membered rings, while the three remaining "2,1" isomers exhibit a *syn* relationship. The IF scaffold exhibits a variety of symmetries: the [1,2-*a*] isomer is only centrosymmetric, the [1,2-*b*] isomer exhibits rotational symmetry, and the [2,1-*a*], [2,1-*b*], and [2,1-*c*] isomers possess a mirror plane. As such, each isomer has its own unique ring topology, which in turn has pronounced structural and electronic consequences.

This review will cover the five IF regioisomers and describe common synthetic procedures used to obtain each form, including assorted structural, optoelectronic, and materials properties as available. IFs possessing $sp^3$-hybridization at the bridgehead of the five-membered rings is a burgeoning area of research in the realm of emissive materials worthy of its own review; however, only salient examples will be described. Device information will be presented assuming the reader has a basic optical and electronic materials background. Greater detail can be found in the appropriate references.

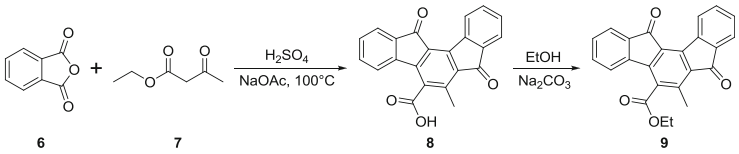


**Scheme 1** Synthesis of Gabriel's [1,2-*a*]IF dione **9** [16]

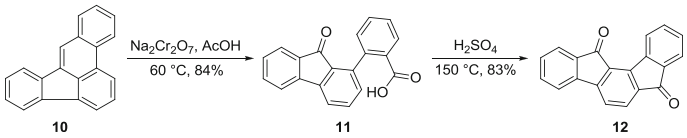


**Scheme 2** Syntheses of parent [1,2-*a*]IF dione **12** [27]

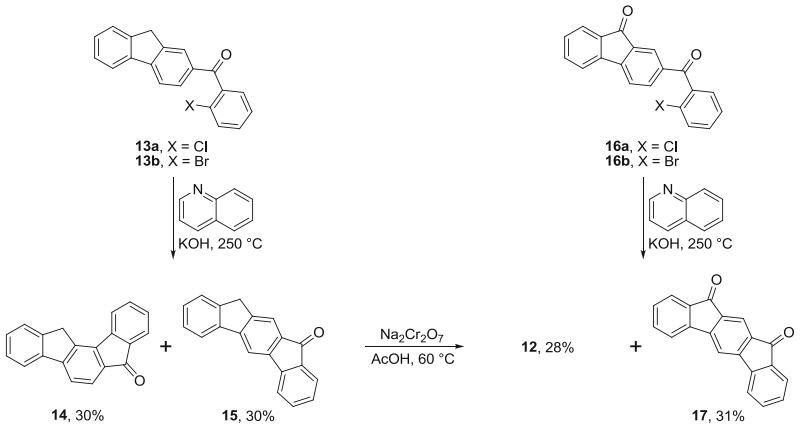


**Scheme 3** Asymmetric synthesis of **12** and [2,1-*b*]IF dione **17** [38–40]

## *1.2 Early Research*

The first reported synthesis of an IF scaffold dates to 1884 when Gabriel condensed 2 equiv. phthalic anhydride (**6**) with ethyl acetoacetonate (**7**) to form carboxylic acid **8** and later ethyl ester **9** (Scheme 1) [16].

In 1955, Chardonnens and Ritter isolated the parent [1,2-*a*]dione **12** through oxidative cleavage of benzo[*e*]acephenanthrylene (**10**) using sodium dichromate to generate 2-fluorenonylbenzoic acid (**11**) followed by ring closure using concentrated sulfuric acid (Scheme 2) [27].

Chardonnens and coworkers later devised a more general pathway to **12** by condensing either indenyl ketone **13a** or **13b**, respectively, with quinoline and NaOH in a stainless steel autoclave at 250 °C to give 7-keto-12-hydroindeno[1,2-*a*]fluorenone (**14**) in 30% yield (Scheme 3) [38–40]. Incidentally, 9-keto-12-hydroindeno[2,1-*b*]

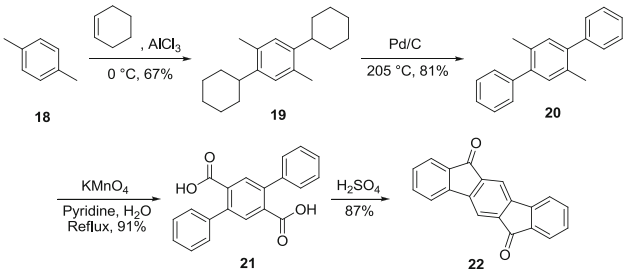


**Scheme 4** Synthesis of parent [1,2-*b*]IF dione **22** [26]

fluorenone (**15**) also formed in equal yield as addition could occur at either the 6- or 8-positions of the fluorene unit. Addition of either indenonyl ketone **16a** or **16b**, respectively, under similar conditions afforded both **12** and parent [2,1-*b*]IF dione **17** in 28% and 31% yield, respectively. Furthermore, oxidation of **14** and **15** using sodium dichromate at elevated temperatures led to the expected diones **12** and **17**. Despite the formation of two discrete condensation products, both **14** and **15** as well as **12** and **17** can be isolated separately either through soxhlet extraction or by selective crystallization. Both techniques take advantage of the key topological differences that the [1,2-*a*] and [2,1-*b*] structures possess – namely, the [2,1-*b*] isomer is more soluble than the [1,2-*a*] isomer. The greater dipole moment induced by the *syn* arrangement of the ketones makes the [2,1-*b*]IF scaffold more amenable to dissolution in polar solvents, allowing for easy separation of the isomers.

The first account of the [1,2-*b*]IF skeleton dates to 1951 when Deuschel alkylated *p*-xylene (**18**) with 2 equiv. cyclohexene to give tricycle **19** (Scheme 4). Treatment with Pd/C afforded 1,4-dimethyl-2,5-diphenylbenzene (**20**). Oxidation of the methyl moieties using potassium permanganate and pyridine generated diacid **21**. Subsequent cyclization using concentrated sulfuric acid gave the parent [1,2-*b*]IF-6,12-dione **22** in 87% yield [26].

Alternatively, passing a stream of chlorine gas in a neat solution of **20** at 185 °C afforded **23** in 46% yield (Scheme 5). A refluxing aqueous solution of $CuCl_2$ also oxidized **23** to dione **22**.

Access to the [1,2-*b*]IF core was also discovered through collapse of the dehydrobenzo[12]annulene scaffold. First described by Eglinton and coworkers in 1960 (Scheme 6), tetrayne **24** underwent a double transannular cyclization when reacted with elemental Na in liquid ammonia to provide octahydroindeno[1,2-*b*] fluorene **25** as a mixture of two isomers in 69% yield [41]. Further treatment with 15% Pd/C aromatized the central ring to afford 6,12-dihydroindeno[1,2-*b*] fluorene (**26**).

Continued work by Deuschel demonstrated that **22** was amenable to nitration using potassium nitrate in concentrated sulfuric acid at 20 °C (Scheme 7) [42]. By varying the amount of electrophile used, [1,2-*b*]IF diones could be nitrated either two (**27**), three (**28**), or four (**29**) times. Reduction of dinitro **27** with aqueous

**Scheme 5** Chlorination/oxidation route to **22** [26]

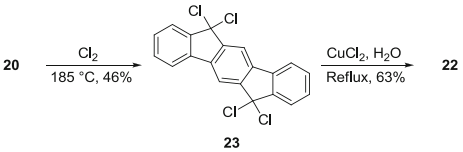


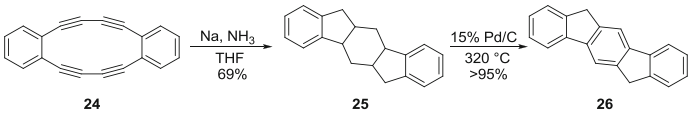


**Scheme 6** Na/$NH_3$-induced transannular cyclization of **24** [41]

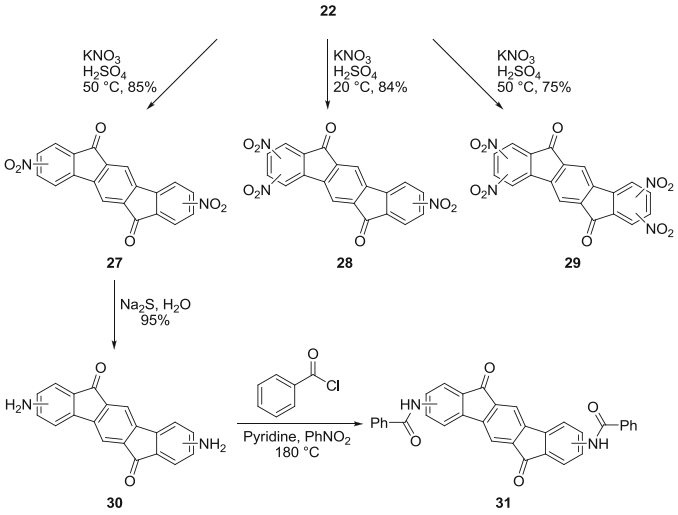


**Scheme 7** Nitration, reduction, and amidation of **22** [42]

sodium sulfide afforded diaminodione **30** in 95% yield, which in turn was amenable to amidation in a pyridine/nitromethane solution at 180 °C to give **31**. While the sites for nitration of **22** were most likely on the peripheral rings, specific information about their exact positions remains unknown.

Chardonnens and Salamin also synthesized a number of substituted [1,2-*b*]IF diones, which were typically made in the same fashion as the [1,2-*a*]IF diones described earlier (Scheme 3) [43]. For example, treatment of 2,5-dibromoterephthalic acid (**32**) with thionyl chloride and subsequent Friedel–Crafts acylation with **33a–d** provided **34a–d** (Scheme 8). Intramolecular arylation at elevated temperatures furnished IF-diones **35a–d** in 20–28% yield. This technique has also been successfully applied to asymmetric 1,3,4-trisubstituted diones as well as 2,3,8,9-tetrasubstituted diones [42].

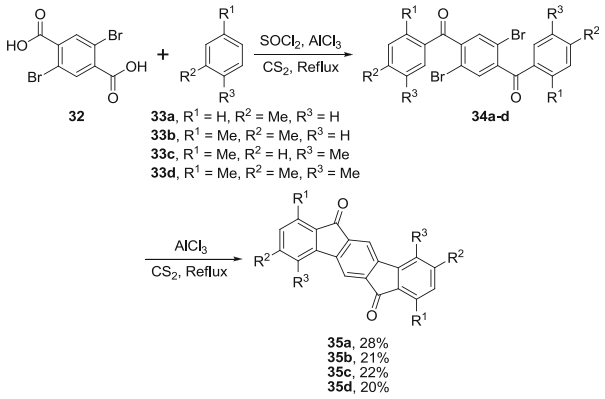


**Scheme 8** Synthesis of 1,3,4,7,9,10-substituted diones **35a–d** [43]

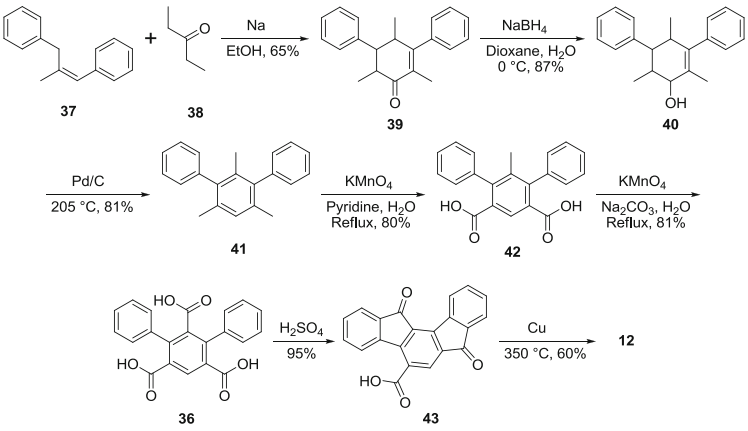


**Scheme 9** Synthesis of **12** via terphenyl tricarboxylic acid precursor **42** [45]

## 2 Indeno[1,2-*a*]fluorenes

### *2.1 Indeno[1,2-a]fluorene-7,12-diones*

The synthetic route utilizing Friedel–Crafts acylation via terphenyldicarboxylic acid precursors to reach the pentacyclic diketone has been applied for the assembly of a multitude of indeno[1,2-*a*]fluorene diones [44]. In most cases, a mixture of [1,2-*a*] and [2,1-*b*] species was formed during the cyclization stage, although in some instances the [1,2-*a*] isomer was the exclusive product. One such example involves tricarboxylic acid precursor **36**, so that the acylation step forms in the correct configuration regardless of direction (Scheme 9) [45]. To achieve this, *cis*-1,3-diphenylpropene (**37**) was reacted with 3-pentanone (**38**) to yield

**Scheme 10** Synthesis of spiro-fused [1,2-*a*]IFs **48a,b** and [2,1-*c*]IFs **49a,b** [46]

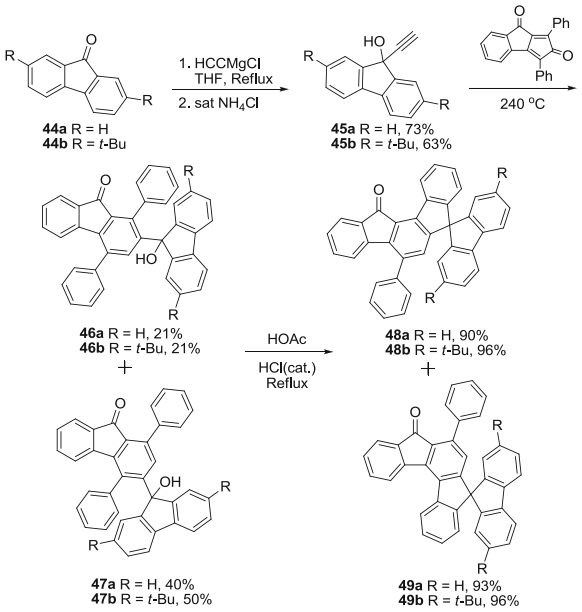


cyclohexenone **39**. Reduction with sodium borohydride afforded cyclohexanol **40** followed by reaction with Pd/C to form 1,3,5-trimethyl-2,4-diphenylbenzene **41**. Oxidation with potassium permanganate, first using pyridine as the base yielding diacid **42**, and then using sodium carbonate, provided triacid **36**. Cyclization in concentrated sulfuric acid afforded 5-carboxyindeno[1,2-*a*]fluorene dione **43** in near quantitative yield. Subsequent decarboxylation using elemental Cu at 350 °C gave **12** as the sole product.

## *2.2 Other Indeno[1,2-a]fluorenes*

Since the initial work of Chardonnens and others, few examples of syntheses of [1,2-*a*]IF derivatives exist outside of patent literature. Shi et al. recently reported [1,2-*a*]IFs **48a,b** and [2,1-*c*]IFs **49a,b** (Scheme 10) [46]. Diels–Alder reaction of alkynes **45a,b**, readily available from fluorenones **44a,b**, provided regioisomeric mixtures of diols **46a,b** and **47a,b**. Subsequent acid-catalyzed Friedel–Crafts condensation gives **48** and **49**. The two derivatives of both regioisomers showed quantum yields in solution of ~60% and showed good thermal stability, with decomposition occurring at temperatures greater than 330 °C.

Minuti and colleagues described the syntheses of cyclophane-fused [1,2-*a*]IFs [47]. Reduction of **50** with sodium borohydride, followed by treatment with $PBr_3$ then LiBr/$LiCO_3$, gave three undetermined intermediates (Fig. 2). This mixture of molecules yielded **51** after treatment with Pd/C in triglyme at 160 °C.

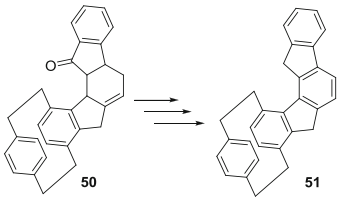


**Fig. 2** Cyclophane-functionalized precursor **50** and [1,2-*a*]IF **51** [47]

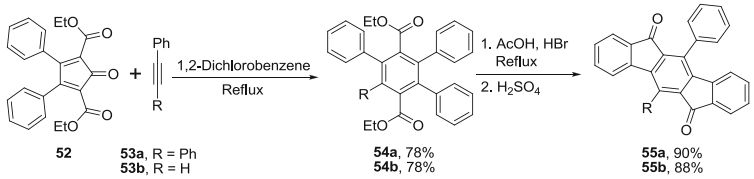


**Scheme 11** Synthesis of IF diones **55a,b** [48]

# 3 Indeno[1,2-*b*]fluorenes

## *3.1 Indeno[1,2-b]fluorene-6,12-diones*

Diels–Alder methods can also be used to generate the terphenyl core that ultimately furnishes [1,2-*b*]IF diones. Wang showed that the [4+2] cycloaddition of cyclopentadienone **52** with either diphenylacetylene (**53a**) or phenylacetylene (**53b**) followed by cheletropic elimination of CO afforded diesters **54a,b** (Scheme 11) [48]. Ester hydrolysis and subsequent Friedel–Crafts ring closure furnished 5,11-diphenyl and 5-phenyl [1,2-*b*]IF diones **55a,b** in 90% and 88% yield, respectively. A noted consequence of this alternative pathway was the suppressed formation of the corresponding [2,1-*c*]IF diones.

Encouraged by the potential semiconducting properties polyacetylenes could offer, Swager reacted **24** and **56a,b** [49], and later Komatsu reacted **56c** [50, 51], with iodine under aerobic conditions to give 5,11-diiodoindeno[1,2-*b*]fluorenediones **57a–d** in 33–95% yield (Scheme 12). The reactivity is reminiscent of Eglinton's earlier transannular cyclization (Scheme 6) but leading to diones in this case due to the reactive nature of the fully-reduced dibenzo-*s*-indacene intermediate (further discussed in Sect. 3.3).

Komatsu and colleagues also demonstrated n-type semiconducting behavior for **57d** in thin-film OFETs [51], a highly desirable characteristic given the relative paucity of organic n-type semiconducting scaffolds compared to p-type molecular motifs. These devices, however, possessed low electron mobilities of $2.93 \times 10^{-5}$ cm$^2$/V·s under vacuum and $6.08 \times 10^{-6}$ cm$^2$/V·s in air.

**Scheme 12** Aerobic iodine-induced transannular cyclization of **57a–d** [49, 50]

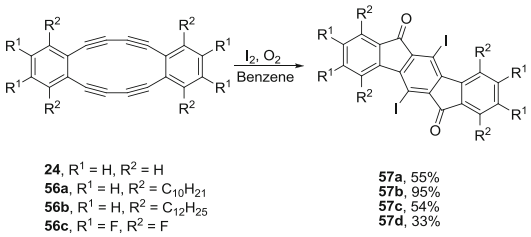


**24**, $R^1$ = H, $R^2$ = H
**56a**, $R^1$ = H, $R^2$ = $C_{10}H_{21}$
**56b**, $R^1$ = H, $R^2$ = $C_{12}H_{25}$
**56c**, $R^1$ = F, $R^2$ = F

**57a**, 55%
**57b**, 95%
**57c**, 54%
**57d**, 33%

**Scheme 13** Preparation of parent dione **22** and 2,8-dihalo IF diones **61a,b** [48, 52]

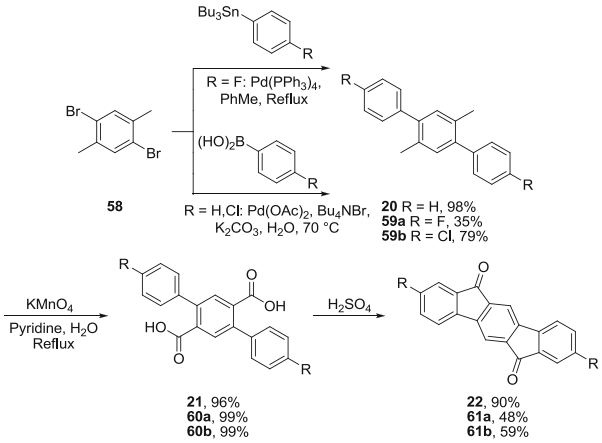


**58**

**20** R = H, 98%
**59a** R = F, 35%
**59b** R = Cl, 79%

**21**, 96%
**60a**, 99%
**60b**, 99%

**22**, 90%
**61a**, 48%
**61b**, 59%

The most common route to IF diones is still based on Deuschels' original 1951 procedure [25]. In 2002, Wang and coworkers modified this synthesis, utilizing a Suzuki cross-coupling reaction to generate terphenyl **20**, which was then oxidized and cyclized as before to yield **22** from 2,5-dibromo-*p*-xylene **58** in 85% yield over three steps (Scheme 13) [48]. Dione **22** could subsequently be reduced to form known 6,12-dihydroindeno[1,2-*b*]fluorene (**26**).

Yamashita and colleagues synthesized **22** and **61a–c** to investigate their utility as n-type semiconducting materials in OFETs [52], inspired by the n-type behavior Komatsu had observed with **57d** [51]. Difluoro- and dichloroterphenyls **59a** and **59b** were formed via either Stille or Suzuki cross-coupling conditions from **58** (Scheme 13). Oxidation with potassium permanganate generated dihalodiacids **60a,b** and then cyclization onto the outside rings afforded dihalodiones **61a,b** in moderate yield. They assessed the performance of these substrates in HMDS-treated OFETs (vapor deposition; bottom-contact; $Si/SiO_2$). **61a** exhibited the best performance, with mobilities as high as 0.17 $cm^2/V{\cdot}s$ and on/off ratio greater than $10^7$, while **22** exhibited no semiconducting behavior.

Marks showed that 2,8-dibromodione **61c** could be made in a slightly different manner (Scheme 14) [37]. Suzuki cross-coupling of methyl 5-bromo-2-iodobenzoate (**62**) with 1,4-dibenzenediboronic acid dipinacolate (**63**) afforded diester **64**; subsequent hydrolysis and cyclization onto the inside ring using concentrated sulfuric acid gave **61c**.

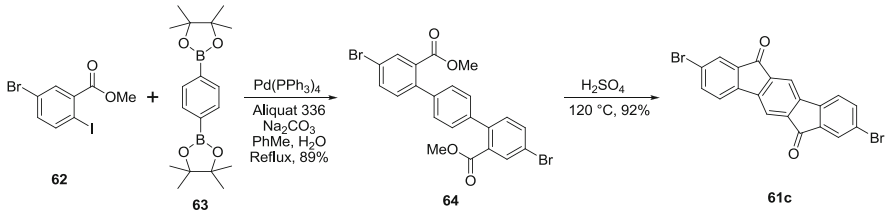


**Scheme 14** Preparation of 2,8-dibromo IF dione **61c** [37]

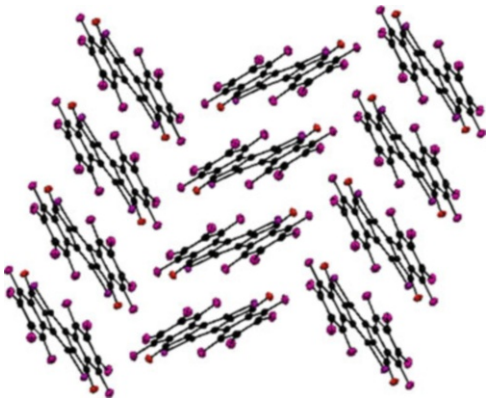

**Fig. 3** Solid state packing of **57d** [51]

Examination of the X-ray data for several [1,2-*b*]IF diones revealed that the extent of halogenation had a dramatic effect on the solid state ordering. For example, perfluoro **57d** exhibited one-dimensional columnar stacking while difluoro **61a** demonstrated face-to-face π-stacking (Fig. 3) [51, 52]. Despite these small structural differences, close contact distances for **57d** and **61a** were found to be 3.31 Å and 3.30 Å, respectively.

Taking advantage of the fortuitous halogenation on the 5- and 11-positions obtained via Swager's iodine-mediated transannular cyclization route (Scheme 13), Haley and coworkers appended a variety of trialkylsilylacetylenes onto **57a**. Sonogashira cross-coupling afforded the 5,11-diethynylindeno[1,2-*b*]fluorene-6,12-diones **65a–f** in 7–61% yield (Scheme 15) [53]. Cyclic voltammetry data illustrated the ability of **65a–f** to accept two electrons reversibly. The half-wave potential for the first reduction occurs at ca. −0.80 V, which is less negative than that of parent **22** (−1.19 V) due to the electron-withdrawing acetylenes but more negative compared to halogenated IF diones **61a–c** (−0.7 V to −0.57 V) and **57d** (−0.45 V). Another advantage of silylacetylene incorporation was a significant increase in solubility, given that minimal solubility in common organic solvents is a hallmark characteristic of nearly all [1,2-*b*]IF diones.

While silyl substitution on the acetylene produced little variance in the optical and electronic properties of **65a–f**, it did have a significant effect on the solid state

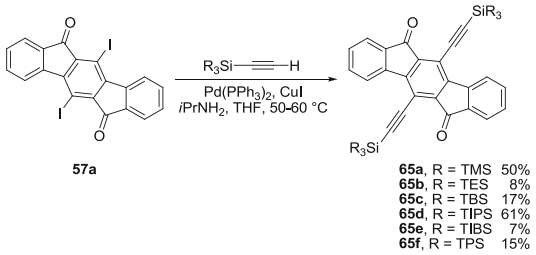


**Scheme 15** 5,11-Diethynyl IF diones **65a–f** [53]

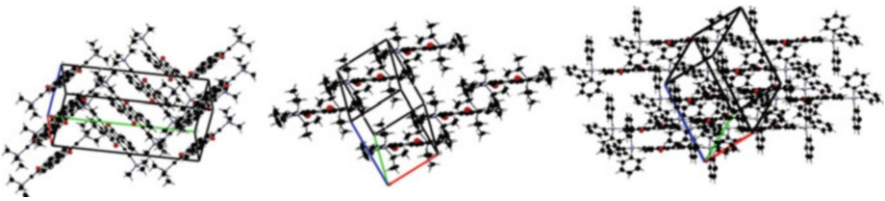

**Fig. 4** Solid state packing of **65a** (*left*), **65d**, *middle*, and **65f** (*right*) [53]

ordering, as three separate packing motifs were observed (Fig. 4). TMS-capped acetylene **65a** possessed herringbone packing, while the larger TPS-capped acetylene **65f** displayed one-dimensional columns without π–π interactions. In accordance with Anthony's observations with 6,13-bis(triisopropylsilylethynyl) pentacene [54], TIPS-capped **65d** exhibited columnar stacking in two dimensions, also known as brick-and-mortar stacking, a packing motif often favorable for charge-transport in materials because it increases the likelihood of significant intermolecular orbital overlap. This was clearly illustrated by comparison of the carbon–carbon close-contact distances of **65a**, **65d**, and **65f**, which were 3.50, 3.40, and 3.77 Å, respectively.

Despite its highly insoluble nature, 2,8-dibromodione **61c** has proven to be a useful precursor for a variety of 2,8-diarylated derivatives, as such species can further provide access to a larger variance of electron-donating/accepting substituents (Scheme 16) [37, 55]. Suzuki or Stille cross-coupling of **61c** with aryls **66a–e** furnished diaryl diones **67a–e** in 43–81% yield.

Marks installed long alkyl groups onto the IF dione core as another method to combat insolubility (Scheme 17) [37]. Kumada cross-coupling of 1,4-dichlorobenzene (**68**) with didodecylmagnesium bromide gave 1,4-didodecylbenzene (**69**). Bromination of **69** yielded 2,5-dibromo-1,4-didodecylbenzene (**70**), which was reacted with boronic acid **71** under Suzuki cross-coupling conditions to afford terphenyl **72**. Cyclization as before with concentrated sulfuric acid at elevated temperatures gave didodecyl dione **73** in 93% yield. Unlike parent **22**, **73** could be directly brominated on the 2- and 8-positions to generate **74** cleanly, which upon further cross-coupling with 2-tributylstannylthiophene (**75**) under standard Stille conditions afforded **76**.

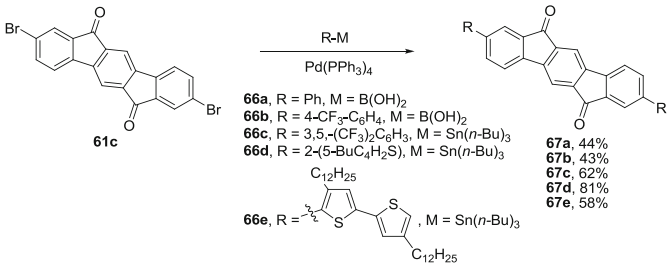


**Scheme 16** Cross-coupling of 2,8-dibromo IF diones **67a–e** [37, 55]

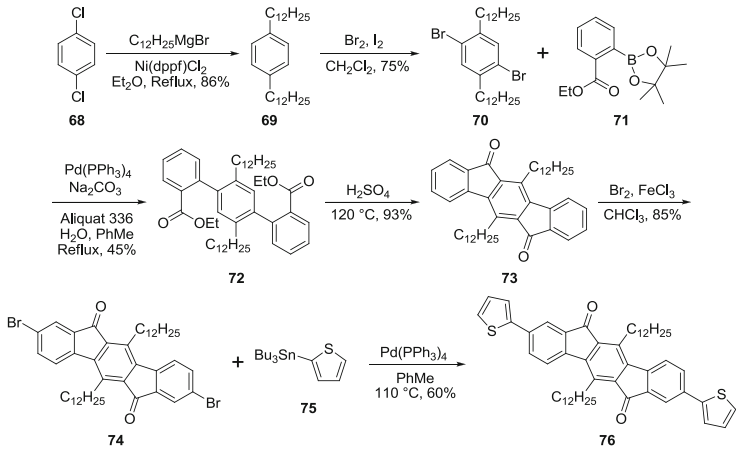


**Scheme 17** Formation of 2,8-dithiophene-5,11-didodecyl IF dione **76** [37]

Like **65a–f**, cyclic voltammetry data for **67d,e**, **73**, and **76** showed that these molecules readily accept electrons at low voltages. Thiophene substitution results in a slight shift of reduction potentials to more negative values with respect to non-thiophene derivative **73**, as well as a small decrease in band gap. In addition, the authors obtained device data for these IF dione derivatives in OTFTs. For example, films of **76** showed ambipolar charge transport, having electron and hole mobilities reaching 0.01 and $6 \times 10^{-4}$ $cm^2/V{\cdot}s$, respectively.

An alternative method to Friedel–Crafts acylation as the final step in dione synthesis involves a Pd-mediated Heck arylation to generate the indeno[1,2-*b*] fluorene skeleton. In 1989, Hellwinkel and Kistenmacher showed that parent and 2,8-di-*tert*-butyl[1,2-*b*]IF diones **22** and **78**, respectively, could be isolated upon reacting precursors **77a,b** with palladium acetate in acetic acid (Scheme 18) [56, 57].

Similarly, Hu and coworkers found that the reaction of dialdehyde **79** with 2 equiv. phenyl and 4-*tert*-butylphenyl boronic acids, **80a**, and **80b**, respectively, in the presence of a custom Pd(II) palladacycle formed diones **22** and **82** in 49% and 58% yield via a two-step, one-pot method (Scheme 19) [58]. Note that the initial step is not a Suzuki cross-coupling reaction; rather addition of the carbonyl and

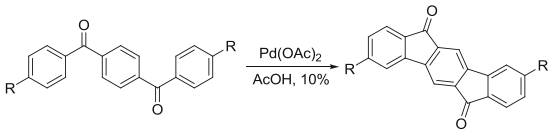


**Scheme 18** $Pd(OAc)_2$-mediated cyclization of **77a,b** [56, 57]

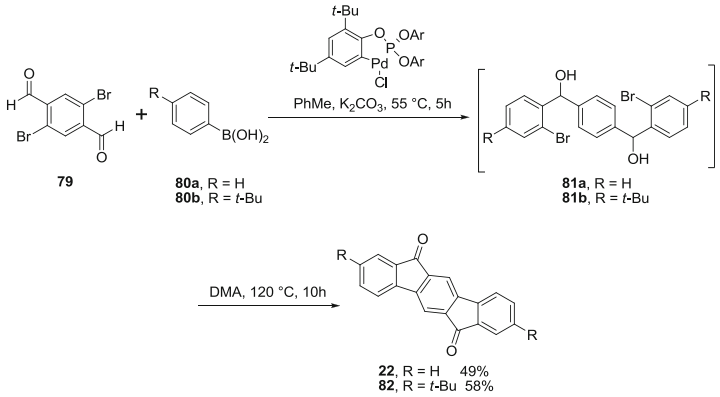


**Scheme 19** Pd-catalyzed preparation of IF diones **22** and **82** [58]

transmetallation of the arylboronic acid to the Pd(II) catalyst is followed by a reductive elimination to give intermediates **81a,b** and generate a Pd(0) species. Switching solvents from toluene to DMA and increasing the temperature promotes oxidative addition of the aryl halide, C–H bond activation of the central aryl ring and subsequent cross-coupling, and then oxidation of the alcohols to ketones gives [1,2-*b*]IF diones **22** and **82** in 49% and 58% yield, respectively, for this complex one-pot cascade reaction.

## *3.2 Indeno[1,2-*b*]fluorene-6,12-olefins*

While not yet as ubiquitous as the above-mentioned diones, olefination at the 6- and 12-positions on the [1,2-*b*]IF scaffold has recently gained interest because of the increased use of the electron-withdrawing dicyanovinylene moiety. This technique was initially described by Gompper in 1987 when dione **22** was reacted with 2 equiv. malononitrile in the presence of $TiCl_4$ to form olefin **83a** (Scheme 20) [59], though no yield was given.

In 2008, Marks expanded the scope of synthesizing IF olefins. Diones **67d,e** and **73** were converted to their corresponding exocyclic olefins **83b**,**c** and **84a** using the $TiCl_4$ method described above (Schemes 21 and 22) [37]. Olefin **84c** was

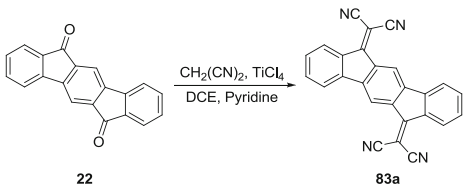


**Scheme 20** Preparation of [1,2-*b*]IF olefin **83a** [59]

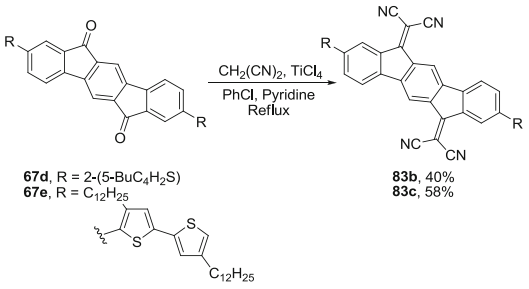


**Scheme 21** Preparation of IF olefins **83b,c** [37]

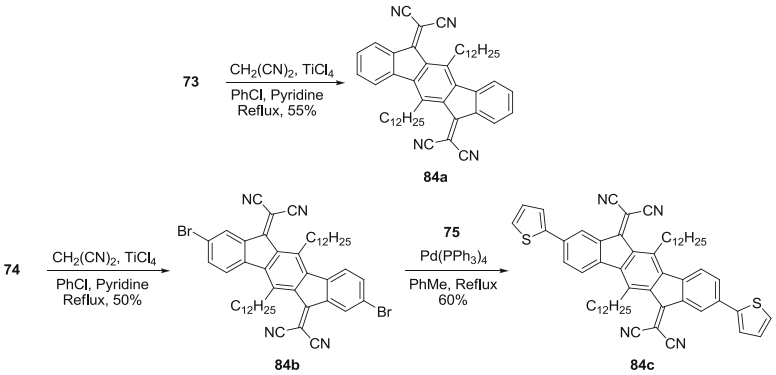


**Scheme 22** Preparation of IF olefins **84a–c** [37]

synthesized through Stille cross-coupling of stannane **75** with olefin **84b** which derived from dione **74** (Scheme 22) [37].

Due to the highly electron deficient dicyanovinylene moiety, **83a–c** and **84b,c** showed consistent stabilization of their HOMO and LUMO levels compared to **67d, e**, **73**, and **76** by approximately 0.15 eV, and 0.6 eV, respectively, as well as a lowered energy gap of approximately 0.5 eV. Furthermore, **83b,c** and **84b,c** exhibited an approximate +0.6 V shift with respect to **67d,e**, **73**, and **76** in reduction potentials. Solid state analysis of **84c** found that the IF core maintains the bond lengths of the three aromatic benzene rings found in *p*-terphenyl. Interestingly,

the exocyclic dicyanovinylene groups contorted the IF core by 13° pointing away from the central alkyl chains. [1,2-*b*]IF dicyanovinylenes **83a–c** and **84a–c** were utilized in thin-film transistors and showed n-type and ambipolar transport. Notably, **83b** showed stable n-type transport in air with mobilities as high as 0.16 $cm^2/V{\cdot}s$.

### *3.3 Fully-Conjugated Indeno[1,2-b]fluorene*

First mentioned by Deuschel as a possible resonance structure of dione **22**, a fully conjugated indeno[1,2-*b*]fluorene (**2**, Fig. 5) might serve as a suitable small molecule analogue of fullerene due to its low-lying LUMO level, subsequently shown by Haley et al. [53, 60]. Furthermore, **2** possesses no *s-cis* diene linkages in its structure, meaning that it should be less susceptible to the deleterious cycloaddition pathways that acenes and fullerenes are susceptible to. Until recently, however, there has been skepticism of the existence of fully conjugated IF species for a number of reasons: (1) the formation of **2** should be energetically costly due to the necessary disruption of the aromaticity of the central benzene ring; (2) IF **2** would possess 20 π-electrons, resulting in the formation of an unfavorable antiaromatic species; and (3) the central rings of **2** would also host a *p*-xylylene (*p*-quinodimethane) core, a notoriously reactive moiety that typically cannot be isolated because of its high tendency to oligomerize/polymerize.

As previously mentioned, Swager and coworkers obtained diones **57a–c** through the iodine-induced transannular cyclization of **24** and **56b,c** in aerobic conditions (Scheme 12) [49]. Under anaerobic conditions, however, another class of products formed that possessed only two aromatic signals in the $^1$H NMR spectrum that were shifted upfield from **57a–c**. Furthermore, they found that exposure to air converted these compounds into **57a–c** in near quantitative yield. Swager deduced the air-sensitive intermediates to be fully conjugated 5,6,11,12-tetraiodoindeno[1,2-*b*]fluorenes **85a–c**, given their highly reactive nature as well as the notable up-field shift of the proton resonances compared to **57a–c** due to their antiaromatic character (Scheme 23). The UV–vis spectrum of **85a** exhibited low energy absorptions of 534 and 571 nm, nearly 250 nm bathochromically shifted from **57a**, attributable to its fully conjugated state.

Studies by Scherf and coworkers in 1996 on the design and structural properties of indeno[1,2-*b*]fluorene polymers (**86a**) came to a similar conclusion [61, 62]. Their argument, based on structurally related 9,9′-bisfluorenes, was that in order to reduce steric hindrance between subunits, the bridging olefinic carbons could lengthen and hence reduce the overall double bond character (**86b**, Fig. 6) [61, 63]. A consequence to such a bond lengthening would be an overall decrease in band gap energy and geometric distortions. Another consequence would be an overall change of the bond structure of the subunit itself. As a model system for **86b**, IF **87a** was prepared and reported to exhibit an absorption spectrum $\lambda_{max}$ of 543 nm; however, no other characterization was reported.

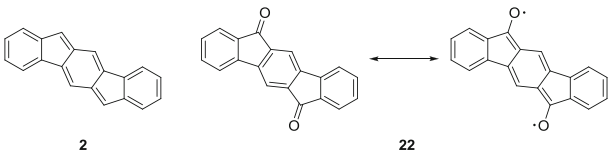


**Fig. 5** Fully conjugated indeno[1,2-*b*]fluorene **2** and resonance structures of **22**

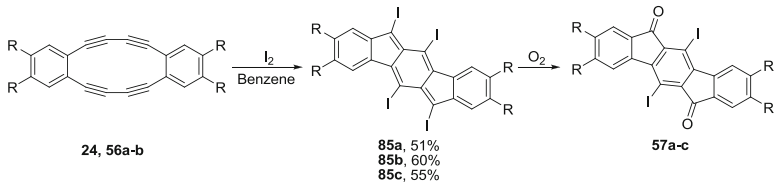


**Scheme 23** Preparation of fully conjugated indeno[1,2-*b*]fluorenes **85a–c** [49]

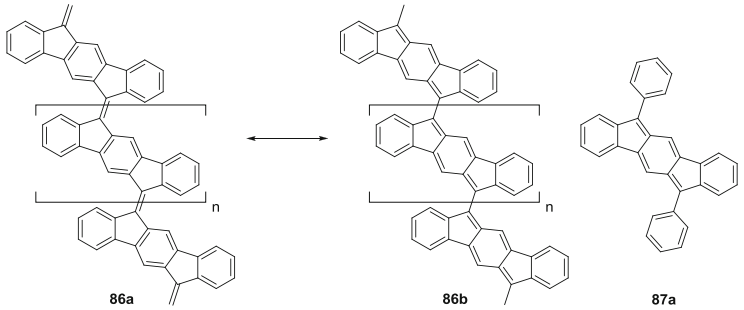


**Fig. 6** Resonance forms of poly(indeno[1,2-*b*]fluorene) **86a,b** and model subunit **87a** [61–63]

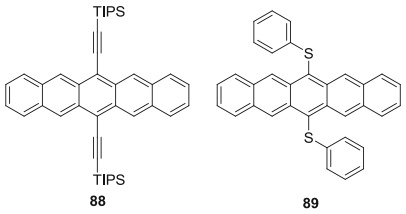


**Fig. 7** Examples of ethynylated (**88**) and heteroatom-substituted (**89**) pentacenes [64, 68]

Works by Anthony [9, 64–67] and Miller [68, 69], among others [70–73], have shown that ethynylogation and/or appending heteroatoms to acenes (e.g., **88**–**89**) results in a marked increase in stability (Fig. 7).

Applying the same rationale and synthetic methodology used to obtain diethynylated pentacenes from pentacene quinone, Haley et al. undertook the synthesis of tetraethynylindeno[1,2-*b*]fluorenes **92a,b** (Scheme 24) using the

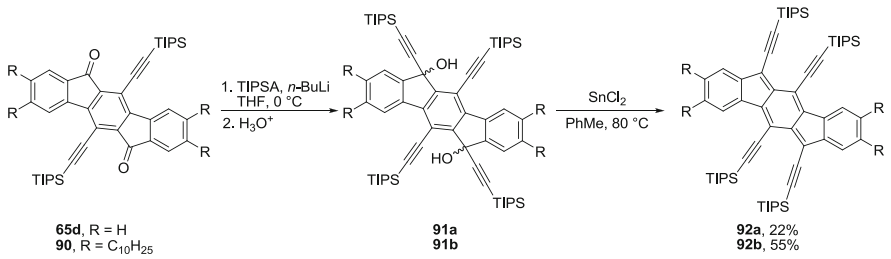


**Scheme 24** Synthesis of fully conjugated 5,6,11,12-tetraethynyl IFs **92a,b** [60]

tetraiodo framework **85a,b** that Swager had already prepared [60]. Unfortunately, direct Sonogashira cross-coupling of (trimethylsilyl)acetylene (TMSA) with **85a,b** did not afford the desired product. Instead, ethynylation of diones **65d** and **90** with the anion of (triisopropylsilyl)acetylene (TIPSA) gave diols **91a,b**; subsequent reduction using anhydrous $SnCl_2$ at elevated temperatures, a common technique used in acene synthesis, afforded compounds **92a,b** in 22% and 55% yield, respectively, over two steps. As observed for **85a–c**, **92a,b** exhibit up-field aromatic chemicals shifts with respect to **65d** and **90**, an indicator of their fully conjugated, anti-aromatic state.

The absorption spectra of **92a,b** showed three low-energy transitions in a pattern with $\lambda_{max}$ values of 594 and 614 nm, respectively, which is roughly a 25 and 45 nm bathochromic shift with respect to **85a** due to the increased conjugation and lower HOMO/LUMO gap caused by the four ethynyl groups. In comparison to **88**, whose low-energy transition $\lambda_{max}$ value is 644 nm, **92a,b** were hypsochromically shifted by 50 and 30 nm, a consequence of having two fewer π-electrons in the anti-aromatic core. Unlike **88,** however, **92a,b** are non-emissive, a trait often observed for antiaromatic molecules.

As with previously mentioned IF diones **65a–f**, **67d,e**, **73**, and **76**, cyclic voltammetry data of **92a** showed first and second reduction potentials of −0.62 V and −1.16 V, respectively, while decyl IF **92b** exhibited potentials of −0.73 and −1.29 V, respectively. Additionally, **92a,b** do exhibit oxidation potentials between 1.10 and 1.30 V, although this process is irreversible. Despite the lack of electron-withdrawing diones, the first reduction potentials of **92a,b** meet or surpass the values of **65a–f**, **67d,e**, **73**, and **76** because a twofold reduction of the indeno[1,2-*b*]fluorene core is extremely favorable as the resultant dianion is a 22 π-electron species where each ring is fully aromatic.

X-Ray analysis of **92a** concluded that there was indeed long and short bond alternation throughout the central portion of the IF core (Fig. 8), which agrees with Scherf's initial hypothesis regarding the internal bond structure of polymer **86** and model compound **87a**. Interestingly, the peripheral benzene rings remain homogenized in length, suggesting that the name dibenzo-*s*-indacene is also a valid descriptor. The bond lengths in the internal three rings show that **92a** is indeed a stable example of a molecule containing a *p*-xylylene core, similar to what was found for Thiele's and Tschitschibabin's hydrocarbons (Fig. 9) [74].

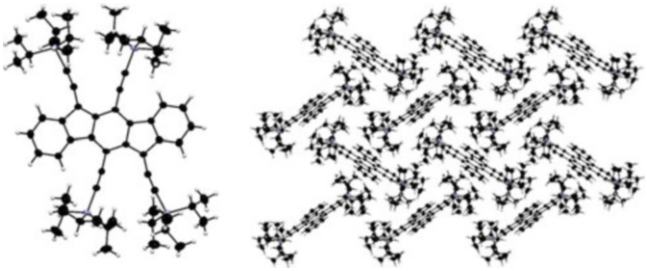

**Fig. 8** X-Ray single crystal structure (*left*) and expanded herringbone crystal packing of **92a** (*right*) [60]

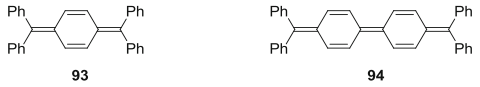


**Fig. 9** Structures of Thiele's (**93**) and Tschitschibabin's (**94**) hydrocarbons [74]

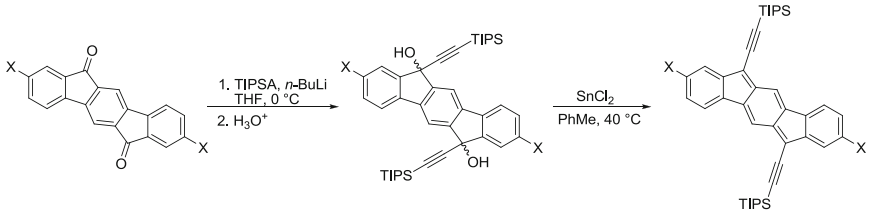


**22**, X = H
**61a**, X = F
**61b**, X = Cl
**61c**, X = Br
**61d**, X = Me
**67a**, X = Ph
**67b**, X = 4-$CF_3C_6H_4$
**67c**, X = 3,5-$(CF_3)_2C_6H_3$
**67d**, X = 2-(5-$BuC_4H_2S$)

**95a-i**

**96a**, 71%
**96b**, 31%
**96c**, 35%
**96d**, 47%
**96e**, 60%
**96f**, 44%
**96g**, 43%
**96h**, 62%
**96i**, 81%

**Scheme 25** Synthesis of 6,12-diethynyl IFs **96a–i** [55]

Examination of the crystal packing indicated that **92a** exhibited an expanded herringbone pattern often found in unsubstituted acenes [75]. This undesirable packing motif is attributable to the steric bulk of the four interdigitated (triisopropylsilyl)ethynyl groups in **92a**.

Regarding the effect of ethynylation on the IF core, computational studies suggested that ethynyl groups on the 5- and 11-positions had only a minor influence on the overall electronics, as their removal changed the calculated HOMO and LUMO energies by +0.02 eV and −0.10 eV, respectively [55]. Functionalization of the favorable 6,12-diethynyl IF scaffold with withdrawing groups on the 2- and 8-positions further lowered the calculated HOMO and LUMO energies to levels that approach those in the fullerene PCBM [7, 8, 76]. Ethynylation of **22**, **61a–d**, and **67a–d** using the lithiate of TIPSA generated mixtures of diol isomers, and subsequent reduction using anhydrous $SnCl_2$ afforded fully conjugated indeno[1,2-*b*]fluorenes **96a–i** in 31–81% yield over two steps (Scheme 25).

**Fig. 10** Solid state packing of **96a** (*left*) and **96h** (*right*) [55]

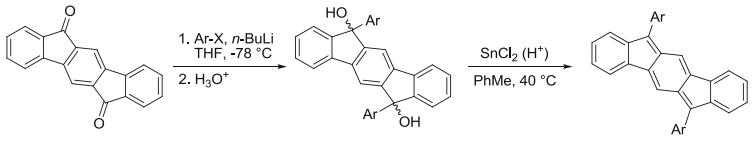


**22**

**97a**, Ar = Ph
**97b**, Ar = 4-OMeC$_6$H$_4$
**97c**, Ar = 2,4,6-Me$_3$C$_6$H$_2$
**97d**, Ar = 4-MeC$_6$H$_4$
**97e**, Ar = 4-FC$_6$H$_4$
**97f**, Ar = 4-ClC$_6$H$_4$
**97g**, Ar = 4-BrC$_6$H$_4$
**97h**, Ar = 4-CF$_3$C$_6$H$_4$
**97i**, Ar = 3,5-(CF$_3$)$_2$C$_6$H$_3$
**97j**, Ar = C$_6$F$_5$
**97k**, Ar = 2,6-F$_2$C$_6$H$_3$
**97l**, Ar = 9-Anthryl

**87a**, 55%
**87b**, 37%
**87c**, 42%
**87d**, 36%
**87e**, 50%
**87f**, 48%
**87g**, 59%
**87h**, 42%
**87i**, 39%
**87j**, 38%
**87k**, 23%
**87l**, 14%

**Scheme 26** Synthesis of 6,12-diaryl IFs **87a–m** [77, 78]

Like **92a,b**, the absorption spectra of **96a–i** showed three low energy transitions with the $\lambda_{max}$ values between 561 and 577 nm, corresponding to a band gap of 2.08−2.15 eV [55]. Cyclic voltammetry measurements exhibited first reduction potentials between −0.7 and −0.5 V and second reduction potentials between −1.2 and −1.0 V, correlating to LUMO energies that range between −4.0 and −4.1 V. Explanation for the lack of HOMO and LUMO energy level variation was due to low orbital density on the 2- and 8-positions, where only weak inductive electronic effects could be invoked.

While removal of ethynyl groups on the 5- and 11-positions did reduce steric hindrance, substitution had a significant impact on the crystal morphology of **96** [55]. Parent **96a** packed without any π-interactions (Fig. 10) where the closest intermolecular distance was an edge to face contact of 3.85 Å. Alternatively, **96h** exhibited one-dimensional columnar stacks with an intermolecular distance of 3.40 Å.

The next series of fully-conjugated indeno[1,2-*b*]fluorenes synthesized by Haley et al. was 6,12-diarylindeno[1,2-*b*]fluorenes (Scheme 26) [77]. Similar to **96a–i**, lithium-halogen exchange with the appropriate aryl halide and reaction with **22** afforded mixtures of stereoisomers **97a–i**. Reduction using anhydrous $SnCl_2$ at elevated temperatures provided **87a–j** in 36–59% yield. The electron-withdrawing

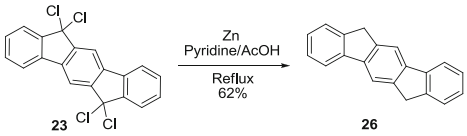


**Scheme 27** Original synthesis of 6,12-dihydroindeno[1,2-*b*]fluorene (**26**) [26]

groups in **97h–j** necessitated the addition of a small amount of trifluoroacetic acid in order for the reaction to proceed in timely fashion.

The absorption spectra for **87a–j** displayed a greater variation in $\lambda_{max}$ values than **96a–i** due to the higher amount of orbital density found on the 6- and 12-positions of the IF core. Cyclic voltammetry data for **87a–j** showed that the diaryl IFs exhibit redox amphoterism, a trait not seen in the previous fully conjugated indeno[1,2-*b*]fluorenes. This is easily observed with 6,12-diphenyl [1,2-*b*]IF **87a**, as it exhibited two reduction peaks and three oxidation peaks. The reduction and oxidation values for **87a–j** corresponded to HOMO and LUMO energies that range between −5.5 to −5.8 eV and −3.6 to −4.0 eV, respectively. Coincidentally, **87e** displayed reduction and oxidation potentials within 0.03 V that of **88**.

Single crystal OFETs were fabricated with microcrystals of **87j** as the active channel [77]. With Au source/drain contacts and Au electrodes, the OFET showed ambipolar charge transport, with saturation hole and electron mobilities of $7 \times 10^{-4}$ and $3 \times 10^{-3}$ $cm^2/V{\cdot}s$, respectively.

Concurrent with the Haley studies, Yamashita et al. reported the synthesis and properties of 6,12-diarylindeno[1,2-*b*]fluorenes **87k–m** as well as **87a** (Scheme 26) [78]. While their molecules exhibited redox amphoterism as well, the Japanese authors reported only a single oxidation and reduction wave for each. Vapor-deposited thin film OFETs of **87k,l** also showed ambipolar charge transport but at diminished mobilities (hole: $1.9 \times 10^{-5}$ and $1.1 \times 10^{-5}$ $cm^2/V{\cdot}s$, respectively; electron: $8.2 \times 10^{-6}$ and $1.6 \times 10^{-6}$ $cm^2/V{\cdot}s$, respectively).

## *3.4 Other Indeno[1,2-b]fluorenes*

First synthesized by Deuschel in 1951 via dehalogenation of **23** (Scheme 27) [26], 6,12-dihydroindeno[1,2-*b*]fluorene (**26**) can be viewed as a planarized *p*-terphenyl derivative. As a result of the enforced geometry, there is greater conjugation between the phenyl rings, which imparts more desirable emissive properties; thus, this core unit has been utilized in a wide variety of molecular and polymeric systems – far too many to be reviewed here. Rather, selected, salient examples will be presented.

Common synthetic routes to **26** typically involve reduction of dione **22**. Another intriguing method, however, involves the use of palladium with *N*-heterocyclic carbene ligand **L** (Scheme 28) [79]. Presumably, the cascade begins with oxidative addition of the aryl halide to the catalyst. Activation of the benzylic C–H bond for

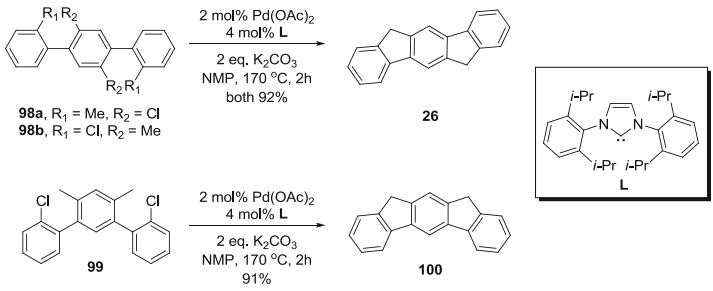


**Scheme 28** Synthesis of **26** and [2,1-*b*]IF **100** [79]

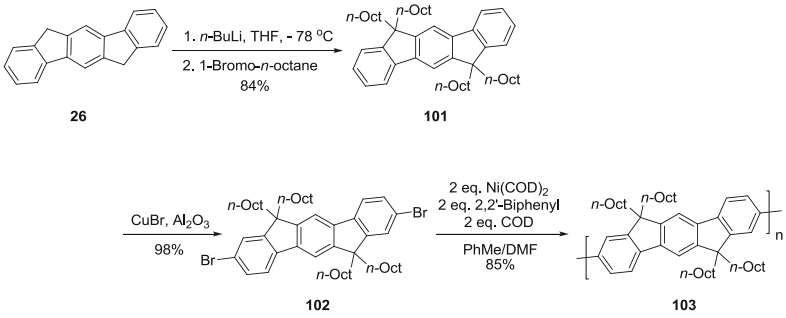


**Scheme 29** Synthesis of polymer **103** starting from **26** [80]

insertion of the metal leads to intramolecular aryl–aryl couplings via subsequent reductive eliminations from the palladium center. This elegant reaction can produce both 6,12-dihydro[1,2-*b*]IFs and 10,12-dihydro[2,1-*b*]IFs in greater than 90% yield from the appropriate terphenyl precursor.

Many synthetic routes are utilized to generate 6,12-functionalized dihydroindeno[1,2-*b*]fluorenes, typically from **22** or **26**. One direct method is base-promoted alkylation of the methylene carbons of **26**. For example, lithiation of **26** followed by treatment with 1-bromooctane gave tetrasubstituted **101** (Scheme 29) [80]. Subsequent bromination at the 2- and 8-positions with CuBr/alumina furnished **102**, which could then be polymerized to form polyindenofluorene **103** linked at the 2- and 8-positions rather than at the 6- and 12-positions as seen in Scherf's polyindenofluorene **85**. Muellen and co-workers found that **103** showed a bathochromic shift in fluorescence compared to polyfluorene (into the visible region) and it formed a liquid crystalline phase at high temperature, possibly making a suitable LED component.

An alternative route to functionalized dihydroindeno[1,2-*b*]fluorenes begins from fluorenone and involves intramolecular Friedel–Crafts alkylation in the final step, leading to spiro-fused derivatives – a method championed by Rault-Berthelot,

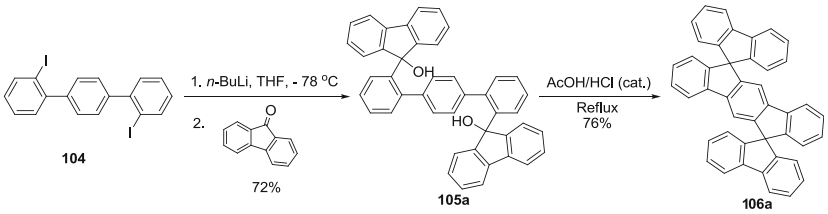


**Scheme 30** Syntheses of dispiro-IF **106a** [28]

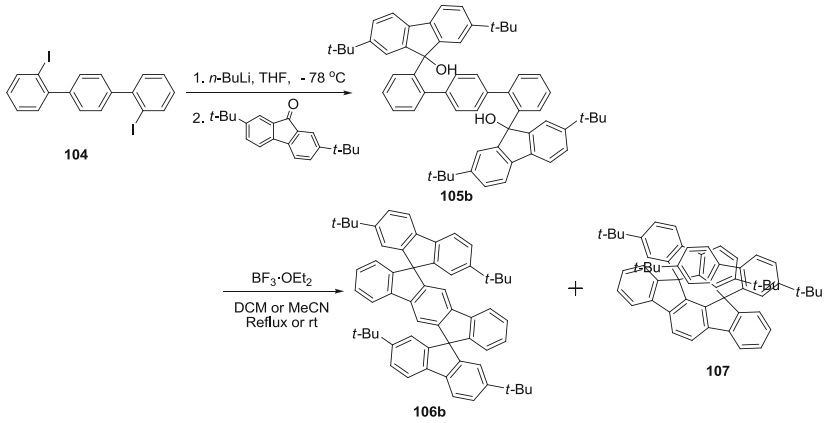


**Scheme 31** Syntheses of dispiro-IFs **106b** and **107** [30]

Poriel, and coworkers. For instance, they prepared dispiro-fused [1,2-*b*]IF **106a** in an attempt to overcome issues in fluorene-utilizing OLEDs involving defects perturbing the color outputs of these devices (Scheme 30) [28, 81]. Beginning with 2,2″-diiodo-*p*-terphenyl (**104**), lithiation and subsequent addition of fluorenone furnished diol **105a**. Treatment with AcOH/HCl at reflux then gave **106a** in 55% yield over the two steps. Devices utilizing **106a** showed improved blue-emission without green contamination from defects [82].

Further investigation by the same group found that, depending on the substrate and reaction conditions, two different products were often produced in this cyclization, thus limiting somewhat the scope of this synthesis to incorporate broader functionalization. When the fluorene moiety possessed steric bulk on the periphery, formation of a second product, the indeno[2,1-*a*]fluorene regioisomer, is favored. Its formation is also typically favored by use of less polar solvents and higher temperatures. In the reaction shown in Scheme 31, **106b** is formed in a ratio with **107** of roughly 3:1 when the reaction is done in DCM but the ratio shifts to 1:2 if the reaction is performed in acetonitrile, regardless of temperature. Adding even more steric bulk on the fluorene favors the [2,1-*a*]IF to an even greater degree, suppressing formation of the [1,2-*b*]IF isomer completely if sufficient bulk exists [30].

**Fig. 11** Spiroxanthene-fused [1,2-*b*]IF **108** [83]

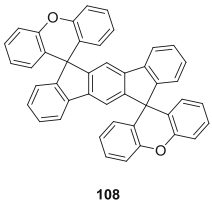


**Fig. 12** Structures of IFs **109** and **110** [84]

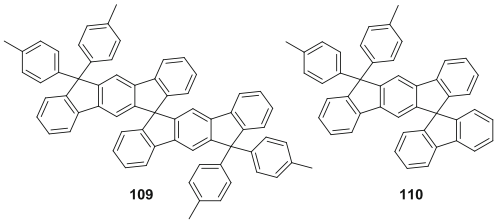


**Fig. 13** IF-oligomer **111** [85]

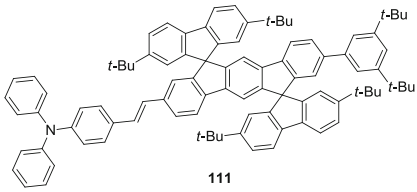


This same group also investigated the use of dispiroxanthene-IF **108** in OLEDs, finding its properties little changed from those of the dispirofluorene-IF derivatives (Fig. 11) [83].

Wong and colleagues found **109** to have a maximum power efficiency ($PE_{max}$) of ~4.0 lumens per watt (lm/W) and external quantum efficiencies (EQE) greater than 8% when used as a red phosphorescent host with $Btp_2Ir(acac)$ in a phosphorescent OLED (PhOLED) (Fig. 12) [84]. The device also showed turn-on voltages of ~2.5–3.0 V. In addition, Wong's group has also synthesized **110** and used it as a host material for a green PhOLED with $ppy_2Ir(acac)$, achieving a EQE of 14% and $PE_{max}$ of >33 lm/W at 10,000 cd/m$^2$ with an operating voltage of 5 V.

Lee and coworkers synthesized IF-oligomer **111** (Fig. 13) [85] and utilized it as a blue dopant in the emitting layer of a blue OLED with maximum power efficiency of 4.8 lm/W and quantum efficiency of 6.4% at 20 mA/cm$^2$ [86].

Ie et al. prepared fluorinated 6,12-dihydro-IF derivatives **112a–g** in an attempt to achieve large electron affinities (EAs) to facilitate n-type charge transport in OFETs (Scheme 32) [87]. With **112d**,**f**,**g** they achieved EAs ca. –3 eV but no device attributes were discussed.

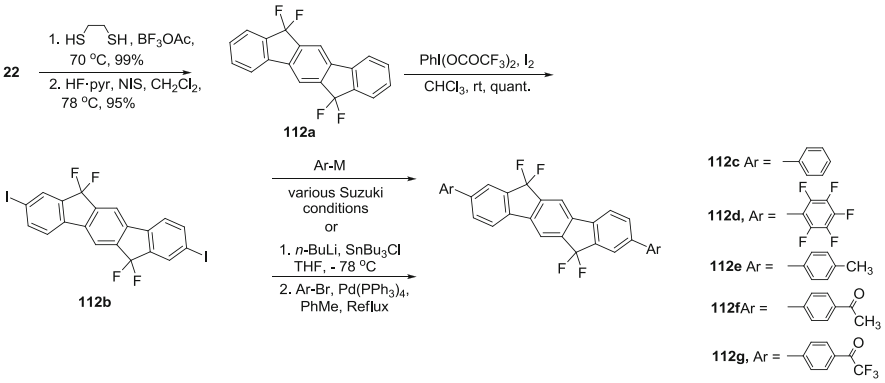


**Scheme 32** Synthesis of 6,12-tetrafluoro [1,2-*b*]IFs **112a–g** [87]

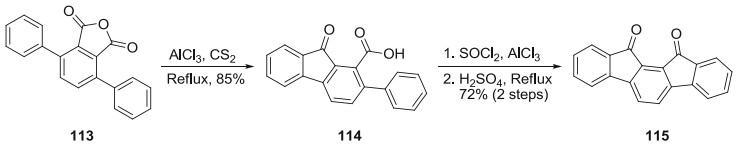


**Scheme 33** Preparation of parent indeno[2,1-*a*]fluorene dione **115** [23, 26]

# 4 Indeno[2,1-*a*]fluorenes

## *4.1 Indeno[2,1-a]fluorene-11,12-diones*

The first account of the indeno[2,1-*a*]fluorene core in the literature dates to 1939 when Weizmann investigated polycyclic structures and their potential carcinogenic properties [23]. Intramolecular Friedel–Crafts acylation of 3,6-diphenylphthalic anhydride (**113**) in refluxing $CS_2$ afforded fluorenone carboxylic acid **114** (Scheme 33). Acid chloride formation and subsequent cyclization in concentrated sulfuric acid generated the parent indeno[2,1-*a*]fluorene dione **115** in 5% yield with respect to **113**. This was reaffirmed by Deuschel in 1951 where **115** is obtained in 72% under the same conditions [26].

Recent work by Rault-Berthelot et al. considered an alternative pathway to **115** (Scheme 34) [33]. Diels–Alder cyclization with *trans*,*trans*-1,4-diphenyl-1,3-butadiene (**116**) and dimethyl acetylenedicarboxylate (**117**) resulted in cyclohexadiene **118** where subsequent oxidation with Pd/C afforded terphenyl **119**. Direct cyclization of **119** using concentrated sulfuric acid does afford **115**, but only in 12% yield. Instead, saponification of **119** to diacid **120** followed by cyclization improves the yield of **115** to 38%.

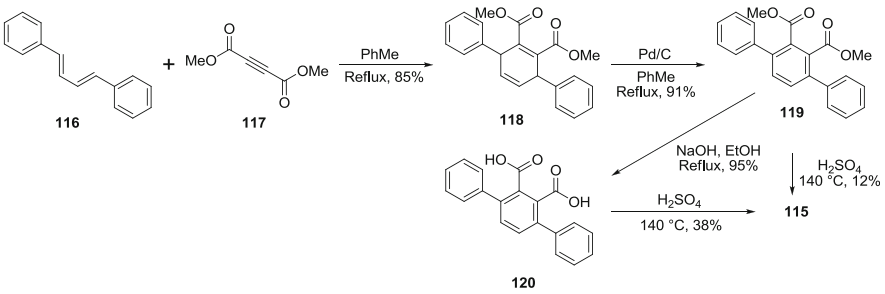


**Scheme 34** Diels–Alder approach to the preparation of **115** [33]


**Fig. 14** Resonance structures of **3**

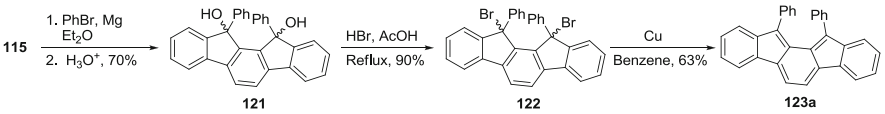


**Scheme 35** Preparation of fully conjugated 11,12-diphenylindeno[2,1-*a*]fluorene **123a** [88]

## *4.2 Fully-Conjugated Indeno[2,1-a]fluorenes*

Like **2**, the indeno[2,1-*a*]fluorene isomer also supports full conjugation, illustrated by **3**, where an *o*-xylylene core (*o*-quinodimethane) is present in the structure (Fig. 14). As such, interest in this structure lies in the potential of the *o*-xylylene core to exist as a stable open shell configuration (**3b**).

Work on **3** originated in 1957 when LeBerre reacted phenylmagnesium bromide with **115** to form diol **121** (Scheme 35) [88]. Refluxing in a hydrobromic acid/acetic acid solution resulted in dibromide **122**, where reduction using elemental Cu afforded diphenylindeno[2,1-*a*]fluorene **123a** in 63% yield. While **123a** readily degraded in aerobic conditions, solutions under an inert atmosphere were said to be stable but no information regarding time was given. However, due to these air-sensitivity issues, no further investigation of its structural or electronic properties was explored.

Recent work by Tobe examined the synthesis of 11,12-dimesitylindeno[2,1-*a*] fluorene **123b**, which was also derived from **115** (Scheme 36) [89]. After reaction of **115** with mesitylmagnesium bromide, diol **124** was reduced with anhydrous $SnCl_2$ in the presence of trifluoroacetic acid at elevated temperatures in toluene to afford **123b** in 48% yield. Fortunately, **123b** was stable at least for 1 week in light and air and showed no reactivity with maleic anhydride. The researchers attributed this

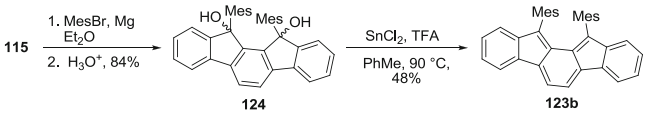


**Scheme 36** Preparation of fully conjugated 11,12-dimesitylindeno[2,1-*a*]fluorene **123b** [89]

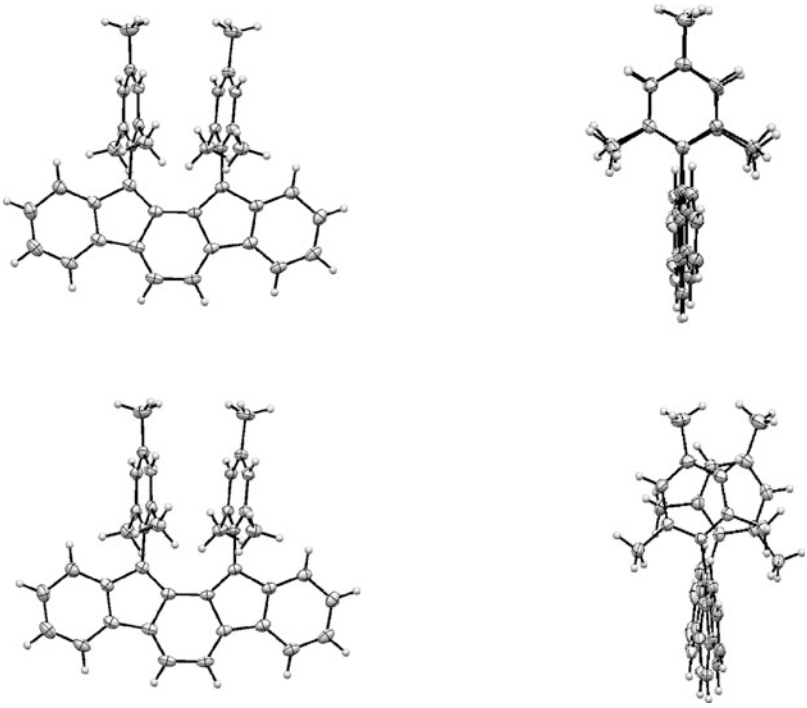

**Fig. 15** Eclipsed (*top*) and staggered (*bottom*) crystal morphs of **123b** [89]

robustness to the bulky mesityl groups adequately shielding the reactive 11- and 12-positions.

The absorption spectra of **123b** showed three distinct transitions in the 480–540 nm domain ($\lambda_{max}$: 537 nm) as well as a low energy tail to 730 nm, affording a 1.70 eV band gap energy. As with the previous mentioned fully conjugated [1,2-*b*]IFs, no fluorescence was observed for **123b**. Cyclic voltammetry data showed that **123b** exhibited both a reversible oxidation and reduction at −1.51 and 0.59 V, respectively.

X-Ray structural data for **123b** clearly showed the indeno[2,1-*a*]fluorene scaffold (Fig. 15). Interestingly, two independent molecules of **123b** were found where the mesityl groups are in either an eclipsed or staggered fashion (top and bottom, respectively), exhibiting a torsion angle of 1.7° and 15.2°, respectively. Examination of the internal bond lengths of **123b** revealed the expected alternating long (1.431 and 1.480 Å) and short (1.359 and 1.391 Å) motif, similar to **92a**.

**Scheme 37** Original preparation of parent indeno [2,1-*b*]fluorene dione **17** [26]

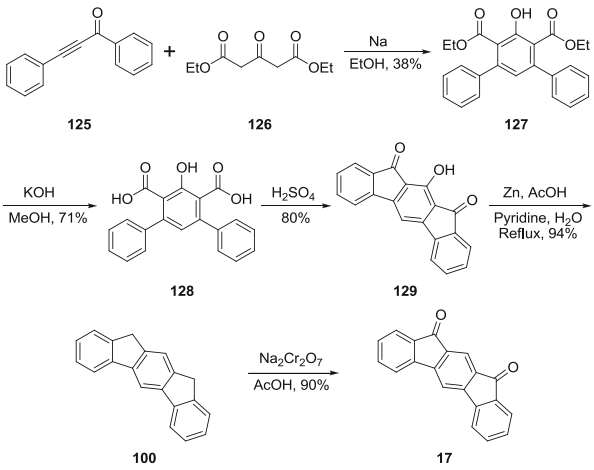


**Scheme 38** Chardonnen's route to **17** [27]

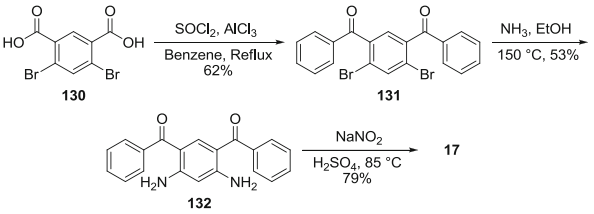


## 5 Indeno[2,1-*b*]fluorenes

### *5.1 Indeno[2,1-*b*]fluorene-10,12-diones*

The first account of 10,12-indeno[2,1-*b*]fluorene dione **17** dates to 1951 when Deuschel condensed phenylbenzoylacetylene (**125**) with ketodiester **126** to afford *m*-terphenyl diester **127** (Scheme 37) [26]. Saponification of **127** to **128** and subsequent ring closure yielded 11-hydroxy-[2,1-*b*]IF dione **129**. Reduction using Zn metal provided 10,12-dihydro [2,1-*b*]IF **100**. A final oxidation with sodium dichromate gave dione **17**.

Chardonnens and Ritter in 1955 reported an alternative pathway to **17** where 4,6-dibromoisophthalic acid (**130**) was converted to the acid chloride and subsequently underwent a twofold Friedel–Crafts acylation with benzene to afford dibromodione **131** (Scheme 38) [27]. Aryl amination of **131** yielded **132** where a subsequent Sandmeyer-mediated cyclization gave **17** in 79% yield. The synthesis of substituted indeno[2,1-*b*]fluorenes has also been explored. As discussed earlier, the [2,1-*b*] isomer was often formed in equal amounts with the corresponding [1,2-*a*] isomer in a multitude of cyclizations performed by Chardonnens and coworkers (Scheme 3) [43].

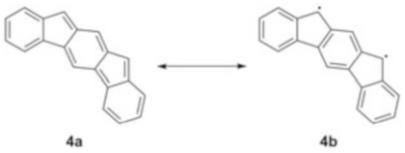


**Fig. 16** Resonance structures of **4**

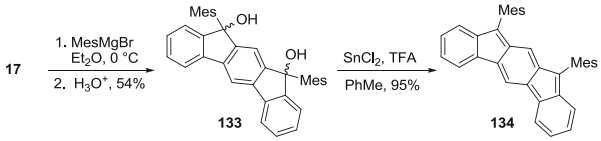


**Scheme 39** Preparation of fully-conjugated 11,12-dimesitylindeno[2,1-*b*]fluorene **134** (Shimizu and Tobe, 2011, private communication)

## 5.2 *Fully-Conjugated Indeno[2,1-*b*]fluorenes*

Full conjugation for the indeno[2,1-*b*]fluorene isomer is also possible (**4**, Fig. 16). However, due to ring positioning, formation of the requisite xylylene core in **4** requires the disruption of two benzene rings rather than one needed for the [1,2-*b*] and [2,1-*a*] isomers. As such, **4** should display an asymmetrical arrangement of the π-system where the D- and E-rings both possess *s-cis* diene linkages. Like the above-mentioned fully conjugated [2,1-*a*] **3**, interest for **4** lies in its ground state biradical character (**4b**).

Currently, only one example of a fully-conjugated indeno[2,1-*b*]fluorene is known and its existence at this time remains unofficial (Shimizu and Tobe, 2011, private communication). Tobe et al. synthesized the molecule in a near identical manner in which **115** was made – IF dione **17** was reacted with 2 equiv. mesitylmagnesium bromide to form diastereomeric diols **133**. Further reaction with $SnCl_2$ in the presence of trifluoroacetic acid yielded 10,12-dimesitylindeno [2,1-*b*]fluorene **134** (Scheme 39). Little is known about this molecule in terms of optoelectronic or structural properties. Due to the presence of the two *s-cis* diene linkages, however, **134** is considerably less stable than its [1,2-*b*] and [1,2-*a*] counterparts.

## 5.3 *Other Indeno[2,1-*b*]fluorenes*

In addition to the spiro-fused [1,2-*b*]IF and [2,1-*a*]IF, Rault-Berthelot and colleagues also synthesized [2,1-*b*] derivative **137** for use in OLED devices (Scheme 40). They found that the compound had one of the highest triplet energies

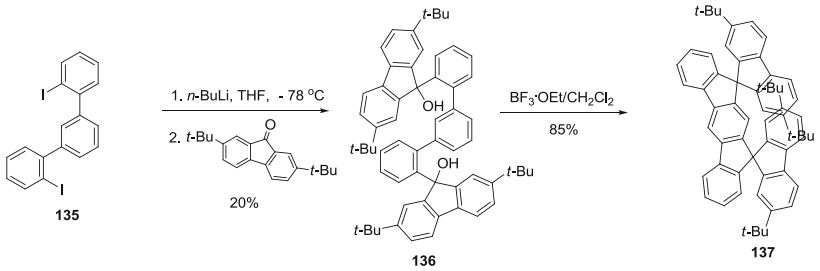


**Scheme 40** Preparation of dispiro-[2,1-*b*]IF derivative **137** [90]

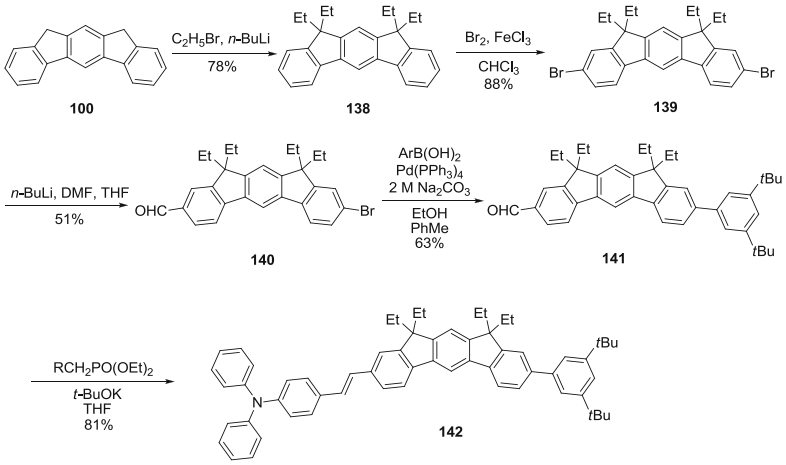


**Scheme 41** Preparation of [2,1-*b*]IF derivative **142** [86]

for a "morphologically-stable pure hydrocarbon" derivative for use in organic electronics [90].

While pursuing their early work on [1,2-*b*] **111**, Lee and colleagues also investigated [2,1-*b*]IFs **138** and **142**. Tetraethyl IF **138** is easily synthesized by treatment of **100** with *n*-BuLi in THF and subsequent addition of 1-bromoethane (Scheme 41) [86]. Lewis acid-catalyzed bromination of **138** in chloroform gives **139**. Treatment of the dibromide with ca. 1.2 equiv. *n*-BuLi in THF then addition of excess DMF gives the monoformylated IF **140**, followed by Suzuki cross-coupling and subsequent Horner–Wadsworth–Emmonds reaction to yield **142** which showed increased planarity with respect to **111**, with a bathochromic shift in fluorescence indicative of a longer conjugation pathway. The quantum yield of **142**, however, was greatly reduced compared to **111** and that, combined with poor overlap with the emission spectrum of the host compound, led to its lower device efficiencies ($PE_{max}$ ~ 1 lm/W, EQE ~ 1.6% at 20 mA/cm$^2$).

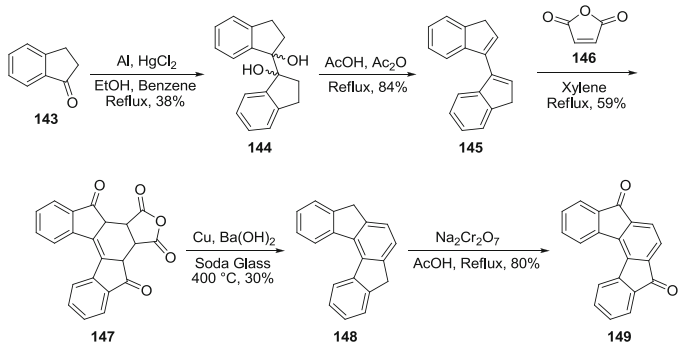


**Scheme 42** Preparation of parent [2,1-*c*]IF dione **149** [91]

# 6 Indeno[2,1-*c*]fluorenes

## *6.1 Indeno[2,1-c]fluorene-5,8-diones*

The first account of the [2,1-*c*]IF dione in the literature occurred in 1961 where work by Ginsburg and Altman investigated the Diels–Alder chemistry regarding bi (cyclopentenes) and bi(cycloheptenes) (Scheme 42) [91]. They found that reaction of indanone **143** in the presence of Al amalgam resulted in pinacol **144**, which was further eliminated in refluxing acetic acid and acetic anhydride to form 3,3′-biindenyl **145**. Cyclization of **145** with maleic anhydride (**146**) afforded anhydride **147**. Decarboxylation of **147** using elemental Cu, barium hydroxide, and soda glass at 400 °C generated 5,8-dihydroindeno[2,1-*c*]fluorene **148**; subsequent oxidation with sodium dichromate in refluxing acetic acid afforded dione **149**.

An alternative route to **149** was devised by Chardonnens and Chardonnens in 1966 where propiophenone (**150**) is converted to pinacol **151** through an aluminum amalgam in refluxing ethyl acetate (Scheme 43) [92]. Double elimination of **151** using acetyl chloride in refluxing acetic anhydride afforded diene **152** which is cyclized with **146** to give anhydride **153**. Aromatization of the central ring using elemental sulfur at 280 °C formed terphenyl anhydride **154**. Saponification to **155** and subsequent decarboxylation using the Lazier catalyst at 215 °C yielded 3,6-dimethyl-1,2-diphenyl benzene (**156**). Oxidation via potassium permanganate in a refluxing solution of water and pyridine formed diacid **157** and further cyclization using concentrated sulfuric acid at elevated temperatures gave **149**.

The few examples of substituted [2,1-*c*]IF diones in the literature are limited to the 1-, 6-, 7-, and 12-positions. For example, work by Wong and coworkers on the investigation of planarized cyclooctatetraenes cyclized diacid **158**, with polyphosphoric acid at elevated temperatures to form dione **159** where the 1- and 12-positions are tethered together with an ethane bridge (Scheme 44) [93].

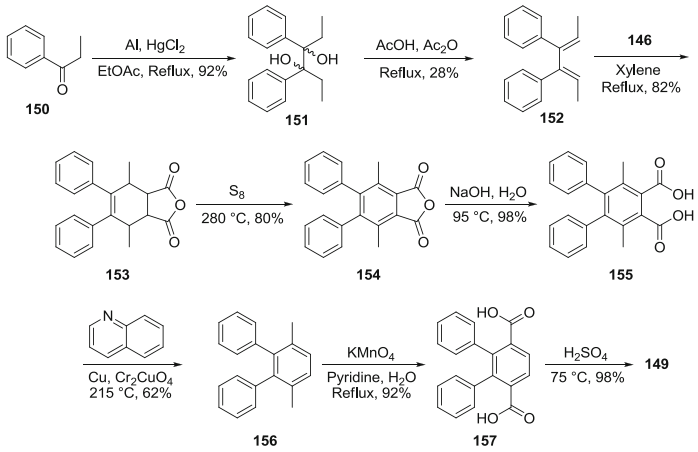


**Scheme 43** Alternate synthesis to **149** [92]

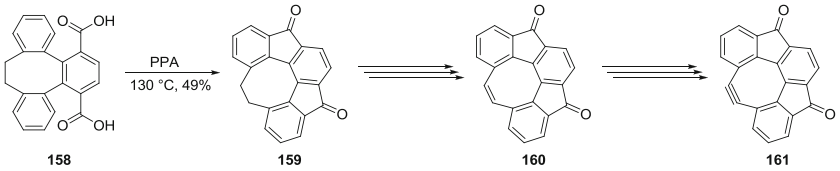


**Scheme 44** Preparation of fused [2,1-*c*]IF diones **159–161** [93]

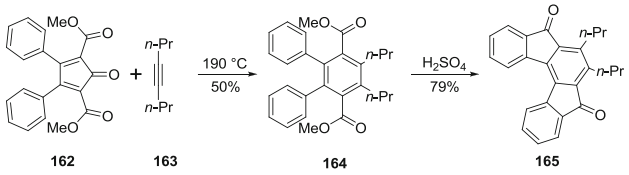


**Scheme 45** Preparation of 6,7,-di-*n*-propyl [2,1-*c*]IF dione **165** [94]

A combination of bromination and elimination reactions on **159** resulted in an unsaturation to ethene- and ethyne-bridged IFs **160** and **161**, respectively.

Wang's group achieved substitution at the 6- and 7-positions of the [2,1-*c*] core by reacting cyclopentadienone **162** with 4-octyne (**163**) in a Diels–Alder reaction to form terphenyl diester **164** (Scheme 45) [94]. Cyclization with concentrated sulfuric acid gave 6,7-di-*n*-propyl [2,1-*c*]IF dione **165** in 79% yield. These results stand in contrast to the observations in Scheme 11 where use of either phenylacetylene or diphenylacetylene gave the corresponding [1,2-*b*] isomer in high yield.

In addition, the same group found that reaction of [2,1-*c*]IFs **165** and **166** with an acetylide nucleophile gave diols **167a,b**; subsequent treatment with $SOCl_2$ induced a cascade cyclization forming [1,2-*a*]IF dimers **168a,b** in low yield (Scheme 46)

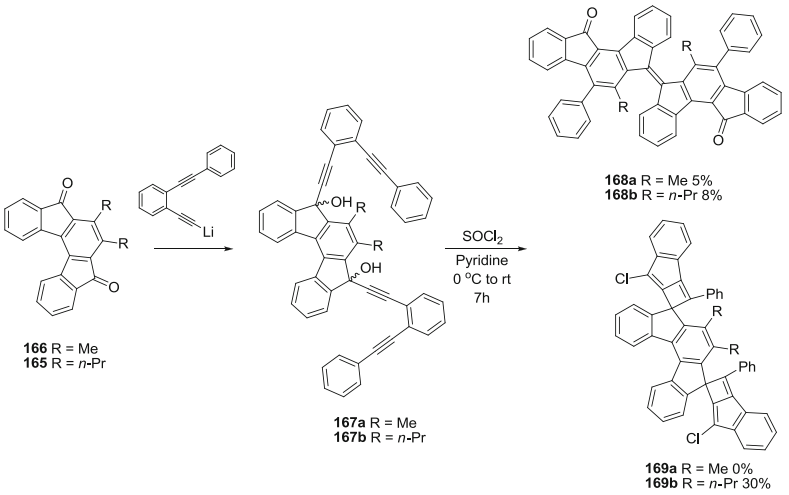


**Scheme 46** Synthesis of dimerized [1,2-*a*]IFs **168a,b** and spiro-fused [2,1-*c*]IFs **169a,b** [94]

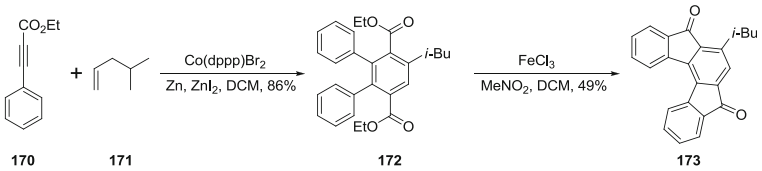


**Scheme 47** Preparation of 6-isobutyl [2,1-*c*]IF dione **173** [95]

[94]. In the reaction that formed **168a**, spiro-fused [2,1-*c*]IF derivative **169a** was not detected, but in the reaction that formed **168b**, highly strained **169b** was the major product.

Isobutyl [2,1-*c*]IF dione **173** was isolated by Hilt and coworkers via a cobalt-mediated [2+2+2] cyclization with 2 equiv. ethyl 3-phenylpropiolate (**170**) and 4-methylpentene (**171**) that gave terphenyl diester **172** in 86% yield (Scheme 47) [95]. Reaction of **172** with an excess of $FeCl_3$ cyclized and aromatized the central ring to afford **173**.

## *6.2 Fully-Conjugated Indeno[2,1-c]fluorenes*

The first example of a fully-conjugated [2,1-*c*]IF (**175**) was recently realized by the Haley group (Fix, Deal, and Haley, 2012, unpublished work). Similar to earlier syntheses by Haley and Tobe, addition of mesityl anion to dione **149** gave **174** as a mixture of stereoisomers. $SnCl_2$ treatment in the succeeding step gave **175** as a green solid, as opposed to the magenta hue common to the fully-conjugated [1,2-*b*]

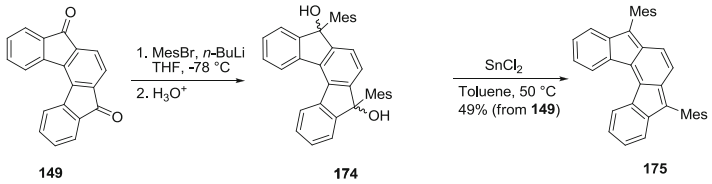


**Scheme 48** Synthesis of 5,8-dimesityl [2,1-*c*]IF **175** (Fix, Deal, and Haley, 2012, unpublished work)

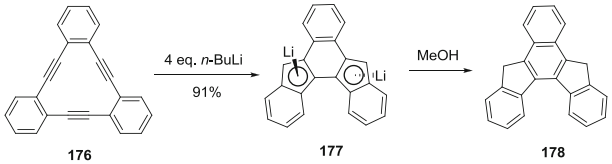


**Scheme 49** Lithium-induced cyclization to form dihydro [2,1-*c*]IF **178** [96]

IFs. The absorption spectrum of **175** displayed a broad region of lower energy transitions ranging from approximately 500 nm to nearly 800 nm with the local $\lambda_{max}$ at 601 nm. Interestingly, and in contrast to the [1,2-*b*]IFs, cyclic voltammetry data showed that arylation/full conjugation in **175** lead to a LUMO that is destabilized with respect to that of parent [2,1-*c*]IF dione **149** (LUMO energies of 3.59 eV and 3.78 eV, respectively). X-Ray crystallographic analysis confirmed the structure **175**, which showed a subtle helical twist to avoid steric interaction of the hydrogen atoms located on carbons 1 and 12. Work on further derivatization of this scaffold is ongoing (Scheme 48).

### *6.3 Other Indeno[2,1-c]fluorenes*

Youngs and Tessier synthesized one of the few [2,1-*c*]IF derivatives not already discussed [96]. Treatment of tribenzocyclotriyne **176** with 4 equiv. *n*-BuLi collapsed the annulene core to furnish the [2,1-*c*]IF dianion **177**; subsequent quenching with MeOH as the proton source afforded the benzo-fused dihydro-IF **178** (Scheme 49).

## 7 Conclusions

Unsurprisingly, given their interesting electronic properties, indenofluorenes, like many PAHs, are experiencing a considerable reemergence into the current literature. While recent attention has mostly pertained to the [1,2-*b*] isomer, it is

reasonable to expect that similar studies will be performed on the remaining isomers as high-yielding synthetic routes to these core structures become increasingly available. Fully conjugated indenofluorenes, too, are of great interest both from a fundamental chemistry standpoint (paratropicity, para-quinodimethane subunit, stability, bonding) as well as potential applications as organic semiconductors (large electron affinities, charge-transport characteristics). Given the large number of indenofluorene papers generated this past decade, the future prospects for this class of molecules indeed look bright.

## References


1. Harvey RG (1997) Polycyclic aromatic hydrocarbons. Wiley-VCH, New York
2. Clar E (1964) Polycyclic hydrocarbons. Academic, London
3. Wise SA, Campbell RM, West WR, Lee ML, Bartle KD (1986) Chem Geol 54:339
4. Müller TJJ, Bunz UHF (eds) (2007) Functional organic materials. Wiley-VCH, Weinheim
5. Müllen K, Scherf U (eds) (2006) Organic light emitting devices: synthesis, properties, and applications. Wiley-VCH, Weinheim
6. Haley MM, Tykwinski RR (eds) (2006) Carbon-rich compounds: from molecules to materials. Wiley-VCH, Weinheim
7. Anthony JE, Facchetti A, Heeney M, Marder SR, Zhan X (2010) Adv Mater 22:3876
8. Bendikov M, Wudl F, Perepichka DF (2004) Chem Rev 104:4891
9. Anthony JE (2006) Chem Rev 106:5028
10. Anthony JE (2008) Angew Chem Int Ed 47:452
11. Herwig P, Kayser CW, Müllen K, Spiess HW (1996) Adv Mater 8:510
12. Wu J, Pisula W, Müllen K (2007) Chem Rev 107:718
13. Kastler M, Pisula W, Wasserfallen D, Pakula T, Müllen K (2005) J Am Chem Soc 127:4286
14. Langa F, Nierengarten JF (eds) (2011) Fullerenes: principles and applications. Royal Society of Chemistry, Cambridge
15. Scott LT (2010) Polycycl Aromat Compd 30:247
16. Gabriel S (1884) Ber Dt Chem Ges 17:1389
17. Errera G (1907) Gazz Chim Ital 37:II:624
18. Errera G (1908) Gazz Chim Ital 38:II:588
19. Errera G, Vaccarino G (1909) Gazz Chim Ital 39:I:1
20. Marotta D (1911) Gazz Chim Ital 41:II:59
21. Radulescu D, Georgescu V (1925) Bull Soc Chim Fr 37:1187
22. Strauss F, Kühnel R, Hansel R (1933) Ber Dt Chem Ges 66:1847
23. Weizmann Ch, Bergmann E, Haskelberg L (1939) J Chem Soc 391
24. Radulescu D, Alexa M (1943) Chem Zentralbl I:622
25. Deuschel W (1951) Helv Chim Acta 35:168
26. Deuschel W (1951) Helv Chim Acta 35:2403
27. Chardonnens L, Ritter R (1955) Helv Chim Acta 38:393
28. Poriel C, Liang J-J, Rault-Berthelot J, Barrière F, Cocherel N, Slawin AMZ, Horhant D, Virboul M, Alcaraz G, Audebrand N, Vignau L, Huby N, Wantz G, Hirsch L (2007) Chem Eur J 13:10055
29. Cocherel N, Poriel C, Rault-Berthelot J, Barrière F, Audbrand N, Slawin AMZ, Vignau L (2008) Chem Eur J 14:11328
30. Poriel C, Barrière F, Thirion D, Rault-Berthelot J (2009) Chem Eur J 15:13304
31. Thirion D, Poriel C, Barrière F, Métivier R, Jeannin O, Rault-Berthelot J (2009) Org Lett 11:4794

32. Cocherel N, Poriel C, Vignau L, Bergamini J-F, Rault-Berthelot J (2010) Org Lett 12:452
33. Thirion D, Poriel C, Rault-Berthelot J, Barrière F, Jeannin O (2010) Chem Eur J 16:13646
34. Cocherel N, Poriel C, Vignau L, Bergamini J-F, Rault-Berthelot J (2011) Org Lett 12:452
35. Usta H, Facchetti A, Marks TJ (2008) Org Lett 10:1385
36. Usta H, Facchetti A, Marks TJ (2008) J Am Chem Soc 130:8580
37. Usta H, Risko C, Wang Z, Huang H, Deliomeroglu MK, Zhukhovitskiy A, Facchetti A, Marks TJ (2009) J Am Chem Soc 131:5586
38. Chardonnens L, Laroche B, Sieber W (1974) Helv Chim Acta 57:585
39. Chardonnens L, Häger J (1974) Helv Chim Acta 57:1472
40. Chardonnens L, Bitsch S, Häger J (1975) Helv Chim Acta 58:503
41. Behr OM, Eglinton G, Galbraith AR, Raphael RA (1960) J Chem Soc 3614
42. Friedrich E, Deuschel W (1956) Chem Ber 89:2794
43. Chardonnens L, Salamin L (1968) Helv Chim Acta 51:1096
44. Chardonnens L, Rody J (1959) Helv Chim Acta 42:1328
45. Chardonnens L, Häger J (1970) Helv Chim Acta 53:843
46. Shi Y, Liu Q, Wu G, Rong L, Tang J (2011) Tetrahedron 67:1201
47. Minuti L, Taticchi A, Marrocchi A, Gacs-Baitz E (2005) Poly Arom Cmpds 25:13
48. Merlet S, Birau M, Wang ZY (2002) Org Lett 4:2157
49. Zhou Q, Carroll PJ, Swager TM (1994) J Org Chem 59:1294
50. Nishinaga T, Nodera N, Miyata Y, Komtasu K (2002) J Org Chem 67:6091
51. Miyata Y, Minari T, Nemoto T, Isoda S, Komatsu K (2007) Org Biomol Chem 5:2592
52. Nakagawa T, Kumaki D, Nishida J-I, Tokito S, Yamashita Y (2008) Chem Mater 20:2615
53. Rose BD, Chase DT, Weber CD, Zakharov LN, Lonergan MC, Haley MM (2011) Org Lett 13:2106
54. Anthony JE, Eaton DL, Parkin SR (2002) Org Lett 4:15
55. Chase DT, Fix AG, Rose BD, Weber CD, Nobusue S, Stockwell CE, Zakharov LN, Lonergan MC, Haley MM (2011) Angew Chem Int Ed 50:11103
56. Hellwinkel D, Kistenmacher T (1989) Liebigs Ann Chem 945
57. Scherf U (1993) Macromol Rapid Commun 14:575
58. Liu T-P, Liao Y-X, Xing C-H, Hu Q-S (2011) Org Lett 13:2452
59. Wolfgang F, Gompper R (1987) Tetrahedron Lett 28:3083
60. Chase DT, Rose BD, McClintock SP, Zakharov LN, Haley MM (2011) Angew Chem Int Ed 50:1127
61. Reisch H, Wiesler U, Scherf U, Tuytuylkov N (1996) Macromolecules 29:8204
62. Reisch H (1995) Ph.D. Thesis, University of Mainz
63. Brunetti F, Gong X, Tong M, Heeger AJ, Wudl F (2010) Angew Chem Int Ed 49:532
64. Anthony JE, Brooks JS, Eaton DL, Parkin SR (2001) J Am Chem Soc 123:9482
65. Payne MM, Parkin SR, Anthony JE (2005) J Am Chem Soc 127:8028
66. Purushothaman B, Parkin SR, Anthony JE (2010) Org Lett 12:2060
67. Purushothaman B, Bruzek M, Parkin SR, Miller A-F, Anthony JE (2011) Angew Chem Int Ed 50:7013
68. Kaur I, Jia W, Kopreski RP, Selvarasah S, Dokmeci MR, Pramanik C, McGreur NE, Miller GP (2008) J Am Chem Soc 130:16274
69. Kaur I, Stein NN, Kopreski RP, Miller GP (2009) J Am Chem Soc 131:3424
70. Tverskoy O, Rominger F, Peters A, Himmel H-J, Bunz UHF (2011) Angew Chem Int Ed 50:3557
71. Bunz UHF (2009) Chem Eur J 15:6780
72. Bunz UHF (2010) Pure Appl Chem 82:953
73. Miao Q (2012) Synlett 326
74. Montgomery LK, Huffman JC, Jurczak EA, Grendze MP (1986) J Am Chem Soc 108:6004
75. Holmes D, Kumaraswamy S, Matzger AJ, Vollhardt KPC (1999) Chem Eur J 5:3399
76. Dong H, Wang C, Hu W (2010) Chem Commun 46:5211

77. Chase DT, Fix AG, Kang SJ, Rose BD, Weber CD, Zhong Y, Zakharov LN, Lonergan MC, Nuckolls C, Haley MM (2012) J Am Chem Soc 134:10349
78. Nishida JI, Tsukaguchi S, Yamashita Y (2012) Chem Eur J 18:8964
79. Hsiao C-C, Lin Y-K, Liu C-J, Wu T-C, Wu Y-T (2010) Adv Synth Catal 352:3267
80. Setayesh S, Marsitzky D, Müllen K (2000) Macromolecules 33:2016
81. Horhant D, Liang J-J, Virboul M, Poriel C, Alcaraz G, Rault-Berthelot J (2006) Org Lett 8:257
82. Poriel C, Rault-Berthelot J, Thirion D, Barrière F, Vignau L (2011) Chem Eur J 17:14031
83. Poriel C, Cocherel N, Rault-Berthelot J, Vignau L, Jeannin O (2011) Chem Eur J 17:12631
84. Chi L-C, Hung W-Y, Chiu H-C, Wong K-T (2009) Chem Commun 3892
85. Lee KH, Kim SO, You JN, Kang S, Lee JY, Yook KS, Jeon SO, Lee JY, Yoon SS (2012) J Mater Chem 22:5145
86. Lee KH, Kim SO, Kang S, Lee JY, Yook KS, Lee JY, Yoon SS (2012) Eur J Org Chem 18:2748
87. Ie Y, Nitani M, Aso Y (2007) Chem Lett 36:1326
88. LeBerre A (1957) Ann Chim 2:371
89. Shimizu A, Tobe Y (2011) Angew Chem Int Ed 50:6906
90. Poriel C, Métivier R, Rault-Berthelot J, Thirion D, Barrière F, Jeannin O (2011) Chem Commun 47:11703
91. Altman Y, Ginsburg D (1961) J Chem Soc 1498
92. Chardonnens L, Chardonnens H (1966) Helv Chim Acta 49:1931
93. Wang X-M, Hou X-L, Zhou Z-Y, Mak TCW, Wong HNC (1993) J Org Chem 58:7498
94. Yang Y, Peterson JL, Wang KK (2003) J Org Chem 68:5832
95. Hilt G, Paul A, Harms K (2008) J Org Chem 73:5187
96. Youngs WJ, Djebli A, Tessier CA (1991) Organometallics 10:2089

Top Curr Chem (2014) 349: 197–248
DOI: 10.1007/128_2012_368

Published online: 14 September 2012

# Closed-Shell and Open-Shell 2D Nanographenes

**Zhe Sun and Jishan Wu**

**Abstract** This chapter describes a series of two-dimensional (2D) expanded arene networks, also known as nanographenes, with either closed-shell or open-shell electronic structure in the ground state. These systems are further categorized into three classes on a basis of different edge structures: those with zigzag edges only, those with armchair edges only, and those possessing both. Distinctive physical properties of these 2D aromatic systems are closely related to their structural characteristics and provide great potential for them as materials for different applications.

**Keywords** Armchair · Graphene · Opto-electronic materials · Polycyclic aromatic hydrocarbons · Radicals · Zigzag

## Contents

1 Introduction ..... 198
2 2D Nanographenes with Only Zigzag Edges ..... 200
2.1 Phenalenyl-Based Open-Shell Systems ..... 201
2.2 Triangulene-Based Triplet Biradicals ..... 215
3 2D Nanographenes with Both Zigzag Edges and Armchair Edges ..... 218
3.1 Rylenes ..... 219
3.2 Anthenes and Periacenes ..... 224

Z. Sun
Department of Chemistry, National University of Singapore, 3 Science Drive 3, Singapore 117543, Singapore

J. Wu (✉)
Department of Chemistry, National University of Singapore, 3 Science Drive 3, Singapore 117543, Singapore

Institute of Materials Research and Engineering, A*Star, 3 Research Link, Singapore 117602, Singapore
e-mail: chmwuj@nus.edu.sg; wuj@imre.a-star.edu.sg

4 2D Nanographenes with Only Armchair Edges ..... 231
4.1 Hexa-*Peri*-Hexabenzocoronene ..... 232
4.2 All-Benzenoid PAHs Larger than HBC ..... 237
5 Conclusion and Outlook ..... 240
References ..... 242

## Abbreviations

| | |
|---|---|
| DDQ | 2,3-Dichloro-5,6-dicyano-1,4-benzoquinone |
| ESR | Electron spin resonance |
| HBC | Hexa-*peri*-hexabenzocoronene |
| HOMO | Highest occupied molecular orbital |
| LUMO | Lowest unoccupied molecular orbital |
| MALDI-TOF | Matrix-assisted laser desorption time-of-flight |
| NIR | Near infrared |
| PDI | Perylene diimide |
| SOMO | Singly occupied molecular orbital |
| SQUID | Superconducting quantum interference device |
| TEMPO | (2,2,6,6-Tetramethylpiperidin-1-yl)oxyl |

## 1 Introduction

Two-dimensional (2D) polyarenes represent one of the most widely studied organic compounds and have attracted increasing attention due to their active role in materials science. From a bottom-up point of view, 2D polyarenes can be viewed as expanded networks by fusion of benzene rings in two-dimensions, which are better described as benzenoid polycyclic aromatic hydrocarbons (PAHs). On the other hand, from a top-down perspective they can be regarded as graphene fragments formed by cutting infinite graphene sheet in different modes; thus they are known as nanographenes. Both viewpoints will produce a series of structurally well-defined molecules with two distinct edge structures – zigzag edge and armchair edge. In this chapter the focus will be on three types of nanographenes divided by the edge structures, i.e., those with zigzag edges only, those with armchair edges only, and those possessing both (e.g., **1**–**3** in Fig. 1).

Fusion of benzene rings in a triangular manner or cutting of graphene in a triangular motif will lead to PAHs with only zigzag edges. No Kekulé structure or closed-shell structure can be drawn for this class of molecule, which inevitably results in one or more unpaired electrons within the molecule. The number of unpaired electrons, or radicals, increases with the size of the framework starting from phenalenyl monoradical to high-spin polyradical systems. The high reactivity derived from open-shell nature of these systems largely impedes their synthesis and isolation, but still, continuous efforts have been made to synthesize and stabilize them due to the desire to understand the interplay of the unpaired electrons and

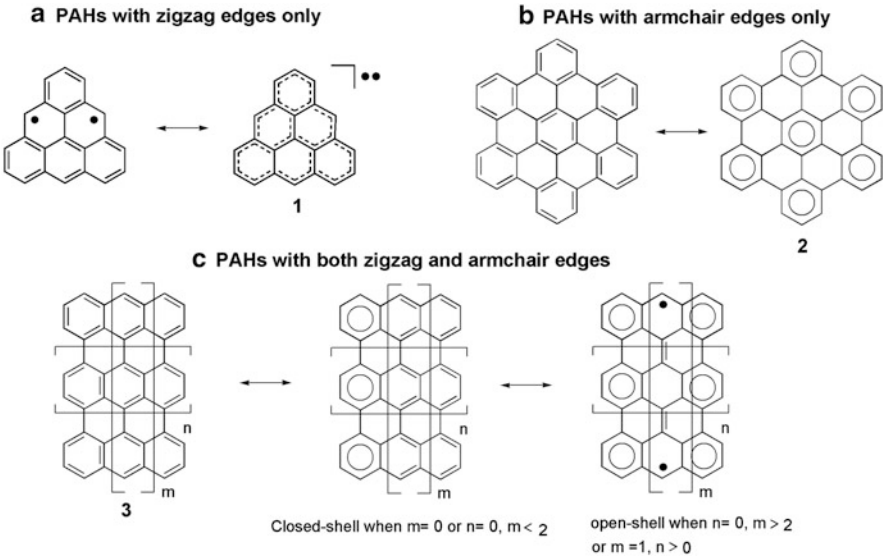


**Fig. 1** Representative structures of PAHs with zigzag edges only (**a**), with armchair edges only (**b**), and with both zigzag and armchair edges (**c**)

delocalized π-electron systems and charge fluctuation, as well as the possibility of using them as molecule-based functional materials [1].

Rectangular-shaped nanographenes are featured by coexistence of zigzag and armchair edges with a typical Kekulé structure. Their structures can be formulated by cycles in a monocyclic system symbolizing the six π-electrons in benzene rings (benzenoid aromatic sextets) according to Clar's aromatic sextet rule [2]. Therefore the determination of stability can be simplified by counting the number of sextet rings for a given system, that is, the more sextet rings the more stable the system. Interestingly, recent theoretical and experimental work indicates that for rectangular PAHs with more than two zigzag edges, such as anthenes and periacenes, a remarkably open-shell biradical character will emerge when the conjugation is extended to some point ($n > 0$ for anthenes and $m > 2$ for periacenes) which originates from a narrowed bandgap and stabilization contribution of forming more Clar's sextet rings in the biradical form (Fig. 1) [3].

Nanographenes with only armchair edges can also be termed "all-benzenoid PAHs" as their structures can be represented as "full" aromatic sextet rings without additional double bonds. It is commonly accepted that the bandgap and stability of PAHs are dependent not only on molecular size but also on the edge structures. Although this class of PAHs possesses large size and extended conjugation, they show high stability and relatively large bandgap due to the existence of the large number of aromatic sextet rings.

Different functionalities and applications are expected for all three types of nanographenes according to their respective intrinsic properties. For example,

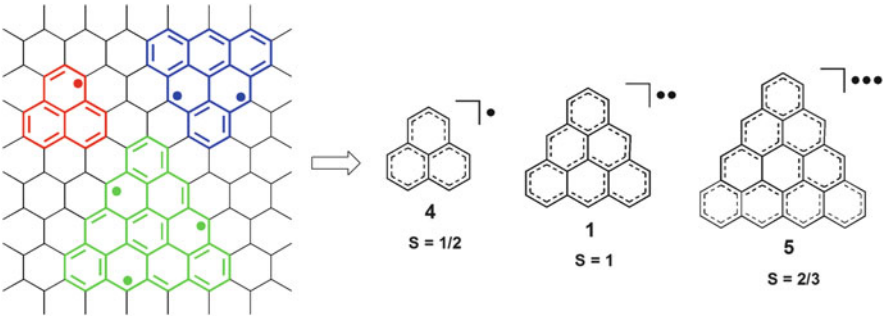


**Fig. 2** Triangular fragments of graphene with open-shell structures

PAHs with only zigzag edges are promising in the field of spintronics and information processing due to their unique magnetic properties, PAHs with both edge structures are attractive as near-infrared (NIR) dyes and ambipolar semiconductors due to their low bandgap and enhanced stability, while the self-assembly behavior and controllable liquid crystal phase of PAHs with only armchair edge make them suitable as electronic materials. In light of this background, we aim to provide an overview of these three types of 2D nanographenes in terms of synthesis, properties, and applications.

## 2 2D Nanographenes with Only Zigzag Edges

As mentioned above, if graphene is cut in a zigzag motif, or in a triangular shape, it will lead to a series of non-Kekulé PAHs possessing one or more unpaired electrons, which can be termed "open-shell graphene fragments" and are very interesting from both theoretical and experimental aspects (Fig. 2). The smallest member in this family, phenalenyl radical **4**, is composed of three benzene rings fused in a triangular manner. It possesses one unpaired electron and spin multiplicity $2S + 1 = 2$. Extension of π-conjugation results in triangulene **1** with two unpaired electrons and a triplet ground state, and further extension leads to larger high spin system **5** (Fig. 2). Apart from the open-shell and non-Kekulé character, these systems have a large delocalization of spin densities over the entire molecule, although the largest coefficiency still resides on the edges of the molecule, which are more exposed than the core.

Inspired by the promising potentialities and applications of these systems in the field of electronics and spintronics [4], the synthesis and functionalization of triangular shaped nanographenes have been intensively investigated for a long time. However, the intrinsic low stability of these open-shell systems largely impedes their isolation as well as application. Fueled by the development of modern synthetic methods and deeper understanding of the decomposing pathways of those radicals, such as dimerization, hydrogen abstraction, and oxidation, chemists have

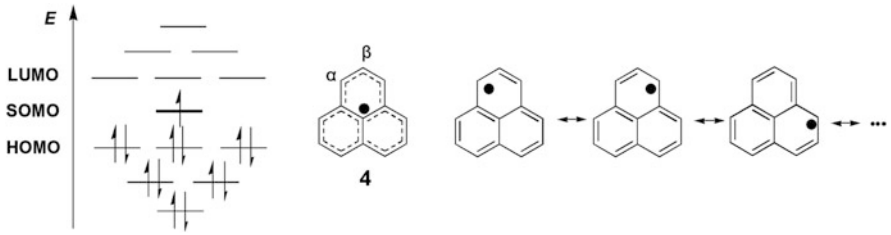


**Fig. 3** Molecular orbital diagram and resonance structures of phenalenyl radical **4**

come up with many methods to stabilize these systems, including steric protection, incorporation of heteroatoms, and fusion with other aromatic skeletons. In addition, it is quite exciting to note that real applications have already been realized in some fields. In the following section we will summarize the recent advances in open-shell PAHs with triangular shapes, including systems based on the phenalenyl radical and the triangulene triplet diradical.

## *2.1 Phenalenyl-Based Open-Shell Systems*

### 2.1.1 Phenalenyl-Based Monoradicals

The phenalenyl radical **4** represents the most fundamental and widely explored member in this family. Unlike typical stable neutral radicals such as TEMPO and α-nitronylnitroxide derivatives with a spin-localized nature, **4** is characterized by a planar, rigid structure with the spin spread over the whole molecular skeleton (Fig. 3). The resonance structures of **4** show that the spin density is predominantly at its α positions, while the spin at the peripheral positions ($\beta$ positions) is much smaller, which can be explained by the spin polarization effect. In addition, **4** exhibits a high amphoteric redox ability with thermodynamically stable cation, neutral radical and anion species. All of these features of **4** lead to new insights in the field of physical chemistry.

The first study of **4** dated back to the 1950s and it was found to be so reactive that it can only be handled in solution under inert conditions [5]. Limited by the kinetic instability of **4** caused by immediate intermolecular σ-bond formation and oxidation by air, phenalenyl chemistry in the past half century has mainly been performed in degassed solutions and under sealed conditions. Therefore, new synthetic approaches and stabilization methods are badly needed to enrich phenalenyl chemistry and to understand its properties in the solid state and crystalline phase.

The pioneering work of stabilizing phenalenyl radicals took advantage of introducing primary alkyl groups, electron-donating and electron-withdrawing groups [6]. Although isolation in the solid phase was not achieved, these systems

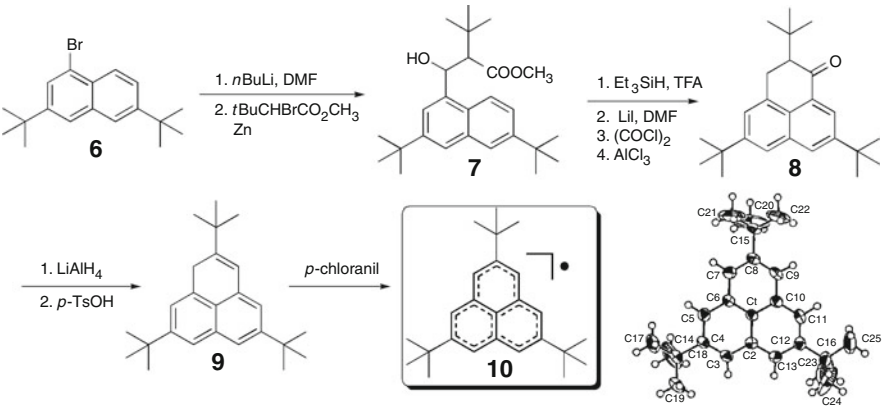


**Scheme 1** Synthetic route and X-ray crystal structure of radical **10** [7]

displayed enhanced stability in solution. The first isolation of phenalenyl in the solid state in air was achieved in 1999 when Nakasuji et al. introduced three *tert*-butyl groups onto the $\beta$ positions. The bulky substituents not only successfully shut down the σ-bond dimerization pathway but also contributed a minimal perturbation effect to the electronic structure of the parent phenalenyl in that the connection positions were $\beta$ positions with negligible spin densities. Therefore, it can be viewed as the most electronically fundamental phenalenyl-based system [7].

As shown in Scheme 1, the synthesis of *tert*-butyl phenalenyl radical **10** started from 2,7-di-*tert*-butylnaphthalene in ten steps. Bromination of 2,7-di-*tert*-butylnaphthalene gave **6** in high yield, which was converted into aldehyde by lithiation followed by reaction with DMF. Successive Reformatsky reaction afforded ester **7**, which upon reduction, hydrolysis, and Friedel-Crafts acylation reaction gave the phenalanone **8**. The key intermediate **9** was then obtained as pale yellow crystals by reduction of **8** and subsequent dehydration. Oxidation of **9** with *p*-chloranil in degassed toluene led to a blue neutral radical solution while similar treatment in hexane gave deep blue needles. This crystal showed high stability in the absence of air, while changing into phenalanone derivatives and other byproducts in 1 week in air.

The ESR spectrum of **10** showed a septet hyperfine structure corresponding to phenalenyl ring protons, and an observed $g_e$ value 2.0028, consistent with genuine spin-doublet hydrocarbon radicals. The X-ray analysis of **10** was reported for the first time for an odd alternant hydrocarbon radical, revealing that it possesses a nearly planar geometry with a slightly distorted $D_{3h}$ symmetry. The molecule formed a π-dimeric pair in staggered alignment of the *tert*-butyl groups to avoid steric repulsion, which also favored the maximum SOMOs overlap. The dimeric pair adopted a herringbone packing motif with interplanar distance ranging from 3.201 to 3.323 Å, much shorter than the sum of the van der Waals radii of the carbon atoms. Such a short distance indicated a strong antiferromagnetic interaction within the π-dimer, which was evidenced by a large antiferromagnetic intermolecular exchange

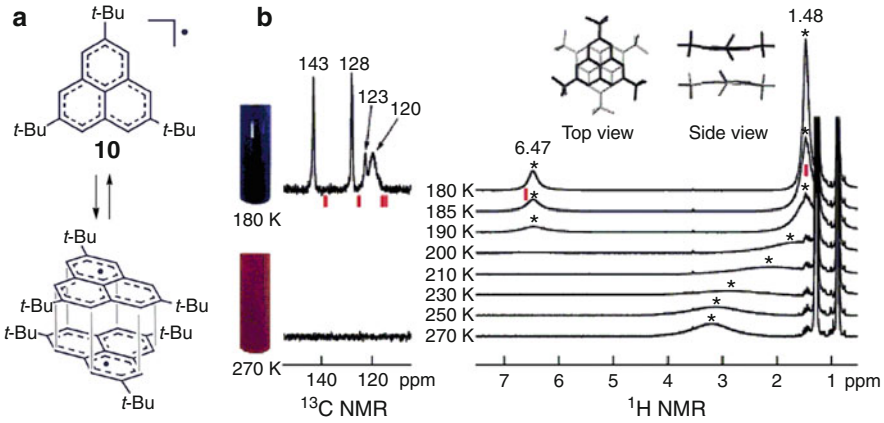


**Fig. 4** (**a**) Schematic representation of the monoradical-π-dimer equilibrium for **10**; (**b**) changes in color, $^{13}C$ and $^{1}H$ NMR spectra in varied temperatures [11]. Reprinted with permission from [11]. Copyright 2006 American Chemical Society

interaction ($2\,J/k_B = -2{,}000$ K) from magnetic susceptibility measurement. This result showed that the π-dimer was spin-singlet in the ground state.

The nature of phenalenyl π-dimer was later investigated by Kochi et al. in more detail from both theoretical and experimental viewpoints [8–10]. Interestingly, the same dimeric behavior was found in solution as that in crystal based on spectroscopic study, especially at lower temperature, leading to the thermochromic phenomenon [11]. In other words, the red purple solution of **10** gradually turned blue upon cooling, which is in accordance with the increase of absorbance in the 530–670 nm region, indicating the formation of dimer. More definite evidence was provided by low temperature $^{1}H$ and $^{13}C$ NMR measurements. In the $^{1}H$ spectrum at higher temperature the aromatic signals were broadened and the *tert*-butyl signals were shifted downfield due to the effect of radical spin, whereas at lower temperature, the diamagnetic dimer became the dominant species, so the aromatic peak became sharp and the *tert*-butyl peak shifted to the normal region. The $^{13}C$ NMR spectrum gave similar observations in the aromatic region due to the presence of paramagnetic species. The molecular weight of the π-dimer was also detected by cold-spray ionization mass spectrometry (CSI-MS) which allows substances ionized at lower temperatures, and this result represented the first detection of a radical dimer with NMR and MS techniques (Fig. 4).

Phenalenyl radical derivatives with other substituents in the periphery, such as alkoxy [12], hydroxyl, amino [13, 14], and N-S-N groups [15], have been prepared and studied. Among them, an interesting example was a perchlorophenalenyl radical **16** with all α-positions and β-positions substituted by chlorine atom. The molecule was firstly prepared by Haddon et al. in 1987 [16] and the X-ray crystal structure was obtained in 2001 [17]. The synthetic route is depicted in Scheme 2, chlorination of acenaphthene **11** affording a mixture of perchloroacenaphthene **12** and perchloroacenaphthylene **13**, and conversion of **13** from **12** can be realized

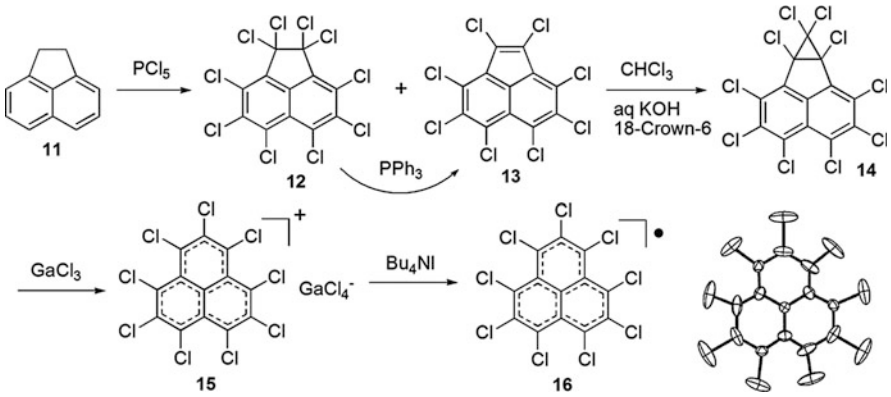


**Scheme 2** Synthetic route and single-crystal structure of perchlorinated phenalenyl radical [16–17]

either by thermolysis or by treatment with $PPh_3$. **13** was then converted to a cyclopropane derivative **14** by addition of dichlorocarbene, and subsequent allyl-rearrangement in the presence of Lewis acid gave phenalenyl cation **15**. Reduction of cation **15** finally afforded **16** as a shiny black hexagonal crystal. The neutral radical **16** possessed a high stability in air. The X-ray analysis was performed on crystals obtained by repeated sublimation under vacuum, and the single molecule was not planar anymore but ruffled into a propeller shape due to the demands of the intramolecular Cl–Cl distance. This molecule stacked in columns separated by 3.78 Å, in sharp contrast to the *tert*-butyl phenalenyl **10** which was dimeric in the solid state with a much closer intermolecular distance. The reason for the long intermolecular distance of **16** was due to the non-planarity which inhibited the formation of 60° rotated stacking motif. The magnetic susceptibility measurements showed that the solid **16** exhibited Curie paramagnetism at 100–380 K and antiferromagnetic below 100 K. Due to the isolation of individual molecules, the solid **16** was a Mott–Hubbard insulator with a room temperature conductivity of $10^{-10}$ S cm$^{-1}$.

Those systems discussed above pointed out a subtle balance on introducing substituents to stabilize the phenalenyl radical, the bulky substituents certainly being necessary to prevent σ-dimerization; however, when the substituents are too bulky they can cut down the communication between the molecules which in the lattice ultimately leads to conductivity. With the aim of obtaining stable neutral radicals with less steric hindrance and extended delocalization, Haddon et al. designed a series of phenalenyl radicals with a disulfide bridge across two neighboring active positions (Fig. 5a). The dithiophenalenyl **17** was first prepared in 1978 by reduction of the corresponding cation species and it survived in the solid state in air for up to 24 h but decomposed quickly in solution [18]. In the crystalline phase, **17** stacked in a sandwich herringbone motif of face-to-face π-dimers with 180° rotation between the two radicals (Fig. 5b). An almost complete superposition of the α carbon atoms can be observed from a perpendicular view, maximizing the

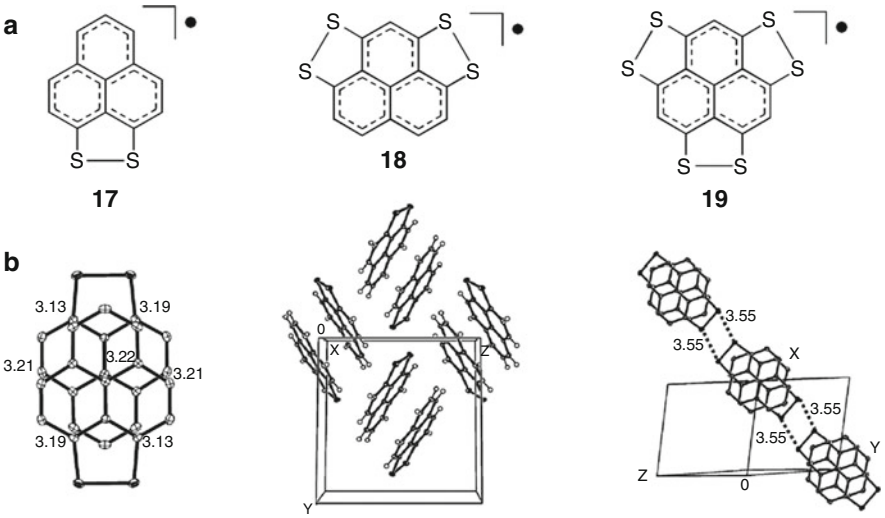


**Fig. 5** (**a**) Structures of phenalenyl radicals with disulfide bridges; (**b**) single-crystal structures of **17** [18–20]. Reprinted with permission from [19]. Copyright 2007 American Chemical Society

overlap of SOMOs. The intermolecular distance in this π-dimer (3.13–3.22 Å) is even shorter than that of **10**, indicating a strong intermolecular interaction. Other contacts in the lattice, such as S-S interactions between different π-dimers, were also observed (Fig. 5b), but the dimers remain isolated with electrons trapped within dimer pairs, which was further demonstrated by the conductivity measurements revealing that this material was an insulator [19]. It is worth noting that, in spite of the absence of bulky substituents, no σ-dimerization was formed in the solid state, showing that extension of spin delocalization indeed provided an alternative way to stabilize neutral radicals. The attempt to prepare a more spin delocalized system, a tetrathiophenalenyl **18**, was performed in 2008; however, the reduction of the corresponding cation led to formation of a closed-shell dimer with an S–S σ bond, and only a weak ESR signal can be observed in solution [20]. The phenalenyl with three disulfide bridges and a threefold symmetrical molecular skeleton, a hexathiophenalenyl **19**, has not been made so far, but was expected to show an extensively spin delocalization nature and intriguing magnetic and electronic properties.

Modifications within the phenalenyl moiety instead of around the phenalenyl unit were also investigated to stabilize the open-shell system; for example, incorporation of heteroatoms such as the nitrogen atom is an effective way to stabilize phenalenyl radical. However, the electronic structure and the spin density can be altered dramatically due to the higher electron negativity of the nitrogen atom and the existence of lone pair electrons; thus it is questionable whether they can be regarded as phenalenyl radicals anymore. On the basis of the position in which nitrogen is introduced, the nitrogen-containing phenalenyl derivatives can be divided into two types: $\alpha$ type and $\beta$ type (Fig. 6). For $\alpha$ type compounds, the spin

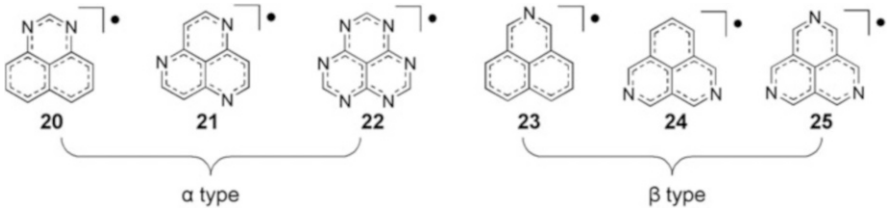


**Fig. 6** Nitrogen-containing phenalenyl radicals [1]

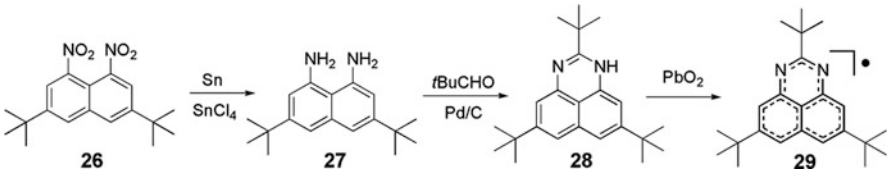


**Scheme 3** Synthetic route to the radical **29** [21]

density distributions are similar to the pristine phenalenyl radicals, with a slight decrease of spin densities on nitrogen atoms. In contrast, $\beta$ type compounds show minimal perturbation on the electronic structure as the nitrogen atoms locate at positions with small and negative spin densities.

The first synthesis and isolation of an $\alpha$ type nitrogen-containing phenalenyl radical, a 2,5,8-tri-*tert*-butyl-1,3-diazaphenalenyl **29**, was achieved in 2002. The synthesis involved reduction of compound **26** followed by condensation with *t*BuCHO and dehydrogenation catalyzed by Pd/C. Oxidation with $PbO_2$ and recrystallization led to a green crystal of **29**. The crystal exhibited increased stability in air due to heteroatomic modification [21] (Scheme 3).

Due to the symmetry-broken incorporation of two nitrogen atoms at the two $\alpha$ positions, the X-ray analysis of single crystals of **29** revealed formation of an angled face-to-face *syn*-dimer structure and a strongly asymmetric bonding nature in the crystal that showed large temperature factors and high anisotropy at 296 K (Fig. 7). These features were associated with a continuous color change from 100 K to 300 K. The crystal was colorless or an extremely pale green at 100 K, which gradually deepened at higher temperature and finally became dark green at 300 K. This behavior is very rare not only in organic radicals but also in metal complexes, making the crystal of **29** a molecular color thermometer. With the help of X-ray single-crystal analysis and temperature dependant polarized electronic spectra, this unconventional dynamic behavior was found to originate from the coexistence of $\sigma$-bonded and $\pi$-bonded dimers, separated by an energy gap of 2.62 kcal $mol^{-1}$. The temperature dependent polarized electronic spectra showed that the $\sigma$-dimer and $\pi$-dimer were colorless and dark green, respectively, so the continuous color change originated from the change of population of the two dimers with respect to temperature. The presence of two dimers was further supported by room temperature ESR measurement of the solid, which showed signals attributed

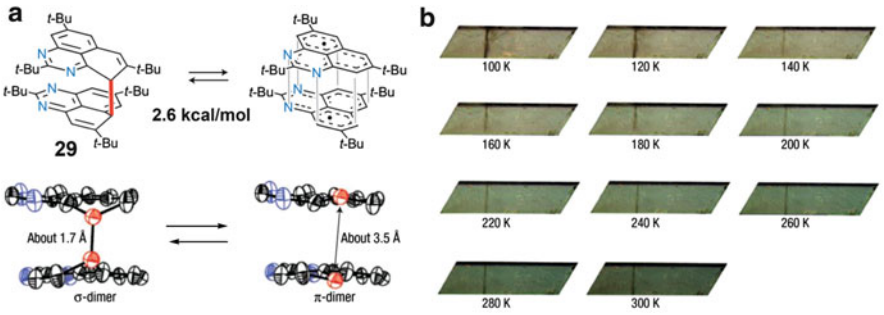


**Fig. 7** (**a**) Chemical structure and X-ray single-crystal structure of σ-dimer and π-dimer for **29**; (**b**) images of crystal of **29** in the range of temperature between 100 K and 300 K [22]. Reprinted with permission from [22]. Copyright 2008 Nature Publishing Group

to the thermally accessible triplet state. This is the first example where the energy levels of an organic radical with three energy states have been experimentally located. On the other hand, radical **10** did not show any thermochromism in the crystalline phase, suggesting that the symmetry lowering of the spin distribution plays a pivotal role to form a σ-dimer and π-dimer equilibrium [22].

A highly symmetrical nitrogen-containing phenalenyl **22** with all α positions replaced by nitrogen atoms is a very interesting motif in that the nitrogen atoms are directed radially and can form coordination and hydrogen bonds to the outside. Due to the largely decreased HOMO energy level, the anion of this compound possesses high stability and can be isolated as stable crystals at room temperature in air [23]. Two *β* type azaphenalenyls **23** and **30** were prepared by Rubin et al. For **23**, the substitution of carbon with nitrogen increases the stability in degassed solution, but the low stability in air and in the solid state hampered its isolation in the crystalline form [24]. On the other hand, radical **30** exhibited high stability both in the solid state and in air, but a dechlorinated dimer connected with a C=C bond was found to form. The ESR measurements and density functional theory (DFT) calculations of those radicals indicated large spin densities on the α positions, which is similar to the pristine phenalenyl radical [25] (Fig. 8).

The above-mentioned systems possess similar electronic structures with phenalenyl radicals, having large positive spin densities on the α positions. In contrast, introduction of two oxygen atoms will lead to a brand new series of radicals termed "oxophenalenoxyls" [26]. These neutral radicals are different from phenalenyl radicals in the following aspects: (1) the *β*, *β*-substituted isomer can be represented as triradical structure and is much less stable than the α, *β*-substituted or α, α-substituted isomers which can be represented as monoradicals; (2) high stability can be expected for the α, α-substituted isomer due to the extensive delocalization of radicals and unique topological symmetries; (3) most of the spin densities and coefficients of SOMO are centered on the *β* carbons and the oxygen atoms, and significant SOMO level lowering compared to phenalenyl systems imply a high electron accepting ability, which is the key factor for applications as electrode active materials in secondary batteries.

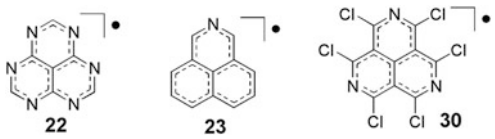


**Fig. 8** Other nitrogen-containing phenalenyl radicals [23–25]

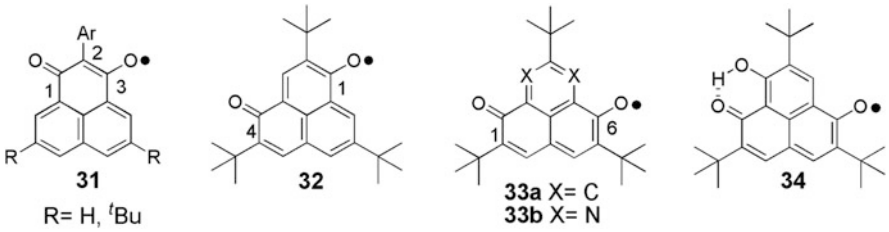


**Fig. 9** Oxophenalenoxyl radicals [27–34]

So far, several types of oxophenalenoxyl systems have been prepared (Fig. 9). Among them, the 3-oxophenalenoxyl **31**, having two oxygen atoms at 1,3-positions of the phenalenyl skeleton, appeared to be quite unstable and oxidation of the corresponding hydroxyl precursors generally led to closed-shell σ-dimers. Pyrolysis of the σ-dimer gave the neutral radical in solution, although this radical could not be isolated [27–30]. The trend of formation of such a σ-dimer was explained by the large spin density distribution at the 2-position and oxygen atoms. In sharp contrast, the 4- and 6-oxophenalenoxyl derivatives **32** and **33a** with oxygen atoms at the 1,4- and 1,6-positions are expected to perform higher thermodynamic stability due to the extensive spin delocalization [31]. Introduction of *tert*-butyl groups as steric protection further increases the kinetic stability of those systems which enables them to be handled in air [32]. With the same strategy, the 7-hydroxy-6-oxophenalenoxyl derivative **34** was prepared as the first neutral radical with an intramolecular hydrogen bond [33]. A 7,9-diaza-6-oxophenalenoxyl derivative **33b** was designed and represented an interesting motif to construct bridging ligands for intermolecular networks. However, this radical is extremely sensitive to sunlight even at very low temperatures which may be due to a lowering of SOMO energy level and decrease of the SOMO-LUMO gap [34].

The ability of oxophenalenoxyl radicals to form functional organic materials was also examined by tetrathiafulvalene (TTF) molecule as an electron donor. It was found that TTF-substituted oxophenalenoxyl radicals exhibited tunable intramolecular electron transfer (IET) by moderate change of external environments such as solvent and temperature in solution, leading to "spin center transfer" accompanied by solvato-/thermochromism (Fig. 10). There were two species involved in this process, a neutral radical **35** existing in dichloromethane solution with most of the spin localized on oxophenalenoxyl motif, and a zwitterionic radical **36** existing in trifluoroethanol solution with spin localized on TTF moiety as radical cation species.

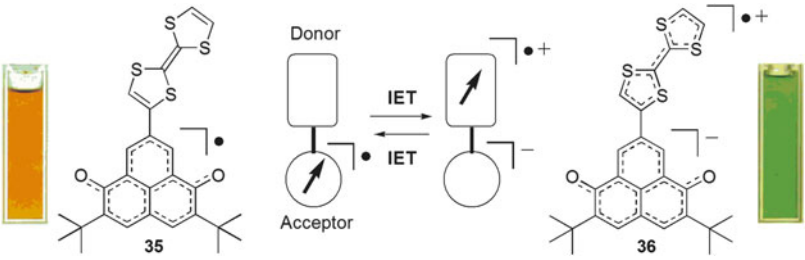


**Fig. 10** Spin center transfer between neutral radical and zwitterionic radical [35]. Reprinted with permission from [35]. Copyright 2002 John Wiley and Sons

This behavior was visualized by a color change from orange to dark green. These two species were also characterized by ESR measurements. Moreover, the 100% interconversion was controllable in a 50 K temperature range (243–293 K) from one species to the other by controlling the ratio of dichloromethane and trifluoroethanol. This unprecedented phenomenon is the first known spin switching phenomenon in a purely organic open-shell molecular system [35].

### 2.1.2 Extended Systems Based on Bis- and Trisphenalenyls

Another interesting molecular design towards stable phenalenyl radicals is to link two phenalenyl moieties with an aromatic bridge to produce singlet biradical compounds having a Kekulé structure as a structural resonance. These systems were initially studied by Murata and Nakasuji and further investigated by Kubo et al. [36]. There are two factors that account for the enhanced stability of these systems; one is the intrinsic delocalization of the phenalenyl moiety and the other is the aromatic stabilization by recovery of one more Clar's aromatic sextet ring from the quinoid form to the biradical form. The biradical character of these compounds has a pronounced effect on their electronic, magnetic, and solid state properties, and the moderate stability increased the likelihood of using them as materials. Computational calculation represents another powerful tool to disclose the open-shell nature, and parameters such as biradical character index, crystal geometry, exchange interaction, and spin density are very informative in exploring the biradical nature.

A series of bis(phenalenyl) compounds were prepared since 1983 when the first member of this family, a pentalenodiphenalene (PDPL, **37**), was synthesized by Nakasuji et al. (Fig. 11a) [39]. This molecule exhibited amphoteric multistage redox properties with a numerical sum $E_{sum}$ as small as 0.99 eV. However, the neutral state of **37** was substantially destabilized by the electronic contribution of the 8π-electron antiaromatic pentalene subunit. Subsequently, indacenodiphenalene (IDPL, **38a**) with one benzene ring fused in the center was developed, and various substituents were introduced to improve the solubility [40, 41]. These compounds were featured by a singlet biradical character in the ground state. The line broadening

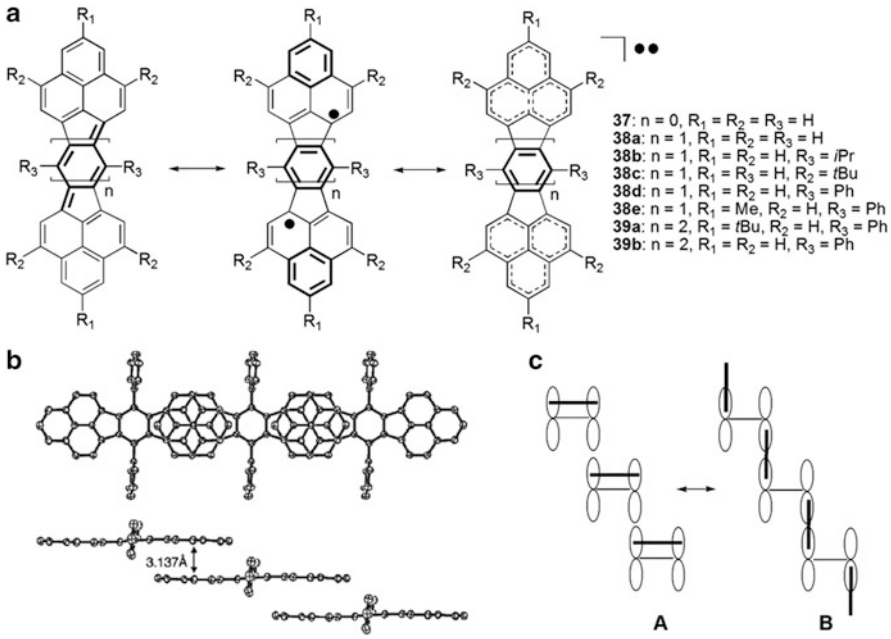


**Fig. 11** (**a**) Resonance forms of bis(phenalenyls) with different aromatic linkers; (**b**) crystal structure of **38d** [37]; (**c**) the RVB model for the electronic structure of **38e** [38]

in the NMR spectra at elevated temperatures as well as line sharpening at lower temperatures indicated a thermally accessible triplet species, and the small singlet-triplet energy gap can be determined by solid state ESR and SQUID measurements. One of the most salient features derived from a profound biradical character was the strong intermolecular interactions in the solid state. In 2005, Kubo reported a phenyl-substituted IDPL **38d** and its packing motif in the solid state, initiating a hot discussion on the interacting motif between and within those systems. The crystal structure of **38d** demonstrated one-dimensional chains in staggered stacking mode with an average π–π distance of 3.137 Å, which is significantly shorter than the van der Waals contact of carbon atoms (3.4 Å) (Fig. 11b). This packing mode will maximize the SOMO–SOMO overlapping between the radicals, leading to stabilized intermolecular orbitals that correspond to intermolecular covalency [37]. Further evidence of the coexistence of intermolecular and intramolecular interactions was provided by Huang from a theoretical perspective [42]. They found that the participation of unpaired electrons in intermolecular π–π bonding made them partially localized on phenalenyl units but less available for intramolecular delocalization, i.e., the intermolecular interaction is more predominant. With the aim of better understanding the intermolecular and intramolecular spin-spin interactions, Shimizu et al. attempted to alter the magnitude of the interactions by varying the external conditions such as molecular structure, temperature, and pressure. Interestingly, they found a larger intermolecular separation (3.225 Å) when introducing a methyl group

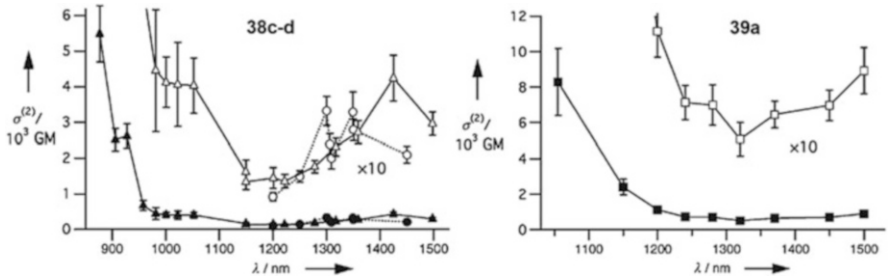


**Fig. 12** Two-photon absorption spectra of **38c** (*circles*), **38d** (*triangles*) and **39a** (*squares, right*) [45]. Reprinted with permission from [45]. Copyright 2007 John Wiley and Sons

to the $\beta$ positions of **38e**, and a similar increase in the π–π distance was also observed with increasing temperature. A decreased π–π distance would improve the intermolecular orbital overlap and strengthen the intermolecular bond interaction; however, it would also weaken the intramolecular interaction by making unpaired electrons more localized. As a result, the electronic structure of the 1D chain can be depicted by the resonating valence bond (RVB) model as a superposition of a resonance balance between intramolecular bonding (A) and intermolecular bonding (B) (Fig. 11c) [38]. A naphthalene-linked bis(phenalenyl) **39a** with even larger biradical character was synthesized by Kubo et al. [43]. The HOMO–LUMO gap of this compound was determined by cyclic voltammetry as 1.04 eV and the singlet-triplet gap was estimated as 1,900 K by SQUID measurements, both smaller than that of **38d** (1.15 eV and 2,200 K), in agreement with its larger biradical character. Compound **39b** without a *tert*-butyl bulky group was prepared to minimize the steric hindrance and to study the intermolecular interaction in the crystalline phase; the packing of **39b** adopted similar stepped mode with **38d** in the 1D chain and the intermolecular bonding was stronger than the intramolecular one due to the spin-localized nature on the phenalenyl moieties and can be more adequately described as muticenter bonding [44].

Theoretical studies pointed out many intriguing potentialities of singlet biradical systems, one of them being a high second hyperpolarizability, a quantity closely related to two-photon absorption (TPA) capabilities. This prediction was later proved by experimental results, which showed maximum TPA cross-section values up to (424 ± 64) GM at 1,425 nm for **38d** and (890 ± 130) GM at 1,500 nm for **39a**, which are comparable to similar TPA chromophores with strong donor or accepter peripheral groups and are among the best for pure hydrocarbons without donor and acceptor substituents, thus providing new insights into the design criteria of TPA materials (Fig. 12a) [45]. Moreover, balanced ambipolar charge transport of the thin films of **38d** was reported by Chikamatsu et al., presumably due to the amphoteric redox properties and strong intermolecular communications. Notably, despite the strong intermolecular interaction as discussed above, only moderate electron and hole mobilities of up to $10^{-3}$ $cm^2$ $V^{-1}$ $s^{-1}$ were observed as a result of the amorphous structure and poor crystallinity of the film [46]. However, these exciting results still indicate a promising future for these biradicals in materials science.

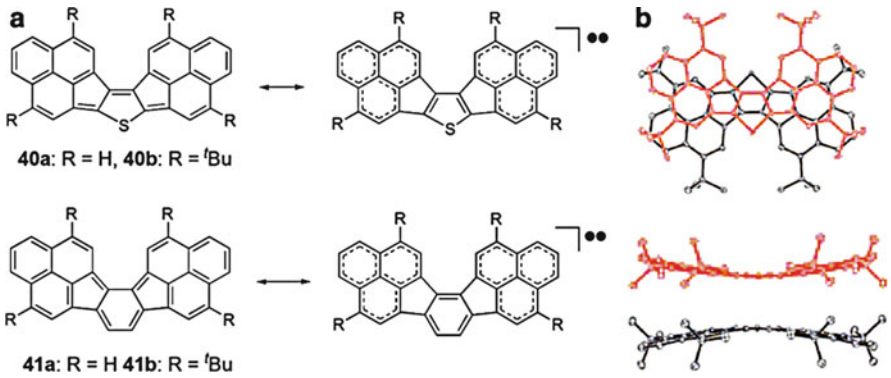


**Fig. 13** (**a**) Bis(phenalenyls) linked by thiophene and benzene; (**b**) single-crystal structures of **40b** [47, 48]

Other aromatic systems, such as the thiophene unit, can also be used as bridges for the bis(phenalenyl) systems. The thiophene fused bis(phenalenyl) **40** was synthesized in 2004 and the X-ray analysis revealed the formation of a dimeric pair with a bent structure for each monomer [47]. Accommodation of a doubly excited configuration into the ground state configuration will stabilize this system by suppressing four-electron repulsion arising from interaction between fully occupied orbitals. Fusion of phenalenyl to alternative positions in the benzene ring led to compound **41** with even larger biradical character [48], and the order of the biradical character is **38a** < **40a** < **41a**. An energy lowering of 7.08 kJ $mol^{-1}$ and 35.38 kJ $mol^{-1}$ from closed-shell form to open-shell form were calculated for **40a** and **41a**, respectively, suggesting that the ground state of these molecules is singlet biradical [49] (Fig. 13).

An interesting concept was recently tested in Kubo's group, in which two phenalenyl moieties are linked through a five-membered ring to produce a monoradical system **42a** [50]. As shown in Fig. 14, the resonance structures indicated a highly delocalized nature of this molecule, and the high stabilization was strong enough to stabilize this system even in absence of steric protection. The calculation results agreed well with this conclusion, showing an evenly distributed spin density throughout the whole molecular backbone. The extensive delocalization of unpaired electrons also suppressed the formation of σ-dimer. A well-defined multiline ESR spectrum was observed at room temperature, the intensity of which remained unchanged even at −90 °C, indicating no σ-dimer formation upon cooling. The butyl-substituted compound **42b** was also prepared to increase the solubility and to obtain a single crystal. X-ray analysis indicated the formation of π dimers in the solid state (Fig. 14), and the SOMO of the π dimer would be split into bonding and antibonding molecular orbitals due to the strong antiferromagnetic coupling of the unpaired electrons.

A "head-to-head" fusion of two phenalenyl moieties will generate a series of interesting polycyclic hydrocarbons named "zethrenes" due to their unique Z-shaped

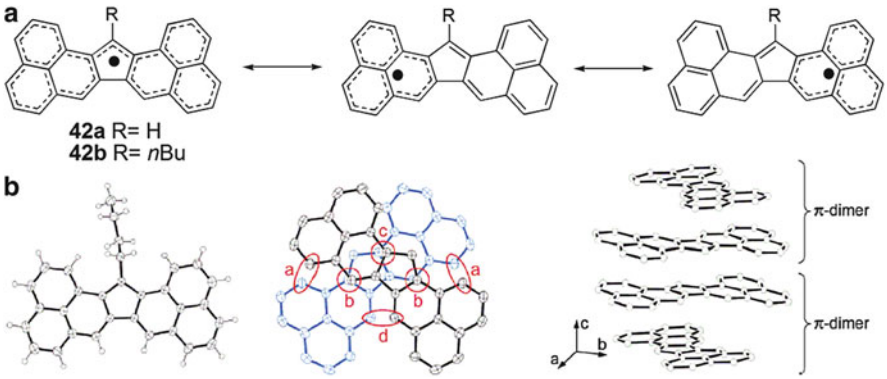


**Fig. 14** (**a**) Resonance structures of radical **42**; (**b**) single-crystal structures of **42b** [50]. Reprinted with permission from [50]. Copyright 2011 American Chemical Society

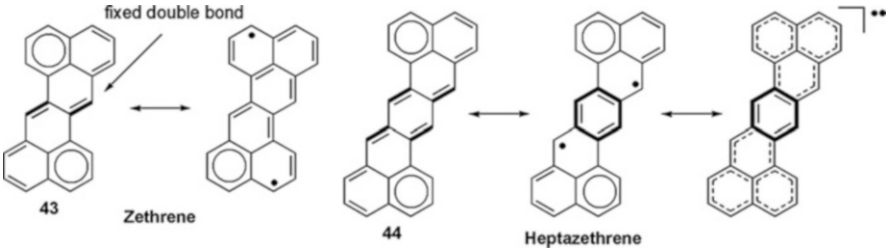


**Fig. 15** Resonance structures of zethrene and heptazethrene

molecular skeleton (Fig. 15). On the basis of the number of fused six-membered rings, longitudinal homologues of zethrene are defined as heptazethrene and octazethrene with two phenalenyl rings separated by benzene or naphthalene units, respectively, in a similar Z-shape manner. The family of zethrenes is featured by the fixed double bond structure in the central part and a singlet biradical character as illustrated by the resonance structures shown in Fig. 15. The biradical form of zethrene is destabilized by losing one sextet ring, but for heptazethrene and higher homologues it will be stabilized by gaining one more sextet ring as well as delocalization.

Although the attempt to make zethrene compounds was performed by Clar more than 50 years ago, the low stability derived from existence of fixed double bond and the biradical character obscures their practical applications. Very recently, stable zethrene derivatives with the most reactive 7, 14-positions blocked by substituents were prepared independently by Tobe [51] and Wu's group [52]. Tobe's synthesis took advantage of iodine promoted transannular cyclization reaction from the tetradehydro[10]annulene precursor **45**, which gave the 7, 14-diiodozethrene intermediate that could be subjected to Sonogashira coupling reaction (Fig. 16). However, the formation of zethrene by this strategy generally suffered from low yield. In 2010, Y.-T. Wu's group developed an even more straightforward and effective way

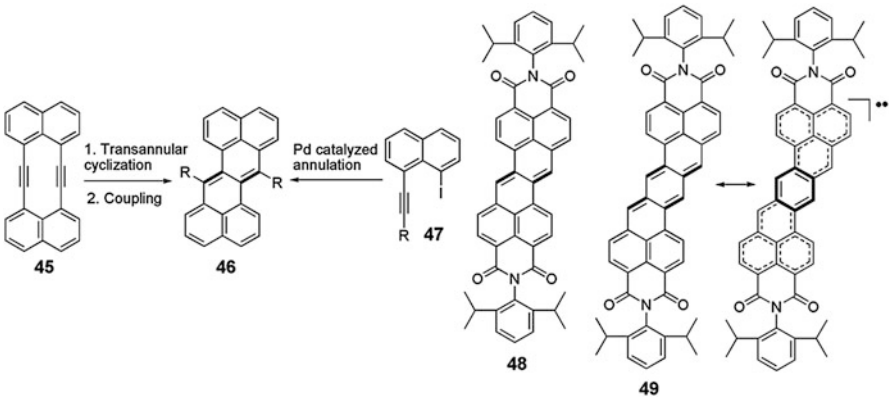


**Fig. 16** Two synthetic approaches to the zethrene derivatives **46**, and the structures of zethrene diimide **48** and heptazethrene diimide **49** [51–54]

to construct the zethrene core by homoannulation reaction from the precursor **47** using a Pd catalyst system. The transformation yield could be enhanced by up to 73%, which was quite impressive considering the forming of zethrene core and the introduction of substituents were realized in one step. At the same time, a novel zethrene derivative with two carboxylic imide groups located along the longer molecular axis (**48**) was synthesized by our group [53]. The introduction of electron-withdrawing groups successfully enhanced stability by lowering the HOMO energy level, and a 100-nm bathochromic shift in the absorption spectrum was also observed. Notably, in contrast to the theoretical predictions, none of the above-mentioned zethrene derivatives display open-shell behavior in the ground state.

Inspired by the prediction that higher homologues of zethrene (e.g., heptazethrene and octazethrene) will possess greater biradical character, our group finally synthesized the first stable heptazethrene derivative, a heptazethrene diimide **49** (Fig. 16) after many tries [54]. On the basis of calculations, the energy of singlet biradical form of **49** was located 5.8 and 7.5 kcal $mol^{-1}$ lower than the closed-shell quinoid and triplet form and thus defined a singlet biradical ground state. The $^{1}H$ NMR spectra showed line broadening at room temperature and line sharpening at low temperatures, due to the existence of thermally accessible triplet species. The UV–vis absorption spectrum gave a lower energy band, and a HOMO-LUMO gap as small as 0.99 eV was determined by cyclic voltammetry, attributed to a biradical ground state. It is noteworthy that compound **49** exhibited good stability in solution which resulted from a synergetic effect of radical delocalization and electron-withdrawing effect of the substituents.

Fusion of three phenalenyl moieties onto one benzene ring will lead to a monoradical system **50a** with a large delocalization of the electron over the whole molecule (Fig. 17) [55, 56]. Although good stability is expected after kinetic stabilization by *tert*-butyl groups, compound **50b** was found to decompose in 1 day

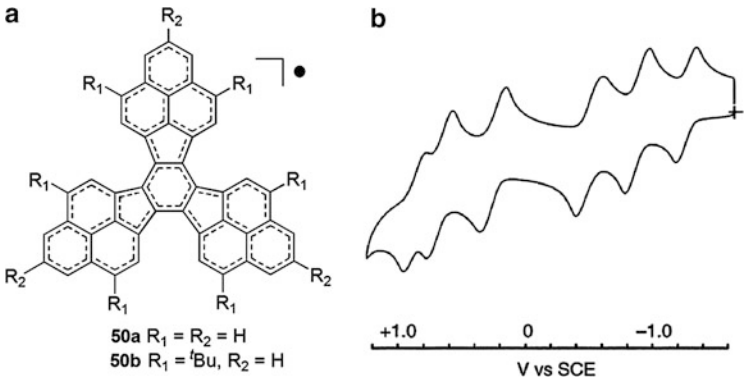


**Fig. 17** (**a**) Structure of trisphenalenyl radical **50**; (**b**) cyclic voltammogram of **50b** [55, 56]

in air. The neutral radical gave six reversible one-electron redox waves (Fig. 17b), providing evidence for the formation of stable monovalent, divalent, and trivalent species, which is one of the rare examples of compounds with six-stage amphoteric redox behavior.

## *2.2 Triangulene-Based Triplet Biradicals*

The higher order analogue of phenalenyl is the $C_3$-symmetric polycyclic hydrocarbon **1** known as triangulene, which represents the most fundamental non-Kekulé polynuclear benzenoid compounds with at least two carbon atoms not participating in the double bond network, giving rise to an open-shell electronic structure. According to theoretical calculations, a triplet ground state is expected due to the topological degeneracy of non-bonding molecular orbitals (NBMOs) with a non-disjoint nature [57]. Theoretical studies also predicted large spin densities at the edge sites, indicating its high reactivity in the neutral state. Notably, it is predicted that the triangulene system can lead to formation of a π-stacked radical polymer with a large SOMO–SOMO overlap and high molecular symmetry, which will enhance the electron and hole mobilities and may serve as potential building blocks to construct thermoresponsive and photoresponsive conductive and magnetic materials [4, 58]. But above all, the stability issue has to be carefully examined.

The first attempt to synthesize triangulene was made by Clar, but only polymerized product was obtained due to its kinetic instability [59]. In 1977, a closed-shell dianion of triangulene was achieved and detected by NMR measurements [60]. In 2001, Nakasuji et al. applied the same strategy that stabilizes the phenalenyl radical to the triangulene system, by introducing bulky *tert*-butyl groups on three vertexes of the triangle, with the aim of increasing kinetic stability and minimizing the electronic perturbation. The synthetic route was shown in Scheme 4 and the biradical species was generated by treating the

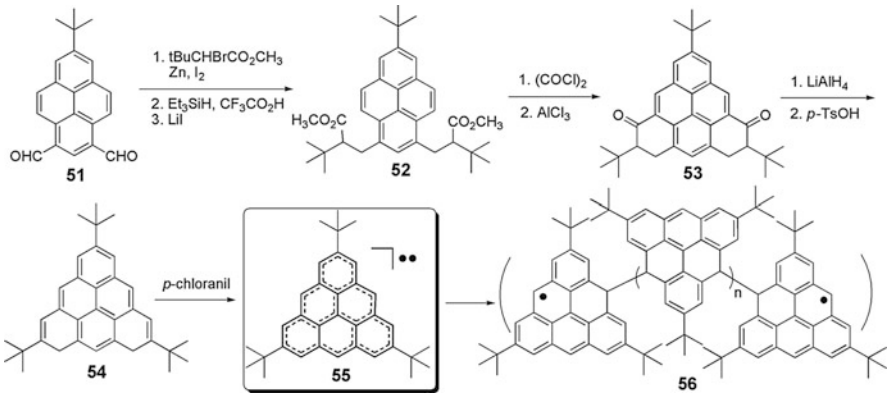


**Scheme 4** Synthetic route to tri-*tert*-butyl triangulene biradical **55** [61]

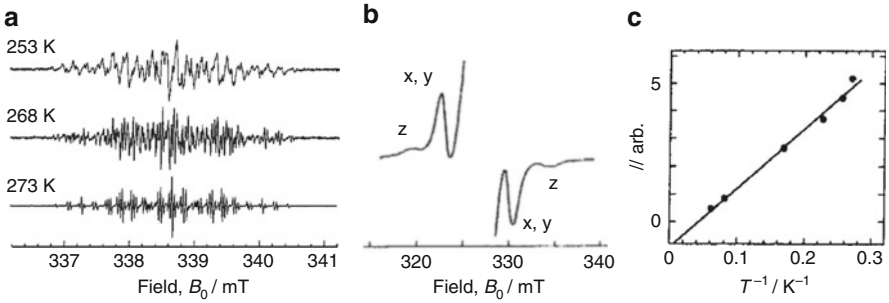


**Fig. 18** Characterization of **55** by variable temperature ESR spectroscopy [61]. Reprinted with permission from [61]. Copyright 2001 American Chemical Society

dihydrotriangulene **54** precursor with *p*-chloranil. Unfortunately, the triangulene system is more reactive than phenalenyl and cannot be fully stabilized by partial blocking. The oxidation of **54** by *p*-chloranil was monitored by ESR spectra at variable temperatures (Fig. 18a) and rapid freezing of sample at an intermediate stage gave a superposition of a doublet monoradical species and a fine-structure ESR spectrum of a typical triplet state which was attributed to compound **55**, a genuine hydrocarbon structure with a threefold rotation axis (Fig. 18b). The linear dependence of the triplet signal intensity I on 1/T (Fig. 18c) showed that the triplet was the ground state which was in agreement with theoretical calculations [61]. Although this work is a significant contribution towards understanding the nature of the triangulene triplet biradical, the long-standing issue of isolating stable triangulene biradicals in the crystalline state still needs further stabilization methods.

Similar to the phenalenyl system, substitution of oxygen atoms at strategic positions of triangulene leads to a series of novel open-shell compounds called "trioxytriangulenes," with their electronic structures significantly different from the parent triangulene. The different redox species are shown in Fig. 19 and the neutral

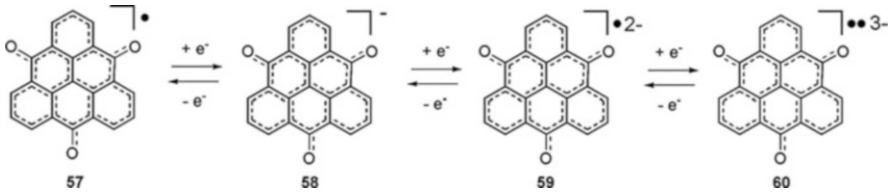


**Fig. 19** Redox species of trioxytriangulene

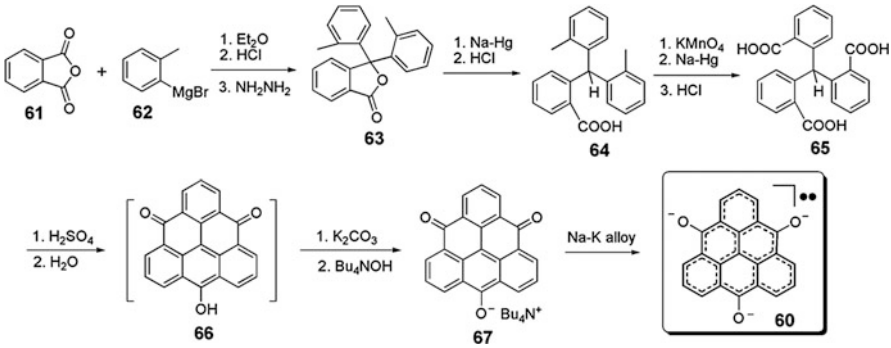


**Scheme 5** Synthesis of biradical trianion **60** [62, 63]

radical **57** possesses a similar electronic structure with 6-oxophenalenoxyl radical mentioned above, in contrast to the diradical trianion **60** with a triplet biradical ground state.

The triplet ground state trioxytriangulene biradical compounds were prepared by Bushby by reduction of the corresponding ketones (Scheme 5). The biradical trianion species **60** exhibited high stability in degassed solution even at room temperature, due to the extension of delocalization and protection from dimerization [62, 63]. Compound **60** was triplet in the ground state as determined by ESR spectroscopy, while other unsymmetric derivatives appeared to be ESR silent and singlet in the ground state [64]. The introduction of heteroatoms was believed to lift the degeneracy of the NBMOs, causing a kinetic exchange interaction that dominates over dynamic spin polarization in the parent π systems.

Organic open-shell compounds have shown some promise as electrode-active materials in secondary batteries. Since oxophenalenoxyl systems have already shown a high performance to this end, some trioxytriangulene neutral radical systems, such as *tert*-butyl and bromo-substituted derivatives **68** and **69**, were recently prepared by Morita et al. [65]. Such molecules possessed a SOMO and two degenerate LUMOs as shown in Fig. 20. Compound **68** gave a high capacity of 311 $Ahkg^{-1}$, exceeding those of Li-ion batteries in the first discharge process. Compared to **68**, the bromo-substituted **69** showed improved output voltage and cycle performance, indicating a tunable performance on the basis of chemical modification. These results pointed out a high potentiality of organic open-shell systems for applications in superbatteries with high energy densities.

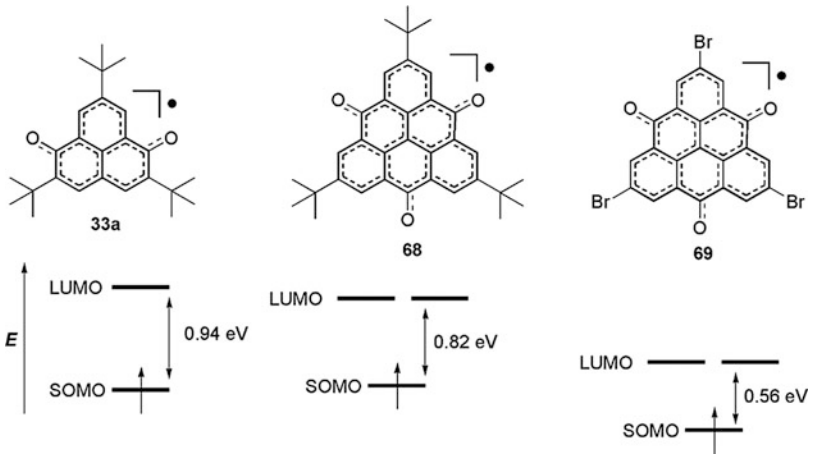


**Fig. 20** Structures and energy diagrams for monoradicals **33a**, **68**, and **69** [65]

## 3 2D Nanographenes with Both Zigzag Edges and Armchair Edges

The rectangular fragments of graphene possess the structural character of coexistence of both zigzag and armchair edges (Fig. 1). In contrast to the above-mentioned all zigzag edged open-shell PAHs, 2D aromatic systems falling into this category can all be depicted as closed-shell Kekulé structures, and the presence of armchair edges provides enhanced stability. Meanwhile, the existence of zigzag edges leads to a narrowed bandgap, which endows them with attracting properties such as charge transporting capability and long wavelength absorption and emission. For systems with more than two zigzag edges, a crossover from closed-shell all-Kekulé form to open-shell biradical form in the ground state will take place with the extension in conjugation, due to the decrease in bandgap which facilitates the double excitation and the aromatic stabilization of the open-shell structure (formation of more sextet benzenoid rings for biradical form). There are several basic units of this class of finite nanographenes. Rylenes are those with two zigzag edges and extended conjugation along the armchair edges, or *peri*-fused naphthalenes. Anthenes are those with three zigzag edges and extended armchair edges, or *peri*-fused anthracenes. Periacenes are those with two armchair edges and extended zigzag edges. More important, the coexistence of both zigzag and armchair edges results in a combination of moderate stability and intriguing electronic properties, making these PAHs highly favorable for applications in dye chemistry and materials science. The examples of using rylenes and anthenes as semiconductors and dyes are already abundant while more are expected, and the recent advances in open-shell systems provide new insights in the field of magnetic materials and nonlinear optics. In the following section, three types of 2D aromatic networks, namely rylenes, anthenes, and periacenes, will be summarized and discussed.

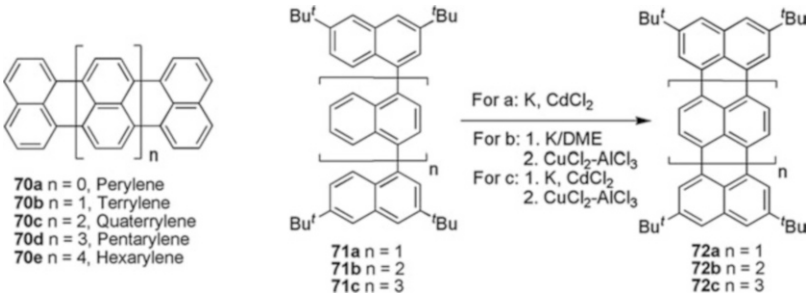


**Scheme 6** Structures of rylenes and synthesis of tetra-*tert*-butyl rylenes [66, 67]

## *3.1 Rylenes*

Rylenes are large PAHs in which two or more naphthalene units are *peri*-fused together by single bonds. Only one aromatic sextet benzenoid ring can be drawn for each naphthalene unit and two zig-zag edges exist at the terminal naphthalene units. On the basis of numbers of fused naphthalenes, rylenes can be termed as perylene, terrylene, and so on (Scheme 6). In pursuit of stable dyes with high extinction coefficients and long-wavelength absorption/emission, rylenes have received a great deal of attention. Among them, perylene **70a** and its imide derivatives have shown obvious advantages including outstanding chemical, thermal, and photochemical inertness, and are already well investigated and documented. So in this part, discussion will be focused on higher order rylenes with lower bandgap and longer wavelength absorption and emission, as well as their applications as materials.

The preparation of more highly ordered rylenes generally suffered from two main obstacles. First of all, high order rylenes are electron-rich π-systems and are relatively unstable upon exposure to air, so mild conditions are needed to construct these systems. Moreover, due to the rigid molecular backbone and high tendency to aggregate in solution, poor solubility is expected and it is essential to introduce substituents to suppress the aggregation and increase solubility. In search of mild conditions to synthesize higher rylenes, a variety of intramolecular cyclodehydrogenation methods have been developed. These include oxidative cyclodehydrogenation using $FeCl_3$, or a combination of $CuCl_2$-$AlCl_3$ as Lewis acid as well as oxidant, and reductive cyclodehydrogenation via anion radical mechanism promoted by base. In 1990, four *tert*-butyl groups were designed in Müllen's group to resolve the solubility problem of rylenes, and the enhanced solubility allowed the investigation of physical properties in solution for the first time for terrylene **72a**, quaterrylene **72b**, and pentarylene **72c** (Scheme 6) [66, 67]. The synthesis of terrylene derivative **72a** was achieved by treatment of the precursor **71a** with potassium followed by oxidation with anhydrous cadmium chloride, while the preparation of **72b** and **72c** took a stepwise manner by an initial reductive cyclodehydrogenation to generate partially cyclized intermediate followed by

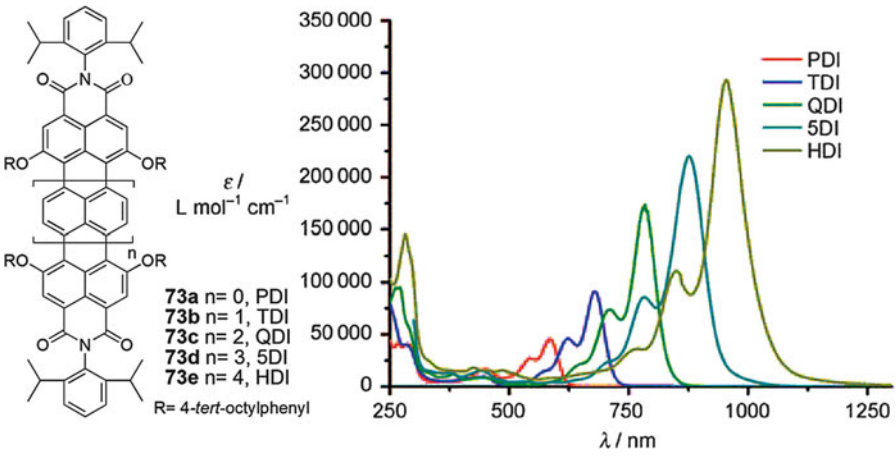


**Fig. 21** Structures and absorption spectra of the tetraphenoxy-substituted rylenediimides **73a–e** in $CHCl_3$ [68]. Reprinted with permission from [68]. Copyright 2010 John Wiley and Sons

oxidative cyclodehydrogenation to give the final product. A significant bathochromic shift in absorption spectrum was observed from **72a** to **72c** due to the elongation of the conjugation.

Although the *tert*-butyl group plays an important role in solubilizing rylenes, the scope is limited to quaterrylene. The solubility of the substituted pentarylene **72c** is strongly decreased which prevents the measurement of its $^1$H NMR spectrum. Alternatively, a breakthrough of making stable and soluble high order rylene derivatives was achieved by introducing dicarboxylic imide functional groups. The electron-withdrawing nature of imide stabilizes the electron-rich rylene core by reducing the electron density, and the bulky groups such as the diisopropylphenyl group can be introduced on the imide end to prevent dye aggregation (Fig. 21). Further substitution can be realized in the bay region of the rylene core with the development of new synthetic strategies, which further increases the solubility. The improved stability and solubility make the preparation of higher rylene bisimides, namely pentarylene bisimide, hexarylene bisimide, heptarylene bisimide, and octarylene bisimide, practically possible. Moreover, additional bathochromic shift in absorption was observed for rylene bisimides compared to parent rylenes due to intramolecular donor-acceptor interaction. The extension of conjugation along the long molecular axis of the rylene bisimides generally induces a bathochromic shift of about 100 nm per additional naphthalene unit, along with a nearly linear increase in extinction coefficient (Fig. 21) [68].

Two approaches were available for the preparation of quaterrylene bisimides, taking advantage of either intramolecular cyclization or intermolecular dimerization reactions. These two methods were developed independently in Müllen's and Langhals' groups. As shown in Scheme 7, Müllen's intramolecular approach started from bromination of perylene monoimide **74**, which was subjected to Yamamoto coupling reaction to produce precursor **76**, and the quaterrylene bisimide **77** was

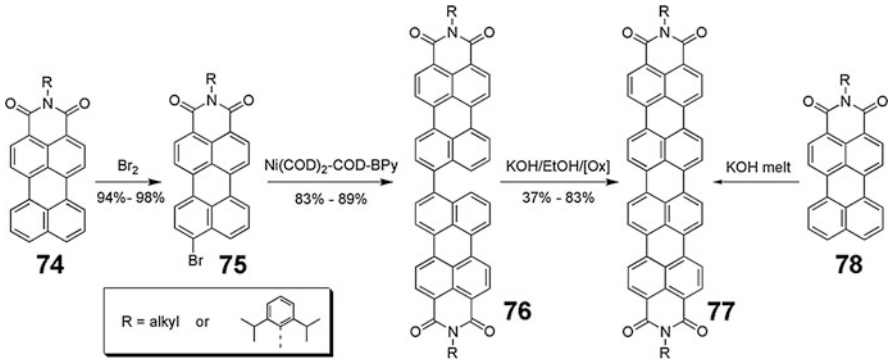


**Scheme 7** Two synthetic routes to quarterrylene bisimides **77** [69, 70]

then obtained by heating **76** in molten KOH in the presence of an added oxidizing agent. Enhanced solubility can be realized by nucleophilic substitution with bulky phenoxy groups in the bay region [69]. In parallel, Langhals reported a one-step dimerization from perylene monoimide **78** inspired by the formation of perylene bisimide from naphthalene monoimide. Reaction of **78** in alkali melt proceeded to give quaterrylene bisimide with swallow tail substituents [70].

The pursuit of higher order rylene bisimides continued and the next two members in this family, pentarylene bisimide **73d** and hexarylene bisimide **73e**, were synthesized in Müllen's group on the basis of two different synthetic methods (Scheme 8) [71]. The first construction concept was called the "nitronaphthalene method" in which one nitronaphthalene unit was attached to a perylenedicarboximide, whereupon the nitro group could be reduced and transformed into iodo group to afford precursor **83**. Subsequently, homocoupling of **83** or Suzuki coupling with perylenedicarboximide **79** yielded **82b** and **82a** which, upon cyclization, generated hexarylene bisimide **73e** and pentarylene bisimide **73d**. This method generally suffered from low overall yield due to the low yield in Sandmeyer reaction, so an alternative method named the "bisbromorylene method" was developed in which two perylenedicarboximides **79** were coupled to a bisbromonaphthalene **80a** or bisbromoperylene **80b** and fused in a one-step or two-step sequence to form the corresponding compounds **73d** and **73e**. The absorption maxima of **73d** and **73e** were located at 877 and 930 nm, respectively, and these two dyes had extremely high extinction coefficients (up to 235,000 $M^{-1}$ $cm^{-1}$ for **73d** and 293,000 $M^{-1}$ $cm^{-1}$ for **73e**), which are the highest values reported among all the known organic dyes in the NIR spectral region. Despite relatively low band gaps, **73d** and **73e** displayed remarkable stability and their solution remained the same over weeks in sunlight. More importantly, nearly no absorption for **73d** and **73e** could be detected in the visible region. All of the outstanding properties mentioned above qualified them as promising NIR dyes for many technological applications, such as security printing.

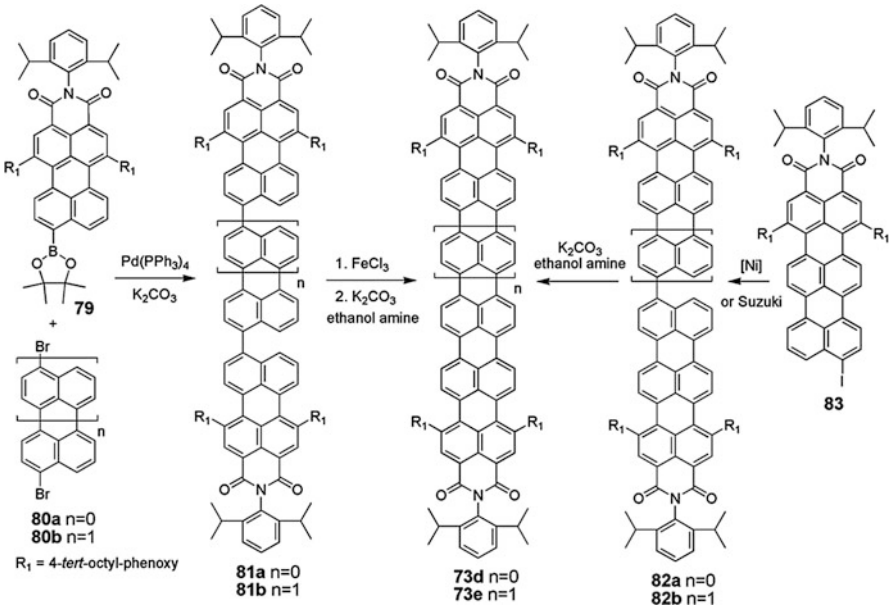


**Scheme 8** Two synthetic routes to pentarylene bisimides and hexarylene bisimides [71]

*N*-Annulation at the armchair edge of the perylene moiety represents another interesting concept to construct high order rylenes, in that additional side chains can be easily introduced to improve the solubility. New opto-electronic properties are expected due to the electron-donating nature of amines. From the year 2009, a series of poly(peri-*N*-annulated perylenes) up to hexarylene **84b** were achieved in Wang's group (Fig. 22), and oxidative ring fusion driven by DDQ/$Sc(OTf)_3$ was found to be very effective for this system due to the electron-rich property of *N*-annulated perylene core [72, 73]. These dyes displayed large dipole moments that may favor the formation of highly ordered supramolecular structures, which may lead to enhanced charge carrier mobilities. In parallel to this work, the carboximide derivative **85** (Fig. 22) was developed in our group, and the presence of imide group not only enhanced the stability of the core by lowering the high-lying HOMO energy level, but also allowed the introduction of the bulky diisopropylphenyl group which helped to increase the solubility together with the branched alkyl chain at the amine site [74]. An alternative intramolecular Michael addition reaction-based cyclodehydrogenation strategy by mild base was applied to synthesize **85**, due to the existence of the electron-withdrawing imide group. Compound **85** exhibited absorption at in the NIR region and emitted strong fluorescence with quantum yield up to 55% in dichloromethane. Such a high quantum yield is remarkable given that many NIR absorbing dyes usually exhibit low fluorescence quantum yield.

Rylene bisimide compounds can be functionalized in different manners to fit different applications due to the existence of multiple modification sites at imide

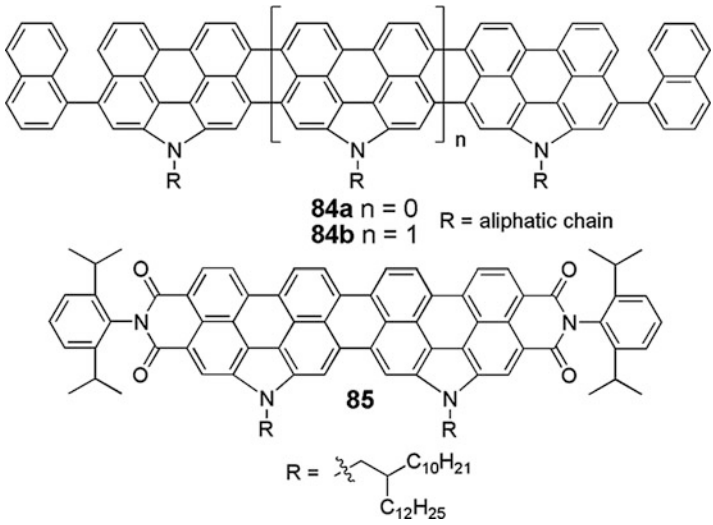


**Fig. 22** Structures of *N*-annulated rylenes [72–74]

ends and bay regions. The important role of rylene bisimides as fluorescent dyes in biological systems have attracted considerable attention because of their excellent chemical and photostability compared to commercial dyes. Moreover, higher order rylene bisimides display absorption and strong emission at the far-red to NIR region which prevents interference from self-absorption of biomolecules. The largest obstacle for aromatic organic dyes to be used in biological systems is to achieve sufficient water solubility while maintaining a high fluorescence quantum yield, as aromatic chromophores are prone to aggregate in aqueous media. Endeavors are made in this area in Müllen's group and some water soluble terrylene bisimide dyes such as **86** and **87** are already available for protein labeling (Fig. 23) [75]. Applications of high order rylene bisimides as semiconducting materials in the fields of organic solar cells and field-effect transistors (FETs) have also been examined. Higher rylenes are expected to display a larger π-conjugation and a concomitant better light-harvesting property, so compound **88** (Fig. 23) was prepared and tested in dye-sensitized solar cell (DSSC) devices [76]. Despite a remarkably broad photocurrent action spectrum arising from its absorption behavior, a moderate efficiency of 2.4% has been achieved, which is attributed to the low voltage caused by the dye's incompatibility with additives. The field effect transistor property was initially studied based on an *n*-type semiconductor molecule **89** (Fig. 23), and the vapor-deposited films of **89** on Si-$SiO_2$ substrates exhibited a maximum FET electron mobility of around 0.07 $cm^2\ V^{-1}\ s^{-1}$ and an on/off ratio in excess of $10^4$, indicating the potential of terrylene molecule for FET applications [77]. Recently, Bao's group successfully developed a scalable synthesis of swallow tailed quaterrylene bisimides **90a** and **90b** (Fig. 23) which can be processed from solution [78]. The pressure-assisted thermal cleavage of swallow tails yielded films

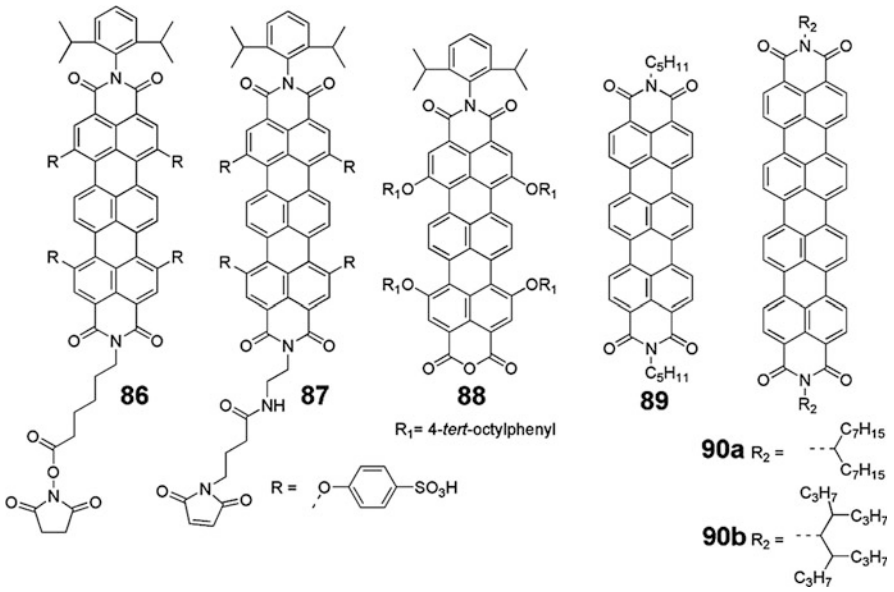


**Fig. 23** Examples of rylenes as functional materials [75–78]

with significantly reduced surface roughness and void space, leading to electron mobility up to 0.088 $cm^2\ V^{-1}\ s^{-1}$. This method opens up a new route toward the solution based fabrication of the crystalline thin films of sparingly soluble higher rylene bisimides.

High order rylenes represent extension of conjugation along the longer molecular axis, while lateral extension of conjugation of perylene bisimides leads to another intriguing 2D aromatic network. A series of triply linked oligo-perylene bisimides **91**–**95** were reported in Wang's group (Fig. 24), and the conjugation can be expanded up to four perylene bisimides fused together at the bay region [79–81]. These systems were synthesized by copper-involved condensation of tetrabromo (chloro)-perylene bisimides along the bay region under different conditions. Due to the two possible coupling positions, there are structural isomers for higher analogues. These fully conjugated graphene-type compounds display broad and red-shifted absorption and strong electron-accepting ability.

## *3.2 Anthenes and Periacenes*

The same fusion mode with anthracene instead of naphthalene leads to another type of extended 2D aromatic network termed "anthene". When two anthracene units are fused together by three single bonds between neighboring anthryls, it is called bisanthene (**96**), and longer homologues are named teranthene (**97**) and

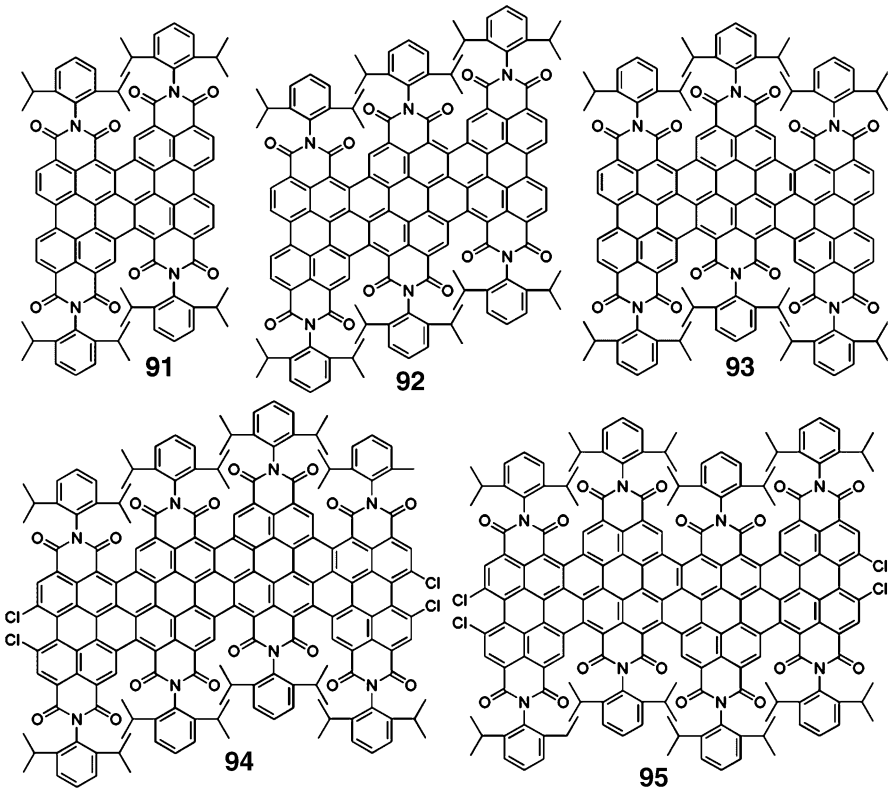


**Fig. 24** Structures of laterally extended perylene bisimides [79–81]

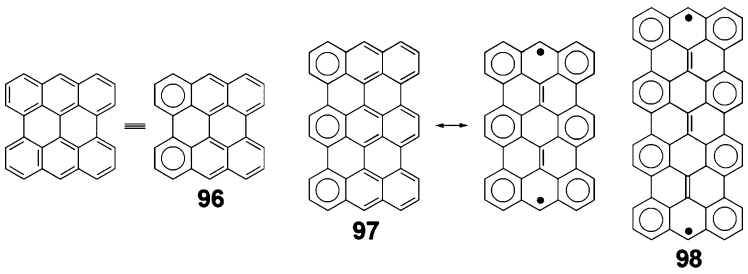


**Fig. 25** Structures of anthenes

quateranthene (**98**) accordingly (Fig. 25). Due to the extension of conjugation and the presence of more zigzag edges, this class of compound shows further decreased HOMO–LUMO gaps and lower stability compared to rylenes. Notably, anthenes from teranthene on will exhibit large singlet biradical character in the ground state, stemming from narrowed HOMO–LUMO gap and recovery of more sextet benzenoid rings. In the course of seeking experimental investigation of the crossover

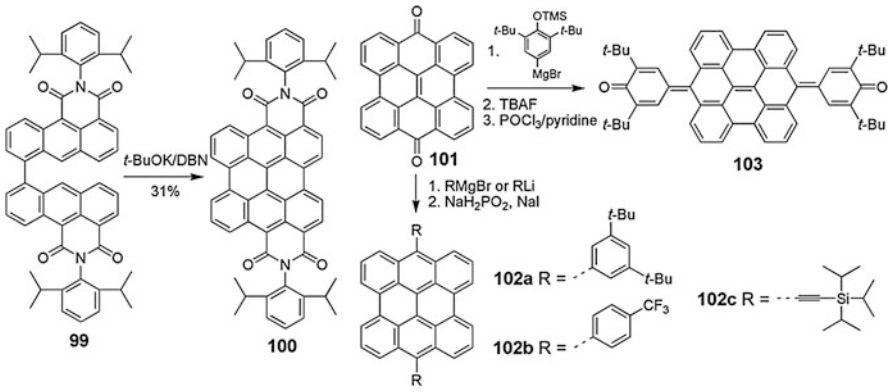


**Scheme 9** Different synthetic methods to stable bisanthenes [82–84]

from closed-shell to open-shell in a series of homologues of Kekulé PAHs, anthenes represent an excellent prototype since the radicals will have fixed positions on the zigzag edges in order to draw the maximum sextet benzenoid rings, which minimize the influence of migration and delocalization. Therefore, the discussion of biradical character can be concentrated on the energy balance between the formal loss of the double bond and the aromatic stabilization, which provides more intriguing properties and functionalities for the anthene family. Moreover, special and intriguing properties derived from open-shell characters provide new potential functionalities in materials science.

The first member of anthenes, bisanthene, was firstly reported by Clar and the improved synthesis was recently developed by Bock's and our groups. The parent bisanthene was a blue color compound with low stability owing to its high-lying HOMO energy level, and the most reactive sites are the *meso*-positions of the zigzag edges which readily undergo addition reaction with the singlet oxygen in air. Therefore, it is essential to do modifications on the zigzag edges in order to obtain stable and soluble bisanthene derivatives to allow further study and applications.

Systematic research was conducted in our group to stabilize bisanthene by different strategies as shown in Scheme 9. The first approach is to introduce electron-withdrawing imide groups onto the zigzag edges, which was proven to be an effective concept to stabilize extended PAHs [82]. The bisanthene bisimide compound **100** was achieved from precursor **99** by base-promoted cyclization reaction in moderate yield, and it displayed good stability with no significant change in solution exposed to air. Moreover, as was the case in other systems, **100** exhibited a red shift of 170 nm at the absorption maximum compared with parent **96**, indicating that **100** can be used a promising candidate for NIR absorbing materials.

An alternative approach was synchronously developed in our group by means of *meso*-substitution with aryl or alkyne substituents to block the reactive sites [83]. Based on this consideration, three *meso*-substituted bisanthenes **102a–102c** were prepared by nucleophilic addition of aryl or alkyne Grignard reagent to the

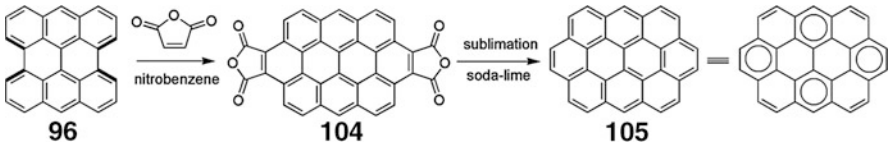


**Scheme 10** Synthesis of ovalene from bisanthene [85]

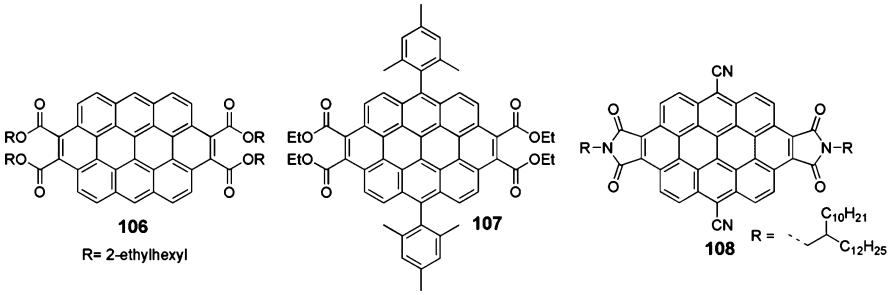


**Fig. 26** Structures of substituted ovalenes [86–88]

bisanthenequinone **101** followed by reduction/aromatization of the as-formed diol. The obtained compounds not only showed enhanced stability and solubility but also exhibited absorption and emission in the NIR region as well as amphoteric redox behavior, which qualified them as NIR dyes and hole/electron transporting materials. The same synthetic strategy was also applied to prepare quinoidal bisanthene **103**, which can be regarded as a rare case of stable and soluble nanographene with a quinoidal character [84]. An intense NIR absorption and amphoteric redox behaviors were also observed for compound **103**.

Since bisanthene has a diene character at the bay regions, Diels-Alder reaction can take place which allows easy access to more extended aromatic systems. For example, Diels–Alder cycloaddition reactions with maleic anhydride as dienophiles followed by oxidative dehydrogenation and decarboxylation gave compound **105**, namely ovalene, as an insoluble material (Scheme 10) [85]. As two more sextet benzenoid rings can be drawn for ovalene compared to bisanthene, ovalene is more stable than bisanthene with larger HOMO-LUMO gap, in spite of a larger molecular size and more extended conjugation. One general approach towards soluble ovalene derivatives is to attach solubilizing and/or bulky groups onto the rigid ovalene core. A series of soluble ovalene derivatives **106** and **107** as shown in Fig. 26 was obtained by twofold oxidative Diels-Alder reactions with different electron-withdrawing dienophiles [86, 87]. An interesting example is our recent report on preparation of large disc-like 7,14-dicyano-ovalene diimide **108** [88]. Due to the attachment of electron-withdrawing imide and cyano groups, **108** exhibited n-type character and high electron mobilities of up to 1.0 $cm^2\ V^{-1}\ s^{-1}$ in $N_2$ and 0.51 $cm^2\ V^{-1}\ s^{-1}$ in air atmosphere were achieved in solution processing FET devices. This device performance from **108** is better than most solution processible n-type semiconductors reported so far.

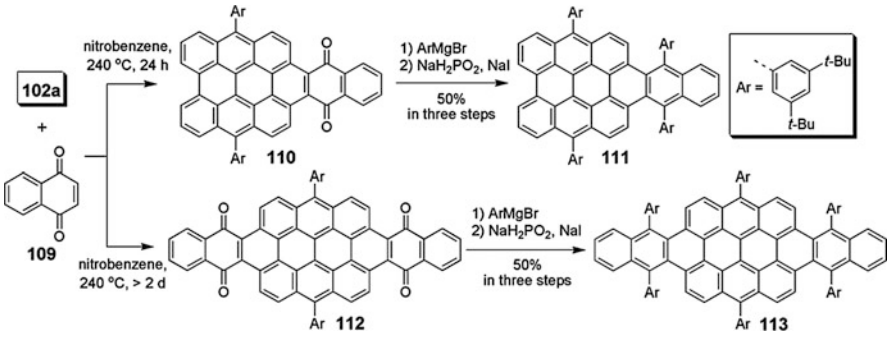


**Scheme 11** Synthesis of laterally extended bisanthenes [89]

The synthetic approach taking advantage of Diels-Alder reaction makes it possible to extend the π-system further by using different dienophiles. For example, using 1,4-naphthaquinone **109** as dienophile led to bisanthene adducts **110** and **112**, whereupon nucleophilic addition of Grignard reagents followed by reductive aromatization gave compounds **111** and **113** (Scheme 11) [89]. Early studies by Müllen and coworkers revealed that *bay*-annulation of rylenes leads to hypsochromic shifts of absorption compared to their parent rylene molecules. For this system, a slight bathochromic shift was observed compared with *meso*-substituted bisanthenes owing to the additionally higher conjugation along the long molecular axis. The emission spectra of **111** and **113** showed mirror symmetry with their absorption spectrum, and relatively moderate photoluminescence quantum yields of 0.45 and 0.38 were measured for dyes **111** and **113**, indicating a potentiality of these compounds as NIR organic light-emitting diodes (OLEDs).

Fusion of three anthracene units leads to teranthene, which is a longer homologue of bisanthene and a big challenge in terms of synthetic difficulty and stability issues. Recently, the first teranthene derivative **119** was obtained in Kubo's group [90]. As shown in Scheme 12, nucleophilic addition of lithium reagent **114** to 1,5-dichloroanthraquinone **115** followed by reductive aromatization with NaI/$NaH_2PO_2$ gave the teranthryl derivative **116**. Cyclization combined with demethylation of **116** was carried out with KOH/quinoline to give the partially ring-closed quinone **117** which was treated with mesitylmagnesium bromide in the presence of $CeCl_3$ and further underwent reductive aromatization to generate partially cyclized compound **118**. The last cyclization was promoted by DDQ/$Sc(OTf)_3$ followed by quenching the reaction with hydrazine to give **119** as a dark-green solid. Compound **119** exhibited moderate stability in solution with a half-life of around 3 days upon exposure to air at room temperature. Like other open-shell PAHs with singlet biradical ground state, the $^1$H NMR spectrum showed temperature dependence with a line broadening at room temperature.

X-ray analysis revealed an effective $D_{2h}$ symmetry for the teranthene core, with two mesityl groups nearly perpendicular (Fig. 27). A prominent biradical character was also reflected by the geometry and bond length of the teranthene in comparison

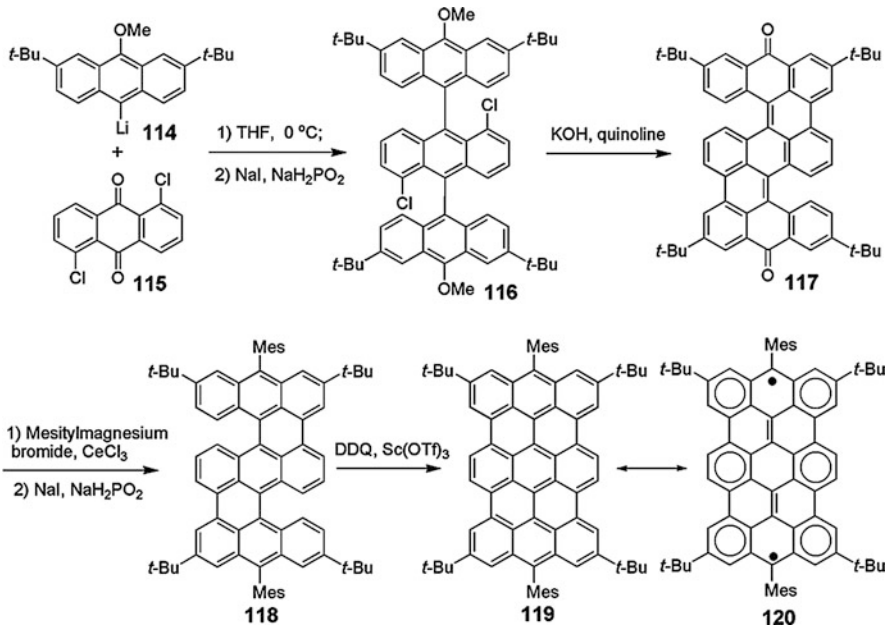


**Scheme 12** Synthesis of teranthene derivative [90]

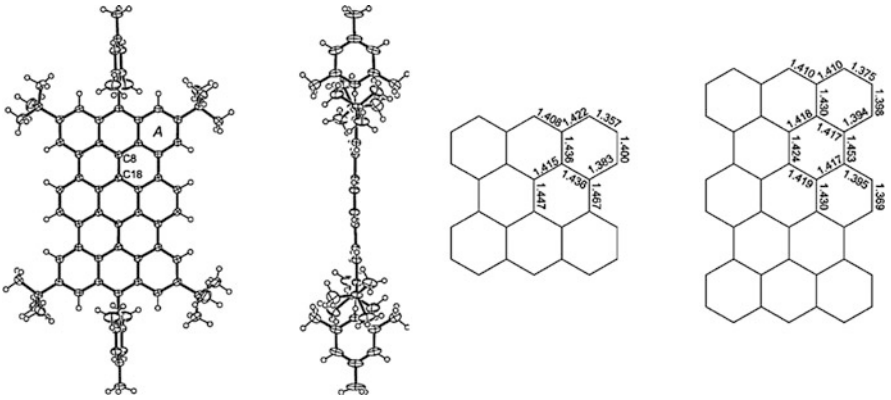


**Fig. 27** X-Ray crystal structures of teranthene **119** and bond length of bisanthene and teranthene [90]. Reprinted with permission from [90]. Copyright 2010 American Chemical Society

with the bisanthene. The bond length of $C_8$–$C_{18}$ was 1.424 Å, being significantly shorter than $sp^2$ C–C single bond (1.467 Å) and the corresponding one in bisanthene (1.447 Å), which resulted from the enforcement of biradical resonance contribution (**120**). Alternatively, from an energy point of view, the lost C–C π-bond energy of 270 kJ $mol^{-1}$ can be fully compensated by three times the aromatic stabilization energy of 90 kJ $mol^{-1}$, suggesting that both Kekulé and biradical forms contribute equally to the ground state.

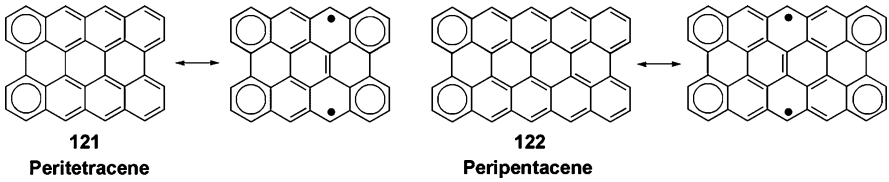


**Fig. 28** Structures of periacenes

Periacenes refer to those PAHs with constant armchair edges and growing zigzag edges, for example, *peri*-fusion of tetracene leads to peritetracene **121** and *peri*-fusion of pentacene results in peripentacene **122** (Fig. 28). Perylene and bisanthene can also be regarded as members of this family. Theoretical calculations by Jiang pointed out a crossover from nonmagnetic phase to antiferromagnetic phase starting from peritetracene, and an open-shell ground state is therefore expected (Fig. 28) [91]. Unfortunately, as the inverse dependence of stability with conjugation length is remarkably larger compared to anthenes and rylenes, the preparation of periacenes has not yet been achieved. The only experimental evidence of peripentacene was the mass spectroscopic peak of gas-phase disproportionation products [92].

On the way to making stable and characterizable peripentacene derivatives, some preliminary results were achieved in our group. The synthetic concept is based on nucleophilic addition followed by aromatization, as well as ring closing reactions, which is similar to the preparation of stable bisanthenes. For this purpose, the bispentacenequinone **124**, obtained from dimerization of pentacenyl monoketone **123**, was subjected to nucleophilic addition of triisopropylsilylethynyl lithium reagent followed by reductive aromatization with $NaI/NaH_2PO_2$ to give the cruciform 6,6′-dipentacenyl **125** (Scheme 13) [93]. Interestingly, compound **125** exhibits two face-to-face π-stacking axes in a single crystal and this allows two-directional isotropic charge transport, representing a new concept in semiconductor design. FET mobilities up to 0.11 $cm^2\ V^{-1}\ s^{-1}$ were obtained based on vapor-deposited thin films. Subsequent study was conducted by applying oxidative photocyclization of **124** to obtain fused bispentacenequinone **126** [94]. However, the subsequent nucleophilic reaction of compound **126** with excess Grignard reagent of 1-bromo-3,5-di-*tert*-butylbenzene in anhydrous THF followed by acidification in air did not generate the desired 1,2-addition adduct. Alternatively, an unexpected 1,4-Michael addition product **127** was obtained and confirmed by X-ray single-crystal analysis. Further treatment of **127** with excess Grignard reagent followed by acidification in air gave the tetraaryl-substituted fused bispentacenequinone **128**. Single-crystal analysis revealed that there are $\alpha$, $\beta$-unsaturated ketone structures in the fused bispentacenequinones **126** and **127**, which may explain the unusual Michael additions. So far, synthesis of peritetracene derivatives was not reported and only one potential precursor, i.e., monobromo-tetracene dicarboximide, was reported by our group [95].

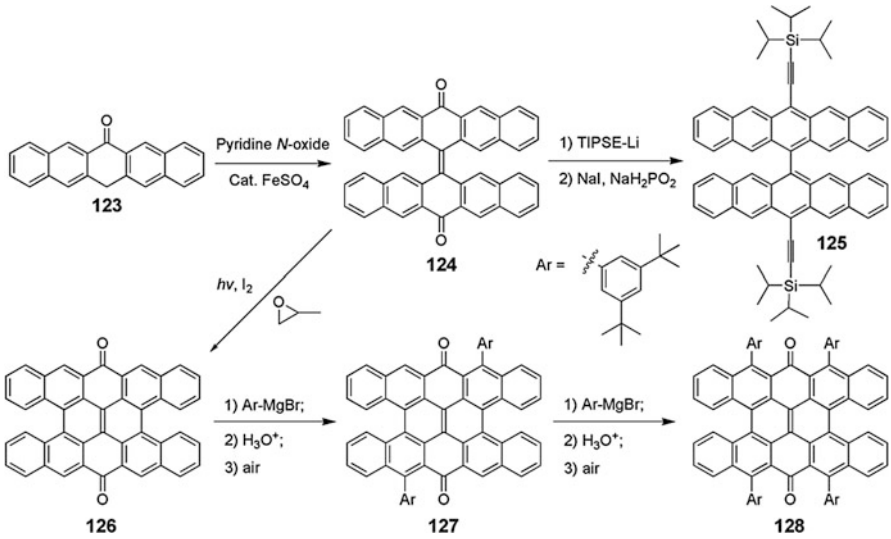


**Scheme 13** Preliminary studies towards peripentacene [93, 94]

## 4 2D Nanographenes with Only Armchair Edges

2D graphene fragments with a fully armchair edge structure generally exhibit high stability and a large band gap, as their chemical structures can be depicted in an all-benzenoid manner with no additional isolated double bond existing. Among this class of PAHs, hexa-*peri*-hexabenzocoronene (HBC) represents the most famous and widely investigated 2D aromatic system. HBC can be viewed as "superbenzene" due to its $D_{6h}$ symmetry and more extended π-conjugation, and in total seven sextet benzenoid rings can be drawn in this structure. The intrinsic properties of HBC can be regarded as a "double-bladed sword" from two aspects: (1) the all-benzoid feature renders a high stability; on the other hand the resulting large band gap is unfavorable in many material applications; (2) the strong intermolecular π–π interaction and self-organization behavior makes HBC attractive in organic electronic devices, but also leads to an extremely low solubility. Therefore, rational design of the HBC derivatives with appropriate molecular size and functional groups is highly desirable. Stimulated by the synthetic breakthroughs achieved by Müllen's group, a boost was achieved in the last decade on synthesizing HBC derivatives and seeking their applications as electronic materials, and similar synthetic approaches are also applied as bottom-up methods to obtain well-defined larger all-benzenoid graphene fragments. In the following section, HBC derivatives and its higher homologue will be summarized and discussed. Since two comprehensive reviews are available on this topic, only a brief overview and selected examples will be given here [96, 97].

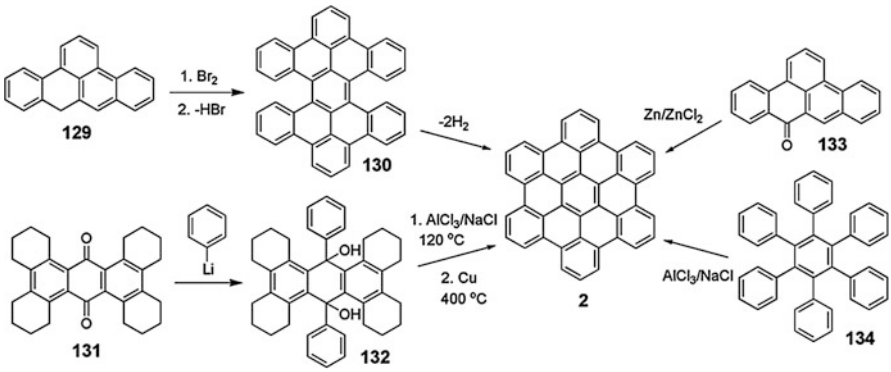


**Scheme 14** Synthesis of HBC in old times [98–100]

## *4.1* *Hexa*-Peri-*Hexabenzocoronene*

The optimization of synthesis for parent HBC has taken a long time, and a number of precursors were developed to construct HBC core in the past (Scheme 14). The first synthesis of parent HBC was reported by Clar in 1958 [98]. The bromination of 2.3,7.8-dibenzoperinaphthene **129** in benzene gave a dark brown precipitate in which three bromine atoms were added. The precipitate was heated at 153 °C and resulted in the formation of tetrabenzoperopyrene **130**. The absorption spectrum of the dilute HBC solution in trichlorobenzene exhibits three typical bands: a low-energy α-band at around 440 nm, a *β*-band at 360 nm, and a *p*-band at 387 nm. Orange-yellow phosphorescence with a very long lifetime in a frozen solid solution of HBC in trichlorobenzene at low temperature was also observed. These properties are typical for PAHs. Two alternative approaches were then reported by Halleux et al., the condensation and the concomitant cyclization of 2.3,7.8-dibenzoperinaphthone **133** with $Zn/ZnCl_2$ as well as oxidative cyclodehydrogenation of hexaphenylbenzene **134** by an $AlCl_3$/NaCl melt which afforded HBC in low yields [99]. A new synthesis of HBC was reported by Schmidt and coworkers in 1986; reaction of quinone **131** with phenyllithium afforded diol **132**, which was cyclized in $AlCl_3$/NaCl melt followed by aromatization with Cu at 400 °C to give HBC in 0.4% yield [100].

Although efforts have been made to obtain HBC from a variety of precursors, the above-mentioned methods all suffered from low overall yield and complicated experimental workup. Later, a milder and more effective approach developed in Müllen's group led to a golden age of HBC synthesis and applications. As shown in Scheme 15, the substituted hexaphenyl benzene **136** was synthesized by $Co_2(CO)_8$-promoted cyclotrimerization of diphenylacetylene **135**, which subsequently underwent oxidative cyclodehydrogenation to give the fused HBC derivatives **137** in high yields. The key step in this reaction sequence is the oxidative cyclodehydrogenation of branched hexaphenylbezene, which can be achieved by Cu(II) salts such as $CuCl_2$ and $Cu(OTf)_2$ combined with $AlCl_3$. Milder Lewis acid $FeCl_3$ has also proved to be effective to promote solely oxidative cyclization of

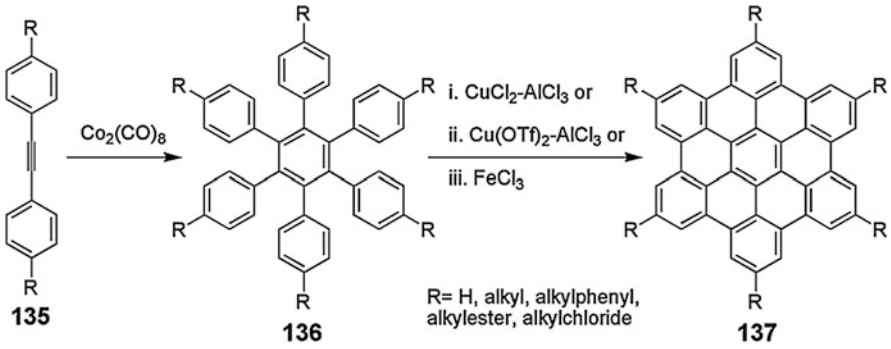


**Scheme 15** Müllen's synthesis of HBC derivatives [101–103]

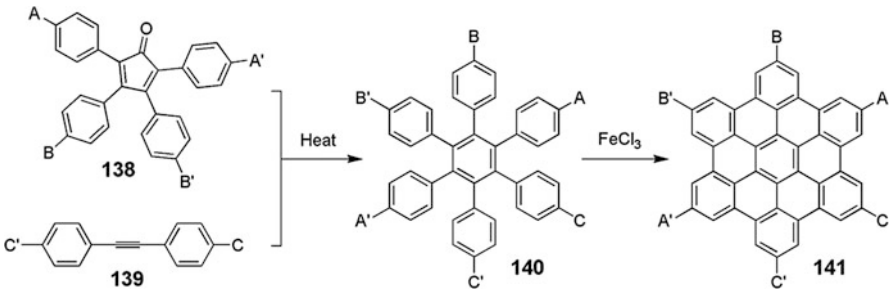


**Scheme 16** Synthesis of HBC derivatives with low symmetry [104, 105]

hexaphenylbezene into HBC because $FeCl_3$ possesses an oxidation potential sufficient for the C–C bond formation [101–103]. The significance of this synthetic sequence lies not only in the large enhancement of the reaction yields, but also allows introduction of various substituents in the periphery, thus realizing increased solubility, processability, and controllable self-assembly.

The HBC derivatives **141** with low symmetry were synthesized by an alternative route, following a synthetic route including Diels-Alder cycloaddition between tetraphenylcyclopentadienone derivatives **138** and diphenylacetylene derivatives **139**, and subsequent oxidative cyclodehydrogenation of low symmetric precursor **140** with $FeCl_3$ (Scheme 16) [104, 105]. Based on this synthetic strategy, HBCs possessing solubilizing chains and one or several bromine atoms with different symmetries were synthesized. The presence of bromine atoms allows further functionalizations by transition metal-catalyzed coupling reactions such as Kumada, Suzuki, Hagihara, Negishi, and Buchwald coupling reactions. The attachment of different functionalities leads to a more exact control of the order of HBC molecules in the bulk state, the alignment of the discs on the surface, and the intramolecular binary energy/electron transport. In addition, both of the above-mentioned synthetic methods are quite versatile and are applicable for a large variety of precursors, which makes the preparation of extended graphene fragments practically possible.


**Scheme 17** Synthesis of non-planar peralkoxylated HBC [106]

Based on a novel synthetic concept, plenty of HBC derivatives with different substituents in the peripheries were synthesized to serve different purposes. Among them, most of the HBC derivatives are deemed planar due to the planarity of the aromatic core. In contrast, an interesting example is the peralkoxylated HBC **144** which adopted nonplanar aromatic backbones due to the steric congestions between the substituents at the bay regions. The synthetic route involved $Co_2(CO)_8$-assisted cyclotrimerization and the subsequent oxidative cyclization of **143** with $FeCl_3$ (Scheme 17). Single-crystal analysis revealed that the outer phenyl rings flip up and down in an alternating manner with respect to the inner core and a significant deviation from planarity with a maximum angle of 16.8°, which resulted in a "double-concave" conformation. This nonplanar HBC represented a good supramolecular host for nonplanar fullerene and electron-deficient perfluorobenzene, which was proven by the analysis of cocrystals of compound **144** and fullerene $C_{60}$, indicating that $C_{60}$ was perfectly included by the complementary double-concave geometry with a 1D columnar structure [106].

Very recently a novel HBC derivative **151** with $C_3$-symmetry was developed (Scheme 18) [107]. In this synthetic sequence, the HBC core **150** was first constructed, where the methylene chloride functional groups in **150** provided the possibility to convert into triphosphate derivative **151**, which allowed the synthesis of the so-called octupolar HBC chromophores with "push-pull" motif by threefold Wittig–Horner reactions between triphosphate derivative and corresponding benzaldehyde derivatives. Notably, these chromophores exhibited large TPA cross-sections up to 16,718 GM (at 760 nm), which are among the best of TPA chromophores. The TPA properties were found to depend on the electron-acceptor strength, the solvent polarity, and the concentration. These chromophores added a new design concept of using large PAHs as potential TPA chromophores in the future.

As mentioned above, the HBC derivatives substituted with alkyl chains can form self-assembled 1D columnar structures due to strong π–π interactions between the rigid aromatic core and the nanoscale phase separation between the rigid core and the flexible alkyl chains at the periphery, which facilitates the overlap of π-orbitals between neighboring planes and maximizes the charge transport ability along the 1D columns. Therefore the control of supramolecular order of HBC derivatives

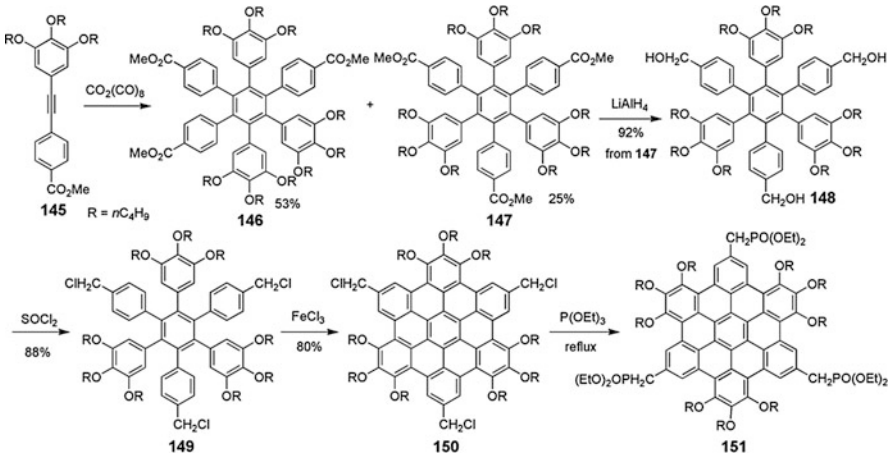


**Scheme 18** Synthesis of threefold HBC derivative **151** [107]

over macroscopic dimensions is essential to obtain optimized performance in device applications. Furthermore, alkyl chain substituted nanosized graphenes are able to self-heal structural defects due to their liquid crystalline (LC) character, and can be processed from solution because of their high solubility. Inspired by these merits, a great number of HBC derivatives have been developed with different sizes, symmetries, and substitutions. Three major methods have been utilized to tune their LC phase. The first is a well-developed way in which the length and branching of the alkyl chains are adjusted. The long and branched chains tend to decrease the phase transition temperature. The isotropic temperatures are higher than 450 °C for the *n*-alkyl substituted HBCs **152a** [108] while the dove-tailed chains substituted HBC **152b** shows an isotropic temperature below 46 °C [109] (Fig. 29). The second method is to tune the molecular size. A wide-range columnar liquid crystalline phase from room temperature up to >400 °C was observed in the dodecylphenyl substituted HBC **152c** [110] whereas further increasing the size of the aromatic core results in broader columnar liquid crystalline phases which cannot become isotropic melt below 600 °C. The third method is to introduce functional groups or additional non-covalent interactions at the side chains. For instance, additional hydrogen bonding units were introduced in **154**, which significantly enhanced the self-assembling abilities of the HBC and thus endowed it with excellent gelation ability [111]. Also interesting is compound **153**, in which the local dipoles are presented [112]. As a result, the solution processing onto a substrate resulted in the formation of exceptionally long fibrous microstructures. The rational control of the LC phase is beneficial to enhance the charge transporting properties of materials, qualifying them as promising organic materials for organic electronic devices such as FETs and solar cells.

It is well known that disc-like PAHs, such as HBCs, are able to self-assemble into one-dimensional columnar structures; the random orientation of assembles, however,

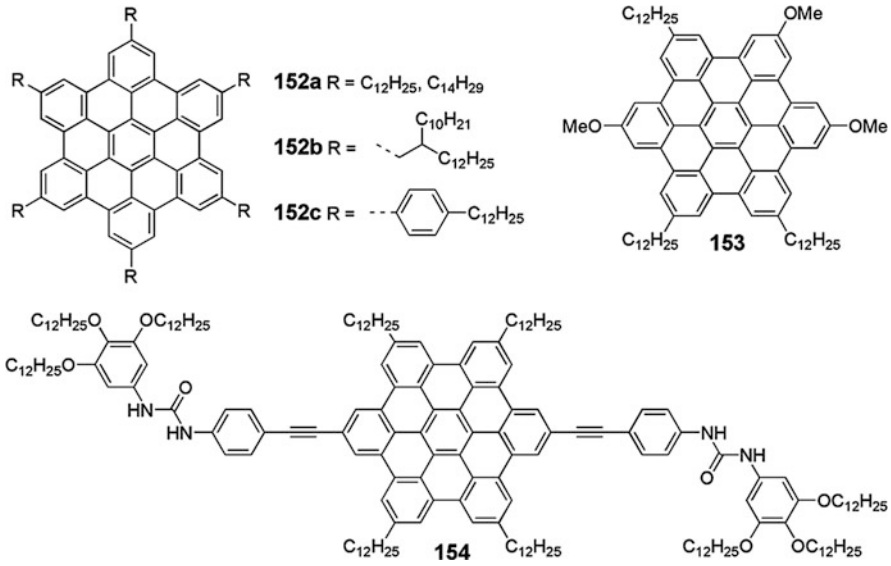


**Fig. 29** HBC derivatives with controlled liquid crystalline mesophases and self-assembly [108–112]

inevitably causes low device performance. There are two types of alignment of columnar discs on substrates: homogeneous edge-on (column axis parallel to a substrate) and homeotropic face-on (column axis perpendicular to a substrate). Generally, for FETs an edge-on organization is required to allow charge carriers to drift along the column axis direction from the source electrode to the drain electrode under controlled gate voltage. However, for photovoltaic devices the face-on arrangement of the discs is preferred that allows faster charge transport between the top and bottom electrodes and favors the photovoltaic performance. Furthermore, the donor columns are accompanied by homeotropically aligned acceptor columns in photovoltaic devices. Techniques including zone-casting, solution-casting on preoriented and friction-deposited poly(tetrafluoroethylene) (PTFE) surfaces, and Langmuir and Langmuir-Blodgett (LB) techniques are developed to induce uniform order in the alignment of the discs and improve device performance.

Many examples are available of using HBC derivatives in organic electronics, and one representative example is Schmidt-Mende's report, in which HBC **155** was used as the donor while perylene diimide was used as the acceptor to build a bulk heterojunction (BHJ) device that leads to an external quantum efficiency of 34% at 490 nm and a power efficiency up to 2%. This remarkable device performance for discotic small molecules is due to efficient photo-induced charge transfer between the HBC and PDI, as well as effective transport of charges through vertically segregated perylene and HBC aromatic systems [113]. Another example is the introduction of 9,9-dioctylfluorenyl moiety at the periphery of HBC as replacement of alkyl chains, which always show negative effects on charge transport in the bulk

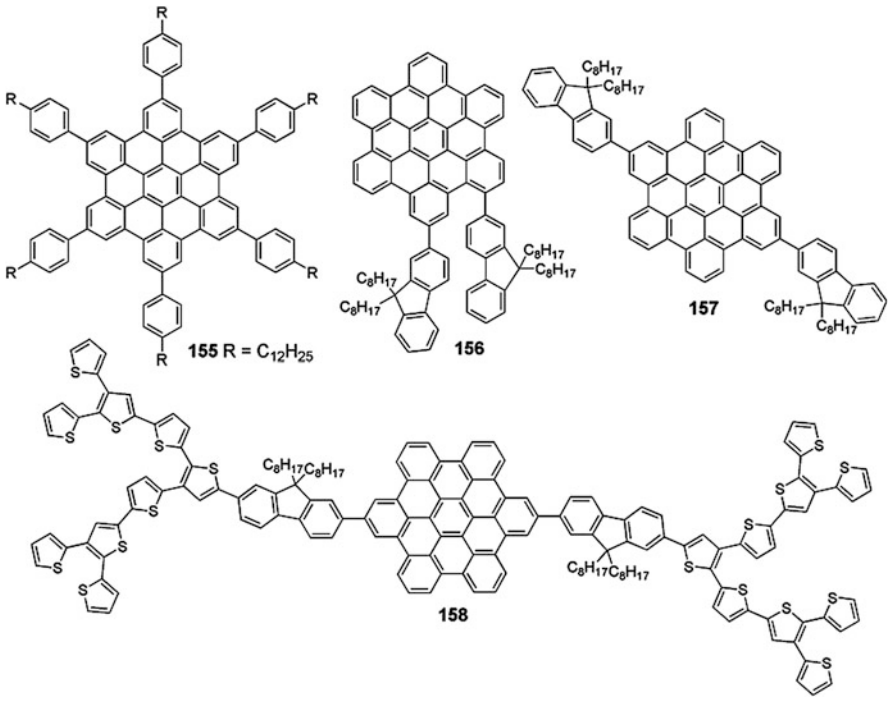


**Fig. 30** HBC derivatives used in organic electronics [113–116]

material by creating an insulating domain around the π–π stacked columnar core. Compounds **156** and **157** exhibited pronounced self-assembly properties and good device results. For instance, a field-effect mobility of $2.8 \times 10^{-3}$ $cm^2$ $V^{-1}$ $s^{-1}$ and a power conversion efficiency of 1.5% were achieved for **157**, which are fairly impressive for HBC-based materials [114, 115]. In subsequent studies, a series of thiophene dendrons were introduced to extend the effective conjugation to produce a thiophene-fluorene co-oligomer substituted HBC **158**, which showed a broader absorption between 250 and 550 nm. The corresponding BHJ devices showed good performance with power conversion efficiency of 2.5%. This is attributed to the enhanced light harvesting property as well as the formation of ordered morphology in solid state induced by the self-assembly of the HBC molecules [116] (Fig. 30).

## *4.2 All-Benzenoid PAHs Larger than HBC*

Taking advantage of $FeCl_3$ or $Cu(OTf)_2$-$AlCl_3$ mediated oxidative cyclodehydrogenation reactions, larger all-benzenoid PAHs with variable shapes and sizes are accessible. Increasing the size of the highly planar HBC core is predicted to improve the π–π intermolecular interaction due to the large overlap of the π-surface

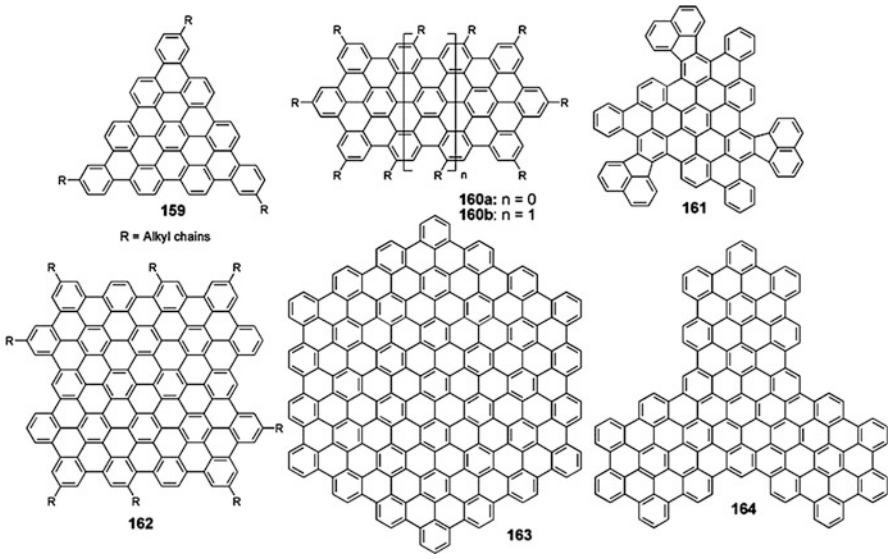


**Fig. 31** Extended HBCs with different shapes and sizes [117–121]

which is beneficial to enhance its charge carrier mobility in terms of FET applications. A general design concept involves preparation of appropriate branched oligophenylenes by Diels-Alder reaction or cyclotrimerization, followed by oxidative cyclodehydrogenation to fuse the phenyl rings for planarization. The possibility of structures and the extension of conjugations seem infinite, but, inevitably, there are restrictions and limitations. For example, incomplete cyclization happens when the size of oligophenylene precursors reaches a certain point, and the ineluctable low solubility arising from extension of π-conjugation not only precludes the reliable structural characterization in the solution but also makes the applications for those systems unrealistic.

Despite all these obstacles, the pursuit of larger graphene fragments never stops and a large number of extended all-benzenoid PAHs of different sizes, shape, and symmetries were obtained from bottom-up synthetic methods and some of the representative examples are listed in Fig. 31. A triangle-shaped PAH **159** was synthesized in 2008 by using $FeCl_3$ mediated cyclodehydrogenation reactions [117], and the introduction of the swallow tailed substituents to the $D_{3h}$ symmetric core facilitated purification and control of the thermotropic properties and fabrication of efficient photovoltaic devices. Systematically increasing the molecular size of HBC by fusion of three aromatic sextet rings in one direction produces a homologue series **160a**, **b** containing 60 and 78 carbon atoms. The synthesis of these systems adopted a similar Diels-Alder reaction and cyclodehydrogenation reaction sequence via a multistep procedure, and the alkyl-substituted derivatives were soluble in organic solvents [118, 119]. The C90 disc **161** containing five-membered rings, together with the C150 disc **164**, which is the largest molecule

with threefold symmetry, were reported in 2004 [120]. Due to the existence of five-membered rings, **161** was nonplanar and therefore offered the possibility of subsequently making bowl-shaped molecules by flash vacuum pyrolysis. Both compounds were characterized by MALDI-TOF spectroscopy, solid-state UV–vis absorption, and Raman spectroscopy. The rectangular PAH **162** was synthesized and for this $D_{2h}$ symmetric compound, long flexible phytyl chains were required to guarantee sufficient solubility in normal organic solvents for various characterizations. Giant molecule **163** with 222 carbon atoms is by far the largest PAH structure characterized to date, and the UV/vis spectrum of insoluble molecule **163** recorded as thin film shows absorption covering the complete visible range of the electronic spectrum, with the absorption maximum at 765 nm. The broad and unstructured pattern of the band can be explained by the large number of electronic transitions taking place in this giant PAH **163** and strong aggregation in solids, thus leading to the continuum-like appearance in the visible range [121].

One-dimensional graphitic ribbons **168** were synthesized under oxidative cyclodehydrogenation conditions from the soluble branched polyphenylene precursor **167** as shown in Scheme 19 [122]. Although the insolubility of **168** prevented standard spectroscopic structure elucidation, the electronic properties were investigated by solid-state UV–vis, Raman, and infrared spectroscopy. A wide and featureless absorption band covering the visible range of the spectrum with an absorption maximum of approximately 800 nm was observed, indicating the highly extended conjugated framework. **168** represented the first example of a two-dimensional highly conjugated all-benzenoid graphene ribbon.

As mentioned above, HBC can be viewed as "superbenzene" as it possesses the same shape and symmetry as benzene but enlarged conjugation. In this regard, a series of "superbenzene" analogues, including "superphenylene", "supernaphthalene", "superphenalene", and "supertriphenylene", were prepared (Fig. 32). A series of oligomers up to the trimer of HBC **169** were prepared by either Yamamoto coupling or oxidative cyclodehydrogenation from corresponding branched oligophenylenes [123]. The UV–vis and fluorescence spectra of dimer and trimer are very similar to individual HBC units, which is understandable considering the large torsion angle between HBC units and small atomic orbital coefficients of the bridgehead carbons. The synthesis of "supernaphthalene" **170a** was firstly reported in 1998 utilizing the $AlCl_3/CuCl_2$ system as cyclodehydrogenation condition [124]. However, partially fused species and chlorinated adducts arising from this method inevitably led to poor reproducibility. Later, a derivative **170b** carrying two *tert*-butyl groups was prepared in a novel approach, in which the *tert*-butyl groups induced a significant deviation from planarity of the aromatic backbone [125]. Together with the solubilizing effects of alkyl chains, **170b** exhibited high solubility and effective suppression of aggregation which allowed the first recording of structure-rich UV–vis and a resolved $^1$H NMR spectrum for aromatic systems twice as large as HBC. Upon removal of *tert*-butyl groups, the solubility decreased dramatically, accompanied with a loss of well-resolved band structure and a bathochromic shift of the absorption spectrum due to the recovery of planarity. PAHs with threefold symmetry, such as "superphenalene" **171** and "supertriphenylene" **172**, were also achieved [126, 127].

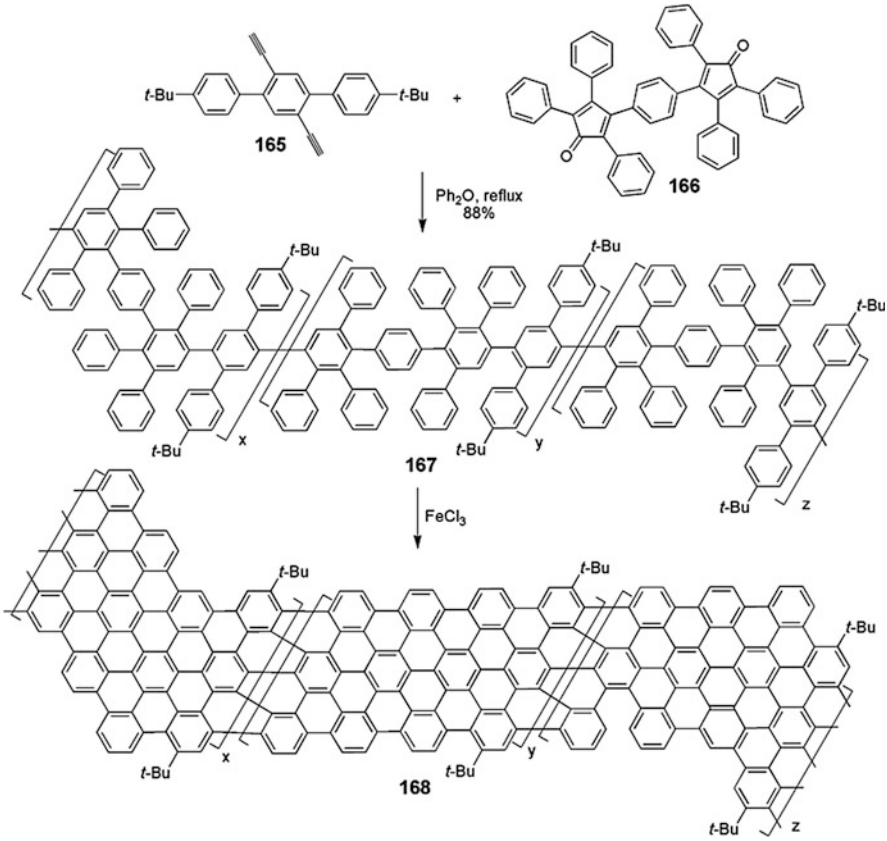


**Scheme 19** Synthesis of polymeric graphite ribbon [122]

## 5 Conclusion and Outlook

So far, three types of 2D nanographenes with different edge structures have been described. The physical properties of these systems, such as optical properties, electronic properties, solid state packing motif, and stability are largely dependent on the types of edge structures (zigzag or armchair) and are tunable upon appropriate chemical modification (e.g., introduction of proper substituents). From the course of development of these 2D aromatic systems, one clue is quite clear: the rational design of synthesis and the isolation of the stable form in solution and crystalline phase are the preconditions for establishing a proper structural-property relationship, and an understanding of the latter is the basis of eventual applications.

For open-shell systems with all zigzag peripheries, the synthetic method and stabilization are long-standing issues but recently a large breakthrough is achieved. Due to the inherent instability, seeking of efficient synthetic approaches and stabilization forces are still the mainstream in this area. Nevertheless, it is exciting

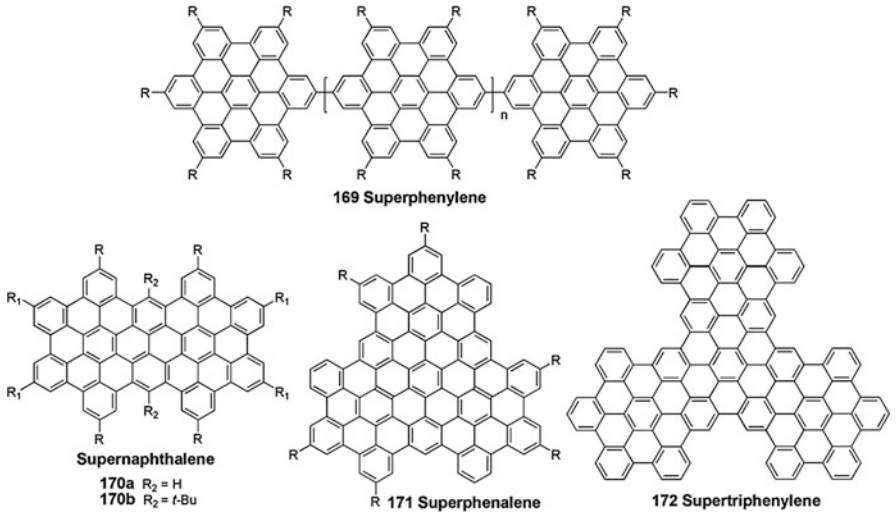


**Fig. 32** Extended structures based on "superbenzene" [123–127]

to note applications such as spintronics, TPA, and ambipolar FET have already emerged. These applications, although still in their infancy, are far beyond what was imagined half a century ago and point to a bright future for these systems as materials.

2D nanographenes with both zigzag and armchair edges still represent the most intensively studied and widely used materials as they are beneficial from the coexistence of both edge structures which leads to a combination of enhanced stability and favorable electronic properties. Moreover, the readily available synthetic methods for certain systems, such as rylenes, make the access of a series of homologues possible and guarantee the systematic establishment of structural-property relationships. In addition, recent studies on extended networks with singlet biradical characters provide new insight from both fundamental study and application aspects.

All benzenoid PAHs enjoyed a golden age in the past 20 years due to their exceptional stability, intriguing self-assembly behavior, and applications as electronic materials. Enthusiastic efforts are also being made to achieve larger graphene fragments from a bottom-up approach. However, the device performances obtained so far for these materials are in general not yet comparable to the other oligomer and polymer-based organic semiconductors. Better device performance may be the target for the future, which requires synergistic cooperation between chemists, physicists, and engineers.

**Acknowledgement** We acknowledge the financial support from A*Star BMRC grant (No. 10/1/21/19/642), MOE AcRF Tier 2 Grant (MOE2011-T2-2-130) and IMRE Core Funding (IMRE/10-1P0509).

## References


1. Morita Y, Nishida S (2010) Phenalenyls, cyclopentadienyls, and other carbon-centered radicals. In: Hicks RG (ed) Stable radicals: fundamentals and applied aspects of odd-electron compounds. Wiley, Chichester
2. Clar E (1972) The aromatic sextet. Wiley-VCH, London
3. Lambert C (2011) Towards polycyclic aromatic hydrocarbons with a singlet open-shell ground state. Angew Chem Int Ed 50:1756–1758
4. Morita Y, Suzuki S, Sato K, Takui T (2011) Synthetic organic spin chemistry for structurally well-defined open-shell graphene fragments. Nat Chem 3:197–204
5. Reid DH (1958) Stable π-electron systems and new aromatic structures. Tetrahedron 3:339–352
6. Nakasuji K, Yamaguchi M, Murata I, Yamaguchi K, Fueno T, Ohya-Nishiguchi H, Sugano T, Kinoshita M (1989) Synthesis and characterization of phenalenyl cations, radicals, and anions having donor and acceptor substituents: three redox states of modified odd alternant systems. J Am Chem Soc 111:9265–9267
7. Goto K, Kubo T, Yamamoto K, Nakasuji K, Sato K, Shiomi D, Takui T, Kubota M, Kobayashi T, Yakusi K, Ouyang J (1999) A stable neutral hydrocarbon radical: synthesis, crystal structure, and physical properties of 2,5,8-tri-*tert*-butyl-phenalenyl. J Am Chem Soc 121:1619–1620
8. Lü JM, Rosokha SV, Kochi JK (2003) Stable (long-bonded) dimers via the quantitative self-association of different cationic, anionic, and uncharged π-radicals: structures, energetics, and optical transitions. J Am Chem Soc 125:12161–12171
9. Small D, Zaitsev V, Jung Y, Rosokha SV, Head-Gordon M, Kochi JK (2004) Intermolecular π-to-π bonding between stacked aromatic dyads. Experimental and theoretical binding energies and near-IR optical transitions for phenalenyl radical/radical versus radical/cation dimerizations. J Am Chem Soc 126:13850–13858
10. Zaitsev V, Rosokha SV, Head-Gordon M, Kochi JK (2006) Steric modulations in the reversible dimerizations of phenalenyl radicals via unusually weak carbon-centered π- and σ-bonds. J Org Chem 71:520–526
11. Suzuki S, Morita Y, Fukui K, Sato K, Shiomi D, Takui T, Nakasuji K (2006) Aromaticity on the pancake-bonded dimer of neutral phenalenyl radical as studied by MS and NMR spectroscopies and NICS analysis. J Am Chem Soc 128:2530–2531
12. Haddon RC, Hirani AM, Kroloff NJ, Marshall JH (1983) 1,3,4,9-Tetramethoxyphenalenyl system. J Org Chem 48:2115–2117
13. Pagni RM, Pagni RM (1989) Substituent effects on the stability of carbodications. Tetrahedron Lett 30:2727–2730
14. Pagni RM, Pagni RM, Haddon RC, Chichester SV (1990) The role of substituents on carbodication stability. J Org Chem 55:5595–5601
15. Kaplan ML, Haddon RC, Hirani AM, Schilling FC, Marshall JH (1981) Phenaleno[1,9-*cd*][1,2,6]thiadiazinium cation. J Org Chem 46:675–678
16. Haddon RC, Chichester SV, Stein SM, Marshall JH, Mujsce AM (1987) Perchloro-*7H*-cycloprop[*a*]acenaphthylene and the perchlorophenalenyl system. J Org Chem 52:711–712
17. Koutentis PA, Chen Y, Cao Y, Best TP, Itkis ME, Beer L, Oakley RT, Cordes AW, Brock CP, Haddon RC (2001) Perchlorophenalenyl radical. J Am Chem Soc 123:3864–3871
18. Haddon RC, Wudl F, Kaplan ML, Marshall JH, Cais RE, Bramwell FB (1978) 1,9-Dithiophenalenyl system. J Am Chem Soc 100:7629–7633
19. Beer L, Mandal SK, Reed RW, Oakley RT, Tham FS, Donnadieu B, Haddon RC (2007) The first electronically stabilized phenalenyl radical: effect of substituents on solution chemistry and solid-state structure. Cryst Growth Des 7:802–809
20. Beer L, Reed RW, Robertson CM, Oakley RT, Tham FS, Haddon RC (2008) Tetrathiophenalenyl radical and its disulfide-bridged dimer. Org Lett 10:3121–3123

21. Morita Y, Aoki T, Fukui K, Nakazawa S, Tamaki K, Suzuki S, Fuyuhiro A, Yamamoto K, Sato K, Shiomi D, Naito A, Takui T, Nakasuji K (2002) A new trend in phenalenyl chemistry: a persistent neutral radical, 2,5,8-tri-*tert*-butyl-1,3-diazaphenalenyl, and the excited triplet state of the gable syn-dimer in the crystal of column motif. Angew Chem Int Ed 41:1973–1976
22. Morita Y, Suzuki S, Fukui K, Nakazawa S, Kishida H, Okamoto H, Naito A, Sekine A, Ohashi Y, Shiro M, Sasaki K, Shiomi D, Sato K, Takui T, Nakasuji K (2008) Thermochromism in an organic crystal based on the coexistence of σ- and π-dimers. Nat Mater 7:48–51
23. Suzuki S, Morita Y, Fukui K, Sato K, Shiomi D, Takui T, Nakasuji K (2005) Hexaazaphenalenyl anion revisited: a highly symmetric planar π system with multiple-networking ability for self-assembled metal complexation. Inorg Chem 44:8197–8199
24. Zheng S, Lan J, Khan SI, Rubin Y (2003) Synthesis, characterization, and coordination chemistry of the 2-azaphenalenyl radical. J Am Chem Soc 125:5786–5791
25. Zheng S, Thompson JD, Tontcheva A, Khan SI, Rubin Y (2005) Perchloro-2,5,8-triazaphenalenyl radical. Org Lett 7:1861–1863
26. Morita Y, Nishida S, Kawai J, Takui T, Nakasuji K (2008) Oxophenalenoxyl: novel stable neutral radicals with a unique spin-delocalized nature depending on topological symmetries and redox states. Pure Appl Chem 80:507–517
27. Hatanaka K, Morita Y, Ohba T, Yamaguchi K, Takui T, Kinoshita M, Nakasuji K (1996) Detection of new neutral radicals: 2-phenyl- and 2-p-methoxyphenyl-3-oxophenalenoxyl radicals. Tetrahedron Lett 37:873–876
28. Morita Y, Nishida S, Kawai J, Fukui K, Nakazawa S, Sato K, Shiomi D, Takui T, Nakasuji K (2003) Redox-based spin diversity: a reversible topological spin switching in oxophenalenoxyl systems. Polyhedron 22:2209–2213
29. Morita Y, Nishida S, Fukui K, Hatanaka K, Ohba T, Sato K, Shiomi D, Takui T, Yamamoto G, Nakasuji K (2005) 2-Aryl substituted 3-oxophenalenoxyl radicals: π-spin structures and properties evaluated by dimer structure. Polyhedron 24:2194–2199
30. Nishida S, Morita Y, Ohba T, Fukui K, Sato K, Takui T, Nakasuji K (2007) Control in spin-delocalization into the 2-substituted π-systems in 3-oxophenalenoxyl neutral radicals: evaluation by their dimeric structures and DFT calculations. Tetrahedron 63:7690–7695
31. Morita Y, Kawai J, Fukui K, Nakazawa S, Sato K, Shiomi D, Takui T, Nakasuji K (2003) Topological symmetry control in spin density distribution: spin chemistry of phenalenyl-based neutral monoradical systems. Org Lett 5:3289–3291
32. Morita Y, Ohba T, Haneda N, Maki S, Kawai J, Hatanaka K, Sato K, Shiomi D, Takui T, Nakasuji K (2000) New persistent radicals: synthesis and electronic spin structure of 2,5-di-*tert*-butyl-6-oxophenalenoxyl derivatives. J Am Chem Soc 122:4825–4826
33. Morita Y, Maki S, Fukui K, Ohba T, Kawai J, Sato K, Shiomi D, Takui T, Nakasuji K (2001) New stable neutral radical with intramolecular hydrogen bonding: synthesis and characterization of 2,5,8-tri-*tert*-butyl-7-hydroxy-6-oxophenalenoxyl. Org Lett 3:3099–3102
34. Morita Y, Suzuki S, Kawai J, Nishida S, Fukui K, Nakazawa S, Sato K, Shiomi D, Takui T, Nakasuji K (2003) Generation and properties of 2,5,8-tri-tert-butyl-6-oxo-7,9-diazaphenalenoxyl. Synth Met 137:1209–1210
35. Nishida S, Morita Y, Fukui K, Sato K, Shiomi D, Takui T, Nakasuji K (2005) Spin transfer and solvato-/thermochromism induced by intramolecular electron transfer in a purely organic open-shell system. Angew Chem Int Ed 44:7277–7280
36. Nakasuji K, Kubo T (2004) Multi-stage amphoteric redox hydrocarbons based on a phenalenyl radical. Bull Chem Soc Jpn 77:1791–1801
37. Kubo T, Shimizu A, Sakamoto M, Uruichi M, Yakushi K, Nakano M, Shiomi D, Sato K, Takui T, Morita Y, Nakasuji K (2005) Synthesis, intermolecular interaction, and semiconductive behavior of a delocalized singlet biradical hydrocarbon. Angew Chem Int Ed 44:6564–6568

38. Shimizu A, Uruichi M, Yakushi K, Matsuzaki H, Okamoto H, Nakano M, Hirao Y, Matsumoto K, Kurata H, Kubo T (2009) Resonance balance shift in stacks of delocalized singlet biradicals. Angew Chem Int Ed 48:5482–5486
39. Nakasuji K, Yoshida K, Murata I (1983) Design and synthesis of a highly amphoteric condensed hydrocarbon with the highest reduction potential: pentaleno[l,2,3-*cd*:4,5,6-*c'd'*] diphenalene. J Am Chem Soc 105:5136–5137
40. Murata I, Sasaki S, Klabunde KU, Toyoda J, Nakasuji K (1991) Synthesis of a highly amphoteric s-indaceno[1,2,3-*cd*:5,6,7-*c'd'*]diphenalene: switching between diatropism and paratropism due to changes in oxidation level. Angew Chem Int Ed Engl 30:172–173
41. Ohashi K, Kubo T, Masui T, Yamamoto K, Nakasuji K, Takui T, Kai Y, Murata I (1998) 4,8,12,16-Tetra-*tert*-butyl-*s*-indaceno[1,2,3-*cd*:5,6,7-*c'd'*]diphenalene: a four-stage amphoteric redox system. J Am Chem Soc 120:2018–2027
42. Huang J, Kertesz M (2007) Intermolecular covalent $\pi$–$\pi$ bonding interaction indicated by bond distances, energy bands, and magnetism in biphenalenyl biradicaloid molecular crystal. J Am Chem Soc 129:1634–1643
43. Kubo T, Shimizu A, Uruichi M, Yakushi K, Nakano M, Shiomi D, Sato K, Takui T, Morita Y, Nakasuji K (2007) Singlet biradical character of phenalenyl-based Kekulé hydrocarbon with naphthoquinoid structure. Org Lett 9:81–84
44. Shimizu A, Kubo T, Uruichi M, Yakushi K, Nakano M, Shiomi D, Sato K, Takui T, Hirao Y, Matsumoto K, Kurata H, Morita Y, Nakasuji K (2010) Alternating covalent bonding interactions in a one-dimensional chain of a phenalenyl-based singlet biradical molecule having Kekulé structures. J Am Chem Soc 132:14421–14428
45. Kamada K, Ohta K, Kubo T, Shimizu A, Morita Y, Nakasuji K, Kishi R, Ohta S, Furukawa S, Takahashi H, Nakano M (2007) Strong two-photon absorption of singlet diradical hydrocarbons. Angew Chem Int Ed 46:3544–3546
46. Chikamatsu M, Mikami T, Chisaka J, Yoshida Y, Azumi R, Yase K (2007) Ambipolar organic field-effect transistors based on a low band gap semiconductor with balanced hole and electron mobilities. Appl Phys Lett 91:043506
47. Kubo T, Sakamoto M, Akabane M, Fujiwara Y, Yamamoto K, Akita M, Inoue K, Takui T, Nakasuji K (2004) Four-stage amphoteric redox properties and biradicaloid character of tetra-tertbutyldicyclopenta[*b;d*]thieno[1,2,3-*cd*;5,6,7-*c'd'*]diphenalene. Angew Chem Int Ed 43:6474–6479
48. Kubo T, Yamamoto K, Nakasuji K, Takui T (2001) Tetra-*tert*-butyl-*as*-indaceno[1,2,3-*cd*:6,7,8-*c'd'*]diphenalene: a four-stage amphoteric redox system. Tetrahedron Lett 42:7997–8001
49. Kubo T, Sakamoto M, Nakasuji K (2005) Biradicaloid character of phenalenyl-based aromatic compounds with a small HOMO–LUMO gap. Polyhedron 24:2522–2527
50. Kubo T, Katada Y, Shimizu A, Hirao Y, Sato K, Takui T, Uruichi M, Yakushi K, Haddon RC (2011) Synthesis, crystal structure, and physical properties of sterically unprotected hydrocarbon radicals. J Am Chem Soc 133:14240–14243
51. Umeda R, Hibi D, Miki K, Tobe Y (2009) Tetradehydrodinaphtho[10]annulene: a hitherto unknown dehydroannulene and a viable precursor to stable zethrene derivatives. Org Lett 11:4104–4106
52. Wu TC, Chen CH, Hibi D, Shimizu A, Tobe Y, Wu YT (2010) Synthesis, structure, and photophysical properties of dibenzo-[de, mn]naphthacenes. Angew Chem Int Ed 49:7059–7062
53. Sun Z, Huang KW, Wu J (2010) Soluble and stable zethrenebis(dicarboximide) and its quinone. Org Lett 12:4690–4693
54. Sun Z, Huang KW, Wu J (2011) Soluble and stable heptazethrenebis(dicarboximide) with a singlet open-shell ground state. J Am Chem Soc 133:11896–11899
55. Kubo T, Yamamoto K, Nakasuji K, Takui T, Murata I (1996) Hexa-*tert*-butyltribenzodecacyclenyl: a six-stage amphoteric redox system. Angew Chem Int Ed Engl 35:439–441

56. Kubo T, Yamamoto K, Nakasuji K, Takui T, Murata I (2001) 4,7,11,14,18,21-Hexa-*t*-butyltribenzodecacyclenyl radical: a six-stage amphoteric redox system. Bull Chem Soc Jpn 74:1999–2009
57. Borden WT, Davidson ER (1977) Effects of electron repulsion in conjugated hydrocarbon diradicals. J Am Chem Soc 99:4587–4594
58. Fukui K, Inoue J, Kubo T, Nakazawa S, Aoki T, Morita Y, Yamamoto K, Sato K, Shiomi D, Nakasuji K, Takui T (2001) The first non-Kekulé polynuclear aromatic high-spin hydrocarbon: generation of a triangulene derivative and band structure calculation of triangulene-based high-spin hydrocarbons. Synth Met 121:1824–1825
59. Clar E, Stewart DG (1953) Aromatic hydrocarbons. LXV. Triangulene derivatives. J Am Chem Soc 75:2667–2672
60. Hara O, Tanaka K, Yamamoto K, Nakazaw T, Murata Y (1977) The chemistry of phenalenium systems: XXV the triangulenyl dianion. Tetrahedron Lett 18:2435–2436
61. Inoue J, Fukui K, Kubo T, Nakazawa S, Sato K, Shiomi D, Morita Y, Yamamoto K, Takui T, Nakasuji K (2001) The first detection of a Clar's hydrocarbon, 2,6,10-tri-*tert*-butyltriangulene: a ground-state triplet of non-Kekulé polynuclear benzenoid hydrocarbon. J Am Chem Soc 123:12702–12703
62. Allinson G, Bushby RG, Paillaud JL (1993) ESR spectrum of a stable triplet π biradical: trioxy triangulene. J Am Chem Soc 115:2062–2064
63. Allinson G, Bushby RG, Paillaud JL, Thornton-Pett M (1995) Synthesis of a derivative of triangulene; the first non-Kekulé polynuclear aromatic. J Chem Soc Perkin Trans 385–390
64. Allinson G, Bushby RG, Jesudason MV, Thornton-Pett M, Taylor M (1997) The synthesis of singlet ground state derivatives of non-Kekulé polynuclear aromatics. J Chem Soc Perkin Trans 2 147–156
65. Morita Y, Nishida S, Murata T, Moriguchi M, Ueda A, Satoh M, Arifuku K, Sato K, Takui T (2011) Organic tailored batteries materials using stable open-shell molecules with degenerate frontier orbitals. Nat Mater 10:947–951
66. Bohnen A, Koch KH, Lüttke W, Müllen K (1990) Oligorylene as a model for "poly (perinaphthalene)". Angew Chem Int Ed Engl 29:525–527
67. Koch KH, Müllen K (1991) Synthesis of tetraalkyl-substituted oligo(l,4-naphthylene)s and cyclization to soluble oligo(*peri*-naphthylene)s. Chem Ber 124:2091–2100
68. Weil T, Vosch T, Hofkens J, Peneva K, Müllen K (2010) The rylene colorant family—tailored nanoemitters for photonics research and applications. Angew Chem Int Ed 49:9068–9093
69. Quante S, Müllen K (1995) Quaterrylenebis(dicarboximides). Angew Chem Int Ed Engl 34:1323–1325
70. Langhals H, Schönmann G, Feiler L (1995) A two-step synthesis of quaterrylenetetracarboxylic bisimides-novel NIR fluorescent dyes. Tetrahedron Lett 36:6423–6424
71. Pschirer NG, Kohl C, Nolde F, Qu J, Müllen K (2006) Pentarylene- and hexarylenebis (dicarboximide)s: near-infrared-absorbing polyaromatic dyes. Angew Chem Int Ed 45:1401–1404
72. Li Y, Wang Z (2009) Bis-N-annulated quaterrylene: an approach to processable graphene nanoribbons. Org Lett 11:1385–1387
73. Li Y, Gao J, Motta SI, Negri F, Wang Z (2010) Tri-N-annulated hexarylene: an approach to well-defined graphene nanoribbons with large dipoles. J Am Chem Soc 132:4208–4213
74. Jiao C, Huang K, Zhang K, Luo J, Chi C, Wu J (2009) Bis-*N*-annulated quaterrylenebis (dicarboximide) as a new soluble and stable near-infrared dye. Org Lett 11:4508–4511
75. Peneva K, Mihov G, Nolde F, Rocha S, Hotta J, Braeckmans K, Hofkens J, Uji-I H, Herrmann A, Müllen K (2008) Water-soluble monofunctional perylene and terrylene dyes: powerful labels for single-enzyme tracking. Angew Chem Int Ed 47:3372–3375
76. Edvinsson T, Pschirer N, Schöneboom J, Eickemeyer F, Boschloo G, Hagfeldt A (2009) Photoinduced electron transfer from a terrylene dye to $TiO_2$: quantification of band edge shift effects. Chem Phys 357:124–131

77. Petit M, Hayakawa R, Shirai Y, Wakayama Y, Hill JP, Ariga K, Chikyow T (2008) Growth and electrical properties of N, N′-bis(n-pentyl)terrylene-3,4:11,12-tetracarboximide thin films. Appl Phys Lett 92:163301
78. Oh JK, Lee WY, Noe T, Chen WC, Könemann M, Bao Z (2011) Solution-shear-processed quaterrylene diimide thin-film transistors prepared by pressure-assisted thermal cleavage of swallow tails. J Am Chem Soc 133:4204–4207
79. Qian H, Wang Z, Yue W, Zhu D (2007) Exceptional coupling of tetrachloroperylene bisimide: combination of Ullmann reaction and C-H transformation. J Am Chem Soc 129:10664–10665
80. Qian H, Negri F, Wang C, Wang Z (2008) Fully conjugated tri(perylene bisimides): an approach to the construction of *n*-type graphene nanoribbons. J Am Chem Soc 130:17970–17976
81. Zhen Y, Wang C, Wang Z (2010) Tetrachloro-tetra(perylene bisimides): an approach towards N-type graphene nanoribbons. Chem Commun 46:1926–1928
82. Yao J, Chi C, Wu J, Loh KP (2009) Bisanthracene bis(dicarboxylic imide)s as soluble and stable NIR dyes. Chem Eur J 15:9299–9302
83. Li J, Zhang K, Zhang X, Chi C, Wu J (2010) meso-Substituted bisanthenes as soluble and stable near-infrared dyes. J Org Chem 75:856–863
84. Zhang K, Huang K, Li J, Chi C, Wu J (2009) A soluble and stable quinoidal bisanthene with NIR absorption and amphoteric redox behavior. Org Lett 11:4854–4857
85. Clar E (1949) Synthesen von benzologen des perylens und bisanthens. Chem Ber 82:46–60
86. Saïdi-Besbes S, Grelet É, Bock H (2006) Soluble and liquid-crystalline ovalenes. Angew Chem Int Ed 45:1783–1786
87. Fort EH, Scott LT (2010) One-step conversion of aromatic hydrocarbon bay regions into unsubstituted benzene rings: a reagent for the low-temperature, metal-free growth of single-chirality carbon nanotubes. Angew Chem Int Ed 49:6626–6628
88. Li J, Chang JJ, Tan HS, Jiang H, Chen X, Chen Z, Zhang J, Wu J (2012) Disc-like 7, 14-dicyano-ovalene-3,4:10,11-bis(dicarboximide) as a solution-processible *n*-type semiconductor for air stable field-effect transistor. Chem Sci 3:846–850
89. Li J, Jiao C, Huang K, Wu J (2011) Lateral extension of π conjugation along the bay regions of bisanthene through a Diels–Alder cycloaddition reaction. Chem Eur J 17:14672–14680
90. Konishi A, Hirao Y, Nakano M, Shimizu A, Botek E, Champagne B, Shiomi D, Sato K, Takui T, Matsumoto K, Kurata H, Kubo T (2010) Synthesis and characterization of teranthene: a singlet biradical polycyclic aromatic hydrocarbon having Kekulé structures. J Am Chem Soc 132:11021–11023
91. Jiang D, Sumpter BG, Dai S (2007) First principles study of magnetism in nanographenes. J Chem Phys 127:124703
92. Roberson LB, Kowalik J, Tolbert LM, Kloc C, Zeis R, Chi X, Fleming R, Wilkins C (2005) Pentacene disproportionation during sublimation for field-effect transistors. J Am Chem Soc 127:3069–3075
93. Zhang X, Jiang X, Luo J, Chi C, Chen H, Wu J (2010) A cruciform 6,6'-dipentacenyl: synthesis, solid-state packing and applications in thin-film transistors. Chem Eur J 16:464–468
94. Zhang X, Li J, Qu H, Chi C, Wu J (2010) Fused bispentacenequinone and its unexpected Michael addition. Org Lett 12:3946–3949
95. Yin J, Zhang K, Jiao C, Li J, Chi C, Wu J (2010) Synthesis of functionalized tetracene dicarboxylic imides. Tetrahedron Lett 51:6313–6315
96. Wu J, Müllen K (2006) All-benzenoid polycyclic aromatic hydrocarbons: synthesis, self-assembly and applications in organic electronics. In: Haley MM, Tykwinski RR (eds) Carbon-rich compounds. WILEY-VCH Verlag GmbH & Co. KGaA, Weinheim
97. Wu J, Pisula W, Müllen K (2007) Graphenes as potential material for electronics. Chem Rev 107:718–747
98. Clar E, Ironside CT (1958) Hexabenzocoronene. Proc Chem Soc 1958, 150

99. Halleux A, Martin RH, King GSD (1958) Syntheses dans la série des dérivés polycycliques aromatiques hautement condensés. L'hexabenzo-1,12; 2,3; 4,5; 6,7; 8,9; 10,11-coronène, le tétrabenzo-4,5; 6,7; 11,12; 13,14-péropyrène etle tétrabenzo-1,2; 3,4; 8,9; 10,11-bisanthène. Helv Chim Acta 41:1177–1183
100. Hendel W, Khan ZH, Schmidt W (1986) Hexa-peri-benzocoronene, a candidate for the origin of the diffuse interstellar visible absorption bands? Tetrahedron 42:1127–1134
101. Müller M, Kübel C, Müllen K (1998) Giant polycyclic aromatic hydrocarbons. Chem Eur J 4:2099–2109
102. Stabel A, Herwig P, Müllen K, Rabe JP (1995) Diodelike current–voltage curves for a single molecule-tunneling spectroscopy with submolecular resolution of an alkylated, *peri*-condensed hexabenzocoronene. Angew Chem Int Ed Engl 34:1609–1611
103. Kübel C, Eckhardt K, Enkelmann V, Wegner G, Müllen K (2000) Synthesis and crystal packing of large polycyclic aromatic hydrocarbons: hexabenzo[bc, ef, hi, kl, no, qr]coronene and dibenzo[fg, ij]phenanthro[9,10,1,2,3-pqrst]pentaphene. J Mater Chem 10:879–886
104. Ito S, Wehmeier M, Brand JD, Kübel C, Epsch R, Rabe JP, Müllen K (2000) Synthesis and self-assembly of functionalized hexa-*peri*-hexabenzocoronenes. Chem Eur J 6:4327–4342
105. Fechtenkötter A, Tchebotareva N, Watson MD, Müllen K (2001) Discotic liquid crystalline hexabenzocoronenes carrying chiral and racemic branched alkyl chains: supramolecular engineering and improved synthetic methods. Tetrahedron 57:3769–3783
106. Wang Z, Dötz F, Enkelmann V, Müllen K (2005) "Double-concave" graphene: permethoxylated hexa-*peri*-hexabenzocoronene and its cocrystals with hexafluorobenzene and fullerene. Angew Chem Int Ed 44:1247–1250
107. Zeng Z, Guan Z, Xu QH, Wu J (2011) Octupolar polycyclic aromatic hydrocarbons as new two-photon absorption chromophores: synthesis and application for optical power limiting. Chem Eur J 17:3837–3841
108. Herwig P, Kayser CW, Müllen K, Spiess HW (1996) Columnar mesophases of alkylated hexa-*peri*-hexabenzocoronenes with remarkably large phase widths. Adv Mater 8:510–513
109. Pisula W, Kastler M, Wasserfallen M, Mondeshki M, Piris J, Schnell I, Müllen K (2006) Relation between supramolecular order and charge carrier mobility of branched alkyl hexa-*peri*-hexabenzocoronenes. Chem Mater 18:3634–3640
110. Fechtenkötter A, Saalwächter K, Harbison MA, Müllen K, Spiess HW (1999) Highly ordered columnar structures from hexa-*peri*-hexabenzocoronenes-synthesis, X-ray diffraction, and solid-state heteronuclear multiple-quantum NMR investigations. Angew Chem Int Ed 38:3039–3042
111. Dou X, Pisula W, Wu J, Bodwell GJ, Müllen K (2008) Reinforced self-assembly of hexa-*peri*-hexabenzocoronenes by hydrogen bonds: from microscopic aggregates to macroscopic fluorescent organogels. Chem Eur J 14:240–249
112. Feng X, Pisula W, Takase M, Dou X, Enkelmann V, Wagner M, Ding N, Müllen K (2008) Synthesis, helical organization, and fibrous formation of $C_3$ symmetric methoxy-substituted discotic hexa-*peri*-hexabenzocoronene. Chem Mater 20:2872–2874
113. Schmidt-Mende L, Fechtenkötter A, Müllen K, Moons E, Friend RH, MacKenzie JD (2001) Self-organized discotic liquid crystals for high-efficiency organic photovoltaics. Science 293:1119–1122
114. Wong WWH, Jones DJ, Yan C, Watkins SE, King S, Haque SA, Wen X, Ghiggino KP, Holmes AB (2009) Synthesis, photophysical, and device properties of novel dendrimers based on a fluorene-hexabenzocoronene (FHBC) core. Org Lett 11:975–978
115. Wong WWH, Singh TB, Vak D, Pisula W, Yan C, Feng X, Williams EL, Chan KL, Mao Q, Jones DJ, Ma CQ, Müllen K, Bäuerle P, Holmes AB (2010) Solution processable fluorenyl hexa-*peri*-hexabenzocoronenes in organic field-effect transistors and solar cells. Adv Funct Mater 20:927–938
116. Wong WWH, Ma CQ, Pisula W, Yan C, Feng X, Jones DJ, Müllen K, Janssen RAJ, Bäuerle P, Holmes AB (2010) Self-assembling thiophene dendrimers with a

hexa-*peri*-hexabenzocoronene core-synthesis, characterization and performance in bulk heterojunction solar cells. Chem Mater 22:457–466
117. Feng X, Liu M, Pisula W, Takase M, Li J, Müllen K (2008) Supramolecular organization and photovoltaics of triangle-shaped discotic graphenes with swallow-tailed alkyl substituents. Adv Mater 20:2684–2689
118. Iyer VS, Yoshimura K, Enkelmann V, Epsch R, Rabe JP, Müllen K (1998) A soluble C60 graphite segment. Angew Chem Int Ed 37:2696–2699
119. Böhme T, Simpson CD, Müllen K, Rabe JP (2007) Current–voltage characteristics of a homologous series of polycyclic aromatic hydrocarbons. Chem Eur J 13:7349–7357
120. Wu J, Tomović Ž, Enkelmann V, Müllen K (2004) From branched hydrocarbon propellers to *C3*-symmetric graphite disks. J Org Chem 69:5179–5186
121. Simpson CD, Brand JD, Berresheim AJ, Przybilla L, Räder HJ, Müllen K (2002) Synthesis of a giant 222 carbon graphite sheet. Chem Eur J 8:1424–1429
122. Wu J, Gherghel L, Watson MD, Li J, Wang Z, Simpson CD, Kolb U, Müllen K (2003) From branched polyphenylenes to graphite ribbons. Macromolecules 36:7082–7089
123. Wu J, Watson MD, Tchebotareva N, Wang Z, Müllen K (2004) Oligomers of hexa-*peri*-hexabenzocoronenes as "super-oligophenylenes": synthesis, electronic properties, and self-assembly. J Org Chem 69:8194–8204
124. Müller M, Kübel C, Morgenroth F, Iyer VS, Müllen K (1998) Oligophenylenes as building blocks for well-defined graphite subunits. Carbon 36:827–831
125. Wasserfallen D, Kastler M, Pisula W, Hofer WA, Fogel Y, Wang Z, Müllen K (2006) Suppressing aggregation in a large polycyclic aromatic hydrocarbon. J Am Chem Soc 128:1334–1339
126. Tomović Ž, Watson MD, Müllen K (2004) Superphenalene-based columnar liquid crystals. Angew Chem Int Ed 43:755–758
127. Iyer VS, Wehmeier M, Brand JD, Keegstra MA, Müllen K (1997) From hexa-*peri*-hexabenzocoronene to "superacenes". Angew Chem Int Ed 36:1604–1607

Top Curr Chem (2014) 349: 249–290
DOI: 10.1007/128_2012_415

Published online: 28 March 2013

# Molecular Belts

**Paul J. Evans and Ramesh Jasti**

**Abstract** Rigid hydrocarbon macrocycles with radially-oriented π-systems and continuous conjugation have attracted great interest in recent years. These molecular belts have novel optoelectronic properties and host–guest behavior. Certain belts may also ultimately lead to a rational synthesis of carbon nanotubes. The high strain associated with the nonplanar, conjugated backbones requires the development of new synthetic methods, and clever synthetic design. Herein we describe the synthetic history and properties of these structurally simple but synthetically challenging molecules.

**Keywords** Cyclacene · Cycloparaphenylene · Cycloparaphenyleneacetylene · Cyclophenacene · Molecular belt · Picotube

## Contents

1 Radially Oriented π-Systems ..... 250
2 Hydrocarbon "Picotube" ..... 250
3 Cycloparaphenyleneacetylenes ..... 252
  3.1 First Synthesis by Kawase ..... 253
  3.2 CPPAs as Novel Host Molecules ..... 254
  3.3 Synthesis of More Reactive CPPAs ..... 256
4 Cycloparaphenylenes ..... 259
  4.1 Early Attempts Towards Cycloparaphenylenes ..... 260
  4.2 First Synthesis of Cycloparaphenylene ..... 261
  4.3 Subsequent Syntheses: A New Field Emerges ..... 264
  4.4 Better Synthetic Control and New CPP Sizes ..... 267
  4.5 Host–Guest Behavior of [10]CPP·$C_{60}$, a Fullerene Peapod ..... 274
  4.6 Functionalized Cycloparaphenylenes ..... 275
5 "Top-Down" Synthesis of [10]Cyclophenacene ..... 278

P.J. Evans and R. Jasti (✉)
Jasti Lab, Boston University, Boston, MA, USA
e-mail: pevans@gmail.bu.edu

6 Cyclacenes ..... 280
6.1 Towards the Synthesis of $[6]_{12}$Cyclacene ..... 281
6.2 Towards the Synthesis of $[6]_8$Cyclacene ..... 283
6.3 [6.8]Cyclacene ..... 284
6.4 Buckybelts ..... 285
References ..... 287

## 1 Radially Oriented π-Systems

Molecules with nonplanar p-orbitals have attracted great interest in recent years due to their fascinating electronics, challenging synthesis, and favorable supramolecular properties [1]. Many of these, such as the calixarenes, cyclotriveratriline, and corranulenes maintain their electron-rich cavities only weakly and can planarize or otherwise deform through rotation or bowl inversion [2]. In contrast, a perplexing and synthetically challenging arrangement, theorized more than 80 years ago, comprises shape-persistent hydrocarbon hoops consisting of all sp or $sp^2$ hybridized carbon atoms [3]. These rigid hoops possess unique π-systems that are geometrically forced into the center of the molecule (carbon nanotube-like) rather than above and below the plane of the molecule (graphene-like, Fig. 1).

The strain associated with these belt systems from nonplanarity renders them challenging synthetic targets. The simplest of this class are the cyclo[*n*]carbons, allotropes of carbon consisting of a macrocycle of all sp-hybridized atoms (Fig. 2).

Cyclo[18]carbon was observed by Diederich and coworkers under mass spectroscopic conditions by the threefold *retro*-Diels–Alder liberation of anthracene from the cleverly designed and stable annulene **1**. The all-carbon product, however, proved to be transient [4–6]. In spite of the reactivity of cyclocarbon, several complex hydrocarbon belts of this type have succumbed to organic synthesis and many more remain in the sights of synthetic chemists (Fig. 3). Herein we provide a review of the synthetic challenges, successful syntheses, and fascinating properties of this novel class of rigid hoops.

## 2 Hydrocarbon "Picotube"

In 1996, Herges reported the groundbreaking first bottom-up organic synthesis of a fully conjugated, aromatic hydrocarbon with a radial π-system [7]. The so-called "picotube" is a hydrocarbon with the formula $C_{56}H_{32}$ formed easily by the photo-induced ring expansion of tetradehydrodianthracene **2** [7]. Proceeding through tandem [2+2] and retro-[2+2] cycloadditions, tetraanthraceneylidene (TDDA) **3** can be obtained in 16% yield after purification (Fig. 4).

The resulting hydrocarbon "picotube" was found to be extremely stable to oxidation and methodology to close the remaining fjord regions to form a [4,4] carbon nanotube **4** has yet to be developed. Herges attempted this challenging

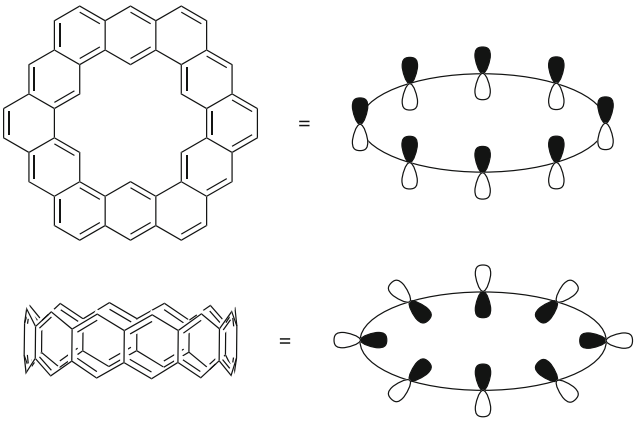

**Fig. 1** PAH isomers and p-orbital orientations of $C_{48}H_{24}$: graphene-like kekulene (*top*) and nanotube-like $[6]_{12}$cyclacene (*bottom*)

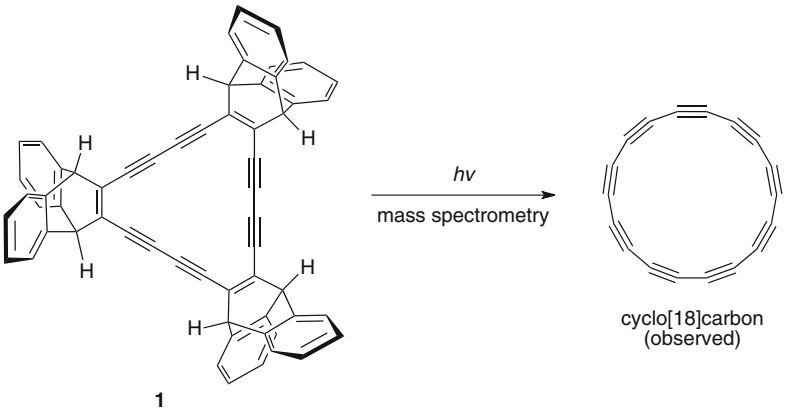


**Fig. 2** The first synthesis of a cyclo[*n*]carbon by Diederich et al. [4]

closure through standard chemical cyclodehydrogenation (e.g., Schöll, etc.) which only led to polymerization. Flash vacuum pyrolysis at 800°C, however, yielded 40% of the interesting rearrangement product **5** with a convoluted structure and a calculated ground state energy 52 kcal/mol more stable than that of the picotube (Fig. 5) [8].

The picotube did prove to be susceptible to Friedel–Crafts functionalization to prepare chiral derivatives [9]. The authors propose this as a general method for the functionalization of carbon nanotubes. The cavity of these picotubes is quite small for the encapsulation of hydrocarbons as is seen with cycloparaphenyleneacetylenes and cycloparaphenylenes, but it has been calculated to be an appropriate guest for a (9,9) carbon nanotube (CNT), though empirical data has not yet been

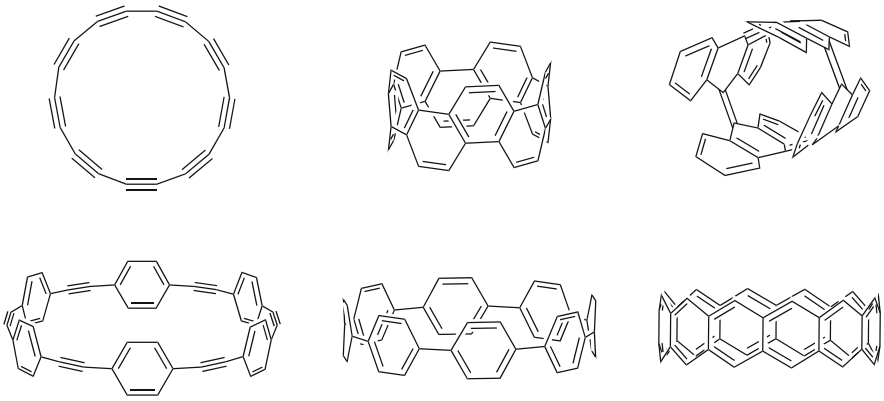

**Fig. 3** Representative molecular belts (clockwise from top *left*, cyclocarbon, cyclophenacene, picotube, cyclacene, cycloparaphenylene, and cycloparaphenyleneacetylene)

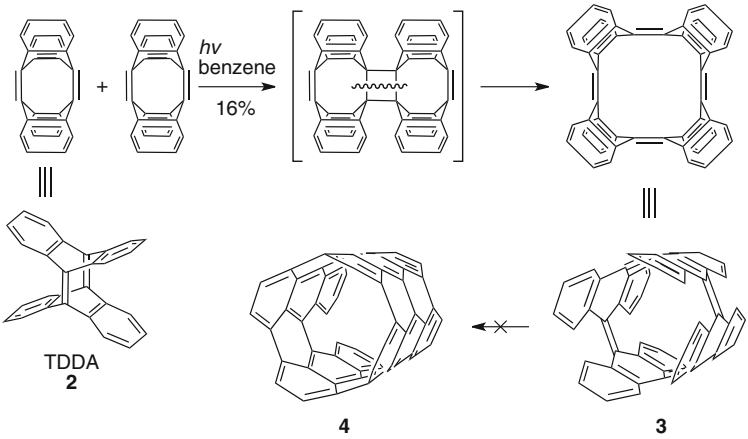


**Fig. 4** Picotube synthesis from TDDA [7]

obtained [10]. In addition to the milestone synthesis, this picotube has attracted the interest of chemists studying its novel vibrational and spectroscopic properties [11–13].

## 3 Cycloparaphenyleneacetylenes

Cycloparaphenyleneacetylenes (CPPAs) are hydrocarbon belts consisting of alkyne and phenyl moieties in differing proportions. By breaking up longer polyyne chains, responsible for the high reactivity of the cyclocarbons, with phenyl rings, one arrives at more stable hydrocarbon macrocycles [4, 14].

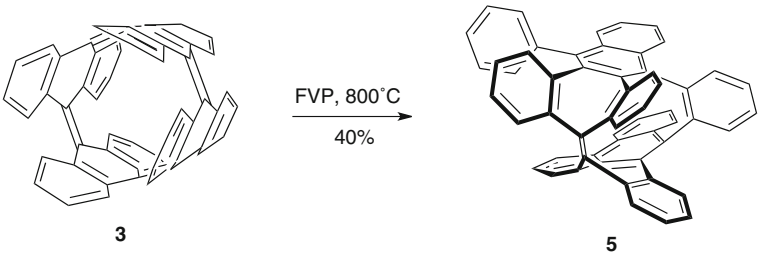


**Fig. 5** Flash vacuum pyrolysis rearrangement of **3** [8]

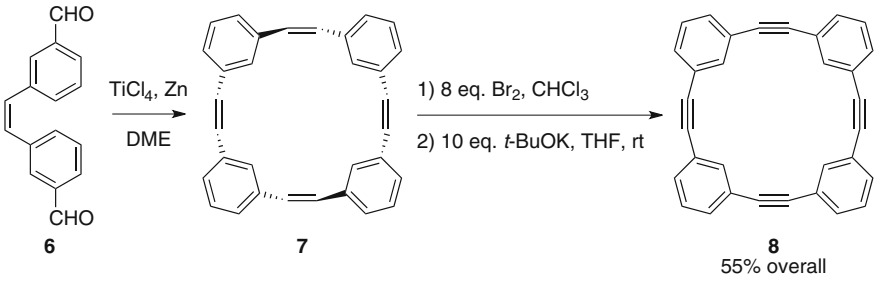


**Fig. 6** Kawase's synthesis of [4]CMPA [15]

## *3.1 First Synthesis by Kawase*

En route to the synthetically elusive CPPA belts, Kawase reported the synthesis of strained [4]cyclometaphenyleneacetylene ([4]CMPA) in 1996 (**8**, Fig. 6). This planar isomer of [4]CPPA was prepared through a McMurry coupling, bromination, and elimination sequence [15].

Having proved this synthesis tractable for the formation of bent alkynes, a similar approach was applied to synthesize [6]CPPA and [8]CPPA (**12** and **13**, Fig. 7). The "shotgun"-style macrocyclization reaction of 4,4′-diformyl-*Z*-stilbene under McMurry conditions provided moderate yields of macrocycles **9**–**11** (Fig. 7). These macrocycles were then subjected as a mixture to the same bromination/elimination sequence that provided [4]CMPA [15].

Macrocycles **10** and **11** were converted efficiently to yield [6]CPPA and [8]CPPA for the first time (17% overall yield, 4:1 **12**:**13**) [16]. Owing to their strained, electron-rich nature, these belts were observed to oxidize upon storage and [6]CPPA was shown to decompose explosively upon heating in air. Interestingly, the [4]CPPA precursor **9** was found to undergo only addition of *tert*-butoxide or THF (when used as solvent) at the reactive site (Fig. 8) [15].

This reactivity indicates that, while appropriate for the introduction of moderate strain, smaller CPPAs are unobtainable by basic elimination [14].

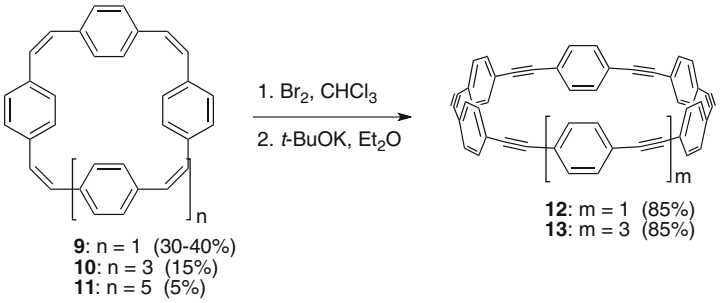


**Fig. 7** Kawase's synthesis of [6]CPPA and [8]CPPA [16]

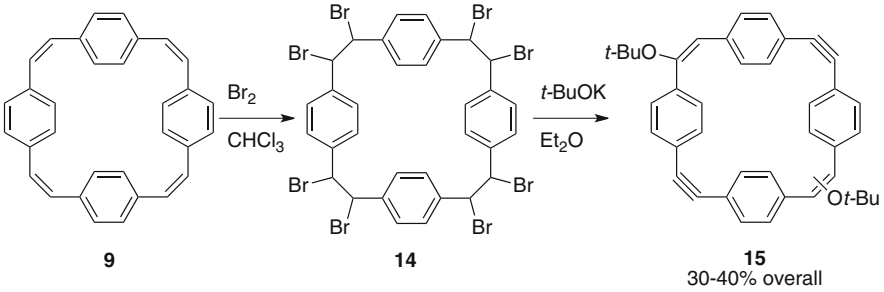


**Fig. 8** Failed conversion of **9** to [4]CPPA [14]

## *3.2 CPPAs as Novel Host Molecules*

Having overcome the challenge of [6]CPPA and [8]CPPA with his landmark synthesis, Kawase improved upon these methods to prepare large quantities of [6]–[9] CPPA. With ample material in hand, the Kawase lab sought to exploit the unique, electron-rich cavity present in these rigid molecular belts [16]. Kawase showed for the first time that CPPAs can form all-hydrocarbon inclusion complexes with appropriate guests [17]. By co-crystallizing [6]CPPA and [8]CPPA with hexamethylbenzene and toluene respectively, crystal structures of a 1:1 **12** · HMB and 1:4 **13** · tol complexes were obtained (Fig. 9).

Though the host–guest interaction in both of these complexes was quite weak, with the toluene complex efflorescing at room temperature, the improved air-stability of the complexes as compared to the CPPAs indicated a favorable electronic interaction within the CPPA cavities [17]. The authors attribute this affinity to the electron-rich nature of the molecules' interior. Furthermore, important crystallographic information about the diameters of these molecular belts was available for the rational design of stronger host–guest complexes. With preliminary proof of the CPPAs' host activity, and in light of the then recent discovery of carbon nanotube fullerene peapod complexes, Kawase correctly ascertained that [6]CPPA was approximately the right size to host fullerene $C_{60}$. Indeed, mixtures of **12** and $C_{60}$

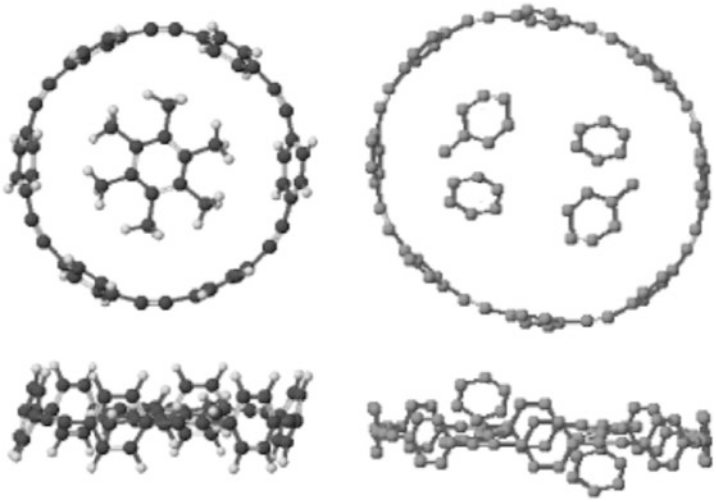

**Fig. 9** Crystal structures of **12** HMB and **13** tol [17]

yielded very strong inclusion complexes with a Gibbs activation energy for dissociation ($\Delta G^{\ddagger}$) of 9.9 ± 0.3 kcal/mol [18]. This interaction is assumed to be stronger then the calix[8]arene–$C_{60}$ complex that is used to purify $C_{60}$ from carbon soot on a commercial scale [19, 20]. The authors attribute the strength of this interaction to polar electrostatic interactions of the CPPA π-system with the electron-deficient [5:6] fusions in fullerene. Furthermore, the complex of bis (ethoxycarbonyl)methanofullerene and [6]CPPA was crystallized and X-ray crystallographic data confirmed the orientation of the CPPA phenyl rings in proximity to the [5:6] fullerene fusions (Fig. 10).

This structure also revealed that the fullerene is only partially encapsulated, with an average intermolecular distance of 3.4 Å, similar to the interlayer distance in multi-walled carbon nanotubes and multi-layer graphene. From this discovery, Kawase was able to investigate further the dynamics of the [6]CPPA–fullerene interaction [21] and also to synthesize naphthyl- derivatives of CPPAs with deeper cavities and stronger interactions such as **16–18** (Figs. 11 and 12) [22, 23] (Table 1).

With experience synthesizing CPPA–fullerene complexes, Kawase went on to design and isolate an onion complex of naphthyl substituted [9]CPPA and [6]CPPA with $C_{60}$ (Fig. 13) [24].

Similar multilayer arrangements are manufactured by "top-down" methods (multi-walled carbon nanotubes, buckyonions) but this was the first example of the assembly of such a structure from the bottom up [25, 26]. Furthermore, at the time it represented the first double inclusion complex of three synthetically accessible organic molecules [24]. Kawase found that, like the previous CPPA–fullerene complexes, the intermolecular distance in this onion complex was 3.2 Å, closely resembling the equivalent distance in carbon materials. This observation demonstrated further proof that discrete, small molecule belts can be accurate models of larger carbon structures.

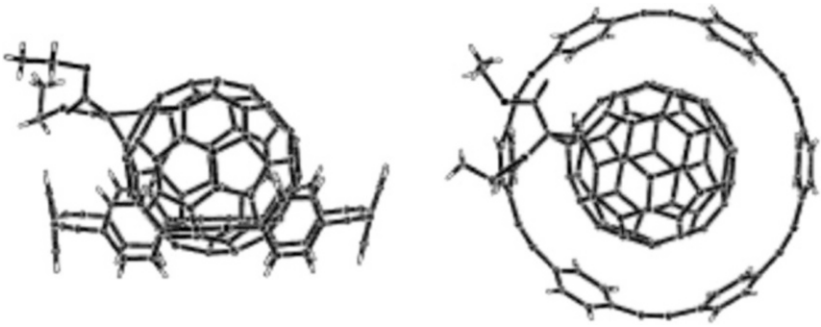

**Fig. 10** Crystal structure of a [6]CPPA fullerene complex [21]

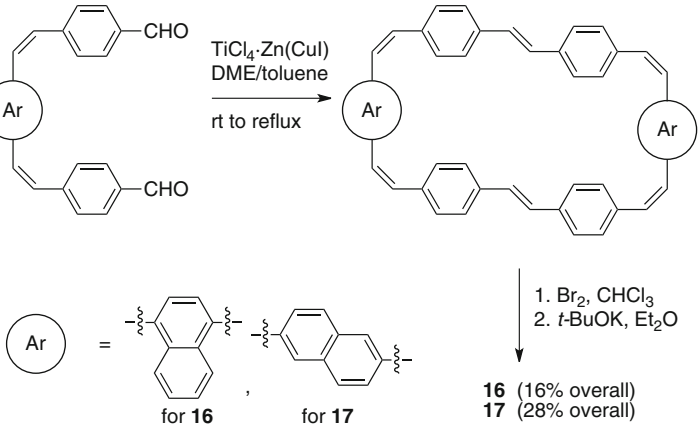


**Fig. 11** Modified CPPA synthesis for π-extended hoops [22, 23]

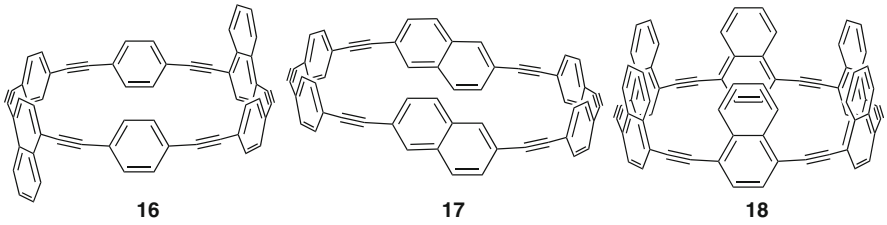


**Fig. 12** Extended CPPAs synthesized by Kawase et al. [22, 23]

## *3.3 Synthesis of More Reactive CPPAs*

The stability of CPPAs to oxidative and polymeric decay falls with increasing length of the polyyne segments [27]. As such, there is an inherent challenge in synthesizing nanohoops with a higher ratio of sp to $sp^2$ carbons, approximating the

**Table 1** Dissociation energy (kcal/mol) for CPPA fullerene

| CPPA | $\Delta G^{\ddagger}$ with $C_{60}$ | $\Delta G^{\ddagger}$ with $C_{70}$ |
|---|---|---|
| [6]CPPA[a] | 9.9 ± 0.2 | 9.6 ± 0.2 |
| [7]CPPA[a] | <9 | <9 |
| **16**[a] | 10.8 ± 0.3 | 10.1 ± 0.2 |
| **17**[a] | <9 | 11.9 ± 0.8 |
| **18**[b] | 14.1 ± 0.3 | |

[a][22]
[b][23]

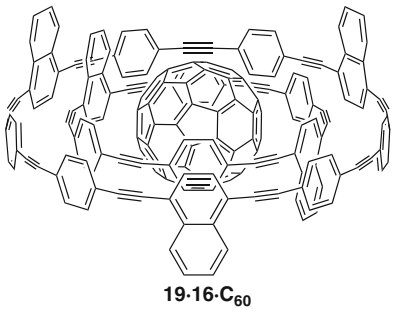


**Fig. 13** A CPPA–fullerene onion complex [24]

very reactive cyclocarbons [4–6]. These approaches have hinged upon masking either the phenyl rings [28–30] or one or more alkynes [31] as curved moieties that can be converted to the desired functionality after macrocyclization.

Both Hopf and Tsuji attempted the synthesis of [$n_2$]CPPAs (having two alkynes per phenyl ring and $n$ phenyl rings) using masked aromatic rings [28–30]. Hopf reported attempts towards [$2_2$]CPPA and [$3_2$]CPPA using *syn*-substituted 1,4-cyclohexadienes to install curvature (Fig. 14). Structure **20** was synthesized by double addition of lithium trimethylsilylacetylide into benzoquinone followed by methylation of the resulting diol. After deprotecting the alkynes, Glaser–Ellington conditions at high dilution ($4 \times 10^{-5}$ M) offered low yields of macrocycles **21** and **22**.

Conversion of these to the corresponding CPPAs has not been reported, presumably due to a lack of appropriate aromatization methods [28, 32].

Tsuji had success in the synthesis of [$6_2$]CPPA using Dewar benzenes as masked aromatic rings which can be irreversibly aromatized by irradiation in the final synthetic step (Fig. 15) [30, 33]. Tsuji's approach consists of the synthesis of Dewar benzene derivative **24** by [2+2] cycloaddition of 1,2-dichloroethylene to dimethylacetylenedicarboxylate. This adduct was then reduced and protected as the cyclohexyl ketal **26**, which is resistant to photoisomerization. Elimination afforded a mix of dichlorides **27** and **28** which were easily separated by chromatography [29].

Tsuji proved the usefulness of this building block in the synthesis of less strained phenylacetylene macrocycles [29, 33]. Sonogashira alkynylation, Glaser–Ellington

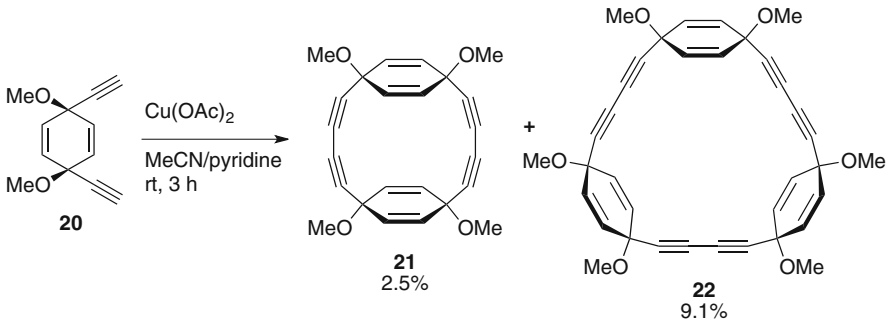


**Fig. 14** Hopf's synthesis of putative CPPA precursors **21** and **22** [28]

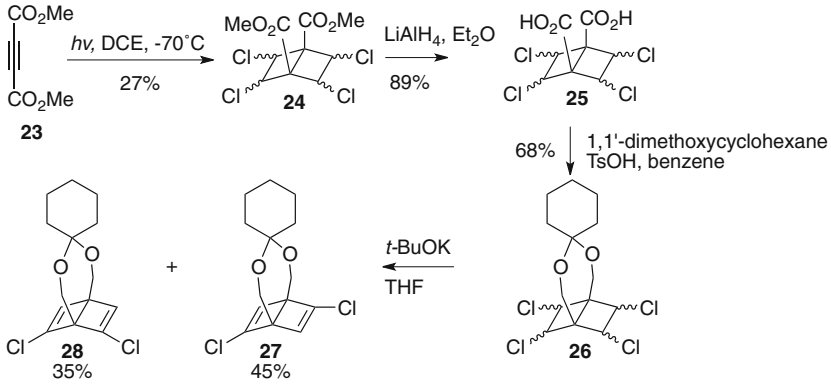


**Fig. 15** Synthesis of Dewar benzene derivatives [29]

dimerization, and Glaser–Ellington macrocyclization afforded **31** which was quantitatively converted by photoirradiation to dodecasilyl [$6_2$]CPPA comprising the first synthesis of a substituted [$n_2$]CPPA (Fig. 16) [30].

While this remains the most unsaturated CPPA ever isolated (stable on the order of days), evidence of the formation of cyclocarbon-like [$2_6$]CPPA was reported "by Tobe". [4.3.2]Propelatriene units are known to undergo photoinduced *retro* [2+2] addition to yield indane and the corresponding alkyne [34]. Having employed a similar strategy en route to cyclocarbon, these masked alkynes were chosen to provide curvature to the CPPA macrocyclic precursors **35** and **36** (Fig. 17).

Fragments **33** and **34** were synthesized by Sonogashira coupling with 1,4-diiodobenzene and 1,4-diiodo-2,3,5,6-tetrachlorobenzene, respectively, followed by deprotection and dilute oxidative coupling to offer **35** and **36**. Under mass spectroscopic conditions, irradiation of the macrocycle generated the highly unstable [$2_6$]CPPA [31]. Interestingly, when using furan as solvent, **37** was obtained as a quickly decomposing orange solid.

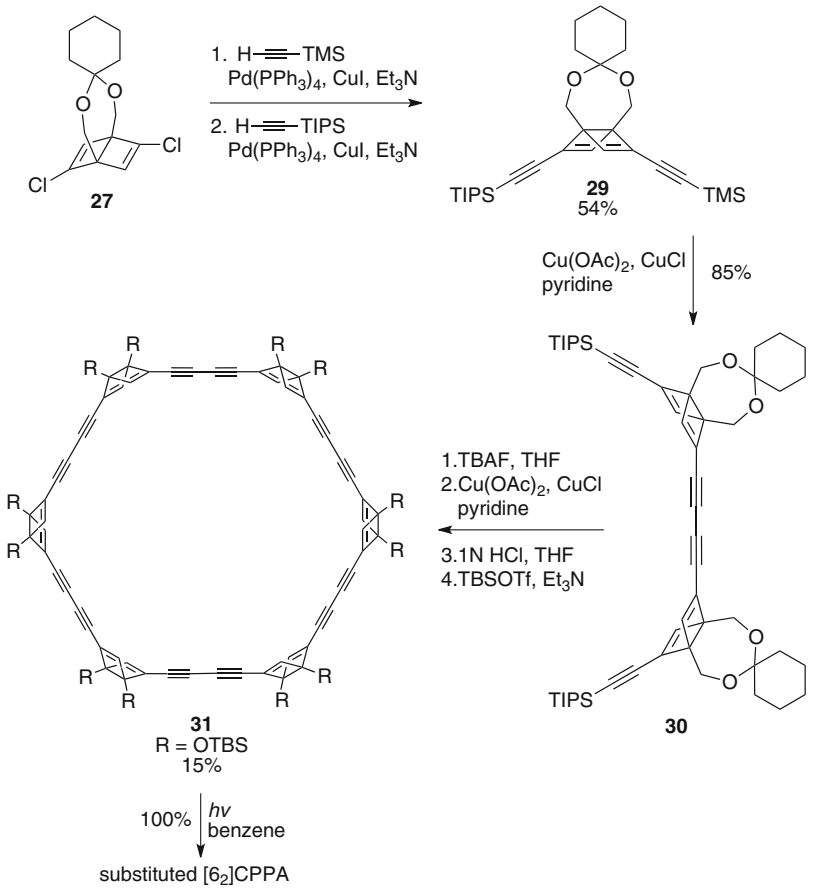


**Fig. 16** Synthesis of CPPA precursor **31** and conversion to a CPPA derivative [29]

## 4 Cycloparaphenylenes

Recently, there has been an explosion of research and new syntheses surrounding the cycloparaphenylenes (CPPs) [32, 35–58]. These conjugated macrocycles are comprised of sequential benzene rings bonded covalently at the *para* positions. As such, they represent the smallest unit cycle of an armchair nanotube (Fig. 18).

These "carbon nanohoops" have been envisioned as seeds for the growth of extended nanotube structures as well as novel, porous, semiconducting, and fluorescent materials in their own right [36, 53, 56, 57].

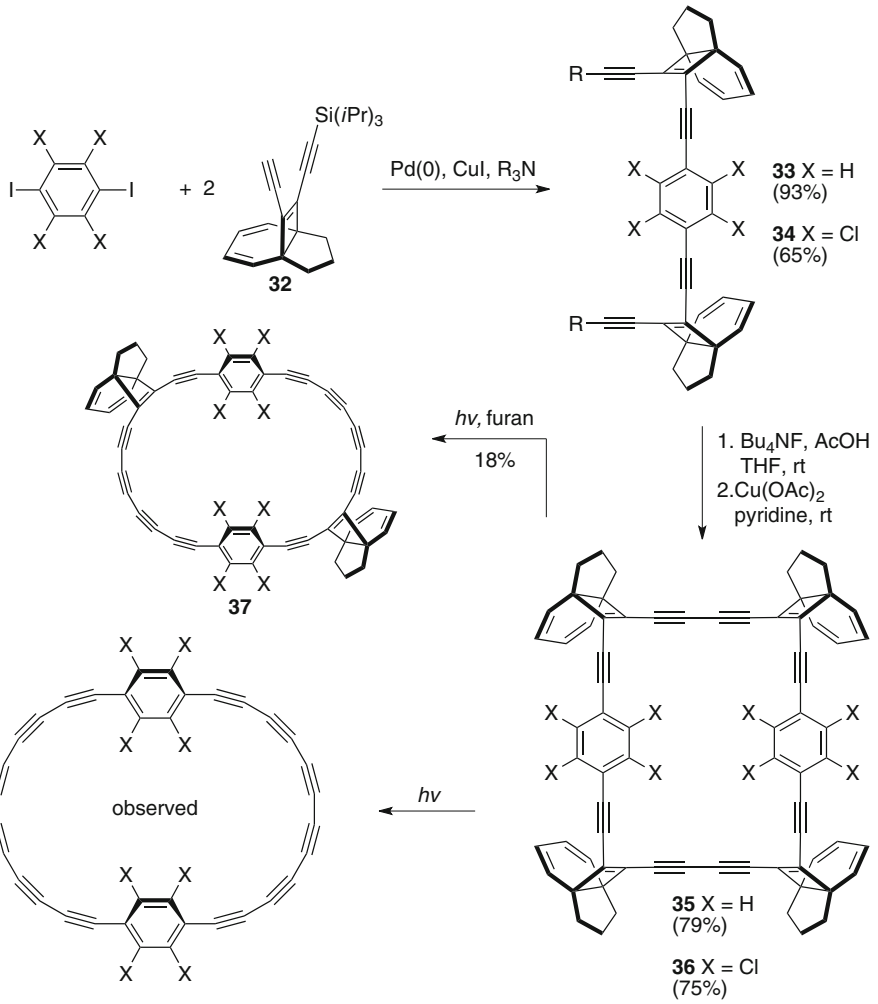


**Fig. 17** Tobe's synthesis of [$2_6$]CPPA [34]

## *4.1 Early Attempts Towards Cycloparaphenylenes*

The first published attempt at the synthesis of any CPP was reported in 1934 by Parekh et al. [3]. Having synthesized the parent macrocycle, *p*,*p*-diphenylenetetrasulfide, **38**, the thermal liberation of 4 equiv. of sulfur (as copper sulfides and sulfur oxides) upon heating with copper in air was attempted (Fig. 19). Only partial desulfination was observed, however, probably owing to the extreme strain associated with the resulting [2]cycloparaphenylene.

Almost 60 years later, Vögtle and coworkers published three inspiring, synthetic routes towards CPP [59]. First, in a similar fashion to the attempts towards [2]CPP

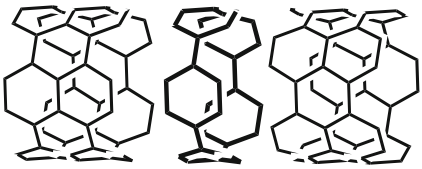

**Fig. 18** Cycloparaphenylene envisioned as the unit-cycle of an armchair nanotube (double bonds omitted for clarity)

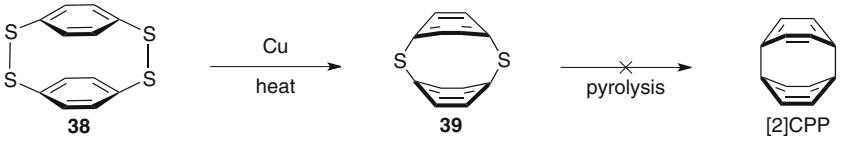


**Fig. 19** Parekh's attempted synthesis of [2]CPP [3]

by Parekh, Vögtle accessed hexaphenyl pentasulfate macrocycle **40** in 65% yield (Fig. 20a).

However, thermal cleavage of the sulfide bonds again proved difficult. It is assumed that, while efficient in many cases for the buildup of strain [60], this motif is inadequate to access the highly rigid, bent aromatic backbone of the CPPs. Vögtle et al. then revised their synthesis to target the less energetic [8]CCP and [10]CPP. To do so, the oligomeric phenyleneethyleneacetylene macrocycles **41** were synthesized from a tetra-Wittig reaction in dilute conditions meant to quell polymerization (Fig. 20b). Vögtle's vision for these macrocycles was that [4+2] cycloadditions to the ene–yne moieties would build in the final four phenyl rings and yield the corresponding carbon nanohoops. However, these attempts were never successful. Lastly, Vögtle prepared substituted L-shaped cyclohexanes **42** and **43** with the intent to oxidize these to phenyl rings after cyclic oligomerization, but failed to arrive at the corresponding macrocycles (Fig. 20c). This cyclohexane approach would later be employed successfully by Itami et al. [35].

## *4.2 First Synthesis of Cycloparaphenylene*

After eluding synthesis for over 70 years, the pioneering synthesis of [9]CPP, [12]CPP, and [18]CPP was reported by Jasti and Bertozzi [32]. Using cyclohexadienes as masked aryl rings, Jasti envisioned a final reductive aromatization from macrocycles of the type **46**–**48**. These aromatization reactions were expected to be highly exothermic and appropriate for building in considerable strain (Fig. 21).

To employ this method, diiodide **44** was easily synthesized on a large scale without chromatography via the addition of benzoquinone into a molar excess of lithiated diiodobenzene followed by methylation with sodium hydride and iodomethane. A portion of this diiodide was then converted to the bisboronate **45** and "shotgun" Suzuki–Miyaura cross-coupling at high dilution offered a mixture of macrocycles. These macrocycles were easily separated by standard chromatographic procedures.

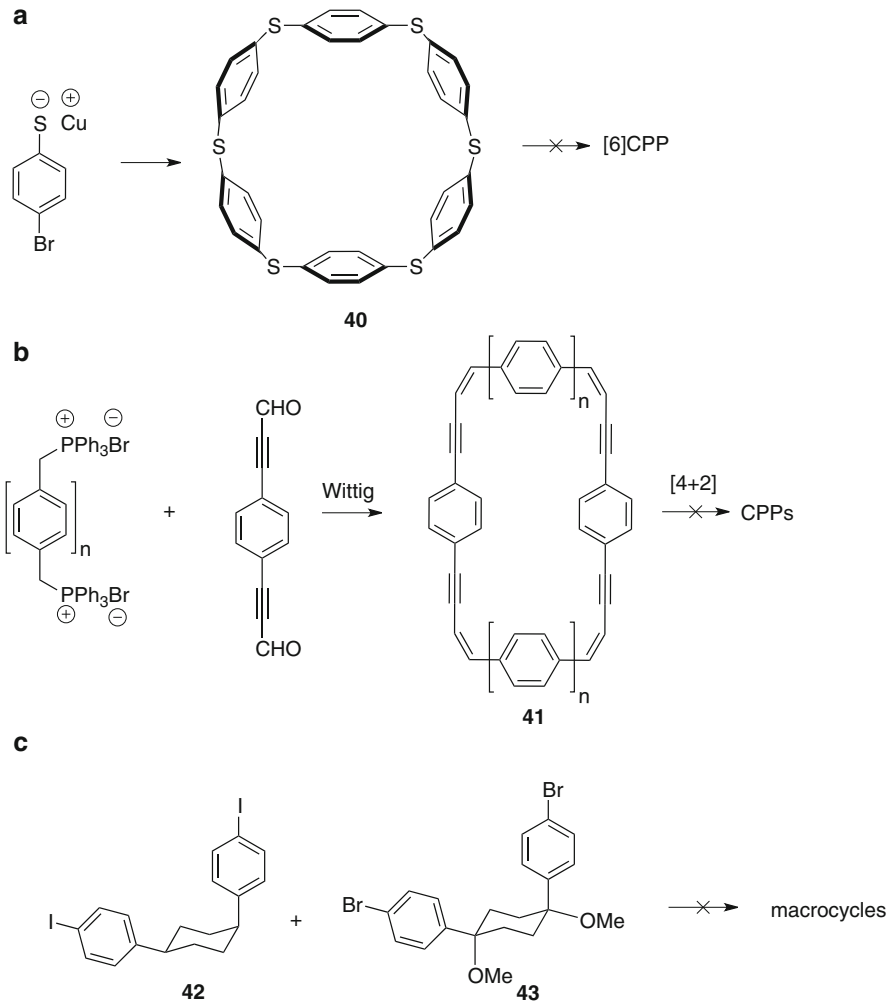


**Fig. 20** Vögtle's attempted syntheses of cycloparaphenylenes [59]

It is interesting to note that the nine-membered macrocycle must be the result of homocoupling of the corresponding nine-membered bisboronate. With these macrocycles in hand, Jasti developed a reductive aromatization technique that circumvented the 1,2-phenyl shift observed under acidic or Lewis acidic conditions for similar systems (Fig. 22) [61].

Treating a solution of the desired macrocycle with lithium naphthalenide at −78°C for 30 min offered the corresponding CPPs in moderate yield [32]. The electron-transfer mechanism of this reduction prevents rearrangement by circumventing carbocation intermediates, and builds in an amazing amount of strain

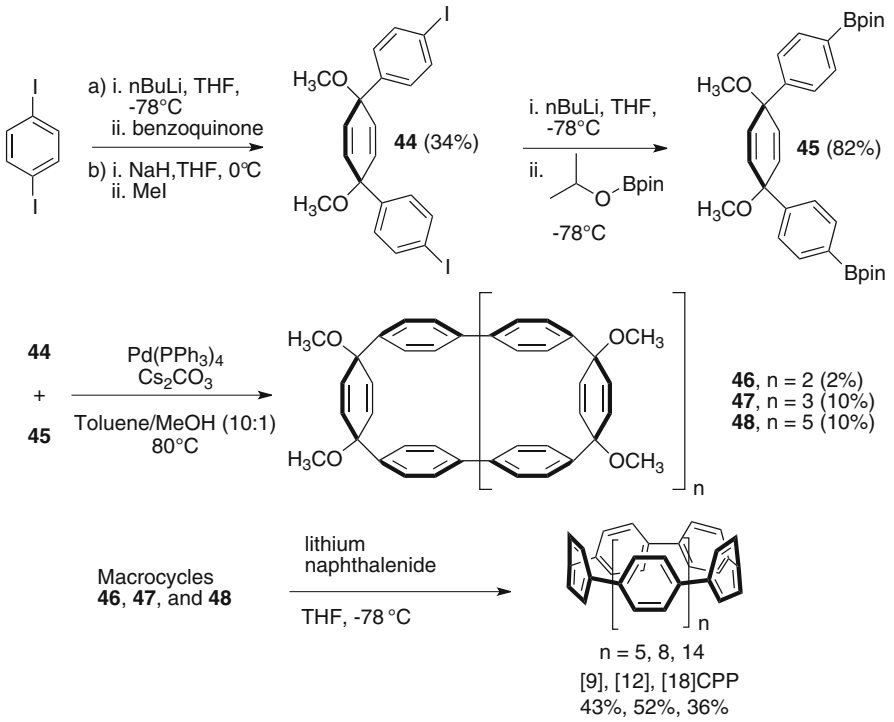


**Fig. 21** The first synthesis of [9]-, [12]-, and [18]cycloparaphenylene [32]

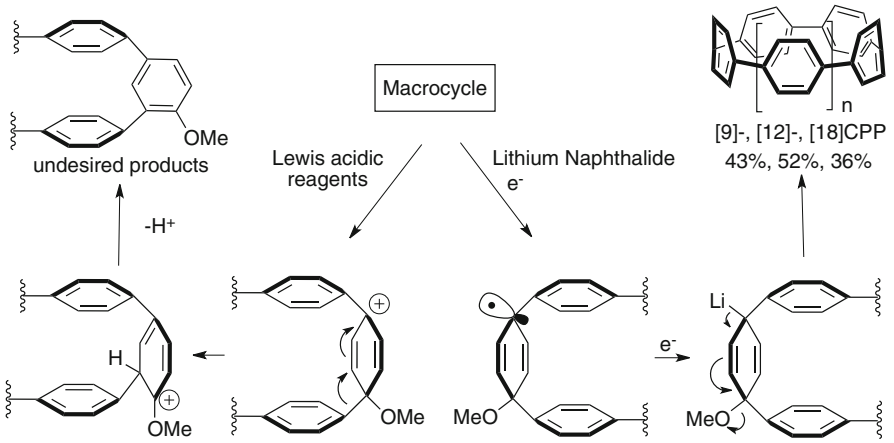


**Fig. 22** Aromatization reaction and proposed mechanism [32]

at low temperatures (total calculated strain energy for [9]CPP: 69 kcal/mol). Using this procedure, Jasti synthesized 1.8, 4.2, and 1.6 mg of [9]CPP, [12]CPP, and [18] CPP for the first time.

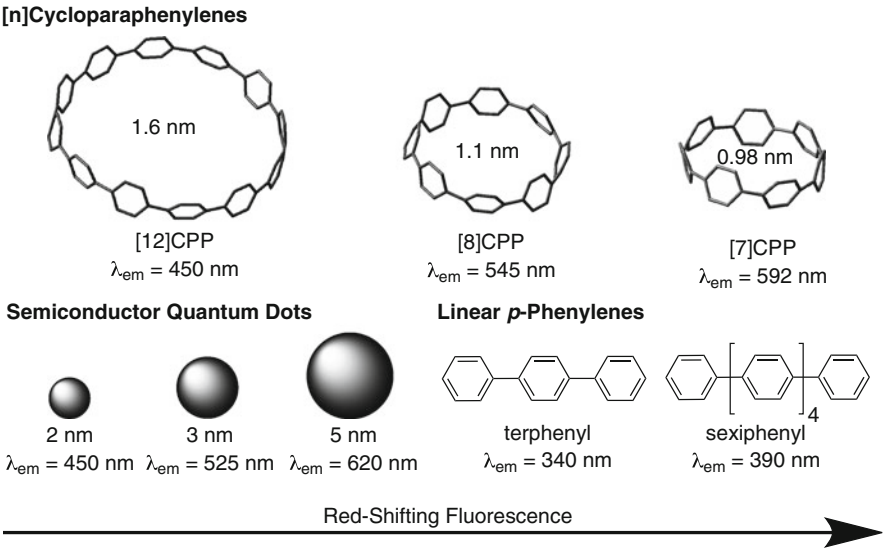


**Fig. 23** Fluorescence trends in quantum dots, CPPs and OPPs [43]

With the elusive hydrocarbons finally in hand, Jasti obtained optical data for these highly fluorescent aromatics and observed a similar absorbance for all diameters (338–339 nm) and a fluorescence red shift with decreasing diameter. The largest absorbance-emission shift, [9]CPP, is approximately 160 nm [32]. Oligoparaphenylenes (OPPs), the linear analogues of CPPs, show a blue fluorescence shift with decreasing length, following a "particle in a box" optoelectronic model [62]. Quantum dots also exhibit blue shifted fluorescence with decreasing size. The odd trend for carbon nanohoops was attributed to the increased $sp^3$ character of the smaller CPPs allowing for greater relaxation in the excited state, as well as the diminished conjugation effects when considering these cyclic, infinitely conjugated molecules. As will be seen, the fluorescence of all CPPs behaves in the same way and has been a current topic of interest (Fig. 23) [38, 48, 57, 58].

## *4.3 Subsequent Syntheses: A New Field Emerges*

In the years following the landmark synthesis by Jasti and Bertozzi, both the Itami group at Nagoya University and Yamago and coworkers at Kyoto University developed new synthetic routes to the cycloparaphenylenes.

In 2009, Itami et al. reported the selective synthesis of [12]CPP using methods inspired by Vögtle [35]. To do so, Itami synthesized bisboronate **50** and MOM-protected **49**. This protecting group simplifies purification. Reaction of a tenfold

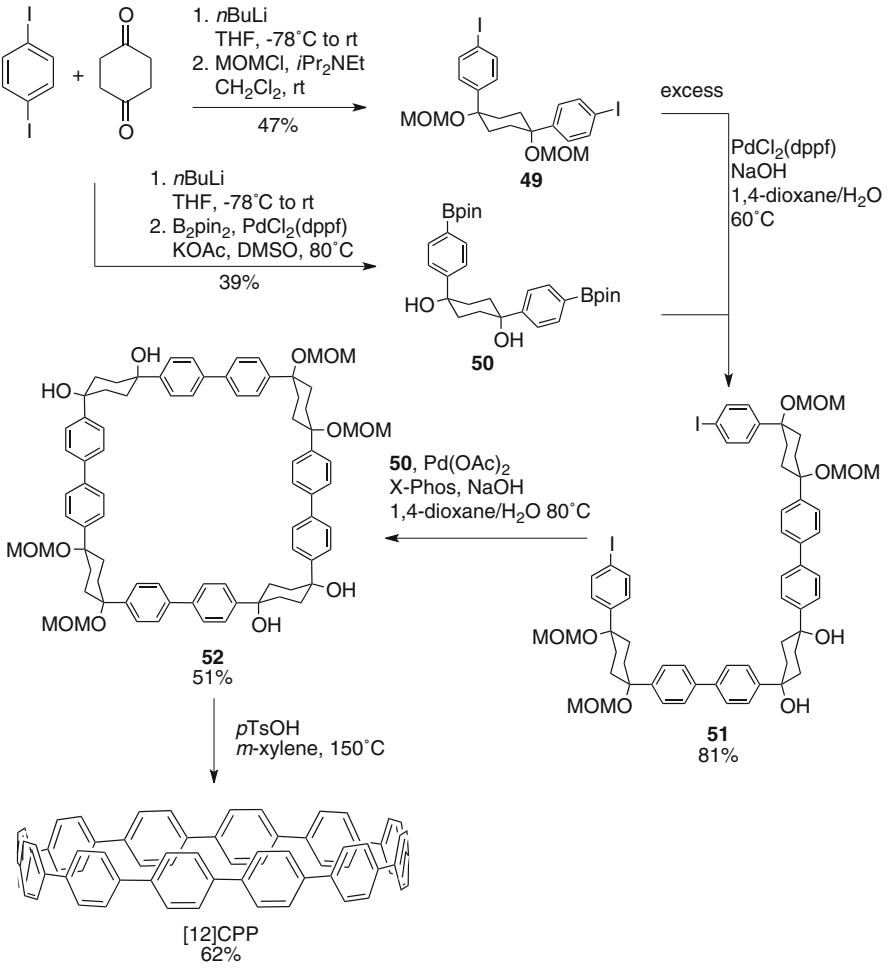


**Fig. 24** Itami's synthesis of [12]CPP [35]

molar excess of **49** with **50** under appropriate palladium coupling conditions favored the formation of 9-membered diiodide **51**. Dilute coupling of **51** with bisboronate **50** yielded selectively the 12-membered macrocycle (Fig. 24).

To aromatize the cyclohexane rings in this CPP precursor, Itami employed harsh but effective microwave conditions using stoichiometric *para*-toluenesulfonic acid at 150°C to achieve the sequential deprotection of the alcohols, acidic elimination, and oxidation of the resulting cyclohexadienes to aryl rings. Using this motif, Itami obtained 4.1 mg of [12]CPP alone [35]. This methodology has recently been employed by Tokyo Chemical Industry, who now offers [12]CPP of 90% purity for $999.00 per 10 mg (TCI, product number C2449). It is an incredible achievement

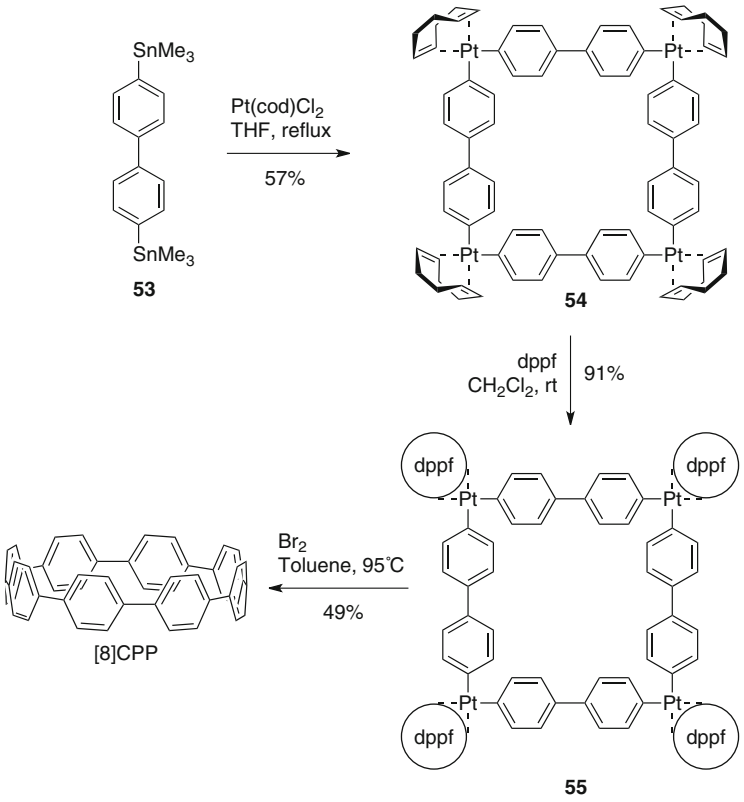


**Fig. 25** Yamago's synthesis of [8]CPP [63]

that such a strained hydrocarbon, which was envisioned decades ago, has become commercially available so shortly after its first synthesis. It seems evident, therefore, that interest in these structures is not limited to synthetic chemists.

In 2010, Yamago et al. entered the field of carbon nanohoop synthesis, reporting the challenging synthesis of [8]CPP, the smallest and most strained CPP at the time of publication. Unlike Itami and Jasti, who relied on masked aromatic rings to relieve strain in the macrocyclic CPP precursors, Yamago employed an organometallic approach (Fig. 25). By reacting 4,4′-bis(trimethyl)stannylbiphenyl **53** with dichloro(cycloocta-1,5-diene)platinum(II), Yamago was able to generate square-shaped macrocycle **54** with very little strain energy [63].

After ligand exchange to 1,1′-bis(diphenylphosphino)ferrocene, (dppf) reductive elimination with bromine led cleanly to 2.0 mg of [8]CPP in three straightforward steps. This reductive elimination builds in an incredible 74 kcal/mol of strain energy in a single reaction. Yamago observed that this new, smaller cycloparaphenylene followed the optical trend observed by Jasti having an absorption maximum at 338 nm and an even larger absorbance–emission shift of 200 nm [63].

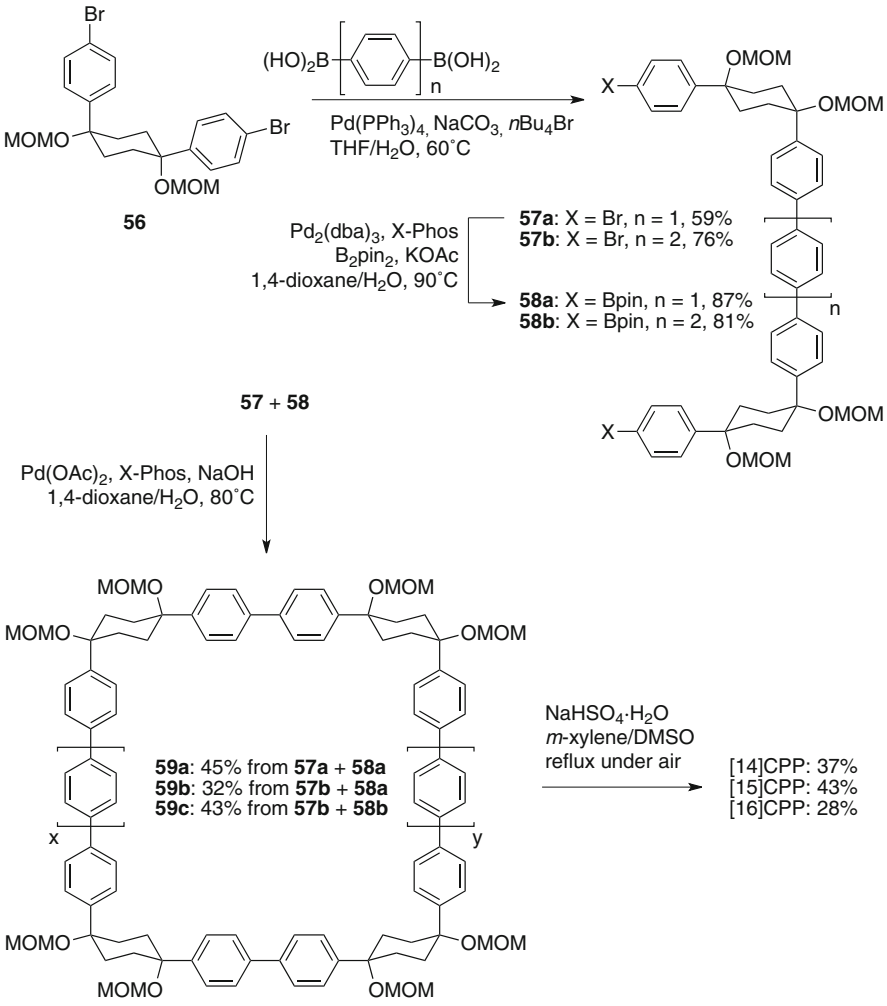


**Fig. 26** Itami's synthesis of [14]CPP, [15]CPP, and [16]CPP [36]

## *4.4 Better Synthetic Control and New CPP Sizes*

With three unique synthetic strategies, each lab pushed forward to create new sizes of cycloparaphenylene and to do so selectively. In 2010, Itami reported a modified synthesis that offered access to [14]CPP, [15]CPP, and [16]CPP selectively via U-shaped dibromide precursors with seven or eight rings (Fig. 26) [36]. These new intermediates **57a** and **57b** were the products of palladium coupling of a molar excess of **56** with 1,4-phenylboronic acid or 4,4′-biphenylboronic acid.

Either of these dibromides can then be converted to the corresponding bisboronates **58a** and **58b** by palladium-mediated borylation and Suzuki coupled

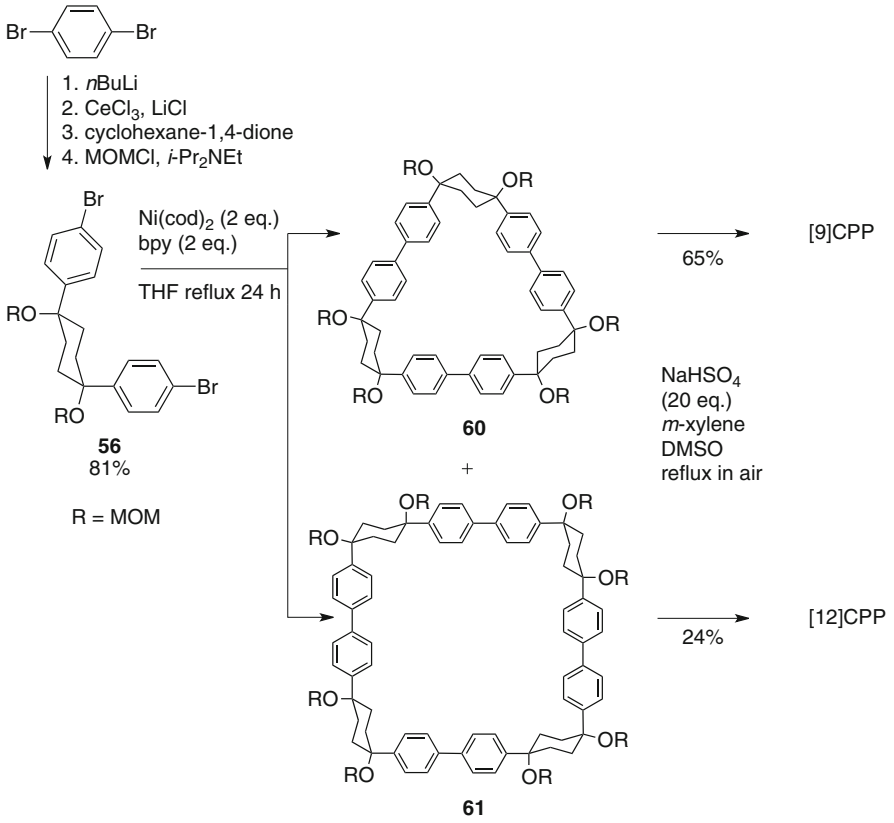


**Fig. 27** Nickel "shotgun" synthesis of [9]CPP and [12]CPP [41, 42]

in a 7+7, 7+8, or 8+8 fashion to offer 2.0, 2.2, and 2.5 mg of [14]CPP, [15]CPP, and [16]CPP respectively after acidic aromatization. The authors propose that chair-flipping accounts for increased flexibility, facilitating the 7+8 macrocyclization [36].

Itami went on to report a new synthesis of [12]CPP based on the "shotgun" homocoupling of dihalide **56** with bis(cyclooctadiene)nickel(0) in the presence of 2,2′-bipyridyl. This new approach circumvented the synthesis of a boronate and also the need for palladium catalysis, albeit stoichiometric nickel is required (Fig. 27). With these synthetic advantages, Itami was able to synthesize **61**, the macrocyclic precursor to [12]CPP on a gram scale. In addition, the authors report that with this synthesis they were able to produce 0.5 g in total of [12]CPP from combined reaction products [36].

At the time of publication, the "shotgun" coupling in this synthesis was reported only for the [12]CPP macrocycle. However, upon investigation of what was originally thought to be linear oligomeric byproducts, it was found that the triangular nine-membered macrocycle **60** also forms in similar yields to the [12]CPP precursor (Fig. 27) [42].

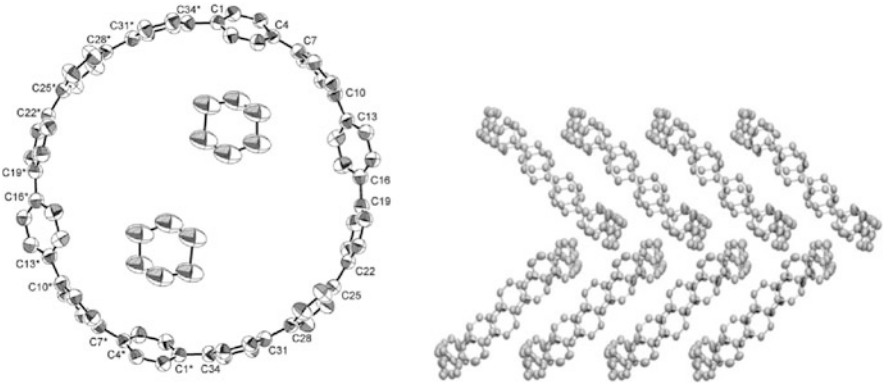


**Fig. 28** Crystal structure (*left*) and packing orientation (*right*) of [12]CPP [41]

The availability of [9]CPP and [12]CPP on a more significant scale allowed for the analysis of their molecular structures by single crystal X-ray diffraction for the first time (Fig. 28). These slightly disordered structures were refined enough to confirm the benzenoid structure of [12]CPP with *ipso–ipso* bond lengths of 1.481 Å and also hint at the trend towards quinoidal structures in smaller CPPs showing shortening of the *ipso–ipso* bond lengths of [9]CPP to 1.468 Å, still longer than the expected region for alkene bonds. In addition, it was shown that the crystal packing of [12]CPP favors a herringbone pattern with channels clearly visible from the appropriate angle, but not strictly nanotube-like [41, 42].

Yamago also published a synthesis of new CPP sizes in 2011 [38]. By utilizing 4,4′-bis(trimethyl)stannylbiphenyl and 4,4′-bis(trimethyl)stannylterphenyl as starting materials, Yamago showed that [8]CPP and [12]CPP can be selectively formed by his platinum-mediated synthesis and also that using a "shotgun" mixture of both provides a mixture of metallocycles which can be converted to the CPPs then separated by preparatory GPC to offer [8]–[13]CPP (Fig. 29).

The formation of [13]CPP is interesting in that it implies the formation of either a 2 + 2 + 3 + 3 + 3 or a 2 + 2 + 2 + 2 + 2 + 3 macrocycle. With these several sizes in hand, Yamago determined the optical characteristics by UV/vis and fluorescence spectroscopy and the oxidation potentials of these CPPs by cyclic voltammetry. The absorbance of all the synthesized CPPs was similar, centered around 338 nm, and the fluorescence followed the emission-shift trend observed by Jasti (Fig. 30) [32]. It was theorized that the relaxation and relief of strain in the excited state geometry of these molecules accounts for the observed shift [57].

The oxidation potentials were shown to be lower with decreasing size. This trend is indicative of the increasing quinodimethane structure and therefore polyene character of the smaller CPPs. These CV observations also correlate well with Yamago's calculated HOMO–LUMO gap, which narrows with decreasing size (Fig. 31). The opposite trend is calculated for OPPs [38].

In an effort to probe the interesting properties of even smaller carbon nanohoops, Jasti published the first synthesis of [7]CPP [43]. This very strained polyphenylene

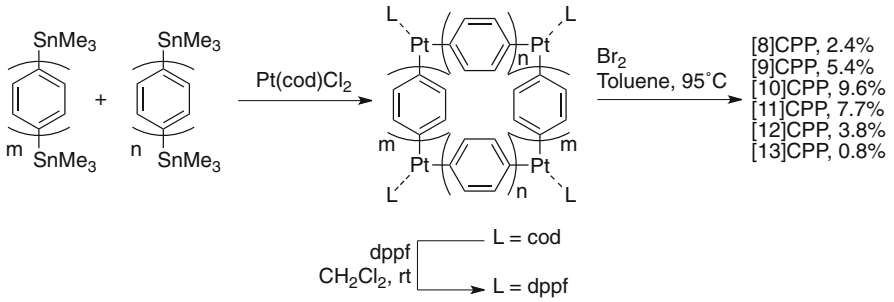


**Fig. 29** Yamago's selective and random synthesis of [8]–[13]CPP [38]

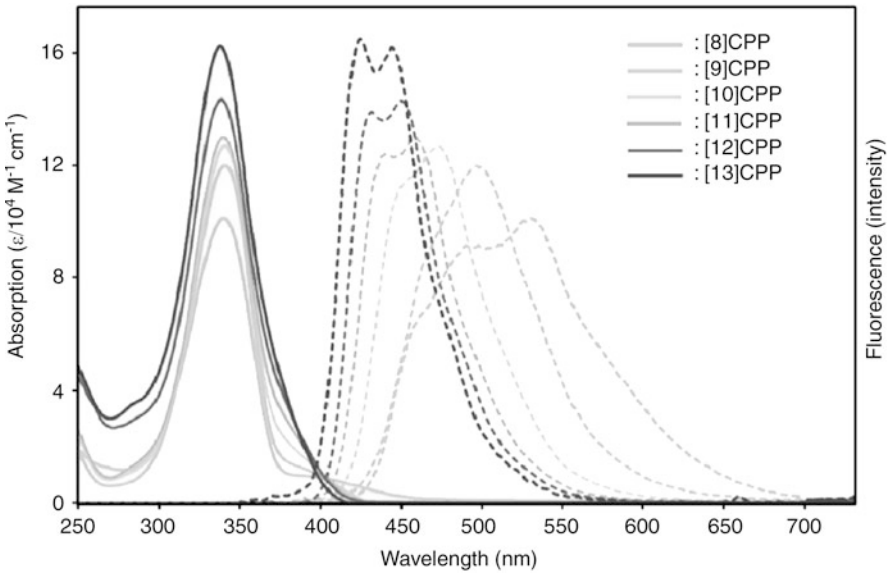


**Fig. 30** Size dependent fluorescence red shift as observed by Yamago [38]

(83 kcal/mol) was assembled using sequential, selective Suzuki coupling reactions. Unsymmetric dihalide **64** was synthesized by the *syn*-selective addition of lithiated 1,4-bromochlorobenzene to **63** after deprotonation of the free alcohol (Fig. 32).

The deprotonation with sodium hydride imparts diastereoselectivity consistent with an electrostatic model in which the anionic nucleophile approaches from the opposite face of the existing negative charge. A portion of this dihalide was then converted by selective lithiation to the boronate **65**. Under standard palladium coupling conditions this boronate and **64** were coupled in a chemoselective manner to offer dichloride **66** without the need for an excess of reactants. Switching to Buchwald's S-Phos as a ligand, this dichloride was closed to macrocycle **67** by reaction of 1,4-phenylboronic acid bis(pinacol) ester at high dilution. The strained

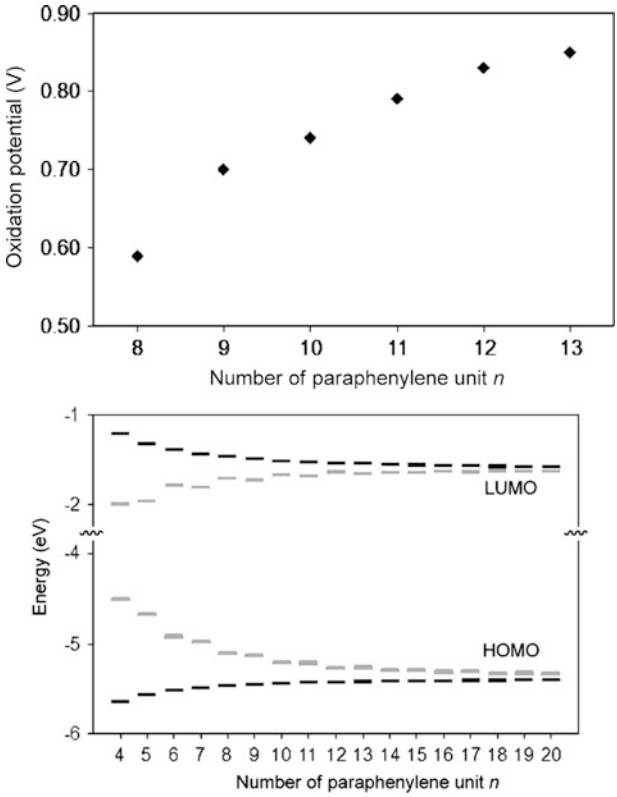


**Fig. 31** *Top*: observed oxidation potential of [*n*]CPP. *Bottom*: calculated HOMO–LUMO gaps for [*n*]CPP (*gray*) and [*n*]OPP (*black*) [38]

terphenyl in the resulting macrocycle explains the relatively low macrocyclization yield. Even so, this molecule was easily aromatized using sodium naphthalenide at −78°C, yielding 1.0 mg of [7]CPP. The final step of any CPP synthesis must necessarily introduce a large amount of strain. These results highlight the reductive aromatization methodology as quite capable of generating large amounts of strain energy at low temperatures. Interestingly, [7]CPP displays an orange fluorescence, further red-shifted than [8]CPP and with a very low quantum yield, following the trends observed in larger carbon nanohoops [43].

A revision of the [7]CPP synthesis to incorporate more curvature in the precursors would allow for the construction of even smaller CPPs, approaching the theoretical limit of the benzenoid structure [64]. With this in mind, Jasti developed a sequential lithium addition/oxidative dearomatization strategy by which tightly-curved dibromide **70** can be obtained on a multigram scale (Fig. 33) [49].

The addition of lithiated 4-bromo, 4′-*tert*-butyldimethylsilyl biphenyl to **63** followed by methylation and deprotection offered **68** which could be subjected to

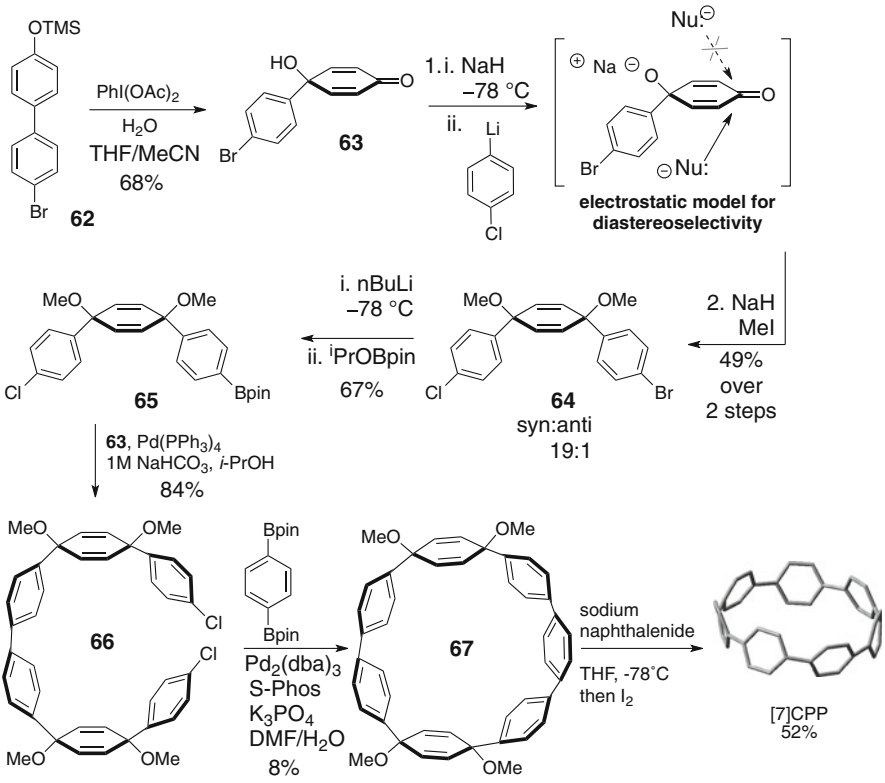


**Fig. 32** Jasti's synthesis of record-breaking [7]CPP [43]

a second oxidative dearomatization to produce **69**. Diastereoselective addition of lithiated 1,4-dibromobenzene to **69** gives the desired dibromide **70** in a highly scalable fashion. Moreover, the increased Suzuki reactivity of bromine vs chlorine led to the application of Buchwald-ligand free palladium(0) coupling with 1,4-phenylboronic acid bis(pinacol) ester to macrocycle **71** with an incredible distorted terphenyl unit evident in the crystal structure (Fig. 34) [49].

Once again, single-electron reduction was employed to aromatize the cyclohexadiene moieties in this macrocycle and [6]CPP was obtained. This is notable because it remains the smallest and most synthetically challenging CPP synthesized to date with a diameter of only 8.1 Å and 97 kcal/mol of strain energy. Also, at 15 mg, it represents the most of any CPP synthesized in one reaction by mass and moles. The optical properties followed the expected trends with no detectable fluorescence, an artifact of the unusual photophysical pathways in smaller CPPs. Most interestingly, single crystal X-ray analysis revealed that, unlike any published, larger CPP structure, [6]CPP organizes very well in the crystalline lattice into tubular nanotube-like rods (Fig. 35) [49].

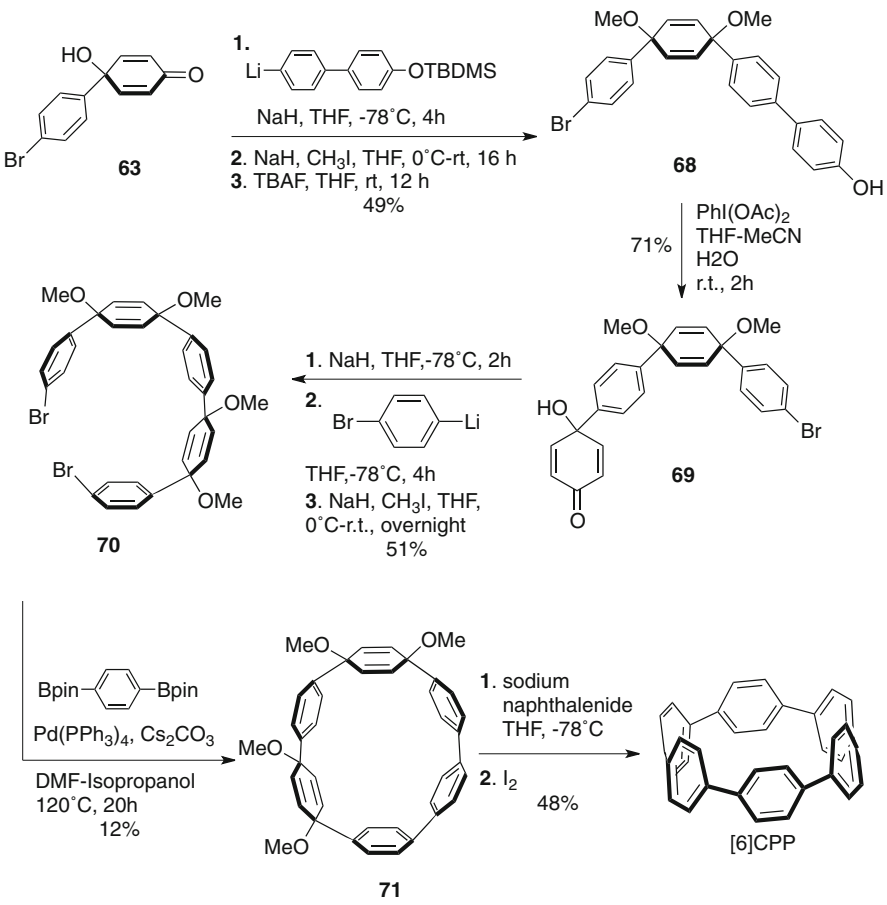


**Fig. 33** The first synthesis of [6]CPP, the smallest to date [49]

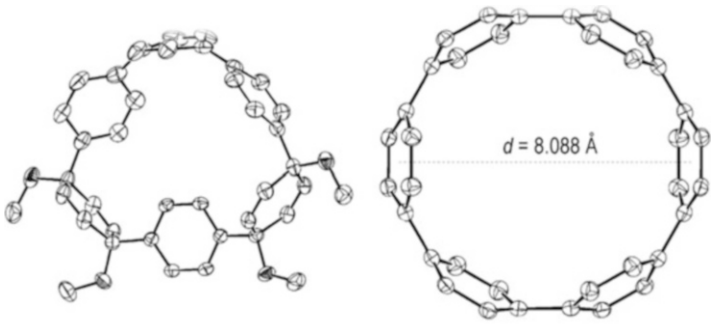


**Fig. 34** Crystal structure of highly-strained **71** (*left*) and [6]CPP (*right*) [49]

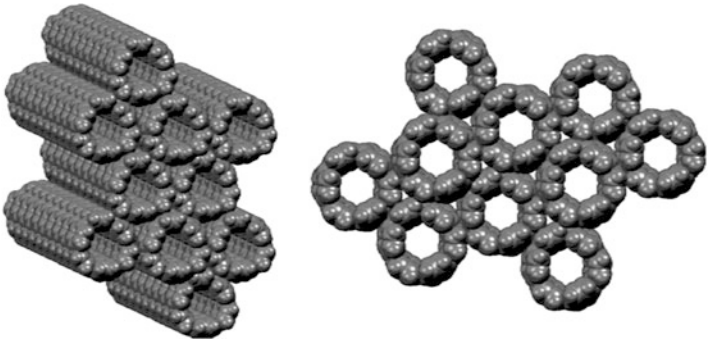

**Fig. 35** Crystal packing of [6]CPP showing tubular arrangement [49]

This has obvious implications in the synthesis of extended nanotube structures.

Most recently, Itami reported the selective syntheses of [9]CPP, [10]CPP, [11]CPP, and [13]CPP using modifications of previously reported methods [45]. This is notable in that it contains the first example of intramolecular macrocyclizations to offer [9]CPP, [11]CPP, and [13]CPP precursors (Fig. 36).

These strategies yield approximately 5 mg of the desired hydrocarbons in good to moderate yields [45].

## *4.5 Host–Guest Behavior of [10]CPP·$C_{60}$, a Fullerene Peapod*

The first and only example of a host–guest complex with cycloparaphenylene was assembled by Yamago and coworkers [37]. In this work, solid fullerene $C_{60}$ was ingeniously added to an NMR sample of the product mixture from the "shotgun" synthesis of [8–13]CPP in $CDCl_3$. The monitored proton spectrum showed the downfield shift of only the signal corresponding to [10]CPP (Fig. 37).

Yamago concluded that this shift indicated the size-selective encapsulation of the fullerene guest by [10]CPP. Similar NMR trends were seen in the CPPA·$C_{60}$ experiments [18, 22]. Yamago was able to confirm by optical data a 1:1 complex of [10]CPP with $C_{60}$ with a dissociation energy of 14.1 kcal/mol, identical to Kawase's π-extended CPPA **18** with $C_{60}$. Moreover, computational analysis showed that the CPP–fullerene intermolecular distance was 3.35 Å, which corresponds with the interlayer distance in graphene and multi-walled carbon nanotubes, as well as CNT–fullerene peapods and CPPA·$C_{60}$. Unlike CNTs, the discrete synthesis of single sizes of CPP made possible the application of their inward-facing π-system to offer a single length of fullerene peapod in high purity.

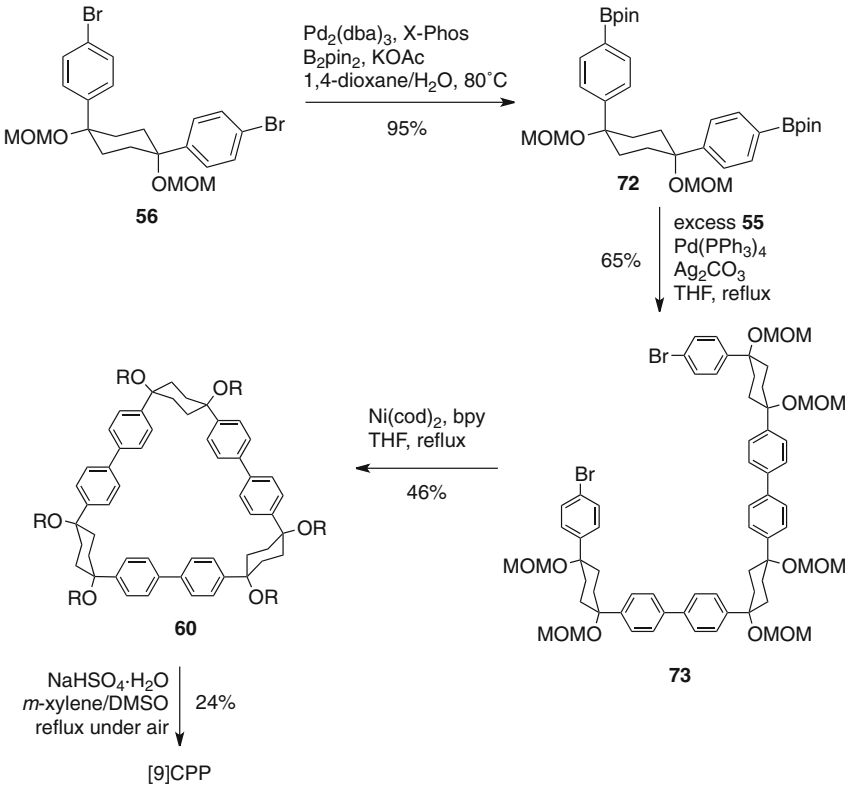


**Fig. 36** Representative intramolecular macrocyclization route to [9]CPP [45]

## *4.6 Functionalized Cycloparaphenylenes*

In 2011, Itami et al. expanded the field of cycloparaphenylene synthesis to include a new class of macrocycle [40]. Representing the smallest unit cycle of a [14, 15] chiral carbon nanotube, naphthalene-included [13]CPPN, was synthesized by modifying the selective synthesis of [12]CPP as developed by the Itami laboratory (Fig. 38). It was rationalized that this new molecule racemized between the M and P isomers at room temperature via rotation of the 2,6-naphthyl moiety through the center of the CPP cavity. It is, however, possible that a smaller CPPN may have restricted isomerization. In principle, the extension of these and other arene-included CPPs could lead to a host of CNT chiralities.

A much more complete model of ultrashort chiral CNTs was synthesized later that year by Isobe et al. [39]. While not, strictly speaking, a cycloparaphenylene, these cyclocrysenylenes (CC) exhibit atropisomerism, with rotation of each chrysenylene unit through the [4]CC cavity geometrically disfavored. These macrocycles were synthesized with an organometallic approach, similar to that used by Yamago (Fig. 39).

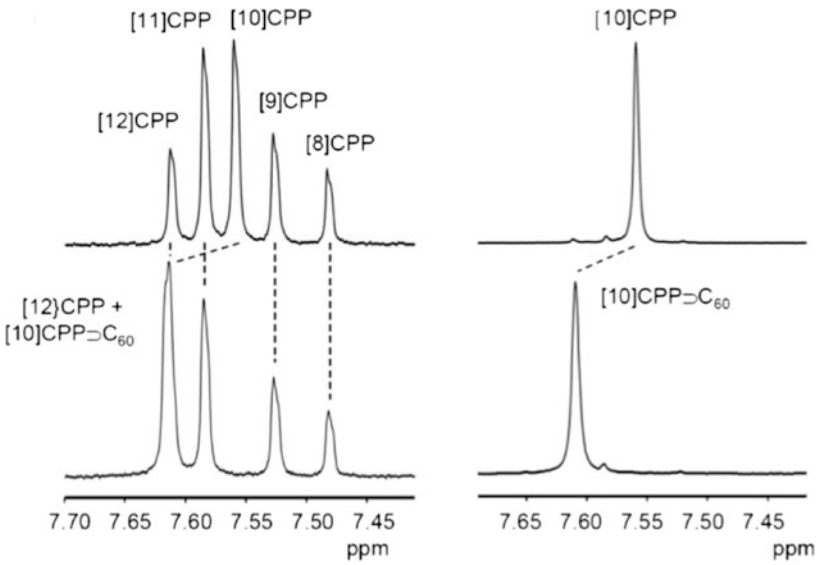


**Fig. 37** Formation of [10]CPP·$C_{60}$ observed by $^{1}$H NMR [37]

Isobe started with hexyl-functionalized dibromo crysene **76**, and accessed the metallocycle **78** via the diboronate **77** using platinum chloride and cesium fluoride. Reductive elimination with triphenylphosphine offered the hydrocarbon **79** cleanly.

Given that the rotation of the aromatic domains of this macrocycle through the cavity is highly disfavored at room temperature (even in the absence of the solubilizing hexyl chains), they represent side wall portions of (10,10), (11,9), and (12,8) carbon nanotubes depending on isomerization (Fig. 40) [44].

Isobe observed that above 100°C a single atropisomer, isolated by HPLC, will scramble to yield all six isomers. Models such as [4]CC with extended π-systems bring us closer to the synthesis of an ultrashort CNT. One can envision, with an appropriate extension strategy, employing Isobe's synthesis to produce selectively armchair (10,10) and chiral (11,9) and (12,8) nanotubes from a single precursor [44].

Along this route to carbon nanohoop elongation, the first π-extended cycloparaphenylene was synthesized by the Itami lab in 2012 [47]. Using the quinone addition and reductive aromatization motif developed by Jasti, dibromide **82** was synthesized by addition to naphthoquinone and macrocyclized using a nickel-catalyzed "shotgun" approach. This macrocyclization gave a poor yield (2%) of the desired nine-membered cyclic oligomer **83** which was painstakingly isolated from the reaction mixture. Single-electron reductive aromatization with granular lithium metal offered the first benzannulated CPP, [9]CN (Fig. 41).

Itami reported the fascinating observation that the proton NMR spectrum of this compound is highly convoluted, indicating restricted rotation of the naphthalene rings through the center of the molecule [47]. Progress towards the closure of the fjord regions in [9]CN to offer the first example of a short CNT obtained by organic synthesis is no doubt underway.

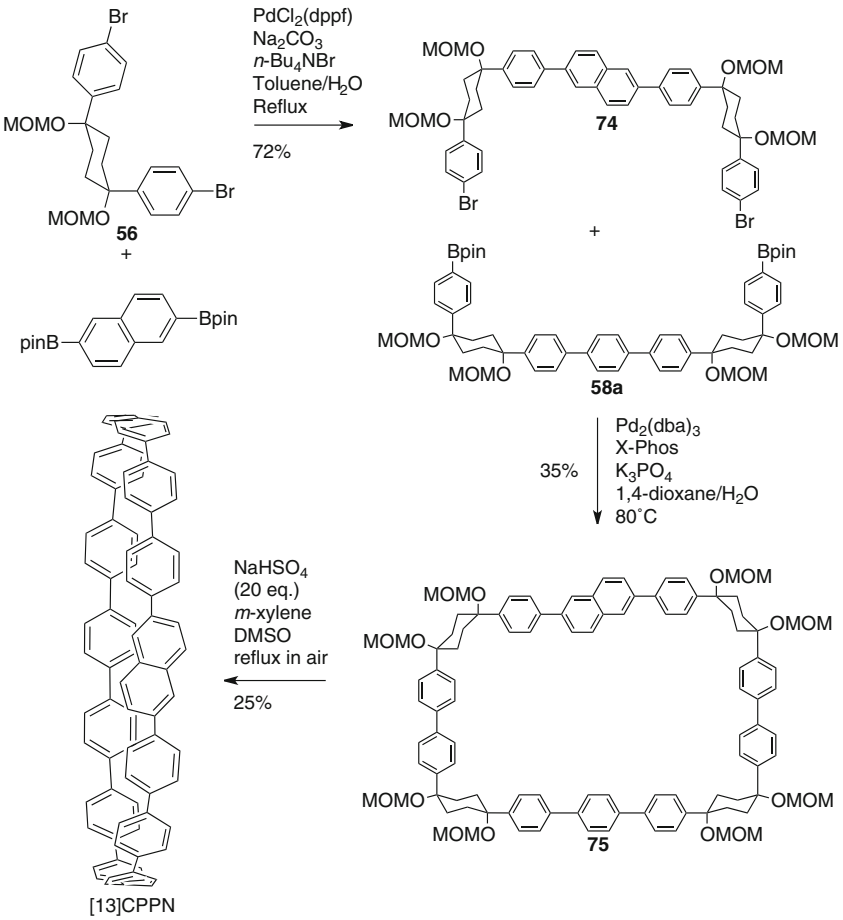


**Fig. 38** Itami's synthesis of [13]CPPN [40]

Another path in which the science of cycloparaphenylenes is expanding is via the inclusion of heteroatoms into the CPP backbone. Itami reported the synthesis of [18]CPP with two 2,2′-bipyridyl units replacing four of the phenyl rings in the CPP structure (Fig. 42) [46]. This [14,4]CPPy was synthesized using established methodology developed by the Itami group and shows a pH dependent fluorescence that can be reversibly red shifted by addition of acid. These preliminary results may open a door towards the controllable fluorescence of nitrogen-doped CPPs.

With their fluorescent properties, high conjugation, and host capability, these nitrogen substituted CPPs are attractive materials for use as ligands and in metal-organic structures. Indeed cycloparaphenylene synthesis in general is a new and wildly exciting frontier in hydrocarbon synthesis. Material science applications of carbon nanohoops are limited, at the moment, only by the availability of large quantities of these unique molecules.

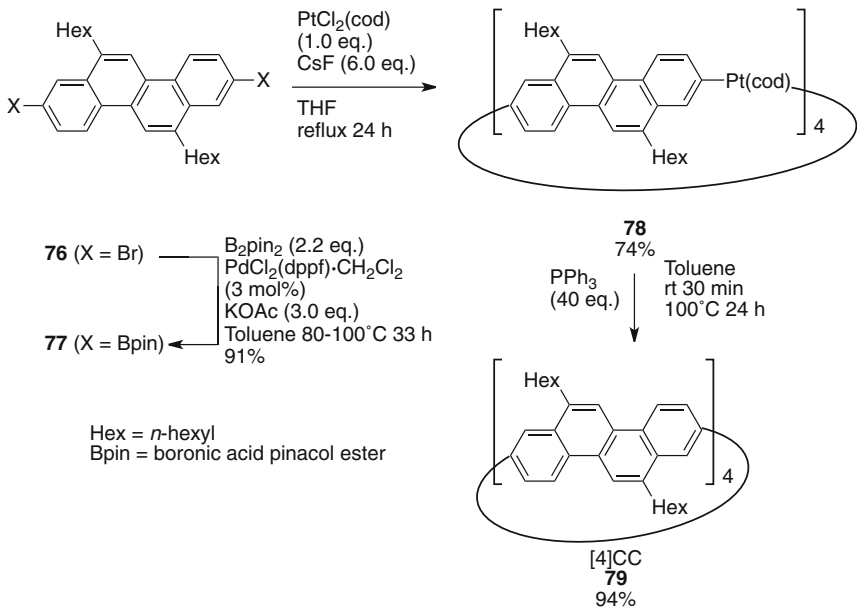


**Fig. 39** Synthesis of a chiral nanohoop with atropisomerism [39]

We have so far focused on single-stranded molecular belts which all display some degree of structural rotation. It is easy to envision molecular belts with two or more strands and a rotationally constrained ladder-type backbone. Discussion of these two-stranded molecular belts follows.

## 5 "Top-Down" Synthesis of [10]Cyclophenacene

One approach to the synthesis of double-stranded aromatic belts is the degradation of higher-order carbon materials with atomistic accuracy. There is only one example of this type in the literature. Nakamura and coworkers developed controllable fullerene chemistry and were able to synthesize successfully a [10]cyclophenacene derivative by the careful selective substitution of the north and south poles of $C_{60}$ fullerene (Fig. 43) [65–68].

The north pole of the fullerene was methylated by reaction with methyl cuprate. This methylated fullerene, **86**, was then converted to cyano-fullerene **87** to prevent formation of the cyclopentadienyl anion by deprotonation in subsequent steps. Derivative **87** was treated with a phenyl cuprate to yield phenyl-substituted **88** with an electronically isolated [10]cyclophenacene. Removal of the cyano group and oxidation gave the penta-oxygenated derivative **90**, which could be easily

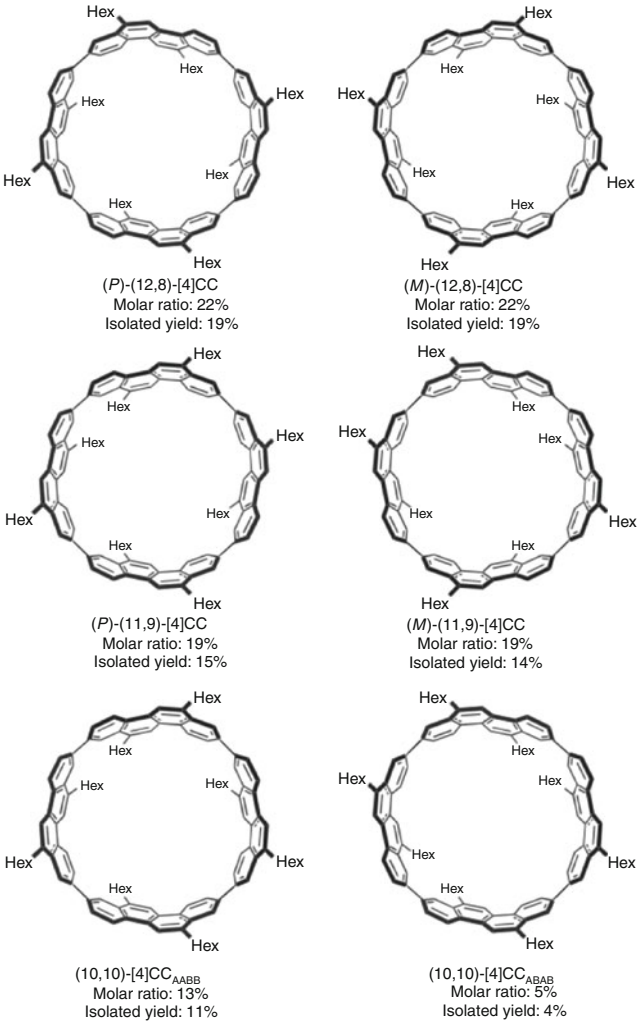


**Fig. 40** Isomers of [4]CC [44]

crystallized for X-ray diffraction studies. Nakamura found that this molecule had remarkable bond consistency. While fullerene exhibits bond length alternation, the 20 π-electrons in the *cis*-annulene equator appeared to be fully delocalized with bond lengths of 1.40 and 1.43 Å. The outer double bonds are much shorter, conforming more to a Kekulé structure than a graphitic model and may be explained by the geometric constraint of the fullerene skeleton. NCIS calculations also confirmed the aromaticity of this novel structure [68]. For the first time, this synthesis validated the idea that discrete, double-stranded aromatic belts can be systematically constructed with organic synthesis. These modified fullerene structures were found to be fluorescent with a quantum yield of $\phi = 0.18$ and a

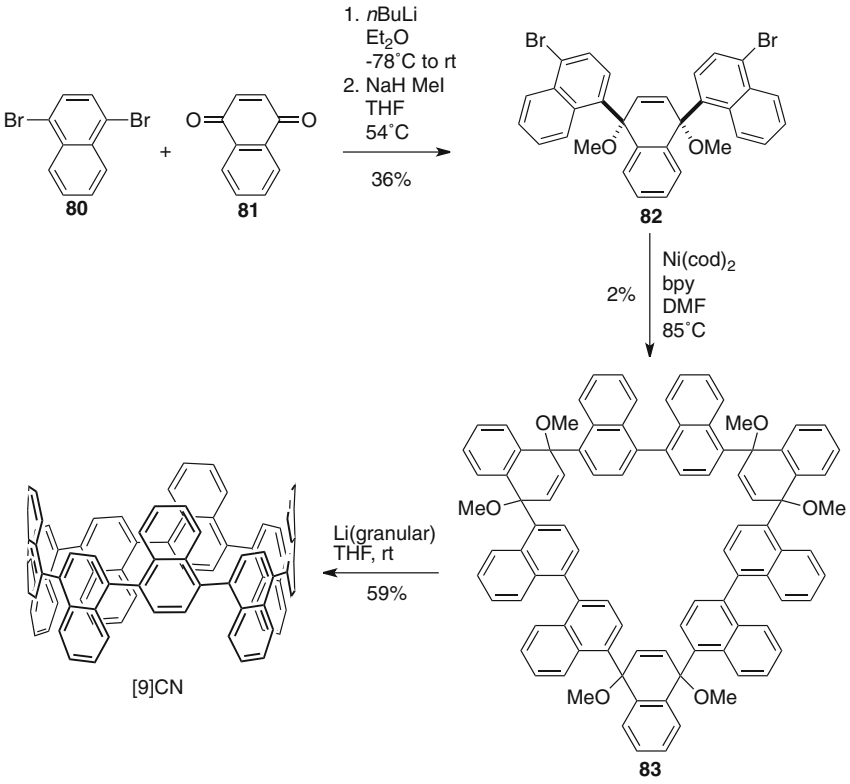


**Fig. 41** Synthesis of a benzannulated CPP, [9]CN [47]

long fluorescence lifetime of $\tau = 65$–$75$ ns [66]. These cores have been functionalized and applied as chromophores [69]. Nakamura's synthesis opened the way for a host of selectively-functionalized fullerenes containing both molecular belts and corrannulene derivatives [66, 67], and the properties of these have been extensively studied and employed in liquid crystal and OLED applications [65, 70].

## 6 Cyclacenes

Just as cycloparaphenylenes and cyclophenacenes represent the unit cycles of armchair carbon nanotubes of the type $(n,n)$, cyclacenes are the shortest possible members of the zigzag nanotube family of $(n,0)$ (Fig. 44).

To date there has been no synthesis of these incredibly strained, fully fused structures. There have, however, been notable attempts that provide insight to the difficult synthesis and unstable nature of these elusive hydrocarbons.

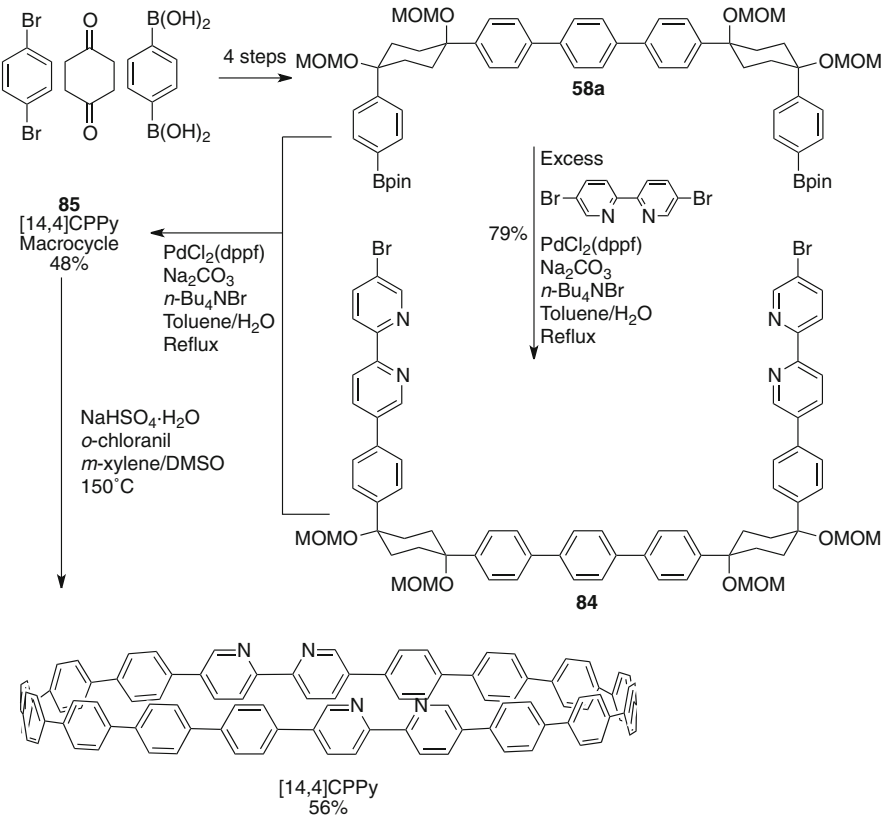


**Fig. 42** Synthesis of [14,4]CPPy [46]

## *6.1 Towards the Synthesis of $[6]_{12}$Cyclacene*

Two notable attempts at synthesizing cyclacenes have been made, the first by Stoddart towards $[6]_{12}$cyclacene in 1992 and the second by Cory towards $[6]_8$cyclacene in 1996 [71, 72]. Stoddart was simply able to build the complex macrocycle Kohnkene **93** in 17% total yield by the sequential reaction of 2 equiv. each of carefully selected but easily synthesized bisdiene **91** and dienophile **92** (Fig. 45) [71].

The electron densities favor only the Diels–Alder addition to the bottom face of the *exo*-diene and the top face of the bicyclic dienophile moieties, thereby yielding **93** under high temperature and pressure. Deoxygenation with low-valent titanium followed by dehydration with acetic anhydride yielded the partially-saturated cyclophane **94**. Given the propensity of linear acenes to oxidative decomposition, the late stage, harsh acidic oxidation, in this synthesis likely prohibited the formation

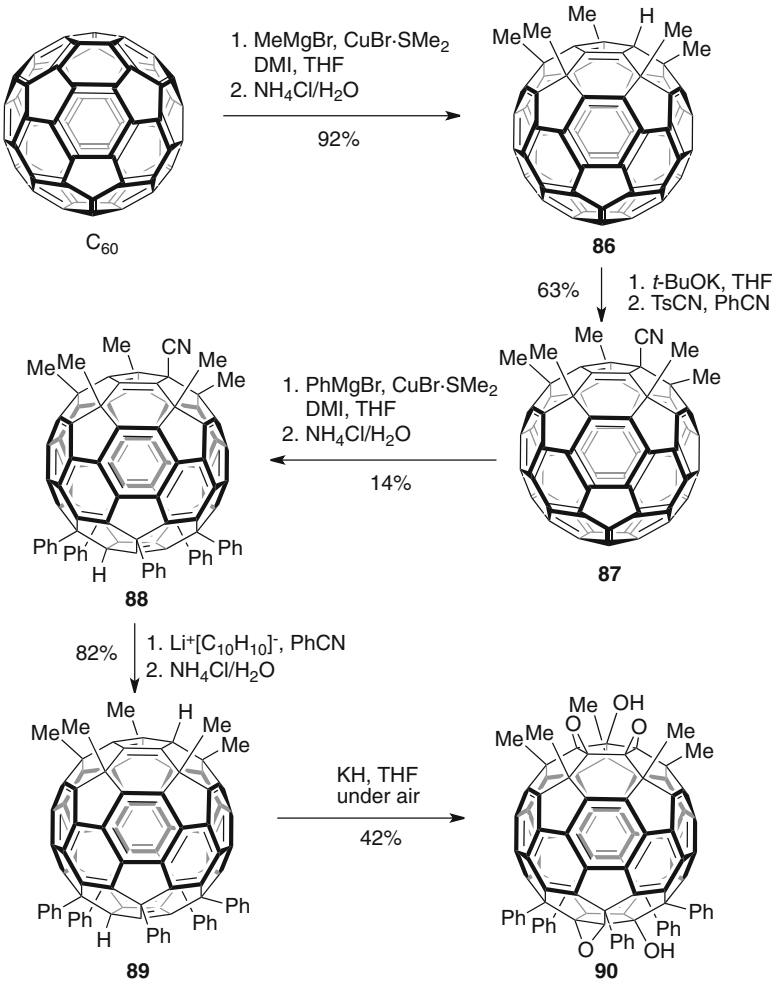


**Fig. 43** Synthesis of substituted [10]cyclophenacene by modification of $C_{60}$ fullerene [67, 68]

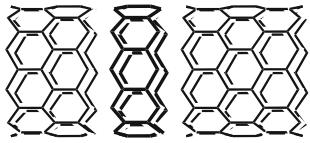

**Fig. 44** Cyclacene envisioned as the unit-cycle of a zigzag nanotube (double bonds omitted for clarity)

of longer acene moieties by way of spontaneous decomposition in the reaction media. Insolubility and large energy requirements due to strain buildup may have also prevented the oxidation of eight additional carbons and conversion to $[6]_{12}$cyclacene [71].

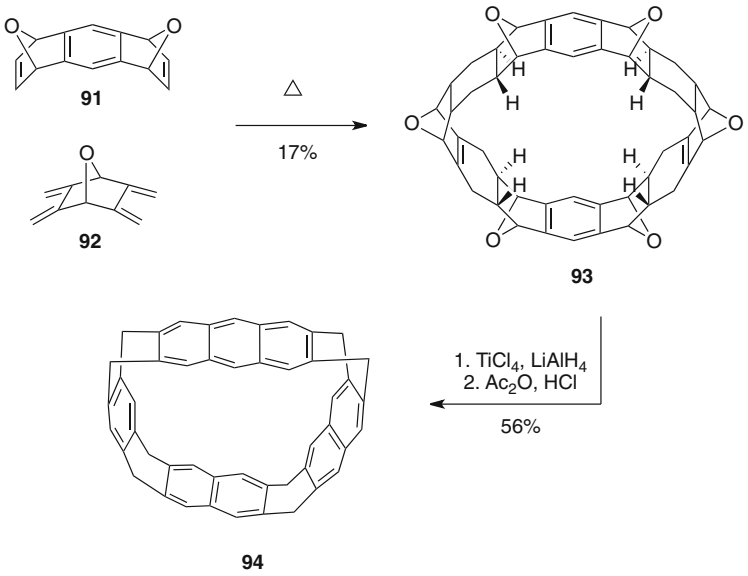


**Fig. 45** Stoddart's attempted synthesis of $[6]_{12}$cyclacene [71]

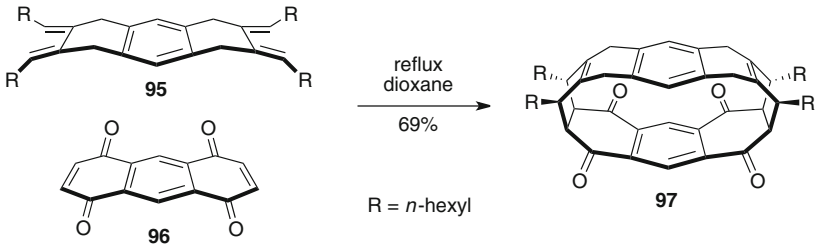


**Fig. 46** Cory's attempted synthesis of $[6]_8$cyclacene [72]

## 6.2 *Towards the Synthesis of $[6]_8$Cyclacene*

In 1996, Cory reported attempts to access $[6]_8$cyclacene from macrocycle **97** (Fig. 46). Building upon the macrocyclization work of Schlüter, this molecule was easily synthesized from the reaction of flexible bisdiene **95** with rigid and planar anthrodiquinone **96** [73].

In this way Cory avoided issues of diastereoselectivity and was able to isolate **97** in 69% yield. Alkyl chains were used to avoid the problem of solubility encountered by Stoddart [72]. Several attempts were made to convert unstrained **97** into $[6]_8$cyclacene including a host of oxidation and deoxygenation conditions, but formation of the cyclacene was never observed [72]. Again, only pathways with oxidative and acidic conditions in the final steps were explored. As previously mentioned, the desired product is likely very unstable in such conditions.

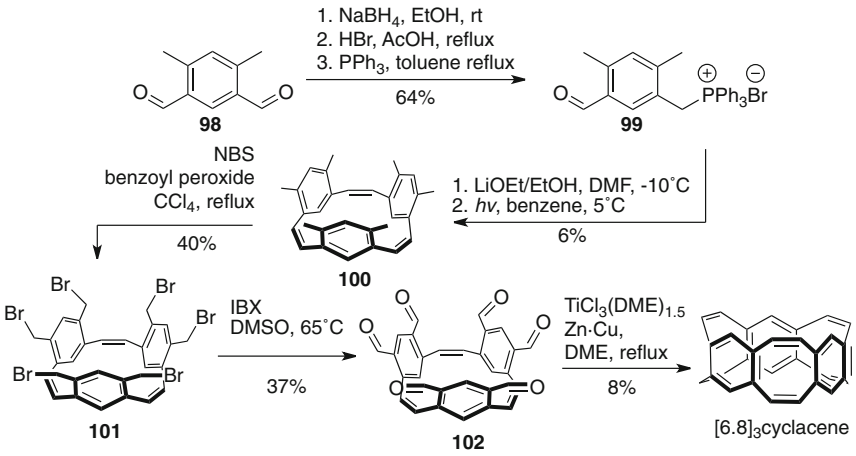


**Fig. 47** Glieter's synthesis of $[6.8]_3$cyclacene [74]

Though the carbon skeleton was assembled in these two attempts, so far there is no successful synthesis of any [6]cyclacene. This enticing molecule—the shortest possible carbon nanotube, with a highly strained skeleton and double trannulene system—will surely not remain an unsolved synthetic problem indefinitely.

## *6.3 [6.8]Cyclacene*

The instability of the [6]cyclacenes is due both to their highly distorted geometry and their calculated singlet–triplet gaps, which narrow with increasing size, falling to near-degeneracy at $[6]_8$cyclacene. To circumvent these unfavorable properties, Glieter employed a moving target approach, proposing that a belt with alternating fused benzene and cyclooctatetraene rings would posses more stable electronics. The boat conformation of the cyclooctatetraene moieties should both alleviate strain and contort the π-system to increase the filled-unfilled orbital gap [74].

This stability was confirmed by the synthesis of $[6.8]_3$cyclacene via a Wittig macrocyclization and McMurry coupling sequence (Fig. 47).

Dialdehyde **96** was converted to the corresponding phosphine salt **99** and dilute macrocyclization followed by irradiation of the resulting *E*/*Z* isomer mixture coalesced into the all-*Z* **101**. Following bromination and oxidation, McMurry conditions closed down the remaining eight-membered rings to offer $[6.8]_3$cyclacene with the majority of hexaaldehyde **102** presumably oligomerizing in the reaction mixture [74].

This cyclacene was found to have $D_{3h}$ symmetry with boat-like cyclooctatetraenes and almost planar benzene rings (Fig. 48) [74].

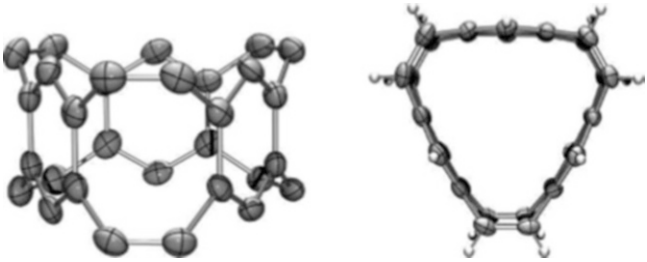

**Fig. 48** Crystal structure of $[6.8]_3$cyclacene showing boat-like cyclooctatetraene moieties [74]

It was estimated that this bending disrupts the conjugation around the cyclacene, diminishing it to about 31% [74]. Even though this structure is electronically distinct from the highly-conjugated [6]cyclacenes, it possesses inward-facing π-orbitals and represents an important step forward in the synthesis of hydrocarbon belts as models for short carbon nanotubes.

## *6.4 Buckybelts*

Over the years, the Schlüter lab has synthesized several saturated belts, including the $[6]_{18}$cyclacene framework [75]. When it became clear that [6]cyclacenes were too reactive to isolate, Schlüter proposed and found evidence for the formation of a buckybelt **110** having the structure of the equator region of fullerene $C_{84}$ (Fig. 49) [76–78].

Reaction of hydrocarbon dienophile **103** with diene synthon **104** gave a greater than 90% yield of *endo* and *exo* adducts which were separated by benchtop chromatography. Generation of benzyne followed by trapping with furan and reaction with tetracyclone offered *syn* and *anti* products **106** and **107** from both *endo* and *exo* **105** respectively in 30% yield over three steps. Heating of both pure *exo* and pure *endo* **106** and **107** separately both led cleanly to the belt **108** having the framework of the target aromatic hydrocarbon. Treatment with *para*-toluenesulfonic acid installed four alkenes to offer **109**. Subsequent conversion of **109** to the desired belt, however, was not observed under acidic conditions, and is yet to be realized [76, 78]. In 2008 it was shown that, upon fragmentation of tetraacetate derivative **111** in a mass spectrometer, the parent ion for **110**, $m/z = 932$ can be observed, confirming the production, if transient, of the desired buckybelt (Fig. 50).

As such, the synthesis of a fully aromatic, two-stranded hydrocarbon belt remains a fascinating challenge in the realm of synthetic organic chemistry.

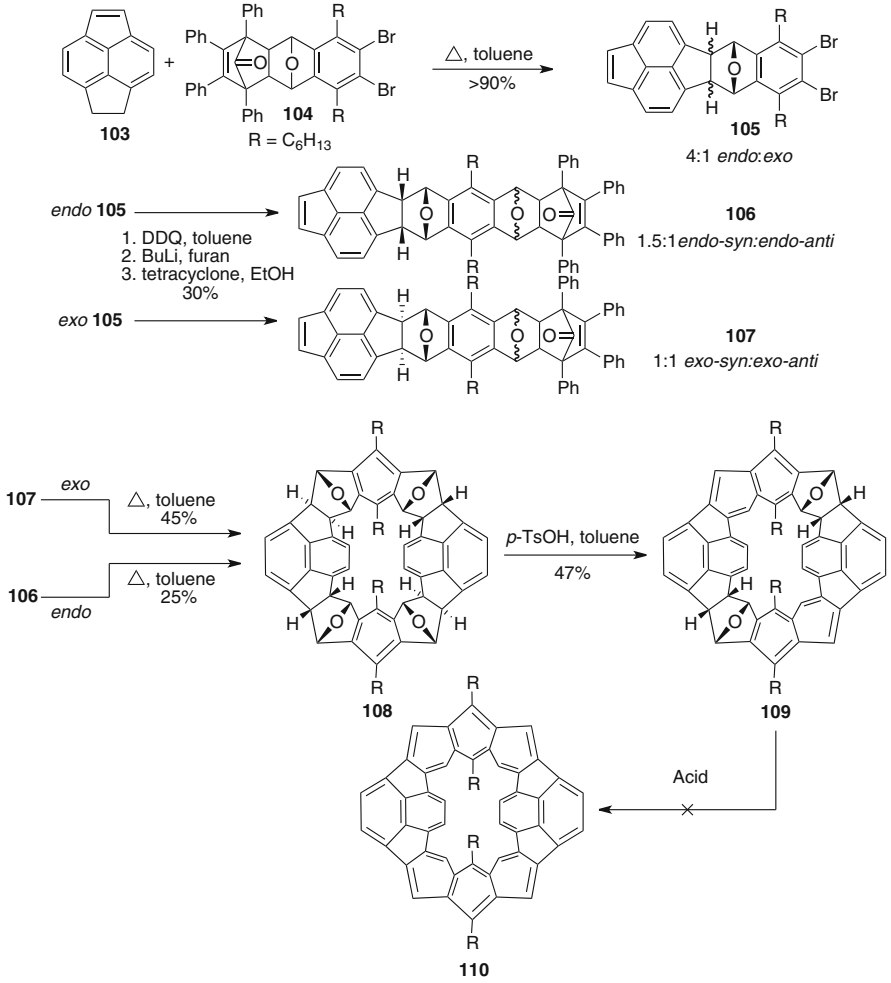


**Fig. 49** Schlüter's synthesis of a buckybelt precursor [76]

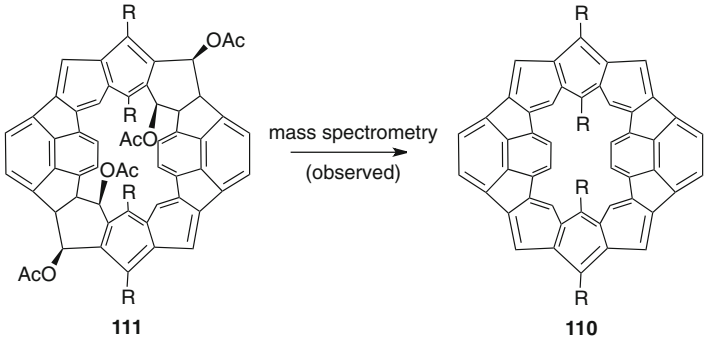


**Fig. 50** Observation of a buckybelt under mass spectrometric conditions [78]

## References


1. Scott LT (2003) Conjugated belts and nanorings with radially oriented p orbitals. Angew Chem Int Ed 42(35):4133–4135
2. Kawase T, Kurata H (2006) Ball-, bowl-, and belt-shaped conjugated systems and their complexing abilities: exploration of the concave-convex π-π interaction. Chem Rev 106 (12):5250–5273
3. Parekh VC, Guha PC (1934) J Indian Chem Soc 11:95–100
4. Diederich F, Rubin Y, Knobler CB, Whetten RL, Schriver KE, Houk KN, Li Y (1989) All-carbon molecules: evidence for the generation of cyclo[18]carbon from a stable organic precursor. Science 245(4922):1088–1090
5. Rubin Y, Knobler CB, Diederich F (1990) Precursors to the cyclo[n]carbons: from 3,4-dialkynyl-3-cyclobutene-1,2-diones and 3,4-dialkynyl-3-cyclobutene-1,2-diols to cyclobutenodehydroannulenes and higher oxides of carbon. J Am Chem Soc 112(4):1607–1617
6. Tobe Y, Fujii T, Matsumoto H, Naemura K, Achiba Y, Wakabayashi T (1996) A new entry into cyclo[n]carbons: [2+2] cycloreversion of propellane-annelated dehydroannulenes. J Am Chem Soc 118(11):2758–2759
7. Kammermeier S, Jones PG, Herges R (1996) Ring-expanding metathesis of tetradehydroanthracene—synthesis and structure of a tubelike, fully conjugated hydrocarbon. Angew Chem Int Ed 35(22):2669–2671
8. Deichmann M, Näther C, Herges R (2003) Pyrolysis of a tubular aromatic compound. Org Lett 5(8):1269–1271
9. Herges R, Deichmann M, Wakita T, Okamoto Y (2003) Synthesis of a chiral tube. Angew Chem Int Ed 42(10):1170–1172
10. Rosenkranz N, Thomsen C (2009) Molecular dynamics simulations of picotube peapods. Physica Status Solidi (B) 246(11–12):2622–2625
11. Rosenkranz N, Machón M, Herges R, Thomsen C (2008) Vibrational properties of four consecutive carbon picotubes. Physica Status Solidi (B) 245(10):2145–2148
12. Rosenkranz N, Machón M, Herges R, Thomsen C (2008) Vibrational properties of semitrimer picotubes. Chem Phys Lett 451(4–6):249–251
13. Machón M, Reich S, Maultzsch J, Okudera H, Simon A, Herges R, Thomsen C (2005) Structural, electronic, and vibrational properties of (4,4) picotube crystals. Phys Rev B 72 (15):155402
14. Kawase T, Darabi HR, Oda M (1996) Cyclic [6]- and [8]paraphenylacetylenes. Angew Chem Int Ed 35(22):2664–2666
15. Kawase T, Ueda N, Darabi HR, Oda M (1996) [2.2.2.2]Metacyclophane-1,9,17,25-tetrayne. Angew Chem Int Ed 35(13–14):1556–1558
16. Kawase T, Ueda N, Tanaka K, Seirai Y, Oda M (2001) The newly modified McMurry reaction toward the improved synthesis of cyclic paraphenylacetylenes. Tetrahedron Lett 42 (32):5509–5511
17. Kawase T, Seirai Y, Darabi HR, Oda M, Sarakai Y, Tashiro K (2003) All-hydrocarbon inclusion complexes of carbon nanorings: cyclic [6]- and [8]paraphenyleneacetylenes. Angew Chem Int Ed 42(14):1621–1624
18. Kawase T, Tanaka K, Fujiwara N, Darabi HR, Oda M (2003) Complexation of a carbon nanoring with fullerenes. Angew Chem Int Ed 115(14):1662–1666
19. Atwood JL, Koutsantonis GA, Raston CL (1994) Purification of C60 and C70 by selective complexation with calixarenes. Nature 368(6468):229–231
20. Suzuki T, Nakashima K, Shinkai S (1994) Very convenient and efficient purification method for fullerene (C60) with 5,11,17,23,29,35,41,47-octa-tert-butylcalix[8]arene-49,50,51,52,53,54,55,56-octol. Chem Lett 23(4):699–702
21. Kawase T, Fujiwara N, Tsutumi M, Oda M, Maeda Y, Wakahara T, Akasaka T (2004) Supramolecular dynamics of cyclic [6]paraphenyleneacetylene complexes with [60]- and

[70]fullerene derivatives: electronic and structural effects on complexation. Angew Chem Int Ed 43(38):5060–5062
22. Kawase T, Tanaka K, Seirai Y, Shiono N, Oda M (2003) Complexation of carbon nanorings with fullerenes: supramolecular dynamics and structural tuning for a fullerene sensor. Angew Chem Int Ed 42(45):5597–5600
23. Kawase T, Oda M (2006) Complexation of carbon nanorings with fullerenes. Pure Appl Chem 78(4):831–839
24. Kawase T, Tanaka K, Shiono N, Seirai Y, Oda M (2004) Onion-type complexation based on carbon nanorings and a buckminsterfullerene. Angew Chem Int Ed 116(13):1754–1756
25. Iijima S (1991) Helical microtubules of graphitic carbon. Nature 354(6348):56–58
26. Ugarte D (1992) Curling and closure of graphitic networks under electron-beam irradiation. Nature 359(6397):707–709
27. Armitage JB, Entwistle N, Jones ERH, Whiting MC (1954) Researches on acetylenic compounds. Part XLI. The synthesis of diphenylpolyacetylenes. J Chem Soc (Resumed) 147–154
28. Srinivasan M, Sankararaman S, Hopf H, Varghese B (2003) Synthesis of buta-1,3-diyne-bridged macrocycles with (Z)-1,4-diethynyl1,4-dimethoxycyclohexa-2,5-diene as the building block. Eur J Org Chem 2003(4):660–665
29. Ohkita M, Ando K, Suzuki T, Tsuji T (2000) Syntheses of acetylenic oligophenylene macrocycles based on a novel Dewar benzene building block approach. J Org Chem 65 (14):4385–4390
30. Ohkita M, Ando K, Tsuji T (2001) Synthesis and characterization of [46]paracyclophane-dodecayne derivative. Chem Commun 24:2570–2571
31. Tobe Y, Furukawa R, Sonoda M, Wakabayashi T (2001) [12.12]Paracyclophanedodecaynes C36H8 and C36Cl8: the smallest paracyclophynes and their transformation into the carbon cluster ion C36−. Angew Chem Int Ed 40(21):4072–4074
32. Jasti R, Bhattacharjee J, Neaton JB, Bertozzi CR (2008) Synthesis, characterization, and theory of [9]-, [12]-, and [18]cycloparaphenylene: carbon nanohoop structures. J Am Chem Soc 130(52):17646–17647
33. Ohkita M, Ando K, Yamamoto K-i, Suzuki T, Tsuji T (2000) First Dewar benzene approach to acetylenic oligophenylene macrocycles: synthesis and structure of a molecular rectangle bearing two spindles. Chem Commun (1):83–84
34. Tobe Y, Fujii T, Matsumoto H, Tsumuraya K, Noguchi D, Nakagawa N, Sonoda M, Naemura K, Achiba Y, Wakabayashi T (2000) [2+2]Cycloreversion of [4.3.2]propella-1,3,11-trienes: an approach to cyclo[n]carbons from propellane-annelated dehydro[n]annulenes. J Am Chem Soc 122(8):1762–1775
35. Takaba H, Omachi H, Yamamoto Y, Bouffard J, Itami K (2009) Selective synthesis of [12]cycloparaphenylene. Angew Chem Int Ed 48(33):6112–6116
36. Omachi H, Matsuura S, Segawa Y, Itami K (2010) A modular and size-selective synthesis of [n]cycloparaphenylenes: a step toward the selective synthesis of [n, n] single-walled carbon nanotubes. Angew Chem Int Ed 49(52):10202–10205
37. Iwamoto T, Watanabe Y, Sadahiro T, Haino T, Yamago S (2011) Size-selective encapsulation of C60 by [10]cycloparaphenylene: formation of the shortest fullerene-peapod. Angew Chem Int Ed 50(36):8342–8344
38. Iwamoto T, Watanabe Y, Sakamoto Y, Suzuki T, Yamago S (2011) Selective and random syntheses of [n]cycloparaphenylenes (n = 8–13) and size dependence of their electronic properties. J Am Chem Soc 133(21):8354–8361
39. Hitosugi S, Nakanishi W, Yamasaki T, Isobe H (2011) Bottom-up synthesis of finite models of helical (n, m)-single-wall carbon nanotubes. Nat Commun 2:492
40. Omachi H, Segawa Y, Itami K (2011) Synthesis and racemization process of chiral carbon nanorings: a step toward the chemical synthesis of chiral carbon nanotubes. Org Lett 13 (9):2480–2483

41. Segawa Y, Miyamoto S, Omachi H, Matsuura S, Šenel P, Sasamori T, Tokitoh N, Itami K (2011) Concise synthesis and crystal structure of [12]cycloparaphenylene. Angew Chem Int Ed 50(14):3244–3248
42. Segawa Y, Senel P, Matsuura S, Omachi H, Itami K (2011) [9]Cycloparaphenylene: nickel-mediated synthesis and crystal structure. Chem Lett 40(4):423–425
43. Sisto TJ, Golder MR, Hirst ES, Jasti R (2011) Selective synthesis of strained [7]cycloparaphenylene: an orange-emitting fluorophore. J Am Chem Soc 133(40):15800–15802
44. Hitosugi S, Nakanishi W, Isobe H (2012) Atropisomerism in a belt-persistent nanohoop molecule: rotational restriction forced by macrocyclic ring strain. Chem Asian J 7:1550–2
45. Ishii Y, Nakanishi Y, Omachi H, Matsuura S, Matsui K, Shinohara H, Segawa Y, Itami K (2012) Size-selective synthesis of [9]-[11] and [13]cycloparaphenylenes. Chem Sci 3:2340–2345
46. Matsui K, Segawa Y, Itami K (2012) Synthesis and properties of cycloparaphenylene-2,5-pyridylidene: a nitrogen-containing carbon nanoring. Org Lett 14(7):1888–1891
47. Yagi A, Segawa Y, Itami K (2012) Synthesis and properties of [9]cyclo-1,4-naphthylene: a π-extended carbon nanoring. J Am Chem Soc 134(6):2962–2965
48. Segawa Y, Fukazawa A, Matsuura S, Omachi H, Yamaguchi S, Irle S, Itami K (2012) Combined experimental and theoretical studies on the photophysical properties of cycloparaphenylenes. Org Biomol Chem 10:5979–84
49. Xia J, Jasti R (2012) Synthesis, characterization, and crystal structure of [6]cycloparaphenylene. Angew Chem Int Ed 51(10):2474–2476
50. Swager TM, Han GD (2011) The smaller the redder. Synfacts 2011(12):1309–1309
51. Sisto TJ, Jasti R (2012) Overcoming molecular strain: synthesis of [7]cycloparaphenylene. Synlett 23(EFirst):483–489
52. Li H-B, Page AJ, Irle S, Morokuma K (2012) Theoretical insights into chirality-controlled SWCNT growth from a cycloparaphenylene template. Chemphyschem 13(6):1479–1485
53. Tian X, Jasti R (2011) Cycloparaphenylenes: the shortest possible segments of armchair carbon nanotubes. In: Petrukhina MA, Scott LT (eds) Fragments of fullerenes and carbon nanotubes. Wiley, Hoboken, pp 291–309
54. Bachrach SM, Stück D (2010) DFT study of cycloparaphenylenes and heteroatom-substituted nanohoops. J Org Chem 75(19):6595–6604
55. Segawa Y, Omachi H, Itami K (2010) Theoretical studies on the structures and strain energies of cycloparaphenylenes. Org Lett 12(10):2262–2265
56. Jasti R, Bertozzi CR (2010) Progress and challenges for the bottom-up synthesis of carbon nanotubes with discrete chirality. Chem Phys Lett 494(1–3):1–7
57. Sundholm D, Taubert S, Pichierri F (2010) Calculation of absorption and emission spectra of [n]cycloparaphenylenes: the reason for the large Stokes shift. Phys Chem Chem Phys 12 (11):2751–2757
58. Wong BM (2009) Optoelectronic properties of carbon nanorings: excitonic effects from time-dependent density functional theory. J Phys Chem C 113(52):21921–21927
59. Friederich R, Nieger M, Vögtle F (1993) Auf dem Weg zu makrocyclischen para-phenylenen. Chem Ber 126(7):1723–1732
60. Ellis KK, Wilke B, Zhang Y, Diver ST (2000) A new method for the synthesis of imidazolidinone- and benzimidazolone-containing [2.2]cyclophanes. Org Lett 2(24):3785–3788
61. Alonso F, Yus M (1992) Easy synthesis of 2,4-dialkyl substituted phenols and anisoles from p-bensoquinone. Tetrahedron 48(13):2709–2714
62. Nijegorodov NI, Downey WS, Danailov MB (2000) Systematic investigation of absorption, fluorescence and laser properties of some p- and m-oligophenylenes. Spectrochim Acta A Mol Biomol Spectrosc 56(4):783–795
63. Yamago S, Watanabe Y, Iwamoto T (2010) Synthesis of [8]cycloparaphenylene from a square-shaped tetranuclear platinum complex. Angew Chem Int Ed 49(4):757–759
64. Jagadeesh MN, Makur A, Chandrasekhar J (2000) The interplay of angle strain and aromaticity: molecular and electronic structures of [0n]paracyclophanes. J Mol Model 6(2):226–233

65. Matsuo Y, Sato Y, Hashiguchi M, Matsuo K, Nakamura E (2009) Synthesis, electrochemical and photophysical properties, and electroluminescent performance of the octa- and deca(aryl) [60]fullerene derivatives. Adv Funct Mater 19(14):2224–2229
66. Matsuo Y, Tahara K, Morita K, Matsuo K, Nakamura E (2007) Regioselective eightfold and tenfold additions of a pyridine-modified organocopper reagent to [60]fullerene. Angew Chem Int Ed 46(16):2844–2847
67. Matsuo Y, Tahara K, Sawamura M, Nakamura E (2004) Creation of hoop- and bowl-shaped benzenoid systems by selective detraction of [60]fullerene conjugation. [10]Cyclophenacene and fused corannulene derivatives. J Am Chem Soc 126(28):8725–8734
68. Nakamura E, Tahara K, Matsuo Y, Sawamura M (2003) Synthesis, structure, and aromaticity of a hoop-shaped cyclic benzenoid [10]cyclophenacene. J Am Chem Soc 125(10):2834–2835
69. Zhang X, Matsuo Y, Nakamura E (2008) Light emission of [10]cyclophenacene through energy transfer from neighboring carbazolylphenyl dendrons. Org Lett 10(18):4145–7
70. Li C-Z, Matsuo Y, Nakamura E (2009) Luminescent bow-tie-shaped decaaryl[60]fullerene mesogens. J Am Chem Soc 131(47):17058–17059
71. Ashton PR, Brown GR, Isaacs NS, Giuffrida D, Kohnke FH, Mathias JP, Slawin AMZ, Smith DR, Stoddart JF, Williams DJ (1992) Molecular LEGO. 1. Substrate-directed synthesis via stereoregular Diels-Alder oligomerizations. J Am Chem Soc 114(16):6330–6353
72. Cory RM, McPhail CL (1996) Transformations of a macrocyclic cyclophane belt into advanced [8]cyclacene and [8]cyclacene triquinone precursors. Tetrahedron Lett 37(12):1987–1990
73. Godt A, Enkelmann V, Schlüter A-D (1989) Double-stranded molecules: a [6] beltene derivative and the corresponding open-chain polymer. Angew Chem Int Ed 28(12):1680–1682
74. Esser B, Rominger F, Gleiter R (2008) Synthesis of [6.8]3cyclacene: conjugated belt and model for an unusual type of carbon nanotube. J Am Chem Soc 130(21):6716–6717
75. Kintzel O, Luger P, Weber M, Schlüter AD (1998) Ring-chain equilibrium between an [18] cyclacene derivative and a ladder oligomer. Eur J Org Chem 1998(1):99–105
76. Neudorff WD, Lentz D, Anibarro M, Schlüter AD (2003) The carbon skeleton of the belt region of fullerene C84 (D2). Chemistry 9(12):2745–2757
77. Denekamp C, Etinger A, Amrein W, Stanger A, Stuparu M, Schlüter AD (2008) Towards a fully conjugated, double-stranded cycle: a mass spectrometric and theoretical study. Chemistry 14(5):1628–1637
78. Stuparu M, Lentz D, Rüegger H, Schlüter AD (2007) Exploring the chemistry of a double-stranded cycle with the carbon skeleton of the belt region of the C84 fullerene. Eur J Org Chem 2007(1):88–100

# Index


**A**
Acenaphth[3,2,1,8-*fghij*]-as-indaceno [3,2,1,8,7,6-*pqrstuv*]picene, 106
Acenaphthalene, 66
Acenaphtho[1,2,3-*bcd*]corannulene, 95
Acenaphtho[3,2,1,8-*ijlkm*]diindeno [4,3,2,1-*cdef*:1′,2′,3′,4′-*pqra*] triphenylene, 106
Acenes, 1, 126, 159
Amidohelicene, 49
Anelli oxidation, 22
Annulation, 142
Anthenes, 224
Anthracenes, 2
  benzannulated, 58
  twisted, 56
Arenes, twisted, 31, 33
Armchair, 197
Aryl–aryl-coupling, 137
Arynes, 126

**B**
Benzene, 1
Benzo[*e*]acephenanthrylene, 162
Benzo[*g*]acecorannulene, 90
Benzocorannulenes, 88
Benzohexacene, 10
Benzopentahelicene, tetramethyl-substituted, 53
Benzo[*c*]phenanthrene, 31, 32, 47
4,5-Bi(3,5-dimethylphenyl)triphenylene, 36
Bisanthene, 224
Bisanthenequinone, 227
Bisbromoperylene, 221
Bis(chloromethyl)-6,6′-dimethylbiphenyl, 34
Bispentacenequinones, 230
Bisphenalenyls, 209
4,5-Bis(2-pyridyl)benzo[c]phenanthrene, 50
13,14-Bis(2-pyridyl)pentaphene, 38
4,5-Bis(2-pyridyl)phenanthrene-3,6-diols, 38
4,5-Bis(2-pyridyl)phenanthrenes, 37, 50
Bowl-shaped molecules, 64
Bowl-to-bowl inversion barriers, 96
Bromocorannulene, 70
Buckminsterfullerene, 95
Buckyballs, 64
Buckybelts, 285
Buckybowls, 63, 110
  hexabenzocoronene-based, 111
  4-*tert*-butyl-1,5,8-trimethylphenanthrene, 36

**C**
Calixarenes, 250
Carbon nanotubes, 63, 64, 112, 251
Catalysis, 121
Chemical vapor deposition (CVD), 121
Circumtrindene, 107, 108
Corannulene cyclophane, 94
Corannulenes, 63, 65, 250
  annelated, 85
  clip, 96
Coronene, 125, 129
Coupling reactions, 121
Cross-coupling, 137
Cyclacenes, 249, 252, 280
Cyclo[18]carbon, 250
Cyclocrysenylenes (CC), 275

Cycloparaphenylene, 249
Cycloparaphenyleneacetylenes, (CPPAs), 249, 251, 252
Cycloparaphenylenes (CPPs), 251, 259
  functionalized, 275
Cyclopentacorannulene, 85, 96
Cyclopentadienone, 66, 126
Cyclophenacene, 249
[10]Cyclophenacene, 278
Cyclotrimerization, 132
Cyclotriveratriline, 250

**D**
Decachlorocorannulene, 75
Decachlorophenanthrene, 44
Decafluorophenanthrene, 44
Decakis(1-pentynyl)corannulene, 114
Decakis(phenylthio)corannulene, 81
Decamethylanthracene, 57
Decamethylcorannulene, 79
Decaphenylanthracene, 31
Decaphenylcorannulene, 80
7,10-Diacetylfluoranthene, 66
1,12-Dialkylbenzo[*c*]phenanthrenes, 47
1,14-Dialkyldibenzo[*c,g*]phenanthrenes, 52
4,5-Dialkylphenanthrenes, 34
1,12-Diarylbenzo[*c*]phenanthrenes, 50
1,14-Diaryldibenzo[*c,g*]phenanthrenes, 54
6,12-Diarylindeno[1,2-*b*]fluorenes, 178
4,5-Diarylphenanthrenes, 36
  diindeno-fused, 39
4,5-Diaryltriphenylenes, 37
4*a*,10*a*-Diazoniaanthra[1,2-*a*]anthracene diperchlorate, 50
Diazoniapentaphene diperchlorate, 37
Dibenz[*1,9;2,3*]anthrone, 124
Dibenzoanthracene-9,10-diyl, 2
Dibenzo[*a,g*]corannulene, 89
Dibenzoperinaphthene, 232
Dibenzo[*c,g*]phenanthrenes, 1,14-disubstituted, 31
  twisted, 52
Dibenzophenanthrolines, 45
2,7-Dibromo-4,5-bis(2-pyridyl)phenanthrene-3,6-diol, 38
Dibromocorannulenes, 68
2,4-Di(*tert*-butyl)-5,7-dimethylphenanthrene, 35
1,10-Dicarboxy-3,8-diphenyl-4,7-phenanthroline, 44
Dichloro(cycloocta-1,5-diene)platinum(II), 266
Dichlorocorannulene, 67
7,14-Dicyano-ovalene diimide, 227
Dideuteriocyclopentacorannulene, 88
Diels–Alder, 2, 4, 6, 8, 11, 16, 18, 20, 53, 66, 87, 96, 126, 148, 149
4,5-Diethylphenanthrene, 36
Difluorobenzo-[*s*]picene, 108
4,5-Dihalophenanthrenes, 43
4,5-Diheteroarylphenanthrenes, 42
Dihydrobenzohexacenes, 10
Dihydrocyclopenta[*b,c*]dibenzo[*g,m*]corannulene, 96
Dihydroheptacenes, 9
Dihydrohexacene, 3
6,12-Dihydroindeno[1,2-*b*]fluorene, 163
Dihydropentacene, 2
Dihydrotriangulene, 216
Dihydroxyanthracene-1,4(2*H*,3*H*)-dione, 4
Diindenocorannulenes, 93
Diindolophenanthroline, 46
Diiodobisanthracene, 149
Diisopropylbenzo[*c*]phenanthrenes, 50
11,12-Dimesitylindeno[2,1-*a*]fluorene, 185
1,14-Dimethoxydibenzo[*c,g*]phenanthrene, 55
1,12-Dimethylbenzo[*c*]phenanthrene, 31, 32
1,12-Dimethylbenzo[*c*]phenanthrene-5-acetic acid, 47
2,5-Dimethylcorannulene, 67
13,14-Dimethyldibenzo[*b,j*][4,7]phenanthroline, 44
1,14-Dimethyldibenzo[*c,g*]phenanthrenes, 53
1,4-Dimethyl-2,5-diphenylbenzene, 163
4,5-Dimethylphenanthrene, 31, 33
Dinaphthosumanenes, 105
1,12-Diphenylbenzo[*c*]phenanthrene, diindeno-fused, 52
Diphenylcorannulene, 71
17,18-Diphenyldibenzo[*a,o*]pentaphene, 40
1,14-Diphenyldibenzo[*c,g*]phenanthrene, 54
14,15-Diphenyldibenzo[*f,j*]picene, 54
2,8-Dithiophene-5,11-didodecyl IF dione, 171
Dye-sensitized solar cell (DSSC) devices, 223

**E**
End-to-end twists, 31
Epoxypolyacenequinones, 126
Ethynylhelicenes, 50
Exfoliation, 121

**F**
Ferrocenes, helical, 54
Fluoranthenes, 8,9-disubstituted, 67
2-Fluorenonylbenzoic acid, 162
Fullerene peapod, 274

**G**
Graphene, 63, 121, 122, 131–151, 197, 255, 274
Graphite ribbon, 240

**H**
Helical aromatics, 31
Hemifullerene, 105
Heptacenequinone, 14
Heptacenes, 3, 9, 14–28
  substituted, 14
Heptazethrene, 213
Heptazethrene diimide, 214
Heterobuckybowls, sumanene-type, 101
Hexa[7]circulene, 112
Hexabenzocoronene (HBC), 124, 142
Hexacenes, 3, 14, 22, 28
  substituted, 7
Hexacosahydroheptacene, 11
Hexafluorosumanene, 99
Hexa(4-iodophenyl)-*peri*-hexabenzocoronene, 135
Hexa-*peri*-hexabenzocoronene (HBC), 231, 232
Hexaphenylheptacene, 18
Hexaphenylpentasulfate macrocycle, 261
Hexaphenyltetrabenzo[*a,c,l,n*]pentaacene, 59
Hexarylene bisimides, 222
Hydrocarbons, alternant, 1
  molecular-bowl, aromatic, 63

**I**
Indacenodiphenalene (IDPL), 209
Indacenopicenes, 108
Indeno[1,2-*a*]fluorene-7,12-diones, 165
Indeno[1,2-*b*]fluorene, 159
Indeno[1,2-*b*]fluorene-6,12-diones, 167
Indeno[1,2-*b*]fluorene-6,12-olefins, 172
Indeno[2,1-*a*]fluorene-11,12-diones, 183
Indeno[2,1-*b*]fluorene-10,12-diones, 186
Indeno[2,1-*c*]fluorene-5,8-diones, 189
Indenocorannulenes, 91
Indenofluorenes (IFs), 159, 160
Iodonorbornanone, 100
Isocorannulenofuran, 87
4-Isopropyl-1,5,8-trimethylphenanthrene, 36
7-Keto-12-hydroindeno[1,2-*a*]fluorenone, 162
9-Keto-12-hydroindeno[2,1-*b*]fluorenone, 162

**L**
Light emitting diodes, 159, 160, 228
Lithium(silylacetylide), 14

**M**
Methylcorannulene, 70
1-Methylnaphthalene, 10
Molecular belts, 249
Molecular ribbon, 126
Multi(phenylthio)corannulenes, 83

**N**
Nanographenes, 112, 199
  2D, 197
Naphthacene, 276
Naphthalene-2,3-dicarbaldehyde, 4
Naphthalenes, 2, 3, 56, 67, 219, 224
  twisted, 56
Naphthosumanenes, 104
Naphthyne, 126
Nonacenes, 21
  silylethynyl substituted, 23
  thioaryl substituted, 26

**O**
Octacene, 21
Octahydroindeno[1,2-*b*]fluorene, 163
Octakis(arylthio)naphthalenes, 57
Octamethylnaphthalene, 31, 57
Octaphenyldibenzo[*a,c*]naphthalene, 59
Octapyrrolylnaphthalene, 57
Octazethrene, 213
N-Octyldibenzo[*d,m*]-1,2-corannulimide, 90
Oligoparaphenylenes (OPPs), 264
Open-shell systems, phenalenyl-based, 201
Opto-electronic materials, 197
Organic electronics, 159
Organic field-effect transistors (OFETs)
Organic light-emitting diodes (OLEDs)
Organic synthesis, 121
Ovalenes, 227
Oxophenalenoxyl radicals, 208

**P**
Penta(*tert*-butyl)corannulene, 81
Pentacenes, 1–27, 175
Pentachlorocorannulene, 75, 76
Pentahelicene, 52
Pentahelicenebisbenzoquinone, 56
Pentaindenocorannulene, 93
Pentakis(arylethynyl)corannulenes, 114
Pentakis(2-biphenylyl)corannulene, 112
Pentakis(Bpin)corannulene, 76, 112
Pentakis(diethylene glycol methyl ether) corannulene, 77
Pentakis(phenylthio)corannulene, 81, 114

Pentakis(trifluoromethyl)corannulene, 76
Pentalenodiphenalene (PDPL), 209
Pentamanisylcorannulene, 82, 114
Pentarylene, 219
Periacenes, 224, 230
Peripentacene, 230
Peritetracene, 230
Perylene monoimide, 220
Perylenedicarboximides, 221
Phenalene, 86
Phenanthrenes, 33
  twisted, 34
1,10-Phenanthroline-1,10-dioxides, 47
Phenanthrolines, 1,10-disubstituted, 44
Phenylbenzoylacetylene, 186
Photocyclizations, 142
Photovoltaics (OPVs)
Picotubes, 249, 250
Polyacene, 126
Polyarenes, 159
Polyaryl hydrocarbons, 159
Polycyclic aromatic hydrocarbons (PAHs), 121, 124, 159, 197
Poly(indeno[1,2-*b*]fluorene), 175
Polymers, 1
Poly(peri-*N*-annulated perylenes), 222
Postfunctionalization, 147

**Q**
Quantum dots, 264
Quateranthene, 225
Quaterrylene, 219
Quaterrylene bisimides, 220

**R**
Radicals, 197
Resonating valence bond (RVB) model, 210
Ribbons, twisted, 127
Ring-closing metathesis, 146
Ruthenium(II) bis(terpyridine) complexes, 41
Rylene bisimides, 221
Rylenes, 219, 228

**S**
Semibuckminsterfullerenes, 95, 110
Semiconducting materials, 2
Solubility, 149
Spectroscopy, 1
Sumanenes (tricyclopenta[*def*,*jkl*,*pqr*] triphenylene), 63, 97
Sumanenetrione, 104
Superbenzene, 129, 231, 239
Superbenzenoids, 130
Supernaphthalene, 128, 129, 239
Superphenalene, 239
Superphenylene, 239
Supertriphenylene, 129, 239
Surface-assisted methods, 149

**T**
Teranthene, 224
Terphenyl, 159, 167, 170, 173, 179, 183, 264, 271
Tetraanthraceneylidene (TDDA), 250, 252
Tetrabenzocoronene, 142
Tetrabenzoperopyrene, 232
Tetrabenzopyracylene, 109
Tetrabromocorannulene, 68, 75
Tetracene, 3
Tetradehydro[10]annulene, 213
Tetradehydrodianthracene, 250
Tetraethynylindeno[1,2-*b*]fluorenes, 175
Tetrahydroheptacenes, 10
Tetraindenopyrene, 109, 110
Tetrakis(bromomethyl)fluoranthene, 67
Tetramethylbenzopentahelicene, 54
Tetramethylidene-bicyclo[2.2.2]oct-2-ene, 11
Tetramethyl-4,7-phenanthroline, 44
Tetraphenyl-9,16-bis[4-(2-ethylhexyloxy) phenyl]heptacene, 18
Tetraphenylcyclopentadienones, 57, 128, 233
Triangulene, 215
Triazasumanenes, 102
Trimethyl-1-phenanthreneacetic acid, 34
Trinaphthosumanene, 105
Trioxytriangulenes, 216
Trisanthracene, 138
Trisaryne, 127
Trisilasumanene, 101
Trisphenalenyls, 209
Trithiasumanene, 101
Two-photon absorption (TPA), 210

**X**
Xylylsumanene, 99

**Z**
Zethrenes, 212
Zigzag, 197